UNIVERSITY OF CALIFORNIA

SANTA CRUZ

1. MEDICINAL CHEMISTRY OF A SMALL MOLECULE DRUG LEAD: TAMOXILOG
2. ELECTRONIC COMMUNICATION THROUGH RUTHENIUM NANOPARTICLES: SYNTHESIS OF CUSTOM LIGANDS AND NANOPARTICLES

A dissertation submitted in partial satisfaction
of the requirements for the degree of

DOCTOR OF PHILOSOPHY

in

CHEMISTRY

by

Nathaniel Benjamin Zuckerman

June 2012

The Dissertation of Nathaniel B. Zuckerman is approved:

_____
Professor R. Scott Lokey, Chair

_____
Professor Joseph P. Konopelski

_____
Professor Roger G. Linington

_____
Tyrus Miller
Vice Provost and Dean of Graduate Studies

TABLE OF CONTENTS

LIST OF FIGURES

CHAPTER 1:

CHAPTER 2:

CHAPTER 4:

LIST OF TABLES

CHAPTER 1:

CHAPTER 2:

CHAPTER 3:

CHAPTER 4:

LIST OF SCHEMES

CHAPTER 1:

CHAPTER 2:

CHAPTER 3:

CHAPTER 4:

ABSTRACT

Nathaniel B. Zuckerman

1. Medicinal Chemistry of a Small Molecule Drug Lead: Tamoxilog
2. Electronic Communication Through Metal Nanoparticles: Synthesis of Custom Ligands and Nanoparticles

1. Compound NSC-670224, previously shown to be toxic to *Saccharomyces cerevisiae* at low micromolar concentrations, potentially acts via a mechanism of action related to that of tamoxifen (NSC 180973), a widely utilized breast cancer drug. The structure of NSC-670224, previously thought to be a 2,4-dichloro arene, was established as the 3,4-dichloro arene, and a focused library of analogues were synthesized and biologically evaluated in conjunction with the UCSC Chemical Screening Center. The synthesis of a biotinylated affinity probe was also completed in order to extract the protein target(s) of NSC-670224 from yeast and human cell lines in collaboration with the Hartzog lab (UCSC MCD Biology)

2. Stabilization of ruthenium nanoparticles (Ru NPs) through carbene bound ligands has led to a simple and effective means to generate new materials with unique optoelectronic properties. The affinity of freshly prepared Ru NPs to diazo compounds, specifically octyl diazoacetate (ODA), provides a robust nanostructure that can be further functionalized via metathesis of terminal olefins to generate these unique materials. Carbene-stabilized Ru NPs have provided insights into the nature of extended conjugation and intraparticle charge delocalization through covalently bound

probes (e.g., ferrocene and pyrene). The growing interest to study electronic communication through Ru NPs has lead to collaborative, multidisciplinary efforts between analytical (Shaowei Chen lab, UCSC), theoretical (Haobin Wang Lab, NMSU), and synthetic organic chemists (Konopelski Lab, UCSC). With this powerful collaboration, new methods to generate stabilized Ru NPs, testing theory with experiment, and efficient means to functionalize NPs have been investigated. The syntheses of custom ligands and their applications to nanoparticle-mediated electronic communication are reported.

DEDICATION AND ACKNOWLEDGEMENT

I am greatly appreciative to have had the opportunity to work for Professor Joseph P. Konopelski. His guidance, provision of freedom in the laboratory, and availability to discuss chemistry were pivotal to my success in graduate school. I would also like to thank Professor Shaowei Chen for the opportunity to work on the collaborative research grant toward nanoparticle-mediated electronic communication. Under the guidance of Professor Chen, former postdoctoral researcher, Dr. Wei Chen, and graduate students Xiongwu “Mike” Kang, and Yang Song were excellent teammates of mine for efficient and high impact research leading to many publications together. I am very grateful for discussions with Dr. James W. Lewis on proper light sources and measurement of these sources for the molecular photoswitch project. Also, I am grateful to Professor Roberto Bogomolni for providing the lamps for studying the molecular photoswitch, to Dr. Allen Oliver, Dr. David Rogow, and Honghan Fei (Scott Oliver lab) for solving all of my X-ray crystal structures, and to Jim Loo and Steven Loveridge (Crews lab) for assistance with NMR and mass spectrometry.

The efforts of many people with varying backgrounds were necessary in the tamoxilog project, and their work must be acknowledged. Thanks to Professor R. Scott Lokey (dissertation committee chair) for including me on this project and supporting my expanded involvement in developing a library of compounds and an affinity probe. Screening of my synthesized compounds

was conducted by Dr. Nadine C. Gassner, Walter M. Bray, and their undergraduate associates in the UCSC Chemical Screening Center. Additional screening against yeast and attempts to identify tamoxilog's target protein(s) were conducted by Dr. Tiffani K. Quan under the guidance of Professor Grant A. Hartzog (UCSC MCD Biology). Analysis of the yeast gene deletion data (Ron Davis lab, Stanford) was conducted by Professor Joshua M. Stuart (UCSC BME). Purification by preparative HPLC of the hexanoate and biotinylated affinity probe were conducted by Arthur Rand (Lokey lab). Assistance with LCMS for the SAR library was afforded by Laura Sanchez (Linington lab).

The opportunity to teach undergraduate organic chemistry was a great experience, and I am thankful for expert guidance from Dr. Daniel R. Palleros, Professor Claude F. Bernasconi, Professor Rebecca Braslau, Professor Joseph P. Konopelski, and Professor Roger G. Linington (dissertation committee member).

Graduate school would not have been complete without the support and camaraderie of my fellow graduate colleagues Jaime Saavedra, Michael Anderson, Eric Evans, Brandon Heilman, and Kenny Ikei. The good times were plenty, but just as important it was great to share the ups and downs of graduate school with such a great group of guys/chemists. It was great to work with my fellow lab mates, Stephanie Stepp Curzon, William Hewitt, Dr. Max Mahoney, Dr. Yvette Mimieux Vaske, and Dr. Jessica Garcia. Special

appreciation goes to my mentor, Dr. Lauren Brown. It was also a great experience to work with Dr. Michael Egger (German postdoctoral researcher) and Professor Kenya Nekata (Japanese Professor) as visiting researchers in our lab. Thanks to my hardworking undergraduate researchers Andrew Myers and Evan Nguyen.

Last, but certainly not least, I would like to dedicate this dissertation to my fantastic, understanding, and beautiful wife, Celeste, and to our soon to be born son, Benjamin Emmett Zuckerman. Much appreciation for their support in all fashions is due to my parents, Alfreda and Lawrence, my brother and sister, Adam and Malinda, my in-laws, Zenaida and Arthur Rosete, and to Laura Zuckerman, Eric Rosete, Chad Cataylo, Kristine, Daniel and Cameron Louie. I am very lucky to have such a loving family.

CHAPTER 1: Medicinal Chemistry of a Small Molecule Drug Lead: Tamoxilog

1.1 Drug Discovery and High-Throughput Screening with Yeast

Advances in pharmaceutical drug discovery throughout history have taken many forms. From folk medicine to natural product isolation, to combinatorial chemistry and receptor expression, attempts to efficiently find new drugs have been an important and necessary evolutionary process. No single process is the answer; the cutting edge of drug discovery is defined by the aggregate of intersecting scientific fields and techniques.

The process of drug discovery from start to finish requires a daunting amount of capital and labor, which often times leads to losses of hundreds of millions of dollars when a drug fails to gain approval or must be pulled in late clinical trials.[1] Drug companies believe that understanding a drug's target and mechanism of action can greatly reduce the number of failures. It has become evident that academia and industry can reduce the investment/risk within a drug lead by working together.[2]

Within our own department, the many forms of drug discovery are unified with the UCSC Chemical Screening Center. It is here that biologists, chemists, engineers and industry professionals (to name a few disciplines) utilize High-Throughput Screening (HTS) capabilities to maximize efficiency towards assay development and, ultimately, drug lead discovery. HTS is a first step approach that both academia and industry employ to ease risk.

Specifically, this thesis will elaborate upon the use of yeast-based HTS methods toward drug discovery.

Yeast is widely chosen as a model biological system for eukaryotic studies. The most commonly used species is that of *Sacchromyces cerevisiae*.[3] Yeast contain many genes that are homologous with human genes implicated in disease states, and much effort has been focused on developing HT methods for genomic analysis.[4]

One such development is the creation of the *Sacchromyces* genome deletion project, which has developed libraries of mutants for nearly all possible open reading frames (ORFs) within the *S. cerevisiae* genome, with the ultimate goal of determining the function of every gene.[5,6] Deletion mutants were created by replacing a single ORF with the *KanMX* gene[5] and a unique "barcode" (two 20 nucleotide sequences that flank the *KanMX* gene). Since the creation of yeast deletion strain libraries, methods have been developed to discover new drug targets and mechanisms. Unperturbed *S. cerevisiae* is considered wild-type (wt) as compared to these deletion mutants.

In 1996, the *Sacchromyces* genome deletion project began and has since led to seminal publications in 1999 and 2002 on the utility of the developed mutant libraries towards determining gene function.[5,6] In these publications, non-essential and essential genes for yeast viability were determined by using phenotypic analysis under varying growth conditions. A

simple artifact of this determination, as mentioned by the authors, is that essential genes in yeast without a human homolog would be prime candidates for antifungal targets. Additionally, another usage of the deletion library would be to probe the gene targets of known therapeutics.

By examining well-characterized therapeutics against the yeast gene deletion series, validation of the technique was made when yeast targets homologous to the known human target of the drug were identified.[11] In this study, a set of heterozygous deletion mutants were competitively grown in the presence of drug, and those strains showing growth reduction relative to other strains (reduced fitness) were indicated as being sensitive to the drug. In addition to hitting the known targets, perhaps more importantly, off-targets were identified implicating alternative modes of action for a given drug. The study also showed relationships between drugs not previously seen by comparison of the developed chemogenomic profiles (compound interactions with its group of sensitive genes defines its chemogenomic profile). This could potentially lead to new uses for a drug, identification of side-effect causality, and additionally affected biological pathways (other than the protein target).

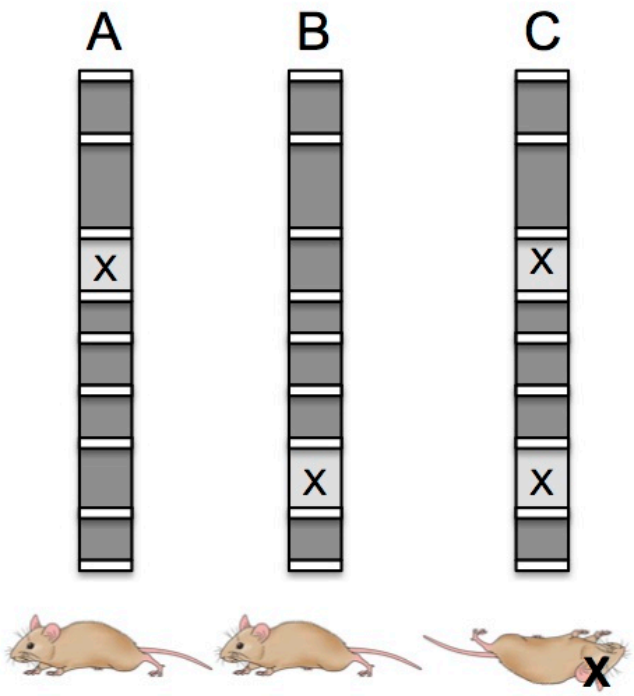

Figure 1.1 Synthetic Lethality Organism **A** has one gene knockout and survives. Organism **B** has a different gene knockout and survives. Combine those two knockouts in one organism and cause death to the organism and a synthetic lethal has been developed.

Looking outside of distinct interactions with single mutant libraries can expand upon the chemogenomic profile. Cell processes are thought to interact and there are many instances whereby multiple pathways lead to a similar cell function. One way to link pathways, and potentially drug mode of action, is to map genetic interactions by the use of a synthetic genetic interaction (SGI) network. Tong and co-workers set out to map genetic interactions with the use of double deletion mutants in the hope to identify "synthetic lethals."[7] A synthetic lethal interaction is described as the effect of lethality on a double deletion mutant strain, that wouldn't be lethal for either of the single deletion mutants alone. The synthetic lethality produced implies

mutually compensating pathways.[8] A general example to explain synthetic lethality is that there are three pathways that produce Ac-CoA in mice and knocking out one pathway won't necessarily be lethal (due to upregulation and compensation by other pathways), but by removing two portions of different pathways producing Ac-CoA, lethality may be induced (pictorial example Figure 1.1). The many synthetic lethal interactions identified by Tong and co-workers have lead to a refinement of chemical genetic profiles, and a powerful means for drug target screening as evidenced by a pathway-to-drug approach published recently by Lokey, Stuart and co-workers (contrary to the more typical drug-to-pathway approach).[8]

1.2 Tamoxifen and Tamoxilog: A Collaborative Investigation

The success and utility of the *Sacchromyces* gene deletion library is undeniable, but for most investigations, it is not necessarily a cost effective starting point. A simple, yet effective, HT method developed by members of our screening center takes advantage of the robust character of wt-yeast, to single out potent drug leads.[9] This HT method is complementary to the previously described gene deletion libraries. To briefly describe the method, an agar plate impregnated with wt-yeast is pinned in 384-well format with compounds of interest (the library). "Hits" are detected as a "halo" or zone of cell death around the pin spot, and a plate reader quantifies their toxicity.

An initial screen of the National Cancer Institute's Diversity Set I, Mechanistic Set and Natural Products Set, comprising a total of 3,104

synthetic compounds and natural products, identified 46 hits. Many of those compounds have unknown activity against yeast, while others, like tamoxifen (NSC 180973, anti-breast cancer drug), are known to interact with yeast without full understanding of mechanism.[10,11,12]

With a narrow field of compounds and their relationships to be determined, utilization of the Davis group's yeast gene deletion library (Stanford Biochemistry/Genetics)[13] was a feasible next step. Our interest in probing the utility of the *Sacchromyces* gene deletion library expands upon the use of data for solely well-characterized compounds. Although tamoxifen can be considered as well characterized, it is not necessarily thoroughly understood when considering potential off targets, as seen by the numerous publications that indicate previously unknown gene interactions with yeast.[10,11,12] In the case of the 46 compounds screened, synthetic lethality of the various mutants was analyzed by the Stuart group (UCSC BME)[14] to develop a chemical genetic profile. The profile for each hit can be compared amongst the group of hits to identify similar chemical genetic profiles, or in other words, compounds that may be targeting similar or related biological pathways. The power of this particular approach is that a compound with an unknown mode of action may share a chemical genetic profile with a compound with known function. As depicted in Figure 1.2, tamoxifen (**1.1**) and the previously biologically undescribed compound NSC-670224 (**1.2**) appeared to have similar chemical genetic profiles as determined by a

computational genomic approach performed by the Stuart lab. The determination of a similar chemogenetic profile between tamoxifen and NSC-670224 leads one to believe that these two compounds share a similar mode of action towards a previously unknown target for tamoxifen. Further evaluation of the synthetic genetic interaction data led to an implication of function relating to chromatin remodeling (a recent publication by Ashworth and co-workers[15] implicates a compendium of tamoxifen related genes, some of them are chromatin related). Therefore, the structural determination of NSC-670224 and synthesis of analogs for development of SAR are required to biologically investigate the relationship between both compounds.

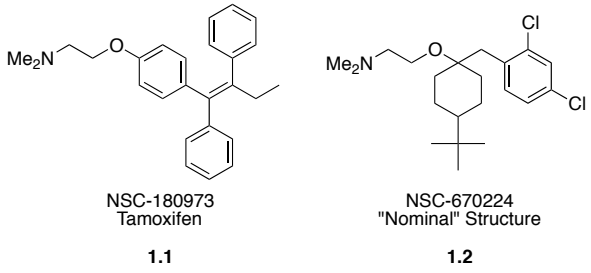

Figure 1.2 Structures of Tamoxifen and NCI compound NSC-670224

Thus, an investigative approach to test this hypothesis ensued, utilizing the expertise of the Hartzog lab (UCSC MCD Biology).[16] The Hartzog lab specializes in yeast as a model system for the study of chromatin related factors, and is therefore a perfect match in this collaborative effort to define the possible link between tamoxifen and NSC-670224.

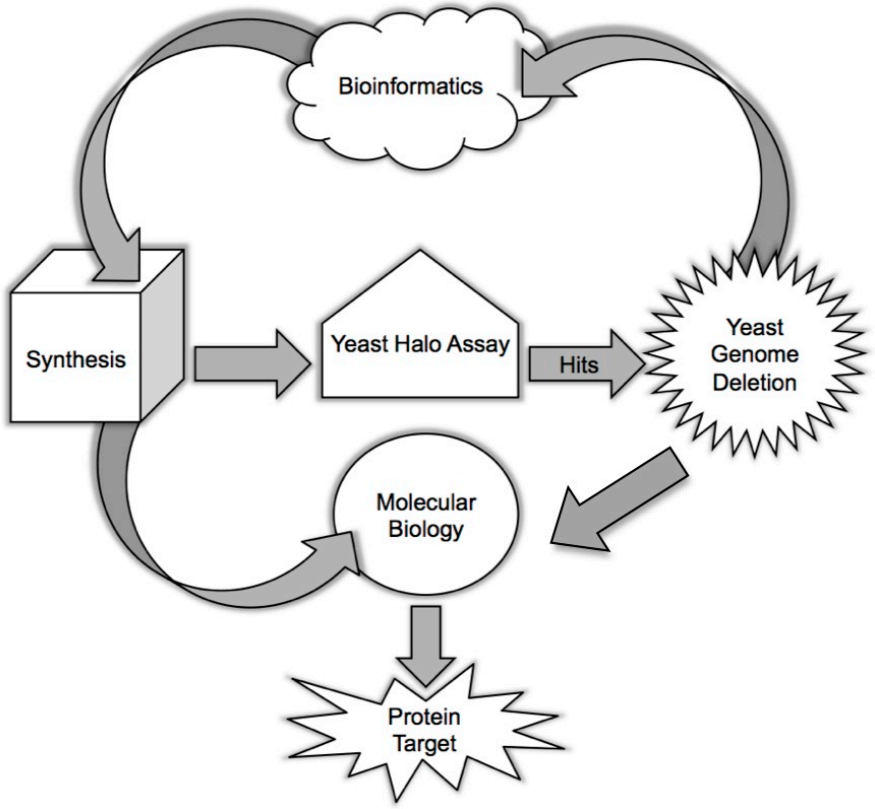

Figure 1.3 Collaboration Diagram UCSC Chemical Screening Center and UCSC Chemistry Lokey Group (Yeast Halo Assay); Stanford Biochemistry/Genetics Davis Group (Yeast Genome Deletion); UCSC BME Stuart Group (Bioinformatics); UCSC Chemistry Konopelski Group (Synthesis); UCSC MCD Biology Hartzog Group (Molecular Biology)

Due to the limited quantities of NSC-670224 provided by the National Cancer Institute (NCI), it was necessary to synthesize more compound for the Hartzog group to carry out their biochemical studies. Therefore, our lab was consulted for the synthesis of NSC-670224. As will be seen, the seemingly simple task of synthesizing both isomers of NSC-670224 spawned the additional development of a small library of compounds and a biotinylated affinity probe.

The collaborations for this project are summarized in the flowchart above, Figure 1.3.

1.3 A Brief History and Background of Tamoxifen and its Uses

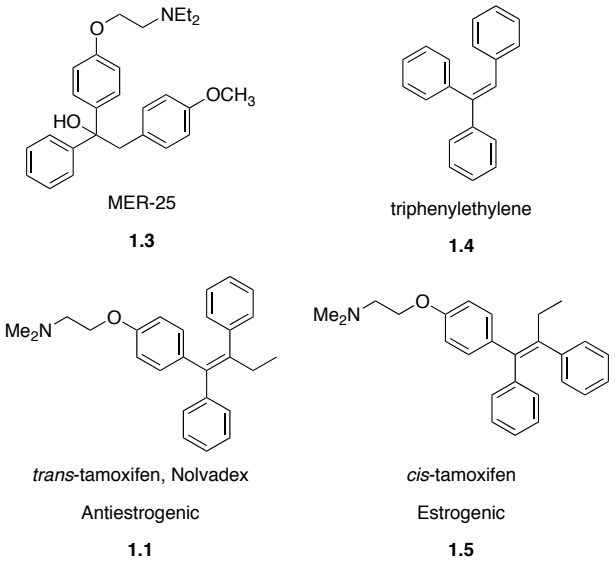

Figure 1.4 Early antiestrogens (top) and both isomers of tamoxifen (bottom)

The use of tamoxifen (antiestrogen/selective estrogen receptor [ER] modulator) as treatment for breast cancer dates back to the early 1970's, but its discovery was nearly 20 years in the making.[17] In 1958, the first non-steroidal antiestrogen compound, MER-25 (Figure 1.4), was reported by Thompson and co-workers and would be focused toward the use as a "morning after" pill.[18] However, the effects of MER-25 on mice turned out to have an opposite effect on women (in addition to its toxicity). In continuing studies, additional antiestrogen compounds were developed, including that of tamoxifen (at the time I.C.I. 46,474, and later sold as Nolvadex) and related structures (Figure 1.4).[19,] Many syntheses of both geometric isomers of tamoxifen, **1.1** and **1.5**, have been developed to date[20,21,22] (*cis*- and *trans*-isomer also shown to have opposing pharmacological effects[23]). The use of

these compounds to treat breast cancer was proposed by Walpole in the 1960's based on the documented and established link between estrogen and breast cancer growth.[18] Thus began many concurrent studies and clinical trials leading to *trans*-tamoxifen's approval for use in women in 1973 (FDA approval for use in the U.S. in 1977). Today, tamoxifen is still widely prescribed for preventative and adjuvant treatment of breast cancer, and research for alternative uses and mechanisms of action continues.

Tamoxifen is most effective when given to women with estrogen dependent breast cancer due to tamoxifen's specific binding to the estrogen receptor of mammary carcinoma cells.[24,25] This specificity toward cancer cells is important because the blocking of all ER containing cells could lead to other deleterious side-effects including osteoporosis and increased circulating cholesterol.[26,27] Tamoxifen is thus described as a selective ER modulator because calcium uptake and cholesterol levels, which depend on estrogen, are not impinged upon. In fact, tamoxifen has been shown to maintain good cholesterol and reduce "bad" cholesterol, as well as increasing bone density significantly in post-menopausal women. Noting the benefits of tamoxifen leads to the point that it is also can increase the risk of endometrial cancer. Thus, the trade-offs for chemotherapy are still evident with tamoxifen.

In addition to the type of breast cancer, the age and fertitility of a woman are factors in the prescription and use of tamoxifen to maximize effectiveness.[28] Regardless of this modulation, an extended period of use

(five years) of tamoxifen is most beneficial for the prevention of recurrence and has even been given to high-risk women for preventative purposes.[25] Despite the decrease in mortality that tamoxifen provides for women suffering from ER-positive breast cancer, there are many cases where a resistance to treatment has developed.[29] In addition, the existence of ER-negative forms of breast cancer are less likely to respond to tamoxifen.[28] There is still a thought that tamoxifen can be used or will lead to the discovery of new treatments based on a better understanding of selective ER modulation and/or unknown off-ER targets. This fact is evidenced by the multitude of ongoing research studies regarding tamoxifen.

Given the available data, the benefits of tamoxifen for women suffering from ER-negative breast cancer would seem to be at a minimum, based on tamoxifen's selective ER modulation. However, studies regarding the induction of apoptosis in ER-positive and negative breast cancer cells using a micromolar concentration of tamoxifen showed that in both cases apoptosis occurred.[30] More importantly, when estradiol was introduced under these same conditions, apoptosis was still induced for the ER-negative cell line and not for the ER-positive, suggesting a non-estrogen receptor related mechanism of action. This and other studies of tamoxifen and ER-negative breast cancer rationalize the current investigation into the target of NSC-670224.

It is understood that yeast do not contain a human estrogen receptor, and therefore tamoxifen's toxicity toward yeast would appear to be an interesting result. However, different strains of yeast, including *Candida albicans*[31] and *Sacchromyces cerevisiae*,[32] contain an estrogen binding protein that has low affinity for tamoxifen or other non-steroidal antiestrogens. With these findings combined, it has been proposed that other mechanisms of action (outside of antiestrogenic activity) are responsible for tamoxifen's ability to inhibit growth of yeast, which may be homologous to higher eukaryotes such as humans. It has also been stated that tamoxifen's tendency to kill a eukaryote such as yeast is reason to be skeptical in prescribing tamoxifen over extended periods of time (on top of some of the side-effects).[33] Whether or not the growth inhibition of yeast by tamoxifen is a corollary to malfunction in women is not understood at all, and can only be one consideration since tamoxifen has different functions across different species. Thus, probing alternative pathways affected by tamoxifen in yeast may lead to useful pathways with homologous functions in humans, which may include an alternative pathway to eliminate ER-negative breast cancer.

One example in the literature whereby function in yeast for a known drug corresponds to a similar and new function in tamoxifen (off ER-target) was exemplified by the work of Boone and co-workers.[10] Amiodarone and tamoxifen were shown to have similar chemical-genetic profiles by screening against a pool of tagged yeast deletion strains. The cytotoxicity of amiodarone

and tamoxifen towards yeast was shown to affect Ca^{2+} homeostasis similar to amiodarone's mode of action in humans. Therefore, the homologous mechanisms between humans and yeast for amiodorane suggest this novel activity for tamoxifen is an overlap of human biological pathways between the two drugs.

1.4 Proposed Synthesis of NSC-670224 Diastereomers and Synthesis of Non-chlorinated Derivatives

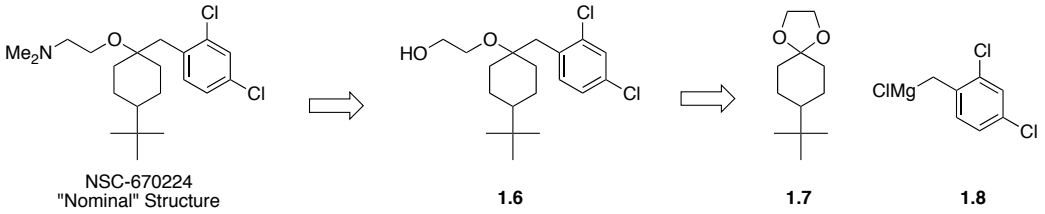

NSC-670224
"Nominal" Structure

1.2 **1.6** **1.7** **1.8**

Scheme 1.1 Retrosynthesis of **1.2** utilizing a patent procedure

Although NSC-670224 is a synthetic compound, the NCI library does not define its origin and stereochemistry, but instead only provides a planar structure. Based on the ^{1}H-NMR spectrum of the NCI sample of NSC 670224 (as received), it is clear that the compound is one diastereomer. Therefore, to define the stereochemistry and provide more sample for biological studies, a synthetic route was devised and is depicted retrosynthetically in Scheme 1.1. Both diastereomers of **1.2** would come from the separate alcohols of **1.6**. Grignard addition using prepared 2,4-dichlorobenzylmagnesium choride (**1.8**) to ketal **1.7** would provide the mixed alcohols.

Similar compounds have been synthesized and are reported in the patent literature.[34] The general synthetic approach begins with the reaction of the desired benzyl Grignard and a cyclic ketal of 4-*t*-butylcyclohexanone to give a mixture of primary alcohols. This mixture is then tosylated and the leaving group displaced with dimethylamine. Within the patent, only phenyl, *p*-tolyl and *p*-fluorophenyl benzyl Grignards were utilized, and it was envisioned that this particular route might be feasible for NSC-670224. However, prior to attempts in our lab to synthesize NSC-670224, Lokey undergraduate student Robert Weber, was unable to reliably produce Grignard reagent from 2,4-dichlorobenzyl halide (no specific procedures found through Scifinder). Thus, based on our expertise in total synthesis we undertook the synthetic task.

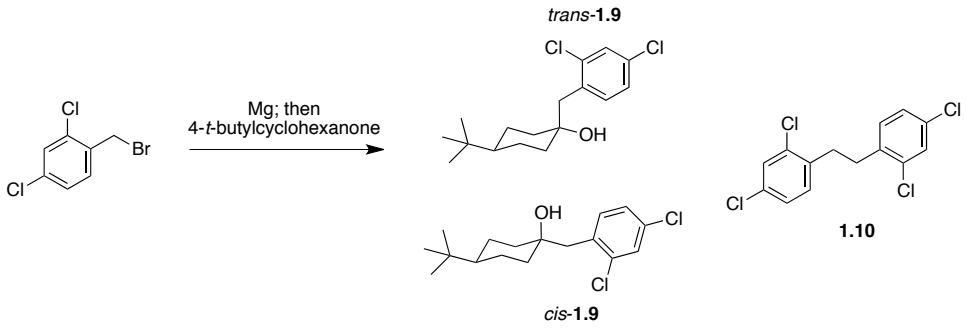

Scheme 1.2 Grignard Approach Reaction of 4-*t*-butylcyclohexanone with 2,4-dichlorobenzyl Grignard reagent

Typically, benzyllic Grignard preparation leads to a fair share of Würtz homocoupling side product due to the facile nature in which the Mg inserts at the benzylic center and subsequent reaction with starting material (in addition to other one electron processes). This problem is exacerbated by the addition of additional electron withdrawing groups on the aromatic ring, and thus the

"usual manner"[33] of generating a Grignard from 2,4-dichlorobenzyl halide is not a consistently efficient process. An initial attempt to generate the appropriate Grignard was successful and was quenched with 4-*t*-butylcyclohexanone (Scheme 1.2) to give a seperable mixture (column chromatography) of diasteromeric tertiary alcohols, *cis* and *trans*-**1.9**, along with homocoupled product **1.10**. However, additional attempts were not as high yielding and in anticipation of needing multiple equivalents of Grignard in the sluggish reaction with ketal, a new means of benzyllic Grignard preparation was investigated. Prior to attempting a new route, practicalities of diastereomer purification and stereochemical determination were pursued using a modified procedure towards the known benzyl compounds.

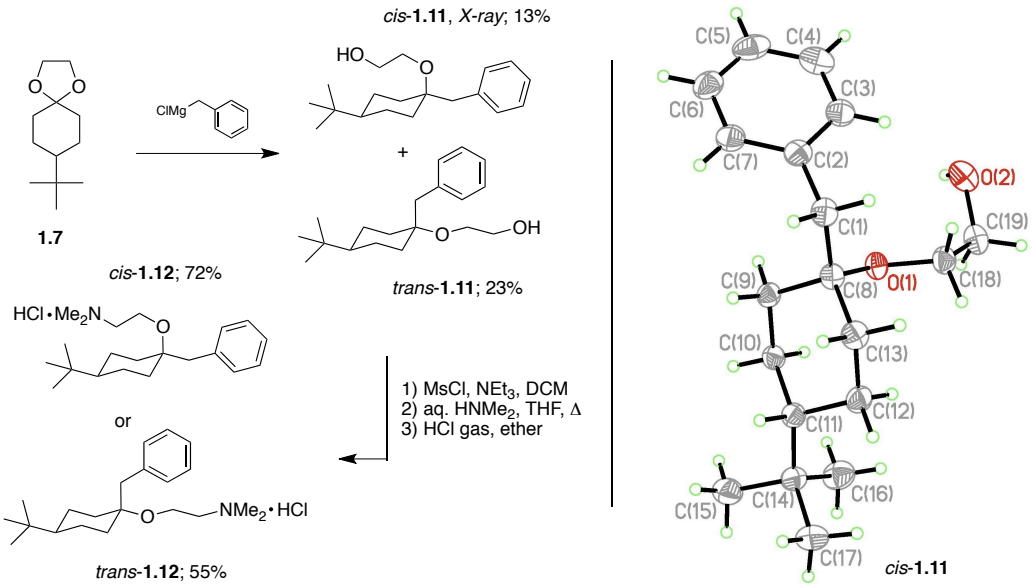

Scheme 1.3 Synthesis of Benzyl Derivatives and stereochemical determination via *X-ray* of **1.11**

Commercially available benzylmagnesium chloride and the ethylene ketal of 4-*t*-butylcyclohexanone (prepared in one step from a literature

procedure) were refluxed together in a 5:1 ratio of Grignard to **1.7** over a period of 16 h (Scheme 1.3). After cooling and quenching the reaction mixture, the two diastereomers were separated by column chromatography. After determining that the *cis* and *trans*-**1.11** could be separated, the task of determining stereochemistry of the eluted compounds was the next issue. With hundreds of milligrams of each diastereomer available, 2D NMR techniques were a viable option. However, the first eluted compound proved to be highly crystalline upon evaporation from a mixture of hexanes and dichloromethane, and thus X-ray crystallography was used to determine its stereochemistry (Scheme 1.3). Based on the angle and orientation of the aromatic ring to the cyclohexane ring it was clear that the first eluted alcohol was the *cis*-isomer (*t*-butyl and ether side-chain relative to one another). Therefore, the second eluted compound, which was an oil, was determined to be the *trans*-isomer by process of elimination. Subsequent mesylation and displacement with dimethylamine on the individual alcohols was conducted in accordance with a literature procedure.[35] For ease of storage and purification, *cis* and *trans*-**1.12** were converted to the hydrochloride salts via HCl gas in ether, followed by recrystallization (slow evaporation DCM/hexanes). The synthesis of these two compounds would provide a valuable piece of SAR data as will be evidenced in a later section.

1.5 Synthesis and Identification of Nominal NSC-670224

In order to take advantage of the ketal opening to effect a short synthesis of the desired compounds, the unique properties of Mg reagents seems necessary. Due to the difficulties in preparing benzyllic Grignards and in particular those with electron withdrawing groups, the literature was consulted for specific methods. The field of study that deals with alternate Grignard preparation, specifically for benzyllic species, is by no means vast and focuses on activated Magnesium preparation. Two seemingly viable areas include Rieke Grignard preparation[36] and Mg-anthracene.[37]

The utility of Rieke magnesium towards benzyllic Grignard preparation appears to be possible due to the ability of the highly activated metal to undergo carbon-halide insertion at low temperature. However, examples of Rieke magnesium and benzylic Grignard reagents with low homocoupling are not evident in the literature. More recently, Rieke has shown the ability to prepare benzylic organo-Mn reagents in high yield with very low homocoupling (~1%) side-products. Unfortunately, the reactivity of Mn reagents towards ketal electrophiles is far less than Mg reagents. The substrate scope reported in the paper focuses on additions to acid chlorides and aldehydes with poor yields when reacted with ketones. Alternatively, the preparation of Mg-anthracene complexes undergoes smooth carbon-halide insertion with minimal Würtz coupling. Also, the reaction undergoes clear color changes that indicate reaction progress. However, the complex

formation requires the use of highly activated magnesium, which in itself can be difficult to attain due to the need for glove-box techniques. The ratio of preparation to reactivity in both cases is not desirable and thus focus moved towards other organometallic nucleophiles.

While investigating the preparation of benzyllic Grignard reagents, it became evident that organozinc reagents may be of great utility in this synthesis for a number of reasons. The work of Knochel and co-workers in the area of benzyllic organozinc reagents[38] describes a process that does not require glove boxes and utilizes minimal purification and preparation of commercially available materials. The principle behind the benzylic organozinc preparation is two-fold. Firstly, LiCl greatly accelerates the process of Mg insertion when generating organomagnesium compounds in THF, and therefore, THF (available from our laboratory's solvent system) can be used in place of diethyl ether (must be distilled freshly). Secondly, in addition to LiCl, $ZnCl_2$ is also present and is consumed as soon as Grignard reagent is formed. Since the organozinc reagents are not as nucleophillic as their Mg counterparts, the homocoupled side-product is greatly reduced (reported as less than 5% in literature examples).[39] With a proposed organozinc reagent in place, a revised synthesis was necessary to take into account the reduced reactivity of the nucleophile.

Ketals are generally not good enough electrophiles for organozinc reagents. Therefore, zincate addition to 4-*t*-butylcyclohexanone directly was

envisioned. The tertiary alcohols could then be separated and reacted with 1-chloro-2-*N,N*-dimethylamino ethane.[40] Alternatively, if this reactivity proved to be less than satisfactory, a longer route utilizing allylation was also proposed.

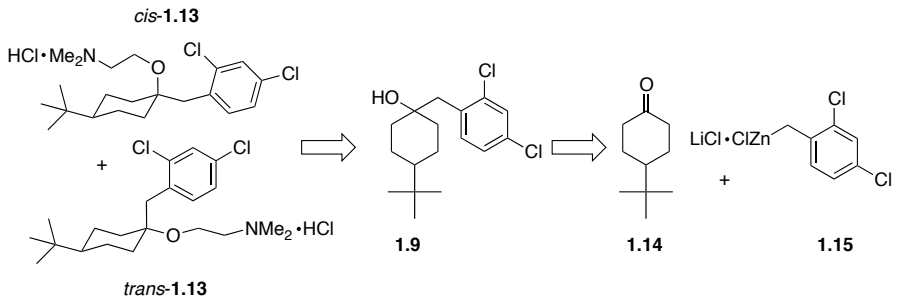

Scheme 1.4 Organozinc Retrosynthetic Approach of *cis* and *trans*-**1.13** starting from organozinc reagent

With the idea of using organozinc reagents firmly in hand, analysis of Knochel's publications revealed a few small hurdles to overcome. Although organozinc reagents are known to be strong enough nucleophiles to react with ketones, this was not evidenced in Knochel's publications where aldehydes were the primary example of electrophiles.[39] Additionally, dihalogenated benzyl species were not generated as examples of organozinc reagents. Retrosynthetically, amines **1.13** would be derived from tertiary alcohols **1.9**. Compound **1.15** would be prepared under Knochel's conditions and reacted with commercially available ketone, **1.14** (Scheme 1.4).

Despite these facts, the preparation of organozinc **1.15** from **1.16** using the method of Knochel and co-workers turned out to be very efficient and highly reproducible. In addition, compound **1.15** underwent facile addition to 4-*t*-butylcyclohexanone when using two or more equivalents of the organozinc

reagent. The tertiary alcohols produced, *cis* and *trans* **1.9**, could be separated by column chromatography and taken on individually towards the two possible diastereomers of NSC-670224. In order to keep the synthesis relatively short, **1.17** was envisioned to undergo Williamson ether synthesis with the tertiary alcohols **1.9**. Within the literature, there is some precedence for reacting this electrophile with tertiary alcohols utilizing NaH as base with heating in DMF,[41] but it was understood this reaction may be sluggish. Compound **1.17** was synthesized in one step according to a literature procedure, and due to the volatility of this particular compound, it was prepared and isolated directly as the hydrochloride salt.

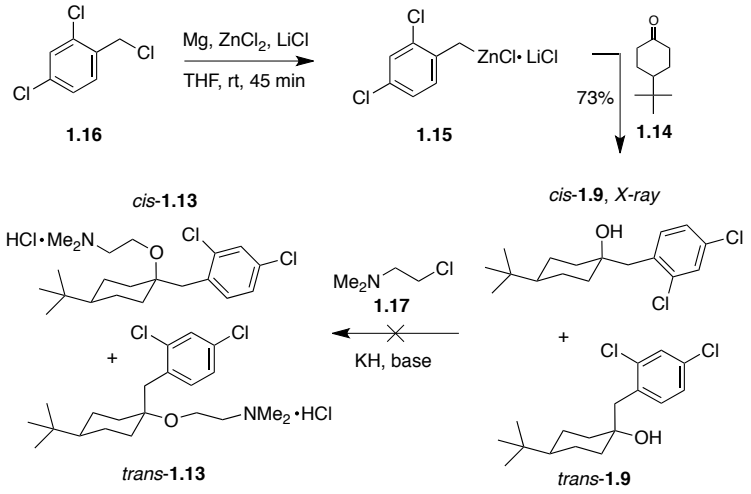

Scheme 1.5 Williamson Ether Synthesis attempt toward *cis* and *trans*-**1.13**

Initial attempts using a published procedure to generate the desired ether linkage with DMF and NaH returned only decomposed product (Scheme 1.5), while running the reaction at room temperature returned only starting material. Changing to the stronger base KH did not provide **1.13** at room

temperature. Thus, the electrophilicity of **1.17** did not appear to be good enough for our needs, as it is hard to believe that KH or NaH were not strong enough bases to deprotonate our tertiary alcohol. Again, an alternate synthesis was in order whereby the lesser effective nucleophilicity of our hindered tertiary alcohol must be compensated with a better electrophile.

Since the ultimate goal was to provide material and verify stereochemistry of NSC-670224, the focus turned away from the shortest route possible. Therefore, allylation of the tertiary alcohol, osmylation/oxidative cleavage/reduction of the alkene, and mesylation/displacement of the primary alcohol was proposed. Each of these steps is potentially high yielding and is well elaborated in the literature, and would provide intermediates that could be advanced by alternative methods if necessary.

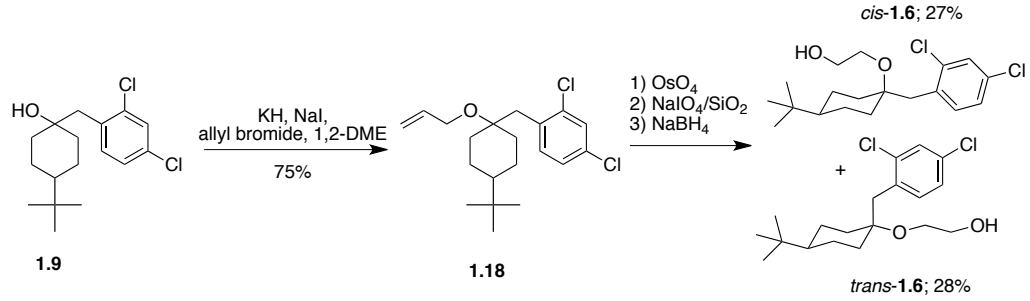

Scheme 1.6 Allylation Synthesis of *cis* and *trans*-**1.6** from allylated tertiary alcohol **1.9**

Unlike **1.17**, allyl bromide proved to be an excellent electrophile, and the allylation procedure by Sauer et al.[42] provided high yields on a multitude of similar substrates. This particular procedure utilizes the strong base KH to deprotonate the hindered alcohol at low temperature followed by the addition

of excess allyl bromide. The reactivity of allyl bromide is enhanced further by the inclusion of a catalytic amount of flame dried NaI (Finkelstein conditions). Sauer's allylation conditions for the mixture of alcohols **1.9** to give the mixture of allyl ethers **1.18** are summarized in Scheme 1.6. Generation of a diol with OsO_4 and oxidative cleavage to the aldehyde with $NaIO_4$ on silica gel[43] gave the crude aldehyde, which was readily reduced to the primary alcohol with $NaBH_4$ in methanol to give *cis* and *trans*-**1.6**. From here the same procedure used for the benzyl compounds of mesylation and displacement of **1.6** with dimethylamine could be performed to give both diastereomers of **1.13** (Scheme 1.7).

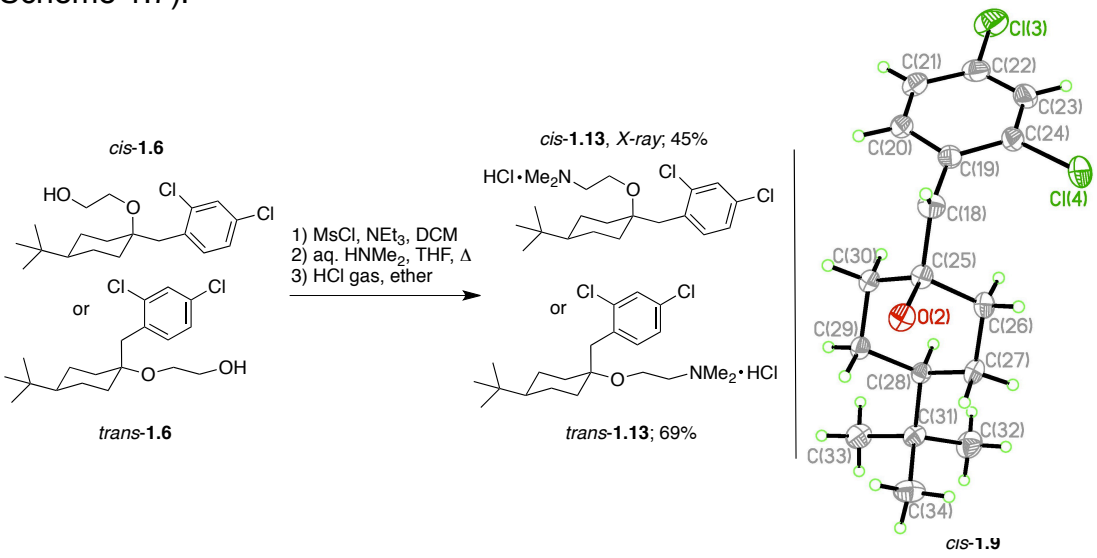

Scheme 1.7 Amination of *cis* and *trans*-**1.6** and ORTEP of *cis*-**1.9**

With a proven synthesis in hand, and the desire to possibly apply this synthesis to more derivatives down the road, we wondered if the tertiary alcohols could be taken through as a mixture and separated as the primary alcohols. This would certainly be more efficient than running each step on

individual intermediates and seemed feasible since the benzyl compounds were separated by column chromatography. Sure enough, each reaction was conducted successfully on the mixture of compounds and could be separated as the primary alcohols. Although the intermediates were not separated at each step, pure fractions of each diastereomer were isolated and fully characterized ($^{1}H/^{13}C$ NMR, IR, mp, HRMS, and TLC analysis). One particular interesting property of these compounds was that the TLC analysis showed that each diastereomer consistently followed the same polarity trends from one intermediate to another.

The stereochemistry was again determined by X-ray analysis of the most crystalline intermediate, which turned out to be the first-eluted tertiary alcohol, **1.6** (Scheme 1.7). As was the case for the benzyl compound elucidated by X-ray, this tertiary alcohol was also the *cis*-compound (in both cases they were the first eluted from the column). With the stereochemistry defined, each primary alcohol was then individually subjected to mesylation and displacement with dimethylamine followed by formation of the hydrochloride salt. At this point, it seemed that a simple comparison of the ^{1}H NMR spectra to that of the NCI sample would verify the true identity of NSC-670224.

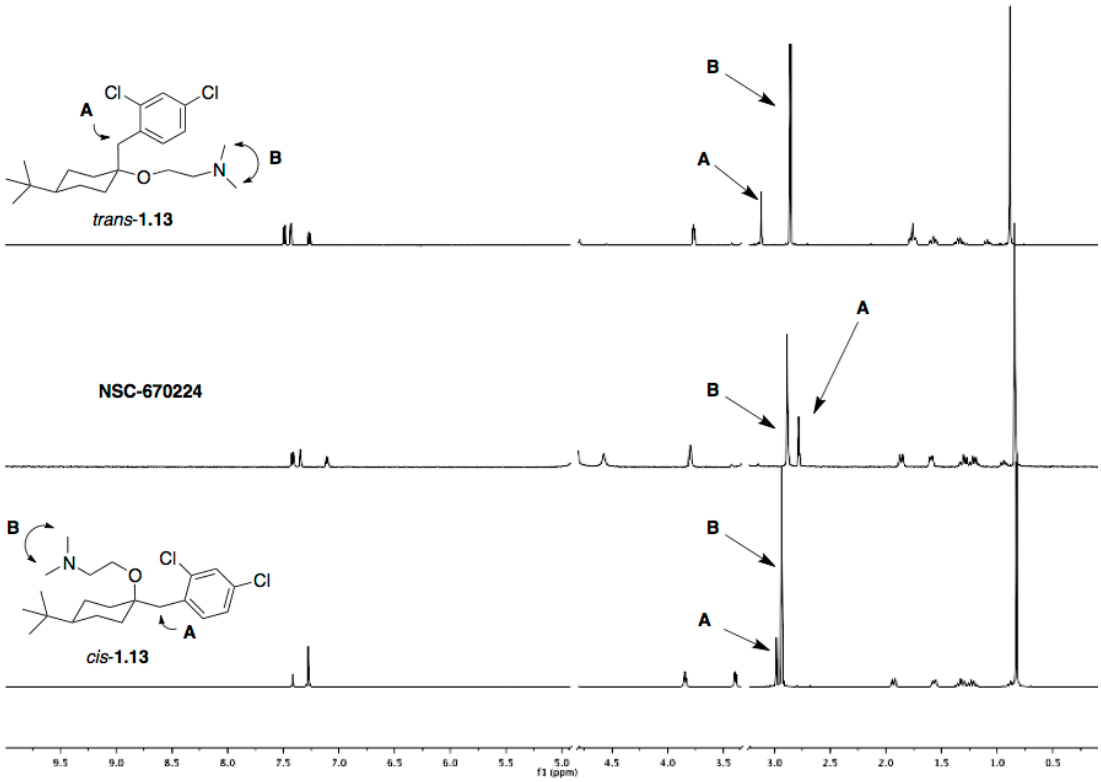

Figure 1.5 Stacked ^{1}H-NMR Traces of 2,4-dichloroinated compounds vs. NSC-670224. Solvent peaks for CD_3OD have been omitted from the spectra for clarity.

Interestingly, the comparison of the spectra (Figure 1.5) did not provide the answer we were looking for, but instead raised concern that the NCI compound was not as advertised. Upon first glance, all of the components of the molecule were present across the three spectra. However, the aromatic region of *trans*-**1.13** appeared to match the NCI sample, while the cyclohexyl region appeared to match *cis*-**1.13**. The benzyl methylene protons and the dimethylamine protons (**A** and **B** respectively in Figure 1.5) did not match either of the diastereomers, but were in fact transposed (later on, this phenomenon would be determined). Alternative methods to define the difference between the three compounds were pursued.

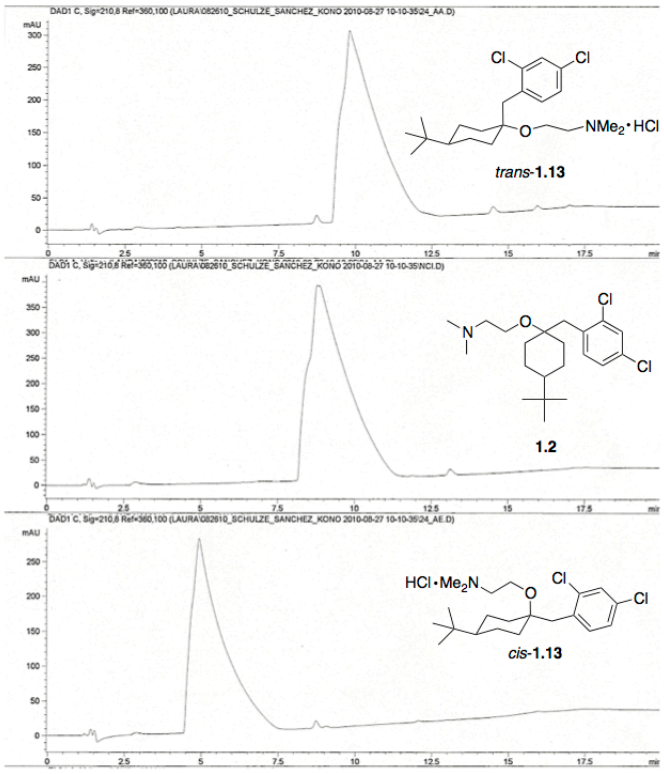

Figure 1.6 LCMS Traces of *trans*-**1.13**, NSC-670224 (**1.2**) and *cis*-**1.13**

With the help of Laura Sanchez of the Linington Lab, it was determined by LCMS (Figure 1.6) that the compounds were all in fact different, as determined by their retention times, but were all isomers of one another (by mass and isotope pattern). These results lead us back to the NMR spectra to determine an alternate atom connectivity that would not drastically change the spectral representation. The most obvious isomeric alteration would be to change the positions of the chlorine atoms on the aromatic ring. The splitting pattern of the aromatic region for the NSC-670224 is indicative of 2,4-disubstitution whereby two doublets and a doublet-of-doublet are represented. However, 3,4-disubstitution would also give a similar pattern.

Since the final compounds and the NSC-670224 were highly crystalline hydrochloride salts, an attempt to attain X-ray quality crystals was undertaken.

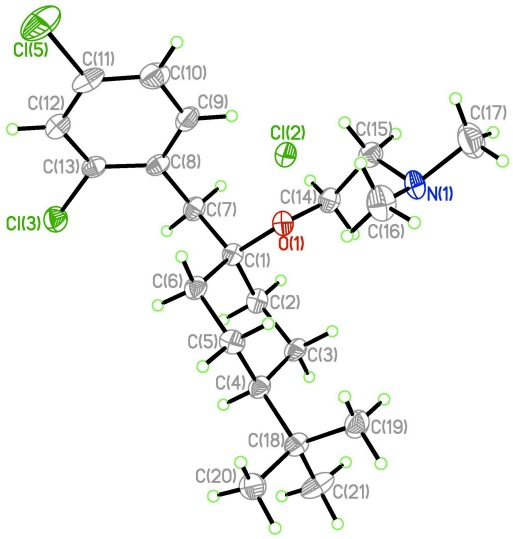

Figure 1.7 ORTEP of *cis*-**1.13**

Slow evaporation of solvent provided seemingly good crystals for the *cis*-compound and the NCI compound and thus they were subjected to X-ray analysis. Only the synthetic sample returned quality data (Figure 1.7), while the NCI sample appeared to have severe twinning making the elucidation difficult for our crystallographer, Dr. David Rogow. David suggested growing the crystals more slowly or under different solvent conditions. However, this did not improve the X-ray data and the help of our former crystallographer, Dr. Allen Oliver, was sought. In fact, Allen was able to solve the structure enough to determine the chlorine atoms were not on the 2,4-positions of the aromatic ring but were instead at the 3,4-positions. Allen also found that the structures were difficult to refine because of a large amount of disorder about the choline

side-chain. With the NMR data and Allen's insight, the synthesis of the 3,4-dichlorinated analogs was pursued. From all of this, two more derivatives were collected towards an eventual SAR study, and the synthesis was expected to translate well to the 3,4-dichlorinated compounds.

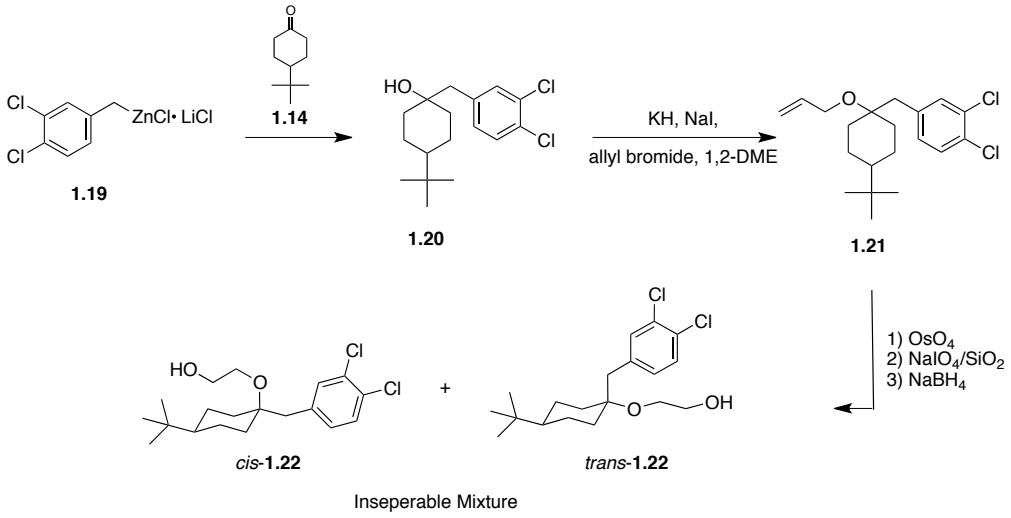

Scheme 1.8 Synthesis of *cis* and *trans*-1.22 via organozinc reagents

Commercially available 3,4-dichlorobenzyl chloride underwent zincate formation under Knochel conditions[38] with ease to give **1.19** and similarly added to 4-*t*-butylcyclohexanone (Scheme 1.8). Similarly to the 2,4-dichloro compounds, the mixture of diastereomers of **1.20** was taken through the same synthetic sequence to give allyl ethers **1.21** with anticipation of separating at the primary alcohol intermediates. However, efficient separation by column chromatography of *cis* and *trans*-**1.22** was not successful and purification of the tertiary alcohols was more thoroughly investigated.

Subsequent synthesis of **1.20** on a multigram scale brought forth a fortunate characteristic of these intermediates. Following reaction workup, the

crude oil was placed under high vacuum overnight, and the next day it was apparent that crystals were crashing out of solution. Analysis by proton NMR of the filtered crystals revealed they consisted of one diastereomer. Efforts to develop a streamlined purification of the crude reaction mixture ensued.

A majority of the crude oil consisted of 3,4-dichlorotoluene due to the excess amount of organozinc used in the reaction. The nonpolar impurities were washed away by vacuum filtration with hexanes through a silica gel plug, and the remaining alcohols were washed through with ethyl acetate. TLC of the remaining mixture and visualization with sulfuric acid/vanillin stain, showed the presence of some unreacted starting ketone. Interestingly, the ketone impurity falls between the two alcohols and slightly overlaps the more nonpolar compound. Crude NMR revealed that the starting ketone presence was minimal, but more importantly, the alcohol it overlapped with was the highly crystalline compound. Removal of ethyl acetate and solvation of the oil in heptanes gave the first-eluted alcohol as pure crystals after cooling on ice and vacuum filtration. The mother liquor was evaporated and chromatographed to provide the remaining alcohol. Each alcohol was taken through the remaining synthetic sequences individually, but alternative alkene oxidation was investigated to reduce contact with OsO_4.

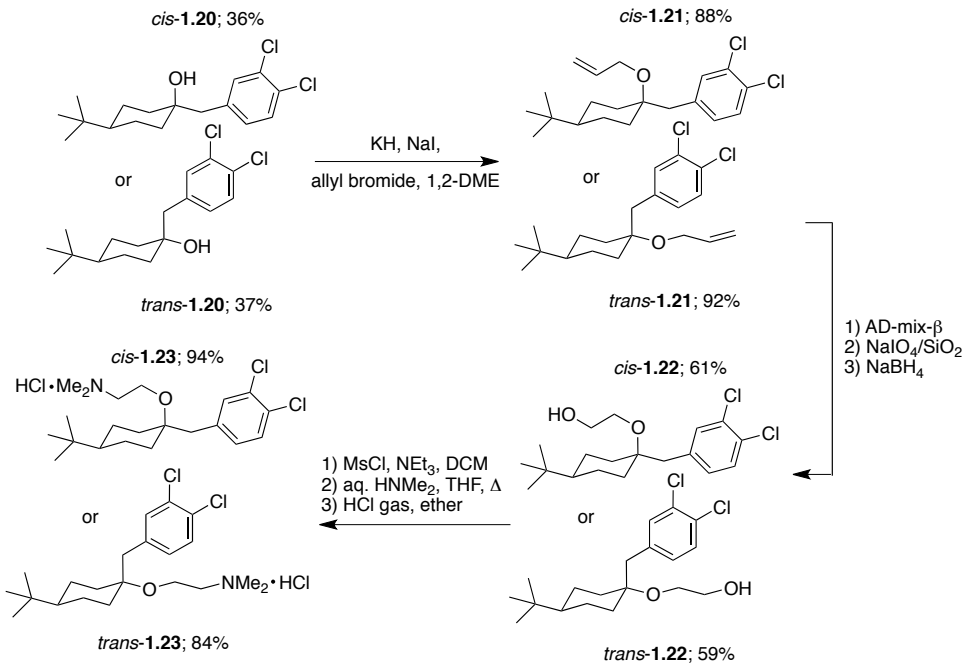

Scheme 1.9 Synthesis of *cis* and *trans*-**1.23**

Previously, OsO_4 dissolved in *t*-butanol was used in catalytic amounts in the presence of excess amounts of oxidant (4-*N*-methylmorpholine-*N*-oxide, 4-NMO). The workup in this particular instance required careful decontamination steps over a large number of pieces of glassware. The use of AD-mix-β as an alternate source of osmium for dihydroxylation appeared to be a good method to reduce possibilities of contamination as Sharpless and co-workers present an *in-situ* precipitation of the osmium salts following the completion of dihydroxylation.[44] Therefore, the toxic by-products could be filtered away and the resulting diol taken through the next steps. From **1.21** to **1.22**, the three steps including AD-mix-β gives only a moderately improved yield over the previously described process for the 2,4-dichloro compounds, which may be due to the poor solubility of the alkene in the mixed solvent

system commonly used for Sharpless dihydroxylation (*t*-butanol/water). Nevertheless, the required primary alcohols were in hand and were *N*,*N*-dimethylated in the usual manner to give *cis* and *trans*-**1.23** (Scheme 1.9).

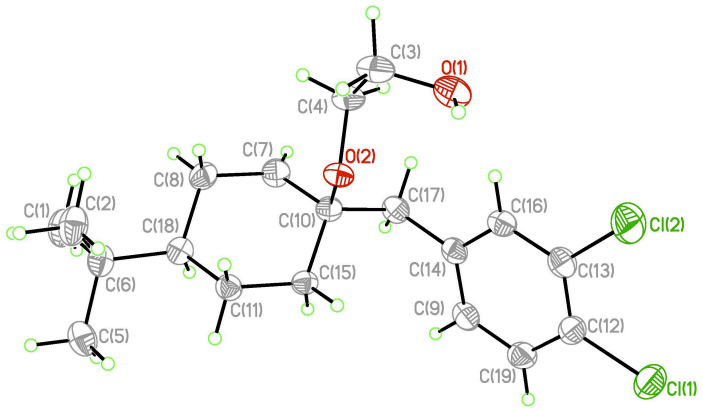

Figure 1.8 ORTEP diagram of *cis*-**1.22**

Stereochemical assignment of the 3,4-dichlorinated derivatives was determined through X-ray analysis of the first-eluted primary alcohol, **1.22**, and the trend continued to hold true, as this too was the *cis*-isomer (Figure 1.8). Final determination of the identity of NSC-670224 by comparing ^{1}H-NMR spectra was not immediately evident. Although the aromatic and cyclohexane ring regions appeared to be a near match for the *cis*-isomer, the ethanol side chain was alarmingly different. The methylene protons were much farther downfield and the benzyl methylene protons/*N*,*N*-dimethyl protons were transposed. At this point, it was hypothesized the differences seen by NMR were concentration dependent due to the limited amounts of NCI sample analyzed (~1 mg/mL NCI sample vs. ~25 mg/mL as prepared) and the possibility of an intermolecular π-cation interaction between the ammonium

species and aromatic ring at higher concentrations. By lowering the concentration of the NMR sample the *cis*-isomer spectra matched the NCI provided sample of NSC-670224 (Figure 1.9).

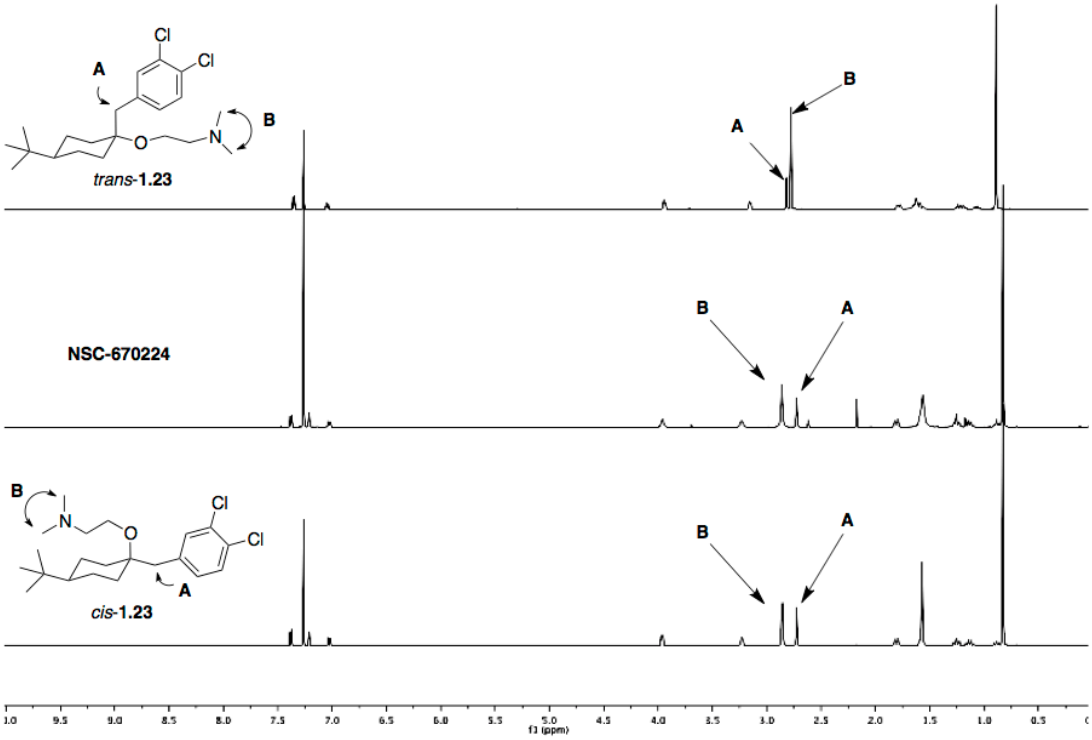

Figure 1.9 Stacked ^{1}H-NMR traces and identification of NSC-670224 as *cis*-**1.23**

1.6 Initial SAR Studies: NSC-670224, Related Derivatives and Tamoxifen vs. wt-Yeast

Work towards the synthesis of NSC-670224 not only provided more sample and stereochemical identity, but also provided five additional analogs to be tested against wt-yeast. Dr. Tiffani Quan and Walter Bray ran each analog and tamoxifen against wt-yeast at different concentrations to determine the IC_{50} values. Their data is summarized below in Figure 1.10 and 1.11 respectively. Interestingly, all of the compounds show lethality against

yeast, with clear trends for SAR development. First of all, the non-chlorinated compounds are far less active against yeast, which indicates that substitution about the aromatic ring is important for activity (Table 1.1). All of the 2,4- and 3,4-dichlorinated derivatives are more potent than tamoxifen, while the 2,4- and 3,4-analogs also share the fact that the *trans*-isomer is slightly more potent than its *cis*-isomer. Of all the compounds tested, the 3,4-dichlorinated isomers are the most active, with the *trans*-isomer being the overall most active compound. It is the *trans*-isomer that would be known as “tamoxilog” and used as a model for further SAR studies due to its activity profile.

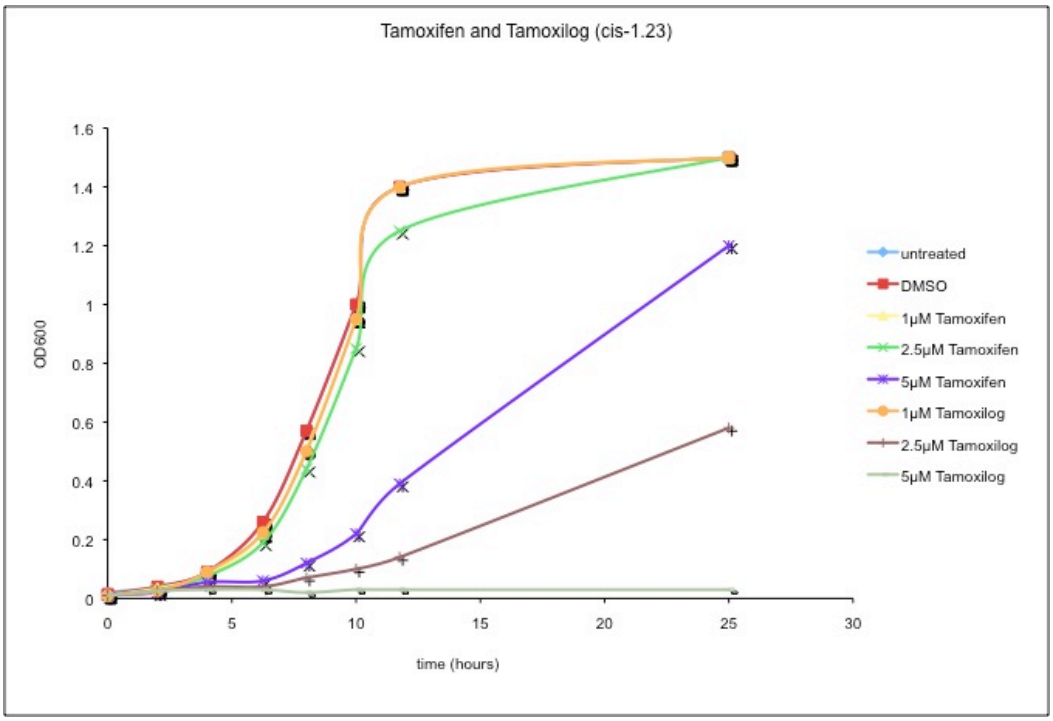

Figure 1.10 Tamoxifen vs Tamoxilog Average growth of wild type yeast cells over 24 h at various concentrations of agent, as measured by optical density of 600 nm.

Table 1.1 Tamoxifen and Synthetic Derivative Lethality Studies on Wild Type *S. cerevisiae*

Compound	**LC_{50} (μM)**
cis-**12** (benzyl)	26
trans-**12** (benzyl)	29
cis-**13** (2,4-dichloro)	6.7
trans-**13** (2,4-dichloro)	2.5
cis-**23** (NSC 670224)	3.2
trans-**23** ('tamoxilog')	2.3
Tamoxifen	4.1

1.7 Synthesis of Derivatives at the Choline Side Chain

The inadvertent creation of the original SAR series lead us to a more focused development of tamoxilog analogs. The next obvious position to vary on tamoxilog would be to that of the choline side chain. How would the addition of chain length, bulk, and hydrogen acceptors alter the overall efficacy of tamoxilog? Before answering that question, the derivatives had to be synthesized.

Five new derivatives were proposed that could all originate from a previously derived intermediate along the synthesis of tamoxilog. Most simply, four of the derivatives would require only changing the amine in the final mesylate displacement step. These derivatives would include pyrrolidine, piperidine, morpholine and *N*-methylpiperazine. The fifth derivative would test

the effect of length on activity by synthesizing a one carbon extension, or homolog.

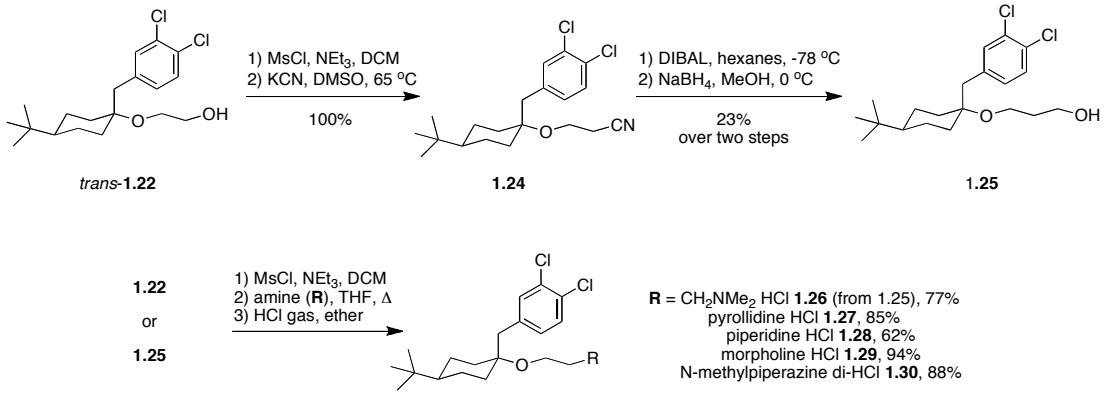

Scheme 1.10 Synthesis of analogs

This homolog synthesis would prove to be non-trivial and was focused on utilizing the remaining primary alcohol **1.22** as starting material (as opposed to hydroboration of the previous allyl ether). Synthesis of the cyano compound **1.24** proceeded in quantitative yield with KCN and mesylate,[45] but reduction of the nitrile to the primary amine with LAH provided only tertiary alcohol in return. Order of addition and reducing the temperature did not change the outcome of this reduction and therefore a milder reducing agent was employed. Reduction with DIBAL and hydrolysis of the imine species to the aldehyde was moderately successful.[46] Although reductive amination could certainly be used at this point, the aldehyde was not purified, but instead the crude mixture was reduced with $NaBH_4$ to give **1.25**. Amination in the usual manner provided the desired homolog **1.26** as well. Reaction of **1.22** through the normal sequence with various amines afforded **1.27**-**1.30**.

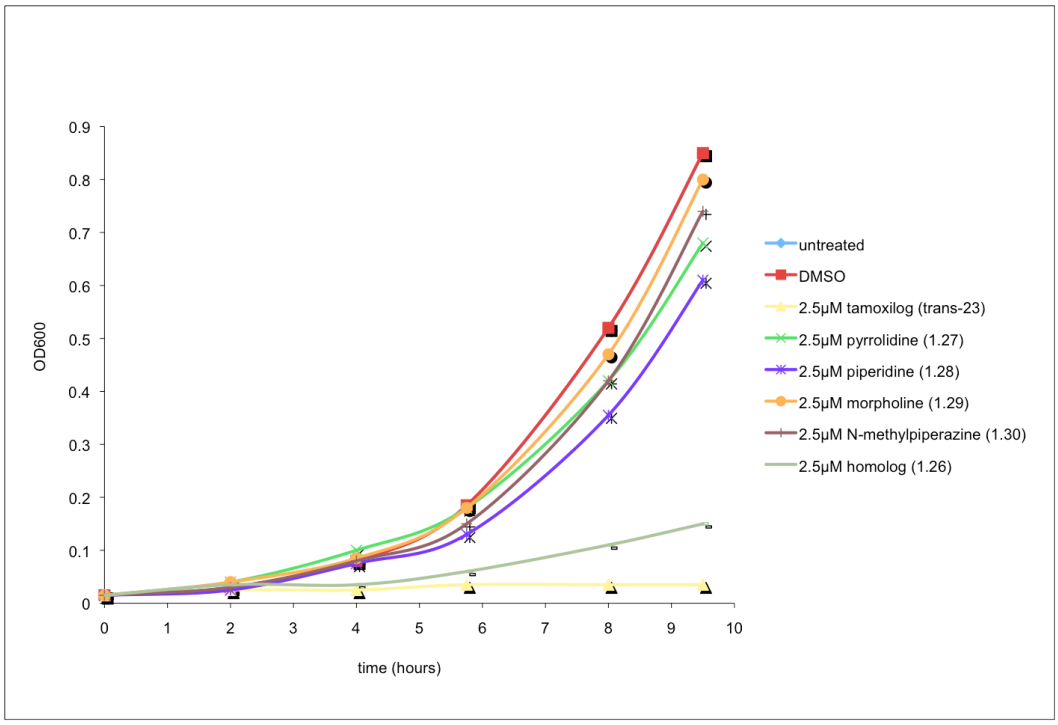

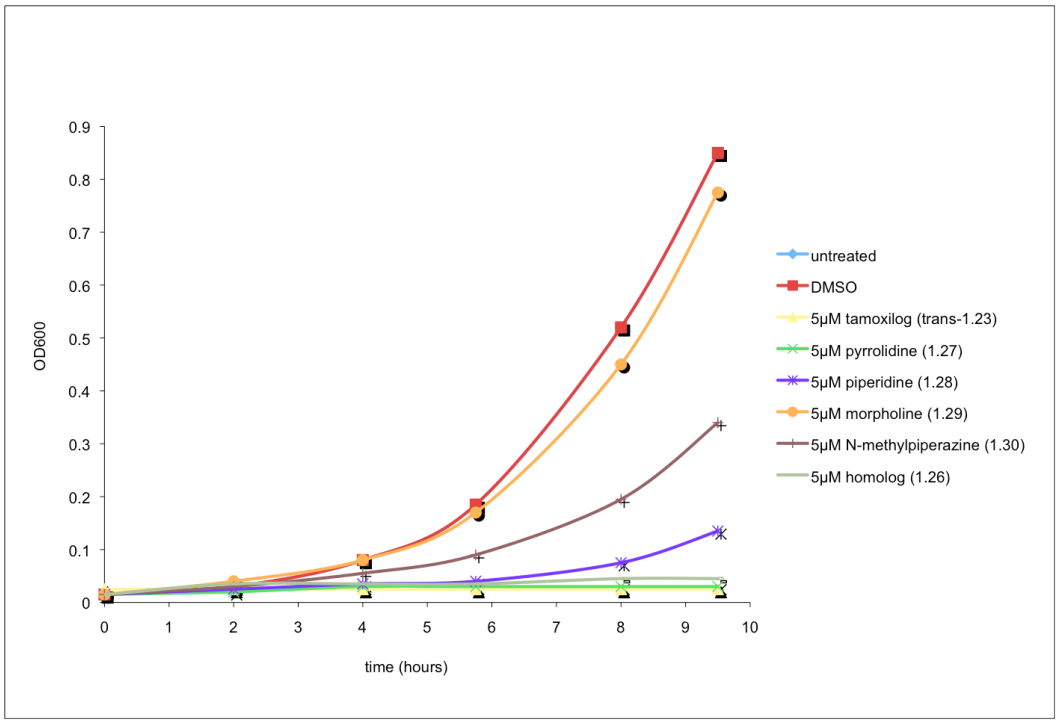

Figure 1.11 Average Growth of Wild-type Yeast Cells over 9.5 h at 2.5 (top) and 5 μM (bottom) concentration of agent, as measured by optical density of 600 nm.

Dr. Quan tested each of the new derivatives against wt-yeast at three different drug concentrations and the trends of the LC_{50} data were analyzed for further insight into the SAR of tamoxilog. Only the drug concentrations, which exhibited cell death for any drug, are represented in Figure 1.11. None of the derivatives completely inhibit wt-yeast growth at 2.5 μM drug concentration, and the homolog is the only derivative that appears to have viable lethality at the same concentration. When looking at the activity profile at 5 μM, it appears that an increase in ring size and the presence of additional hydrogen bond acceptors greatly inhibits drug activity. The pyrollidine derivative, homolog and tamoxilog show complete growth inhibition over the length of the experiment, while piperidine is the next most effective with an onset of cell viability around six hours. The *N*-methylpiperazine derivative appears to have some growth inhibition while the morpholine derivative appears to be completely inactive at 5 μM drug concentration. These trends are interesting, but ultimately, the original substitution is the most active.

1.8 Design and Synthesis of Biotinylated Tamoxilog

The initial goal of this synthesis was to secure reasonable supplies of NSC-670224. In the process, a somewhat more active isomer, tamoxilog, was identified. However, the ultimate goal of the tamoxilog project has been to identify the target of NSC-670224 either in yeast or breast cancer cells and to possibly identify an unknown target(s) for tamoxifen and/or tamoxilog. To this point, all indirect methods to identify the target of tamoxilog have been

inconclusive. Commonly, direct methods for target identification are used in addition to indirect methods, and thus the development of an affinity probe[47,48] had always been a possibility. However, until SAR studies were completed, there was insufficient data to design a proper probe.

The most commonly used and simple affinity probe for protein pull-down studies has been the attachment of a biotin molecule to an unobtrusive/inactive portion of the drug, separated by a variable linker. Complexity of the affinity probe can be altered by the inclusion of photo-sensitive warheads like benzophenone or diazarines for the covalent attachment to the protein target, and/or the addition of fluorophores for fluorescence detection (on gel or in-vivo).[49] For our purposes, the first generation affinity probe would use a commercially available pegylated biotin linker that would connect to tamoxilog through an ester linkage via a pendant alcohol attached to the *t*-butyl group. This would provide a convergent approach with two "expensive" molecules, but would also provide a milder alternative method of biotin cleavage (dilute base vs. boiling SDS)[49] once impurities have been washed away from the attached protein.

Of course, there are potential pitfalls to a simplified affinity probe without the alternative means of target identification/isolation (fluorophore/warhead). Affinity probes are subject to on/off kinetics of the small molecule and protein when a covalent interaction between the two does not occur, and the proteins can be inadvertently washed away during elution

steps because of this effect. Additionally, the abundance of target protein may be extremely small.[48] One or both of these possibilities could greatly reduce the success of a simple biotinylated probe, but would not necessarily eliminate its efficacy.

Most importantly, the point of attachment to tamoxilog must be determined using the SAR data, and as long as this point is innocuous and does not eliminate activity, the handle could be used to attach to a variety of linkers if necessary. Overall, there are three "simple" points of attachment to tamoxilog: the aryl ring, side chain and the *t*-butyl group. The SAR data suggests that the aryl ring and the choline side chain are highly involved in binding to the protein target and would not be a good point to insert a functional handle. Therefore, the *t*-butyl group was chosen to install a pendant alcohol to form an ester linkage to a biotinylated linker.

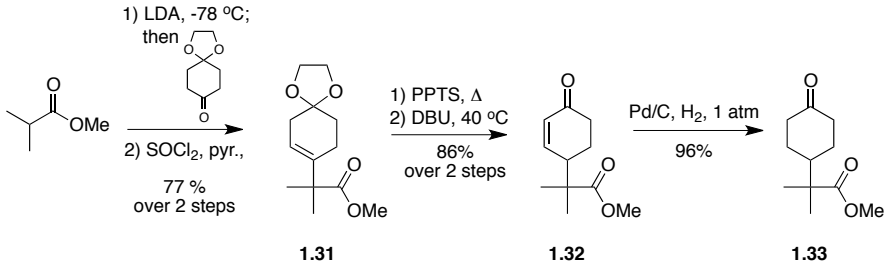

Scheme 1.11 Synthesis of dicarbonyl **1.33**

The synthetic challenge of the probe lies within the installment of the alcohol handle on the *t*-butyl group. Using the method of Engel and Schexnayder, deprotonation of methyl isobutyrate with LDA and the introduction of the mono-ethylene glycol protected 1,4-diketocyclohexane

gave the corresponding alcohol.[50] After work-up, the crude alcohol was dehydrated with thionyl chloride in pyridine to give alkene **1.31** in 73% yield over two steps. Attempts to reduce the tri-substituted double bond of compound **1.31** were unsuccessful; even at elevated pressures. However, attempts to deprotect the ketal with catalytic PTSA gave a mixture of the deprotected trisubstituted alkene along with the α,β-unsaturated isomer, which could be reduced at atmospheric pressure. Due to the appearance of a significant amount of an unknown side-product under catalytic PTSA conditions, **1.31** was deprotected with PPTS in refluxing acetone/water to eliminate the production of this unwanted side-product.[51] The crude alkene was isomerized in refluxing dichloromethane with DBU to give α,β-unsaturated ketone **1.32** in 88% yield over two steps.[52] Finally, reduction of **1.32** with Pd/C and hydrogen at 1 atm gave keto-methyl ester **1.33** in 96% yield.

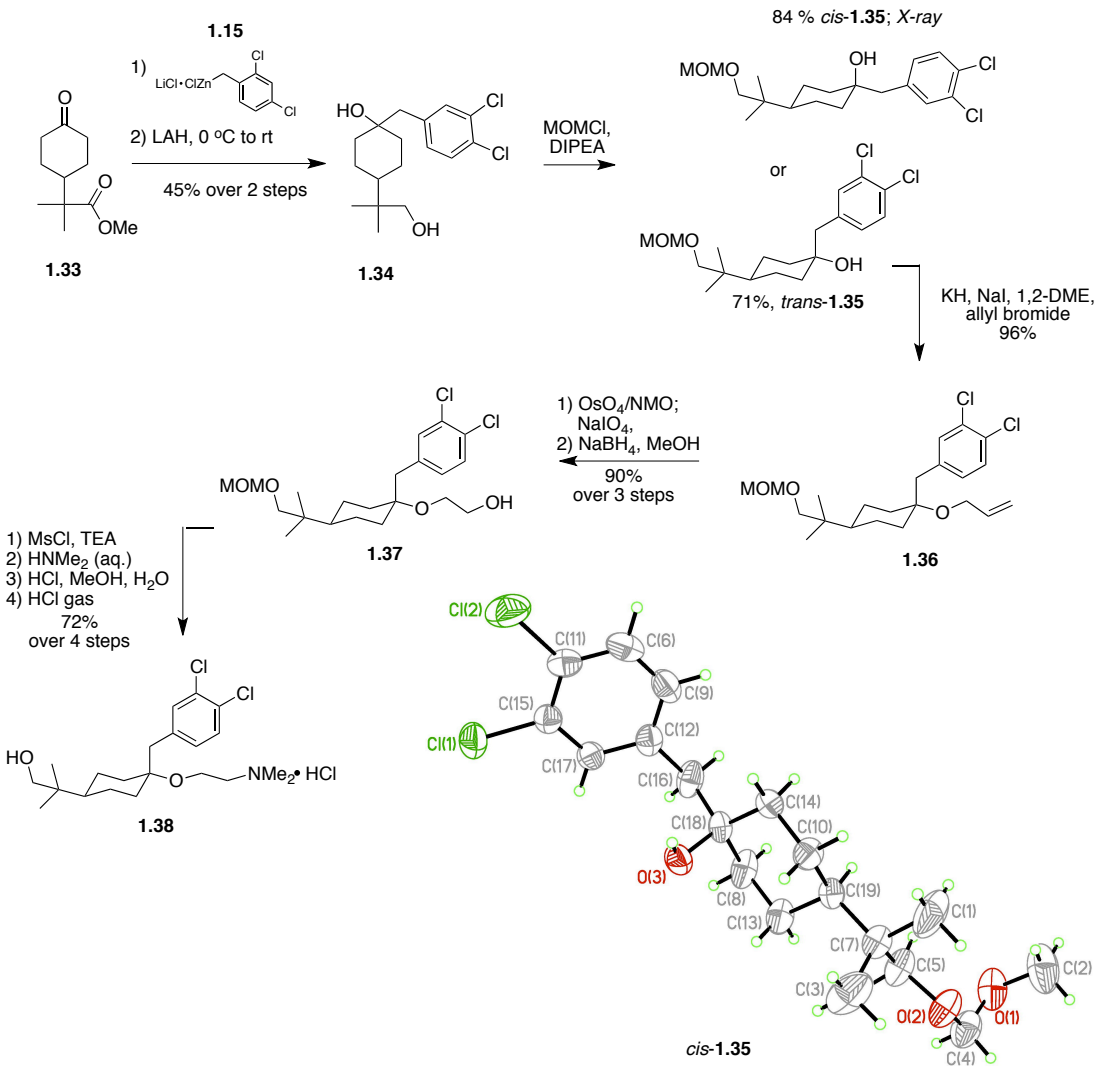

Scheme 1.12 Synthesis of alcohol functionalized tamoxilog (**1.38**)

It was originally envisioned that the methyl ester would mask the alcohol through the remaining steps. However, introduction of the aryl substituent, **1.15**, to **1.33** using Knochel's conditions provided the desired tertiary alcohols as an inseparable mixture. Therefore, the crude mixture was reduced with $LiAlH_4$ to give the mixture of diols **1.34**, which could be separated efficiently by column chromatography. The *cis* and *trans*

diastereomers of **1.34** were mono-protected with MOM-Cl to give *cis*-**1.35** and *trans*-**1.35** in 84% and 71% yield respectively. Although it was envisioned that only the *trans* diastereomer would be taken all the way through to the affinity probe, *cis*-**1.35** was found to give X-ray quality crystals, thus allowing for the stereochemical determination of each species. Allylation of *trans*-**1.35** with KH, allyl bromide and catalytic NaI gave allyl ether **1.36** in 96% yield. Conversion of the allyl ether to primary alcohol **1.37** was conducted over three steps in 90% yield in accordance to a published procedure by Cossy et al.[53] Mesylation and displacement with dimethylamine of **1.37** gave crude MOM protected amine, which was deprotected in a mixture of HCl/methanol/water. The oil that remained after deprotection was passed through a deactivated silica gel column (1% triethylamine in eluent) to give the free amine. The amine was converted to the hydrochloride salt with HCl gas in ether, and after recrystallization, the desired alcohol **1.38** was obtained in 72% yield over four steps.

To test the reasoning/SAR of the *t*-butyl appended alcohol handle, a simple hexanoate ester was synthesized from **1.38** (Scheme 1.13). Yeast growth inhibition experiments run by Prof. Grant Hartzog showed the hexanoate was still effectively active with an LC_{50} of 13.0 μM. The hydrophobic nature of the "greasy" hexanoate chain may have been the culprit of reduced activity of **1.39**, yet the compound was deemed sufficiently efficacious to proceed to the affinity probe.

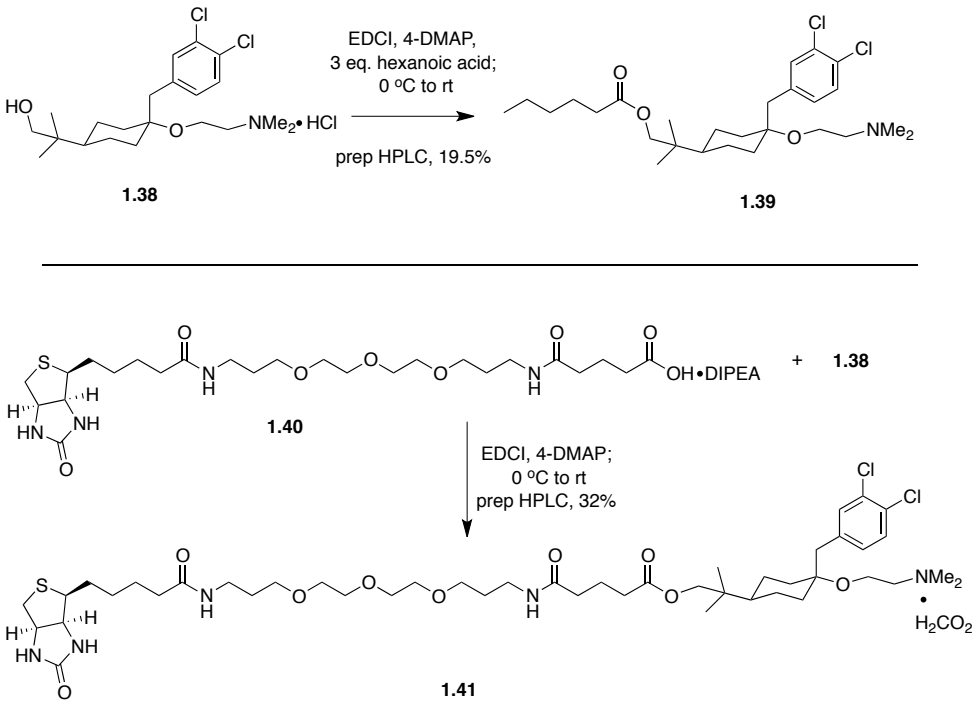

Scheme 1.13 Synthesis of hexanoate **1.39** and biotinylated affinity probe **1.41**

It has been shown that a linker must have a proper length (dependent upon the accessibility or distance to the binding pocket) and to be hydrophilic in order to reduce interference with the target binding. Commercially available linker **1.40** was chosen due to its length and polyethyleneglycol (PEG) units. A coupling procedure between the biotinlyated linker **1.40** and alcohol **1.38** (1:1.5), using EDCI and catalytic 4-DMAP, returned only a few mg of coupled product **1.41** due to difficult separation from starting alcohol (prep HPLC, Art Rand, Lokey group). Therefore, it was determined that only a slight excess of **1.38** should be used for an efficient separation by preparative HPLC, which gave the affinity probe **1.41** in 32% yield with enough material to run multiple immunoprecipitation experiments.

1.9 Isolation and Identification of Tamoxilog Protein Target

With our biotinylated affinity probe, standard pulldown techniques could be employed, as conducted by Dr. Tiffani Quan.[54] Dr. Quan attempted to immunoprecipitate any interactions between tamoxilog and proteins in yeast whole cell extracts (WCE) in an unbiased approach. Biotin-tamoxilog was preincubated with streptavidin beads and then incubated with WCE followed by a series of washes and then elution via acid-base cleavage of the ester linkage connecting the biotin to the tamoxilog. Elutions were then separated via SDS-PAGE and associated proteins identified by mass spectrometry.

With the help of a colleague at UCSF, Dr. Quan was able to reproducibly pull down the same protein target in multiple trials with **1.41** as confirmed by MS analyses. Dr. Quan identified Acc1 (acetyl CoA carboxylase), Fas1 (fatty acid synthase beta subunit), Fas2 (fatty acid synthase alpha subunit), Kap123 (importin beta 4), Kap104 (importin beta 2), and Kap119 (nonsense mediated decay protein 5) in her immunoprecipitation experiments with whole yeast cell extracts, and believes the first three proteins listed fit into her working hypothesis. She is currently trying to identify mammalian homologs. The findings of her research on tamoxilog and tamoxifen are currently being summarized and a manuscript prepared.

1.10 Conclusion

In an effort to identify a new target of tamoxifen, many pitfalls have been surpassed while other challenges remain. Many of the challenges lie within the interworking of a multidisciplinary collaboration. In particular, the design of an affinity probe could have been more refined with the inclusion of photolyzable “warheads” capable of covalently binding to the protein target. The alcohol-appended tamoxilog (**1.38**) is set up well for any second-generation affinity probes that may be pursued in the future. However, it appears the simple biotinylated linker was sufficient for our current purposes.

This work is detailed in an article entitled, “Structural determination of NSC 670224, synthesis of analogs and biological evaluation.”[55]

Experimentals

General Methods

Standard syringe techniques using flame and/or oven-dried glassware were utilized for syntheses under an atmosphere of dry nitrogen. All melting points are uncorrected. Proton NMR spectra were run in the specified deuterated solvents at 500 MHz, while carbon NMR were run at 125 MHz. The chemical shifts are reported in parts per million, and ^{1}H and ^{13}C spectra were calibrated against residual solvent peaks as follows: $CDCl_3$ (δ 7.26, 77.2), CD_3OD (δ 3.31, 49.0). The following abbreviations will be used throughout: s = singlet, d = doublet, t = triplet, q = quartet, p = pentet, m =

multiplet, app = apparent, THF = tetrahydrofuran, DCM = dichloromethane, DMSO = dimethylsulfoxide, EtOAc = ethyl acetate, DME = 1,2-dimethoxyethane, DMF = *N,N*-dimethylformamide, MeOH = methanol, 4-DMAP = 4-*N,N*-dimethylaminopyridine, EDCI-HCl = 1-(3-Dimethylaminopropyl)-3-ethylcarbodiimide hydrochloride, LAH = lithium aluminum hydride, aq. = aqueous, sat. = saturated, con. = concentrated, h = hour, and min = minutes. Anhydrous toluene, THF and DCM were obtained from a solvent purification system. DME was distilled over sodium metal/benzophenone and was stored over 4Å molecular sieves. Dimethylformamide was pretreated with activated (flame-dried under vacuum) 4Å molecular sieves overnight and then distilled below 70 °C under vacuum. Hexanes was distilled from CaH_2 and stored over 4 Å molecular sieves. Allyl bromide and benzyl halides were passed through a neutral alumina plug immediately before use. All amines were distilled over CaH_2 and stored over KOH. All other solvents and reagents were used as received unless otherwise noted.

Diastereomers are referred to as *cis* and *trans* throughout based on the relative positions between the *t*-butyl group and the alkoxy substituents.

***Caution:** *Osmium tetroxide is extremely toxic and should only be handled in the hood along with reviewing the MSDS and standard operating procedures prior to use. Disposable gloves and aprons should be worn (in addition to regular PPE) and disposed of as hazardous waste (as well as paper towels,*

pipettes, etc.) All glassware and washing solutions were treated with a saturated solution of sodium bisulfite and/or canola oil. Waste generated from this reaction was disposed of in a dedicated waste container.

General Procedure A: Mesylation, Amination and HCl Salt Formation.

The preparation of the amine hydrochloride salts was adapted from a previously published procedure by Hay et al.[35] Primary alcohol (2.0 mmol) was dissolved in DCM (anhydrous, 20 mL) and stirred under dry nitrogen. Triethylamine (362 mL, 2.6 mmol) and methanesulfonyl chloride (185 mL, 2.4 mmol) were then added and the resulting mixture was allowed to stir at room temperature for 2 h. The reaction was then diluted with DCM (20 mL) and washed with water and brine. The combined organic layer was dried with $MgSO_4$, filtered and evaporated to give the mesylate, which was taken on without purification. The crude mesylate was dissolved in THF (20 mL) and aq. dimethylamine (40 wt. %, 5.1 mL, 40 mmol) and refluxed for 16 h. The reaction was allowed to cool and the solvent was evaporated at reduced pressure. The residue was taken up in EtOAc, which was washed with water (3x), dried with $MgSO_4$, filtered and evaporated. Formation of the hydrochloride salt was performed by taking the residue up in ether and bubbling HCl gas (drop-wise addition of conc. H_2SO_4 to NH_4Cl) through the solution. Evaporation of the ether and recrystallization from DCM/hexanes gave the pure hydrochloride salt.

General Procedure B: Allylation.

The preparation of the allyl ethers was adapted from a previously published procedure by Sauer et al.[42] To a two-neck round bottom flask charged with a stir bar was added NaI (17 mg, 0.11 mmol), which was flame dried under vacuum and cooled under nitrogen. KH in mineral oil (30 wt. %, 543 mg, 4.06 mmol) was added to the flask and was rinsed three times with dry hexanes. Distilled DME (10 mL) was added to the flask and was cooled to 0 ^{o}C prior to addition of pure, or a mixture of, tertiary alcohol(s) (0.88 mmol) in DME (3 mL). The reaction was stirred for 5 min prior to addition of allyl bromide (0.23 mL, 2.63 mmol), which was then allowed to warm gradually to room temperature and stirred overnight. The reaction was cooled to 0 ^{o}C and carefully quenched with aq. sat. NH_4Cl (5 mL) followed by extraction with three portions of DCM. The combined organic fractions were dried with $MgSO_4$, filtered and evaporated to yield crude allyl ether(s). Flash column chromatography on silica yielded the allyl ether(s).

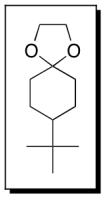

8-*tert*-Butyl-1,4-diaxospiro[4.5]decane (1.7). To a 250 mL round bottom flask fitted with a Dean-Stark apparatus, 4-*tert*-butylcyclohexanone (5.0 g, 32.4 mmol), ethylene glycol (6.0 g, 5.4 mL, 62.1 mmol), and *p*-toluenesulfonic acid monohydrate (0.6 g, 3.2 mmol) were refluxed in toluene (anhydrous, 150 mL) for 16 h under an atmosphere of dry nitrogen. After cooling, the reaction mixture was washed with aq. sat.

$NaHCO_3$, water, and brine. The organic layer was then dried ($MgSO_4$) and evaporated prior to bulb-to-bulb distillation of the crude product to give the known ketal[56] as a clear colorless oil (5.6 g, 88% yield). ^{1}H NMR ($CDCl_3$) δ 3.93 (s, 4H), 1.79-1.71 (m, 4H), 1.49 (app td, *J* = 4.0, 13.0 Hz, 2H), 1.27 (app qd, *J* = 3.0, 13.5 Hz, 2H), 1.02 (tt, *J* = 3.0, 12.0 Hz, 1H), 0.86 (s, 9H); ^{13}C NMR ($CDCl_3$) δ 109.2, 64.4, 64.3, 47.3, 35.4, 32.5, 27.8, 25.0.

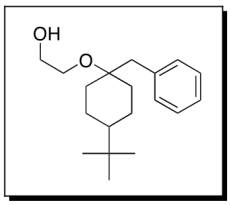

***cis*- and *trans*-2-(1-Benzyl-4-*tert*-butylcyclohexyloxy)-ethanol (1.11).** To a 100 mL round bottom flask fitted with a water-cooled reflux condenser was added **1.7** (500 mg, 2.5 mmol), benzylmagnesium chloride solution (1.0 *M* in ether, 12.6 mL, 12.6 mmol), and toluene (anhydrous, 25 mL). The reaction was allowed to reflux for 20 h followed by quenching at room temperature with aq. sat. NH_4Cl solution. The toluene layer was removed and the aqueous layer was extracted with ether (3x). The combined organic layers were dried with $MgSO_4$, filtered, and evaporated to give the crude mixture of primary alcohols (294 mg, 41% yield). Flash column chromatography was used to separate the two diastereomers, (15% EtOAc in hexanes) whereby *cis*-**1.11** was the first to elute as confirmed by single crystal X-ray diffraction. X-ray quality single crystals were obtained from slow evaporation of a DCM/hexanes solution.

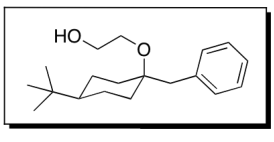

***cis*-1.11** (96 mg, 13% yield), mp 72-74 ^{o}C. IR (thin-film, cm^{-1}) 3429, 3085, 3062, 3028, 2941, 2865, 1604, 1496-

1365, 1126-1051, 762, 720, 700; ^{1}H NMR (500 MHz, $CDCl_3$) δ 7.29-7.15 (m, 5H), 3.78 (q, *J* = 5.0 Hz, 2H), 3.57 (t, *J* = 5.0 Hz, 2H), 2.74 (s, 2H), 2.08 (t, *J* = 6.0 Hz, 1H), 1.82 (dd, *J* = 2.0 Hz, 8.0 Hz, 2H), 1.51-1.48 (m, 2H), 1.28-1.19 (m, 4H), 0.93-0.84 (m, 1H), 0.81 (s, 9H); ^{13}C NMR ($CDCl_3$) δ 137.8, 130.5, 128.0, 126.2, 75.1, 62.4, 61.0, 47.1, 44.2, 34.1, 32.3, 27.4, 22.0; HRMS (ESI) for $C_{19}H_{30}O_2$ [M + Na] calcd, 313.21380, found, 313.21443 (error = 2.0063 ppm).

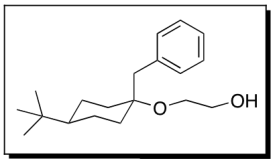

***trans*-1.11** (198 mg, 28% yield), mp 42-45 ^{o}C. IR (thin-film, cm^{-1}) 3429, 3086, 3061, 3027, 2942, 2867, 1601, 1495-1365, 1198, 1093-1055, 985, 892, 772, 754, 713, 698;^{1}H NMR ($CDCl_3$) δ 7.37-7.20 (m, 5H), 3.70 (q, *J* = 5.5 Hz, 2H), 3.57 (t, *J* = 5.0 Hz, 2H), 2.87 (s, 2H), 2.07 (t, *J* = 6.0 Hz, 1H), 1.72 (m, 4H), 1.46 (app td, *J* = 3.5, 13.0 Hz, 2H), 1.26 (app qd, *J* = 3.0, 13.0 Hz, 2H), 1.06 (tt, *J* = 3.5, 12.0 Hz, 1H) 0.90 (s, 9H); ^{13}C NMR ($CDCl_3$) δ 138.0, 130.5, 128.0, 126.2, 76.9, 62.3, 61.1, 47.6, 38.5, 34.4, 32.3, 27.6, 24.3; HRMS (ESI) for $C_{19}H_{30}O_2$ [M + Na] calcd, 313.21380, found, 313.21431 (error = 1.6232 ppm).

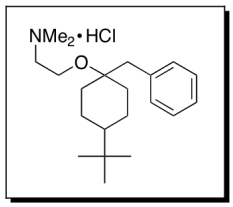

***cis*- and *trans*-3-(1-Benzyl-4-*tert*-butylcyclohexyloxy)-*N*,*N*-dimethylethanamine, hydrochloride (1.12)**. The preparation of the amine hydrochloride salts was conducted in accordance to General Procedure A.

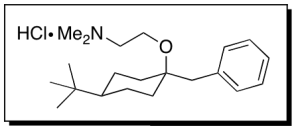

***cis*-1.12** (87 mg, 72% yield), mp 167-169 °C. IR (thin-film, cm^{-1}) 3368, 3079, 3059, 3026, 2943, 2866, 2687, 2479, 1658, 1491-1365, 1185-1063, 989, 957, 924, 882, 832, 763, 703; ^{1}H NMR ($CDCl_3$) δ 7.30-7.27 (m, 2H), 7.22 (tt, *J* = 1.5, 7.5 Hz, 1H), 7.14-7.12 (m, 2H), 3.92 (t, *J* = 5.0 Hz, 2H), 3.24 (t, *J* = 5.0 Hz, 2H), 2.83 (s, 6H), 2.75 (s, 2H), 1.83 (br dd, *J* = 2.5, 14.5 Hz, 2H), 1.54 (br d, *J* = 10.5 Hz, 2H), 1.28 (app td, *J* = 3.5, 13.5 Hz, 2H), 1.11 (app qd, *J* = 3.5, 12.5 Hz, 2H), 0.86 (tt, *J* = 3.0, 12.0 Hz, 1H), 0.80 (s, 9H); ^{13}C NMR (CD_3OD) δ 137.4, 130.3, 127.6, 125.9, 76.5, 57.4, 54.2, 43.4, 42.3, 33.5, 31.7, 26.4, 22.0; HRMS (ESI) for $C_{21}H_{36}NO$ [M + H] calcd, 318.27914, found, 318.28031 (error = 3.6713 ppm).

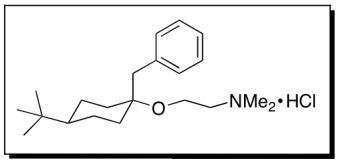

***trans*-1.12** (65 mg, 55% yield), mp 176-178 °C. IR (thin-film, cm^{-1}) 3423, 3010, 2963, 2949, 2866, 2590, 2511, 2459, 1602, 1493-1364, 1110-1003, 931, 715, 702; ^{1}H NMR ($CDCl_3$) δ 12.37 (br s, 1H), 7.20 (m, 5H), 3.90 (t, *J* = 4.5 Hz, 2H), 3.14 (t, *J* = 4.5 Hz, 2H), 2.84 (s, 2H), 2.70 (s, 6H), 1.76-1.70 (m, 4H), 1.52 (app td, *J* = 3.5, 13.0 Hz, 2 H), 1.25 (app qd, *J* = 2.5, 13.0 Hz, 2H), 1.05 (tt, *J* = 3.5, 12.5 Hz, 1H), 0.87 (s, 9H); ^{13}C NMR ($CDCl_3$) δ 137.5, 130.4, 127.9, 126.2, 78.4, 57.5, 55.7, 47.4, 43.6, 39.1, 33.9, 32.2, 27.5, 24.2; HRMS (ESI) for $C_{21}H_{36}NO$ [M + H] calcd, 318.27914, found, 318.28061 (error = 4.6138 ppm).

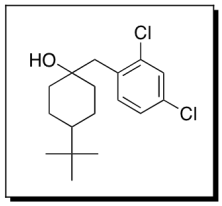

***cis*- and *trans*-4-*tert*-Butyl-1-(2,4-dichlorobenzyl)cyclohexanol (1.9)**. The required benzylic zinc reagent from 2,4-dichlorobenzyl chloride was formed in accordance to a procedure developed by Knochel et al.[38] Solutions of $ZnCl_2$ (1.0 *M*) and LiCl (0.5 *M*) were prepared in anhydrous THF after drying each salt under vacuum at 140 ^oC (5 h). To a two-neck round bottom flask with magnesium turnings (566 mg, 23.6 mmol) and a stir bar, were added 0.5 *M* LiCl in THF (31.6 mL, 15.3 mmol) and 1.0 *M* $ZnCl_2$ in THF (10.2 mL, 10.2 mmol). The reaction mixture was stirred under dry nitrogen at 0 ^oC prior to adding 2,4-dichlorobenzyl chloride (1.3 mL, 9.4 mmol) in one portion. The mixture was then stirred for 45 min at room temperature. In a separate two-neck round bottom flask charged with a stir-bar, 4-*tert*-butylcyclohexanone (727 mg, 4.7 mmol) in THF (anhydrous, 10 mL) was stirred at 0 ^oC under nitrogen. The benzylic zinc reagent was transferred via syringe into the flask containing the ketone and the resulting mixture was stirred overnight at room temperature, after which the reaction was again cooled to 0 ^oC and quenched with aq. sat. NH_4Cl. The mixture was diluted with DCM, which was washed with water, brine, and the organic layer dried with $MgSO_4$. Filtration and evaporation of the organic layer yielded a yellow oil consisting of the expected two isomeric tertiary alcohols, 2,4-dichlorotoluene, and a small portion of unreacted starting ketone. Flash column chromatography using 10% EtOAc in hexanes separated the two diastereomers. The first eluted alcohol was confirmed to be

the *cis* isomer by X-ray analysis, which is consistent with the elution pattern of the benzyl derivatives. The fractions containing the mixture of desired alcohols (1.08 g, 73% yield), but not containing starting ketone, were combined and taken through the next series of synthetic steps. As determined by TLC, pure fractions were taken for analytical purposes. X-ray quality single crystals were obtained from slow evaporation of a DCM/hexanes solution.

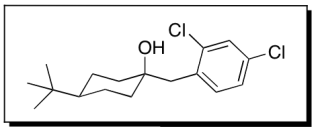

***cis*-1.9** mp 87-89 °C. IR (thin-film, cm^{-1}) 3582, 3437, 3060, 2943, 2867, 1725, 1640, 1588, 1558, 1471-1364, 1320, 1233, 1201, 1172, 1116-1049, 1015, 981, 927, 866-823, 753, 735, 698, 630, 554; ^{1}H NMR ($CDCl_3$) δ 7.38 (d, *J* = 2.0 Hz, 1H), 7.27 (d, *J* = 8.0 Hz, 1H), 7.18 (dd, *J* = 2.0, 8.5 Hz, 1H), 2.88 (s, 2H), 1.65-1.57 (m, 4H), 1.47 (app td, *J* = 4.0, 13.5 Hz, 2H), 1.28 (app qd, *J* = 4.0, 13.5 Hz, 2H), 1.28 (s, 1H), 0.95 (tt, *J* = 3.0, 12.0 Hz, 1H), 0.85 (s, 9H); ^{13}C NMR ($CDCl_3$) δ 135.8, 134.2, 133.5, 132.7, 129.3, 126.7, 71.8, 47.6, 45.6, 37.4, 32.3, 27.5, 22.2; HRMS (ESI) for $C_{17}H_{24}OCl_2$ [M + Na] calcd, 337.10964, found, 337.10815 (error = -4.4264 ppm).

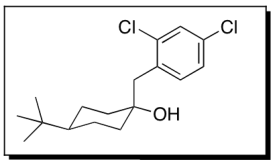

***trans*-1.9** mp 83-84 °C. IR (thin-film, cm^{-1}) 3412, 3071, 2944, 2866, 1640, 1588, 1558, 1472-1365, 1322, 1230, 1195, 1103, 1059, 985, 929, 864-815, 758, 739, 685, 587, 564; ^{1}H NMR ($CDCl_3$) δ 7.39 (d, *J* = 2.5 Hz, 1H), 7.38 (d, *J* = 8.5 Hz, 1H), 7.19 (dd, *J* = 2.5, 8.5 Hz, 1H), 2.99 (s, 2H), 1.79-1.73 (m, 4H), 1.45 (s, 1H), 1.43-1.27 (m, 4H), 1.07 (tt, *J* = 3.5, 12.0 Hz, 1H), 0.90 (s, 9H); ^{13}C NMR

($CDCl_3$) δ 135.7, 134.5, 133.6, 132.8, 129.4, 126.8, 73.1, 47.6, 39.2, 38.5, 27.8, 24.7; HRMS (ESI) for $C_{17}H_{24}OCl_2$ [M + Na] calcd, 337.10964, found, 337.10949 (error = -0.4514 ppm).

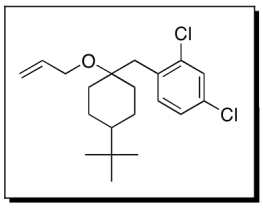

***cis*- and *trans*-1-((1-(Allyloxy)-4-*tert*-butylcyclohexyl) methyl)-2,4-dichlorobenzene (1.18).** The preparation of the allyl ethers was conducted in accordance to General Procedure B. Flash column chromatography on silica using hexanes/DCM (2:1) yielded the mixture of allyl ethers as a clear colorless oil (266 mg, 75% yield). As determined by TLC, pure fractions were taken for analytical purposes.

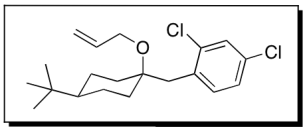

***cis*-1.18** IR (thin-film, cm^{-1}) 3428, 3065, 2948, 2867, 1719, 1659, 1630, 1588, 1472-1365, 1322, 1238, 1175, 1118, 1072-1039, 979, 927, 864, 824, 759, 743, 681, 634; ^1H NMR ($CDCl_3$) δ 7.36-7.35 (d, *J* = 2.0 Hz, 1H), 7.19-7.14 (m, 2H), 6.02-5.95 (m, 1H), 5.36 (app dq, *J* = 2.0, 17.0 Hz, 1H), 5.17 (app dq, *J* = 2.0, 10.0 Hz, 1H), 4.01 (app dt, *J* = 2.0, 5.0 Hz, 2H), 2.91 (s, 2H), 1.87-1.85 (m, 2H), 1.50-1.48 (m, 2H), 1.33-1.22 (m, 4H), 0.90-0.86 (m, 1H), 0.82 (s, 9H); ^{13}C NMR ($CDCl_3$) δ 135.6, 134.6, 133.2, 129.2, 126.8, 116.0, 76.3, 61.6, 47.3, 39.3, 34.2, 32.4, 27.6, 22.2; HRMS (CI) for $C_{20}H_{28}OCl_2$ $[M - H]^+$ calcd, 353.1439, found, 353.1441 (error = 0.6 ppm).

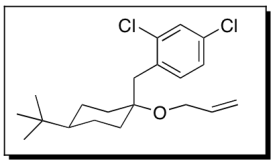

***trans*-1.18** IR (thin-film, cm^{-1}) 3076, 2945, 2862, 2719, 1838, 1722, 1646, 1585, 1555, 1470-1366, 1319-1196, 1122, 1102, 1067, 1023, 990, 916, 864-814, 740, 683-633, 562; ^{1}H NMR ($CDCl_3$) δ 7.55 (d, *J* = 8.5 Hz, 1H), 7.35 (d, *J* = 2.5 Hz, 1H), 7.16 (dd, *J* = 2.5, 8.5 Hz, 1H), 5.98-5.90 (m, 1H), 5.28 (app dq, *J* = 2.0, 17.5 Hz, 1H), 5.14 (app dq, *J* = 2.0, 10.5 Hz, 1H), 4.01 (app dt, *J* = 1.5, 5.5 Hz, 2H), 3.05 (s, 2H), 1.74-1.67 (m, 4H), 1.51 (app td, *J* = 4.0, 14.0 Hz, 2H), 1.31, (app qd, *J* = 3.0, 13.5 Hz, 2H), 1.02 (tt, *J* = 3.5, 12.0 Hz, 1H), 0.88 (s, 9H); ^{13}C NMR ($CDCl_3$) δ 135.9, 135.3, 134.8, 133.4, 132.3, 129.0, 126.8, 115.9, 78.0, 61.8, 47.7, 34.8, 33.6, 32.4, 27.7, 24.3; HRMS (CI) for $C_{20}H_{28}OCl_2$ $[M - H]^+$ calcd, 353.1439, found, 353.1442 (error = 0.8 ppm).

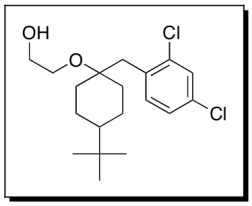

***cis*- and *trans*-2-(4-*tert*-Butyl-1-(2,4-dichloroben-zyl)cyclohex-yloxy)ethanol (1.6).** The mixture of allyl ethers (**1.18**, 429 mg, 1.21 mmol) were dissolved in dioxane (8 mL) and stirred at room temperature. A catalytic amount of OsO_4 (2.5% in *t*-BuOH), and *N*-methylmorpholine-*N*-oxide (205 mg, 1.75 mmol) were added to the reaction while stirring was continued overnight in the dark. The reaction was then cooled to 0 ^{o}C and sodium bisulfite was added. The precipitate was filtered, rinsed with EtOAc, and evaporated to yield the crude diol mixture, which was taken on without further purification.

Silica gel (2.8 g) was added to DCM (anhydrous, 12 mL) with vigorous stirring while $NaIO_4$ (483 mg, mmol) in distilled water (0.5 mL) was added drop-wise to minimize clumping. The mixture was cooled to 0 ^oC and the crude diol was added drop-wise in DCM (2.75 mL) and allowed to stir at room temperature for 3 h. The mixture was filtered through celite, rinsed with 10% MeOH in EtOAc, and evaporated to give the crude aldehyde mixture, which was taken on without further purification.

The crude aldehyde mixture was dissolved in MeOH (anhydrous, 15 mL), stirred under dry nitrogen, and cooled to 0 ^oC prior to the portion-wise addition of $NaBH_4$ (136 mg, 3.63 mmol). The mixture was stirred for 30 min at 0 ^oC and was quenched with water. Removal of the solvent by rotary evaporation left a sticky residue, which was purified by flash column chromatography (15% EtOAc in hexanes) to yield each primary alcohol as a pure diastereomer (238 mg, 55% yield over 3 steps).

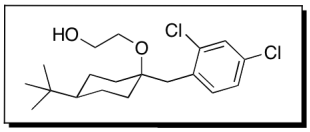

***cis*-1.6** (115 mg, 27% yield), clear colorless oil, IR (thin-film, cm^{-1}) 3422, 2943, 2866, 1638, 1588, 1558, 1471, 1451, 1365, 1319, 1119, 1094, 1049, 981, 963, 927, 892, 821, 753, 735, 698, 627; ^1H NMR ($CDCl_3$) δ 7.35 (d, *J* = 2.0 Hz, 1H), 7.22-7.19 (m, 2H), 3.79 (q, *J* = 5.0 Hz, 2H), 3.57 (t, *J* = 5.0 Hz, 2H), 2.90 (s, 2H), 2.12 (t, *J* = 6.0 Hz, 1H), 1.84 (app d, 2H), 1.50 (app d, 2H), 1.32-1.19 (m, 4H), 0.91-0.83 (m, 1H), 0.81 (s, 9H); ^{13}C NMR ($CDCl_3$) δ 135.6, 134.5, 133.1, 132.6, 129.3, 126.7, 76.1, 62.5, 61.2, 47.1, 39.4, 34.0, 32.5, 27.5, 22.1; HRMS (ESI) for

$C_{19}H_{28}O_2Cl_2$ [M + Na] calcd, 381.13586, found, 381.13706 (error = 3.1564 ppm).

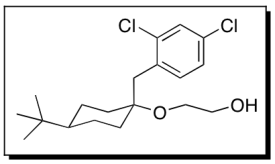

***trans*-1.6** (123 mg, 28% yield), clear colorless oil. IR (thin-film, cm^{-1}) 3401, 2943, 2867, 1640, 1587, 1555, 1470, 1366, 1322, 1264, 1198, 1102, 1052, 984, 888-740; ^1H NMR ($CDCl_3$) δ 7.47 (d, *J* = 8.0 Hz, 1H), 7.37 (d, *J* = 2.0 Hz, 1H), 7.17 (dd, *J* = 2.0, 8.0 Hz, 1H), 3.72-3.68 (m, 2H), 3.52 (t, *J* = 4.5 Hz, 2H), 3.04 (s, 2H), 2.01 (t, *J* = 6.0 Hz, 1H), 1.73-1.67 (m, 4H), 1.52 (app dt, *J* = 4.0, 13.0, 2H), 1.26 (app qd, *J* = 3.5, 13.0 Hz, 2H), 1.02 (tt, *J* = 3.5, 12.0 Hz, 1H), 0.88 (s, 9H); ^{13}C NMR ($CDCl_3$) δ 137.9, 133.6, 133.2, 131.8, 129.3, 126.8, 78.0, 62.6, 47.8, 35.0, 34.5, 32.5, 27.8, 24.4; HRMS (ESI) for $C_{19}H_{28}O_2Cl_2$ [M + Na] calcd, 381.13586, found, 381.13647 (error = 1.6084 ppm).

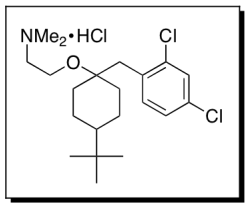

***cis*- and *trans*-2-(4-*tert*-Butyl-1-(2,4-dichlorobenzyl)cyclohex-yloxy)-*N*,*N*-dimethylethanamine hydrochloride (1.13).** Mesylation, alkylation and formation of the hydrochloride salt was performed individually on *cis*-**1.6** and *trans*-**1.6** in accordance to General Procedure A. X-ray quality single crystals were obtained from slow evaporation of a DCM/toluene solution for ***cis*-13**.

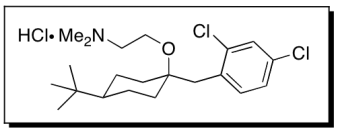

***cis*-1.13** (32 mg, 45% yield), mp 165-167 ^oC. IR (thin-film, cm^{-1}) 3391, 3067, 2942, 2865, 2593, 2470, 1643, 1587, 1559, 1470, 1382, 1364, 1333,

1240-1047, 999-931, 867, 850 827, 752, 734, 698, 660, 628, 556; ^{1}H NMR (CD_3OD) δ 7.42 (dd, *J* = 0.5, 1.5 Hz, 1H), 7.29-7.26 (m, 2H), 3.85 (t, *J* = 5.0 Hz, 2H), 3.39 (t, *J* = 5.0 Hz, 2H), 2.98 (s, 2H), 2.94 (s, 6H), 1.93 (app br dd, *J* = 2.0, 14.0 Hz, 2H), 1.57 (app d, *J* = 11.0 Hz, 2H), 1.32 (app td, *J* = 3.5, 13.5 Hz, 2H), 1.22 (app qd, *J* = 2.0, 12.5 Hz, 2H), 0.91-0.85 (m, 1H), 0.83 (s, 9H); ^{13}C NMR (CD_3OD) δ 135.2, 134.1, 133.4, 132.4, 128.6, 126.4, 77.3, 57.3, 54.4, 42.4, 38.9, 33.3, 31.6, 26.4, 22.1; HRMS (ESI) for $C_{21}H_{34}NOCl_2$ [M + H] calcd, 386.20120, found, 386.20263 (error = 3.7108 ppm).

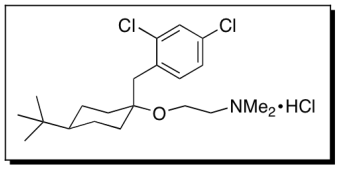

***trans*-1.13** (23 mg, 69% yield), mp 186-188 °C. IR (thin-film, cm^{-1}) 3368, 2967, 2944, 2869, 2837, 2730, 1637, 1584, 1552, 1469-1325, 1198, 1173, 1103, 1052, 1020, 927, 861, 835; ^{1}H NMR ($CDCl_3$) δ 7.37 (d, *J* = 2.0 Hz, 1H), 7.30 (d, *J* = 8.5 Hz, 1H), 7.18 (dd, *J* = 2.0, 8.5 Hz, 1H), 3.90 (t, *J* = 5.0 Hz, 2H), 3.11 (t, *J* = 5.0 Hz, 2H), 3.03 (s, 2H), 2.72 (s, 6H), 1.78-1.70 (m, 4H), 1.62 (app td, *J* = 4.0, 12.5, 2H), 1.28 (app qd, *J* = 2.0, 12.5 Hz, 2H), 1.06 (tt, *J* = 3.5, 12.5 Hz, 1H); ^{13}C NMR (CD_3OD) δ 135.0, 134.3, 133.1, 132.2, 128.4, 126.4, 78.7, 57.3, 54.4, 42.3, 33.8, 33.7, 31.5, 26.4, 23.8; HRMS (ESI) for $C_{21}H_{34}NOCl_2$ [M + H] calcd, 386.20120, found, 386.19996 (error = -3.2027 ppm).

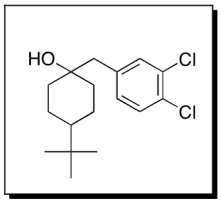

***cis*- and *trans*-4-*tert*-Butyl-1-(3,4-dichlorobenzyl)cyclo-hexanol (1.20).** To a two-neck round bottom flask with a stir

bar was added magnesium turnings (2.2 g, 90 mmol), 0.5 *M* LiCl in THF (90 mL, 45 mmol), and 1.0 *M* $ZnCl_2$ (39.7 mL, 39.7 mmol). The reaction mixture was stirred under nitrogen at 0 ^oC prior to adding 3,4-dichlorobenzyl chloride (5.0 mL, 36.1 mmol) in one portion. The mixture was then stirred for 45 min at room temperature with occasional cooling on an ice bath. In a separate two-neck round bottom flask charged with a stir-bar, 4-*tert*-butylcyclohexanone (2.78 g, 18.0 mmol) in THF (anhydrous, 15 mL) was stirred at 0 ^oC under nitrogen. The benzylic zinc reagent was transferred via syringe into the flask containing the ketone and was stirred overnight at room temperature, after which the reaction was again cooled to 0 ^oC and quenched with aq. sat. NH_4Cl. The mixture was diluted with DCM, which was washed with water, brine, and the organic layer dried with $MgSO_4$. Filtration and evaporation of the organic layer yielded a yellow oil consisting of the two tertiary alcohols (*cis* and *trans*), 3,4-dichlorotoluene, and a small portion of unreacted starting ketone. The oil was loaded onto a plug of silica and 300 mL of hexanes was flushed through a vacuum filter to remove the majority of nonpolar impurities. The vacuum flask was exchanged and 300 mL of EtOAc was passed through to collect the crude tertiary alcohol mixture. Evaporation of the polar fraction and cooling caused the less polar tertiary alcohol isomer to crystallize. Collection of the crystals by vacuum filtration (wash with cold heptane) and flash column chromatography of the remaining oil (10% EtOAc in hexanes) separated the two diastereomers (4.16 g, 73% yield).

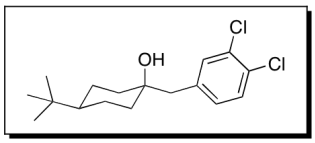

***cis*-1.20** (2.07 g, 36% yield), clear colorless oil. IR (thin-film, cm^{-1}) 3435, 2943, 2867, 1638, 1558, 1471-1364, 1318, 1131, 1071, 1031, 1016, 983, 927, 868, 825, 739, 667; ^{1}H NMR ($CDCl_3$) δ 7.35 (d, *J* = 8.0 Hz, 1H), 7.31 (d, *J* = 2.0 Hz, 1H), 7.04 (d, *J* = 2.0, 8.0 Hz, 1H), 2.66 (s, 2H), 1.61-1.58 (m, 4H), 2.36 (app td, *J* = 4.0, 13.5 Hz, 2H), 1.27 (app qd, *J* = 3.5, 13.0 Hz, 2H), 1.16 (s, 1H), 0.92(tt, *J* = 3.0, 12.0 Hz, 1H), 0.84 (s, 9H); ^{13}C NMR ($CDCl_3$) δ 138.0, 132.6, 132.2, 130.7, 130.2, 130.1, 70.8, 49.5, 47.9, 37.7, 32.6, 27.7, 22.5; HRMS (ESI) for $C_{17}H_{24}OCl_2$ [M + Na] calcd, 337.10964, found, 337.10968 (error = 0.1122 ppm).

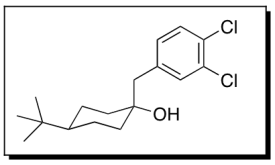

***trans*-1.20** (2.09 g, 37% yield), mp 118-119 ^{o}C. IR (thin-film, cm^{-1}) 3368, 2933, 2865, 1591, 1560, 1473, 1456, 1395, 1366, 1316, 1233, 1197, 1130, 1055, 1032, 984, 931, 867, 826, 815, 740, 715, 578; ^{1}H NMR ($CDCl_3$) δ 7.36 (d, *J* = 8.0 Hz, 1H), 7.35 (d, *J* = 2.0 Hz, 1H), 7.08 (dd, *J* = 2.0, 8.0 Hz, 1H), 2.76 (s, 2H), 1.76-1.71 (m, 4H), 1.37 (app td, *J* = 3.5, 13.0 Hz, 2H), 1.28 (s, 1H), 1.20 (app qd, *J* = 3.0, 13.5 Hz, 2H), 1.08 (tt, *J* = 3.0, 12.0 Hz), 0.90 (s, 9H); ^{13}C NMR ($CDCl_3$) δ 138.2, 132.6, 132.2, 130.7, 130.3, 130.2, 72.3, 47.8, 41.8, 38.8, 32.5, 27.9, 24.7; HRMS (ESI) for $C_{17}H_{24}OCl_2$ [M + Na] calcd, 337.10964, found, 337.10822 (error = -4.2187 ppm).

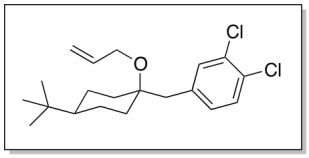

***cis*- 4-((1-(Allyloxy)-4-*tert*-butylcyclohexyl)methyl)-1,2-dichlorobenzene (*cis*-1.21).** The synthesis of the allyl ether was conducted on the pure diastereomer in accordance to General Procedure B. (0.63 g, 88% yield), clear colorless oil. IR (thin-film, cm^{-1}) 3079, 3014, 2943, 2865, 1646, 1591, 1559, 1472, 1450, 1394, 1365, 1124, 1064, 1032, 919, 822; ^{1}H NMR ($CDCl_3$) δ 7.32 (d, *J* = 8.0 Hz, 1H), 7.22 (d, *J* = 2.0 Hz, 1H), 6.97 (dd, *J* = 2.0, 8.0 Hz, 1H), 6.00-5.93 (m, 1H), 5.34 (app dq, *J* = 2.0, 17.0 Hz, 1H), 5.18 (app dq, *J* = 1.5, 10.5 Hz, 1H), 3.98 (dd, *J* = 1.5, 4.0 Hz, 2H), 2.68 (s, 2H), 1.81 (app dd, *J* = 2.0, 14.0 Hz, 2H), 1.50 (br d, *J* = 11.0 Hz, 2H), 1.29 (app qd, *J* = 2.0, 13.0 Hz, 2H), 1.18 (app td, *J* = 3.5, 13.0 Hz, 2H), 0.88 (tt, *J* = 3.0, 12.0 Hz, 1H), 0.83 (s, 9H); ^{13}C NMR ($CDCl_3$) δ 138.4, 135.3, 132.3, 131.9, 130.2, 129.9, 129.8, 116.1, 75.2, 61.7, 47.5, 43.2, 34.6, 32.5, 27.7, 22.3; HRMS (CI) for $C_{20}H_{28}OCl_2$ $[M - H]^+$ calcd, 353.1439, found, 353.1445 (error = 1.7 ppm).

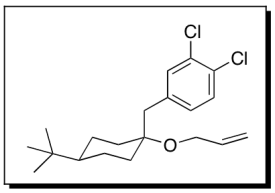

***trans*-1.21** The synthesis of the allyl ether was conducted on the pure diastereomer in accordance to General Procedure B. (1.58 g, 92% yield), clear colorless oil. IR (thin-film, cm^{-1}) 3078, 3013, 2943, 2866, 2721, 1646, 1590, 1559, 1473, 1422, 1394, 1366, 1317, 1290, 1261, 1237, 1197, 1132, 1071, 1031, 994, 919, 888, 859, 826, 814, 749, 714, 688, 669, 578; ^{1}H NMR ($CDCl_3$) δ 7.33-7.31 (m, 2H), 7.06 (dd, *J* = 2.0, 8.5 Hz, 1H),

5.96-5.88 (m, 1H), 5.27 (app dq, *J* = 2.0, 17.0 Hz, 1H), 5.15 (app dq, *J* = 2.0, 10.0 Hz, 1H), 4.01 (app dt, *J* = 1.5, 5.0 Hz, 2H), 2.81 (s, 2H), 1.74-1.72 (m, 2H), 1.69-1.66 (m, 2H), 1.49 (app td, *J* = 4.0, 13.0 Hz, 2H), 1.17 (app qd, *J* = 3.5, 13.5 Hz, 2H), 1.05 (tt, *J* = 3.0, 12.5 Hz, 1H), 0.89 (s, 9H); ^{13}C NMR ($CDCl_3$) δ 138.5, 135.8, 132.6, 131.9, 130.2, 129.8, 116.0, 61.9, 47.8, 37.5, 34.5, 32.5, 27.8, 24.5; HRMS (CI) for $C_{20}H_{28}OCl_2$ $[M - H]^+$ calcd, 353.1439, found, 353.1443 (error = 1.1 ppm).

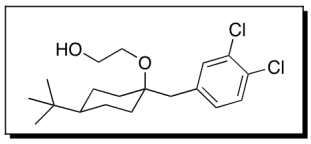

***cis*- 2-(4-*tert*-Butyl-1-(3,4-dichlorobenzyl)cyclo-hexyloxy)-ethanol (1.22).** Dihydroxylation of allyl ether *cis*-**1.21** was adapted from a previously published procedure by Sharpless and co-workers. To a round bottom flask charged with a stir bar was added 6.8 mL of 1:1 *t*-BuOH/H_2O and AD-mix-β (0.95 g). The mixture was cooled to 0 ^{o}C and *cis*-**1.21** (0.24 g, 0.68 mmol) was added drop-wise in *t*-BuOH (2 mL). Stirring was continued at room temperature overnight and in the dark. The mixture was cooled to 0 ^{o}C and sodium sulfite (1.02 g) was added and stirred at room temperature for 1 h. Filtration through celite and rinsing with EtOAc provided the crude diol, which was taken on without further purification.

Subsequent oxidative cleavage and reduction of the crude aldehyde were performed similarly to the above procedure for the 2,4-dichloro analogue. Flash column chromatography required loading with 20% EtOAc in

hexanes, followed by 40% EtOAc. Thus, elution of the *cis* isomer before the *trans* isomer was consistent throughout. X-ray quality single crystals were obtained from slow evaporation of a DCM/hexanes solution. (0.15 g, 61% yield over 3 steps), mp 109-110 ^{o}C. IR (thin-film, cm^{-1}) 3400, 2942, 2865, 1591, 1558, 1472, 1394, 1365, 1319, 1131, 1072, 1031, 984, 926, 892, 823, 741, 665; ^{1}H NMR ($CDCl_3$) δ 7.33 (d, *J* = 8.0 Hz, 1H), 7.26 (d, *J* = 2.0 Hz, 1H), 6.99 (dd, *J* = 2.0, 8.0 Hz, 1H), 3.78 (q, *J* = 5.0 Hz, 2H), 3.54 (t, *J* = 4.5 Hz, 2H), 2.68 (s, 2H), 2.00 (t, *J* = 6.0 Hz, 1H), 1.79 (br d, *J* = 11.5 Hz, 2H), 1.52 (br d, *J* = 10.0 Hz, 2H), 1.28-1.17 (m, 4H), 0.92-0.85 (m, 1H), 0.82 (s, 9H); ^{13}C NMR ($CDCl_3$) δ 138.2, 132.3, 131.9, 130.1, 130.0, 75.0, 62.5, 61.3, 47.3, 43.3, 34.5, 32.6, 27.7, 22.2; HRMS (ESI) for $C_{19}H_{28}O_2Cl_2$ [M + Na] calcd, 381.13586, found, 381.13557 (error = -0.7529 ppm).

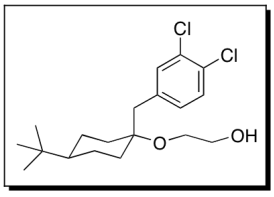

***trans*-1.22** The synthesis of the primary alcohol was conducted on the pure *trans*-**1.21** under similar conditions for *cis*-**1.22** above (0.34 g, 59% yield over 3 steps), mp 102-103 ^{o}C. IR (thin-film, cm^{-1}) 3054, 2943, 2867, 1590, 1472, 1394, 1366, 1318, 1261, 1198, 1131, 1078, 1030, 916, 853, 762, 736, 687, 668, 610, 579; ^{1}H NMR ($CDCl_3$) δ 7.33 (m, 2H), 7.07 (dd, *J* = 2.0, 8.0 Hz, 1H), 3.72 (m. 2H), 3.54 (t, *J* = 4.5 Hz, 2H), 2.81 (s, 2H), 1.95 (t, *J* = 6.0 Hz, 1H), 1.76-1.74 (m, 2H), 1.65-1.63 (m, 2H), 1.48 (app td, *J* = 4.0, 13.0 Hz, 2H), 1.19 (app qd, *J* = 3.0, 13.0 Hz, 2H), 1.05 (tt, *J* = 3.0, 12.5 Hz, 1H), 0.89 (s,

9H); ^{13}C NMR ($CDCl_3$) δ 138.4, 132.4, 132.0, 130.3, 130.1, 129.9, 77.0, 62.5, 61.4, 47.7, 38.0, 34.3, 32.4, 27.8, 24.5; HRMS (ESI) for $C_{19}H_{28}O_2Cl_2$ [M + Na] calcd, 381.13586, found, 381.13707 (error = 3.1826 ppm).

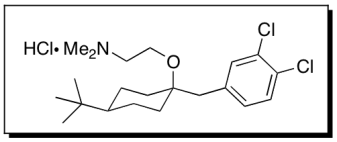

NSC- 670224/*cis*-2-(4-*tert*-Butyl-1-(3,4-dichloro-benzyl)-cyclohexyloxy)-*N*,*N*-dimethylethan-amine HCl (*cis*-1.23). Mesylation, alkylation and formation of the hydrochloride salt was performed in accordance to General Procedure A. (60.5 mg, 94% yield), mp 192-194 ^{o}C. IR (thin-film, cm^{-1}) 3401, 3013, 2945, 2866, 2607, 2467, 1634, 1559, 1471, 1393, 1365, 1126, 1093, 1030, 998, 825, 733; ^{1}H NMR ($CDCl_3$) δ 7.31 (d, *J* = 8.0 Hz, 1H), 7.26 (d, *J* = 2.0 Hz, 1H), 6.97 (dd, *J* = 2.0, 8.0 Hz, 1H), 3.53 (t, *J* = 5.0 Hz, 2H), 2.67 (s, 2H), 2.55 (t, *J* = 5.0 Hz, 2H), 2.31 (s, 6H), 1.79 (app br d, *J* = 12.0 Hz, 2H), 1.49 (app br d, *J* = 11.5 Hz, 2H), 1.26 (app qd, *J* = 2.5, 13.5 Hz, 2H), 1.15 (app td, *J* = 3.0, 13.0 Hz, 2H), 0.89-0.85 (m, 1H), 0.82 (s, 9H); ^{13}C NMR ($CDCl_3$) δ 137.4, 132.0, 131.7, 130.3, 129.9, 129.8, 76.6, 57.5, 55.7, 46.8, 43.6, 42.9, 33.6, 32.2, 27.3, 22.3; HRMS (ESI) for $C_{21}H_{34}NOCl_2$ [M + H] calcd, 386.20120, found, 386.20311 (error = 4.9537 ppm).

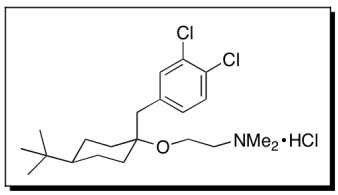

***trans*-1.23/Tamoxilog**. Mesylation, alkylation and formation of the hydrochloride salt was conducted in accordance to General Procedure A (24.9 mg, 84% yield), mp 116-118 ^{o}C. IR (thin-film, cm^{-1}) 3391, 2944, 2868, 2675, 2461,

1730, 1590, 1470, 1392, 1366, 1259, 1198, 1129, 1099, 1029, 995, 927, 888-666; ^{1}H NMR ($CDCl_3$) δ 12.61 (br s, 1H), 7.35 (d, *J* = 8.0 Hz, 1H), 7.26 (d, *J* = 2.0 Hz, 1H), 7.04 (dd, *J* = 2.0, 8.0 Hz, 1H), 3.94 (t, *J* = 4.5 Hz, 2H), 3.15 (t, *J* = 4.5 Hz, 2H), 2.81 (s, 2H), 2.77 (s, 6H), 1.79-1.77 (app br dd, *J* = 2.0, 14.0 Hz, 2H), 1.64-1.56 (m, 4H), 1.20 (app qd, *J* = 3.5, 12.5 Hz, 2H), 1.05 (tt, *J* = 3.0, 12.0 Hz, 1H), 0.88 (s, 9H); ^{13}C NMR ($CDCl_3$) δ 137.9, 135.4, 132.4, 130.6, 130.4, 129.93, 129.87, 78.5, 57.9, 55.9, 47.4, 43.9, 38.7, 33.5, 32.3, 27.6, 24.3; HRMS (ESI) for $C_{21}H_{34}NOCl_2$ [M + H] calcd, 386.20120, found, 386.20017 (error = -2.6589 ppm).

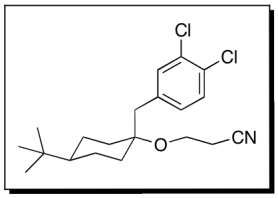

***trans*-3-(4-*tert*-Butyl-1-(3,4-dichlorobenzyl)cyclo-hexyloxy) propanenitrile (1.24).** The preparation of the nitrile was adapted from a previously published procedure by Fuwa et al. *Trans*-**1.22** (75 mg, 0.21 mmol) was dissolved in DCM (anhydrous, 15 mL) and stirred under dry nitrogen. Triethylamine (45 mL, 0.25 mmol) and methanesulfonyl chloride (20 mL, 0.32 mmol) were then added and allowed to stir at room temperature for 2 h. The reaction was then diluted with DCM (15 mL) and washed with water and brine. The organic layer was then dried with $MgSO_4$, filtered and evaporated to give the corresponding mesylate, which was taken on without purification. The crude mesylate was then dissolved in DMSO (anhydrous, 2 mL) with KCN (51 mg, 0.78 mmol) and was stirred at 65 ^{o}C for 2 h. The reaction was allowed to cool and was diluted

with EtOAc (20 mL), washed with water (4 x 5 mL) and brine. After drying and evaporation, the crystalline product **1.24** could be used without further purification (76 mg, quantitative yield), mp 69-70 ^{o}C. IR (thin-film, cm^{-1}) 3054, 2943, 2868, 2251, 1590, 1559, 1473, 1393, 1366, 1321, 1261, 1198, 1131, 1093, 1030, 876, 816, 739, 687, 668, 579; ^{1}H NMR ($CDCl_3$) δ 7.34 (d, *J* = 8.0 Hz, 1H), 7.31 (d, *J* = 2.0 Hz, 1H), 7.10 (dd, *J* = 2.0, 8.0 Hz, 1H), 3.62 (t, *J* = 6.5 Hz, 2H), 2.80 (s, 2H), 2.53 (t, *J* = 6.5 Hz, 2H), 1.75 (app br dd, *J* = 2.0, 12.0 Hz, 2H), 1.63-1.60 (app br d, *J* = 12.0 Hz, 2H), 1.51 (app td, *J* = 4.0, 12.0 Hz, 2H), 1.18 (app qd, *J* = 3.0, 12.0 Hz, 2H), 1.04 (tt, *J* = 3.0, 12.0 Hz, 1H), 0.89 (s, 9H); ^{13}C NMR ($CDCl_3$) δ 137.9, 132.2, 131.7, 130.1, 130.0, 129.7, 118.1, 77.9, 55.7, 47.4, 38.7, 33.4, 32.2, 27.5, 24.2, 19.5; HRMS (ESI) for $C_{20}H_{27}NOCl_2$ [M + Na] calcd, 390.13619, found, 390.13795 (error = 4.5079 ppm).

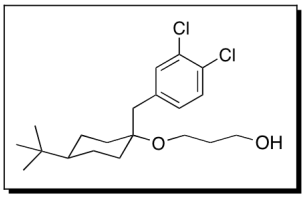

***trans*-3-(4-*tert*-Butyl-1-(3,4-dichlorobenzyl)cyclo-hexyloxy) propan-1-ol (1.25).** The preparation of the primary alcohol from **1.24** was adapted from a previously published procedure by Marshall et al. To a two-neck round bottom flask under dry nitrogen was added **1.24** (100 mg, 0.27 mmol) in dry hexanes (10 mL). The solution was cooled to -78 ^{o}C with a dry ice/acetone bath and DIBAL (1.0 *M* in hexanes, 54 mL, 0.54 mmol) was added drop-wise and allowed to stir for 30 min, at which point the reaction was allowed to warm to

room temperature and stirred 3 h prior to quenching with ethyl formate (60 mL; stir 1 h). Finally, the solution was added to sat. aq. NH_4Cl solution and extracted with EtOAc. Drying of the organic layer and filtration gave the crude aldehyde, which was taken on for reduction without further purification.

The crude aldehyde was dissolved in MeOH (anhydrous, 10 mL) and cooled to 0 ^oC prior to portion-wise addition of $NaBH_4$. After stirring for 30 min, the reaction was quenched with water and the solvent evaporated. The residue was purified by flash column chromatography (loaded with hexanes, elute with 15% EtOAc in hexanes) to yield the primary alcohol **1.25** (23.1 mg, 23% yield over 2 steps, unoptimized), clear colorless oil. IR (thin-film, cm^{-1}) 3400, 2943, 2867, 1472; ^1H NMR ($CDCl_3$) δ 7.35-7.32 (m, 2H), 7.06 (d, *J* = 8.0 Hz, 1H), 3.76 (t, *J* = 5.5 Hz, 2H), 3.64 (t, *J* = 5.5 Hz, 2H), 2.80 (s, 2H), 1.82 (p, *J* = 5.5 Hz, 2H), 1.74 (app br d, *J* = 12.0 Hz, 2H), 1.67 (app br d, *J* = 12.5 Hz, 2H), 1.50 (app td, *J* = 3.0, 13.0 Hz, 2H), 1.24-1.13 (m, 3H), 1.08-1.02 (m, 1H), 0.89 (s, 9H); ^{13}C NMR ($CDCl_3$) δ 132.3, 131.9, 130.2, 129.9, 77.2, 62.4, 59.8, 47.7, 37.7, 34.2, 32.4, 27.7, 25.7, 24.4; HRMS (ESI) for $C_{20}H_{30}O_2Cl_2$ [M + Na] calcd, 395.15151, found, 395.15313 (error = 4.1071 ppm).

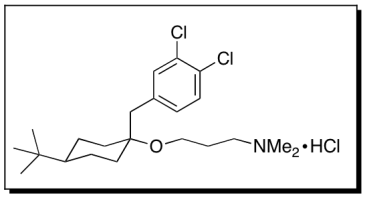

***trans*-3-(4-*tert*-Butyl-1-(3,4-dichlorobenzyl)cyc-lohex-yloxy)-*N*,*N*-dimethylpropan-1-amine hydrochloride (1.26).** Mesylation, alkylation and

formation of the hydrochloride salt from **1.25** was performed in accordance to General Procedure A (11.8 mg, 77% yield), mp 146-148 ^{o}C. IR (thin-film, cm^{-1}) 3400, 2943, 2867, 2689, 2472, 1628, 1588, 1472, 1393, 1365, 1316, 1259, 1198, 1130, 1076, 1028, 932, 888, 812, 688, 666; ^{1}H NMR (CD_3OD) δ 7.41 (d, *J* = 8.0 Hz, 1H), 7.37 (d, *J* = 2.0 Hz, 1H), 7.13 (dd, *J* = 2.0, 8.0 Hz, 1H), 3.58 (t, *J* = 5.5 Hz, 2H), 3.14 (m, 2H), 2.87 (s, 2H), 2.85 (s, 6H), 1.94-1.89 (m, 2H), 1.73 (app br d, *J* = 13.0 Hz, 2H), 1.63 (app br d, *J* = 12.5 Hz, 2H), 1.51 (app td, *J* = 4.0, 13.0 Hz, 2H), 1.17 (app qd, *J* = 2.0, 13.5 Hz, 2H), 1.05-0.99 (tt, *J* = 3.0, 12.0 Hz, 1H), 0.90 (s, 9H); ^{13}C NMR ($CDCl_3$) δ 138.4, 132.6, 131.4, 130.1, 130.0, 129.9, 57.1, 56.6, 47.6, 43.1, 38.7, 33.7, 32.4, 27.7, 25.6, 24.3; HRMS (ESI) for $C_{22}H_{36}NOCl_2$ [M + H] calcd, 400.21685, found, 400.21633 (error = -1.2917 ppm).

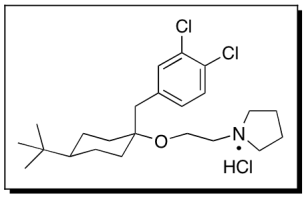

***trans*-1-(2-(4-*tert*-Butyl-1-(3,4-dichlorobenzyl)cyclohex-yloxy)ethyl)pyrrolidine hydrochloride (1.27).** Mesylation, alkylation and formation of the hydrochloride salt from *trans*-**1.22** was performed in accordance to General Procedure A replacing dimethylamine with pyrollidine (26.6 mg, 85% yield), mp 148-151 ^{o}C. IR (thin-film, cm^{-1}) 3391, 2945, 2868, 2609, 2478, 1591, 1471, 1393, 1363, 1314, 1262, 1196, 1098, 1050, 1026, 875, 814; ^{1}H NMR ($CDCl_3$) δ 12.4 (br s, 1H), 7.35 (d, *J* = 8.5 Hz, 1H), 7.26 (under $CDCl_3$, 1H), 7.04 (dd, *J* = 2.0, 8.5 Hz, 1H), 3.94 (t, *J* = 5.0 Hz, 2H),

3.66 (app br s, 2H), 3.19 (app br s, 2H), 2.81 (s, 2H), 2.77-2.74 (m, 2H), 2.14-2.13 (m, 2H), 2.01-1.96 (m, 2H), 1.79-1.77 (app br d, *J* = 12.5 Hz, 2H), 1.63-1.60 (m, 5H), 1.24-1.15 (m, 2H), 1.06 (tt, *J* = 3.0, 12.0 Hz, 1H), 0.88 (s, 9H); ^{13}C NMR ($CDCl_3$) δ 138.2, 132.5, 131.7, 130.0, 129.9, 78.3, 56.4, 55.3, 54.5, 47.3, 38.7, 33.4, 32.2, 27.5, 24.2, 23.2; HRMS (ESI) for $C_{23}H_{36}NOCl_2$ [M + H] calcd, 412.21685, found, 412.21657 (error = -0.6719 ppm).

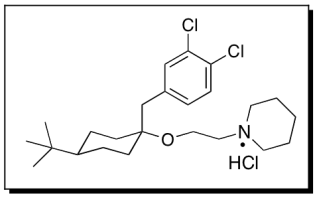

***trans*-1-(2-(4-*tert*-Butyl-1-(3,4-dichlorobenzyl)-cyclohex-yloxy)ethyl)piperidine hydrochloride (1.28).** Mesylation, alkylation and formation of the hydrochloride salt from *trans*-**1.22** was performed in accordance to General Procedure A replacing dimethylamine with piperidine (20.2 mg, 62 % yield), mp 188-189 ^{o}C. IR (thin-film, cm^{-1}) 3406, 2945, 2868, 2626, 2494, 2197, 1629, 1558, 1470, 1390, 1366, 1325, 1198, 1130, 1097, 1053, 1028, 924, 729, 688, 639; ^{1}H NMR ($CDCl_3$) δ 12.07 (br s, 1H), 7.34 (br d, *J* = 8.0 Hz, 1H), 7.24 (d, *J* = 2.0 Hz, 1H), 7.03 (dd, *J* = 2.0, 8.0 Hz, 1H), 3.96 (app br s, 2H), 3.45 (br d, *J* = 11.0 Hz, 2H), 3.07 (app br s, 2H), 2.79 (s, 2H), 2.58 (app br q, *J* = 8.5 Hz, 2H), 2.19 (app br q, *J* = 13.0 Hz, 2H), 1.84 (br d, *J* = 4.0 Hz, 1H), 1.78-1.72 (m, 4H), 1.60-1.56 (m, 4H), 1.36-1.28 (m, 1H), 1.24-1.15 (m, 2H), 1.05 (tt, *J* = 3.0, 12.5 Hz, 1H), 0.87 (s, 9H); ^{13}C NMR ($CDCl_3$) δ 138.2, 132.7, 131.7, 130.4, 130.2, 130.0, 78.5, 57.8, 55.9, 54.4, 47.6, 39.0, 33.5, 32.4, 27.7,

24.4, 22.8, 22.1; HRMS (ESI) for $C_{24}H_{38}NOCl_2$ [M + H] calcd, 426.23250, found, 426.23314 (error = 1.5085 ppm).

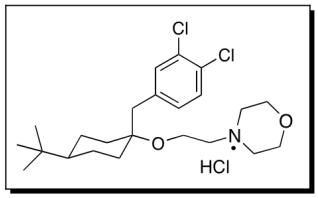

***trans*-4-(2-(4-*tert*-Butyl-1-(3,4-dichlorobenzyl)-cyclohex-yloxy)ethyl)morpholine hydrochloride (1.29).** Mesylation, alkylation and formation of the hydrochloride salt from *trans*-**1.22** was performed in accordance to General Procedure A replacing dimethylamine with morpholine (30.6 mg, 94% yield), mp 180-181 ^{o}C. IR (thin-film, cm^{-1}) 3391, 2947, 2867, 2648, 2582, 2474, 1590, 1455, 1391, 1366, 1200, 1134, 1091, 1060, 1029, 984, 922, 858; ^{1}H NMR ($CDCl_3$) δ 7.36 (d, *J* = 8.0 Hz, 1H), 7.25 (d, *J* = 2.0 Hz, 1H), 7.05 (dd, *J* = 2.0, 8.0 Hz, 1H), 4.22 (t, *J* = 12.0 Hz, 2H), 4.02 (t, *J* = 4.0 Hz, 2H), 3.87 (dd, *J* = 2.5, 13.0 Hz, 2H), 3.36 (br d, *J* = 12.0 Hz, 2H), 3.13 (d, *J* = 3.5 Hz, 2H), 2.88-2.81 (m, 2H), 2.81 (s, 2H), 1.80 (br d, *J* = 13.5 Hz, 2H), 1.63-1.58 (m, 4H), 1.21 (app qd, *J* = 5.0, 12.0 Hz, 2H), 1.05 (tt, *J* = 3.0, 12.0 Hz, 1H), 0.89 (s, 9H); ^{13}C NMR ($CDCl_3$) δ 137.9, 132.4, 131.6, 130.2, 129.9, 129.8, 78.5, 63.7, 58.0, 55.7, 53.0, 47.3, 38.7, 33.4, 32.2, 27.5, 24.2; HRMS (ESI) for $C_{23}H_{36}NO_2Cl_2$ [M + H] calcd, 428.21176, found, 428.21294 (error = 2.7519 ppm).

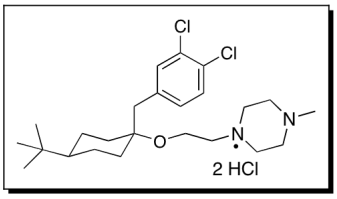

***trans*-1-(2-(4-*tert*-Butyl-1-(3,4-dichlorobenzyl)-cyclohex-yloxy)ethyl)-4-methylpiperazine di-hydrochloride (1.30).** Mesylation, alkylation and formation of the dihydrochloride salt from *trans*-**1.22** was performed in accordance to General Procedure A replacing dimethylamine with *N*-methylpiperazine (31.6 mg, 88% yield), mp 204-205 ^{o}C. IR (thin-film, cm^{-1}) 3400, 2942, 2867, 2371, 1637, 1472, 1456, 1393, 1365, 1318, 1197, 1130, 1102, 1027, 977, 914, 883, 812, 744, 668; ^{1}H NMR ($CDCl_3$) δ 7.42 (d, *J* = 8.0 Hz, 1H), 7.27 (d, *J* = 1.5 Hz, 1H), 7.09 (app d, *J* = 8.0 Hz, 1H), 3.96 (m, 6H), 3.59 (br d, *J* = 12.0 Hz, 2H), 3.45 (br d, *J* = 12.0 Hz, 2H), 3.26 (br s, 2H), 2.89 (s, 3H), 2.83 (s, 2H), 1.79 (br d, *J* = 13.0 Hz, 2H), 1.67 (br d, *J* = 12.5 Hz, 2H), 1.58-1.53 (m, 2H), 1.24-1.16 (m, 2H), 1.08 (tt, *J* = 3.0, 12.0 Hz, 1H), 0.88 (s, 9H); ^{13}C NMR ($CDCl_3$) δ 137.8, 132.1, 131.8, 130.3, 130.2, 130.1, 78.9, 57.6, 55.7, 49.9, 49.4, 47.3, 43.1, 38.4, 33.6, 32.2, 27.5, 24.2; HRMS (ESI) for $C_{24}H_{39}N_2OCl_2$ [M + H] calcd, 441.24340, found, 441.24532 (error = 4.3602 ppm).

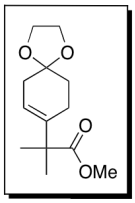

Methyl 2-methyl-2-(1,4-dioxaspiro[4.5]dec-7-en-8-yl)propa-noate (1.31). Diisopropylamine (7.00 mL, 50.0 mmol) was dissolved in THF (anhydrous, 100 mL) and cooled to -78 ^{o}C while *n*-BuLi (2.5 M, 20.0 mL, 50.0 mmol) was added drop-wise and stirred for 15 min. Methyl isobutyrate (5.75 mL, 10.0 mmol) was then added neat and

allowed to stir for 20 min at -78 ^{o}C. Commercially available 1,4-cyclohexanedione monoethyleneacetal (7.8 g, 10.0 mmol, freshly recrystallized from heptane) was dissolved in a minimal amount of anhydrous THF and added drop-wise to the prepared methyl isobutyrate anion. Stirring was continued for 2 h at -78 ^{o}C and aq. sat. NH_4Cl solution was added while cold and allowed to warm to room temperature. The reaction was then extracted with EtOAc (3x) and the combined organic layers were washed with water and brine. Drying of the organic layer with $MgSO_4$ followed by filtration and evaporation yielded the crude product as a yellow oil, which was loaded onto a pad of silica and vacuum filtered with a 1:1 hexanes/EtOAc solution. This crude product was taken on to the dehydration step.

The crude alcohol was dissolved in pyridine (anhydrous, 150 mL) and cooled with an ice bath before an excess of thionyl chloride (4.2 mL, 57.4 mmol) was added drop-wise. The reaction was allowed to come to room temperature overnight before being poured over crushed ice and subsequently extracted with DCM (3x). The combined organic layers were washed with water and brine, and dried with $MgSO_4$. After evaporation to yield the crude product as a yellow oil, flash column chromatography (3:1 hexanes/EtOAc) yielded pure ketal **1.31** (8.8 g, 73% yield), as a clear colorless oil. IR (thin-film, cm^{-1}) 3439, 3054, 2978, 2950, 2879, 2675, 1731, 1665, 1467, 1432, 1374, 1253, 1193, 1141, 1116, 1061, 1037, 995, 976, 943, 919, 864, 836; ^{1}H NMR ($CDCl_3$) δ 5.49-5.48 (m, 1H), 3.97-3.94 (m, 4H), 3.65

(s, 3H), 2.32-2.31 (m, 2H), 2.16-2.13 (m, 2H), 1.73 (t, *J* = 5.5 Hz, 2H), 1.30 (s, 6H); ^{13}C NMR ($CDCl_3$) δ 177.3, 139.7, 118.3, 107.8, 64.4, 52.0, 47.4, 35.9, 32.3, 31.4, 24.9, 24.5; HRMS (ESI) for $C_{13}H_{20}O_4$ [M + Na] calcd, 263.12538, found, 263.12604 (error = 2.5065 ppm).

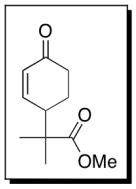

Methyl 2-methyl-2-(4-oxocyclohex-2-enyl)propanoate (1.32). Ketal **1.31** (6.1 g, 25.4 mmol) was dissolved in 9:1 acetone/water (175 mL) containing PPTS (8.9 g, 35.4 mmol). The mixture was stirred under reflux for 2 days and the reaction was cooled and evaporated under reduced pressure. The crude product was taken up in EtOAc and washed with water (3x) and brine. The organic layer was dried with $MgSO_4$, filtered, and evaporated before being vacuum filtered through a plug of silica gel with 1:1 hexanes/EtOAc.

Isomerization of the tri-substituted alkene to the desired α,β-unsaturated alkene was conducted by refluxing the crude product in DCM (anhydrous, 150 mL) with DBU (10.2 mL, 68.6 mmol). The reaction mixture turned dark in color and was refluxed for 2 h. After cooling to room temperature, the reaction mixture was washed with a 2.0 *M* solution of NaH_2PO_4 (5x). The combined aqueous layers were extracted with EtOAc (3x) and combined with the DCM layer. The combined organic layers were washed with brine, dried with $MgSO_4$, filtered and evaporated to give the crude product as a brown oil. Flash column chromatography (3:1

hexanes/EtOAc) furnished the desired α,β-unsaturated ketone **1.32** (4.4 g, 88% yield over two steps), as a clear colorless oil. IR (thin-film, cm^{-1}) 3032, 2978, 2956, 2879, 1731, 1681, 1613, 1465-1369, 1305, 1259-1124, 1070, 979, 853, 817, 773, 735; ^{1}H NMR ($CDCl_3$) δ 6.82 (dt, *J* = 2.0, 10.5 Hz, 1H), 6.05 (ddd, *J* = 1.0, 3.0, 10.0 Hz, 1H), 3.71 (s, 1H), 2.81 (app dp, *J* = 2.5, 11.0 Hz, 1H), 2.56-2.51 (m, 1H), 2.41-2.34 (m, 1H), 2.02-1.97 (m, 1H), 1.81-1.72 (m, 1H), 1.23 (s, 3H), 1.21 (s, 3H); ^{13}C NMR ($CDCl_3$) δ 199.4, 177.3, 151.3, 130.5, 52.3, 45.2, 44.0, 37.7, 24.6, 22.6, 22.4; HRMS (ESI) for $C_{11}H_{16}O_3$ [M + Na] calcd, 219.09917, found, 219.10015 (error = 4.4926 ppm).

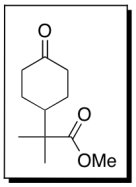

Methyl 2-methyl-2-(4-oxocyclohexyl)propanoate (1.33). Compound **1.32** (6.0 g, 30.6 mmol) was dissolved in THF (anhydrous, 150 mL) and purged with dry nitrogen prior to the addition of Pd/C (10%, 65 mg, 6.2 mmol). The reaction was stirred 24 h under 1 atm of hydrogen and carefully vacuum filtered through a pad of celite. Evaporation of solvent yielded a clear colorless oil, which crystallized upon standing (5.8 g, 96% yield), mp 54-55 ^{o}C. IR (thin-film, cm^{-1}) 2950, 2879, 1720, 1547, 1465, 1448, 1432, 1390, 1369, 1333, 1264, 1190, 1176, 1135, 1100, 1086, 998, 982, 952, 883, 842, 795, 773; ^{1}H NMR ($CDCl_3$) δ 3.66 (s, 3H), 2.40-2.27 (m, 4H), 2.06 (app tt, *J* = 3.0, 12.5 Hz, 1H), 1.92-1.86 (m, 2H), 1.46 (d, *J* = 5.0 Hz, 2H), 1.14 (s, 6H); ^{13}C NMR ($CDCl_3$) δ 211.4, 178.1, 51.9,

45.2, 43.8, 41.1, 27.6, 22.3; HRMS (ESI) for $C_{11}H_{18}O_3$ [M + Na] calcd, 221.11482, found, 221.11417 (error = -2.9205 ppm).

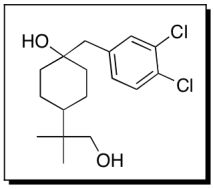

1-(3,4-Dichlorobenzyl)-4-(1-hydroxy-2-methylpropan-2-yl)cyclohexanol (1.34). To a two-neck round bottom flask with a stir bar was added magnesium turnings (1.2 g, 50.0 mmol), 0.5 *M* LiCl in THF (50 mL, 25.0 mmol), and 1.0 *M* $ZnCl_2$ (22.0 mL, 22.0 mmol). The reaction mixture was stirred under dry nitrogen at 0 ^oC prior to adding 3,4-dichlorobenzyl chloride (2.77 mL, 20.0 mmol) in one portion. The mixture was then stirred for 45 min at room temperature with occasional cooling on an ice bath. In a separate two-neck round bottom flask charged with a stir-bar, ketoester **1.33** (2.0 g, 10.0 mmol) in THF (anhydrous, 10 mL) was stirred at 0 ^oC under dry nitrogen. The benzylic zinc reagent was transferred via syringe into the flask containing the ketone and was stirred overnight at room temperature, after which the reaction was again cooled to 0 ^oC and quenched with aq. sat. NH_4Cl. The mixture was diluted with DCM, which was washed with water, brine, and the organic layer dried with $MgSO_4$. Filtration and evaporation yielded the crude product mixture as a colorless oil.

The crude mixture was taken up in THF (anhydrous, 10 mL) and added drop-wise to an ice cooled mixture of LAH (1.14 g, 30.0 mmol) in THF (anhydrous, 50 mL). The reaction was allowed to come to room temperature and stirring continued for 3 h. Standard LAH quenching techniques using one

part water, one part 10% NaOH, and three parts water at 0 °C gave a slurry which was vacuum filtered through celite. After rinsing the celite bed with EtOAc, the solvent was evaporated. Flash column chromatography (1:1 hexanes/EtOAc) yielded the separated diol diastereomers as white crystalline solids (1.49 g, 45% yield, over 2 steps). The structural assignment for each diol was determined using the X-ray structure of the first eluted mono-MOM protected compound (*cis*-**1.35**).

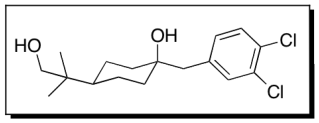

***cis*-1-(3,4-dichlorobenzyl)-4-(1-hydroxy-2-methyl-propan-2-yl)cyclohexanol (*cis*-1.34).** (0.70 g), mp 141-142 °C. IR (thin-film, cm^{-1}) 3368, 2937, 2871, 1592, 1562, 1471, 1443, 1393, 1130, 1031, 824; ^1H NMR (CD_3OD) δ 7.37-7.36 (m, 2H), 7.10 (dd, *J* = 2.0, 8.0 Hz, 1H), 3.28 (s, 2H), 2.63, (s, 2H), 1.57 (br d, *J* = 10.5 Hz, 2H), 1.48 (br d, *J* = 10.5 Hz, 2H), 1.41-1.31 (m, 4H), 1.23-1.18 (m, 1H), 0.79 (s, 6H); ^{13}C NMR (CD_3OD) δ140.1, 133.6, 132.4, 131.6, 130.9, 130.7, 71.6, 70.7, 50.3, 43.7, 38.1, 38.0, 22.9, 22.3; HRMS (ESI) for $C_{17}H_{24}O_2Cl_2$ [M + Na] calcd, 353.10456, found, 353.10436 (error = -0.5574 ppm).

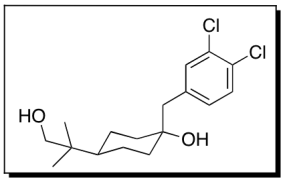

***trans*-1-(3,4-Dichlorobenzyl)-4-(1-hydroxy-2-methyl-propan-2-yl)cyclohexanol (*trans*-1.34).** (0.79 g), mp 122-124 °C. IR (thin-film, cm^{-1}) 3477, 3063, 2937, 2874, 1591, 1561, 1471, 1443, 1393, 1364, 1210, 1147, 1130, 1110, 1047, 985, 917, 870, 825, 738; ^1H NMR (CD_3OD) δ 7.39 (d, *J* = 2.0 Hz, 1H), 7.35 (d, *J* =

8.5 Hz, 1H), 7.13 (dd, *J* = 2.0, 8.0 Hz, 1H), 3.31 (s, 2H), 2.75 (s, 2H), 1.66 (br d, *J* = 9.5 Hz, 4H), 1.38-1.22 (m, 5H); ^{13}C NMR (CD_3OD) δ 140.3, 133.7, 132.4, 131.6, 129.9, 130.7, 72.8, 70.8, 43.9, 42.3, 39.1, 37.8, 25.1, 22.4; HRMS (ESI) for $C_{17}H_{24}O_2Cl_2$ [M + Na] calcd, 353.10456, found, 353.10432 (error = -0.6707 ppm).

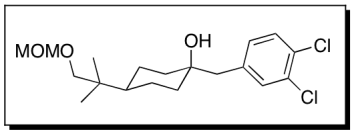

***cis*-1-(3,4-Dichlorobenzyl)-4-(1-(methoxymeth-oxy)-2-methylpropan-2-yl)cyclohexanol (*cis*-1.35).** A solution of *cis*-diol **1.34** (166 mg, 0.5 mmol) was dissolved in DCM (anhydrous, 10 mL) with Hunig's base (350 mL, 2.0 mmol). Chloromethyl methyl ether (MOM-Cl, 42 mL, 0.55 mmol) was added to the reaction mixture and the solution was allowed to stir at room temperature overnight. Methanol was added to quench any unreacted MOM-Cl and the solvent was evaporated. Flash column chromatography (3:1 hexanes/EtOAc) yielded the desired mono-protected MOM ether as a crystalline solid. X-ray quality single crystals were obtained from slow evaporation of a DCM/hexanes solution. (158 mg, 84% yield), mp 95-97 ^{o}C. IR (thin-film, cm^{-1}) 3477, 3063, 2937, 2874, 2773, 1591, 1561, 1471, 1443, 1393, 1364, 1210, 1147, 1130, 1110, 1047, 985, 917, 870, 825, 738; ^{1}H NMR ($CDCl_3$) δ 7.31 (d, *J* = 8.0 Hz, 1H), 7.28 (d, *J* = 2.0 Hz, 1H), 7.01 (dd, *J* = 2.0, 8.0 Hz, 1H), 4.56 (s, 2H), 3.32 (s, 3H), 3.23 (s, 2H), 2.62 (s, 2H), 1.58-1.52 (m, 4H), 1.38-1.2 (m, 6H), 0.84 (s, 6H); ^{13}C NMR ($CDCl_3$) δ 137.8, 132.4,

132.0, 130.5, 130.1, 129.9, 96.8, 75.7, 70.7, 55.2, 49.4, 43.0, 37.4, 36.3, 22.5, 22.0; HRMS (ESI) for $C_{19}H_{28}O_3Cl_2$ [M + Na] calcd, 397.13077, found, 397.12955 (error = -3.0761 ppm).

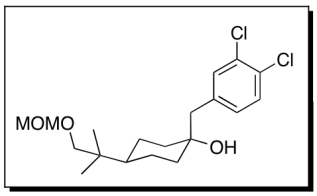

***trans*-1-(3,4-Dichlorobenzyl)-4-(1-(methoxymeth-oxy)-2-methylpropan-2-yl)cyclohexanol (*trans*-1.35).** A solution of *trans*-diol **1.34** (663 mg, 2.0 mmol) was dissolved in DCM (anhydrous, 40 mL) with Hunig's base (1.4 mL, 8.0 mmol). MOM-Cl (154 mL, 2.0 mmol) was added to the reaction mixture and the solution was allowed to stir at room temperature overnight. Methanol was added to quench any unreacted MOM-Cl and the solvent was evaporated. Flash column chromatography (7:3 hexanes/EtOAc) yielded the desired mono-protected MOM ether as a crystalline solid (530 mg, 71% yield), mp 75-76 ^{o}C. IR (thin-film, cm^{-1}) 3401, 2934, 2873, 1592, 1558, 1473, 1392, 1208, 1148, 1109, 1047, 918, 824, 743; ^{1}H NMR ($CDCl_3$) δ 7.36 (d, *J* = 8.0 Hz, 1H), 7.34 (d, *J* = 2.0 Hz, 1H), 7.08 (dd, *J* = 2.0, 8.0 Hz, 1H), 4.61 (s, 2H), 3.36 (s, 3H), 3.29 (s, 2H), 2.77 (s, 2H), 1.72 (br d, *J* = 10.5 Hz, 4H), 1.42-1.35 (m, 3H), 1.28 (s, 1H), 1.26-1.21 (m, 2H), 0.92 (s, 6H); ^{13}C NMR ($CDCl_3$) δ 138.0, 132.5, 132.2, 130.7, 130.2, 130.1, 96.9, 75.8, 72.2, 55.4, 43.0, 41.7, 38.6, 36.3, 24.3, 22.7; HRMS (ESI) for $C_{19}H_{28}O_3Cl_2$ [M + Na] calcd, 397.13077, found, 397.13062 (error = -0.3818 ppm).

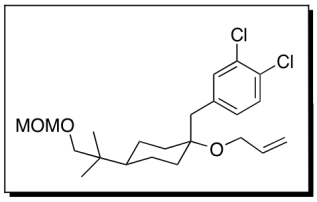

4-(((*trans*)-1-(Allyloxy)-4-(1-(methoxymethoxy)-2-methylpropan-2-yl)cyclohexyl)methyl)-1,2-dichlorobenzene (*trans*-1.36). The allyl ether was synthesized in accordance to General Procedure B. Flash column chromatography on silica using hexanes/EtOAc (9:1) yielded the allyl ether as a clear colorless oil (280 mg, 96% yield), clear colorless oil. IR (thin-film, cm^{-1}) 3368, 3078, 2939, 2872, 2769, 1646, 1591, 1558, 1473, 1392, 1365, 1319, 1207, 1148, 1109, 1048, 919, 822, 749; ^{1}H NMR ($CDCl_3$) δ 7.33-7.31 (m, 2H), 7.06 (dd, *J* = 2.0, 8.0 Hz, 1H), 5.95-5.87 (m, 1H), 5.27 (app dq, *J* = 2.0, 17.0 Hz, 1H), 5.14 (app dq, *J* = 2.0, 9.0 Hz, 1H), 4.61 (s, 2H), 3.99 (app dt, *J* = 1.5 Hz, 5.0 Hz, 2H), 3.36 (s, 3H), 3.28 (s, 2H), 2.81 (s, 2H), 1.69 (app br t, *J* = 15.0 Hz, 4H), 1.51 (app td, *J* = 4.0, 13.0 Hz, 2 H), 1.37 (app tt, *J* = 3.0, 12.0 Hz, 1H), 1.22 (app qd, *J* = 3.0, 13.0 Hz, 2H), 0.91 (s, 6H); ^{13}C NMR ($CDCl_3$) δ 138.4, 135.7, 132.6, 131.8, 130.1, 129.8, 116.0, 96.9, 76.9, 75.8, 61.8, 55.4, 43.1, 37.5, 36.3, 34.4, 24.1, 22.6; HRMS (ESI) for $C_{22}H_{32}O_3Cl_2$ [M + Na] calcd, 437.1621, found, 437.1631 (error = 2.35 ppm).

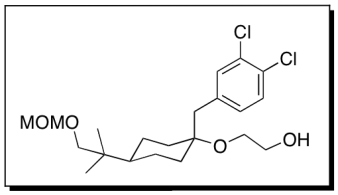

2-((*trans*)-1-(3,4-Dichlorobenzyl)-4-(1-(methoxymethoxy)-2-methylpropan-2-yl)cyclohexyloxy)-ethanol (*trans*-1.37). Allyl ether **1.36** (277 mg, 0.67 mmol) was dissolved in a 9:1 acetone/water mixture (15 mL) and OsO_4 (2.5% in *t*-BuOH, 136 mL, 0.013 mmol) and *N*-methylmorpholine-*N*-oxide (136 mg,

1.16 mmol) were added to the reaction mixture. Stirring (in dark) was continued overnight at room temperature. A solution of $NaIO_4$ (287 mg, 1.34 mmol) in water (3.5 mL) was added to the dark reaction mixture and stirring was continued for 4 h prior to vacuum filtration and evaporation of solvent under reduced pressure. The residue was taken up in EtOAc and was washed with a 10% solution of sodium thiosulfate followed by washing with water and brine. The organic layer was dried, filtered and evaporated to yield crude aldehyde.

The crude aldehyde was taken up in MeOH (anhydrous, 10 mL) and was cooled in an ice bath. Sodium borohydride (114 mg, 2.0 mmol) was added in portions and the reaction was stirred for 30 min. A few drops of acetic acid were added to quench the reaction and the solvent was removed under reduced pressure. The residue was taken up in EtOAc and washed with water (3x) and brine. The organic layer was dried ($MgSO_4$), filtered and evaporated to give crude alcohol. Purification by flash column chromatography with hexanes/EtOAc (2:1) yielded the desired primary alcohol (253 mg, 90% yield), clear colorless oil. IR (thin-film, cm^{-1}) 3435, 2939, 2872, 1591, 1559, 1473, 1393, 1365, 1208, 1148, 1107, 1048, 984, 918, 891, 820, 734; ^1H NMR ($CDCl_3$) δ 7.32 (d, *J* = 8.5 Hz, 1H), 7.33 (d, *J* = 2.0 Hz, 1H), 7.07 (dd, *J* = 2.0, 8.5 Hz, 1H), 4.60 (s, 2H), 3.77 (app q, *J* = 4.5 Hz, 2H), 3.53 (t, *J* = 4.5 Hz, 2H), 3.35 (s, 3 H), 3.28 (s, 2H), 2.81 (s, 2H), 1.98 (t, *J* = 6.0 Hz, 2H), 1.72 (app br d, *J* = 11.0 Hz, 2H), 1.64 (app br d, *J* = 12.5

Hz, 2H), 1.49 (app td, *J* = 4.0, 13.0 Hz, 2H), 1.36 (app tt, *J* = 3.0, 12.0 Hz, 1H), 1.23 (app qd, *J* = 3.0, 13.0, 2H), 0.91 (s, 6H); ^{13}C NMR ($CDCl_3$) δ 138.3, 132.4, 131.9, 130.3, 130.0, 129.9, 96.8, 75.7, 62.4, 61.3, 55.3, 43.0, 37.9, 36.2, 34.1, 24.0, 22.5; HRMS (ESI) for $C_{21}H_{32}O_4Cl_2$ [M + Na] calcd, 441.1570, found, 441.1577 (error = 1.62 ppm).

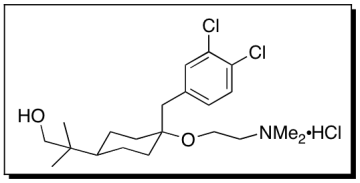

2-((*trans*)-4-(3,4-Dichlorobenzyl)-4-(2-(dimethyl-amino)ethoxy)cyclohexyl)-2-methylpropan-1-ol, hydrochloride salt (*trans*-1.38). Protected primary alcohol **1.37** (230 mg, 0.55 mmol) was dissolved in DCM (anhydrous, 20 mL) and stirred under dry nitrogen. Triethylamine (100 mL, 0.72 mmol) and methanesulfonyl chloride (51 mL, 0.66 mmol) were then added and the resulting mixture was allowed to stir at room temperature for 2 h. The reaction was then diluted with DCM (20 mL) and washed with water and brine. The combined organic layer was dried with $MgSO_4$, filtered and evaporated to give the mesylate, which was taken on without purification. The crude mesylate was dissolved in THF (20 mL) and aq. dimethylamine (40 wt. %, 1.4 mL, 11.0 mmol) and refluxed for 20 h. The reaction was allowed to cool and the solvent was evaporated at reduced pressure. The residue was taken up in EtOAc, which was washed with water (3x), dried with $MgSO_4$, filtered and evaporated. The crude amine was taken up in MeOH/water (85/15, 25 mL) and con. HCl was added (1.2 mL) with stirring and was continued for 24 h. Evaporation of

the solvent left a thick yellow oil which was then taken up in EtOAc/THF and dried with Na_2SO_4. Vacuum filtration and evaporation of solvent left the crude material as a yellow oil. This oil was purified by flash pipette column (9:1 $CHCl_3$/MeOH, then 90:9:1 $CHCl_3$/MeOH/triethylamine) and phosphomolybdic acid stain was used to visualize the pure amine fractions by TLC. The pure fractions were evaporated and formation of the hydrochloride salt was performed by taking the residue up in ether and bubbling HCl gas (H_2SO_4 added drop-wise to NH_4Cl) through the solution. Evaporation of the ether and recrystallization from minimal MeOH/$CHCl_3$ gave the pure hydrochloride salt **1.38** (174 mg, 72% yield over four steps); mp 199-200 ^oC. IR (thin-film, cm^{-1}) 3348, 2935, 2862, 2594, 2478, 1469, 1393, 1093; ^1H NMR (CD_3OD) δ 7.43 (d, *J* = 8.0 Hz, 1H), 7.41 (d, *J* = 2.0 Hz, 1H), 7.20 (dd, *J* = 2.0, 8.0 Hz, 1H), 3.80 (t, *J* = 5.0 Hz, 2H), 3.33 (s, 2H), 3.32 (t, *J* = 5.0 Hz, 2H, overlap with solvent peak), 2.92 (s, 2H), 2.89 (s, 6H), 1.76-1.69 (m, 4H), 1.61-1.50 (m, 2H), 1.40-1.29 (m, 4H), 0.87 (s, 6H); ^{13}C NMR (CD_3OD) δ 140.2, 133.6, 132.7, 131.8, 131.2, 79.7, 70.8, 59.0, 56.0, 44.0, 43.9, 38.8, 38.0, 35.0, 25.1, 22.6; HRMS (ESI) for $C_{21}H_{34}NO_2Cl_2$ [M + H] calcd, 402.19611, found, 402.19717 (error = 2.6317 ppm).

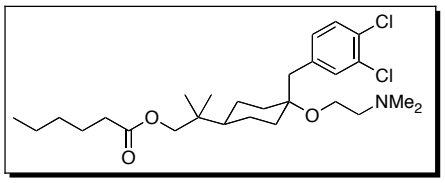

2-((*trans*)-4-(3,4-Dichlorobenzyl)-4-(2-(dimethylamino)ethoxy)cyclohexyl)-2-methylpropyl hexanoate (1.40). 4-DMAP (5.0 mg, 0.04 mmol) was added to a solution of hexanoic acid (10.05 μL, 0.09 mmol) and DMF (anhydrous, 0.7 mL). The solution was cooled with an ice bath and EDCI-HCl (15.4 mg, 0.08 mmol) was added and stirred for 45 min. Alcohol **27** (11.7 mg, 0.027 mmol) was dissolved in DMF (anhydrous, 1.5 mL) and added to the cooled reaction mixture. Stirring was continued for 16 h while allowing the reaction to warm to room temperature. The mixture was diluted to 5 mL with CH_3CN (0.1 % formic acid) and purified by preparative HPLC (reverse phase, C18 column, CH_3CN/water with 0.1% formic acid) (2.4 mg, 19.5 % yield), soapy film. IR (thin-film, cm^{-1}) 3368, 2938, 2871, 2818, 2768, 1735, 1648, 1589, 1471, 1393, 1377, 1167, 1097; ^1H NMR ($CDCl_3$) δ 7.38 (d, *J* = 2.0 Hz, 1H), 7.33 (d, *J* = 8.0 Hz, 1H), 7.07 (dd, *J* = 2.0, 8.0 Hz, 1H), 3.87 (s, 2H), 3.55 (t, *J* = 6.0 Hz, 2H), 2.79 (s, 2H), 2.50 (t, *J* = 6.0 Hz, 2H), 2.33 (t, *J* = 7.5 Hz, 2H), 2.29 (s, 6H), 1.70-1.61 (m, 5H), 1.48 (app td, *J* = 4.0, 13.0 Hz, 2H), 1.36-1.17 (m, 8H), 0.92 (s, 6H), 0.90 (t, *J* = 7.0 Hz, 3H); ^{13}C NMR ($CDCl_3$) δ 174.2, 138.4, 132.6, 131.9, 130.2, 130.0, 129.8, 71.3, 59.8, 58.5, 45.8, 43.6, 37.8, 35.9, 34.6, 34.1, 31.5, 25.0, 24.1, 22.5, 14.1; HRMS (ESI) for $C_{27}H_{44}NO_3Cl_2$ [M + H] calcd, 500.26928, found, 500.27137 (error = 4.1846 ppm).

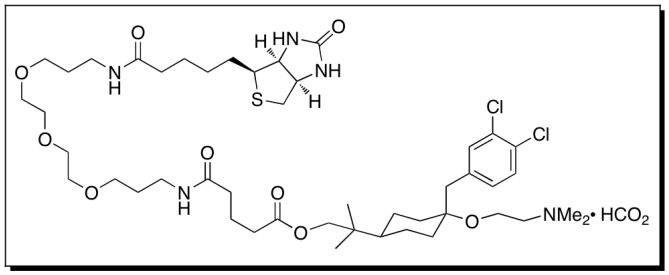

Biotinylated probe 1.41. To a solution of the commercially available biotin linker, O-(*N*-Biotinyl-3-aminopropyl)-O'-(*N*-diglycolyl-3-aminopropyl)-diethyleneglycol diisopropylethylamine salt (77.1 mg, 0.11 mmol), in DMF (anhydrous, 1 mL) was added 4-DMAP (7 mg, 0.55 mmol) and EDCI-HCl (21 mg, 0.11 mmol) at 0 ^{o}C. The reaction mixture was purged with dry nitrogen and stirred for 30 min. Alcohol **1.38** (51.8 mg, 0.11 mmol) was dissolved in DMF (anhydrous, 1 mL) and sonicated to suspend the alcohol. This slurry was added drop-wise to the reaction mixture with vigorous stirring and was allowed to warm to room temperature overnight. The reaction mixture was diluted to 5 mL with CH_3CN (0.1 % formic acid) and purified by preparative HPLC (reverse phase, C18 column, CH_3CN/water with 0.1% formic acid) (32.6 mg, 32 % yield). IR (thin-film, cm^{-1}) 3284, 3081, 2937, 2868, 1726, 1697, 1646, 1551, 1470, 1370, 1261, 1099, 923, 732; ^{1}H NMR ($CDCl_3$) δ 8.51 (s, 1H), 7.31 (d, *J* = 2.0 Hz, 1H), 7.31 (d, *J* = 8.5 Hz, 1H), 7.03 (dd, *J* = 2.0, 8.5 Hz, 1H), 6.70 (t, *J* = 5.0 Hz, 1H), 6.57 (t, *J* = 5.0 Hz, 1H), 6.28 (s, 1H), 5.59 (s, 1H), 4.48 (1H), 4.29 (1H), 3.84 (s, 2H), 3.63-3.56 (m, 8H), 3.53 (app q, *J* = 6.0 Hz, 4H), 3.31 (app q, *J* = 5.5 Hz, 4H), 3.14-3.11 (m, 1H), 2.88 (dd, *J* = 5.0, 13.0 Hz, 1H), 2.77 (s, 2H), 2.74-2.70 (m, 3H), 2.42 (s, 6H), 2.39 (t, *J* = 8.0 Hz, 2H), 2.21 (t, *J* = 7.5 Hz, 2H), 2.17 (t, *J* = 7.5 Hz, 2H), 1.94 (p, *J* = 7.0, 8.0 Hz, 2 H), 1.75 (p, *J* =

7.0, 6.0 Hz, 2H), 1.72-1.61 (m, 10H), 1.52-1.39 (m, 4H), 1.30-1.16 (m, 4H), 0.89 (s, 6H); ^{13}C NMR ($CDCl_3$) δ 173.6, 173.3, 172.4, 168.6, 163.9, 138.3, 132.5, 131.8, 130.2, 130.0, 129.9, 71.4, 70.6, 70.1, 69.9, 61.9, 60.3, 58.7, 57.8, 55.8, 45.1, 43.3, 40.7, 38.0, 37.9, 37.7, 36.1, 35.9, 35.6, 33.8, 33.75, 29.2, 29.1, 28.3, 28.2, 25.8, 24.0, 22.4, 21.2; HRMS (ESI) for $C_{46}H_{75}O_9N_5Cl_2S$ [M + H] calcd, 944.4735, found, 944.4732 (error = -0.35 ppm).

Yeast Studies. *Growth Assays.* Wild type cells (strain BY4741[57]) were grown in YPD media at 30 ºC. Cells were counted with a hemocytometer and cultures were diluted to 8 x 10^5 cells/mL. The desired concentration of tamoxifen, tamoxilog and related compounds (5μM) or DMSO was added and cultures were incubated at 30 ºC with rotation. Optical density at 600 nm was recorded every 1.5-2h, starting at the time of dilution.

LC_{50} Values. Strain BY4741 (195μL) was plated into a 96 well plate at an OD_{600} of 0.1. Desired compound (5μL) was added to each well and two-fold serial dilutions of each compound were tested. OD_{600} readings were taken every 30 min with an EnVision plate (PerkinElmer). After 16 h of incubation the OD_{600} was plotted against concentration in Prism (GraphPad) to generate a dose response curve and calculate the LC_{50}.

1.12 Crystal Structure Data

Acknowledgement

The single crystal X-ray diffraction data in this work were recorded on an instrument supported by the National Science Foundation, Major Research

Instrumentation (MRI) Program under Grant No. CHE-0521569.

Table 1.2 Crystal data and structure refinement for *cis*-**1.11**.

Identification code	***cis*-1.11**	
Empirical formula	C19 H30 O2	
Formula weight	290.43	
Temperature	150(2) K	
Wavelength	0.71073 Å	
Crystal system	Monoclinic	
Space group	p2(1)/c	
Unit cell dimensions	a = 12.194(2) Å	α = 90°
	b = 19.725(4) Å	β = 98.53(3)°
	c = 7.1971(14) Å	γ = 90°
Volume	1712.0(6) $Å^3$	
Z	4	
Density (calculated)	1.127 $g.cm^{-3}$	
Absorption coefficient (μ)	0.071 mm^{-1}	
F(000)	640	
Crystal size	20 × 20 × 10 mm^3	
ω range for data collection	1.98 to 25.35°	
Index ranges	$-14 \le h \le 14$, $-23 \le k \le 23$, $-8 \le l \le 8$	
Reflections collected	15493	
Independent reflections	3134 [R_{int} = 0.0756]	
Completeness to θ = 25.35°	100.0 %	
Absorption correction	Empirical	

Max. and min. transmission	0.7457 and 0.6695
Refinement method	Full-matrix least-squares on F^2
Data / restraints / parameters	3134 / 0 / 195
Goodness-of-fit on F^2	1.014
Final R indices [I>2σ(I)]	$R_1 = 0.0473$, $wR_2 = 0.0985$
R indices (all data)	$R_1 = 0.0957$, $wR_2 = 0.1202$
Largest diff. peak and hole	0.171 and -0.224 $e^{-}.Å^{-3}$

Table 1.3 Atomic coordinates and equivalent isotropic displacement parameters ($Å^2$) for *cis*-**1.11**. U(eq) is defined as one third of the trace of the orthogonalized U_{ij} tensor.

	x	y	z	U(eq)
O(1)	0.62837(11)	0.05866(6)	0.86697(18)	0.027(1)
C(8)	0.66259(16)	0.12421(10)	0.8028(3)	0.026(1)
O(2)	0.46025(12)	-0.04941(8)	0.7888(2)	0.039(1)
C(14)	0.97612(17)	0.12728(10)	1.2185(3)	0.030(1)
C(9)	0.67260(16)	0.16907(10)	0.9767(3)	0.026(1)
C(10)	0.76521(16)	0.14731(10)	1.1311(3)	0.027(1)
C(13)	0.77591(16)	0.11999(11)	0.7378(3)	0.030(1)
C(2)	0.46115(17)	0.16390(11)	0.6883(3)	0.029(1)
C(1)	0.57649(17)	0.15186(11)	0.6428(3)	0.030(1)
C(11)	0.87808(16)	0.14419(10)	1.0625(3)	0.027(1)
C(12)	0.86836(17)	0.09738(11)	0.8907(3)	0.031(1)
C(3)	0.38254(18)	0.11223(11)	0.6707(3)	0.034(1)
C(7)	0.42982(18)	0.22725(11)	0.7458(3)	0.035(1)

C(18)	0.63352(18)	0.00201(10)	0.7439(3)	0.031(1)
C(19)	0.57728(18)	-0.05767(11)	0.8171(3)	0.034(1)
C(4)	0.27599(19)	0.12423(13)	0.7069(3)	0.042(1)
C(6)	0.32394(19)	0.23934(13)	0.7834(3)	0.040(1)
C(15)	0.98494(18)	0.18172(12)	1.3714(3)	0.042(1)
C(17)	1.08612(17)	0.12832(12)	1.1384(3)	0.041(1)
C(16)	0.96356(19)	0.05830(11)	1.3080(3)	0.043(1)
C(5)	0.2471(2)	0.18816(14)	0.7635(3)	0.044(1)
H(2)	0.4384(7)	-0.0479(13)	0.889(3)	0.059
H(9A)	0.6028	0.1683	1.0261	0.031
H(9B)	0.6860	0.2154	0.9408	0.031
H(10A)	0.7478	0.1030	1.1773	0.033
H(10B)	0.7693	0.1791	1.2348	0.033
H(13A)	0.7714	0.0885	0.6335	0.036
H(13B)	0.7945	0.1642	0.6922	0.036
H(1A)	0.6042	0.1944	0.6003	0.036
H(1B)	0.5712	0.1203	0.5385	0.036
H(11)	0.8923	0.1898	1.0174	0.032
H(12A)	0.9381	0.0973	0.8411	0.037
H(12B)	0.8538	0.0515	0.9287	0.037
H(3)	0.4019	0.0692	0.6342	0.041
H(7)	0.4814	0.2623	0.7592	0.042
H(18A)	0.7103	-0.0090	0.7366	0.037
H(18B)	0.5972	0.0134	0.6186	0.037
H(19A)	0.5962	-0.0984	0.7535	0.041
H(19B)	0.6036	-0.0630	0.9503	0.041

H(4)	0.2238	0.0895	0.6934	0.050
H(6)	0.3047	0.2821	0.8222	0.048
H(15A)	1.0524	0.1754	1.4571	0.064
H(15B)	0.9227	0.1782	1.4384	0.064
H(15C)	0.9853	0.2258	1.3147	0.064
H(17A)	1.1466	0.1217	1.2384	0.062
H(17B)	1.0944	0.1713	1.0792	0.062
H(17C)	1.0861	0.0927	1.0476	0.062
H(16A)	0.9596	0.0237	1.2135	0.065
H(16B)	0.8969	0.0577	1.3642	0.065
H(16C)	1.0263	0.0500	1.4028	0.065
H(5)	0.1755	0.1963	0.7880	0.053

Table 1.4 Anisotropic displacement parameters $(Å)^2$ for *cis*-**1.11**. The anisotropic displacement factor exponent takes the form:
$-2\pi^2[h^2 a^{*2} U_{11} + ... + 2 h k a^* b^* U_{12}]$

	U_{11}	U_{22}	U_{33}	U_{23}	U_{13}	U_{12}
O(1)	0.0330(8)	0.0237(8)	0.0243(7)	-0.0030(6)	0.0069(6)	-0.0012(6)
C(8)	0.0281(12)	0.0232(11)	0.0265(11)	0.0015(9)	0.0073(9)	-0.0016(9)
O(2)	0.0423(10)	0.0450(10)	0.0315(9)	-0.0031(8)	0.0101(7)	-0.0118(8)
C(14)	0.0259(12)	0.0285(12)	0.0358(13)	0.0006(10)	0.0044(10)	0.0012(9)
C(9)	0.0265(11)	0.0255(11)	0.0262(11)	-0.0016(9)	0.0071(9)	-0.0001(9)
C(10)	0.0282(12)	0.0266(11)	0.0270(11)	-0.0037(9)	0.0054(9)	-0.0004(9)
C(13)	0.0329(13)	0.0320(13)	0.0263(12)	-0.0012(10)	0.0100(10)	-0.0015(10)
C(2)	0.0325(12)	0.0352(13)	0.0172(11)	0.0017(9)	-0.0001(9)	0.0050(10)

C(1)	0.0365(13)	0.0286(12)	0.0246(11)	0.0018(9)	0.0041(10)	0.0009(10)
C(11)	0.0265(12)	0.0222(11)	0.0329(12)	-0.0004(9)	0.0080(10)	-0.0021(9)
C(12)	0.0281(12)	0.0322(12)	0.0347(13)	-0.0029(10)	0.0109(10)	0.0015(10)
C(3)	0.0372(14)	0.0362(13)	0.0269(12)	0.0018(10)	-0.0007(10)	0.0017(11)
C(7)	0.0359(14)	0.0375(14)	0.0291(12)	-0.0009(10)	-0.0036(10)	0.0040(11)
C(18)	0.0340(13)	0.0297(12)	0.0292(12)	-0.0065(10)	0.0071(10)	0.0002(10)
C(19)	0.0454(15)	0.0273(12)	0.0304(12)	-0.0019(10)	0.0055(11)	-0.0026(11)
C(4)	0.0355(14)	0.0533(16)	0.0350(14)	0.0055(12)	0.0008(11)	-0.0063(12)
C(6)	0.0422(15)	0.0460(15)	0.0301(13)	-0.0039(11)	-0.0014(11)	0.0148(12)
C(15)	0.0342(13)	0.0488(16)	0.0418(14)	-0.0065(12)	-0.0020(11)	0.0001(11)
C(17)	0.0279(13)	0.0479(15)	0.0489(15)	0.0000(12)	0.0061(11)	-0.0005(11)
C(16)	0.0412(14)	0.0419(15)	0.0464(15)	0.0111(12)	0.0034(12)	0.0056(12)
C(5)	0.0331(14)	0.0709(19)	0.0267(13)	0.0052(12)	0.0015(11)	0.0150(13)

Table 1.5 Bond lengths [Å] for *cis*-**1.11**.

atom-atom	distance	atom-atom	distance
O(1)-C(18)	1.433(2)	O(1)-C(8)	1.455(2)
C(8)-C(9)	1.523(3)	C(8)-C(13)	1.525(3)
C(8)-C(1)	1.538(3)	O(2)-C(19)	1.421(3)
C(14)-C(16)	1.523(3)	C(14)-C(15)	1.530(3)
C(14)-C(17)	1.537(3)	C(14)-C(11)	1.550(3)
C(9)-C(10)	1.524(3)	C(10)-C(11)	1.531(3)
C(13)-C(12)	1.521(3)	C(2)-C(7)	1.388(3)
C(2)-C(3)	1.392(3)	C(2)-C(1)	1.509(3)
C(11)-C(12)	1.533(3)	C(3)-C(4)	1.383(3)

C(7)-C(6)	1.379(3)	C(18)-C(19)	1.497(3)
C(4)-C(5)	1.387(3)	C(6)-C(5)	1.371(3)

Table 1.6 Bond angles [°] for *cis*-**1.11**.

atom-atom-atom	angle	atom-atom-atom	angle
C(18)-O(1)-C(8)	117.10(14)	O(1)-C(8)-C(9)	104.30(15)
O(1)-C(8)-C(13)	111.37(16)	C(9)-C(8)-C(13)	108.54(17)
O(1)-C(8)-C(1)	110.90(16)	C(9)-C(8)-C(1)	111.83(16)
C(13)-C(8)-C(1)	109.80(16)	C(16)-C(14)-C(15)	108.87(19)
C(16)-C(14)-C(17)	108.59(17)	C(15)-C(14)-C(17)	106.75(18)
C(16)-C(14)-C(11)	112.55(18)	C(15)-C(14)-C(11)	109.54(17)
C(17)-C(14)-C(11)	110.36(17)	C(8)-C(9)-C(10)	113.33(16)
C(9)-C(10)-C(11)	112.39(16)	C(12)-C(13)-C(8)	113.71(16)
C(7)-C(2)-C(3)	118.0(2)	C(7)-C(2)-C(1)	120.9(2)
C(3)-C(2)-C(1)	121.07(19)	C(2)-C(1)-C(8)	116.60(16)
C(10)-C(11)-C(12)	108.58(17)	C(10)-C(11)-C(14)	114.13(16)
C(12)-C(11)-C(14)	114.42(17)	C(13)-C(12)-C(11)	111.54(17)
C(4)-C(3)-C(2)	120.7(2)	C(6)-C(7)-C(2)	121.4(2)
O(1)-C(18)-C(19)	109.32(16)	O(2)-C(19)-C(18)	111.24(18)
C(3)-C(4)-C(5)	119.9(2)	C(5)-C(6)-C(7) 1	19.9(2)
C(6)-C(5)-C(4)	120.0(2)		

Table 1.7 Torsion angles [°] for *cis*-**1.11**.

atom-atom-atom-atom	angle	atom-atom-atom-atom	angle
C(18)-O(1)-C(8)-C(9)	-167.77(16)	C(18)-O(1)-C(8)-C(13)	-50.9(2)
C(18)-O(1)-C(8)-C(1)	71.7(2)	O(1)-C(8)-C(9)-C(10)	65.9(2)
C(13)-C(8)-C(9)-C(10)	-52.9(2)	C(1)-C(8)-C(9)-C(10)	-174.19(16)
C(8)-C(9)-C(10)-C(11)	56.1(2)	O(1)-C(8)-C(13)-C(12)	-60.5(2)
C(9)-C(8)-C(13)-C(12)	53.8(2)	C(1)-C(8)-C(13)-C(12)	176.31(16)
C(7)-C(2)-C(1)-C(8)	94.0(2)	C(3)-C(2)-C(1)-C(8)	-87.1(2)
O(1)-C(8)-C(1)-C(2)	60.7(2)	C(9)-C(8)-C(1)-C(2)	-55.3(2)
C(13)-C(8)-C(1)-C(2)	-175.83(18)	C(9)-C(10)-C(11)-C(12)	-55.2(2)
C(9)-C(10)-C(11)-C(14)	175.82(16)	C(16)-C(14)-C(11)-C(10)	61.0(2)
C(15)-C(14)-C(11)-C(10)	-60.3(2)	C(17)-C(14)-C(11)-C(10)	-177.54(17)
C(16)-C(14)-C(11)-C(12)	-65.0(2)	C(15)-C(14)-C(11)-C(12)	173.78(17)
C(17)-C(14)-C(11)-C(12)	56.5(2)	C(8)-C(13)-C(12)-C(11)	-57.1(2)
C(10)-C(11)-C(12)-C(13)	55.4(2)	C(14)-C(11)-C(12)-C(13)	-175.84(16)
C(7)-C(2)-C(3)-C(4)	0.9(3)	C(1)-C(2)-C(3)-C(4)	-177.93(19)
C(3)-C(2)-C(7)-C(6)	-0.5(3)	C(1)-C(2)-C(7)-C(6)	178.41(19)
C(8)-O(1)-C(18)-C(19)	-170.23(16)	O(1)-C(18)-C(19)-O(2)	73.1(2)
C(2)-C(3)-C(4)-C(5)	-0.7(3)	C(2)-C(7)-C(6)-C(5)	-0.2(3)
C(7)-C(6)-C(5)-C(4)	0.5(3)	C(3)-C(4)-C(5)-C(6)	0.0(3)

Table 1.8 Hydrogen bonds for *cis*-**1.11** [Å and °].

D-H...A	d(D-H)	d(H...A)	d(D...A)	<(DHA)
O(2)-H(2)...O(1)#1	0.81	2.05	2.852(2)	170.9

Symmetry transformations used to generate equivalent atoms:
#1 -x+1,-y,-z+2

Table 1.9 Crystal data and structure refinement for *cis*-**1.9**.

Identification code	*cis*-**1.9**	
Empirical formula	C17 H22.50 Cl2 O	
Formula weight	313.75	
Temperature	150(2) K	
Wavelength	0.71073 Å	
Crystal system	Monoclinic	
Space group	P2(1)/c	
Unit cell dimensions	a = 11.895(12) Å	α = 90°
	b = 12.704(14) Å	β = 102.245(15)°
	c = 22.58(2) Å	γ = 90°
Volume	3335(6) $Å^3$	
Z	8	
Density (calculated)	1.250 $g.cm^{-3}$	
Absorption coefficient (μ)	0.383 mm^{-1}	
F(000)	1332	
Crystal size	0.200 × 0.100 × 0.050 mm^3	
ω range for data collection	2.26 to 28.29°	
Index ranges	$-15 \leq h \leq 15$, $-16 \leq k \leq 16$, $-30 \leq l \leq 29$	
Reflections collected	37006	
Independent reflections	8260 [R_{int} = 0.0287]	

Completeness to θ = 28.29°	99.8 %
Absorption correction	Empirical
Max. and min. transmission	0.7457 and 0.6856
Refinement method	Full-matrix least-squares on F^2
Data / restraints / parameters	8260 / 0 / 367
Goodness-of-fit on F^2	1.044
Final R indices [I>2σ(I)]	R_1 = 0.0402, wR_2 = 0.1109
R indices (all data)	R_1 = 0.0496, wR_2 = 0.1188
Largest diff. peak and hole	0.868 and -0.624 $e^-.Å^{-3}$

Table 1.10 Atomic coordinates and equivalent isotropic displacement parameters ($Å^2$) for *cis*-**1.9**. U(eq) is defined as one third of the trace of the orthogonalized U_{ij} tensor.

	x	y	z	U(eq)
Cl(1)	0.11211(4)	0.21841(3)	0.09882(2)	0.035(1)
Cl(2)	-0.02217(4)	0.07348(4)	-0.12636(2)	0.043(1)
Cl(3)	-0.04678(4)	0.04051(5)	0.26031(2)	0.051(1)
Cl(4)	0.25873(4)	0.34828(4)	0.25731(2)	0.042(1)
O(1)	0.47278(9)	0.08017(8)	0.06827(5)	0.023(1)
O(2)	0.51361(10)	0.36404(8)	0.45156(5)	0.025(1)
C(2)	0.22344(13)	0.05492(11)	0.05662(7)	0.022(1)
C(29)	0.57539(13)	0.14076(11)	0.47157(7)	0.022(1)
C(26)	0.49598(13)	0.26218(12)	0.36068(7)	0.024(1)
C(31)	0.74724(13)	0.06755(12)	0.42988(7)	0.024(1)
C(3)	0.22916(13)	-0.01697(12)	0.01057(7)	0.026(1)
C(6)	0.05969(13)	0.13503(13)	-0.01180(8)	0.028(1)
C(25)	0.44444(13)	0.28307(11)	0.41603(7)	0.021(1)

C(28)	0.62493(12)	0.11708(11)	0.41579(6)	0.020(1)
C(1)	0.30958(13)	0.04827(12)	0.11626(7)	0.023(1)
C(13)	0.50718(14)	0.08675(12)	0.17838(7)	0.025(1)
C(27)	0.61785(13)	0.21729(11)	0.37743(7)	0.024(1)
C(30)	0.45257(12)	0.18279(11)	0.45392(7)	0.021(1)
C(7)	0.13526(13)	0.12906(12)	0.04399(7)	0.024(1)
C(11)	0.59797(13)	0.26791(12)	0.18038(7)	0.024(1)
C(19)	0.23016(13)	0.25730(12)	0.36275(7)	0.024(1)
C(18)	0.32128(13)	0.32737(12)	0.39909(7)	0.026(1)
C(5)	0.07079(14)	0.06384(14)	-0.05621(7)	0.029(1)
C(8)	0.42249(12)	0.11017(11)	0.11854(6)	0.020(1)
C(14)	0.70908(14)	0.33606(14)	0.19063(7)	0.030(1)
C(4)	0.15405(14)	-0.01374(13)	-0.04546(7)	0.029(1)
C(20)	0.17157(13)	0.18613(13)	0.39237(7)	0.026(1)
C(33)	0.75388(15)	-0.02224(13)	0.47567(8)	0.032(1)
C(12)	0.61931(13)	0.14844(12)	0.18522(7)	0.027(1)
C(21)	0.08676(14)	0.11970(14)	0.36195(8)	0.030(1)
C(23)	0.11038(15)	0.19510(15)	0.26765(8)	0.034(1)
C(24)	0.19586(14)	0.25978(13)	0.29968(7)	0.028(1)
C(9)	0.40275(13)	0.22831(11)	0.11334(7)	0.022(1)
C(10)	0.51504(13)	0.28983(12)	0.11992(7)	0.024(1)
C(32)	0.77198(16)	0.02052(15)	0.37143(9)	0.037(1)
C(22)	0.05731(14)	0.12496(15)	0.29962(8)	0.033(1)
C(34)	0.84078(15)	0.14803(14)	0.45527(9)	0.036(1)
C(15)	0.78052(18)	0.31898(18)	0.25455(8)	0.047(1)
C(16)	0.78483(17)	0.3097(2)	0.14587(9)	0.049(1)

C(17)	0.6760(2)	0.45287(16)	0.18422(12)	0.052(1)
H(29A)	0.5760	0.0770	0.4952	0.026
H(29B)	0.6236	0.1923	0.4967	0.026
H(26A)	0.4975	0.3275	0.3386	0.029
H(26B)	0.4470	0.2131	0.3341	0.029
H(3A)	0.2855	-0.0689	0.0178	0.031
H(6A)	0.0025	0.1862	-0.0191	0.033
H(28A)	0.5736	0.0654	0.3916	0.024
H(1A)	0.3286	-0.0252	0.1249	0.028
H(1B)	0.2735	0.0744	0.1481	0.028
H(13A)	0.4711	0.1040	0.2119	0.030
H(13B)	0.5244	0.0120	0.1805	0.030
H(27A)	0.6688	0.2700	0.3998	0.028
H(27B)	0.6443	0.2017	0.3406	0.028
H(30A)	0.4036	0.1293	0.4311	0.025
H(30B)	0.4244	0.1971	0.4904	0.025
H(11A)	0.5575	0.2868	0.2124	0.029
H(18A)	0.3040	0.3946	0.4108	0.032
H(4A)	0.1596	-0.0629	-0.0753	0.034
H(20A)	0.1905	0.1833	0.4345	0.032
H(33A)	0.6920	-0.0708	0.4619	0.048
H(33B)	0.7478	0.0059	0.5143	0.048
H(33C)	0.8260	-0.0582	0.4795	0.048
H(12A)	0.6591	0.1265	0.1540	0.033
H(12B)	0.6685	0.1324	0.2242	0.033
H(21A)	0.0503	0.0724	0.3831	0.036

H(23A)	0.0893	0.1988	0.2256	0.041
H(9A)	0.3631	0.2509	0.1445	0.026
H(9B)	0.3537	0.2441	0.0743	0.026
H(10A)	0.4980	0.3645	0.1168	0.029
H(10B)	0.5519	0.2710	0.0870	0.029
H(32A)	0.7134	-0.0299	0.3552	0.055
H(32B)	0.8457	-0.0136	0.3801	0.055
H(32C)	0.7724	0.0756	0.3424	0.055
H(34A)	0.9132	0.1126	0.4679	0.054
H(34B)	0.8215	0.1833	0.4894	0.054
H(34C)	0.8464	0.1987	0.4245	0.054
H(15A)	0.8008	0.2459	0.2600	0.070
H(15B)	0.7364	0.3395	0.2837	0.070
H(15C)	0.8493	0.3607	0.2601	0.070
H(16A)	0.8103	0.2380	0.1515	0.073
H(16B)	0.8504	0.3557	0.1527	0.073
H(16C)	0.7414	0.3189	0.1052	0.073
H(17A)	0.7431	0.4953	0.1983	0.079
H(17B)	0.6198	0.4678	0.2079	0.079
H(17C)	0.6443	0.4686	0.1424	0.079

Table 1.11 Anisotropic displacement parameters $(Å)^2$ for *cis*-**1.9**. The anisotropic displacement factor exponent takes the form:
$-2\pi^2[h^2 a^{*2} U_{11} + ... + 2 h k a^* b^* U_{12}]$

	U_{11}	U_{22}	U_{33}	U_{23}	U_{13}	U_{12}
Cl(1)	0.0355(2)	0.0356(2)	0.0364(2)	-0.0050(2)	0.0116(2)	0.0056(2)
Cl(2)	0.0371(2)	0.0609(3)	0.0252(2)	0.0106(2)	-0.0062(2)	-0.0129(2)
Cl(3)	0.0363(2)	0.0683(3)	0.0480(3)	-0.0249(3)	0.0098(2)	-0.0148(2)
Cl(4)	0.0435(3)	0.0484(3)	0.0336(2)	0.0198(2)	0.0068(2)	0.0022(2)
O(1)	0.0263(5)	0.0230(5)	0.0213(5)	-0.0016(4)	0.0055(4)	-0.0002(4)
O(2)	0.0307(6)	0.0187(5)	0.0278(6)	-0.0051(4)	0.0079(4)	-0.0063(4)
C(2)	0.0214(7)	0.0218(7)	0.0227(7)	0.0035(6)	0.0036(5)	-0.0044(5)
C(29)	0.0242(7)	0.0217(7)	0.0197(7)	0.0018(5)	0.0063(5)	-0.0014(5)
C(26)	0.0308(8)	0.0208(7)	0.0205(7)	0.0019(6)	0.0071(6)	0.0014(6)
C(31)	0.0235(7)	0.0224(7)	0.0275(8)	0.0010(6)	0.0081(6)	-0.0002(6)
C(3)	0.0230(7)	0.0233(7)	0.0306(8)	0.0003(6)	0.0049(6)	-0.0028(6)
C(6)	0.0215(7)	0.0299(8)	0.0314(8)	0.0087(6)	0.0038(6)	0.0004(6)
C(25)	0.0250(7)	0.0178(6)	0.0214(7)	-0.0025(5)	0.0062(5)	-0.0015(5)
C(28)	0.0220(7)	0.0180(6)	0.0199(7)	-0.0009(5)	0.0062(5)	-0.0031(5)
C(1)	0.0256(7)	0.0218(7)	0.0213(7)	0.0037(6)	0.0022(6)	-0.0028(6)
C(13)	0.0291(8)	0.0219(7)	0.0218(7)	0.0038(6)	-0.0011(6)	-0.0020(6)
C(27)	0.0284(8)	0.0216(7)	0.0233(7)	0.0019(6)	0.0116(6)	-0.0003(6)
C(30)	0.0230(7)	0.0207(7)	0.0204(7)	-0.0004(5)	0.0076(5)	-0.0019(5)
C(7)	0.0248(7)	0.0242(7)	0.0250(7)	0.0020(6)	0.0068(6)	-0.0019(6)
C(11)	0.0279(7)	0.0252(7)	0.0186(7)	-0.0008(6)	0.0030(6)	-0.0058(6)
C(19)	0.0244(7)	0.0246(7)	0.0248(7)	0.0009(6)	0.0061(6)	0.0065(6)

C(18)	0.0274(8)	0.0209(7)	0.0311(8)	-0.0034(6)	0.0067(6)	0.0037(6)
C(5)	0.0238(7)	0.0384(9)	0.0218(7)	0.0075(6)	0.0007(6)	-0.0099(6)
C(8)	0.0225(7)	0.0192(6)	0.0182(7)	0.0008(5)	0.0025(5)	-0.0014(5)
C(14)	0.0306(8)	0.0341(8)	0.0234(8)	-0.0002(6)	0.0025(6)	-0.0113(7)
C(4)	0.0286(8)	0.0317(8)	0.0254(8)	-0.0035(6)	0.0058(6)	-0.0089(6)
C(20)	0.0251(7)	0.0320(8)	0.0235(7)	0.0007(6)	0.0073(6)	0.0045(6)
C(33)	0.0311(8)	0.0266(8)	0.0393(10)	0.0072(7)	0.0104(7)	0.0054(6)
C(12)	0.0268(8)	0.0262(7)	0.0247(8)	0.0022(6)	-0.0031(6)	-0.0023(6)
C(21)	0.0266(8)	0.0341(8)	0.0328(9)	-0.0020(7)	0.0120(7)	-0.0001(7)
C(23)	0.0291(8)	0.0485(10)	0.0234(8)	-0.0020(7)	0.0032(6)	0.0068(7)
C(24)	0.0275(8)	0.0327(8)	0.0253(8)	0.0068(6)	0.0071(6)	0.0070(6)
C(9)	0.0243(7)	0.0188(6)	0.0222(7)	0.0015(5)	0.0034(5)	0.0005(5)
C(10)	0.0275(7)	0.0195(7)	0.0239(7)	0.0030(6)	0.0016(6)	-0.0030(6)
C(32)	0.0384(9)	0.0386(9)	0.0366(10)	-0.0020(8)	0.0170(8)	0.0083(8)
C(22)	0.0238(8)	0.0399(9)	0.0338(9)	-0.0099(7)	0.0055(6)	0.0015(7)
C(34)	0.0251(8)	0.0330(9)	0.0481(11)	-0.0002(8)	0.0047(7)	-0.0048(7)
C(15)	0.0477(11)	0.0591(12)	0.0271(9)	0.0019(9)	-0.0045(8)	-0.0278(10)
C(16)	0.0356(10)	0.0757(15)	0.0357(10)	-0.0071(10)	0.0105(8)	-0.0201(10)
C(17)	0.0498(12)	0.0337(10)	0.0701(15)	0.0000(10)	0.0037(11)	-0.0193(9)

Table 1.12 Bond lengths [Å] for *cis*-**1.9**.

atom-atom	distance	atom-atom	distance
Cl(1)-C(7)	1.744(2)	Cl(2)-C(5)	1.733(2)
Cl(3)-C(22)	1.734(2)	Cl(4)-C(24)	1.744(2)
O(1)-C(8)	1.442(2)	O(2)-C(25)	1.449(2)

C(2)-C(7)	1.393(2)	C(2)-C(3)	1.396(2)
C(2)-C(1)	1.512(2)	C(29)-C(30)	1.527(2)
C(29)-C(28)	1.529(2)	C(26)-C(25)	1.528(2)
C(26)-C(27)	1.529(3)	C(31)-C(34)	1.530(2)
C(31)-C(33)	1.530(2)	C(31)-C(32)	1.533(3)
C(31)-C(28)	1.555(2)	C(3)-C(4)	1.386(3)
C(6)-C(5)	1.377(3)	C(6)-C(7)	1.386(2)
C(25)-C(30)	1.526(2)	C(25)-C(18)	1.540(2)
C(28)-C(27)	1.532(2)	C(1)-C(8)	1.548(2)
C(13)-C(12)	1.526(2)	C(13)-C(8)	1.534(2)
C(11)-C(10)	1.531(2)	C(11)-C(12)	1.539(3)
C(11)-C(14)	1.556(2)	C(19)-C(20)	1.396(2)
C(19)-C(24)	1.396(3)	C(19)-C(18)	1.504(2)
C(5)-C(4)	1.382(3)	C(8)-C(9)	1.520(2)
C(14)-C(16)	1.527(3)	C(14)-C(15)	1.527(3)
C(14)-C(17)	1.534(3)	C(20)-C(21)	1.381(3)
C(21)-C(22)	1.378(3)	C(23)-C(22)	1.381(3)
C(23)-C(24)	1.386(3)	C(9)-C(10)	1.527(2)

Table 1.13 Bond angles [°] for *cis*-**1.9**.

atom-atom-atom	angle	atom-atom-atom	angle
C(7)-C(2)-C(3)	116.31(15)	C(7)-C(2)-C(1)	123.96(14)
C(3)-C(2)-C(1)	119.73(14)	C(30)-C(29)-C(28)	111.61(13)
C(25)-C(26)-C(27)	112.73(13)	C(34)-C(31)-C(33)	108.40(15)
C(34)-C(31)-C(32)	109.02(15)	C(33)-C(31)-C(32)	107.42(15)

C(34)-C(31)-C(28)	112.38(14)	C(33)-C(31)-C(28)	110.60(13)
C(32)-C(31)-C(28)	108.89(14)	C(4)-C(3)-C(2)	122.45(16)
C(5)-C(6)-C(7)	118.82(16)	O(2)-C(25)-C(30)	108.74(14)
O(2)-C(25)-C(26)	107.28(13)	C(30)-C(25)-C(26)	108.96(13)
O(2)-C(25)-C(18)	106.07(13)	C(30)-C(25)-C(18)	112.84(12)
C(26)-C(25)-C(18)	112.70(13)	C(29)-C(28)-C(27)	108.52(13)
C(29)-C(28)-C(31)	114.73(13)	C(27)-C(28)-C(31)	112.88(12)
C(2)-C(1)-C(8)	114.88(13)	C(12)-C(13)-C(8)	112.71(13)
C(26)-C(27)-C(28)	112.67(12)	C(25)-C(30)-C(29)	112.43(12)
C(6)-C(7)-C(2)	122.54(15)	C(6)-C(7)-Cl(1)	116.11(13)
C(2)-C(7)-Cl(1)	121.33(13)	C(10)-C(11)-C(12)	107.95(12)
C(10)-C(11)-C(14)	113.45(13)	C(12)-C(11)-C(14)	114.59(14)
C(20)-C(19)-C(24)	115.84(15)	C(20)-C(19)-C(18)	119.81(15)
C(24)-C(19)-C(18)	124.33(15)	C(19)-C(18)-C(25)	117.17(14)
C(6)-C(5)-C(4)	121.09(15)	C(6)-C(5)-Cl(2)	118.55(14)
C(4)-C(5)-Cl(2)	120.36(14)	O(1)-C(8)-C(9)	106.46(12)
O(1)-C(8)-C(13)	109.74(14)	C(9)-C(8)-C(13)	108.75(12)
O(1)-C(8)-C(1)	109.96(12)	C(9)-C(8)-C(1)	112.36(13)
C(13)-C(8)-C(1)	109.50(13)	C(16)-C(14)-C(15)	107.84(18)
C(16)-C(14)-C(17)	108.97(17)	C(15)-C(14)-C(17)	107.87(17)
C(16)-C(14)-C(11)	112.43(15)	C(15)-C(14)-C(11)	110.27(14)
C(17)-C(14)-C(11)	109.34(16)	C(5)-C(4)-C(3)	118.72(16)
C(21)-C(20)-C(19)	122.93(16)	C(13)-C(12)-C(11)	111.83(14)
C(22)-C(21)-C(20)	118.62(16)	C(22)-C(23)-C(24)	118.42(17)
C(23)-C(24)-C(19)	122.85(16)	C(23)-C(24)-Cl(4)	116.64(14)
C(19)-C(24)-Cl(4)	120.50(14)	C(8)-C(9)-C(10)	112.34(13)

C(9)-C(10)-C(11)	112.24(13)	C(21)-C(22)-C(23)	121.33(17)
C(21)-C(22)-Cl(3)	119.48(15)	C(23)-C(22)-Cl(3)	119.19(15)

Table 1.14 Torsion angles [°] for *cis*-**1.9**.

atom-atom-atom-atom	angle	atom-atom-atom-atom	angle
C(7)-C(2)-C(3)-C(4)	1.9(2)	C(1)-C(2)-C(3)-C(4)	-178.78(14)
C(27)-C(26)-C(25)-O(2)	64.12(16)	C(27)-C(26)-C(25)-C(30)	-53.43(16)
C(27)-C(26)-C(25)-C(18)	-179.49(12)	C(30)-C(29)-C(28)-C(27)	56.23(15)
C(30)-C(29)-C(28)-C(31)	-176.49(12)	C(34)-C(31)-C(28)-C(29)	-74.62(17)
C(33)-C(31)-C(28)-C(29)	46.67(17)	C(32)-C(31)-C(28)-C(29)	164.49(13)
C(34)-C(31)-C(28)-C(27)	50.41(18)	C(33)-C(31)-C(28)-C(27)	171.70(13)
C(32)-C(31)-C(28)-C(27)	-70.48(17)	C(7)-C(2)-C(1)-C(8)	-92.94(19)
C(3)-C(2)-C(1)-C(8)	87.78(18)	C(25)-C(26)-C(27)-C(28)	55.37(17)
C(29)-C(28)-C(27)-C(26)	-54.92(16)	C(31)-C(28)-C(27)-C(26)	176.74(12)
O(2)-C(25)-C(30)-C(29)	-61.44(15)	C(26)-C(25)-C(30)-C(29)	55.19(16)
C(18)-C(25)-C(30)-C(29)	-178.83(12)	C(28)-C(29)-C(30)-C(25)	-58.55(16)
C(5)-C(6)-C(7)-C(2)	1.1(2)	C(5)-C(6)-C(7)-Cl(1)	-177.50(12)
C(3)-C(2)-C(7)-C(6)	-2.6(2)	C(1)-C(2)-C(7)-C(6)	178.06(14)
C(3)-C(2)-C(7)-Cl(1)	175.94(11)	C(1)-C(2)-C(7)-Cl(1)	-3.4(2)
C(20)-C(19)-C(18)-C(25)	87.22(18)	C(24)-C(19)-C(18)-C(25)	-94.76(19)
O(2)-C(25)-C(18)-C(19)	-178.73(12)	C(30)-C(25)-C(18)-C(19)	-59.77(19)
C(26)-C(25)-C(18)-C(19)	64.17(18)	C(7)-C(6)-C(5)-C(4)	1.2(2)
C(7)-C(6)-C(5)-Cl(2)	-178.71(12)	C(12)-C(13)-C(8)-O(1)	61.49(17)
C(12)-C(13)-C(8)-C(9)	-54.60(17)	C(12)-C(13)-C(8)-C(1)	-177.73(13)

C(2)-C(1)-C(8)-O(1)	-52.92(17)	C(2)-C(1)-C(8)-C(9)	65.46(17)
C(2)-C(1)-C(8)-C(13)	-173.58(13)	C(10)-C(11)-C(14)-C(16)	-66.1(2)
C(12)-C(11)-C(14)-C(16)	58.5(2)	C(10)-C(11)-C(14)-C(15)	173.50(16)
C(12)-C(11)-C(14)-C(15)	-61.9(2)	C(10)-C(11)-C(14)-C(17)	55.05(19)
C(12)-C(11)-C(14)-C(17)	179.66(16)	C(6)-C(5)-C(4)-C(3)	-1.9(2)
Cl(2)-C(5)-C(4)-C(3)	178.00(12)	C(2)-C(3)-C(4)-C(5)	0.3(2)
C(24)-C(19)-C(20)-C(21)	1.6(2)	C(18)-C(19)-C(20)-C(21)	179.80(14)
C(8)-C(13)-C(12)-C(11)	57.10(18)	C(10)-C(11)-C(12)-C(13)	-55.88(17)
C(14)-C(11)-C(12)-C(13)	176.66(13)	C(19)-C(20)-C(21)-C(22)	-1.0(2)
C(22)-C(23)-C(24)-C(19)	-0.3(3)	C(22)-C(23)-C(24)-Cl(4)	-179.09(13)
C(20)-C(19)-C(24)-C(23)	-0.9(2)	C(18)-C(19)-C(24)-C(23)	-179.04(15)
C(20)-C(19)-C(24)-Cl(4)	177.85(12)	C(18)-C(19)-C(24)-Cl(4)	-0.2(2)
O(1)-C(8)-C(9)-C(10)	-63.47(15)	C(13)-C(8)-C(9)-C(10)	54.71(17)
C(1)-C(8)-C(9)-C(10)	176.10(12)	C(8)-C(9)-C(10)-C(11)	-58.12(17)
C(12)-C(11)-C(10)-C(9)	56.45(17)	C(14)-C(11)-C(10)-C(9)	-175.43(13)
C(20)-C(21)-C(22)-C(23)	-0.3(3)	C(20)-C(21)-C(22)-Cl(3)	178.67(12)
C(24)-C(23)-C(22)-C(21)	0.9(3)	C(24)-C(23)-C(22)-Cl(3)	-178.05(13)

Table 1.15 Crystal data and structure refinement for *cis*-**1.13**.

Identification code	*cis*-**1.13**
Empirical formula	C42 H66 Cl6 N2 O2
Formula weight	843.67
Temperature	150(2) K
Wavelength	0.71073 Å
Crystal system	Monoclinic

Space group	P2(1)/n	
Unit cell dimensions	a = 18.308(9) Å	α = 90°
	b = 10.588(5) Å	β = 94.192(6)°
	c = 23.636(11) Å	γ = 90°
Volume	4570(4) $Å^3$	
Z	4	
Density (calculated)	1.226 $g.cm^{-3}$	
Absorption coefficient (μ)	0.411 mm^{-1}	
F(000)	1800	
Crystal size	0.15 × 0.10 × 0.03 mm^3	
ω range for data collection	2.11 to 21.30°	
Index ranges	$-18 \leq h \leq 18$, $-10 \leq k \leq 10$, $-23 \leq l \leq 24$	
Reflections collected	27749	
Independent reflections	5076 [R_{int} = 0.0483]	
Completeness to θ = 21.30°	99.1 %	
Absorption correction	Empirical	
Max. and min. transmission	0.7446 and 0.6797	
Refinement method	Full-matrix least-squares on F^2	
Data / restraints / parameters	5076 / 0 / 478	
Goodness-of-fit on F^2	1.017	
Final R indices [I>2σ(I)]	R_1 = 0.0362, wR_2 = 0.0825	
R indices (all data)	R_1 = 0.0500, wR_2 = 0.0906	
Largest diff. peak and hole	0.518 and -0.356 $e^-.Å^{-3}$	

Table 1.16 Atomic coordinates and equivalent isotropic displacement parameters ($Å^2$) for *cis*-**1.13**. U(eq) is defined as one third of the trace of the orthogonalized U_{ij} tensor.

	x	y	z	U(eq)
Cl(1)	0.26090(5)	0.33114(8)	0.11816(3)	0.038(1)
Cl(2)	0.53976(4)	0.28075(7)	0.05997(3)	0.032(1)
Cl(3)	0.35857(4)	0.16465(8)	0.26814(3)	0.033(1)
Cl(4)	0.32990(5)	0.61651(9)	0.30118(4)	0.052(1)
Cl(5)	0.56620(6)	-0.08947(9)	0.39180(4)	0.056(1)
Cl(6)	0.69066(5)	0.72420(10)	0.20507(4)	0.052(1)
O(1)	0.46065(10)	-0.12444(17)	0.11353(8)	0.022(1)
O(2)	0.55911(11)	0.37513(19)	0.28531(9)	0.030(1)
N(1)	0.55986(13)	-0.2903(2)	0.04894(10)	0.028(1)
N(2)	0.69843(14)	0.2601(3)	0.19563(11)	0.039(1)
C(1)	0.40237(15)	-0.0402(3)	0.12811(12)	0.022(1)
C(8)	0.46795(16)	0.0387(3)	0.22028(12)	0.024(1)
C(5)	0.31531(16)	-0.2276(3)	0.12892(12)	0.026(1)
C(31)	0.30596(18)	0.4720(3)	0.20910(13)	0.030(1)
C(4)	0.27246(16)	-0.1813(3)	0.07439(12)	0.024(1)
C(25)	0.57373(16)	0.3939(3)	0.43501(13)	0.032(1)
C(18)	0.23214(16)	-0.2892(3)	0.04022(12)	0.026(1)
C(7)	0.43395(17)	0.0734(3)	0.16219(12)	0.026(1)
C(2)	0.35781(16)	0.0060(3)	0.07474(12)	0.025(1)
C(15)	0.57416(17)	-0.1596(3)	0.07188(13)	0.029(1)
C(36)	0.62601(17)	0.2756(3)	0.21925(14)	0.037(1)

C(33)	0.39918(18)	0.4008(3)	0.15046(13)	0.027(1)
C(29)	0.43360(17)	0.5229(3)	0.23546(13)	0.029(1)
C(3)	0.32358(16)	-0.1027(3)	0.03968(12)	0.024(1)
C(28)	0.49420(17)	0.5781(3)	0.27476(13)	0.034(1)
C(23)	0.47724(16)	0.4194(3)	0.35331(13)	0.032(1)
C(19)	0.28530(17)	-0.3877(3)	0.01979(13)	0.033(1)
C(6)	0.35348(16)	-0.1214(3)	0.16276(12)	0.025(1)
C(27)	0.59187(17)	0.5442(3)	0.35362(13)	0.033(1)
C(10)	0.56214(18)	-0.0736(3)	0.27788(14)	0.037(1)
C(14)	0.50617(16)	-0.0803(3)	0.07180(12)	0.026(1)
C(20)	0.17783(17)	-0.3541(3)	0.07717(14)	0.034(1)
C(9)	0.53141(17)	-0.0340(3)	0.22598(13)	0.031(1)
C(30)	0.35967(18)	0.5302(3)	0.24443(13)	0.030(1)
C(34)	0.45131(17)	0.4574(3)	0.18707(13)	0.028(1)
C(24)	0.51354(17)	0.3289(3)	0.39695(14)	0.035(1)
C(22)	0.53110(16)	0.4808(3)	0.31620(13)	0.028(1)
C(12)	0.46650(17)	0.0336(3)	0.32293(13)	0.028(1)
C(26)	0.62862(17)	0.4525(3)	0.39681(13)	0.033(1)
C(32)	0.32729(17)	0.4075(3)	0.16260(13)	0.027(1)
C(11)	0.52863(18)	-0.0389(3)	0.32571(14)	0.034(1)
C(21)	0.18795(19)	-0.2350(3)	-0.01165(14)	0.043(1)
C(35)	0.62213(18)	0.3944(3)	0.25533(14)	0.037(1)
C(40)	0.5504(2)	0.2423(4)	0.51495(17)	0.061(1)
C(37)	0.6996(2)	0.1378(4)	0.16320(16)	0.057(1)
C(41)	0.6533(2)	0.3922(4)	0.52605(16)	0.059(1)
C(16)	0.52546(19)	-0.3729(3)	0.09053(14)	0.040(1)

C(13)	0.43722(16)	0.0720(3)	0.27018(13)	0.024(1)
C(38)	0.7169(2)	0.3671(4)	0.15866(16)	0.054(1)
C(17)	0.62936(19)	-0.3495(3)	0.03273(16)	0.049(1)
C(42)	0.6589(2)	0.2091(4)	0.46017(19)	0.067(1)
C(39)	0.60914(18)	0.3089(3)	0.48318(15)	0.041(1)
H(5A)	0.2811	-0.2709	0.1531	0.031
H(5B)	0.3524	-0.2900	0.1187	0.031
H(31A)	0.2558	0.4767	0.2168	0.036
H(4A)	0.2338	-0.1225	0.0865	0.029
H(25A)	0.5498	0.4657	0.4540	0.038
H(7A)	0.4715	0.1148	0.1405	0.031
H(7B)	0.3943	0.1354	0.1666	0.031
H(2A)	0.3185	0.0630	0.0860	0.031
H(2B)	0.3901	0.0551	0.0511	0.031
H(15A)	0.5965	-0.1660	0.1112	0.035
H(15B)	0.6098	-0.1170	0.0488	0.035
H(36A)	0.6161	0.2010	0.2427	0.044
H(36B)	0.5875	0.2796	0.1876	0.044
H(33A)	0.4128	0.3581	0.1175	0.033
H(3A)	0.3628	-0.1575	0.0267	0.029
H(3B)	0.2955	-0.0684	0.0057	0.029
H(28A)	0.4738	0.6473	0.2969	0.041
H(28B)	0.5318	0.6149	0.2517	0.041
H(23A)	0.4402	0.3726	0.3289	0.038
H(23B)	0.4514	0.4862	0.3733	0.038
H(19A)	0.2578	-0.4535	-0.0017	0.049

H(19B)	0.3129	-0.4256	0.0526	0.049
H(19C)	0.3193	-0.3469	-0.0047	0.049
H(6A)	0.3836	-0.1583	0.1951	0.030
H(6B)	0.3159	-0.0668	0.1784	0.030
H(27A)	0.5711	0.6160	0.3740	0.039
H(27B)	0.6291	0.5783	0.3294	0.039
H(10A)	0.6054	-0.1234	0.2806	0.044
H(14A)	0.5198	0.0088	0.0797	0.031
H(14B)	0.4792	-0.0842	0.0340	0.031
H(20A)	0.1479	-0.4143	0.0541	0.051
H(20B)	0.1460	-0.2904	0.0927	0.051
H(20C)	0.2048	-0.3990	0.1084	0.051
H(9A)	0.5544	-0.0573	0.1928	0.038
H(34A)	0.5013	0.4516	0.1791	0.034
H(24A)	0.5351	0.2572	0.3770	0.042
H(24B)	0.4760	0.2946	0.4208	0.042
H(12A)	0.4441	0.0568	0.3564	0.034
H(26A)	0.6668	0.4980	0.4206	0.040
H(26B)	0.6529	0.3844	0.3764	0.040
H(21A)	0.1593	-0.3025	-0.0310	0.065
H(21B)	0.2215	-0.1984	-0.0377	0.065
H(21C)	0.1548	-0.1692	0.0005	0.065
H(35A)	0.6664	0.4031	0.2817	0.044
H(35B)	0.6169	0.4708	0.2312	0.044
H(40A)	0.5733	0.2013	0.5489	0.092
H(40B)	0.5258	0.1786	0.4902	0.092

H(40C)	0.5144	0.3044	0.5260	0.092
H(37A)	0.6911	0.0673	0.1887	0.086
H(37B)	0.7475	0.1275	0.1477	0.086
H(37C)	0.6612	0.1391	0.1321	0.086
H(41A)	0.6706	0.3413	0.5590	0.088
H(41B)	0.6222	0.4609	0.5383	0.088
H(41C)	0.6954	0.4278	0.5083	0.088
H(16A)	0.4775	-0.3385	0.0983	0.060
H(16B)	0.5570	-0.3764	0.1259	0.060
H(16C)	0.5193	-0.4582	0.0748	0.060
H(38A)	0.7197	0.4453	0.1809	0.082
H(38B)	0.6790	0.3756	0.1274	0.082
H(38C)	0.7643	0.3511	0.1432	0.082
H(17A)	0.6502	-0.2984	0.0033	0.074
H(17B)	0.6192	-0.4348	0.0181	0.074
H(17C)	0.6643	-0.3542	0.0661	0.074
H(42A)	0.6749	0.1503	0.4906	0.101
H(42B)	0.7017	0.2500	0.4457	0.101
H(42C)	0.6320	0.1626	0.4294	0.101

Table 1.17 Anisotropic displacement parameters $(Å)^2$ for *cis*-**1.13**. The anisotropic displacement factor exponent takes the form:
$-2\pi^2[h^2 a^{*2} U_{11} + ... + 2 h k a^* b^* U_{12}]$

	U_{11}	U_{22}	U_{33}	U_{23}	U_{13}	U_{12}
Cl(1)	0.0441(5)	0.0316(5)	0.0353(5)	0.0008(4)	-0.0079(4)	-0.0056(4)

Cl(2)	0.0373(5)	0.0303(5)	0.0286(5)	-0.0029(4)	0.0045(4)	-0.0005(4)
Cl(3)	0.0325(5)	0.0365(5)	0.0296(5)	-0.0021(4)	0.0021(4)	0.0059(4)
Cl(4)	0.0437(6)	0.0704(7)	0.0412(6)	-0.0259(5)	-0.0027(4)	0.0206(5)
Cl(5)	0.0720(7)	0.0553(6)	0.0362(6)	0.0085(5)	-0.0225(5)	0.0084(5)
Cl(6)	0.0417(6)	0.0691(7)	0.0441(6)	-0.0051(5)	-0.0084(4)	0.0044(5)
O(1)	0.0270(12)	0.0182(11)	0.0203(11)	0.0031(9)	0.0044(9)	0.0024(9)
O(2)	0.0256(13)	0.0311(13)	0.0344(13)	-0.0078(11)	0.0020(10)	0.0007(10)
N(1)	0.0303(16)	0.0252(15)	0.0307(16)	-0.0030(13)	0.0100(12)	0.0055(12)
N(2)	0.0311(17)	0.0514(19)	0.0340(17)	-0.0101(15)	0.0031(13)	0.0030(14)
C(1)	0.0247(18)	0.0190(17)	0.0212(17)	0.0009(14)	0.0009(14)	0.0022(14)
C(8)	0.0272(19)	0.0197(17)	0.0247(19)	-0.0039(14)	-0.0035(15)	-0.0039(15)
C(5)	0.0259(18)	0.0243(18)	0.0273(18)	0.0049(15)	0.0020(14)	-0.0005(14)
C(31)	0.032(2)	0.0307(19)	0.027(2)	0.0040(16)	0.0002(16)	0.0097(16)
C(4)	0.0256(18)	0.0238(18)	0.0219(17)	-0.0020(14)	-0.0030(14)	0.0037(14)
C(25)	0.0268(19)	0.0287(19)	0.039(2)	-0.0020(16)	-0.0033(16)	-0.0017(15)
C(18)	0.0281(18)	0.0255(18)	0.0239(18)	-0.0015(15)	-0.0027(15)	0.0002(15)
C(7)	0.0321(19)	0.0208(17)	0.0239(18)	-0.0019(14)	0.0004(15)	0.0008(14)
C(2)	0.0322(19)	0.0215(18)	0.0226(18)	0.0014(14)	0.0018(15)	0.0031(14)
C(15)	0.033(2)	0.0292(19)	0.0249(18)	0.0000(15)	0.0031(15)	-0.0050(16)
C(36)	0.029(2)	0.044(2)	0.037(2)	-0.0083(17)	0.0014(16)	0.0002(16)
C(33)	0.039(2)	0.0217(18)	0.0214(18)	0.0033(14)	0.0023(16)	0.0048(16)
C(29)	0.037(2)	0.0220(18)	0.0270(19)	0.0031(15)	-0.0001(16)	0.0049(15)
C(3)	0.0290(18)	0.0243(18)	0.0183(17)	0.0007(14)	-0.0050(14)	0.0040(14)
C(28)	0.036(2)	0.031(2)	0.035(2)	-0.0054(16)	0.0026(16)	-0.0019(16)
C(23)	0.0230(18)	0.039(2)	0.032(2)	-0.0050(16)	-0.0038(15)	-0.0027(15)
C(19)	0.039(2)	0.0273(19)	0.033(2)	-0.0081(16)	0.0063(16)	-0.0066(16)

C(6)	0.0273(19)	0.0284(18)	0.0192(17)	0.0011(15)	-0.0013(14)	0.0019(15)
C(27)	0.032(2)	0.032(2)	0.034(2)	-0.0052(16)	0.0008(16)	-0.0076(16)
C(10)	0.036(2)	0.032(2)	0.041(2)	-0.0073(17)	-0.0082(18)	0.0080(16)
C(14)	0.0322(19)	0.0218(18)	0.0237(18)	-0.0003(14)	0.0027(15)	0.0005(15)
C(20)	0.030(2)	0.034(2)	0.038(2)	-0.0066(16)	0.0017(16)	0.0019(16)
C(9)	0.033(2)	0.035(2)	0.025(2)	-0.0086(16)	-0.0033(16)	0.0021(16)
C(30)	0.038(2)	0.0281(19)	0.0218(18)	-0.0044(15)	0.0010(16)	0.0107(16)
C(34)	0.0306(19)	0.0266(18)	0.0274(19)	0.0060(16)	0.0049(16)	0.0017(15)
C(24)	0.0278(19)	0.038(2)	0.038(2)	0.0003(17)	-0.0023(16)	-0.0072(16)
C(22)	0.0252(18)	0.0270(19)	0.0306(19)	-0.0068(16)	0.0015(15)	-0.0031(15)
C(12)	0.033(2)	0.0266(19)	0.025(2)	-0.0012(15)	-0.0019(15)	-0.0017(16)
C(26)	0.0287(19)	0.033(2)	0.036(2)	-0.0095(16)	-0.0067(16)	-0.0063(16)
C(32)	0.036(2)	0.0209(18)	0.0240(19)	0.0045(15)	-0.0040(16)	0.0018(15)
C(11)	0.041(2)	0.0294(19)	0.028(2)	0.0026(16)	-0.0143(17)	-0.0045(17)
C(21)	0.050(2)	0.039(2)	0.037(2)	-0.0047(17)	-0.0189(18)	-0.0059(18)
C(35)	0.031(2)	0.043(2)	0.037(2)	-0.0073(17)	0.0029(17)	-0.0032(16)
C(40)	0.060(3)	0.061(3)	0.060(3)	0.027(2)	-0.012(2)	-0.011(2)
C(37)	0.041(2)	0.077(3)	0.053(3)	-0.022(2)	-0.0011(19)	0.016(2)
C(41)	0.067(3)	0.052(3)	0.053(3)	0.015(2)	-0.026(2)	-0.010(2)
C(16)	0.050(2)	0.0253(19)	0.045(2)	0.0013(17)	0.0125(18)	0.0005(17)
C(13)	0.0262(18)	0.0204(17)	0.026(2)	-0.0023(15)	-0.0030(15)	-0.0027(14)
C(38)	0.040(2)	0.080(3)	0.044(2)	-0.002(2)	0.0066(19)	-0.005(2)
C(17)	0.045(2)	0.052(2)	0.052(2)	-0.007(2)	0.0127(19)	0.0144(19)
C(42)	0.057(3)	0.050(3)	0.092(3)	0.014(2)	-0.007(2)	0.010(2)
C(39)	0.037(2)	0.032(2)	0.053(2)	0.0060(18)	-0.0120(18)	-0.0010(17)

Table 1.18 Bond lengths [Å] *cis*-**1.13**.

atom-atom	distance	atom-atom	distance
Cl(1)-C(32)	1.746(3)	Cl(3)-C(13)	1.740(3)
Cl(4)-C(30)	1.743(3)	Cl(5)-C(11)	1.744(3)
O(1)-C(14)	1.416(3)	O(1)-C(1)	1.451(3)
O(2)-C(35)	1.412(4)	O(2)-C(22)	1.450(4)
N(1)-C(16)	1.490(4)	N(1)-C(17)	1.494(4)
N(1)-C(15)	1.502(4)	N(2)-C(36)	1.485(4)
N(2)-C(38)	1.485(5)	N(2)-C(37)	1.506(4)
C(1)-C(6)	1.522(4)	C(1)-C(2)	1.532(4)
C(1)-C(7)	1.537(4)	C(8)-C(13)	1.389(4)
C(8)-C(9)	1.392(4)	C(8)-C(7)	1.511(4)
C(5)-C(6)	1.520(4)	C(5)-C(4)	1.539(4)
C(31)-C(32)	1.375(4)	C(31)-C(30)	1.387(4)
C(4)-C(3)	1.534(4)	C(4)-C(18)	1.555(4)
C(25)-C(26)	1.531(4)	C(25)-C(24)	1.534(4)
C(25)-C(39)	1.556(4)	C(18)-C(19)	1.528(4)
C(18)-C(21)	1.531(4)	C(18)-C(20)	1.533(4)
C(2)-C(3)	1.526(4)	C(15)-C(14)	1.501(4)
C(36)-C(35)	1.524(4)	C(33)-C(32)	1.369(4)
C(33)-C(34)	1.378(4)	C(29)-C(30)	1.387(4)
C(29)-C(34)	1.396(4)	C(29)-C(28)	1.511(4)
C(28)-C(22)	1.542(4)	C(23)-C(22)	1.514(4)
C(23)-C(24)	1.525(4)	C(27)-C(22)	1.525(4)

C(27)-C(26)	1.529(4)	C(10)-C(11)	1.375(5)
C(10)-C(9)	1.377(4)	C(12)-C(11)	1.370(4)
C(12)-C(13)	1.382(4)	C(40)-C(39)	1.528(5)
C(41)-C(39)	1.530(5)	C(42)-C(39)	1.521(5)

Table 1.19 Bond angles [°] for *cis*-**1.13**.

atom-atom-atom	angle	atom-atom-atom	angle
C(14)-O(1)-C(1)	116.3(2)	C(35)-O(2)-C(22)	118.2(2)
C(16)-N(1)-C(17)	109.4(3)	C(16)-N(1)-C(15)	111.9(2)
C(17)-N(1)-C(15)	110.5(2)	C(36)-N(2)-C(38)	112.6(3)
C(36)-N(2)-C(37)	109.5(3)	C(38)-N(2)-C(37)	110.1(3)
O(1)-C(1)-C(6)	104.6(2)	O(1)-C(1)-C(2)	110.9(2)
C(6)-C(1)-C(2)	109.0(2)	O(1)-C(1)-C(7)	110.5(2)
C(6)-C(1)-C(7)	111.9(2)	C(2)-C(1)-C(7)	109.8(2)
C(13)-C(8)-C(9)	116.4(3)	C(13)-C(8)-C(7)	123.0(3)
C(9)-C(8)-C(7)	120.5(3)	C(6)-C(5)-C(4)	113.0(2)
C(32)-C(31)-C(30)	118.2(3)	C(3)-C(4)-C(5)	109.1(2)
C(3)-C(4)-C(18)	114.0(2)	C(5)-C(4)-C(18)	113.2(2)
C(26)-C(25)-C(24)	108.1(3)	C(26)-C(25)-C(39)	114.2(3)
C(24)-C(25)-C(39)	114.4(3)	C(19)-C(18)-C(21)	108.3(3)
C(19)-C(18)-C(20)	109.2(3)	C(21)-C(18)-C(20)	107.3(3)
C(19)-C(18)-C(4)	112.1(2)	C(21)-C(18)-C(4)	110.1(2)
C(20)-C(18)-C(4)	109.7(2)	C(8)-C(7)-C(1)	113.6(2)

C(3)-C(2)-C(1)	112.3(2)	C(14)-C(15)-N(1)	113.1(2)
N(2)-C(36)-C(35)	112.4(3)	C(32)-C(33)-C(34)	118.6(3)
C(30)-C(29)-C(34)	116.1(3)	C(30)-C(29)-C(28)	124.4(3)
C(34)-C(29)-C(28)	119.4(3)	C(2)-C(3)-C(4)	111.2(2)
C(29)-C(28)-C(22)	113.6(3)	C(22)-C(23)-C(24)	113.1(3)
C(5)-C(6)-C(1)	113.6(2)	C(22)-C(27)-C(26)	112.0(3)
C(11)-C(10)-C(9)	118.3(3)	O(1)-C(14)-C(15)	110.2(2)
C(10)-C(9)-C(8)	122.6(3)	C(31)-C(30)-C(29)	122.7(3)
C(31)-C(30)-Cl(4)	116.6(2)	C(29)-C(30)-Cl(4)	120.7(2)
C(33)-C(34)-C(29)	122.6(3)	C(23)-C(24)-C(25)	111.9(3)
O(2)-C(22)-C(23)	103.3(2)	O(2)-C(22)-C(27)	111.2(2)
C(23)-C(22)-C(27)	109.4(3)	O(2)-C(22)-C(28)	110.5(2)
C(23)-C(22)-C(28)	112.4(3)	C(27)-C(22)-C(28)	110.0(2)
C(11)-C(12)-C(13)	118.3(3)	C(27)-C(26)-C(25)	112.1(3)
C(33)-C(32)-C(31)	121.8(3)	C(33)-C(32)-Cl(1)	119.2(2)
C(31)-C(32)-Cl(1)	119.0(3)	C(12)-C(11)-C(10)	121.9(3)
C(12)-C(11)-Cl(5)	119.1(3)	C(10)-C(11)-Cl(5)	119.0(3)
O(2)-C(35)-C(36)	103.6(2)	C(12)-C(13)-C(8)	122.5(3)
C(12)-C(13)-Cl(3)	117.2(2)	C(8)-C(13)-Cl(3)	120.4(2)
C(42)-C(39)-C(40)	108.5(3)	C(42)-C(39)-C(41)	109.7(3)
C(40)-C(39)-C(41)	107.3(3)	C(42)-C(39)-C(25)	111.6(3)
C(40)-C(39)-C(25)	110.8(3)	C(41)-C(39)-C(25)	108.8(3)

Table 1.20 Torsion angles [°] for *cis*-**1.13**.

atom-atom-atom-atom	angle	atom-atom-atom-atom	angle
C(14)-O(1)-C(1)-C(6)	167.9(2)	C(14)-O(1)-C(1)-C(2)	50.5(3)
C(14)-O(1)-C(1)-C(7)	-71.5(3)	C(6)-C(5)-C(4)-C(3)	53.0(3)
C(6)-C(5)-C(4)-C(18)	-178.9(2)	C(3)-C(4)-C(18)-C(19)	63.4(3)
C(5)-C(4)-C(18)-C(19)	-62.1(3)	C(3)-C(4)-C(18)-C(21)	-57.3(3)
C(5)-C(4)-C(18)-C(21)	177.3(3)	C(3)-C(4)-C(18)-C(20)	-175.1(2)
C(5)-C(4)-C(18)-C(20)	59.4(3)	C(13)-C(8)-C(7)-C(1)	-110.2(3)
C(9)-C(8)-C(7)-C(1)	67.2(4)	O(1)-C(1)-C(7)-C(8)	-67.0(3)
C(6)-C(1)-C(7)-C(8)	49.2(3)	C(2)-C(1)-C(7)-C(8)	170.3(2)
O(1)-C(1)-C(2)-C(3)	58.8(3)	C(6)-C(1)-C(2)-C(3)	-55.9(3)
C(7)-C(1)-C(2)-C(3)	-178.8(2)	C(16)-N(1)-C(15)-C(14)	-75.9(3)
C(17)-N(1)-C(15)-C(14)	161.9(3)	C(38)-N(2)-C(36)-C(35)	-60.1(4)
C(37)-N(2)-C(36)-C(35)	177.0(3)	C(1)-C(2)-C(3)-C(4)	59.2(3)
C(5)-C(4)-C(3)-C(2)	-55.7(3)	C(18)-C(4)-C(3)-C(2)	176.7(2)
C(30)-C(29)-C(28)-C(22)	97.6(4)	C(34)-C(29)-C(28)-C(22)	-81.0(4)
C(4)-C(5)-C(6)-C(1)	-53.4(3)	O(1)-C(1)-C(6)-C(5)	-65.9(3)
C(2)-C(1)-C(6)-C(5)	52.8(3)	C(7)-C(1)-C(6)-C(5)	174.4(2)
C(1)-O(1)-C(14)-C(15)	165.4(2)	N(1)-C(15)-C(14)-O(1)	70.8(3)
C(11)-C(10)-C(9)-C(8)	-0.3(5)	C(13)-C(8)-C(9)-C(10)	1.1(5)
C(7)-C(8)-C(9)-C(10)	-176.5(3)	C(32)-C(31)-C(30)-C(29)	-1.7(5)
C(32)-C(31)-C(30)-Cl(4)	177.4(2)	C(34)-C(29)-C(30)-C(31)	2.5(4)
C(28)-C(29)-C(30)-C(31)	-176.1(3)	C(34)-C(29)-C(30)-Cl(4)	-176.5(2)
C(28)-C(29)-C(30)-Cl(4)	4.8(4)	C(32)-C(33)-C(34)-C(29)	-1.1(4)
C(30)-C(29)-C(34)-C(33)	-1.1(4)	C(28)-C(29)-C(34)-C(33)	177.6(3)

C(22)-C(23)-C(24)-C(25)	56.6(4)	C(26)-C(25)-C(24)-C(23)	-55.7(3)
C(39)-C(25)-C(24)-C(23)	175.9(3)	C(35)-O(2)-C(22)-C(23)	-166.9(2)
C(35)-O(2)-C(22)-C(27)	-49.7(3)	C(35)-O(2)-C(22)-C(28)	72.8(3)
C(24)-C(23)-C(22)-O(2)	64.4(3)	C(24)-C(23)-C(22)-C(27)	-54.1(3)
C(24)-C(23)-C(22)-C(28)	-176.5(3)	C(26)-C(27)-C(22)-O(2)	-59.1(3)
C(26)-C(27)-C(22)-C(23)	54.3(3)	C(26)-C(27)-C(22)-C(28)	178.2(3)
C(29)-C(28)-C(22)-O(2)	56.3(3)	C(29)-C(28)-C(22)-C(23)	-58.5(4)
C(29)-C(28)-C(22)-C(27)	179.4(3)	C(22)-C(27)-C(26)-C(25)	-57.7(3)
C(24)-C(25)-C(26)-C(27)	56.6(3)	C(39)-C(25)-C(26)-C(27)	-174.9(3)
C(34)-C(33)-C(32)-C(31)	2.0(4)	C(34)-C(33)-C(32)-Cl(1)	-177.5(2)
C(30)-C(31)-C(32)-C(33)	-0.7(4)	C(30)-C(31)-C(32)-Cl(1)	178.9(2)
C(13)-C(12)-C(11)-C(10)	0.1(5)	C(13)-C(12)-C(11)-Cl(5)	-179.6(2)
C(9)-C(10)-C(11)-C(12)	-0.4(5)	C(9)-C(10)-C(11)-Cl(5)	179.3(2)
C(22)-O(2)-C(35)-C(36)	-168.8(2)	N(2)-C(36)-C(35)-O(2)	-164.9(3)
C(11)-C(12)-C(13)-C(8)	0.8(4)	C(11)-C(12)-C(13)-Cl(3)	-179.7(2)
C(9)-C(8)-C(13)-C(12)	-1.3(4)	C(7)-C(8)-C(13)-C(12)	176.2(3)
C(9)-C(8)-C(13)-Cl(3)	179.1(2)	C(7)-C(8)-C(13)-Cl(3)	-3.4(4)
C(26)-C(25)-C(39)-C(42)	-52.5(4)	C(24)-C(25)-C(39)-C(42)	72.8(4)
C(26)-C(25)-C(39)-C(40)	-173.5(3)	C(24)-C(25)-C(39)-C(40)	-48.2(4)
C(26)-C(25)-C(39)-C(41)	68.7(4)	C(24)-C(25)-C(39)-C(41)	-166.0(3)

Table 1.21 Crystal data and structure refinement for *cis*-**1.22**.

Identification code	*cis*-**1.22**
Empirical formula	C19 H27 Cl2 O2
Formula weight	358.31

Temperature	150(2) K	
Wavelength	0.71073 Å	
Crystal system	Triclinic	
Space group	P-1	
Unit cell dimensions	a = 6.9683(7) Å	α = 69.8640(10)°
	b = 10.9136(11) Å	β = 82.6300(10)°
	c = 13.3343(13) Å	γ = 88.0140(10)°
Volume	944.17(16) $Å^3$	
Z	2	
Density (calculated)	1.260 $g.cm^{-3}$	
Absorption coefficient (μ)	0.351 mm^{-1}	
F(000)	382	
Crystal size	0.125 × 0.105 × 0.075 mm^3	
ω range for data collection	1.99 to 26.73°	
Index ranges	$-8 \leq h \leq 8$, $-13 \leq k \leq 13$, $-16 \leq l \leq 16$	
Reflections collected	9635	
Independent reflections	3957 [R_{int} = 0.0145]	
Completeness to θ = 26.73°	99.0 %	
Absorption correction	Empirical	
Max. and min. transmission	0.7459 and 0.7016	
Refinement method	Full-matrix least-squares on F^2	
Data / restraints / parameters	3957 / 0 / 208	
Goodness-of-fit on F^2	1.046	
Final R indices [I>2σ(I)]	R_1 = 0.0417, wR_2 = 0.1196	
R indices (all data)	R_1 = 0.0462, wR_2 = 0.1238	
Largest diff. peak and hole	0.749 and -0.608 $e^-.Å^{-3}$	

Table 1.22 Atomic coordinates and equivalent isotropic displacement parameters ($Å^2$) for *cis*-**1.22**. U(eq) is defined as one third of the trace of the orthogonalized U_{ij} tensor.

	x	y	z	U(eq)
Cl(1)	0.27346(7)	0.45813(5)	0.68781(4)	0.044(1)
Cl(2)	0.19829(9)	0.15746(5)	0.72967(4)	0.050(1)
O(2)	0.36991(16)	0.10540(11)	0.34167(9)	0.026(1)
O(1)	0.28266(18)	-0.07844(12)	0.56166(10)	0.036(1)
C(19)	0.2460(3)	0.49363(17)	0.48031(15)	0.034(1)
C(18)	0.5615(2)	0.26721(16)	0.05889(13)	0.027(1)
C(17)	0.1289(2)	0.28065(17)	0.32252(14)	0.029(1)
C(16)	0.1713(2)	0.23342(16)	0.51732(14)	0.028(1)
C(15)	0.4760(2)	0.31665(15)	0.23178(13)	0.025(1)
C(14)	0.1727(2)	0.32302(16)	0.41356(13)	0.026(1)
C(13)	0.2042(2)	0.27353(17)	0.60157(14)	0.030(1)
C(12)	0.2404(2)	0.40421(18)	0.58350(15)	0.030(1)
C(11)	0.6372(2)	0.27864(16)	0.15884(13)	0.026(1)
C(10)	0.3007(2)	0.22486(16)	0.26695(13)	0.025(1)
C(9)	0.2118(3)	0.45343(16)	0.39679(14)	0.031(1)
C(8)	0.3992(3)	0.16388(18)	0.09849(14)	0.032(1)
C(7)	0.2353(2)	0.20274(18)	0.16885(14)	0.031(1)
C(6)	0.7207(3)	0.24571(17)	-0.02595(13)	0.031(1)
C(5)	0.8704(3)	0.35664(19)	-0.06227(15)	0.038(1)
C(4)	0.2492(3)	-0.00837(17)	0.37231(15)	0.032(1)

C(3)	0.3217(3)	-0.11215(17)	0.46708(16)	0.035(1)
C(2)	0.6299(3)	0.2462(2)	-0.12525(15)	0.043(1)
C(1)	0.8254(3)	0.11566(19)	0.01826(15)	0.039(1)
H(1D)	0.3841	-0.0859	0.5911	0.053
H(19A)	0.2736	0.5829	0.4669	0.041
H(18A)	0.4996	0.3524	0.0228	0.032
H(17A)	0.0779	0.3566	0.2674	0.035
H(17B)	0.0249	0.2136	0.3506	0.035
H(16A)	0.1475	0.1437	0.5305	0.034
H(15A)	0.5292	0.3182	0.2967	0.030
H(15B)	0.4330	0.4061	0.1932	0.030
H(11A)	0.6922	0.1941	0.1999	0.031
H(11B)	0.7419	0.3452	0.1357	0.031
H(9A)	0.2148	0.5159	0.3264	0.037
H(8A)	0.3482	0.1537	0.0358	0.038
H(8B)	0.4520	0.0789	0.1403	0.038
H(7A)	0.1051	0.2123	0.1534	0.038
H(5A)	0.9711	0.3421	-0.1153	0.057
H(5B)	0.9291	0.3589	0.0000	0.057
H(5C)	0.8069	0.4399	-0.0948	0.057
H(4A)	0.2527	-0.0408	0.3113	0.038
H(4B)	0.1138	0.0134	0.3920	0.038
H(3A)	0.2578	-0.1965	0.4791	0.042
H(3B)	0.4628	-0.1226	0.4513	0.042
H(2A)	0.7307	0.2311	-0.1780	0.064
H(2B)	0.5697	0.3308	-0.1574	0.064

H(2C)	0.5316	0.1769	-0.1036	0.064
H(1A)	0.9237	0.1057	-0.0379	0.059
H(1B)	0.7316	0.0435	0.0405	0.059
H(1C)	0.8878	0.1147	0.0803	0.059

Table 1.23 Anisotropic displacement parameters $(Å)^2$ for *cis*-**1.22**. The anisotropic displacement factor exponent takes the form:
$-2\pi^2[h^2 a^{*2} U_{11} + ... + 2 h k a^* b^* U_{12}]$

	U_{11}	U_{22}	U_{33}	U_{23}	U_{13}	U_{12}
Cl(1)	0.0387(3)	0.0576(3)	0.0471(3)	-0.0317(2)	-0.0045(2)	-0.0023(2)
Cl(2)	0.0681(4)	0.0459(3)	0.0300(3)	-0.0049(2)	-0.0090(2)	0.0001(2)
O(2)	0.0221(6)	0.0235(6)	0.0315(6)	-0.0069(5)	-0.0044(4)	-0.0032(4)
O(1)	0.0287(6)	0.0333(6)	0.0393(7)	-0.0045(5)	-0.0070(5)	-0.0015(5)
C(19)	0.0326(9)	0.0275(8)	0.0419(10)	-0.0145(7)	0.0039(7)	-0.0019(7)
C(18)	0.0279(8)	0.0267(8)	0.0257(8)	-0.0080(6)	-0.0065(6)	0.0034(6)
C(17)	0.0220(8)	0.0317(8)	0.0316(9)	-0.0096(7)	-0.0037(6)	0.0018(6)
C(16)	0.0249(8)	0.0251(8)	0.0329(9)	-0.0084(7)	-0.0010(6)	-0.0006(6)
C(15)	0.0246(8)	0.0248(7)	0.0264(8)	-0.0093(6)	-0.0043(6)	-0.0021(6)
C(14)	0.0184(7)	0.0285(8)	0.0302(8)	-0.0095(6)	0.0001(6)	0.0018(6)
C(13)	0.0252(8)	0.0333(9)	0.0294(8)	-0.0076(7)	-0.0019(6)	0.0016(6)
C(12)	0.0215(8)	0.0377(9)	0.0364(9)	-0.0193(7)	-0.0001(6)	-0.0001(6)
C(11)	0.0237(8)	0.0291(8)	0.0254(8)	-0.0091(6)	-0.0026(6)	-0.0018(6)
C(10)	0.0232(8)	0.0261(8)	0.0267(8)	-0.0088(6)	-0.0054(6)	-0.0001(6)
C(9)	0.0302(9)	0.0268(8)	0.0312(9)	-0.0061(7)	0.0031(7)	0.0016(6)
C(8)	0.0331(9)	0.0349(9)	0.0316(9)	-0.0160(7)	-0.0066(7)	-0.0020(7)

C(7)	0.0231(8)	0.0422(10)	0.0329(9)	-0.0164(7)	-0.0085(7)	-0.0017(7)
C(6)	0.0361(9)	0.0303(8)	0.0232(8)	-0.0068(6)	-0.0047(7)	0.0073(7)
C(5)	0.0377(10)	0.0407(10)	0.0294(9)	-0.0058(8)	0.0013(7)	0.0016(8)
C(4)	0.0294(9)	0.0270(8)	0.0404(10)	-0.0117(7)	-0.0049(7)	-0.0067(7)
C(3)	0.0282(9)	0.0242(8)	0.0496(11)	-0.0085(8)	-0.0039(8)	-0.0023(6)
C(2)	0.0522(12)	0.0504(11)	0.0256(9)	-0.0131(8)	-0.0076(8)	0.0079(9)
C(1)	0.0469(11)	0.0361(10)	0.0323(9)	-0.0107(8)	-0.0043(8)	0.0151(8)

Table 1.24 Bond lengths [Å] for *cis*-**1.22**.

atom-atom	distance	atom-atom	distance
Cl(1)-C(12)	1.7290(18)	Cl(2)-C(13)	1.7377(18)
O(2)-C(4)	1.4320(19)	O(2)-C(10)	1.4527(19)
O(1)-C(3)	1.423(2)	C(19)-C(9)	1.379(3)
C(19)-C(12)	1.383(3)	C(18)-C(8)	1.535(2)
C(18)-C(11)	1.539(2)	C(18)-C(6)	1.552(2)
C(17)-C(14)	1.507(2)	C(17)-C(10)	1.545(2)
C(16)-C(13)	1.385(2)	C(16)-C(14)	1.391(2)
C(15)-C(10)	1.526(2)	C(15)-C(11)	1.531(2)
C(14)-C(9)	1.393(2)	C(13)-C(12)	1.389(3)
C(10)-C(7)	1.535(2)	C(8)-C(7)	1.527(2)
C(6)-C(5)	1.531(3)	C(6)-C(1)	1.535(2)
C(6)-C(2)	1.537(2)	C(4)-C(3)	1.508(3)

Table 1.25 Bond angles [°] for *cis*-**1.22**.

atom-atom-atom	angle	atom-atom-atom	angle
C(4)-O(2)-C(10)	117.05(12)	C(9)-C(19)-C(12)	120.11(16)
C(8)-C(18)-C(11)	107.52(13)	C(8)-C(18)-C(6)	114.44(14)
C(11)-C(18)-C(6)	114.63(14)	C(14)-C(17)-C(10)	115.93(13)
C(13)-C(16)-C(14)	120.77(15)	C(10)-C(15)-C(11)	113.86(13)
C(16)-C(14)-C(9)	118.05(16)	C(16)-C(14)-C(17)	120.93(15)
C(9)-C(14)-C(17)	121.00(15)	C(16)-C(13)-C(12)	120.32(16)
C(16)-C(13)-Cl(2)	118.72(13)	C(12)-C(13)-Cl(2)	120.96(14)
C(19)-C(12)-C(13)	119.37(16)	C(19)-C(12)-Cl(1)	119.22(14)
C(13)-C(12)-Cl(1)	121.39(14)	C(15)-C(11)-C(18)	111.51(13)
O(2)-C(10)-C(15)	104.13(12)	O(2)-C(10)-C(7)	111.77(13)
C(15)-C(10)-C(7)	110.00(13)	O(2)-C(10)-C(17)	110.87(13)
C(15)-C(10)-C(17)	111.66(13)	C(7)-C(10)-C(17)	108.41(13)
C(19)-C(9)-C(14)	121.36(16)	C(7)-C(8)-C(18)	110.93(14)
C(8)-C(7)-C(10)	113.60(14)	C(5)-C(6)-C(1)	108.53(16)
C(5)-C(6)-C(2)	108.05(15)	C(1)-C(6)-C(2)	108.32(16)
C(5)-C(6)-C(18)	109.85(14)	C(1)-C(6)-C(18)	112.15(14)
C(2)-C(6)-C(18)	109.84(15)	O(2)-C(4)-C(3)	108.93(14)
O(1)-C(3)-C(4)	110.82(14)		

Table 1.26 Torsion angles [°] for *cis*-**1.22**.

atom-atom-atom-atom	angle	atom-atom-atom-atom	angle
C(13)-C(16)-C(14)-C(9)	1.2(2)	C(13)-C(16)-C(14)-C(17)	-177.45(15)

C(10)-C(17)-C(14)-C(16)	-83.98(19)	C(10)-C(17)-C(14)-C(9)	97.40(18)
C(14)-C(16)-C(13)-C(12)	-0.4(3)	C(14)-C(16)-C(13)-Cl(2)	179.37(12)
C(9)-C(19)-C(12)-C(13)	1.4(3)	C(9)-C(19)-C(12)-Cl(1)	-177.21(13)
C(16)-C(13)-C(12)-C(19)	-0.9(3)	Cl(2)-C(13)-C(12)-C(19)	179.30(13)
C(16)-C(13)-C(12)-Cl(1)	177.69(13)	Cl(2)-C(13)-C(12)-Cl(1)	-2.1(2)
C(10)-C(15)-C(11)-C(18)	55.48(18)	C(8)-C(18)-C(11)-C(15)	-58.68(17)
C(6)-C(18)-C(11)-C(15)	172.86(13)	C(4)-O(2)-C(10)-C(15)	-167.88(13)
C(4)-O(2)-C(10)-C(7)	-49.17(18)	C(4)-O(2)-C(10)-C(17)	71.90(17)
C(11)-C(15)-C(10)-O(2)	70.67(16)	C(11)-C(15)-C(10)-C(7)	-49.24(18)
C(11)-C(15)-C(10)-C(17)	-169.65(13)	C(14)-C(17)-C(10)-O(2)	63.64(18)
C(14)-C(17)-C(10)-C(15)	-51.99(19)	C(14)-C(17)-C(10)-C(7)	-173.32(14)
C(12)-C(19)-C(9)-C(14)	-0.6(3)	C(16)-C(14)-C(9)-C(19)	-0.7(2)
C(17)-C(14)-C(9)-C(19)	177.96(15)	C(11)-C(18)-C(8)-C(7)	59.59(18)
C(6)-C(18)-C(8)-C(7)	-171.84(14)	C(18)-C(8)-C(7)-C(10)	-57.47(19)
O(2)-C(10)-C(7)-C(8)	-64.81(18)	C(15)-C(10)-C(7)-C(8)	50.35(19)
C(17)-C(10)-C(7)-C(8)	172.69(14)	C(8)-C(18)-C(6)-C(5)	178.06(14)
C(11)-C(18)-C(6)-C(5)	-57.04(18)	C(8)-C(18)-C(6)-C(1)	-61.2(2)
C(11)-C(18)-C(6)-C(1)	63.7(2)	C(8)-C(18)-C(6)-C(2)	59.33(19)
C(11)-C(18)-C(6)-C(2)	-175.77(15)	C(10)-O(2)-C(4)-C(3)	-167.50(14)
O(2)-C(4)-C(3)-O(1)	71.07(18)		

Table 1.27 Crystal data and structure refinement for *cis*-**1.35**.

Identification code	*cis*-**1.35**
Empirical formula	C19 H28 Cl2 O3
Formula weight	375.31

Temperature	296(2) K	
Wavelength	0.71073 Å	
Crystal system	Monoclinic	
Space group	P2(1)/n	
Unit cell dimensions	a = 16.1573(11) Å	α = 90°
	b = 6.3264(4) Å	β = 111.8800(10)°
	c = 20.9453(14) Å	γ = 90°
Volume	1986.8(2) $Å^3$	
Z	4	
Density (calculated)	1.255 $g.cm^{-3}$	
Absorption coefficient (μ)	0.340 mm^{-1}	
F(000)	800	
Crystal size	0.15 × 0.09 × 0.08 mm^3	
ω range for data collection	2.00 to 27.10°	
Index ranges	$-20 \le h \le 20$, $-8 \le k \le 8$, $-26 \le l \le 26$	
Reflections collected	19733	
Independent reflections	4365 [R_{int} = 0.0168]	
Completeness to θ = 27.10°	99.7 %	
Absorption correction	Empirical	
Max. and min. transmission	0.7459 and 0.7103	
Refinement method	Full-matrix least-squares on F^2	
Data / restraints / parameters	4365 / 0 / 217	
Goodness-of-fit on F^2	1.061	
Final R indices [I>2σ(I)]	R_1 = 0.0499, wR_2 = 0.1538	
R indices (all data)	R_1 = 0.0580, wR_2 = 0.1622	
Largest diff. peak and hole	0.513 and -0.539 $e^-.Å^{-3}$	

Table 1.28 Atomic coordinates and equivalent isotropic displacement parameters ($Å^2$) for *cis*-**1.35**. U(eq) is defined as one third of the trace of the orthogonalized U_{ij} tensor.

	x	y	z	U(eq)
Cl(1)	0.61079(4)	0.12720(10)	0.05732(3)	0.062(1)
Cl(2)	0.63383(6)	-0.32424(12)	0.00270(3)	0.080(1)
O(3)	0.93873(9)	0.2636(2)	0.23405(7)	0.051(1)
O(2)	1.37414(10)	0.4302(3)	0.47890(8)	0.062(1)
C(19)	1.15911(12)	0.1841(3)	0.36116(9)	0.041(1)
C(18)	0.96371(12)	0.1028(3)	0.28538(9)	0.041(1)
O(1)	1.41973(11)	0.3149(3)	0.59284(8)	0.069(1)
C(17)	0.75313(12)	0.0287(3)	0.17029(9)	0.042(1)
C(16)	0.88045(13)	-0.0240(4)	0.28205(10)	0.056(1)
C(15)	0.69592(12)	-0.0380(3)	0.10600(9)	0.042(1)
C(14)	1.03574(12)	-0.0369(3)	0.27701(11)	0.048(1)
C(13)	1.08772(14)	0.3341(4)	0.36602(11)	0.055(1)
C(12)	0.82162(12)	-0.1003(3)	0.21186(10)	0.045(1)
C(11)	0.70646(14)	-0.2372(3)	0.08228(11)	0.048(1)
C(10)	1.12287(13)	0.0811(4)	0.28969(11)	0.049(1)
C(9)	0.83130(14)	-0.2990(4)	0.18687(13)	0.055(1)
C(8)	1.00091(13)	0.2187(4)	0.35430(10)	0.058(1)
C(7)	1.25286(13)	0.2867(4)	0.38099(10)	0.048(1)
C(6)	0.77472(17)	-0.3658(3)	0.12279(14)	0.059(1)
C(5)	1.28458(14)	0.3518(5)	0.45615(11)	0.059(1)

C(4)	1.40741(16)	0.4866(5)	0.54819(12)	0.068(1)
C(3)	1.2508(2)	0.4813(7)	0.33764(16)	0.101(1)
C(2)	1.4862(2)	0.1708(6)	0.58930(17)	0.097(1)
C(1)	1.31903(17)	0.1249(6)	0.3739(2)	0.101(1)
H(3D)	0.9368	0.2138	0.1974	0.076
H(19A)	1.1652	0.0707	0.3945	0.049
H(17A)	0.7456	0.1622	0.1859	0.051
H(16A)	0.9000	-0.1457	0.3121	0.067
H(16B)	0.8450	0.0639	0.3001	0.067
H(14A)	1.0140	-0.0946	0.2308	0.057
H(14B)	1.0474	-0.1543	0.3089	0.057
H(13A)	1.1088	0.3996	0.4111	0.066
H(13B)	1.0772	0.4451	0.3320	0.066
H(10A)	1.1129	0.1894	0.2548	0.058
H(10B)	1.1669	-0.0169	0.2857	0.058
H(9A)	0.8766	-0.3881	0.2138	0.066
H(8A)	0.9569	0.3200	0.3564	0.069
H(8B)	1.0106	0.1173	0.3911	0.069
H(6A)	0.7480	-0.4974	0.1292	0.071
H(6B)	0.8113	-0.3991	0.0965	0.071
H(5A)	1.2456	0.4607	0.4618	0.071
H(5B)	1.2821	0.2312	0.4840	0.071
H(4A)	1.4202	0.6254	0.5633	0.082
H(3A)	1.3097	0.5398	0.3514	0.151
H(3B)	1.2111	0.5846	0.3442	0.151
H(3C)	1.2302	0.4421	0.2900	0.151

H(2A)	1.4929	0.0571	0.6212	0.145
H(2B)	1.5420	0.2437	0.6008	0.145
H(2C)	1.4683	0.1150	0.5435	0.145
H(1A)	1.3767	0.1892	0.3864	0.152
H(1B)	1.2992	0.0767	0.3271	0.152
H(1C)	1.3227	0.0070	0.4037	0.152

Table 1.29 Anisotropic displacement parameters $(Å)^2$ for *cis*-**1.35**. The anisotropic displacement factor exponent takes the form:
$-2\pi^2[h^2 a^{*2} U_{11} + ... + 2 h k a^* b^* U_{12}]$

	U_{11}	U_{22}	U_{33}	U_{23}	U_{13}	U_{12}
Cl(1)	0.0603(3)	0.0636(4)	0.0487(3)	0.0043(2)	0.0037(2)	0.0118(2)
Cl(2)	0.1095(6)	0.0663(4)	0.0585(4)	-0.0208(3)	0.0229(4)	-0.0203(4)
O(3)	0.0562(8)	0.0437(7)	0.0432(7)	0.0078(6)	0.0074(6)	0.0076(6)
O(2)	0.0450(8)	0.0935(13)	0.0465(8)	-0.0091(8)	0.0146(6)	-0.0121(8)
C(19)	0.0390(9)	0.0484(10)	0.0370(9)	0.0037(7)	0.0154(7)	0.0050(7)
C(18)	0.0370(8)	0.0493(10)	0.0339(8)	0.0070(7)	0.0119(7)	0.0094(7)
O(1)	0.0580(9)	0.1027(14)	0.0446(8)	-0.0105(9)	0.0156(7)	0.0190(9)
C(17)	0.0415(9)	0.0417(10)	0.0438(9)	-0.0014(8)	0.0163(8)	0.0020(7)
C(16)	0.0412(10)	0.0839(16)	0.0409(10)	0.0131(10)	0.0135(8)	-0.0004(10)
C(15)	0.0417(9)	0.0425(10)	0.0407(9)	0.0031(7)	0.0156(7)	-0.0004(7)
C(14)	0.0424(10)	0.0409(10)	0.0572(11)	-0.0023(8)	0.0159(8)	0.0056(8)
C(13)	0.0453(10)	0.0713(14)	0.0438(10)	-0.0172(10)	0.0126(8)	0.0096(10)
C(12)	0.0373(9)	0.0522(11)	0.0477(10)	0.0103(8)	0.0180(8)	0.0003(8)
C(11)	0.0571(11)	0.0423(10)	0.0488(10)	-0.0044(8)	0.0252(9)	-0.0087(9)

C(10)	0.0427(10)	0.0548(11)	0.0518(11)	-0.0127(9)	0.0219(8)	0.0012(8)
C(9)	0.0481(11)	0.0468(11)	0.0737(14)	0.0169(10)	0.0256(10)	0.0078(9)
C(8)	0.0397(10)	0.0939(17)	0.0391(10)	-0.0115(11)	0.0142(8)	0.0096(10)
C(7)	0.0425(10)	0.0624(12)	0.0406(10)	-0.0031(9)	0.0179(8)	-0.0023(9)
C(6)	0.0697(14)	0.0386(11)	0.0826(16)	-0.0003(10)	0.0433(13)	-0.0022(10)
C(5)	0.0413(10)	0.0913(17)	0.0430(11)	-0.0056(11)	0.0145(8)	-0.0067(10)
C(4)	0.0600(13)	0.0810(18)	0.0535(13)	-0.0207(12)	0.0104(10)	-0.0039(12)
C(3)	0.086(2)	0.130(3)	0.0707(18)	0.0352(19)	0.0122(15)	-0.044(2)
C(2)	0.081(2)	0.130(3)	0.0733(18)	-0.0097(18)	0.0222(15)	0.042(2)
C(1)	0.0404(12)	0.133(3)	0.128(3)	-0.068(2)	0.0288(15)	-0.0045(15)

Table 1.30 Bond lengths [Å] for *cis*-**1.35**.

atom-atom	distance	atom-atom	distance
Cl(1)-C(15)	1.7258(19)	Cl(2)-C(11)	1.732(2)
O(3)-C(18)	1.425(2)	O(2)-C(4)	1.393(3)
O(2)-C(5)	1.433(2)	C(19)-C(13)	1.526(3)
C(19)-C(10)	1.534(3)	C(19)-C(7)	1.555(3)
C(18)-C(14)	1.522(3)	C(18)-C(8)	1.529(3)
C(18)-C(16)	1.545(3)	O(1)-C(4)	1.399(4)
O(1)-C(2)	1.432(3)	C(17)-C(15)	1.385(3)
C(17)-C(12)	1.389(3)	C(16)-C(12)	1.502(3)
C(15)-C(11)	1.388(3)	C(14)-C(10)	1.527(3)
C(13)-C(8)	1.518(3)	C(12)-C(9)	1.393(3)
C(11)-C(6)	1.379(3)	C(9)-C(6)	1.379(4)
C(7)-C(5)	1.520(3)	C(7)-C(3)	1.523(4)

C(7)-C(1) 1.527(3)

Table 1.31 Bond angles [°] for *cis*-**1.35**.

atom-atom-atom	angle	atom-atom-atom	angle
C(4)-O(2)-C(5)	112.64(17)	C(13)-C(19)-C(10)	107.82(15)
C(13)-C(19)-C(7)	114.07(17)	C(10)-C(19)-C(7)	114.66(15)
O(3)-C(18)-C(14)	109.95(15)	O(3)-C(18)-C(8)	105.72(17)
C(14)-C(18)-C(8)	109.80(15)	O(3)-C(18)-C(16)	109.85(15)
C(14)-C(18)-C(16)	112.56(18)	C(8)-C(18)-C(16)	108.71(16)
C(4)-O(1)-C(2)	112.5(2)	C(15)-C(17)-C(12)	121.16(18)
C(12)-C(16)-C(18)	115.69(16)	C(17)-C(15)-C(11)	119.88(18)
C(17)-C(15)-Cl(1)	119.09(15)	C(11)-C(15)-Cl(1)	121.02(15)
C(18)-C(14)-C(10)	113.04(17)	C(8)-C(13)-C(19)	111.47(19)
C(17)-C(12)-C(9)	118.00(19)	C(17)-C(12)-C(16)	119.36(19)
C(9)-C(12)-C(16)	122.62(19)	C(6)-C(11)-C(15)	119.48(19)
C(6)-C(11)-Cl(2)	120.27(17)	C(15)-C(11)-Cl(2)	120.24(17)
C(14)-C(10)-C(19)	111.66(16)	C(6)-C(9)-C(12)	121.0(2)
C(13)-C(8)-C(18)	113.45(16)	C(5)-C(7)-C(3)	108.8(2)
C(5)-C(7)-C(1)	107.7(2)	C(3)-C(7)-C(1)	110.2(3)
C(5)-C(7)-C(19)	107.98(15)	C(3)-C(7)-C(19)	112.03(18)
C(1)-C(7)-C(19)	110.0(2)	C(9)-C(6)-C(11)	120.4(2)
O(2)-C(5)-C(7)	110.32(16)	O(2)-C(4)-O(1)	113.6(2)

Table 1.32 Torsion angles [°] for *cis*-**1.35**.

atom-atom-atom-atom	angle	atom-atom-atom-atom	angle
O(3)-C(18)-C(16)-C(12)	49.2(2)	C(14)-C(18)-C(16)-C(12)	-73.7(2)
C(8)-C(18)-C(16)-C(12)	164.41(19)	C(12)-C(17)-C(15)-C(11)	0.2(3)
C(12)-C(17)-C(15)-Cl(1)	178.80(14)	O(3)-C(18)-C(14)-C(10)	64.8(2)
C(8)-C(18)-C(14)-C(10)	-51.1(2)	C(16)-C(18)-C(14)-C(10)	-172.34(16)
C(10)-C(19)-C(13)-C(8)	58.1(2)	C(7)-C(19)-C(13)-C(8)	-173.29(16)
C(15)-C(17)-C(12)-C(9)	0.2(3)	C(15)-C(17)-C(12)-C(16)	-178.24(17)
C(18)-C(16)-C(12)-C(17)	-89.1(2)	C(18)-C(16)-C(12)-C(9)	92.6(2)
C(17)-C(15)-C(11)-C(6)	-0.8(3)	Cl(1)-C(15)-C(11)-C(6)	-179.40(16)
C(17)-C(15)-C(11)-Cl(2)	178.65(15)	Cl(1)-C(15)-C(11)-Cl(2)	0.1(2)
C(18)-C(14)-C(10)-C(19)	56.4(2)	C(13)-C(19)-C(10)-C(14)	-58.0(2)
C(7)-C(19)-C(10)-C(14)	173.72(17)	C(17)-C(12)-C(9)-C(6)	0.1(3)
C(16)-C(12)-C(9)-C(6)	178.44(19)	C(19)-C(13)-C(8)-C(18)	-56.9(3)
O(3)-C(18)-C(8)-C(13)	-67.1(2)	C(14)-C(18)-C(8)-C(13)	51.5(3)
C(16)-C(18)-C(8)-C(13)	175.05(19)	C(13)-C(19)-C(7)-C(5)	63.1(2)
C(10)-C(19)-C(7)-C(5)	-171.84(19)	C(13)-C(19)-C(7)-C(3)	-56.6(3)
C(10)-C(19)-C(7)-C(3)	68.4(3)	C(13)-C(19)-C(7)-C(1)	-179.5(2)
C(10)-C(19)-C(7)-C(1)	-54.5(3)	C(12)-C(9)-C(6)-C(11)	-0.7(3)
C(15)-C(11)-C(6)-C(9)	1.1(3)	Cl(2)-C(11)-C(6)-C(9)	-178.39(17)
C(4)-O(2)-C(5)-C(7)	-178.3(2)	C(3)-C(7)-C(5)-O(2)	-63.4(3)
C(1)-C(7)-C(5)-O(2)	56.1(3)	C(19)-C(7)-C(5)-O(2)	174.83(19)
C(5)-O(2)-C(4)-O(1)	67.3(3)	C(2)-O(1)-C(4)-O(2)	64.5(3)

References

[1] Tall, A. R.; Yvan-Charvet, L.; Wang, N. *Arterioscler. Thromb. Vasc. Biol.* **2007**, *27*, 257-260.

[2] Miller, G. *Science* **2010**, *329*, 502-504.

[3] Hughes, T. R. *Funct. Integr. Genomics* **2002**, *2*, 199-211.

[4] Norris, J. R.; Ribbons, D. W., Eds.; Yeast Gene Analysis, Volume 36, Methods in Microbiology; Academic Press: London, **2007**.

[5] Giaever, G.; Chu, A. M.; Ni, L.; Connelly, C.; Riles, R.; Véronneau, S.; Dow, S.; Lucau-Danila, A.; Anderson, K.; André, B.; Arkin, A. P.; Astromoff, A.; El Bakkoury, M.; Bangham, R.; Benito, R.; Brachat, S.; Campanaro, S.; Curtiss, M.; Davis, K.; Deutschbauer, A.; Entian, K.-D.; Flaherty, P.; Foury, F.; Garfinkel, D. J.; Gerstein, M.; Gotte, D.; Güldener, U.; Hegemann, J. H.; Hempel, S.; Herman, Z.; Jaramillo, D. F.; Kelly, D. E.; Kelly, S. L.; Kötter, P.; LaBonte, D.; Lamb, D. C.; Lan, N.; Liang, H.; Liao, H.; Liu, L.; Luo, C.; Lussier, M.; Mao, R.; Menard, P.; Ooi, S. L.; Revuelta, J. L.; Roberts, C. J.; Rose, M.; Ross-Macdonald, P.; Scherens, B.; Schimmack, G.; Shafer, B.; Shoemaker, D. D.; Sookhai-Mahadeo, S.; Storms, R. K.; Strathern, J. N.; Valle, G.; Voet, M.; Volckaert, G.; Wang, C.-Y.; Ward, T. R.; Wilhelmy, J.; Winzeler, E. A.; Yang, Y.; Yen, G.; Youngman, E.; Yu, K.; Bussey, H.; Boeke, J. D.; Snyder, M.;Philippsen, P.; Davis, R. W.; Johnston, M. *Nature*, **2002**, *418*, 387-391.

[6] Winzeler, E. A.; Shoemaker, D. D.; Astromoff, A.; Liang, H.; Anderson, K.; André, B.; Bangham, R.; Benito, R.; Boeke, J. D.; Bussey, H.; Chu, A. M.; Connelly, C.; Davis, K.; Dietrich, F.; Dow, S. W.; El Bakkoury, M.; Foury, F.; Friend, S. H.; Gentalen, E.; Giaever, G.; Hegemann, J. H.; Jones, T.; Laub, M.; Liao, H.; Liebundguth, N.; Lockhart, D. J.; Lucau-Danila, A.; Lussier, M.; M'Rabet, N.; Menard, P.; Mittmann, M.; Pai, C.; Rebischung, C.; Revuelta, J. L.; Riles, L.; Roberts, C. J.; Ross-MacDonald, P.; Scherens, B.; Snyder, M.; Sookhai-Mahadeo, S.; Storms, R. K.; Véronneau, S.; Voet, M.; Volckaert, G.; Ward, T. R.; Wysocki, R.; Yen, G. S.; Yu, K.; Zimmermann, K.; Philippsen, P.; Johnston, M.; Davis, R. W. *Science*, **1999**, *285*, 901-906.

[7] Tong, A. H.; Lesage, G.; Bader, G. D.; Ding, H.; Xu, H.; Xin, X.; Young, J.; Berriz, G. F.; Brost, R. L.; Chang, M.; Chen, Y.; Cheng, X.; Chua, G.; Friesen, H.; Goldberg, D. S.; Haynes, J.; Humphries, C.; He, G.; Hussein, S.; Ke, L.; Krogan, N.; Li, Z.; Levinson, J. N.; Lu, H.; Ménard, P.; Munyana, C.; Parsons, A. B.; Ryan, O.; Tonikian, R.; Roberts, T.; Sdicu, A.-M.; Shapiro, J.; Sheikh, B.; Suter, B.; Wong, S. L.; Zhang, L. V.; Zhu, H.; Burd, C. G.; Munro, S.; Sander, C.; Rine, J.; Greenblatt, J.; Peter, M.; Bretscher, R.; Bell, G.; Roth, F. P.; Brown, G. W.; Andrews, B.; Bussey, H.; Boone, C. *Science* **2004**, *303*, 808-813.

[8] Tamble, C. M.; St. Onge, R. P.; Giaever, G.; Nislow, C.; Williams, A. G.; Stuart, J. M.; Lokey, R. S. *Mol. Biosyst.* **2011**, *7*, 2019-2030.

[9] Gassner, N. C.;Tamble, C. M.; Bock, J. E.; Cotton, N.; White, K. N.; Tenney, K.; St. Onge, R. P.; Proctor, M. J.; Giaever, G.; Davis, R. W.; Crews, P.; Holman, T. R.; Lokey, R. S. *J. Nat. Prod.* **2007,** *70,* 383-390.

[10] Parsons, A. B.; Lopez, A.; Givoni, I. E.; Williams, D. E.; Gray, C. A.; Porter, J.; Chua, G.; Sopko, R.; Brost, R. L.; Ho, C.-H.; Wang, J.; Ketela, T.; Brenner, C.; Brill, J. A.; Fernandez, G. E.; Lorenz, T. C.; Payne, G. S.; Ishihara, S.; Ohya, Y.; Andrews, B.; Hughes, T. R.; Frey, B. J.; Graham, T. R.; Andersen, R. J.; Boone, C. *Cell* **2006**, *126*, 611-625.

[11] Lum, P. K.; Armour, C. D.; Stepaniante, S. B.; Cavet, G.; Wolf, M. K.; Butler, J. S.; Hinshaw, J. S.; Garnier, P.; Prestwich, G. D.; Leonardson, A.; Garrett-Engele, P.; Rush, C. M.; Bard, M.; Schimmack, G.; Phillips, J. W.; Roberts, C. J.; Shoemaker, D. D. *Cell*, **2004**, 121-137.

[12] Cardenas, M. E.; Cruz, M. C.; Del Poeta, M.; Chung, N.; Perfect, J. R.; Heitman, J. *Clin. Microbiol. Rev.* **1999**, *12*, 583-611.

[13] Professor Ronald W. Davis website: http://genomics.Stanford.edu/

[14] Professor Joshua M. Stuart website: http://sysbio.soe.ucsc.edu/

[15] Mendes-Pereira, A. M.; Sims, D.; Dexter, T.; Fenwick, K.; Assiotis, I.; Kozarewa, I.; Mitsopoulos, C.; Hakas, J.; Zvelebil, M.; Lord, C. J.; Ashworth, A. *Proc. Natl. Acad. Sci. USA* **2011**, *Early Edition*.

[16] Professor Grant A. Hartzog website: mcd.ucsc.edu/faculty/hartzog.html

[17] Ward, H. W. C. *Br. Med. J.* **1973**, *1*, 13-14.

[18] Lerner, L. J.; Holthaus, J. F.; Thompson, C. R.; *Endocrinology* **1958**, *63*, 295-318.

[19] Jordan, V. C. *Breast Cancer Res. Treat.* **1988**, *11*, 197-209.

[20] Pandey, R. J.; Wakharkar, R. D.; Kumar, P. *Synth. Commun.* **2005**, *35*, 2795-2800.

[21] Itami, K.; Kamei, T.; Yoshida, J. *J. Am. Chem. Soc.* **2003**, *125*, 14670-14671.

[22] Robertson, D. W.; Katzenellenbogen, J. A. *J. Org. Chem.* **1982**, *47*, 2387-2393.

[23] Robertson, D. W.; Katzenellenbogen, J. A.; Long, D. J.; Rorke, E. A.; Katzenellenbogen, B. S. *J. Steroid Biochem.* **1982**, *16*, 1-13.

[24] Patterson, J.; Furr, M. B. B.; Wakeling, A.; Battersby, L. *Breast Cancer Res. Treat.* **1982**, *2*, 363-374.

[25] Jordan, V. C.; Jaspan, T. *J. Endocrinol.* **1976**, *68*, 453-460.

[26] Fisher, B.; Constantino, J. P.; Wickerham, D. L.; Redmond, C.; Kovanah, M.; Cronin, W. M.; Vogel, V.; Robidoux, A.; Dimitrov, N.; Atkins, J.; Daly,

M.; Wiend, S.; T.-C., E.; Ford, L.; Wolmark, N. *J. Natl. Cancer Inst* **1998**, *90*, 1371-1388.

[27] McDonald, C. C.; Alexander, F. E.; Whyte, B. W.; Forest, A. P. Steward, H. J.; *Br. Med. J.***1995***, 311*, 977-980.

[28] Jordan, V. C.; Morrow, M. *Endocr. Rev.* **1999**, *20*, 253-278.

[29] Osborne, C. K.; Coronado, E.; Allred, D. C.; Wiebe, V.; DeGregorio, M. *J. Natl. Cancer Inst.* **1991**, *83*, 1477-1482.

[30] Couldwell, W. T.; Hinton, D. R.; He, S.; Chen, T. C.; Sebat, I.; Weiss, M. H.; Law, R. E. *FEBS Lett.* **1994**, *345, 43-46.*

[31] Madani, N. D.; Malloy, P. J.; Rodriguez-Pombo, P.; Krishnan, A. V.; Feldman, D. *Microbiology* **1994**, *91*, 922-926.

[32] Burshell, A.; Stathis, P. A.; Do, Y.; Miller, S. C.; Feldman, D. *J. Biol. Chem.* **1984**, *259*, 3450-3456.

[33] Gottardis, M. M.; Robinson, S. P.; Satyaswaroop, P. G.; Jordan, V. C. *Cancer Res.* **1988**, *48*, 812-815.

[34] Bok, P. R.; Sambanis, A. British Patent 1 549 122, **1979**.

[35] Hay, M. P.; Pchalek, K.; Prujin, F. B.; Hicks, K. O.; Slim, B. G.; Anderson, R. F.; Shinde, S. S.; Phillips, V.; Denny, W. A.; Wilson, W. R. *J. Med. Chem.* **2007**, *50*, 6654-6664.

[36] Kim, S.-H.; Rieke, R. D. *J. Org. Chem.* **2000**, *65*, 2322-2330.

[37] Harvey, S.; Junk, P. C.; Raston, C. L.; Salem, G. *J. Org. Chem.* **1988**, *53*, 3134-3140.

[38] Piller, F. M.; Metzger, A.; Schade, M. A.; Haag, B. A.; Gavryushin, A.; Knochel, P. *Eur. J. Org. Chem.* **2009**, *15*, 7192-7202.

[39] Metzger, A.; Piller, F. M.; Knochel, P. *Chem. Commun.* **2008**, 5824-5826.

[40] Hall, L. A. R.; Stephens, V. C.; Burckhalter, J. H. *Org. Syn.* **1951**, *31*.

[41] Schenone, S.; Bruno, O.; Ranise, A.; Bondavalli, F.; Cenicola, M. L.; Losasso, C.; Carnevale, M.; Ottavo, R.; D'Antonio, M. *Farmaco* **1990**, *12*, 1309-1325.

[42] Sauer, E. L. O.; Hooper, J.; Woo, T.; Barriault, L. *J. Am. Chem. Soc.* **2007**, *129*, 2112-2119.

[43] Zhang, Y.-L.; Shing, T. K. M. *J. Org. Chem.* **1997**, *62*, 2622-2624.

[44] Sharpless, K. B.; Amberg, W.; Bennani, Y. L. Crispino, G. A.; Hartung, J.; Jeong, K.-Y.; Kwong, H.-L.; Morikawa, K.; Wang, S.-M.; Xu, D.; Zhang, X.-L. *J. Org. Chem.* **1992**, *57*, 2768-2771

[45] Fuwa, H.; Ishigai, K.; Goto, T.; Suzuki, A.; Sasaki, M. *J. Org. Chem.* **2009**, *74*, 4024-4040.

[46] Marshall, J. A.; Andersen, N. H.; Schlicher, J. W. *J. Org. Chem.* **1970**, *35*, 858-861.

[47] Sato, S.; Murata, A.; Shirakawa, T.; Uesugi, M. *Chem. Biol.* **2010**, *17*, 616-623.

[48] Diamandis, E. P.; Christopoulos, T. K. *Clin. Chem.* **1991**, *37*, 625-636.

[49] Moore, L. L.; Fulton, A. M.; Harrison, M. L.; Geahlen, R. L. *J. Proteome Res.* **2004**, *3*, 1184-1190.

[50] Engel, P. S.; Schexnayder, M. A. *J. Am. Chem. Soc.* **1975**, *97*, 145–153.

[51] Carson, C. A.; Kerr, M. A. *Org. Lett.* **2009**, *11*, 777–779.

[52] Gromov, A.; Enev, V.; Mulzer, J. *Org. Lett.* **2009**, *11*, 2884–2886.

[53] Ferrié, L.; Boulard, L.; Pradaux, F.; Bouzbouz, S.; Reymond, S.; Capdevielle, P.; Cossy, J. *J. Org. Chem.* **2008**, *73*, 1864–1880.

[54] Quan,T. K.; Zuckerman, N. B.; Bray, W. M.; Weber, R. J.; Roguev, A.; Krogan, N.J.; Li, R.; Stuart, J. M.; Konopelski, J. P.; Hartzog, G. A.; Lokey, R. S. *Manuscript in Progress* **2011**.

[55] Zuckerman, N. B.; Myers, A. S.; Quan, T. K.; Bray, W. M.; Lokey, R. S.; Hartzog, G. M.; Konopelski, J. P. *ChemMedChem*, **2012**, accepted.

[56] Torok, D. S.; Figueroa, J. J.; Scott, W. J. *J. Org. Chem.* **1993**, *58*, 7274-7276.

[57] Brachmann, C. B.; Davies, A.; Cost, G. J.; Caputo, E.; Li, J.; Hieter, P.; Boeke, J. D. *Yeast* **1998**, *14*, 115-132.

CHAPTER 2: Nanoparticle Mediated Electronic Communication

2.1 Monolayer Protected Clusters: Stabilized Nanoparticles

It is widely accepted that materials at the molecular level have different properties than those same substances at the macro scale. A glaring indication of this fact is exhibited by the powerful catalytic transformations performed by gold salts and complexes,[1] while bulk gold is entirely noble with its classical uses in electronics, currency and jewelry (Figure 2.1). Between the molecular and bulk scale are colloidal species, or nanoparticles (NPs), which also exhibit different properties than their dimensional counterparts. In particular, metal NPs are of great interest due to new electronic, catalytic, optical and physical properties exhibited by these species. However, Brust et al. greatly expanded the potential of metal NPs in 1994 with the advent of thiol-stabilized gold NPs described in their seminal publication.[2]

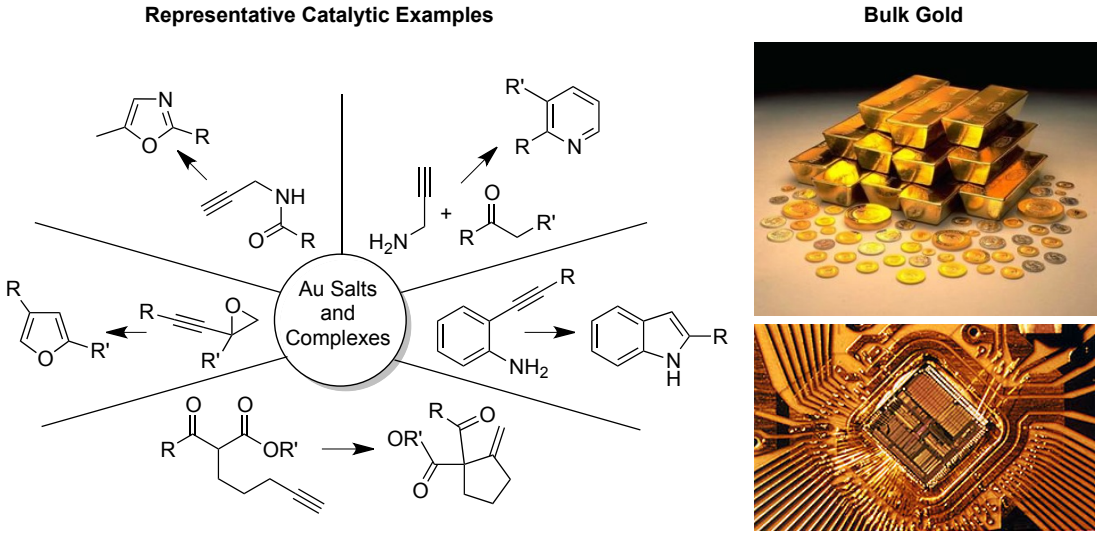

Figure 2.1 Utility of Gold salts and complexes at the molecular level leading to complex organic transformations vs. bulk gold which is stable for everyday use as currency and electronic components.

Stable colloidal species can be prepared and suspended in solution, and these materials have great utility. However, over time, aggregation can occur leading to precipitation and loss of the original intended use. More specifically, metal NPs can be prepared in various sizes in solution, but these "naked" spheres cannot be re-suspended if the solvent is evaporated due to irreversible aggregation. By taking advantage of the strong thiolate/gold interaction, Brust et al. dramatically increased the robustness of gold NPs by encapsulating the metal surface with an organic soluble long-chain monolayer (monolayer protected clusters, or MPCs). These particles can be suspended, dried, and re-suspended multiple times with minimal aggregation. Additionally, this method provided for particle size control and a route to introduce a seemingly endless variety of functionality opposite the thiolate-gold linkage directly, by ligand exchange, or solution phase reactions (Scheme 2.1). Since this first publication, other metal MPCs including, but not limited to, Pt,[3] Ag,[4] and Cu[5] have been successfully protected with thiolate ligands.

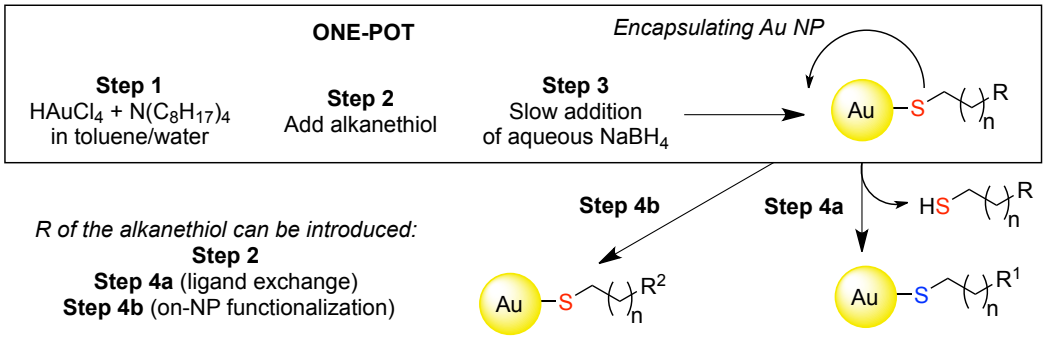

Scheme 2.1 Brust Method Schematic Representation of the Brust method of gold nanoparticle synthesis and the varied means for changing the ligands.

The principle of MPC chemistry has expanded from the use of thiols as ligands toward taking advantage of an element's affinity for different functionalities. As is always the case in nanotechnology research, the impetus for changing the interfacial linkage between ligand and metal is due to a change in material properties. Yang et al. investigated the importance of the monolayer interfacial interaction regarding the particle size and ligand dependence of Pt nanoparticles toward catalytic electro-oxidation of methanol.[6] They found the reaction of interest proceeded more efficiently with the more loosely bound amine ligand as the particle size increased. This was in contrast to a reduced activity as the size increased for thiol-protected Au NPs. Although size and shape can be modified to alter NP properties, this is finite in comparison with the ability to alter the interfacial bonding interaction (arguably more tunable as well). Again, using Au NPs as an example, they not only have a strong affinity for thiolates, but also toward *N*-heterocyclic carbenes (NHC)[7] and alkynes.[8] The electronics of NHC and phosphine ligands in particular can be greatly altered by their own ligand make-up (electron withdrawing/donating capabilities) adding another avenue to fine-tune the ligand-metal interaction.

Changing the ligand or altering its affinity towards the metal NP surface is often independent of the ability to decorate MPCs with interesting compounds ranging from fluorophores (detection of chemical warfare agents),[9] biological compounds (therapeutic applications),[10] and a vast variety

of functional groups.[11] Attaching interesting groups to the exterior end of the protecting ligand of MPCs (Figure 2.2) allows for the development of sensors, devices, and electronic components toward a wide variety of applications. In general, thiolate MPCs functionalized with a fluorophore do not act much differently than the same monomeric molecule in solution due to the lack of interaction between the metal core and the fluorophore. This is due to the fact that the insulating linker between the sulfur atom and the fluorophore disables the interaction between fluorophore and NP. This poses a legitimate question. What if generating a direct interaction between the NP core and the appended molecule of interest can expand the field of MPC studies further? What new properties develop when this molecule of interest is conjugated to other molecules on the same NP? Those are the questions our collaborator, Professor Shaowei Chen proposed, and to which we are involved to help answer.[12]

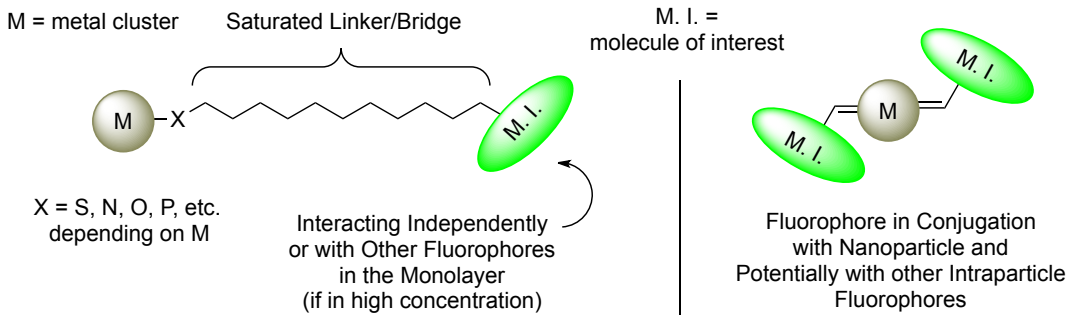

Figure 2.2 MPCs with saturated linkers between the molecules of interest vs. the proposed MPC, whereby molecules of interest are conjugated through the nanoparticle core to one another.

The collaborative partners in the following studies provided expertise in nanoparticle synthesis/analytical characterization (Shaowei Chen group,

UCSC Chemistry),[13] theoretical calculations (Haobin Wang group, New Mexico State University),[14] and organic synthesis (Konopelski group, UCSC Chemistry).

The umbrella for which this idea falls under is coined, “nanoparticle-mediated electronic communcation,”[12] (NPMEC) and the model system is that of the carbene-stabilized ruthenium nanoparticle (Ru NP or Ru MPC).[15] Following the report by Tulevski et al.[16] that described Ru thin-film surfaces undergoing reaction with diazomethane, a postdoc in our lab, Dr. James R. Davies, synthesized a custom diazoacetate ligand for the purpose of generating Ru MPCs in collaboration with the Chen group. Dr. Davies prepared octyldiazoacetate (ODA), whereby the diazo group is stabilized by the acetate functionality, and the eight-carbon chain is long enough to provide a suitable protecting layer for the Ru metal cluster. Just like thiolate or otherwise protected MPCs, ODA protected Ru NPs are soluble in non-polar solvents such as dichloromethane, toluene, and hexanes. The most interesting aspect of ODA protected Ru NPs (Ru=C8 NPs) is of course the carbene interfacial linkage between the ligand and the NP surface, which allows for ligand exchange with other terminal olefins by a metathesis reaction (Nobel Prize in chemistry, 2005). Chen et al. described in the seminal publication on carbene-stabilized Ru NPs[15] that the rate at which the ligand exchange reaction occurred was nearly twice as fast as thiol exchange with Au NPs. Finally, to the point of our collaborative research on NP-

mediated electronic communication, the efficient exchange of olefins onto the Ru=C8 NPs allows for the introduction of interesting and complex molecules with the possibility of conjugation to the Ru core via the carbene linkage.

2.1.1 Synthesis, Ligand Exchange, and Basic Characterization of Ru ODA NPs

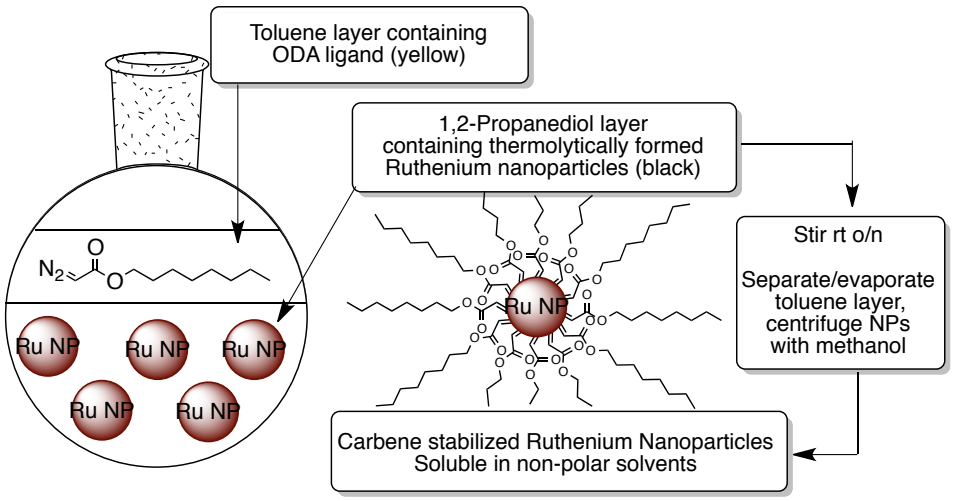

Figure 2.3 Ru ODA NP (Ru=C8) synthesis and purification.

The preparation of carbene-stabilized Ru NPs was developed in the Chen lab (Figure 2.3) and followed a procedure by Viau et al.[17] A solution of $RuCl_3$ was heated to 165 ^oC in 1,2-propanediol in the presence of three equivalents of sodium acetate. During the reaction, distinct color changes occurred evolving a dark brown/black solution that indicated the creation of "naked" Ru NPs via a thermolytic reduction of the $RuCl_3$ salt. The reaction was cooled to room temperature and vigorous stirring was continued along with the addition of three equivalents of ODA in toluene. After stirring the biphasic solution overnight in the dark, the mixture was allowed to settle and

the reaction was judged to be complete when the diol layer was clear. Separation of the black organic layer and evaporation of solvent provided the crude stabilized NPs. Purification of the Ru=C8 NPs is quite simple, utilizing the limited solubility of the MPCs in polar solvents such as ethanol or methanol. Thus, centrifugation of the sample four to five times is sufficient to remove any excess ligand and 1,2-propanediol. UV/Vis and proton NMR judge purity, whereby the characteristic exponential decay seen by UV/Vis (Mie scattering[18]), and the lack of sharp peaks from free ligand symbolizes a successful reaction. The morphology of the NPs can be determined by transmission electron microscopy (TEM), and FTIR spectroscopy can reveal the key stretches for the protecting monolayer including regions of the ligand closest to the particle surface. This last factor will be discussed further in Chapter 3 of this thesis.

Chen et al. demonstrated the ability of metathesis by mixing 11-bromo-1-undecene with the Ru=C8 NPs in DCM (6:1 olefin to particle-bound ligands) over a period of days (Figure 2.4). This simple ligand was chosen due to the fact 1) the α-methylene protons to the bromine will stand out by their relative downfield shift to 3.6 ppm, and 2) those protons are far enough away from the NP surface to be seen in the NMR spectrum. Due to the size of the NPs, the mobility of the ligands is greatly reduced leading to significant broadening of the peaks. Also, the closer to the Ru surface a proton is (or any atom for that matter), the less likely it can be seen by simple NMR techniques. These facts

greatly limit the utility of NMR for characterizing the NP ligands. However, for simple determination of purity, ^{1}H-NMR is sufficient. The absence of signals for vinyl protons and other sharp peaks signifies removal of excess ligand (purified by centrifugation with polar solvent).

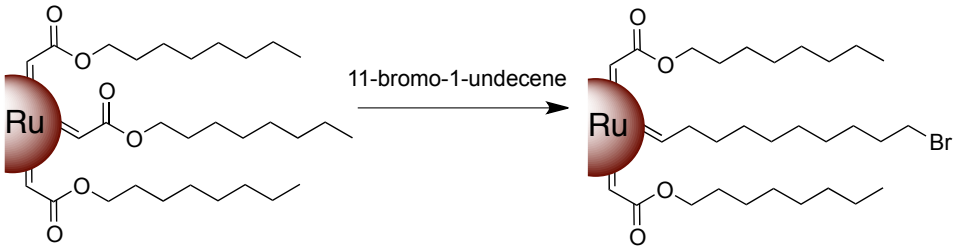

Figure 2.4 Nanoparticle Metathesis with 11-bromo-1-undecene.

It is important to determine the amount of ligand exchange that occurs for analytical purposes, and the Chen lab developed an indirect method.[19,20] The Ru core can be dissolved in a dilute solution of KCN and the organics are extracted and analyzed by NMR. The exact nature of the ligands is unclear following this process, particularly the end formally attached to the NP surface. However, the rest of the molecule remains intact and unique protons from each ligand can be identified in the spectrum and integrated relative to one another to determine a ratio. Typical loading is dependent on the amount of olefin used, size of the molecule, and time of reaction, but generally is not allowed to exceed 20-30% coverage to ensure NP stability.

2.2 Introduction to Nanoparticle Mediated Electronic Communication: Ferrocene-Functionalized Ruthenium Nanoparticles

The methods to detect electronic communication are centered upon electrochemistry and near-infrared spectroscopy (NIR). These techniques are typically used to investigate intervalence charge transfer (IVCT) processes of binuclear to multi-metal centered organometallic complexes whereby the metal atoms are linked through a conjugated organic framework.

One of the simplest examples of an organometallic complex frequently studied with regard to electronic communication is biferrocene.[21,22] The degree of charge transfer at mixed valence for a compound like biferrocene is exemplified by a characteristic voltammetric signature seen when monitoring the redox reaction of the iron centers of each ferrocene moiety (Fe^{2+}/Fe^{3+} transitions). The appearance of two voltammetric waves signifies charge transfer between the two metal centers at mixed valence. Conjugated organic spacers joining two ferrocene moieties allow electronic communication as well, but as will be discussed in the next section of this chapter, a progressively reduced interaction between the metal centers is seen as the distance increases. This reduced interaction is manifested in a lower potential spacing of the two voltammetric waves, which can be used to quantitatively judge efficiency of IVCT. However, if an sp^3 hybridized methylene spacer is placed between two ferrocene moieties, charge transfer is effectively inhibited resulting in a single voltammetric wave. Spectroscopically, IVCT can be

ascribed to a system using characteristic absorption in the NIR region from 1800-1900 nm.[23] It was the hope of our collaborators that these well known techniques used to study IVCT of organometallic complexes could be successfully applied to the larger and more complex system of appropriately functionalized carbene-stabilized Ru NPs. Since ferrocene is a well-characterized compound, it was chosen as a probe for the first study in NP-mediated electronic communication.[24]

Two simple ferrocene probes were chosen and synthesized by Dr. Lauren Brown (Konopelski lab) to functionalize the Ru ODA NPs, including the fully conjugated vinylferrocene and insulated allylferrocene. Chen and co-workers showed that Ru=C8 NPs functionalized with 5.9-21.3% coverage of vinylferrocene exhibited similar charge transfer capabilities averaging a potential spacing of $\Delta E^{o\prime}$ = 0.204 V. As hoped, the appearance of two pairs of voltammetric peaks appeared to indicate IVCT between mixed valence iron centers through the Ru core (Figure 2.5). Comparatively, biferrocene has a $\Delta E^{o\prime}$ value of 0.35 V, and Fc–CH=CH–Fc has a $\Delta E^{o\prime}$ value of 0.17 V. Strong absorption in the NIR at 1930 nm by the vinylferrocene functionalized NPs also indicated mixed valence intraparticle charge transfer.

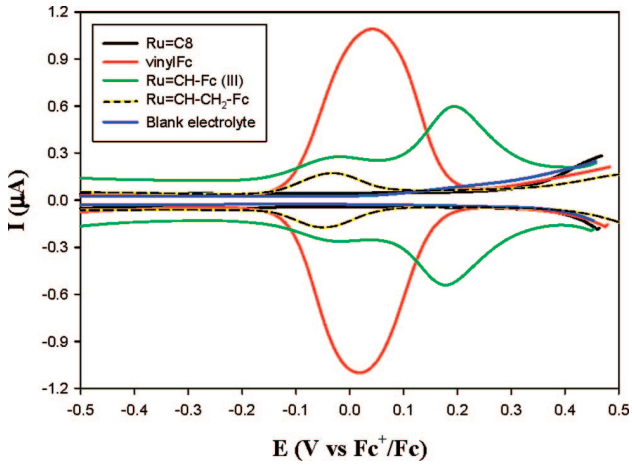

Figure 2.5 Square-wave Voltammograms for all of the species involved with ferrocene-functionalized Ru NP studies. Vinylferrocene monomers were 0.1 mM in DMF, Ru=C8 (4.7 mg/mL), Ru=CH-Fc (5 mg/mL), Ru=CH-CH2-Fc (2 mg/mL) with 0.1 M TBAP. Experimental conditions: Au disk electrode, area 0.3 mm^2, increment of potential 4 mV, amplitude 25 mV, and frequency 15 Hz. Figure reprinted with permission from Chen, W.; Chen, S. W.; Ding, F.; Wang, H.; Brown, L. E.; Konopelski, J. P. *J. Am. Chem. Soc.*, **2008**, *130,* 12156-12162. Copyright 2008, American Chemical Society.

Intervalence charge transfer between the ferrocene moieties was effectively turned off by the insertion of a methylene spacer between the ferrocene and the carbene linkage (allylferrocene functionalized Ru ODA NPs). Again, the expected single voltammetric wave was seen by electrochemistry. Also the lack of two voltammetric peaks with the allylferrocene NPs shows that the electrochemistry of the vinylferrocene NPs is not due to through-space interactions of ferrocene moieties as observed in the self-assembled monolayer of ferrocenyl alkane-thiols.[25] This fact seems to be further corroborated, since similar $\Delta E^{o'}$ values are seen from 5.9-21.3% coverage of vinyl ferrocene. At coverage down to 5.9%, it is not expected that ferrocene moieties would be next to each other on the NP surface with significant insulation from one another by the remaining protecting ligands.

The promising results of these initial experiments generated a continuing and growing collaboration between our group and the Chen/Wang groups. Further study of the mechanisms, properties and expansion of NP-mediated electronic communication was pursued during my tenure in the Konopelski group, whereby synthesis of new and interesting ligands was pursued.

2.3 Bridge-Assisted Electronic Communication

The contributions of efficient charge transfer between metal centers is understood to come from metal-to-metal interactions (close proximity and direct orbital overlap) and through-bond interactions due to metal-ligand-metal overlap. As mentioned before, the distance between the metal centers is important. Equally as important is the nature of the conjugated linker separating the metal centers, and calculations performed by our collaborator, Prof Haobin Wang, explored the efficiency of individual and mixed conduits of varying lengths separating two ferrocene moieties.[26] Due to the similar $\Delta E^{o'}$ values of ethylene bridged ferrocene and ferrocene-functionalized Ru NPs determined empirically, calculations for the simpler organometallic complexes should translate well to the NP systems.

It is understood that the electronics of conjugated organic systems including aryl, alkene, alkyne, and other systems containing heteroatoms are not considered equal. Quantification of this fact by the Wang group is important to how we further investigate the phenomena of NP-mediated

electronic communication. These factors would help to develop ideas toward new ways to prepare ligand-conjugated Ru NPs and methods to control percent ligand incorporation with high accuracy. Not only would this expand upon the usage of Ru ODA NPs, but it would also open the possibility to new systems for studying electronic communication.

Table 2.1 Summary of CDFT calculations for biferrocene and simple organic bridges. Table reprinted with permission from Ding, F.; Wang, H.; Wu, Q.; Voorhis, T. V.; Chen, S. W.; Konopelski, J. P. *J. Phys. Chem A*, **2010**, *114,* 6039-6046. Copyright 2010, American Chemical Society.

Compound	H_{ab} (kcal/mol)	
	Gas Phase	**CH_2Cl_2 (COSMO)**
Fc−Fc^+	3.26	2.03
Fc−CH_2−CH_2−Fc^+	0.88	0.41
Fc−CH=CH−Fc^+	3.22	1.99
Fc−C≡C−Fc^+	2.82	1.69
Fc−triazole−Fc^+	1.82	0.56
Fc−benzene−Fc^+	1.99	1.08
Fc−pyrazine−Fc^+	1.78	0.94
Fc−pyridine−Fc^+	1.85	0.99
Fc−pyrimidine−Fc^+	1.69	0.91

The first calculations presented by Wang and co-workers, using constrained density functional theory (CDFT), included the simple spacers ethyl, ethylene, alkyne, benzene, triazole, pyrazine, pyridine and pyrimidine (Table 2.1). The electronic coupling is reported in kcal/mol or H_{ab}, and is derived in a recent publication by the Wang group.[26] As expected, calculations for the saturated ethyl spacer did not show significant electron transfer between the iron centers. An alkene spacer is only slightly less efficient as a conduit than the biferrocene system, while the alkyne spacer is

not far behind. The benzene, pyrazine, pyridine and pyrimidine spacers are calculated to be about half as good of a conduit than an ethylene spacer. Interestingly, the triazole system was only slightly better than the saturated ethyl linker. This is in contrast to a recent paper whereby phenylaza-crown ethers linked to a fluorophore through a triazole showed induced fluorescence enhancement and quenching in the presence of various metal ions, which strongly suggests significant intramolecular charge delocalization across the extended π-conjugated system.[27]

With respect to the synthetic organic chemist, each of these linkers is considered to be quite useful, due to the ease in which they are synthesized and modified. For example, halogenated alkenyl/aryl and akynyl species undergo assorted Pd-catalyzed coupling reactions that proceed under various mild reaction conditions. Therefore, modification of these functional groups on the Ru NP can be imagined. Additionally, nitrogenated heteroaromatic rings are excellent ligands for a number of transition metals. Organometallic complexes containing these types of ligands could then be considered for electronic communication studies. Triazoles are highly desirable due to the endless number of alkyne or azide compounds that can be used to prepare them under Cu-catalyzed “click” conditions,[28] and the findings of Ast et al. provide further interest to study the utility of the triazole as a conduit for NPMEC.

The calculated efficiencies of each linker appear to eliminate only the triazole from consideration, which would be rather unfortunate. Despite this potential downside for one simple linker, it is still of interest to understand bridges that consist of more than one hetero- or homogeneous units. In particular, when considering the carbene linkage of Ru ODA NPs, the bridging system can be thought to consist of an ethylene flanked by the rest of the conjugated system. This is because the NP conducts charge between the metal centers of interest including two carbenes, all which can be considered equivalent to an ethylene bond. Thus, a carbene-linked *p*-ferrocenyl benzene would be similar to a bridge consisting of benzene-ethene-benzene. Wang and co-workers address this issue by also conducting DFT studies on hybrid-bridged systems (Table 2.2).

Table 2.2 Summary of CDFT calculations for mixed organic bridges. Table reprinted with permission from Ding, F.; Wang, H.; Wu, Q.; Voorhis, T. V.; Chen, S. W.; Konopelski, J. P. *J. Phys. Chem A*, **2010**, *114,* 6039-6046. Copyright 2010, American Chemical Society.

Compound	H_{ab} **(kcal/mol)**	
	Gas Phase	**CH_2Cl_2 (COSMO)**
Fc−CH=CH−C≡C−CH=CH−Fc^+	2.87	1.45
Fc−CH=CH−benzene−CH=CH−Fc^+	2.11	0.91
Fc−CH=CH−triazole−CH=CH−Fc^+	1.43	0.42
Fc−C≡C−triazole−C≡C−Fc^+	0.94	0.25
Fc−benzene−triazole−Fc^+	0.63	0.21
Fc−benzene−pyrazine−Fc^+	1.22	0.49
Fc−CH_2−CH=CH−CH=CH−CH_2−Fc^+	0.10	0.03
Fc−CH_2−CH_2−CH=CH−CH_2−CH_2−Fc^+	0.04	0.01

Alkene-alkyne and alkene-benzene hybrid bridges do not vary greatly from the lesser of the two conduits by themselves as seen by comparing Table 2.1 and 2.2. The triazole hybrid bridges are still calculated to be inefficient conduits. The results of the Wang group's calculations and analysis were applied to our previous ideas as well as potential new projects.

Prior to the DFT paper, we had been working towards the synthesis of terminal alkyne functionalized ligands for the purpose of on-nanoparticle functionalization. The original idea was to generate a compact and linear *p*-diazoethynylbenzene ligand (**2.1**), which would fall under the hybrid-bridge of benzene-alkene-benzene (Figure 2.6). However, similar diazo compounds are typically generated in solution and used immediately due to their instability in the pure form.[29] As mentioned before, ODA is a stable ligand due to the diazo conjugation to the ester moiety. We then envisioned another means for stabilizing the diazo compound while still maintaining a fully conjugated system. The fluorene or compound **2.2** scaffold fit this mold and precedence for di-ethynyl substituted fluorene (**2.3**) compounds exists in the literature.[30] Both of these structures are known to have extremely stable radical and carbene species due to their extended conjugation. Still, the relatively short length of this ligand was a bit concerning when considering the necessity for long carbon chains in protecting the NP from aggregation. It is possible that pi-pi stacking of the aryl units could provide tight packing around the Ru cluster and subsequently deliver the desired stability. Of course, the

fluorene diazo **2.3** could be mixed with ODA to provide partial functionalization and the necessary stability. If successful, the degree of molecule of interest incorporation could be controlled easily as the Cu-catalyzed “click” reaction generally proceeds near quantitatively. As depicted in Figure 2.7, NPs similar to **2.4** could undergo reaction with a variety of azides, including azidoferrocene (**2.5**), to provide triazole functionalized NPs (**2.6**). Not only would these NPs potentially demonstrate NPMEC, but if triazoles were efficient conduits, EC would occur within the ligand as well. Of course, all of this is moot if the calculations for the triazole conduit are valid.

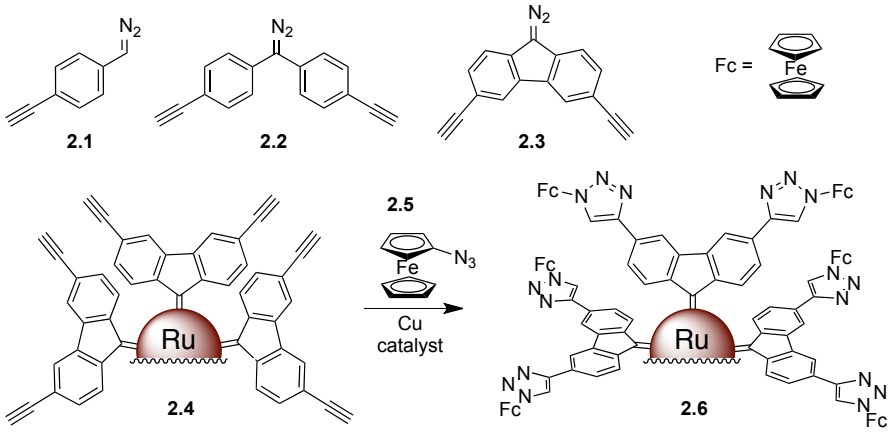

Figure 2.6 Potential Diazo Ligands with handles for alkyne-click modification after nanoparticle stabilization.

In addition to the evaluated bridges, one system that was not considered in the DFT study was the cross-conjugated ketone. This system was considered based on an idea involving a modified Weinreb amide diazo compound **2.7** (Figure 2.7). Similar to ODA, **2.7** would contain a carbene linkage with a long chain carbon tail. The added utility of this ligand would be absolute control over nucleophilic addition to the Weinreb amide while

attached to the NP (**2.8**). Single addition of Grignard and Li anions to the carbonyl would occur due to the stability of the intermediate formed. Additionally, the amount of nucleophile could be adjusted to add as little or as much of the desired molecule while still maintaining NP stability (**2.9**).

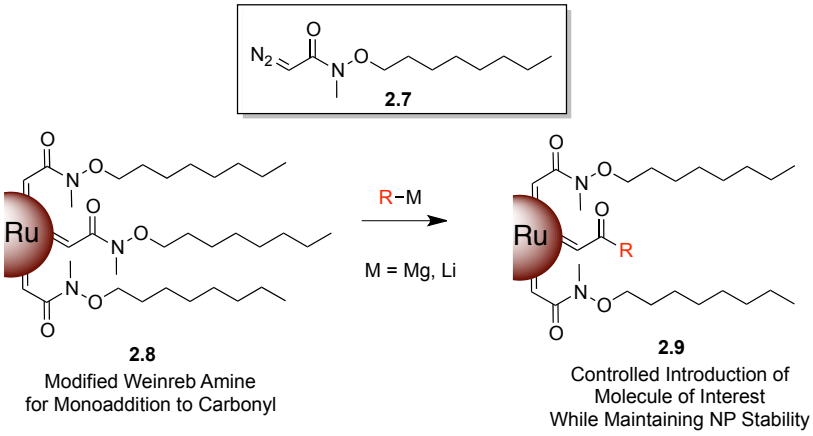

Figure 2.7 Diazo-Weinreb Amide (**2.7**) proposed to stabilize Ru NPs and have the ability for cross-conjugation to conjugated nucleophiles.

These two ideas involving the fluorene or Weinreb amide diazo compounds deserve simple consideration before full implementation. In particular, the results of the DFT studies should be evaluated by experiment utilizing the now well-established Ru ODA NP system. Four model ligands appended with ferrocene were designed for this purpose with a range of compounds involving a good (alkyne), intermediate (benzene), and poor (triazole) conduit. For our own purpose we also included the cross conjugated ketone for electrochemical analysis.

2.3.1 Synthesis of Bridged-Ferrocene Compounds

Two of the four desired compounds were synthesized according to known procedures to give acryloylferrocene (**2.10**) and *p*-ferrocenyl styrene

(**2.13**) as depicted in Scheme 2.2. The addition of vinylmagnesium bromide to ferrocenylaldehyde, followed by oxidation with excess MnO_2 provided **2.10** in 79% yield over two steps. Friedel-Crafts reaction between ferrocene and the tetrafluoroborate stabilized diazonium salt **2.11**,[31] gave **2.12** according to known procedures. Subsequently, the aldehyde was converted to the vinyl group by Wittig reaction to give **2.13** in 34% overall yield.

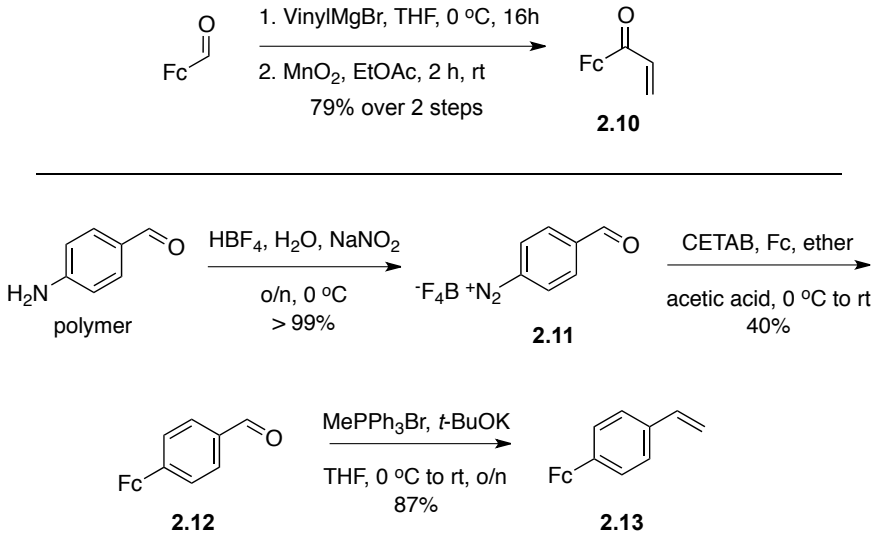

Scheme 2.2 Synthesis of **2.10** and **2.13**.

Both the enyne (**2.16**) and triazole (**2.18**) substituted ferrocene compounds are new compounds that result from the combination of two known precursors in one step each (Scheme 2.3). The synthesis of **2.16** was conducted by coupling vinyl bromide to the known ethynylferrocene (**2.14**)[32] under standard Sonagashira conditions in 81% yield.[33] Compound **2.18** results from the in-situ deprotection of TIPS-enyne (**2.17**)[33] with TBAF in the presence of a catalytic amount of CuI and **2.5**.[34] This reaction is run for two

days in the dark to prevent degradation of the azide. Typical aqueous click conditions using sodium ascorbate and Cu(II) sulfate pentahydrate were unsuccessful in generating **2.18** as seen from a similar reaction in the literature.[35]

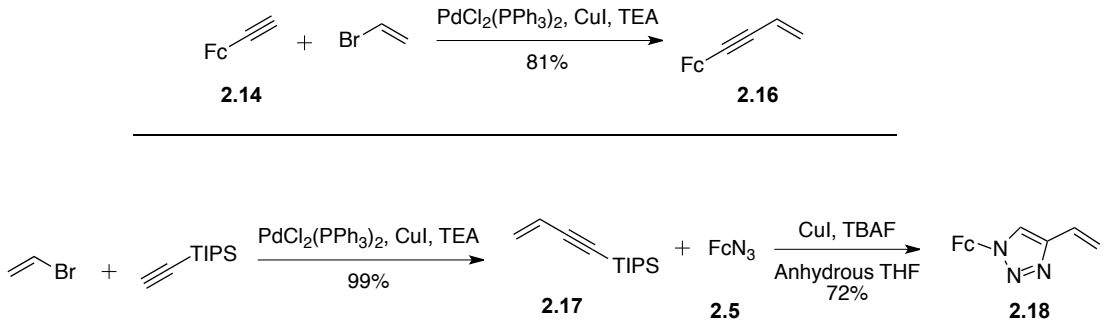

Scheme 2.3 Synthesis of **2.16** and **2.18**.

Each ligand was metathesized onto Ru=C8 NPs prepared in our lab according to the procedure developed by Chen et al.[15] Purification of the functionalized NPs was the same for all samples by precipitating the NPs with methanol from a minimal amount of DCM and centrifuging the particles. Removal of the supernatant and repeating the process 3-4 times (as judged by NMR) provided the NPs as a black residue. Proton NMR showed that excess ligand was removed in the purification process, but it was not clear if the ferrocenylated compounds were incorporated. Monosubstituted ferrocene compounds typically appear as a singlet and two triplets by ^{1}H-NMR around 4.0 ppm. When attached to the Ru NP, the ferrocene signals are suspected to be broadened if seen at all. Very small, broad peaks were seen around 5.1-5.5 ppm following the metathesis reaction for each set of NPs. The

distinguishing protons of the aromatic ring and for the triazole proton were not seen. Incorporation of the ferrocene moieties through metathesis was conclusively determined via electrochemical studies.

2.3.2 Results of Bridged-Ferrocene Capped Ruthenium Nanoparticle Study

Fortunately, when fellow graduate student Xiongwu (Mike) Kang studied the prepared NPs by electrochemistry, it was clear that each new ferrocene ligand was successfully incorporated, due to the appearance of distinct voltammetric peaks. Ordinary Ru=C8 NPs show featureless profiles by electrochemistry. The degree of incorporation was not determined for any of the ligands.

Table 2.3 Summary of Electrochemical data for DFT compounds. Electrochemical data collected by Xiongwu Kang.

Fc-Bridge-RuNP-Bridge-Fc Organic Bridge	$\Delta E^{o\prime}$
2.10 (ketone)	0
2.13 (benzene)	0.159
2.16 (alkyne)	0.187
2.18 (triazole)	0

In summary, the data in Table **2.3** correlated very well with calculations performed by the Wang group. The alkyne was the best conduit, while the benzene linker was slightly worse, followed by only single waves for the triazole and ketone spacers. In this case, comparison to vinyl ferrocene is a good gauge for IVCT, which has a $\Delta E^{o\prime}$ of 0.204 V. Although the ideas

developed regarding the fluorene-alkynyl (**2.3**) and diazo-Weinreb amide (**2.7**) compounds were novel and interesting, their further study was deemed unnecessary in the effort to study NP-mediated electronic communication.

2.4 Pyrene-Functionalized Ruthenium Nanoparticles

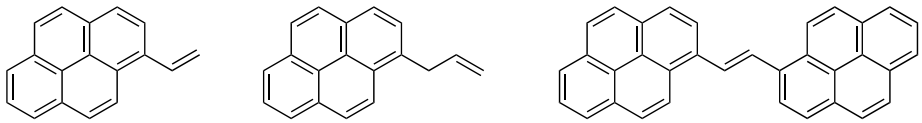

2.19 **2.20** **2.21**

Figure 2.8 Pyrene Compounds for pyrene-functionalized Ru NP studies.

Although ferrocene is a wonderful probe and is great for identifying the presence of electronic communication through our NP system, we had not yet induced the expected prospect of new optoelectronic properties. Our next collaborative venture was to investigate the attachment of the well-known fluorophore, pyrene, to Ru=C8 NPs since pyrene is a highly fluorescent and relatively robust compound with a wide variety of applications in sensing applications. Our goal was to determine if conjugation to the NP core would provide an advantage in the detection of nitroaromatics to a previous report considering monomeric pyrene.[36] Would these new pyrene-functionalized Ru NPs act as a simple summation of monomers?

The approach to investigate this process[37] required the synthesis of 1-vinylpyrene (**2.19**),[38] 1-allylpyrene (**2.20**),[39] and an additional control molecule, (*E*)-1,2-di(pyren-1-yl)ethene (**2.21**) as depicted in Figure 2.8.[40] Clearly, the capacity of **2.19** and **2.20** were proposed to show fluorescence results homologous to the electrochemical results of their ferrocene analogs

once attached to the Ru=C8 NPs. The dimeric species was synthesized for comparison to the **2.19** functionalized Ru=C8 NPs (Ru=VPy), and the **2.20** Ru=C8 NPs (Ru=APy) with hope its fluorescence spectra would be distinctive from Ru=VPy.

2.4.1 Synthesis of Pyrene Ligands, Control Molecule and Functionalized Nanoparticles

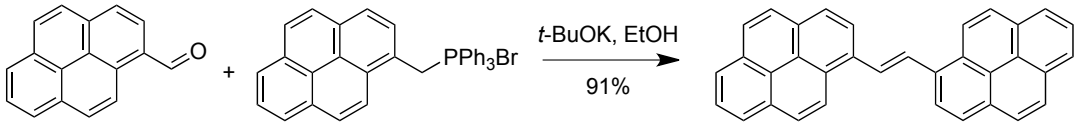

2.22 **2.21**

Scheme 2.4 Synthesis of (*E*)-1,2-di(pyren-1-yl)ethene.

All three pyrene compounds were known and followed relatively straightforward synthetic procedures. **2.19** was synthesized in one step by the Wittig reaction of 1-pyrenecarboxaldehyde and methylenetriphenylphosphorane,[38] and **2.20** was synthesized in one step from the reaction of 1-lithiopyrene and allyl bromide.[39] The only issue for either of these syntheses was that the suggested mixed-solvent system was absolutely necessary for the synthesis of 1-allylpyrene. A 4:1 mixture of diethyl ether/benzene cannot be substituted with THF as 1-lithiopyrene reacts with this solvent.

Synthesis of **2.21** was conducted in accordance to the procedure of Geerts et al.[40] The Wittig reagent **2.22** was formed in three steps from 1-pyrenecarboxaldehyde, and after recrystallization could be subsequently

deprotonated and reacted with another equivalent of 1-pyrenecarboxaldehyde to give the pyrene dimer.

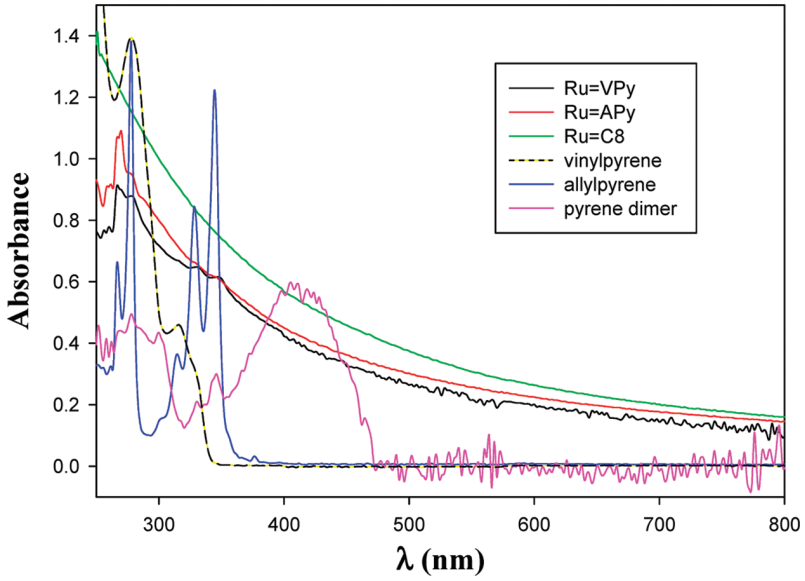

Figure 2.9 UV/Vis of Pyrene NP Studies. Nanoparticle solutions were all 0.1 mg/mL in DMF and monomers 0.1 mM in DMF. Figure reprinted with permission from Chen, W.; Zuckerman, N. B.; Lewis, J. W.; Konopelski, J. P.; Chen, S. W. *J. Phys. Chem C*, **2009**, *113,* 16988-16995. Copyright 2009, American Chemical Society. Spectra collected by Dr. Wei Chen.

Dr. Wei Chen functionalized the Ru=C8 NPs following the previously described metathesis procedure to give Ru=VPy and Ru=APy. By dissolving a portion of the NPs in a dilute KCN solution and analyzing the organic extracts, Dr. Chen determined 26.4 and 22.9% coverage for the Ru=VPy and Ru=APy, respectively. FTIR and UV/Vis appeared to indicate the incorporation of the fluorophores onto the NP surface. Typically, the UV/Vis spectra for Ru=C8 NPs and functionalized Ru NPs are indistinguishable due to Mie scattering and an ordinary exponential decay profile. However, since pyrene is very absorbent in the UV, Ru=VPy and Ru=APy NPs displayed peaks at 266-269, 278, 329, and 349 nm, similar to the monomeric species

(Figure 2.9). The UV/Vis spectrum of pyrene dimer **2.21** showed much less intense peaks at 300 nm and below, but a new and intense peak appeared around 410 nm. This shift towards the visible region is most likely due to the extended conjugation of the π electrons across the entire pyrene dimer system. We hoped this would translate to intraparticle extended conjugation between NP bound pyrene moieties.

2.4.2 Results and Discussion

The most interesting results of this study emerged during the fluorescence experiments on the pyrene-functionalized NPs and **2.21**. From simple comparison of the monomeric and NP species, similarities could be seen that began to tell the tale of possible NP-mediated electronic communication. The fluorescence spectra of the Ru=C8 NPs were completely featureless, but the Ru=VPy and Ru=APy NPs showed distinct fluorescence spectra with clear differences between the two (Figure 2.10A). The Ru=VPy NPs showed two major peaks at 392 and 490 nm in stark contrast to the Ru=APy NPs where only the peak at 392 nm existed. The appearance of these peaks can be explained when compared to the fluorescence spectra of the monomeric species. Both **2.20** and **2.19** have one peak in the same region as the Ru=APy NPs, indicating the attached fluorophores are acting similar to monomeric pyrene species.

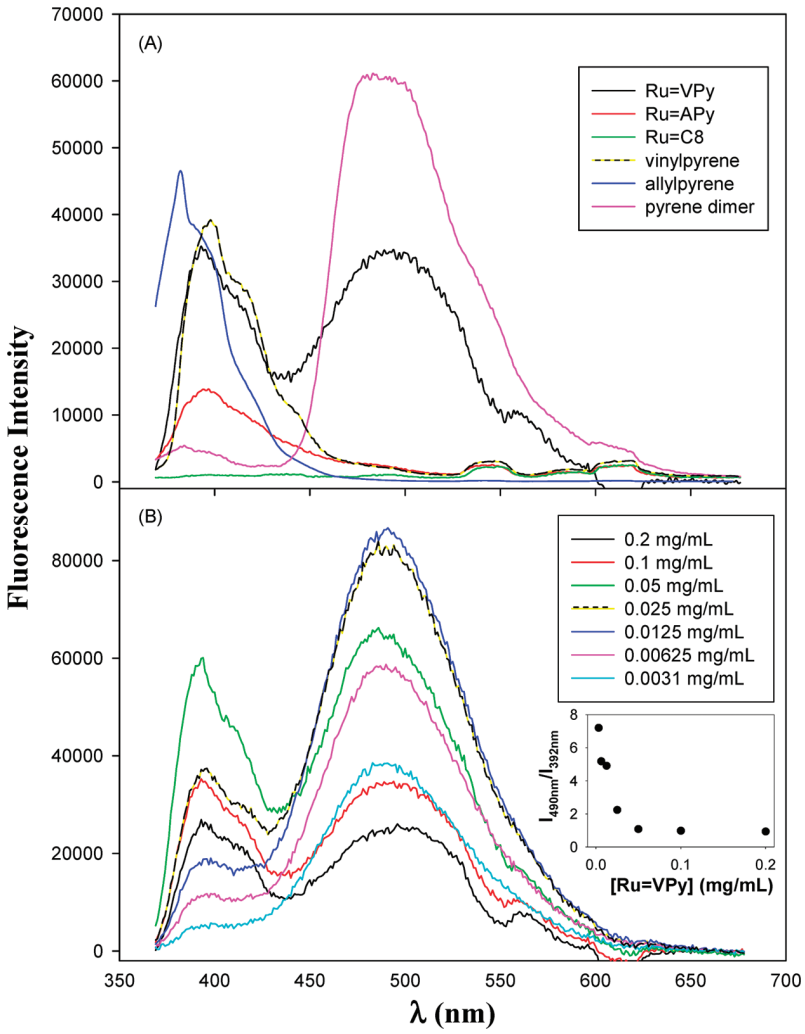

Figure 2.10 Fluorescence Spectra of **2.19** (vinylpyrene), **2.20** (allylpyrene), **2.21** (pyrene dimer), and functionalized NPs. A) Nanoparticle solutions were all 0.1 mg/mL in DMF and monomers 0.1 mM in DMF. B) Ru=VPy at different concentrations in DMF (0.1 mg/mL). Inset shows the variation of the ratio of the intensity of the emission bands at 490 and 392 nm with particle concentration. The excitation wavelength was set at 349 nm for all emission spectra. Figure reprinted with permission from Chen, W.; Zuckerman, N. B.; Lewis, J. W.; Konopelski, J. P.; Chen, S. W. *J. Phys. Chem C*, **2009**, *113,* 16988-16995. Copyright 2009, American Chemical Society. Spectra collected by Dr. James W. Lewis and Dr. Wei Chen.

On the other hand, the spectra of the pyrene dimer **2.22** was very similar to the Ru=VPy NPs. The dimeric species had a lower intensity peak at 384 nm, but an intense peak at 490 nm. These results compared quite favorably to the ferrocene-functionalized Ru NPs, and strongly suggested the

unique fluorescence characteristics are indicative of intraparticle extended conjugation.

Pyrene excimers are known to occur when pyrene moieties are in close proximity to one another, and they too emit in the region of 450-500 nm. It seems unlikely that the bound pyrene moieties would contact each other since they are surrounded and buried amongst the long-chain ligands. To discount excimer formation as a possible cause of the observed unique fluorescence spectra, Dr. Chen and Dr. Lewis collected concentration dependent spectra (Figure 2.10B). If excimer formation were to occur, one would expect an increase in emission as the concentration increased. However, this was not the case as the peak at 490 nm increased in intensity as the concentration decreased.

Dr. Chen conducted the appropriate control experiments to tie the appearance of the new peaks at 490 nm for the fully conjugated Ru=VPy NPs to the carbene linkage of the fluorophore to the metal core. Monitoring the fluorescence spectra of a mixture of Ru=C8 NPs and **2.19** over a period of zero to 92 h, the peak at 392 nm remained constant as the peak for intraparticle extended conjugation emerged and reached a plateau towards the end of the reaction (Figure 2.11). The same process was repeated with Ru=C8 NPs and 1-bromopyrene, which showed no new peaks over a period of 76 hours since this molecule does not undergo reaction with the Ru NPs (Figure 2.12).

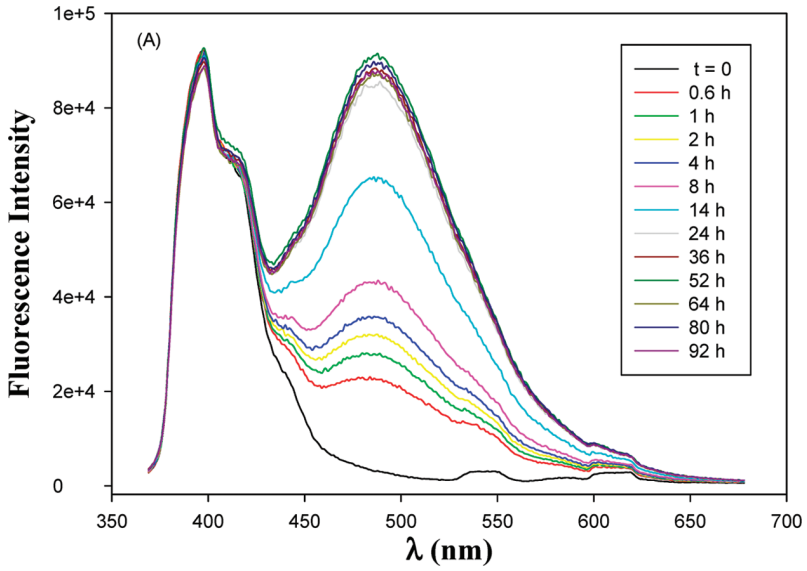

Figure 2.11 Fluorescence spectra for formation of Ru=VPy NPs over time. Ru=C8 NPs (0.01 mg/mL) mixed with 1-vinylpyrene (3 mM) for different periods of time. The excitation wavelength was set at 349 nm. Figure reprinted with permission from Chen, W.; Zuckerman, N. B.; Lewis, J. W.; Konopelski, J. P.; Chen, S. W. *J. Phys. Chem C*, **2009**, *113,* 16988-16995. Copyright 2009, American Chemical Society. Spectra collected by Dr. James W. Lewis and Dr. Wei Chen.

The appearance of the new emission peak at 490 nm for Ru=VPy NPs and the lack of a peak for the Ru=APy NPs in this region indicated novel fluorescence characteristics that are controlled only by the lack of or inclusion of a simple sp^3-hybridized spacer, respectively. The Ru=VPy particles behave similarly to the dimeric pyrene species, but further studies were conducted to potentially capitalize on these unique photoluminescence properties.

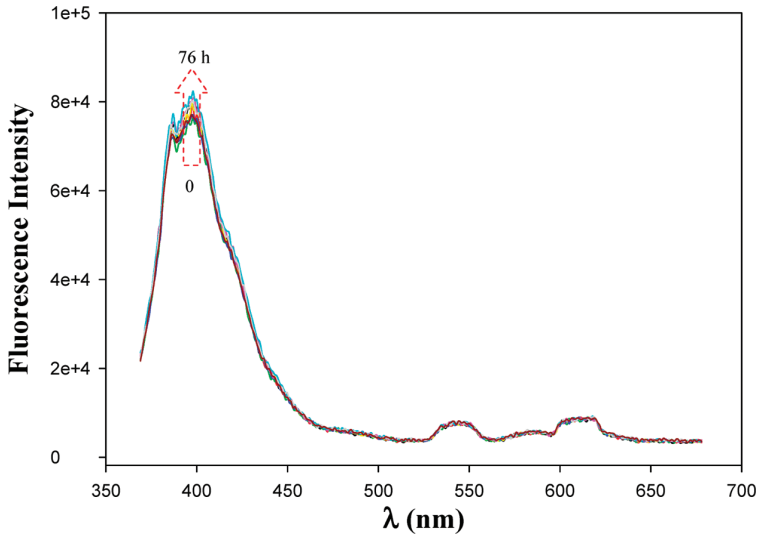

Figure 2.12 Fluorescence spectra for Ru=C8 NPs (0.01 mg/mL) mixed with 1-bromopyrene (3 mM) up to 76 h. The excitation wavelength was 349 nm. Figure reprinted with permission from Chen, W.; Zuckerman, N. B.; Lewis, J. W.; Konopelski, J. P.; Chen, S. W. *J. Phys. Chem C*, **2009**, *113,* 16988-16995. Copyright 2009, American Chemical Society. Spectra collected by Dr. James W. Lewis and Dr. Wei Chen.

2.4.3 Applications of Pyrene-Functionalized NPs as Fluorescence-Based Nitroaromatic Detectors

The collaborative efforts thus far progressively moved from proof of concept to application. Intraparticle IVCT was shown to be possible and of meaningful occurrence with the study of ferrocene-functionalized Ru NPs.[24] Extension of this concept was transferred to the idea of intraparticle extended conjugation[37] and detection of this phenomenon by fluorescence characteristics of carbene-bound pyrene molecules. We then sought out to apply the utility and well-known characteristics of fluorescent pyrene to probe the sensing abilities of nitroaromatic compounds by Ru=VPy and Ru=APy NPs[41] (Figure 2.13) relative to monomeric pyrene species. We believed the pyrene-functionalized NPs (specifically the Ru=VPy NPs) would act

analogously to conjugated polymers, which show amplified detection effects (**2.23**) towards the electron deficient nitroaromatic compounds (**2.24**).[42]

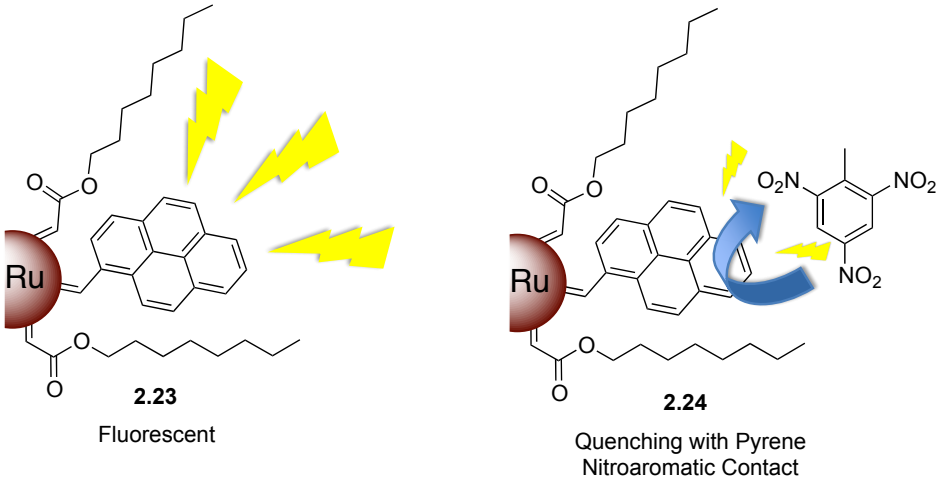

Figure 2.13 Nitroaromatics and Ru=VPy NPs.

Dr. Chen was able to show a marked amplification and increased sensitivity to nitroaromatic compounds for Ru=VPy NPs relative to monomeric pyrene (Figure 2.14A). In particular, as the concentration of 2,4,6-trinitrotoluene (TNT) was increased, the emission peak at 392 nm diminished markedly. The peak at 490 nm, which is attributed to intraparticle extended conjugation, decreased only slightly. More importantly, these NPs appear to show a marked increased sensitivity to TNT relative to other developed chemosensors,[36] and they also appear to show a degree of selectivity towards the detection of TNT over other nitroaromatic compounds tested. The detection also increases with the amount of nitration.

Table 2.4 Quenching constants (K_{SV}) of the Ru=VPy and Ru=APy nanoparticles for varied nitroaromatic compounds. Figure reprinted with permission from Chen, W.; Zuckerman, N. B.; Konopelski, J. P.; Chen, S. W. *Anal. Chem*, **2010**, *82,* 461-465. Copyright 2010, American Chemical Society.

K_{SV} (M^{-1})	Ru=VPy	Ru=APy
Chloronitrobenzene (CNB)	2.71×10^3	2.28×10^2
Nitrobenzene (NB)	6.69×10^3	2.96×10^2
2,6-Dinitrotoluene (2,6-DNT)	1.33×10^4	9.27×10^3
2,4-Dinitrotoluene (2,4-DNT)	1.40×10^4	1.14×10^4
2,4,6-Trinitrotoluene (TNT)	6.40×10^4	1.40×10^4

The characteristics of Ru=APy NPs (Figure 2.14B) were also tested by Dr. Chen and showed moderate quenching of the only emission peak at 394 nm when TNT was added to the solution. From the determined quenching constants (Table 2.4) of the varied nitroaromatic compounds, Ru=APy NPs also showed increasing sensitivity as the nitration increased. However, the quenching constants were much smaller than for Ru=VPy, which may be due to the extended conjugation difference between the two NP systems. Further evidence of this phenomenon was confirmed by similar quenching characteristics by the pyrene dimer **2.21**. The emission peak at 490 nm does not diminish with increasing amounts of nitroaromatics for the dimer as well.

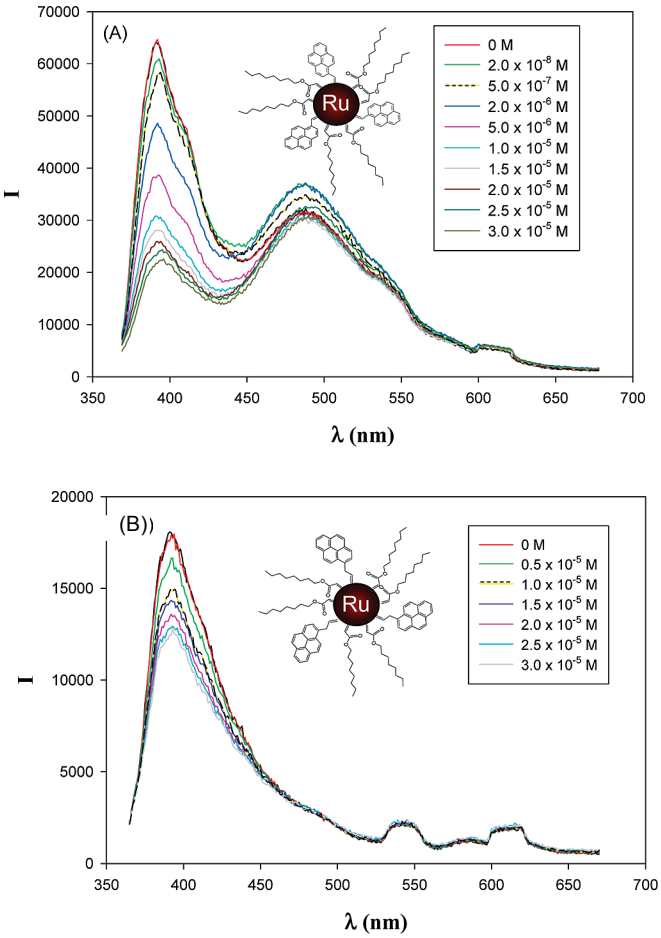

Figure 2.14 Fluorescence Spectra for Ru=VPy (A) and Ru=APy (B) Nanoparticles (0.05 mg/mL in DMF; 16 μM and 19 μM effective pyrene concentration) with TNT at varying concentrations. Excitation wavelength was set at 349 nm. Figure reprinted with permission from Chen, W.; Zuckerman, N. B.; Konopelski, J. P.; Chen, S. W. *Anal. Chem*, **2010**, *82,* 461-465. Copyright 2010, American Chemical Society. Spectra collected by Dr. Wei Chen.

2.5 18-6-Benzocrown-Ether/Pyrene-Functionalized Nanoparticles for Detection of K^+ Ions

Further extension of the application of intraparticle extended conjugation lead to another analytical study utilizing indirect fluorescence quenching of pyrene through a selective binding event away from the fluorophore.[43] Among organic structures, there are many methods for the

selective detection of various small molecules, biological compounds, and ions. The selective detection of ions is probably one of the more difficult tasks to accomplish of the classes just mentioned due to the relatively small differences in size and properties between similarly charged ions.[44] In nature, ion channels have evolved to selectively transport ions into and out of the cell.[45] Of the organic molecules that selectively bind ions, the classical crown-ether moiety comes to mind. In particular, 18-crown-6 binds multiple positively charged ions, but it has the strongest affinity toward K^+ ions.[46] A simple ion sensor was reported, where benzo-15-crown-5 is connected to anthracene via an ethene bridge (**2.25**), and the binding of ions leads to a dramatic increase in fluorescence for Mg^{2+} binding (Figure 2.15).[47] More than ever, with the previous findings of our collaborative studies, the Ru NP core can be thought of as a simple ethylene conduit. Thus, the translation of the anthracene/crown ether sensor should directly translate to our developed carbene-functionalized Ru NPs, but instead the fluorophore of choice in our case is pyrene (**2.26)**.

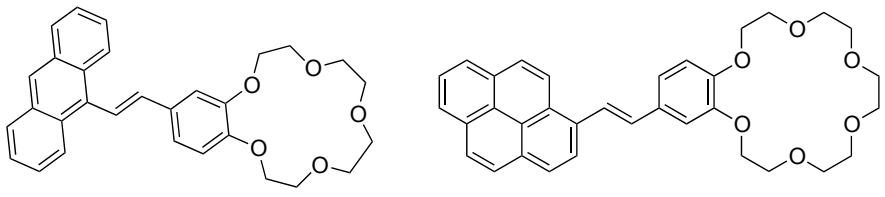

2.25 **2.26**

Figure 2.15 Anthracene/crown ether detector[47] and our pyrene/crown ether conjugate.

Prior to this study, only one molecule of interest was incorporated onto the Ru=C8 NPs via metathesis. The most obvious method to incorporate two

different olefins would be to run one metathesis reaction with a mixture of the molecules of interest. A downside to this method is that it is unknown how the rates of exchange vary between different molecules, and it is therefore difficult to predict what the ratio of incorporation would be when the olefins are added 1:1 relative to one another. The results of the ligand ratios as determined by the KCN method, showed that 1-vinylpyrene (**2.19**) is incorporated much more readily than the commercially available 4-vinylbenzo-18-crown-6 (4:1) to give Ru=VPy/crown ether functionalized NPs (Ru=VPyCE). The successful incorporation of both the fluorophore and the "detector" onto the Ru NP surface via a carbene linkage allowed for the investigation of intraparticle charge delocalization on ion detection.

2.5.1 Synthesis of 2.26 and Cofunctionalized Ru NPs

In addition to cofunctionalizing Ru=C8 NPs with **2.20** (Ru=APyCE) and 4-vinylbenzo-18-crown-6, **2.26** was formed between the two known compounds **2.27** and the ylide of triphenyl(pyren-1-ylmethyl)phosphonium bromide (**2.22**) was synthesized to act as a control (Scheme, 2.5, pyrene-crown ether conjugate). Compound **2.26** was synthesized to investigate photoluminescent contributions from extended conjugation between the pyrene and crown ether. This study is necessary to attempt to deconvolute the contributions from pyrene/pyrene and crown ether/crown ether intraparticle delocalization. Also, NPs were functionalized with only 4-

vinylbenzo-18-crown-6. The possibility for multiple intraparticle extended conjugation pathways required careful analysis of each contributing factor.

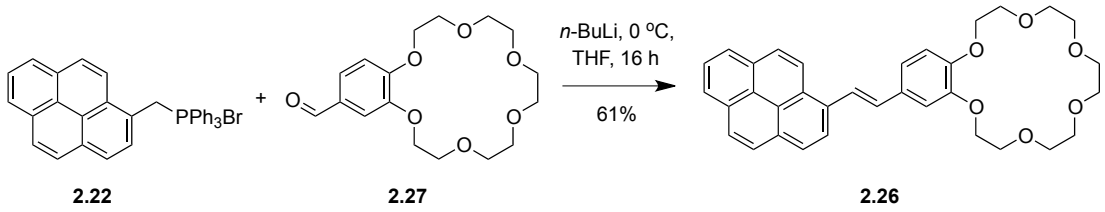

2.22 **2.27** **2.26**

Scheme 2.5 Synthesis of **2.26**.

2.5.2 Results and Discussion

Perchlorate salts of the positively charged ions Li, Na, K and Mg were tested against the various NPs and **2.26**. Upon binding the positively charged ion, delocalizations of charge within the NP was expected to affect the intraparticle extended conjugation and subsequently alter the photoluminescent properties of the functionalized NPs. The spectral changes for the Ru=VPyCE particles were not nearly as drastic as seen in the previous study for the detection of nitroaromatic compounds, but in the presence of different metal salts, there was a preference for K^+ over the other selected ions, as seen by a decrease in fluorescence intensity at 484 nm (Figure 2.16).

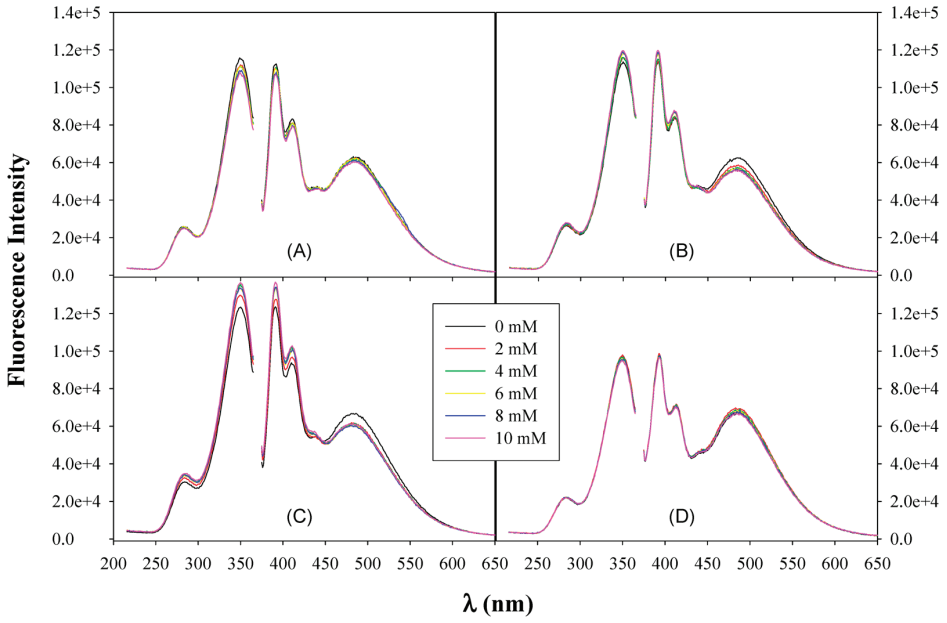

Figure 2.16 Excitation and Emission Spectra of Ru=VPyCE NPs (2 mL, 0.05 mg/mL in DMF) with addition of various amounts of metal salts in DMF (0.1 M): (A) $LiClO_4$, (B) $NaClO_4$, (C) $KClO_4$, and (D) $Mg(ClO_4)_2$. The Excitation wavelength is set at 349 nm. Figure reprinted with permission from Kang, X.; Chen, W.; Zuckerman, N. B.; Konopelski, J. P.; Chen, S. W. *Langmuir*, **2011**, *27,* 12636-12641. Copyright 2011 American Chemical Society.

Interestingly, with similar coverage of crown ether to pyrene, Ru=APyCE NPs showed almost no change with the addition of potassium perchlorate as seen in Figure 2.17. This result appears to eliminate through-space interactions as a means for fluorescent enhancement of the Ru=VPyCE NPs. The solely crown ether-functionalized NPs (Ru=CE NPs) displayed a change in fluorescence when exposed to the various metal salts. Since the Ru=CE NP system can be thought of as a stilbene analog, charge delocalization enhancement effects were not unexpected upon binding. However, the fluorescence intensity was an order of magnitude lower than the Ru=VPyCE NPs suggesting the fluorescence of the pyrene moieties dominates in the confunctionalized system. Lastly, the **2.26** showed a

fluorescence excitation peak at 384 nm and an emission peak at 463 nm. To evaluate the contribution of fluorescence from the benzene and pyrene rings, the Ru=VPyCE NPs were also excited at 384 nm, but new emission peaks were a magnitude lower than the pyrene-pyrene fluorescence contributions (Figure 2.17).

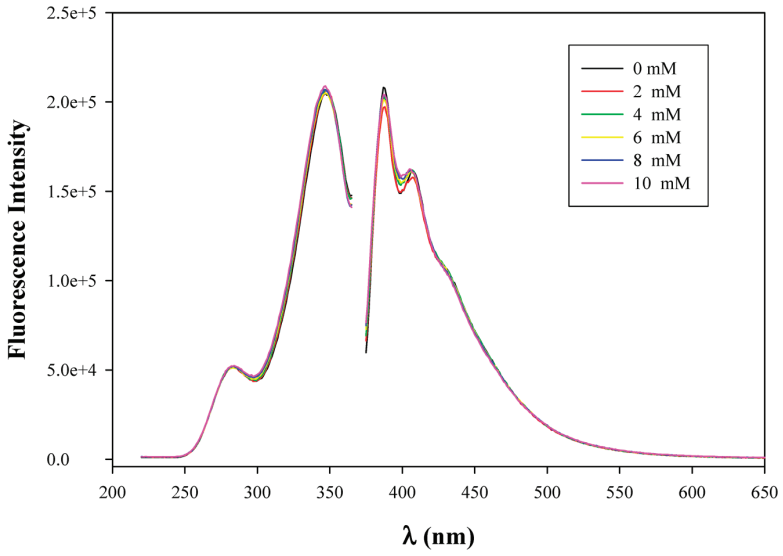

Figure 2.17 Fluorescence of Ru=APyCE NPs (2 mL, 0.05 mg/mL in DMF) with the addition of various amounts of $KClO_4$ in DMF (0.1 M). The Excitation wavelength is set at 349 nm. Figure reprinted with permission from Kang, X.; Chen, W.; Zuckerman, N. B.; Konopelski, J. P.; Chen, S. W. *Langmuir*, **2011**, *27,* 12636-12641. Copyright 2011 American Chemical Society.

With multiple extended conjugation pathways between different fluorescent compounds on the cofuntionalized system, the major contributions were deemed to come from pyrene. By binding positively charged ions and manipulating the extended conjugation system, the energy of the core electrons was altered, and ultimately the fluorescence characteristics were affected.

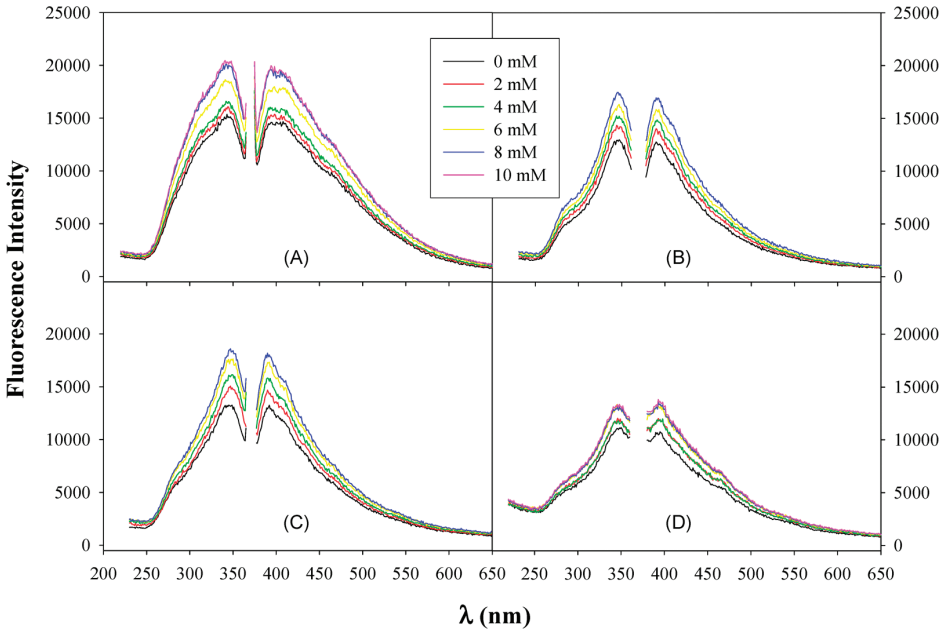

Figure 2.18 Fluorescence of Ru=CE NPs (2 mL, 0.05 mg/mL in DMF) with the addition of various amounts of $KClO_4$ in DMF (0.1 M): (A) $LiClO_4$, (B) $NaClO_4$, (C) $KClO_4$, and (D) $Mg(ClO_4)_2$. The Excitation wavelength is set at 345 nm. Figure reprinted with permission from Kang, X.; Chen, W.; Zuckerman, N. B.; Konopelski, J. P.; Chen, S. W. *Langmuir*, **2011**, *27,* 12636-12641. Copyright 2011 American Chemical Society.

Another pyrene cofunctionalized Ru NP sensor utilizing the same principles was disclosed for the complexation of transition metal ions with histidine moieties.[48] This ligand was synthesized by William Hewitt in our lab and was based on a discovery made by former Konopelski group member, Dr. Yakira Landaverry, that particular functionalized histidine moieties binds Pb^{2+} extremely tightly.[49] Similar trends in fluorescence changes and selectivity were reported for Pb^{2+}, Co^{2+}, and Hg^{2+}.

2.6 Ferrocene-Functionalized Carbon Nanoparticles

IVCT was also shown to exist across carbon nanoparticles (CNP) when the surface was treated with *p*-ferrocenyl diazonium **2.28** and $LiEt_3BH$ (Figure 2.19).[50] The linkage between the aryl ring and the CNPs surface

differs from the previous studies in that it is thought to be a single bond. The $\Delta E^{o\prime}$ was found to only be 0.078 V, which is not nearly as good as any of the Ru carbene studies. This small value is often attributed to through-space interactions, but was discounted by the inclusion of a methylene spacer between ferrocene and aryl ring (**2.29**).

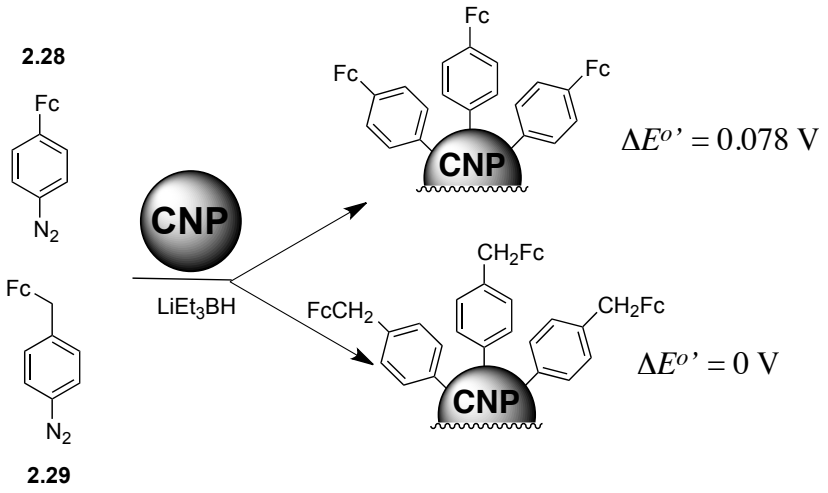

Figure 2.19 Carbon Nanoparticles treated with aryl diazoniums. The CNPs were synthesized and characterized by Yang Song (graduate student, Shaowei Chen lab). The diazonium precursors were synthesized according to literature procedures.[51,52]

2.7 Conclusion

Not only has nanoparticle-mediated electronic communication been demonstrated using electrochemistry and NIR spectroscopy, but expansion of the idea to incorporate fluorescence as a means to demonstrate and detect intraparticle extended conjugation has led to novel means to control photoluminescent properties of carbene-bound moieties. The findings thus far have only begun to scratch the surface of the applications and utility of electronic communication through NPs.

Certainly, from the work described in this thesis chapter, there has been a good fundamental groundwork laid for further advancement in the field of nanoparticle-mediated electronic communication. A simpler and cheaper means to functionalize carbene-stabilized Ru NPs more efficiently and controllably would be a direction worth pursuing. The field of catalysis is also another unexplored direction with these novel carbene-functionalized NPs.

Experimentals

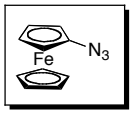

Azidoferrocene (2.5). The synthesis of **2.5** was conducted as previously described by Nesmeyanov et al.[34] Bromoferrocene (1.00 g, 3.59 mmol, 95%) was dissolved in DMF (anhydrous, 20 mL), followed by the addition of NaN_3 (2.00 g, 30.5 mmol) in water (5 mL) and $CuBr_2$ (0.35 g, 1.57 mmol) in water (1.5 mL). The resulting mixture was stirred in the dark for 2 days at room temperature. The brown solution was washed with ether (4 x 10 mL) and the combined organic layers were washed with water (4 x 10 mL). The organic layer was dried ($MgSO_4$), filtered and evaporated under reduced pressure. Recrystallization of the orange residue from pentanes (-78 ^oC) and vacuum filtration yielded **2.5** as yellow needles (0.72 g, 95 % yield), mp = 53-54 ^oC (lit.[34] 53-54 ^oC). IR (thin-film, cm^{-1}) 3110, 2106, 1454, 1409, 1373, 1284, 1163, 1104, 1024, 1001, 916, 822, 741; ^1H ($CDCl_3$) δ 4.29 (s, 5H), 4.26 (t, *J* = 2.0 Hz, 2H), 4.04 (t, *J* = 2.0 Hz, 2H); ^{13}C ($CDCl_3$) δ 69.2, 65.4, 60.7.

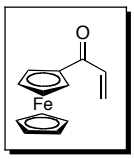

Acryloylferrocene (2.10). Freshly sublimed ferrocenecarboxaldehyde (228 mg, 2.0 mmol) was dissolved in THF (anhydrous, 10 mL) and cooled to 0 ^{o}C. With stirring, vinylmagnesium bromide (5.7 mL, 4.0 mmol, 0.7 *M* in THF) was added drop-wise and the reaction was allowed to warm to room temperature. After 16 h, the reaction was quenched with sat. aq. NH_4Cl solution in an ice bath. The resulting mixture was filtered and the aqueous layer extracted with DCM (3 times). The combined organic layers were dried ($MgSO_4$), filtered and evaporated under reduced pressure to yield the crude alcohol.

The crude alcohol was dissolved in EtOAc (10 mL) and stirred, while MnO_2 (1.74 g, 20 mmole) was added in portions. Stirring was continued for 2 h followed by vacuum filtration through celite. Evaporation of the solvent under reduced pressure and flash column chromatography (20% EtOAc in hexanes) yielded **2.10**. A portion was recrystallized (red needles) from hexanes/DCM for mp analysis (381 mg, 79 % yield), mp = 72-73 ^{o}C (lit.[53] 73.5-74^{o}C). IR (thin-film, cm^{-1}); ^{1}H ($CDCl_3$) δ 6.81 (dd, *J* = 11.0, 18.0 Hz, 1H), 6.45 (dd, *J* = 1.0, 18.0 Hz, 1H), 5.71 (dd, *J* = 1.0, 11.0 Hz, 1H), 4.83 (t, *J* = 2.0 Hz, 2H), 4.57 (t, *J* = 2.0 Hz, 2H), 4.19 (s, 5H); ^{13}C ($CDCl_3$) δ 193.4, 133.2, 126.6, 79.8, 73.1, 70.2, 69.9.

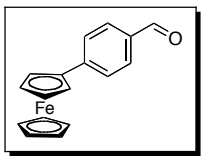

***p*-Ferrocenylbenzaldehyde (2.12)**. The preparation of **2.12** was conducted over two steps beginning with the synthesis

of the diazonium salt from 4-aminobenzaldehyde.[31] Fluoroboric acid (16 mL, 50% in H_2O) was stirred in an Erlenmeyer flask prior to the addition of 4-aminobenzaldehyde (2.42 g, 20.0 mmol). Boiling water (14 mL) was added to the vigorously stirred mixture before cooling the solution to 0 ^oC. Sodium nitrite (2.06 g, mmol) was added slowly in portions and stirring was continued at 0 ^oC until the evolution of gas ceased. The reaction vessel was placed in the refrigerator overnight to yield the diazonium salt as off-white crystals, which were filtered, rinsed with ether and used without further purification (quantitative yield).

Ferrocene (1.58 g, 8.5 mmol) was dissolved in acetic acid (100 mL) and stirred at room temperature. The prepared diazonium salt (3.73 g, 17 mmol) was added to the stirring reaction mixture in portions, at which time the solution became dark in color. The reaction was stirred for 3 h followed by extraction with DCM (3 times). The combined organic layers were washed with sat. $NaHCO_3$ solution and brine prior to drying with Na_2SO_4. Solvent was removed by rotary evaporation and the resulting residue was passed through a plug of silica (25% EtOAc in hexanes). Further purification by flash column chromatography (5% EtOAc in hexanes) yielded **2.12** as red needles (0.98 g, 40% yield), mp = 122-125 ^oC (lit.[54] 121-129 ^oC). IR (thin-film, cm^{-1}) 3104, 1690, 1599, 1105, 828; ^1H ($CDCl_3$) δ 9.97 (s, 1H), 7.79 (d, J = 8.0 Hz, 2H), 7.59 (d, J = 8.0 Hz, 2H), 4.74 (t, J = 2.0 Hz, 2H). 4.43 (t, J = 2.0 Hz, 2H), 4.05

(s, 5H); ^{13}C ($CDCl_3$) δ 191.9, 147.5, 134.2, 130.1, 126.3, 83.0, 70.3, 70.1, 67.2.

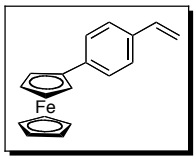

***p*-Ferrocenylstyrene (2.13)**. To a round bottom flask under dry nitrogen was added methyltriphenylphosponium bromide (536 mg, 1.5 mmol) and THF (anhydrous, 5mL). The mixture was stirred and cooled to 0 ^oC prior to the drop-wise addition of *n*-butyllithium (0.63 mL, 1.5 mmol, 2.4 *M* in hexanes). Stirring was continued for 10 min before adding **2.12** (290 mg, 1mmol) in THF (anhydrous, 2 mL). After stirring for 2.5 h at room temperature the reaction was complete (TLC) and quenched with water (1 mL). Vacuum filtration of the reaction mixture through celite and evaporation of the solvent gave the crude alkene. Purification by flash column chromatography (5% EtOAc in hexanes) gave **2.13** as a red-orange amorphous solid (250 mg, 87% yield), mp = 119-120 ^oC (lit.[55] 128-128.5 ^oC recryst. From petroleum ether). IR (thin-film, cm^{-1}) 3115, 3082, 2917, 1690, 1626, 1604, 1522, 1410, 1385, 1278, 1102, 1028, 990, 902, 839, 814; ^1H ($CDCl_3$) δ 7.45 (app dt, *J* = 1.5, 8.0 Hz, 2H), 7.35 (app dt, *J* = 1.5, 8.0 Hz, 2H), 6.72 (dd, *J* = 11.0, 17.5 Hz, 1H), 5.46 (dd, *J* = 0.5, 17.5 Hz, 1H), 5.24 (dd, *J* = 0.5, 11.0 Hz, 1H), 4.66 (t, *J* = 2.0 Hz, 2H), 4.33 (t, *J* = 2.0 Hz, 2H), 4.05 (s, 5H); ^{13}C ($CDCl_3$) δ 139.2, 136.8, 135.4, 126.4, 126.3, 113.0, 85.1, 69.8, 69.2, 66.6.

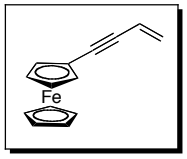

But-3-en-1-ynyl-ferrocene (2.16). The synthesis of enyne **2.16** was adapted from a previously published procedure by Todo et al.[33] Under an inert atmosphere CuI (2 mg), $Pd(PPh_3)_2Cl_2$ (4 mg), triethylamine (3 mL), and ethynylferrocene (217 mg, 1.03 mmol) in THF (anhydrous, 2 mL) were stirred at room temperature. Vinyl bromide (1.55 mL, 1.55 mmol, 1.0 *M* in THF) was added and the red-orange mixture was allowed to stir for 20 h at room temperature. The reaction mixture was quenched with 1N HCl (1 mL) followed by the addition of aq. sat. $NH_4^+Cl^-$ solution (1 mL) and subsequent extraction with ether. The organic layer was dried ($MgSO_4$), filtered, and evaporated under reduced pressure to give the crude enyne. Purification through a short silica column using hexanes as eluent yielded **2.16** as red crystals (197 mg, 81% yield), mp = 51-52 ^oC. IR (thin-film, cm^{-1}) 3096, 3005, 2223, 2199, 1603, 1462, 1410, 1262, 1201, 1106, 1038-955, 913, 819; ^1H ($CDCl_3$) δ 5.94 (dd, *J* = 11.0, 17.5 Hz, 1H), 5.68 (dd, *J* = 2.0, 17.5 Hz, 1H), 5.48 (dd, *J* = 2.0, 11.0 Hz), 4.45 (t, *J* = 2.0 Hz, 2H), 4.24 (s, 5H), 4.23 (t, *J* = 2.0 Hz, 1H); ^{13}C ($CDCl_3$) δ 125.6, 117.8, 89.3, 84.8, 71.5, 70.1, 70.0, 69.0, 65.2.

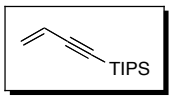

But-3-en-1-ynyl-triisopropylsilane (2.17). The synthesis of **2.17** was conducted as previously described by Todo et al.[33] Under an inert atmosphere CuI (20 mg), $Pd(PPh_3)_2Cl_2$ (37 mg), triethylamine (5 mL), and triisopropysilyl acetylene (0.50 g, 0.62 mL, 2.64 mmol) were

stirred at room temperature. Vinyl bromide (3.95 mL, 3.95 mmol, 1.0 *M* in THF) was added and the ruby-red mixture was allowed to stir for 20 h at room temperature. The reaction mixture was quenched with 1N HCl (2 mL) followed by the addition of sat. aq. NH_4Cl solution (2 mL) and subsequent extraction with ether. The organic layer was dried ($MgSO_4$), filtered, and evaporated under reduced pressure to give the crude enyne. Flash column chromatography using hexanes as eluent yielded **2.17** as a clear colorless oil (0.55 g, 99% yield). IR (thin-film, cm^{-1}) 3101, 3011, 2944, 2866, 2150, 2063, 1608, 1597, 1463, 1103, 952, 919, 883, 677, 661; ^1H ($CDCl_3$) δ 5.83 (dd, *J* = 11.0, 17.5 Hz, 1H), 5.68 (dd, *J* = 2.0, 17.5 Hz, 1H), 5.49, (dd, *J* = 2.0, 11.0 Hz, 1H), 1.11-1.10 (m, 21H);^{13}C ($CDCl_3$) δ 127.7, 117.8, 105.9, 91.5, 18.9, 11.5.

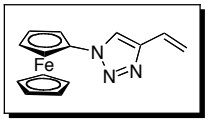

1-Ferrocenyl-4-vinyl-1*H*-1,2,3-triazole (2.18). Compound **2.18** was synthesized utilizing a procedure published by Siemeling et al.[35] To a round bottom flask was added **2.5** (230 mg, 1.0 mmol), THF (anhydrous, 20 mL), **2.17** (313 mg, 1.5 mmol) and CuI (20 mg, 0.1 mmol). A solution of TBAF (1.5 mL, 1.5 mmol, 1.0 *M* in THF) was added and stirring was continued for 2 days in the dark. The solvent was evaporated under reduced pressure and the crude product was dry loaded onto silica gel. Flash column chromatography (hexanes then 10% EtOAc in hexanes) eluted pure **2.18** as a yellow amorphous solid. A small portion was crystallized (yellow needles) for mp analysis by slow evaporation from hexanes/DCM

(201 mg, 72% yield), mp = 148-149 °C. IR (thin-film, cm^{-1}) 3401, 3120, 2923, 1632, 1514, 1410, 1223, 1105, 1039, 995, 921, 820; ^1H ($CDCl_3$) δ 7.72 (s, 1H), 7.52, (dd, *J* = 11.0, 18.0 Hz, 1H), 5.96 (dd, *J* = 1.0, 18.0 Hz, 1H), 5.39 (dd, *J* = 1.0, 11.0 Hz, 1H), 4.84 (t, *J* = 2.0 Hz, 2H), 4.27 (t, *J* = 2.0 Hz, 2H), 4.22 (s, 5H); ^{13}C ($CDCl_3$) δ 146.4, 125.6, 119.8, 116.5, 93.8, 70.4, 66.9, 62.1; HRMS (ESI) for $C_{14}H_{13}N_3Fe$ $[M + H]^+$ calcd, 280.05316, found, 280.05369 (error = 1.8807 ppm).

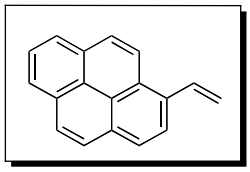

1-Vinylpyrene (2.19). The procedure of Cumming et al. was generally followed.[38] To a two-neck, round bottom flask under N_2 was added methyltriphenylphosphonium bromide (0.85 g, 2.4 mmol) and 18-crown-6 (18.0 mg, 0.07 mmol). A 1.0 *M* solution of potassium *t*-butoxide (2.4 mL, 2.4 mmol in THF) was added and the mixture was further diluted with THF (7.0 mL) and cooled to 0 °C. A solution of 1-pyrenecarboxaldehyde (0.50 g, 2.2 mmol) in THF (3.0 mL) was added drop-wise over 10 min to the cooled solution and was allowed to stir at room temperature overnight. The mixture was filtered and the filter cake dissolved in diethyl ether before being passed through a short bed of neutral alumina. Evaporation yielded a yellow solid, which was further purified to a white solid by flash column chromatography using hexanes as eluent (0.23 g, 47% yield); mp 86-88 °C (lit.[56] 87-89 °C); ^1H NMR (500 MHz, $CDCl_3$) δ 8.41-8.39 (d, *J* = 9.0 Hz, 1H), 8.22-8.20 (sext, *J* = 8.0, 4.5 Hz, 4H), 8.13-8.11 (d, *J*

= 9.0 Hz, 1H), 8.05 (s, 2H), 8.02-7.99 (t, *J* = 7.5 Hz, 1H), 7.83-7.77 (dd, *J* = 11.0, 17.5 Hz, 1H), 6.02-5.98 (d, *J* = 17.0 Hz, 1H), 5.63-5.61 (d, *J* = 11.5 Hz, 1H); ^{13}C NMR (125 MHz, $CDCl_3$) δ 134.4, 132.6, 131.7, 131.2, 131.1, 128.3, 127.8, 127.6, 127.5, 126.2, 125.5, 125.2, 123.9, 123.3, 117.5.

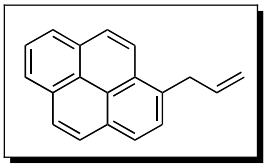

1-Allylpyrene (2.20). The procedure of Takuwa et al. was generally followed.[39] 1-Bromopyrene (100 mg, 0.35 mmol) was stirred in a mixture of anhydrous benzene and diethyl ether (4:1, 2.0 mL) in a two-neck, round bottom flask. The solution was stirred at room temperature under N_2 and *n*-BuLi (2.2 *M* in hexanes, 0.19 mL, 0.53 mmol) was added drop-wise, at which time the mixture became bright yellow. The solution was stirred for 30 min before adding freshly distilled allyl bromide. Following an additional 20 min of stirring, no solid remained in the yellow solution, which was then cooled to 0 ^{o}C and quenched with saturated ammonium chloride solution. The reaction was extracted with ether (3 x 20 mL) and the combined organic layers were washed with water (30 mL), dried with $MgSO_4$, vacuum filtered, and evaporated to yield a yellow oil. Purification by flash column chromatography using hexanes as eluent yielded a pale-yellow oil, which was stored away from light, nitrogen flushed, and in a freezer (52.1 mg, 62% yield); ^{1}H NMR (500 MHz, $CDCl_3$) δ 8.29-8.27 (d, *J* = 9.5 Hz, 1H), 8.22-8.10 (m, 4H), 8.07-7.99 (m, 3H), 7.91-7.89 (d, *J* = 7.5 Hz, 1H), 6.27-6.20 (m, 1H), 5.16-5.13 (dq, *J* = 1.5, 10.0 Hz, 1H), 5.11-5.06

(dq, *J* = 2.0, 17.0 Hz, 1H), 4.14-4.12 (dt, *J* = 1.5, 6.0 Hz, 2H); ^{13}C NMR (125 MHz, $CDCl_3$) δ 137.5, 134.1, 131.6, 131.3, 131.1, 130.3, 129.1, 127.7, 127.60, 127.57, 127.5, 126.9, 126.0, 125.2, 125.1, 125.0, 124.9, 123.8, 116.3, 37.9.

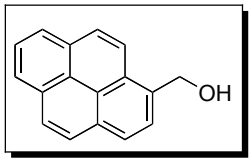

1-Hydroxymethylpyrene. The procedure of Malashikhin and Finney was generally followed.[57] To a round bottom flask charged with a stir bar, 1-pyrenecarboxaldehyde (0.50 g, 2.2 mmol) was stirred at 0 °C in THF. A solution of $NaBH_4$ (0.25 g, 6.5 mmol) in 95% ethanol (15 mL) was prepared along with ten drops of 1 M NaOH. This solution was added to the aldehyde and stirred at 0 °C for 15 min and changed from a yellow-green color to milky-white. The mixture was quenched with 10% HCl (v/v), diluted with water (50 mL) and extracted with CH_2Cl_2 (3 x 30 mL). The combined organic fractions were washed with $NaHCO_3$ and water successively (30 mL each), and dried with $MgSO_4$. Filtration and evaporation gave the desired alcohol, which was used without further purification (0.50 g, 98% yield); mp 122-123 °C (lit.[58] 123-124 °C); ^{1}H NMR (500 MHz, $CDCl_3$) δ 8.40-8.38 (d, *J* = 9.5 Hz, 1H), 8.22-8.16 (m, 4H), 8.08-8.16 (m, 4H), 5.43-5.42 (d, *J* = 5.5 Hz, 2H), 1.88-1.86 (t, *J* = 5.5 Hz, 1H); ^{13}C NMR (125 MHz, $CDCl_3$) δ 128.2, 127.8, 127.7, 126.3, 125.6, 125.0, 123.3, 64.1.

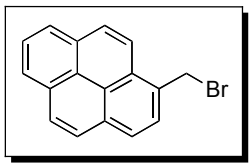

1-Bromomethylpyrene. The procedure of Malashikhin and Finney was generally followed.[57] To a 2-neck round bottom flask under N_2 was added 1-hydroxymethylpyrene (0.50 g, 2.2 mmol) and pyridine (0.09 mL, 1.1 mmol) in anhydrous CH_2Cl_2 (40 mL). The clear solution was stirred at 0 ^oC and phosphorous tribromide (0.10 mL, 1.1 mmol) in CH_2Cl_2 (2.5 mL) was added drop-wise, at which point the solution became cloudy. After stirring for 3 h at 0 ^oC, the reaction was poured into a mixture of ice and CH_2Cl_2 (100 mL). The organic layer was washed with water, saturated $NaHCO_3$, and water (50 mL each). The organic layer was dried with $MgSO_4$, filtered and evaporated to give a pale-yellow solid, which was recrystallized from benzene. According to Geerts and Martin,[40] 1-bromomethylpyrene should be used immediately, as it is not stable (0.54 g, 85% yield), mp 134-135 ^oC (lit.[59] 136-137 ^oC); ^1H NMR (500 MHz, $CDCl_3$) δ 8.40-8.38 (d, *J* = 9.5 Hz, 1H), 8.26-8.22 (m, 3H), 8.13-8.02 (m, 5H), 5.27 (s, 2H); ^{13}C NMR (125 MHz, $CDCl_3$) δ 132.1, 131.4, 130.9, 130.7, 129.2, 128.5, 128.40, 128.32, 128.26, 128.2, 128.0, 127.9, 127.7, 127.6, 127.5, 126.4, 125.8, 125.3, 125.0, 124.9, 124.8, 123.0, 32.4.

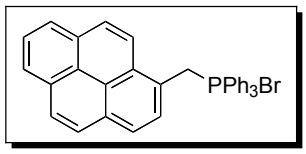

Triphenyl(pyren-1-ylmethyl)phosphonium bromide (2.22). The procedure of Geerts and Martin was generally followed.[40] To a 2-neck round bottom flask under N_2 was added 1-bromomethylpyrene (0.50 g, 1.7 mmol) and

recrystallized triphenylphosphine (0.45 g, 1.7 mmol) in toluene (16 mL). The reaction was stirred at reflux for 2 h in the dark. The product precipitated out of solution as a white solid and was vacuum filtered, washed with toluene, water and dried under vacuum (0.80 g, 85% yield); ^{1}H NMR (500 MHz, CD_3OD), δ 8.18-8.17 (d, *J* = 7.5 Hz, 1H), 8.07-8.04 (t, *J* = 8.0 Hz, 2H), 7.98-7.92 (m, 3H), 7.76-7.73 (m, 3H), 7.71-7.69 (dd, *J* = 2.5, 8.0 Hz, 1H), 7.66 (s, 2H), 7.59-7.50 (m, 12H), 5.58-5.55 (d, *J* = 14.5 Hz, 2H); ^{13}C NMR (125 MHz, CD_3OD), δ 136.5, 135.8, 135.6, 135.5, 133.1, 132.6, 132.1, 132.0, 131.6, 131.4, 131.3, 130.5, 130.4, 129.5, 129.2, 128.3, 127.8, 127.1, 126.8, 125.9, 125.2, 123.4, 121.7, 121.6, 119.3, 118.7, 28.7, 28.3.

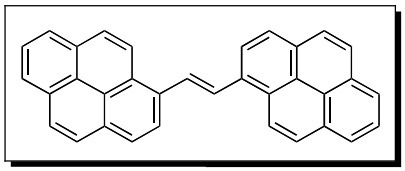

(*E*)-1,2-di(pyren-1-yl)ethane (2.21). The procedure of Geerts and Martin was generally followed.[40] To a 2-neck round bottom flask under N_2 was added triphenyl(pyren-1-ylmethyl)phosphonium bromide (0.72 g, 1.3 mmol), 1-pyrenecarboxaldehyde (0.22 mg, 0.94 mmol), and absolute ethanol (25 mL). The mixture was stirred to dissolution prior to adding *t*-BuOK in THF (0.30 mL, 1.3 mmol, 20 wt. %) at room temperature. Immediately upon addition of the *t*-BuOK solution, the reaction became orange in color and was allowed to stir for 3 h in the dark. Filtration of the light orange solid and subsequent suspension in boiling water gave a yellow-orange solid, which was dried under vacuum. Trituration in hexanes and

filtration gave a yellow powder. Extra care was taken to protect the product from exposure to light and excess heat (0.367 g, 91% yield); mp 306-308 ^{o}C (yellow to orange to brown; lit.[40] 306.5-308 ^{o}C); ^{1}H NMR (600 MHz, $CDCl_3$), δ 8.63-8.62 (d, *J* = 9.0 Hz, 1H), 8.56-8.55 (d, *J* = 7.8 Hz, 1H), 8.51-8.49 (d, *J* = 9.0 Hz, 1H), 8.46 (s, 1H). 8.29-8.27 (d, *J* = 8.4 Hz, 1H), 8.23-8.17 (m, 5H), 8.14-8.10 (m, 3H), 8.05-8.00 (m, 3H), 7.92-7.90 (d, *J* = 9.0 Hz, 1H), 7.82 (s, 1H), 7.73-7.71 (d, *J* = 8.4 zHz, 1H), 7.61-7.60 (d, *J* = 8.4 Hz, 1H).

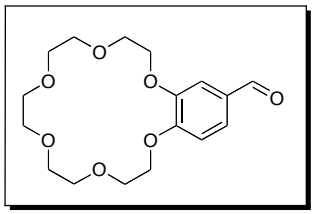

4´-Formylbenzo[18-crown-6] (2.27). The aldehyde was synthesized in one step according to the procedure of D'Souza et al.[60] 3,4-Dihydroxybenzaldehyde (230 mg, 1.67 mmol) was dissolved in dry DMF (10 mL) K_2CO_3 (1.15 g, 8.32 mmol) was added. The resulting mixture was heated to 80 ^{o}C under dry nitrogen and stirred for 30 min prior to the drop-wise addition of pentaethylene glycol di(*p*-toluenesulfonate) (1.0 g, 1.83 mmol) in DMF (2 mL). The reaction mixture was stirred for 20 h at 80 ^{o}C, cooled and the DMF evaporated under a stream of nitrogen. Chloroform was added to the residue followed by filtration through celite. Evaporation of the chloroform under reduced pressure, flash column chromatography (5% methanol in chloroform), and recrystallization from ethanol gave the desired aldehyde (398 mg, 70% yield), mp = 59-61 ^{o}C (lit.[61] 60-62 ^{o}C). IR (thin film, cm^{-1}) 3077, 2877, 1682, 1586, 1511, 1437, 1397, 1355, 1270, 1171, 1124, 1052, 954; ^{1}H

NMR ($CDCl_3$) δ 9.80 (s, 1H), 7.41 (dd, *J* = 1.5, 8.5 Hz, 1H), 7.36 (d, *J* = 1.5 Hz, 1H), 6.93 (d, *J* = 8.5 Hz, 1H), 4.21-4.17 (m, 4H), 3.94-3.92 (m, 4H), 3.91-3.89 (m, 2H), 3.76-3.73 (m, 4H), 3.70-3.67 (m, 4H), 3.54 (s, 4H); ^{13}C NMR ($CDCl_3$) δ 190.8, 154.3, 149.1, 130.0, 126.7, 111.9, 111.1, 70.9, 70.7, 70.6, 70.55, 70.47, 69.2, 69.1, 68.9.

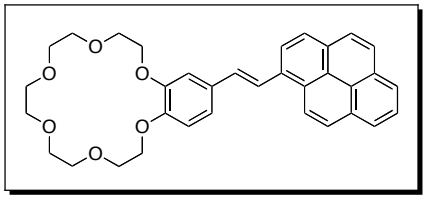

(*E*)-18-(2-(pyren-1-yl)vinyl)-2,3,5,6,8,9,11,12,14,15-decahydrobenzo[*b*][1,4,7,10,13,16]hexaoxacyclooctadecine (2.26). To a round bottom flask under a flow of dry nitrogen and charged with a stir bar was added triphenyl(pyren-1-ylmethyl)phosphonium bromide (88.6 mg, 0.158 mmol) and THF (anhydrous, 10 mL). The mixture was cooled to 0 ^oC and *n*-butyllithium (63 mL, 0.158 mmol, 2.5 *M* in hexanes) was added drop-wise to form the red-orange phosphonium ylide. Stirring was continued for 10 min prior to the addition of **2.27** (48.1 mg, 0.141 mmol) in THF (anhydrous, 2 mL). The reaction was allowed to warm to room temperature and stir for 16 h, at which time the color became iridescent yellow/green. Distilled water (1 mL) was added and the solvent was evaporated under reduced pressure to yield a yellow residue, which was purified by flash column chromatography (10% methanol in chloroform). Further impurities were removed by dissolving the compound in a minimal amount of THF and placing aliquots into micro centrifuge tubes.

Hexanes was added to each aliquot to precipitate **2.26**, followed by centrifugation and subsequent washing of the pellets with a drop of ethanol and hexanes (remaining volume, repeat 3 times). The pellets were combined to give **2.26** as a fluorescent green film or yellow residue (46.7 mg, 61% yield), mp = 106-108 ^{o}C. IR (thin film, cm^{-1}) 3043, 2919, 2872, 1597, 1577, 1514, 1452, 1429, 1354, 1270, 1247, 1130, 954, 845; ^{1}H NMR (CD_2Cl_2) δ 8.54(d, *J* = 9.5 Hz, 1H), 8.34(d, *J* = 8.0 Hz, 1H), 8.21-8.19 (m, 3H), 8.16 (d, *J* = 9.5 Hz, 1H), 8.09-8.01 (m, 4H), 7.33 (d, *J* = 15.5 Hz, 1H), 7.28 (d, *J* = 2.5 Hz, 1H), 7.23 (dd, *J* = 2.5, 8.5 Hz, 1H), 6.94 (d, *J* = 8.0 Hz, 1H), 4.29-4.27 (m, 2H), 4.21-4.19 (m, 2H), 3.94-3.92 (m, 2H), 3.91-3.89 (m, 2H), 3.75-3.72 (m, 4H), 3.69-3.67 (m, 4H), 3.65 (s, 4H); ^{13}C NMR (CD_2Cl_2) δ 149.63, 149.56, 132.8, 132.3, 132.2, 131.6, 131.2, 128.7, 128.0, 127.97, 127.6, 126.6, 125.8, 125.6, 125.5, 124.0, 123.7, 121.0, 113.7, 111.7, 71.1, 71.0, 70.0, 69.9, 69.2, 69.1; HRMS (ESI) calcd for $C_{34}H_{34}O_6K$ $[M + K]^+$ 577.19870, found *m/z* 577.20180.

References

[1] Hashmi, A. S. K.; Hutchings, G. J. *Angew. Chem. Int. Ed.* **2006**, *45*, 7896-7936.

[2] Brust, M.; Walker, M.; Bethell, D.; Schiffrin, D. J.; Whyman, R. *J. Chem. Soc. Chem. Commun.* **1994**, 801-802.

[3] Yee, C.; Scotti, M.; Ulman, A.; White, H.; Rafailovich, M.; Sokolov, S. *Langmuir*, **1999**, *15*, 4314-4316.

[4] Hiramatsu, H.; Osterloh, F. E. *Chem. Mater.* **2004**, *16*, 2509-2511.

[5] Chen, S. W.; Sommers, J. M. *J. Phys. Chem. B* **2001**, *105*, 8816-8820.

[6] Yang, J.; Lee, J. Y.; Too, H.-P. *Analytica Chimica Acta* **2006**, *571*, 206-210.

[7] Vignolle, J.; Tilley, T. D. *Chem. Commun.* **2009**, 7230-7232.

[8] Zhang, S.; Chandra, K. L.; Gorman, C. B. *J. Am. Chem. Soc.* **2007**, *129*, 4876-4877.

[9] Simonian, A. L.; Good, T. A.; Wang, S.-S.; Wild, J. R. *Analytica Chimica Acta*, **2005**, *534*, 69-77.

[10] Petros, R. A.; DeSimone, J. M. *Nat. Rev. Drug Discovery*, **2010**, *9*, 615-627.

[11] Perrier, T.; Saulnier, P.; Benoît, J.-P. *Chem. Eur. J.* **2010**, *16*, 11516-11529.

[12] Chen, S. W.; Konopelski, J. P.; Wang, H. "CRC: Nanoparticle-Mediated Electronic Communication," **2008**, NSF CHE-0832065.

[13] Shaowei Chen group website: www.chem.ucsc.edu/~schen/

[14] Haobin Wang group website: www.chemistry.nmsu.edu/hwang_new.html

[15] Chen, W.; Davies, J. R.; Ghosh, D.; Tong, M. C.; Konopelski, J. P.; Chen, S. *Chem. Mater.* **2006**, *18*, 5253-5259.

[16] Tulevski, G. S.; Myers, M. B.; Hybertsen, M. S.; Steigerwald, M. L.; Nuckolls, C. *Science*, **2005**, *309*, 591-594.

[17] Viau, G.; Brayner, R.; Poul, L.; Chakroune, N.; Lacaze, E.; Fievet-Vincent, F.; Fievet, F. *Chem. Mater.* **2003**, *15*, 486-494.

[18] Creighton, J. A.; Eadon, D. G. *J. Chem. Soc. Faraday Trans.* **1991**, *87*, 3881-3891.

[19] Caruso, F.; Gittins, D. I. *J. Phys. Chem. B*, **2001**, *105*, 6846-6852.

[20] Zhai, J.; Zhai, Y.; Dong, S. *Colloids Surf. A*, **2009**, *335*, 207-210.

[21] Cowan, D. O.; LeVanda, C.; Park, J.; Kaufman, F. *Acc. Chem. Res.* **1973**, *6*, 1-7.

[22] Powers, M. J.; Meyer, T. J. *J. Am. Chem. Soc.* **1978**, *100*, 4393-4398.

[23] Kaim, W.; Klein, A.; Glöckle, M. *Acc. Chem. Res.* **2000**, *33*, 755-763.

[24] Chen, W.; Chen, S. W.; Ding, F.; Wang, H.; Brown, L. E.; Konopelski, J.P. *J. Am. Chem. Soc.* **2008**, *130*, 12156-12162.

[25] Chidsey, C. E. D.; Bertozzi, C. R.; Putvinkski, T. M.; Mujsce, A. M. *J. Am. Chem. Soc.* **1990**, *112*, 4301-4306.

[26] Ding, F.; Wang, H.; Wu, Q.; Van Voorhis, T.; Chen, S. W.; Konopelski, J. P. *J. Phys. Chem. A* **2010**, *114*, 6039-6046.

[27] Ast, S.; Müller, H.; Flehr, R.; Klamroth, T.; Walz, B.; Holdt, H.-J. *Chem. Commun.* **2011**, *47*, 4685-4687.

[28] Kolb, H. C.; Sharpless, K. B. *Drug Discovery Today*, **2003**, *8*, 1128-1137.

[29] Fulton, J. R.; Aggarwal, V. K.; de Vicente, J. *Eur. J. Org. Chem.* **2005**, 1479-1492.

[30] Ipaktschi, J.; Hosseinzadeh, R.; Sclaf, P.; Dreiseidler, E. *Helv. Chim. Acta* **1998**, *81*, 1821-1834.

[31] Lai, L-L.; Ho, C-H.; Lin, Y-J.; Wang, E.; Liu, Y-H.; Wang, Y.; Lin, Y-C.; Cheng, K-L. *Helv. Chim. Acta.* **2002**, *85*, 108-114.

[32] Luo, S.-J.; Liu, Y.-H.; Liu, C.-M.;Liang, Y.-M.; Ma, Y.-X. *Synth. Commun.* **2000**, *30*, 1569-1572.

[33] Todo, H.; Terao, J.; Watanabe, H.; Kuniyasu, H.; Kambe, N. *Chem. Commun.* **2008**, 1332-1334.

[34] Nesmeyanov, A. N.; Drozd, V. N.; Sazonova, V. A. *Dokl. Akad. Nauk SSSR*, **1963**, *150,* 321-324.

[35] Siemeling, U.; Rother, D. *J. Organomet. Chem.* **2009**, *694*, 1055-1058.

[36] Focsanneanu, K.-S.; Scaiano, J. C. *Photochem. Photobiol. Sci*, **2005**, *4*, 817-821.

[37] Chen, W.; Zuckerman, N. B.; Lewis, J. W.; Konopelski, J. P.; Chen, S. W. *J. Phys. Chem. C*, **2009**, *113*, 16988-16995.

[38] Cumming, W. J.; Gaudiana, R. A.; Ingwall, R. T.; Kolb, E. S.; Mehta, P. G.; Minns, R. A. Polaroid Corporation, Cambridge Mass. U. S. Patent 5,414,069; **1995**.

[39] Takuwa, A.; Kanaue, T.; Yamashita, K.; Nishigaichi, Y. *J. Chem. Soc., Perkin Trans. 1*, **1998**, 1309-1314.

[40] Geerts, J. P.; Martin, R H. *Bull. Soc. Chim. Belg.* **1960**, *69*, 563-569.

[41] Chen, W.; Zuckerman, N. B.; Konopelski, J. P.; Chen, S. W. *Anal. Chem.* **2010**, *82*, 461-465.

[42] Yang, Y. F.; Zhou, Y. H.; Cha, C. S. *Electrochim. Acta* **1995**, *40*, 2579-2586.

[43] Kang, X.; Chen, W.; Zuckerman, N. B.; Konopelski, J. P.; Chen, S. W. *Langmuir* **2011**, *27,* 12636-12641.

[44] Kim, H. N.; Ren, W. X.; Kim, J. S.; Yoon, J. *Chem. Soc. Rev.* **2012**, *41*, 3210-3244.

[45] Varma, S.; Sabo, D.; Rempe, S. B. *J. Mol. Biol.* **2008**, *376*, 13-22.

[46] Glendening, E. D.; Feller, D.; Thompson, M. A. *J. Am. Chem. Soc.* **1994**, *116*, 10657-10669.

[47] Shin, E. J. *Chem. Lett.* **2002**, 686-687.

[48] Kang, X.; Li, X.; Hewitt, W. M.; Zuckerman, N. B.; Konopelski, J. P.; Chen, S. W. *Anal. Chem*. **2012**, *84*, 2025-2030.

[49] Landaverry, Y. R. Ph.D. Dissertation, University of California, Santa Cruz, **2007**.

[50] Song, Y.; Kang, X.; Zuckerman, N. B.; Phebus, B. D.; Konopelski, J. P.; Chen, S. W. *Nanoscale* **2011**, *3*, 1984-1989.

[51] Hu, P.; Zhao, K. Q.; and Xu, H. B. *Molecules* **2001**, *6*, M249.

[52] Hu, P.; Zhao, K. Q.; and Xu, H. B. *Molecules* **2001**, *6*, M250.

[53] Hauser, C. R.; Pruett, R. L.; Mashburn, T. A. *J. Org. Chem.* **1961**, *26*, 1800-1801.

[54] Egger, H.; Schloegel, K. *Monatsh. Chem.* **1964**, *6*, 1750-1758.

[55] Traylor, T. G.; Ware, J. C. *J. Am. Chem. Soc.* **1967**, *89*, 2304-2316.

[56] Flowers, R. G.; Nichols, F. S. *J. Am. Chem. Soc.* **1949**, *71*, 3104.

[57] Malashikhin, S.; Finney, N. S. *J. Am. Chem. Soc.* **2008**, *130*, 12846-12847.

[58] Bachmann, W. E.; Carmack, M. *J. Am. Chem. Soc.* **1941**, *63*, 2494-499.

[59] Hariharan, M.; Karunakaran, S. C.; Ramaiah, D. *Org. Lett.* **2007**, *9*, 417-420.

[60] D'Souza, F.; Chitta, R.; Gadde, S.; Zandler, M. E.; McCarty, A. L.; Sandanayaka, A. S. D.; Araki, Y.; Ito, O. *Chem. Eur. J.* **2005**, *11*, 4416-4428.

[61] Smid, J. *Org. Prep. Proceed. Intl.* **1976**, *8*, 193-196.

CHAPTER 3: Alkyne and Vinylidene-Protected Ruthenium Nanoparticles

3.1 Introduction

The examples of NPMEC in Chapter 2 elaborated on the Ru=C linkage and showed that effective overlap between the d_π orbital or the $p_\pi d_\pi$ hybrid orbital of the Ru metal and the π^* orbital of the ligand carbons[1,2] allowed for significant intervalence charge transfer (IVCT) between conjugated ferrocene moieties and extended intraparticle conjugation between particle bound fluorophores. The interfacial bonding interaction, as well as the unique metathesis characteristic of Ru, provided a versatile system for studying NPMEC through the appearance of novel optoelectronic properties. To extend the study of NPMEC we sought an alternative means for stabilizing Ru NPs, while still maintaining the potential for ligand-metal conjugation. We believed the Ru-C≡ system would provide the desired properties via the reaction of Ru and terminal alkynes. The manner in which these two pieces would come together would have to be elaborated based on what is known about organometallic and nanoparticle chemistry.

When looking to the literature for the stabilization of metal NPs via covalent carbon-metal bonds there are few examples.[3] Commonly the methods to stabilize the metal clusters follow a variation of the Brust/Schiffrin method[4] for the formation of thiolate-protected nanoparticles (as described in Chapter 2). Aqueous soluble metal salts are brought into the organic layer with phase transfer catalysts such as tetraoctylammonium bromide (TOABr),

and the reaction mixture is subsequently treated with a thiol and reducing agent. Although the ratio of thiol to gold is thought to control the size of the NPs, TOABr and other surfactants have also been used to stabilize NPs indicating a role in colloidal organization as well.[5]

Single-phase syntheses of metal NPs are also described in the literature.[6,7] The creation of alkanethiol-stabilized Au, Pd, and Ir nanoparticles were all synthesized by the reduction of a solution of the appropriate metal salt and thiol in THF with lithium triethylborohydride, as described by Sokolov and co-workers.[6] The use of common organic solvents and reducing agents in a homogenous synthesis were most attractive for our studies toward the development of alkyne-stabilized Ru NPs.

3.2 Synthesis of Alkyne-Protected Ruthenium Nanoparticles Using Lithium Acetylides

Our first attempt to synthesize alkyne-stabilized Ru NPs utilized a mixture of dried $RuCl_3$ x H_2O (40 ^oC vacuum oven), TOABr, and 1-octyne in anhydrous THF (Figure 3.1). This mixture was vigorously stirred and a 1.0 M solution of lithium triethylborohydride was added drop-wise to the solution, at which point the solution went from deep red to black. Attempts to purify this mixture (Dr. Wei Chen) by the methods previously described for Ru=C8 NPs revealed a complex mixture as seen by proton NMR. The addition of TOABr to aid in NP formation was most certainly ill advised under the reaction

conditions, as $LiEt_3BH$ may lead to Hofmann type elimination of the ammonium salt. Evaluation of a new route toward our goal was imperative.[8]

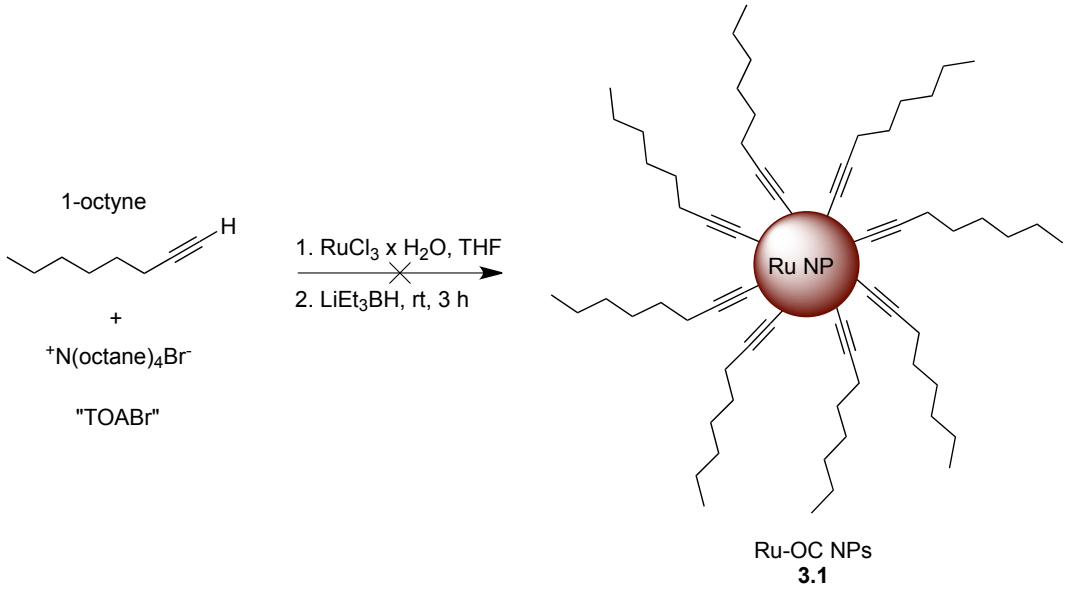

Figure 3.1 Failed attempt toward the synthesis of Ru-OC nanoparticles.

In the second approach to **3.1**, we wanted to remove the alkynyl proton completely to avoid the possibility of adverse effects on the chemical system. Therefore, we chose to work with the lithium acetylide via deprotonation with *n*-BuLi instead of the pure alkyne. The ratio of ligand to Ru was set at 3:1, which would seem excessive on first glance. In particular, one would predict a proper ratio of ligand to metal would be necessary so that some proportion of $RuCl_3$ remains for the formation of the NP core, and a ratio of 3:1 would seemingly produce only trialkynyl organoruthenate species. However, the source of $RuCl_3$ is not anhydrous and our method to dry the metal salt at 40 ^oC in a vacuum oven is insufficient to remove the majority of water molecules. Invariably, reaction of the lithium acetylide of 1-octyne with our “dry” $RuCl_3$

would lead to a mixture of $Ru(octyne)_3$, $RuCl(octyne)_2$, $RuCl_2(octyne)$ and $RuCl_3$. Subsequent treatment of the mixture of complexes with $LiEt_3BH$ was proposed as the reducing step, while any coordinating surfactants such as TOABr were eliminated from the procedure.

The formation of the lithium anion of 1-octyne was performed at -78 ^oC in THF (0.2 M). Following the formation of the lithium acetylide, a solution of the "dry" $RuCl_3$ in THF (0.01 M) was added drop-wise to the vigorously stirring solution. Immediately, the red $RuCl_3$ solution turned green upon mixing with the anion, but as the addition continued, a red-brown color persisted. The reaction was allowed to warm to room temperature and the formed complexes were then reduced over a period of three hours after the slow addition of excess $LiEt_3BH$ over 20 minutes. The solution was dark brown to black, and there were no apparent precipitates after quenching the remaining hydride with water or methanol. Fortunately, the purification of product, which had the characteristics of **3.1**, was performed similarly to the Ru=C8 NPs via centrifugation with ethanol to remove the excess ligands. Similar to Ru=C8 NPs, these were soluble in non-polar solvents such as hexanes, DCM and toluene. Initial characterization of the 1-octyne protected-Ru NPs (Ru-OC) by FTIR (Figure 3.2) and ^1H-NMR (Figure 3.3 B) were very promising.

3.3 Characterization and Properties of Alkyne-Protected Ruthenium Nanoparticles

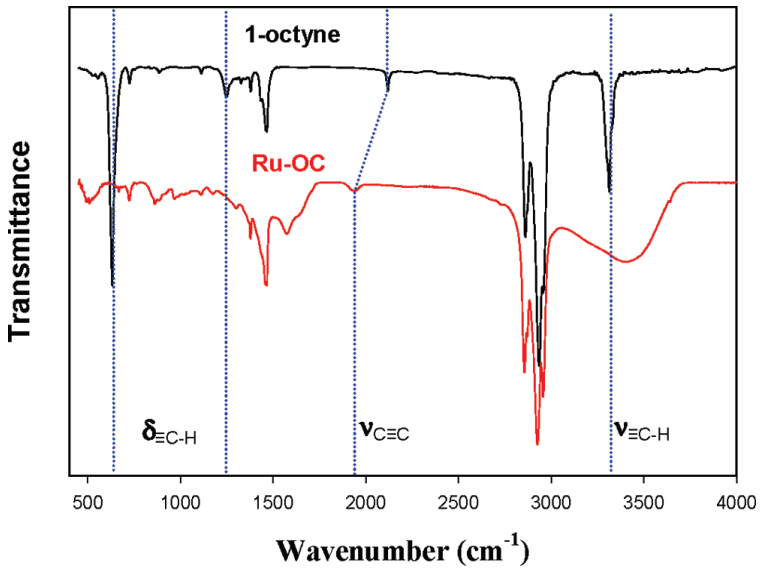

Figure 3.2 FTIR spectra of 1-octyne and Ru-OC nanoparticles. Figure reprinted with permission from Chen, W.; Zuckerman, N. B.; Kang, X.; Ghosh, D.; Konopelski, J. P.; Chen, S. W. *J. Phys. Chem. C* **2010**, *114*, 18146-18152. Copyright 2010, American Chemical Society.

Typically, the organic protecting layer surrounding the metal nanoparticle will look very similar to the monomeric ligand by FTIR. More importantly, the characteristic IR stretches can reveal the means in which the ligand is attached to the NP surface. The comparison of 1-octyne and **3.1** revealed the alkynyl ≡C-H stretch (3313 cm^{-1}), ≡C-H bend overtone (1255 cm^{-1}), and ≡C-H bend fundamental (631 cm^{-1}) were missing from the Ru-OC spectrum. While the C≡C stretch was apparent in both IR spectra, a red-shift from 2119 cm^{-1} to 1936 cm^{-1} from monomeric 1-octyne to the Ru NP bound alkyne was found (Figure 3.2).

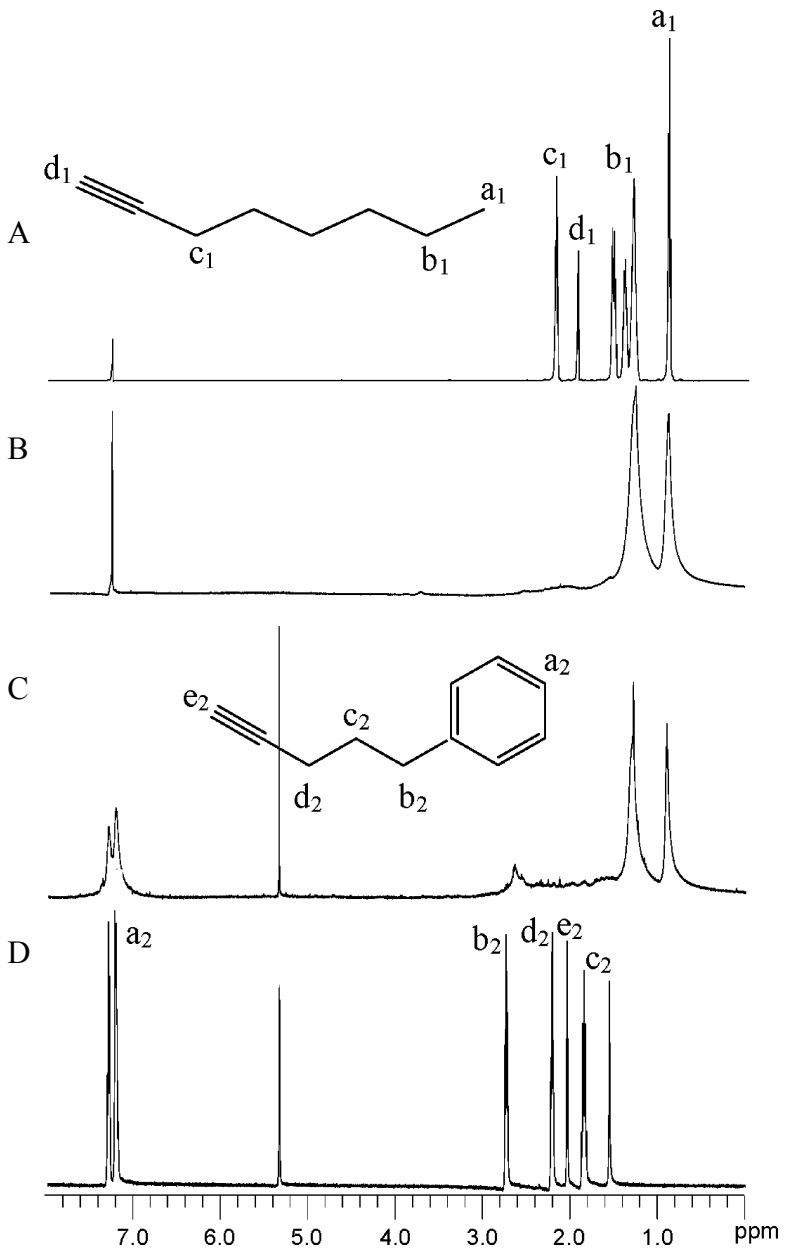

Figure 3.3 NMR Comparison A) ^{1}H-NMR of 1-octyne with labeled protons. B) ^{1}H-NMR of Ru-OC nanoparticles. C) ^{1}H-NMR of 5-phenyl-1-pentyne functionalized Ru-OC nanoparticles. D) ^{1}H-NMR of 5-phenyl-1-pentyne. Figure reprinted with permission from Chen, W.; Zuckerman, N. B.; Kang, X.; Ghosh, D.; Konopelski, J. P.; Chen, S. W. *J. Phys. Chem. C* **2010**, *114*, 18146-18152. Copyright 2010, American Chemical Society.

By ^{1}H-NMR, the broadened peaks for the protecting ligands were visible in the same regions as for 1-octyne. No free ligands were present, as

the peak for the acetylenic proton did not appear in the NMR spectrum of **3.1**. Due to the proximity of the methylene protons α to the alkyne, they were just barely seen as a broad bump around 2.0 ppm (Figure 3.3 B). Although the nature of the ligands could be analyzed by IR and NMR, more specialized techniques were necessary to determine the structure of the NPs themselves.

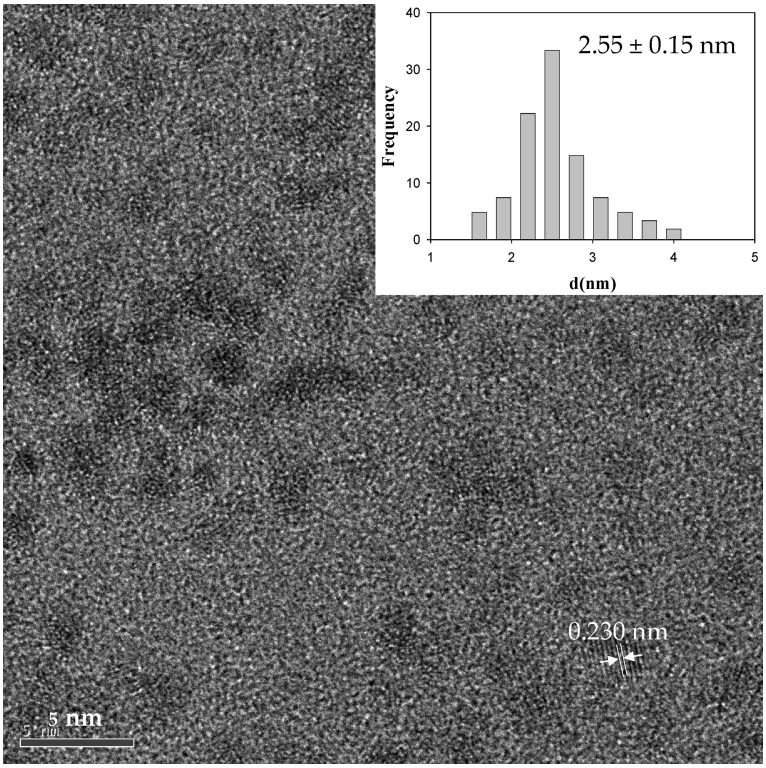

Figure 3.4 TEM Micrograph of Ru-OC Nanoparticles showing fringe measurement. The inset displays the size distribution of the particles. Figure reprinted with permission from Chen, W.; Zuckerman, N. B.; Kang, X.; Ghosh, D.; Konopelski, J. P.; Chen, S. W. *J. Phys. Chem. C* **2010**, *114*, 18146-18152. Copyright 2010, American Chemical Society.

Visual characterization by TEM was used to determine the morphology of the Ru-OC NPs, which showed an average core diameter of 2.55 ± 0.15 nm and a lattice fringe of 0.230 nm indicative of Ru (100) crystalline planes (Figure 3.4). Thus, the derived method was shown to be capable of providing

uniform and air-stable alkyne-protected Ru NPs. In addition to the broad scope of NPMEC, a motivating factor for protecting the Ru core with commercially available alkynes was the reduced cost over preparing octyldiazoacetate (ODA). However, these alkyne-protected Ru NPs would not necessarily replace Ru=C8 NPs due to their very different properties.

Unlike Ru=C8 NPs, when treated with terminal alkenes, **3.1** did not undergo metathesis to incorporate additional ligands of interest onto the Ru surface. However, two new methods were used to incorporate additional ligands by utilizing acetylide species. We first attempted a two-step approach whereby **3.1** was suspended in anhydrous toluene and treated with the lithium anion of 5-phenyl-1-pentyne in the same molar equivalent as used for 1-octyne (Scheme 3.1 A). Since the aryl group of the new ligand is on the terminal end furthest from the nanoparticle surface, we expected to see characteristic proton signals in the aromatic region. This was in fact the case as seen in the stacked spectrum of the functionalized NPs (**3.2**) versus the monomer of 5-phenyl-1-pentyne (Figure 3.3 C and D). Although this was a good proof of concept, this was not necessarily the most efficient route to incorporate a second ligand.

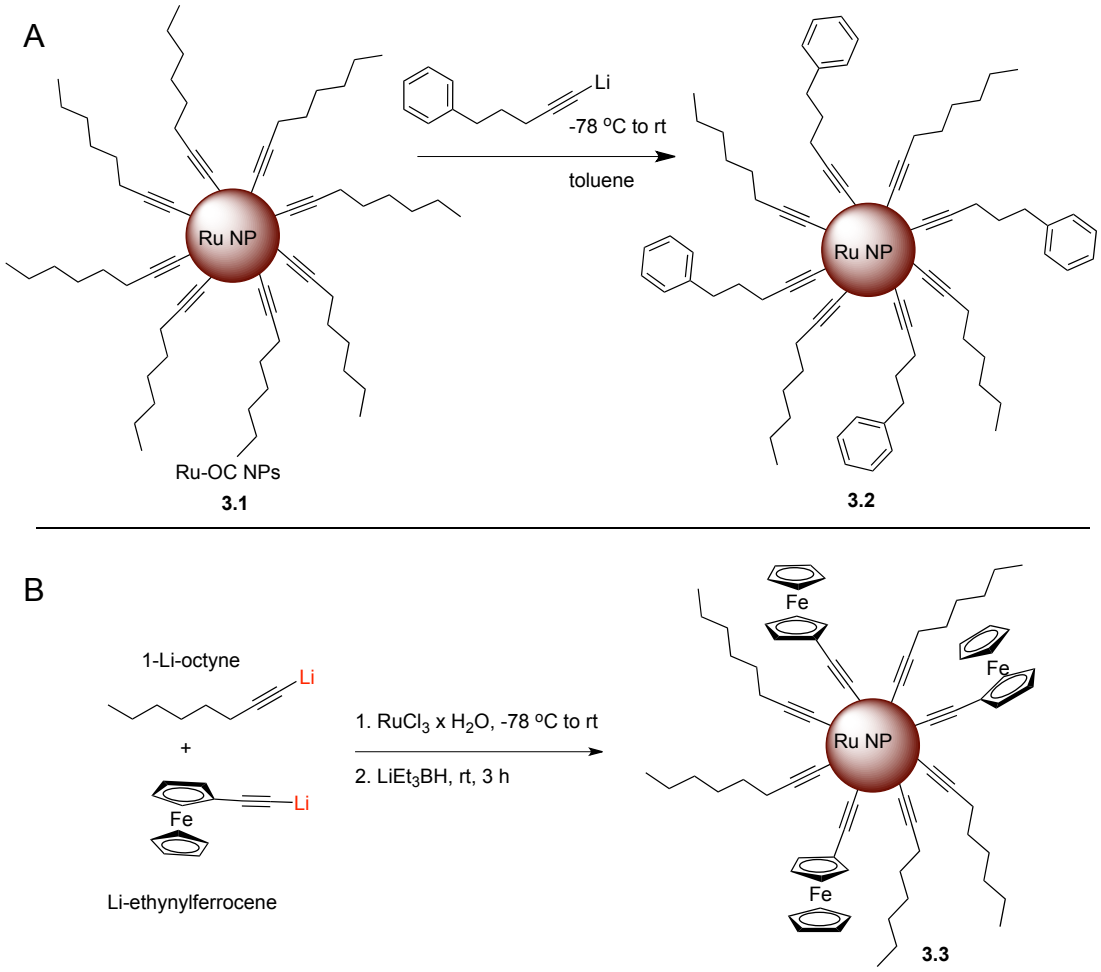

Scheme 3.1 Alkyne NPs A) Functionalization of RuOC nanoparticles with the lithium anion of 5-phenyl-1-pentyne. B) One-step approach to functionalize Ru nanoparticles with two alkynes: 1-octyne and ethynylferrocene.

A simple one step method relied upon reacting a mixture of the lithium anions of protecting ligand (1-octyne) and a ligand of interest (ethynylferrocene) without changing the previously described procedure toward **3.1** (Scheme 3.1 B). With an initial 7:3 mixture of 1-octyne to ethynylferrocene, analysis of the KCN dissolved NPs revealed a final incorporation of ~13% ethynylferrocene to give Ru-OCFc NPs (**3.3**). Additionally, the incorporation of ferrocene moieties around the NP surface

was verified by electrochemical experiments and NIR spectroscopy. Existence of NPMEC was again validated by the appearance of a pair of voltammetric peaks with a $\Delta E^{o'}$ = 0.265 V (Figure 3.5). This was higher than Ru=VFc NPs ($\Delta E^{o'}$ = 0.204 V) and represents better charge delocalization between the alkyne ligands and the Ru NP as compared to the Ru=C8 interfacial bonding interaction. The IVCT for **3.3** was also comparable to the bis-Ru complex Fc-C≡C-Ru_2-C≡C-Fc, which has a $\Delta E^{o'}$ = 0.300 V.[9] Furthermore, the characteristic NIR peak in the region of IVCT appeared upon addition of the oxidant $NOBF_4$ (1687 nm as compared to 1667 nm for the bis-Ru complex, Fc-C≡C-Ru_2-C≡C-Fc).[9]

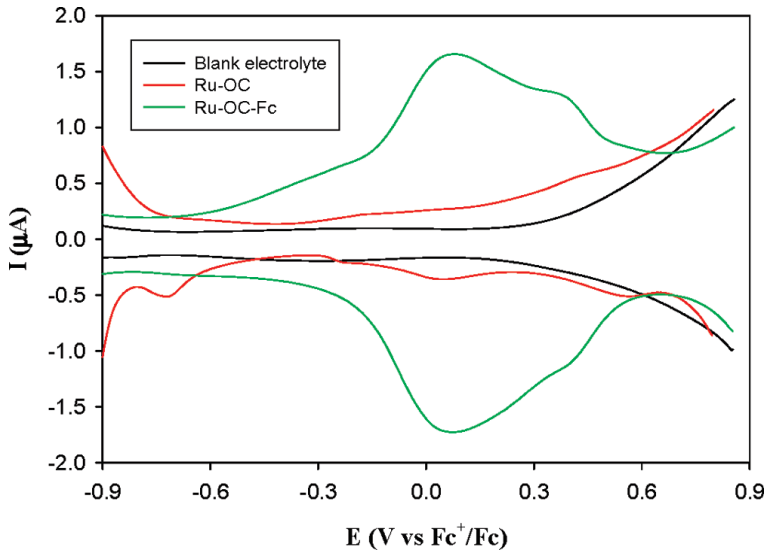

Figure 3.5 Differential Pulse Voltammograms (DPVs) of Ru-OC (red curve) and Ru-OC-Fc (green curve) nanoparticles in dichloromethane (DCM) containing 0.1 M tetrabutylammonium perchlorate (TBAP). The particle concentrations were both 8 mg/mL. The DPV profiles of the blank electrolyte (black curve) were also included in the figure. Au disk electrode area 0.8 mm^2. In the DPV measurements, the dc ramp was 4 mV/s, the pulse amplitude was 50 mV, and the pulse width was 200 ms. Figure reprinted with permission from Chen, W.; Zuckerman, N. B.; Kang, X.; Ghosh, D.; Konopelski, J. P.; Chen, S. W. *J. Phys. Chem. C* **2010**, *114*, 18146-18152. Copyright 2010, American Chemical Society.

Another manner in which Ru-OC NPs (**3.1**) distinguish themselves from Ru=C8 NPs is by their unique photoluminescence (Figure 3.6). Compound **3.1** exhibited clear excitation and emission peaks at 347 and 428 nm in contrast to Ru=C8 NPs which do not show any fluorescence. As was the case for the Ru=VPy study where the dimer displayed comparable fluorescence spectra to the fluorophore-bound NPs, **3.1** showed very similar emission peaks to dimers, trimers and polymers of acetylenes (408 nm).[10] From the observed photoluminescence of **3.1**, it appears that intraparticle charge delocalization can occur due to the alkynyl linkage to the Ru surface.

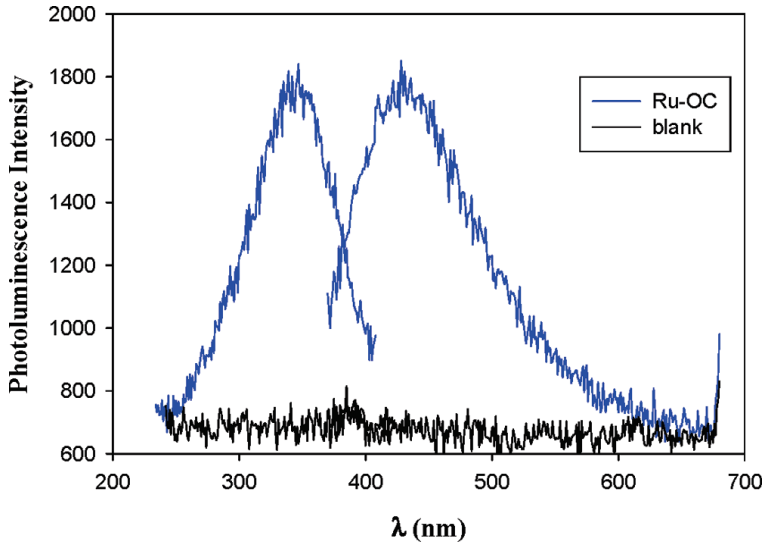

Figure 3.6 Excitation and Emission Spectra of Ru-OC Nanoparticles (blue curves) at a concentration of 0.1 mg/mL in DCM. The corresponding profiles measured with the blank solvent (black curves) were also included. Figure reprinted with permission from Chen, W.; Zuckerman, N. B.; Kang, X.; Ghosh, D.; Konopelski, J. P.; Chen, S. W. *J. Phys. Chem. C* **2010**, *114*, 18146-18152. Copyright 2010, American Chemical Society.

Further study of the molecular capacitance of **3.1** and the controlled oxidation and reduction of the nanoparticle core was investigated by Xiongwu Kang.[11] He showed that the optoelectronic properties of **3.1** could be

controlled by nanoparticle core reduction or oxidation leading to decreased or enhanced bonding order of the particle-bound alkynyl moieties. In essence, the intraparticle conjugation was affected accordingly, leading to enhanced or diminished photoluminescent properties.

3.4 Varied Alkyne Length and Nanoparticle Composition

The length of the alkyne was also varied successfully using decyne and dodecyne as the protecting ligands. Both of these ligands required a 6:1 ligand to $RuCl_3$ ratio as opposed to the 3:1 ratio for **3.1**. Hexyne did not provide stable NPs and precipitated during the workup. Unfortunately, the method was not general to the stabilization of other nanoparticles including Si ($SiCl_4$), Co ($CoCl_2$), Fe ($FeCl_3$), or Ag (AgOTf). Initially, the formation of Fe, Co and Ag NPs by this method looked very promising in that each system ended in a black solution without precipitation following reduction with $LiEt_3BH$. However, upon quenching and workup, precipitation occurred and no soluble nanoparticles could be isolated. The formation of Pd-octyne NPs using $Pd(OAc)_2$ as precursor did provide stable nanoparticles by this method, but other than their formation nothing else was pursued.

As previously mentioned, Ru-OC NPs are cheaper to synthesize than Ru=C8 NPs, which is stabilized with the custom ligand, ODA. However, the two different NP systems should not be seen as better than one another, but instead they should be viewed as two complementary systems. Both are

capable of IVCT and the inclusion of multiple ligand types by varying methods.

3.5 Background of Vinylidene-Protected Nanoparticles

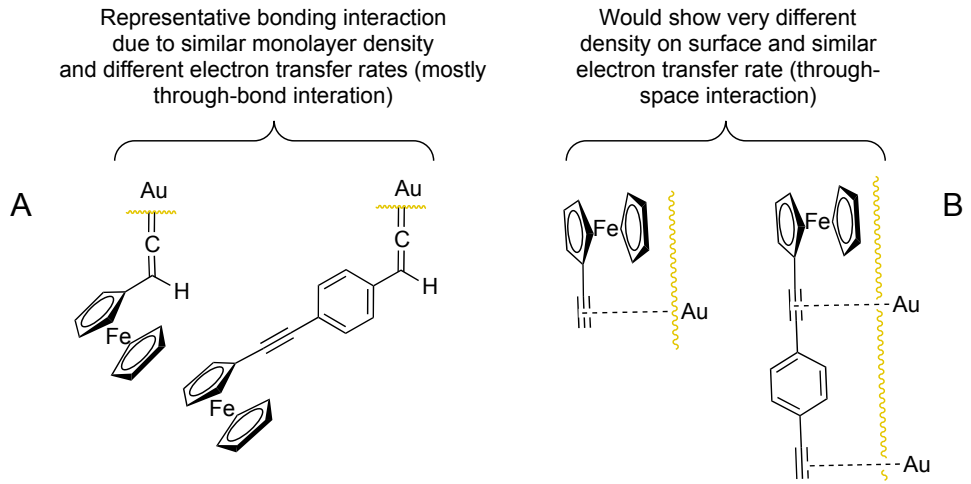

Figure 3.7 Au Vinylidene A) Proposed end-on attachment to Au surface via vinylidene bond. B) Unlikely formation of Au self-assembled monolayer (SAM) due to experimental data by Gorman and co-workers.[13]

Similar to our Ru-OC NPs (**3.1**), gold nanoparticles have been stabilized with terminal alkynes. However, the nature of the interfacial bonding between the alkyne ligand and Au NPs is thought to be a vinylidene species as depicted in a theoretical study[12] and later by experiment on thin film[13] and nanoparticles.[14] The side-on π-interaction between alkyne and Au had to be discounted by Gorman and co-workers[13] due to the calculated density of the packed monolayer as well as the electron transfer rate for alkynyl functionalized ferrocene compounds (Figure 3.7 A and B). Despite the difference in size between the two ligands, their packing was very similar suggesting end on interaction with the gold surface. Additionally, the drop off

in charge transfer rate between the ferrocene and Au surface is indicative of through-bond charge transfer processes and not metal-metal interactions if the ligands were side-on to the Au substrate. Coupled with these findings and ruthenium's affinity towards alkynes, it was proposed that a similar approach could be used for stabilizing the thermolytically produced Ru NPs in a similar fashion to Gorman and co-workers.[13]

3.6 Synthesis and Characterization of Vinylidene-Protected Ru NPs and Comparison to Alkyne-Protected Ru NPs

Similarly to the Au NPs stabilized with alkyne ligands,[13,14] Xiongwu prepared "bare" or preformed Ru NPs via the thermolytic reduction method with 1,2-propanediol and sodium acetate.[15] Upon cooling, a solution of 1-dodecyne in toluene was added with continued vigorous stirring overnight. Just as with Ru=C8 NPs, the toluene layer became black while the diol layer was clear. The nanoparticles were denoted RuHC12 and are soluble in non-polar solvents. Evaluation by TEM, FTIR, and NMR was conducted and we found it necessary to compare these nanoparticles with dodecyne stabilized NPs prepared from the lithium acetylide (RuC12). Through these techniques, the interfacial bond was not distinguishable as an alkyne or vinylidene species. This was not surprising due to the inability to visualize atoms near the surface of the NP via NMR. However, it was surprising that the purported vinylidene species of the RuHC12 NPs could not be seen by FTIR. In fact, the two types of NPs gave nearly identical IR spectra when one would expect to

see clearly distinguishing peaks for C≡C stretch between 1900-2100 cm^{-1} and around 1650 cm^{-1} for the C=C stretch. To possibly explain this phenomenon, the mechanism for the reaction of the Ru NP with terminal alkynes was proposed based on organometallic chemistry studies of Ru-vinylidene species (Scheme 3.2).

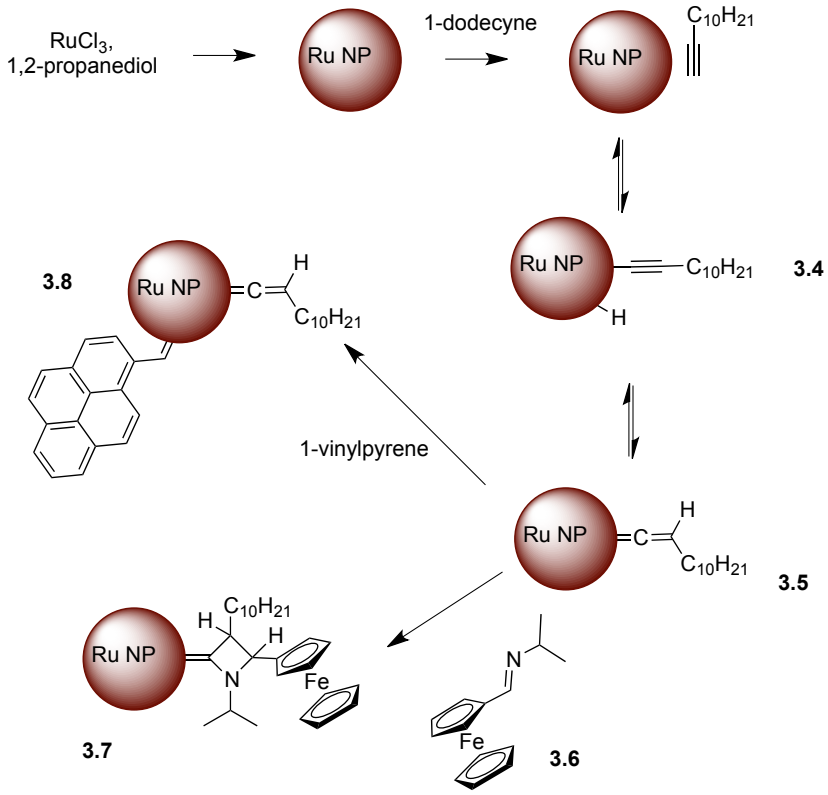

Scheme 3.2 Proposed Mechanism for the formation of RuHC12 nanoparticles, metathesis of RuHC12 nanoparticles with 1-vinylpyrene, and reaction of isopropylimine ferrocene with RuHC12 nanoparticles.

The formation of Ru-vinylidene complexes has been extensively studied in the literature, and the interconversion between alkyne and vinylidene and vice-versa is unequivocally established.[16] The mechanisms for which these transitions occur have also been proposed,[17,18] and involve the coordination of the alkyne via an η^2 configuration followed by insertion of the

metal center between the acetylenic hydrogen and carbon to form a hydridoalkynyl intermediate (analogous to **3.4**). A subsequent 1,2 or 1,3-hydride shift leads to the vinylidene species (**3.5**). When treated with base, a representative organometallic vinylidene is converted to the Ru-alkyne complex,[19,20] and the complex is reverted by treatment with acid.[16,21]

From the above mechanism for the formation of **3.5**, we propose the equilibrium lies more toward the hydridoalkynyl species, **3.4**. We believe this to be the case because of the nearly identical FTIR spectra for **3.1** and the NPs formed from alkyne and "bare" Ru NPs. However, in order for metathesis with olefins to occur as is the case in the generation of **3.8**, the interfacial bonding order of the stabilizing ligand must transition through the vinylidene linkage.

Metal vinylidene complexes have also been shown to undergo 2 + 2 cycloadditions with imines[22,23] via nucleophilic additions to the electrophillic α-carbon.[21] To probe the existence of vinylidene bonding at the nanoparticle interface, we chose to treat the RuHC12 NPs (**3.5**) with isopropyliminferrocene (**3.6**, Scheme 3.2). As atoms close to the NP surface are often difficult to detect, the incorporation of a ferrocene moiety would allow for electrochemical probing of the reaction's occurrence. As a control experiment, RuC12 was also treated with **3.6**. Comparison of the ^{1}H-NMR for **3.5**, **3.5** plus **3.6** (**3.7**), and RuC12 plus **3.6** showed a distinct difference only for **3.7** with an appearance of a broad bump in the region of 4-4.5 ppm

(Figure 3.8 A, B and C). Monosubstituted ferrocene typically appears as a singlet (5H) and two triplets (4H) between 4-5 ppm, so the appearance of a bump in that region was promising. More telling of incorporation of **3.6** onto the RuHC12 NPs were the voltammograms, which showed a pair of peaks for **3.7** and only a featureless profile for the reaction of of RuC12 with **3.6** (Figure 3.9).

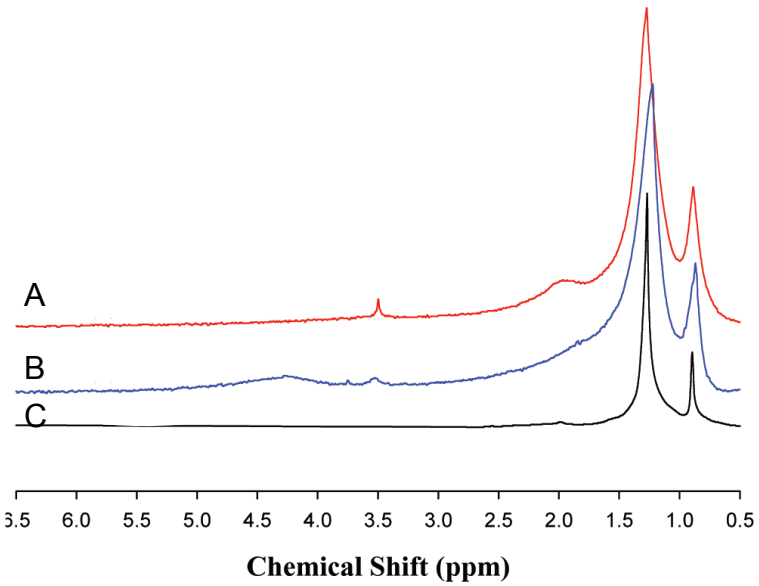

Figure 3.8 ^{1}H-NMR Spectra of the RuHC12 nanoparticles (**3.5**) (A) before and (B) after reactions with **3.6** and (C) the RuC12 nanoparticles after reactions with **3.6**. The nanoparticles were all dissolved in $CDCl_3$ (500 MHz). Figure reprinted with permission from Kang, X.; Zuckerman, N. B.; Konopelski, J. P.; Chen, S. W. *J. Am. Chem. Soc.* **2012**, *134*, 1412-1415. Copyright 2012, American Chemical Society.

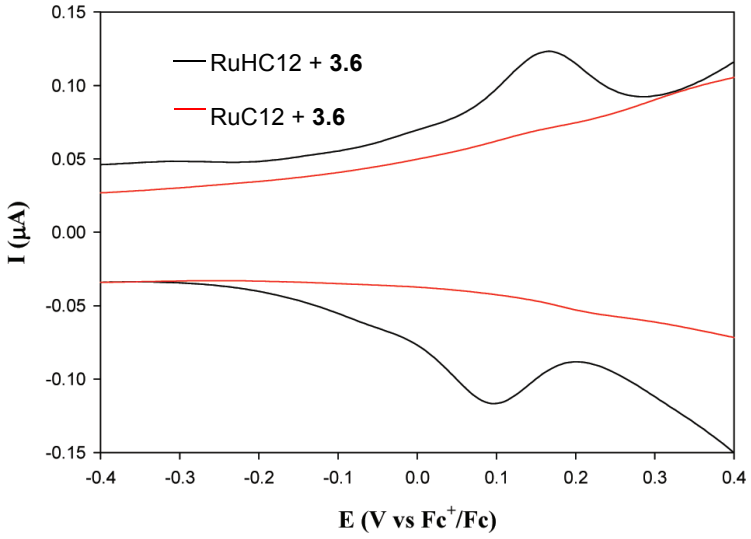

Figure 3.9 Reaction with Imine Ferrocene DPVs of RuHC12 nanoparticles (**3.5**) and RuC12 nanoparticles after reactions with **3.6** in CH_2Cl_2 with 0.1 M TBAP. Conditions: nanoparticle concentration, 3 mg/mL; gold electrode surface area, 0.51 mm2; DC ramp, 4 mV/s; pulse amplitude, 50 mV; pulse width, 200 ms. The potential was calibrated against the formal potential of ferrocene monomers in the same electrolyte solution. Figure reprinted with permission from Kang, X.; Zuckerman, N. B.; Konopelski, J. P.; Chen, S. W. *J. Am. Chem. Soc.* **2012**, *134*, 1412-1415. Copyright 2012, American Chemical Society.

Another manner in which **3.1** and **3.5** are very similar is by their photoluminescent character. Both sets of nanoparticles have excitation and emission peaks at 360 and 440 nm respectively, indicative of intraparticle charge delocalization between the conjugated interfacial linkages. The fluorescence diminished upon formation of **3.7**, alluding to the cycloaddition reaction and formation of a non-fluorescent carbene linkage (Figure 3.10). That the fluorescence did not completely disappear most likely is due to incomplete reaction in the tightly packed environment around the NP surface.

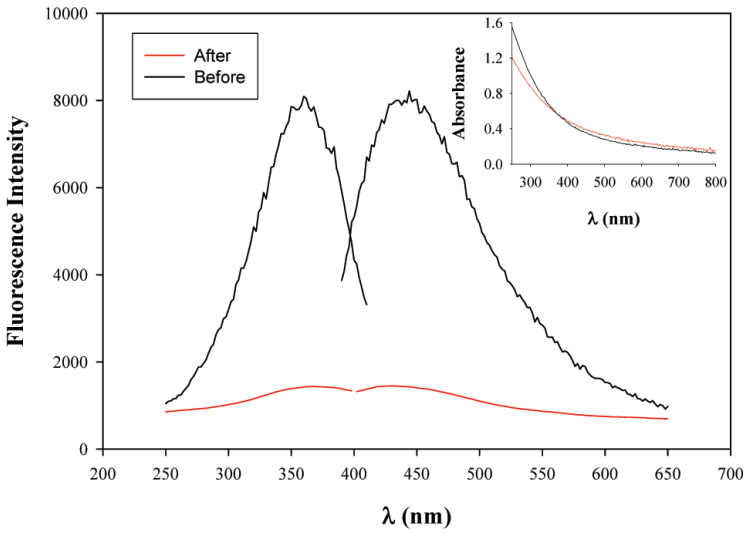

Figure 3.10 Excitation and Emission Spectra of RuHC12 Nanoparticles (**3.5**) in CH_2Cl_2 before (black curves) and after (red curves) reactions with **3.6**. The corresponding UV/vis absorption spectra are shown in the inset. The nanoparticle concentration was 0.1 mg/mL. Figure reprinted with permission from Kang, X.; Zuckerman, N. B.; Konopelski, J. P.; Chen, S. W. *J. Am. Chem. Soc.* **2012**, *134*, 1412-1415. Copyright 2012, American Chemical Society.

Compound **3.5** also underwent metathesis with 1-vinylpyrene, further distinguishing this material from **3.1** and drawing a closer relation to Ru=C8 NPs. The characteristic excitation and emission peaks for **3.8** was consistent with what was seen for Ru=VPy NPs in our previous work. Most notably, the appearance of a small peak around 392 nm (monomeric character) and a large peak around 492 nm (dimeric character) were shown to be a product of intraparticle extended conjugation between the particle bound pyrene moieties (Figure 3.11).

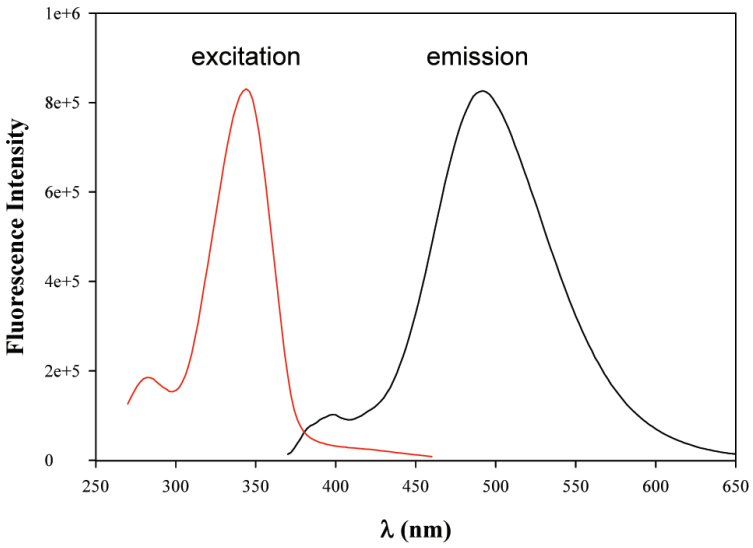

Figure 3.11 Olefin Metathesis Excitation and emission spectra of RuHC12 nanoparticles after the olefin metathesis reaction with 1-vinylpyrene in CH_2Cl_2. The nanoparticle concentration was 0.1 mg/mL. Figure reprinted with permission from Kang, X.; Zuckerman, N. B.; Konopelski, J. P.; Chen, S. W. *J. Am. Chem. Soc.* **2012**, *134*, 1412-1415. Copyright 2012, American Chemical Society.

3.7 Conclusion

Two new methods for functionalizing Ru NPs have been developed. Both methods display the effects of NPMEC due to their unique interfacial bonding interactions with the Ru NP surface. While there is certainly more work to be done in fully characterizing the nature of the alkyne and vinylidene linkages to the NP surface, the utility of both systems is evident and complementary to the more established Ru=C8 NPs. Further probing of the interfacial interactions for both systems may be as simple as reacting the two systems analogously to Ru-vinylidene/hydridoalkyne complexes by treatment with acid and base. A more involved study would use solid-state NMR and the magic-angle spinning (MAS) technique as shown recently for NHC stabilized Ru NPs.[24]

Experimentals

The syntheses of Ru-vinylidene NPs **3.5**, **3.7** and **3.8** were performed by Xiongwu Kang and are described in our publication.[15] Isopropyliminoferrocene (**3.6**) was synthesized according to a literature procedure.[25]

Ruthenium-1-octyne nanoparticles, Ru-OC (3.1). To a two-neck round bottom flask under nitrogen was added 1-octyne (0.14 mL, 0.94 mmol) and THF (5 mL, anhydrous). The solution was cooled to -78 ^{o}C (acetone/dry ice bath) and stirred prior to the drop-wise addition of 2.24 M *n*-BuLi in hexanes (0.42 mL, 0.96 mmol). The reaction was allowed to stir for 1 h. In a separate flask, pre-dried $RuCl_3$ x H_2O (62.2 mg, 0.30 mmol) and THF (30 ml, anhydrous) was stirred and cooled to -78 ^{o}C. The ruthenium salt solution was added to the cooled lithium-octyne anion solution via cannula and the resulting mixture was allowed to warm to room temperature over a period of 1 h. A 1.0 *M* solution of lithium triethylborohydride in hexanes (5.0 mL, 5.0 mmol) was added drop-wise to the reaction mixture and the resulting solution was allowed to stir at room temperature over 3 h. The reaction was cooled with an ice-water bath, quenched with DI water, and the solvent removed under reduced pressure.

1-Decyne and 1-dodecyne could be substituted as protecting ligands, but required twice as many ligands for successful nanoparticle formation.

5-Phenyl-1-pentyne lithium acetylide exchange reaction (3.2). The lithium acetylide of 5-phenyl-1-pentyne (0.14 mL, 0.90 mmol) was generated similarly to 1-octyne in toluene. In a separate round bottom flask under nitrogen, the previously prepared 1-octyne ruthenium nanoparticles were dissolved in toluene (30 mL, anhydrous) and cooled to -78 ^{o}C. Via cannula, the nanoparticle suspension was added to the acetylide solution and allowed to stir for 1 h prior to warming and stirring at room temperature for an additional two hours. The reaction was cooled to 0 ^{o}C, quenched with DI water, and the solvent removed under reduced pressure.

Ethynylferrocene. The syntheses of 1,1-dichloro-2-ferrocenylethene and ethynylferrocene followed the work of Luo et al.[26] To a two-neck round bottom flask under nitrogen was added PPh_3 (5.24 g, 20 mmol), ferrocenecarboxaldehyde (1.07 g, 5 mmol), and CH_3CN (10 mL, anhydrous). The solution was cooled to 0 ^{o}C and CCl_4 was added in one portion. Stirring was continued at room temperature for 30 minutes, followed by an addition of DI water (5 mL). The mixture was then extracted with ether, washed with water, brine, and dried with $MgSO_4$. Following removal of solvent under reduced pressure, the residue was purified on a short column of neutral alumina to give 1,1-dichloro-2-ferrocenylethene (9:1 hexanes/DCM), (0.63 g, 45 % yield), mp 56-57 ^{o}C (lit. 57-58 ^{o}C); ^{1}H NMR (600 MHz, $CDCl_3$) δ 6.53 (s, 1H), 4.58 (t, *J* = 1.8 Hz, 2H), 4.29 (t, *J* = 1.8 Hz, 2H), 4.18 (s, 5H); ^{13}C NMR

(150 MHz, $CDCl_3$) δ 127.3, 116.2, 77.8, 69.3, 69.1; IR (cm^{-1}) 3368, 3111, 3025, 2917, 1786, 1725, 1622, 1408, 1286, 1244, 1191, 1103, 1100, 932, 898, 868, 809, 716, 662.

1,1-Dichloro-2-ferrocenylethene (147 mg, 0.52 mmol) was dissolved in THF (1 mL, anhydrous). The solution was cooled to 0 ^oC and stirred under nitrogen during the drop-wise addition of *n*-BuLi (2.24 *M* in hexanes, 0.43 mL, 1.04 mmol). The reaction was then removed from the ice bath and allowed to stir for 10 min, and was then cooled again to 0 ^oC prior to quenching with DI water (1 mL). The solution was extracted with ether, dried with $MgSO_4$ and the solvent removed under reduced pressure. Purification of the crude product by flash column chromatography was performed using a short column of neutral alumina (9:1 hexanes/DCM). (99.6 mg, 91% yield), mp 52-53 ^oC (lit. 52-53 ^oC); ^1H NMR (600 MHz, $CDCl_3$) δ 4.48 (t, *J* = 1.8 Hz, 2H), 4.24 (s, 5H), 4.21 (t, *J* = 1.8 Hz, 2H), 2.74 (s, 1H); ^{13}C NMR (150 MHz, $CDCl_3$) δ 82.8, 73.8, 71.9, 70.2, 68.9, 64.0; IR (cm^{-1}) 3293, 3095, 2108, 1774, 1647, 1411, 1226, 1106, 1024, 1001, 916, 821, 645, 531.

1-Octyne/ethynylferrocene Ru NPs (3.3). To a two-neck round bottom flask under nitrogen was added 1-octyne (92.9 mL, 0.63 mmol), ethynylferrocene (57.3 mg, 0.27 mmol) and THF (5 mL, anhydrous). The solution was cooled to -78 ^oC (acetone/dry ice bath) and stirred prior to the drop-wise addition of *n*-BuLi (2.24 *M* in hexanes, 0.42 mL, 0.96 mmol). The reaction was allowed to

stir for 1 h. In a separate flask, pre-dried $RuCl_3$ x H_2O (62.2 mg, 0.30 mmol) and THF (30 ml, anhydrous) was stirred and cooled to -78 ^oC. The ruthenium salt solution was added to the cooled, mixed, lithium anion solution via cannula and the resulting mixture was allowed to warm to room temperature over a period of 1 h. A 1.0 *M* solution of lithium triethylborohydride in hexanes (5.0 mL, 5.0 mmol) was added drop-wise to the reaction mixture and the resulting solution was allowed to stir at room temperature over 3 h. The reaction was cooled with an ice-water bath, quenched with DI water, and the solvent removed under reduced pressure.

References

[1] Pruchnik, F. P. Organometallic Chemistry of the Transition Elements; Plenum Press: New York, 1990.

[2] Tsutsui, M.; Courtney, A. *Adv. Organomet. Chem.* **1977**, *16*, 241–282.

[3] Mirkhalaf, F.; Paprotny, J.; Schiffrin, D. J. *J. Am. Chem. Soc.* **2006,** *128,* 7400–7401.

[4] Brust, M.; Walker, M.; Bethell, D.; Schiffrin, D. J.; Whyman, R. *J. Chem. Soc. Chem. Commun.* **1994**, 801-802.

[5] Thomas, K. G.; Zajicek, J.; Kamat, P. V. *Langmuir*, **2002**, *18*, 3722-3727.

[6] Yee, C. K.; Jordan, R.; Ulman, A.; White, H.; King, A.; Rafailovich, M.; Sokolov, J. *Langmuir* **1999,** *15,* 3486-3491.

[7] Brust, M.; Fink, J.; Bethell, D.; Schiffrin, D. J.; Kiely, C. *J. Chem. Soc., Chem. Commun.* **1995,** 1655-1656.

[8] Chen, W.; Zuckerman, N. B.; Kang, X.; Ghosh, D.; Konopelski, J. P.; Chen, S. W. *J. Phys. Chem. C* **2010**, *114*, 18146-18152.

[9] Xu, G. L.; Crutchley, R. J.; DeRosa, M. C.; Pan, Q. J.; Zhang, H. X.; Wang, X. P.; Ren, T. *J. Am. Chem. Soc.* **2005**, *127*, 13354-13363.

[10] Warta, R.; Sixl, H. *J. Chem. Phys.* **1988**, *88*, 95-99.

[11] Kang, X.; Zuckerman, N. B.; Konopelski, J. P. Chen, S. W. *Angew. Chemie Int. Ed.* **2010**, *49*, 9496-9499.

[12] Ford, M. J.; Hoft, R. C.; McDonagh, A. *J. Phys. Chem. B* **2005**, *109*, 20387-20392.

[13] Zhang, S.; Chandra, K. L.; Gorman, C. B. *J. Am. Chem. Soc.* **2007**, *129*, 4876-4877.

[14] Maity, P.; Tsunoyama, H.; Yamauchi, M.; Xie, S.; Tsukuda, T. *J. Am. Chem. Soc.* **2011**, *133*, 20123-20125.

[15] Kang, X.; Zuckerman, N. B.; Konopelski, J. P.; Chen, S. W. *J. Am. Chem. Soc.* **2012**, *134*, 1412-1415.

[16] Bustelo, E.; de los Ríos, I.; Tenorio, M. J.; Puerta, M. C.; Valerga, P. *Monatsh. Chem.* **2000**, *131*, 1311-1320.

[17] de los Ríos, I.; Tenorio, M. J.; Puerta, M. C.; Valerga, P. *J. Am. Chem. Soc.* **1997**, *119*, 6529-6538.

[18] Lynam, J. M. *Chem. Eur. J.* **2010**, *16*, 8238-8247.

[19] Faulkner, C. W.; Ingham, S. L.; Khan, M. S.; Lewis, J.; Long, N. J.; Raithby, P. R. *J. Organomet. Chem.* **1994**, *482*, 139-145.

[20] McDonagh, A. M.; Deeble, G. J.; Hurst, S.; Cifuentes, M. P.; Humphrey, M. G. *J. Chem. Ed.* **2001**, *78*, 232-234.

[21] Bianchini, C.; Masi, D.; Romerosa, A.; Zanobini, F.; Peruzzini, M. *Organometallics* **1999**, *18*, 2376-2386.

[22] Song, Z.; Chrisope, D. R.; Beak, P. *J. Org. Chem.* **1987**, *52*, 3940-3941.

[23] Fischer, H.; Zayed, M. A. *J. Therm. Anal. Calorim.* **2000**, *61*, 897-908.

[24] Lara, P.; Rivada-Wheelaghan, O.; Conejero, S.; Poteau, R.; Philippot, K.; Chaudret, B. *Angew. Chem. Int. Ed.* **2011**, *50* , 12080-12084.

[25] Balogh, J.; Kegl, T.; Parkanyi, L.; Kollar, L.; Ungvary, F.; Skoda-Foldes, R. *J. Organomet. Chem*. **2011**, *696*, 1394-1403.

[26] Luo, S-J.; Liu, Y-H.; Liu, C-M.; Liang, Y-M; Ma, Y-X. *Synth. Commun.* **2000**, *30*, 1569-1572.

CHAPTER 4: Synthesis of a Ferrocene-Functionalized Unsymmetrical Benzo[*b*]thienyl-thienylethene Photoswitch with a Cyclopentene Core

4.1 Introduction to Molecular Switches

As the desire to miniaturize electronic components and devices remains a constant challenge, there is a renewed focus on organic compounds in a move toward the molecular scale. One such group of scaffolds is that of the diarylethenes (Figure 4.1),[1] whose photochromic properties are amenable for use in memory applications.[2,3] The ideal components of the photoswitch scaffold have been well documented over the past 20+ years leading to structures that contain the desirable qualities of: 1) induced reversible ring closure (light, acid,[4] redox[5]), 2) thermal irreversibility and 3) fatigue resistance. Photochromism in the solid state is also a very desirable characteristic. Of the large variety of photoswitches developed over the years, those that contain a perfluorinated cyclopentene bridge have remained superior for use in materials applications.[6]

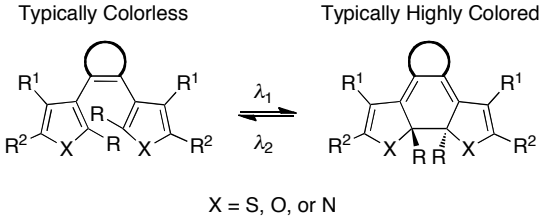

Figure 4.1 General structure of the diarylethene photoswitch.

In general, the syntheses of perfluorocyclopentene-bridged photoswitches (Figure 4.2) have followed the relatively short and moderate yielding pathway utilizing nucleophilic addition of the lithiated aryl subunits to

octafluorocyclopentene (**4.1**). One recent advancement in their syntheses utilizes the Suzuki-Miyaura coupling of the desired boronic acid subunits with the commercially available 1,2-dichlorohexafluorocyclopentene (**4.2**) as described by Shinokubo and co-workers (bottom, Figure 4.2).[7] These procedures predominantly provide only symmetrical compounds without the creation of monoarylated side-products. However, if one requires an unsymmetrical perfluorocyclopentene-bridged photoswitch without the low yield that arises from the separation of a mixture of compounds, there are few such examples. The need for these unsymmetrical compounds is not only attractive for use in materials applications, but also among photoswitches used in biological applications.[8]

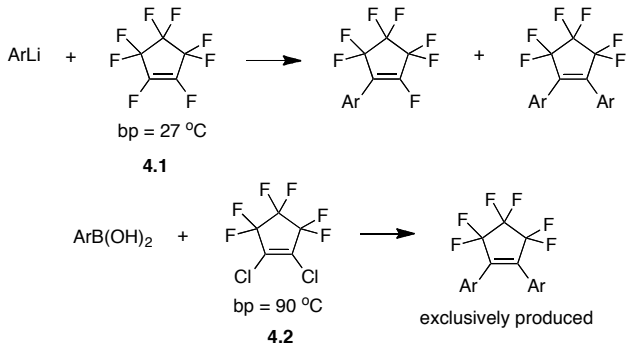

Figure 4.2 Perfluorocyclopentene Photowitch Syntheses (Top) Typical mixtures from anion addition to the volatile octafluorocyclopentane (**4.1**) starting material. (Bottom) Suzuki coupling to the less volatile 1,2-dichlorohexafluorocyclopentane (**4.2**) as published by Shinokubo and co-workers.

Within the last 15 years, there has been an expansion of research regarding the synthesis of perhydrocyclopentene-bridged photoswitches,[9,10,11] largely directed toward the more desirable subunits: thiophene[12] and benzo[*b*]thiophene.[13] Many of these compounds have the key aforementioned

requirements of a desirable photoswitch. Additionally, the syntheses of these compounds are generally more amenable to scale up, are lower in cost, and use reagents that are relatively easy to attain and handle in comparison to their fluorinated counterparts. Entry into the cyclopentene core has focused on the intramolecular ring closure of a suitably substituted 1,5-diketone via the McMurry reaction.

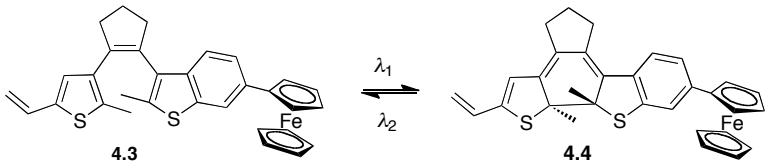

4.3 open form **4.4** closed form

Figure 4.3 Open and Closed Forms of the Desired Photoswitch.

Our interest in pursuing the cyclopentene-bridged photoswitch scaffold was in part due to the tangible characteristics involved in their synthesis, including the aspect of the expanded availability of chemical transformations not currently available for the fluorinated compounds. In particular, we were interested in deriving a synthetic scheme that avoided the separation of mixtures toward the unsymmetrical ferrocene-functionalized compound **4.3** (Figure 4.3). The importance of ferrocene as an analytical tool for monitoring charge transfer processes is an obvious choice for its inclusion on a molecule that isomerizes to a highly conjugated form.[14] Transition metal containing dithienylethene photoswitches represent a small portion of the literature,[15,16] and those which contain ferrocene[17,18,19,20] or an iron center[21,22] are even less frequently described. However, this is the first reported ferrocene containing

photoswitch with a cyclopentene core whereby the metal complex is fused directly to one of the aryl subunits.

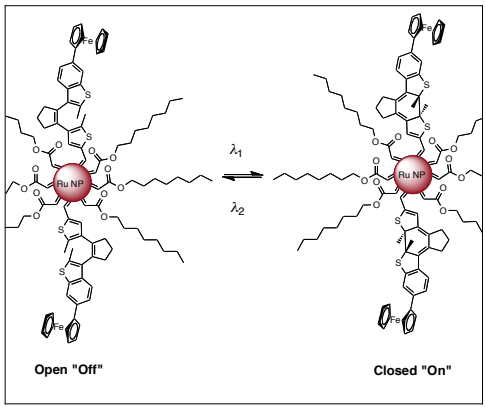

Figure 4.4 Ruthenium Nanoparticles functionalized with the designed photoswitch **4.3** and a depiction of the two potential forms after irradiation with a specific wavelength of light: left, “off,” right, “on.”

Our interest in pursuing the unsymmetrical cyclopentene-bridged photoswitch scaffold **4.3** was driven by our continuing interest in organic monolayer-protected ruthenium nanoparticles.[23,24] In recent publications we have demonstrated that ferrocene moieties conjugated to the metal nanoparticle via ruthenium-carbene bonds display intervalence transfer at mixed valence. Conversely, a single saturated carbon between the ferrocene and nanoparticle negates any communication between the ferrocenyl metal centers. Within this context, compound **4.3** provides an interesting test case. Appended to a ruthenium nanoparticle through olefin metathesis of the terminal alkene, photoisomerization of **4.3** to **4.4** (Figure 4.4) provides for a fully conjugated pathway between the ruthenium core and the ferrocenyl substituent. Reversion to the open form (i.e., **4.3**) breaks the conjugation and any interaction between metal sites.

4.2 Design of Compound 4.3

The design of **4.3** took into consideration the literature on photochromic properties of photoswitches with cyclopentene cores.[8-13] Those switches which contain two thiophene subunits are generally much more susceptible to degradative effects upon prolonged UV irradiation,[12] while those which contain a *bis*-benzo[*b*]thiophene scaffold have comparable photochromic properties to their perfluorocyclopentene analogs (including high thermal stability of the closed forms and repeatable cyclization/cycloreversion).[13] During the course of our research, a patent[25] appeared that implicated molecules containing a cyclopentene core and mixed thiophene/benzo[*b*]thiophene subunits as viable photoswitches, and thus provided the impetus for the design of **4.3**.

4.3 Retrosynthesis of 4.3

As depicted in Scheme 4.1, the convergent synthesis of **4.3** relies heavily on the well precedented intramolecular McMurry reaction of diketones similar to compound **4.5**.[9-13] In our case, the appended functional groups on the thienyl and benzothienyl moieties were to be introduced prior to the McMurry reaction. The decision to functionalize the thiophene with the vinyl group and the benzo[*b*]thiophene with the ferrocene (and not vice versa) was driven by the anticipated reaction conditions needed for coupling of compounds **4.6** and **4.7**. The less expensive lithium anion of **4.6**,[26] derived in three steps from 2-methylthiophene, was expected to be used in excess as

compared with lactol **4.7**.[27] In order to furnish **4.7** via DIBALH reduction, **4.8** or **4.9** would first undergo ferrocenylation via a microwave Stille reaction under CuO mediated Gronowitz conditions.[28] Friedel-Crafts acylation between glutaric anhydride and **4.10**, followed by Weinreb amide or methyl ester formation, would provide **4.8** or **4.9**, respectively.

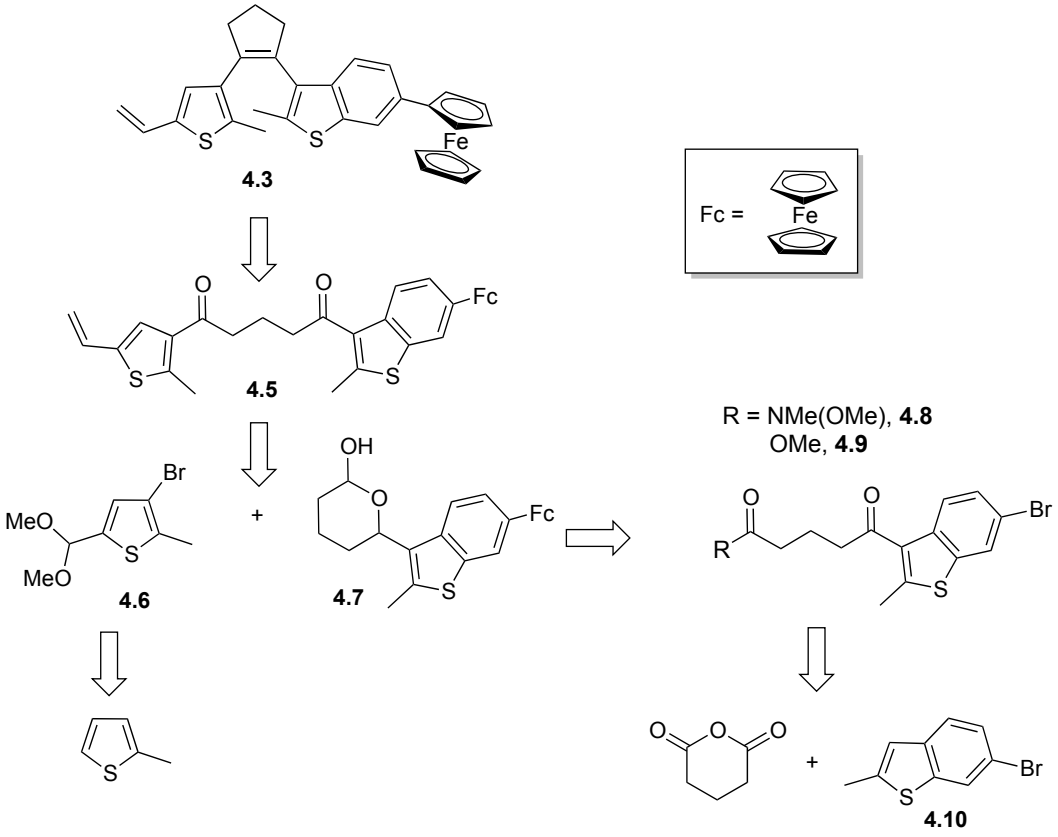

Scheme 4.1 Retrosynthesis of **4.3**

4.4 Synthesis of Benzo[*b*]thiophene Subunits

Known compound **4.11** was chosen as an entryway into the differentiable heterocycle **4.10** (Scheme 4.2). Although desired, a one step reduction from **4.11** to **4.10** with $AlCl_3$ and $LiAlH_4$ was unlikely due to potential

dehalogenation as described for the reduction of a similar molecule.[29] With this fact in mind, a three-step approach to **4.10** was envisioned beginning with the reduction of the ester with $LiAlH_4$. Unfortunately, in addition to desired **4.12a**, there was contamination with 20% of dehalogenated product **4.12b**. Although recrystallization to remove **4.12b** was successful, an alternative reducing agent was sought. Thus, in only five minutes, 2.5 equivalents of lithium dimethylammonium borohydride reduced **4.11** to **4.12a** on a 25 mmol scale without the side reaction of dehalogenation. Mesylation of alcohol **4.12a** followed by subsequent reduction with two equivalents of lithium triethylborohydride yielded **4.10** in 91% yield over two steps.

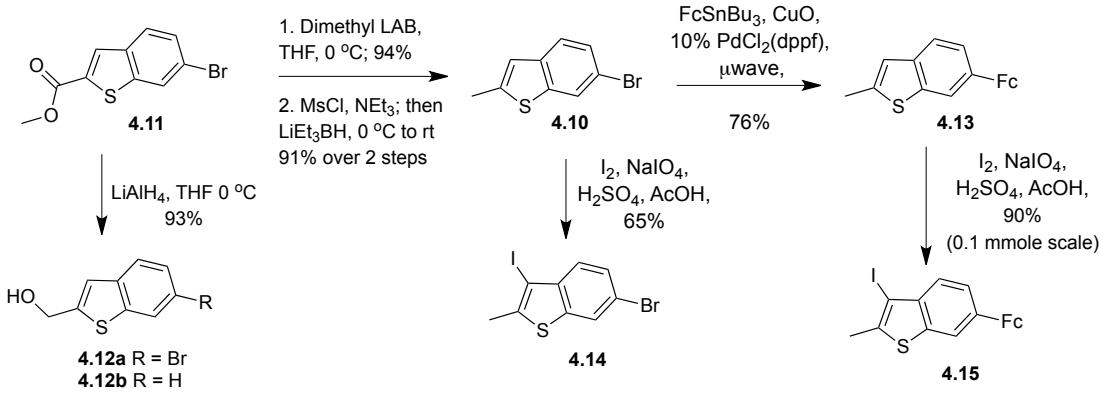

Scheme 4.2 Synthesis of Varied Benzo[*b*]thiophene Subunits.

We decided to further functionalize **4.10** to investigate the potential utility of Weinreb amide **4.8** with benzo[*b*]thiophene nucleophiles. Also, **4.10** was a good substrate to develop Stille coupling conditions for the required aryl-ferrocene coupling reaction. Ferrocene cross-coupling reactions have been reviewed,[30] and particular success for ferrocene/heteroaryl coupling has been seen in the work of Ma and co-workers.[31,32] The Stille coupling between

heteroaryl halides and tributylstannyl ferrocene[33] was shown to be enhanced by an equivalent of CuO in addition to the $Pd(PPh_3)_4$ catalyst. This is very similar to the original work of Gronowitz and co-workers which first showed this effect of CuO and other additives on Stille reactions.[28] Optimization of conditions for the Stille coupling of tributylstannyl ferrocene to **4.10** was conducted in a microwave reactor. Also, a relatively more stable catalyst alternative to $Pd(PPh_3)_4$ was sought, which led to the choice of $PdCl_2$(dppf) based on a procedure given by Guillaneux and Kagan.[33] In only 20 minutes at 140 ^{o}C, compound **4.13** was furnished in 76% yield.

Although **4.10** was anticipated to undergo Friedel-Crafts acylation, it was not believed that **4.13** would be able to do so, due to the competing nature of the ferrocene moiety to also participate in this reaction. However, halogenation at the 3-position of **4.13** or **4.10** would provide two compounds that could be easily converted to the appropriate lithium anion via lithium-halogen exchange for possible addition to **4.8** or its ferrocenylated analog, respectively. The oxidative conditions to iodinate **4.10**[34] to give dihalide **4.14** were successfully used on a 0.1 mmol scale of compound **4.13** to give **4.15** in 90% yield. However, any scale-up led to much lower yields and a black insoluble precipitate. Alternative halogenation methods, either with NBS or NCS, returned only decomposed material in a matter of minutes.

4.5 Acylation of 4.7 and Attempts to Incorporate Second Aryl Subunit

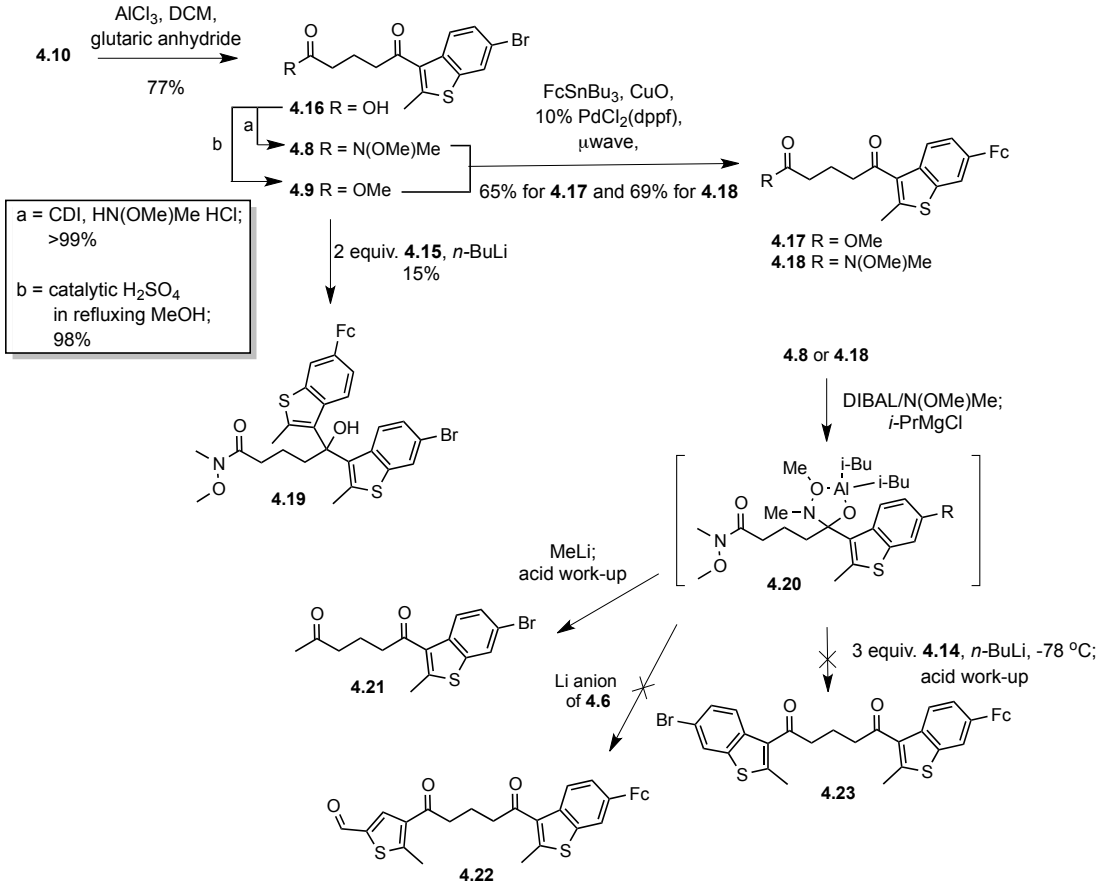

Scheme 4.3 Synthetic Investigation of Weinreb Amide Reactivity.

Friedel-Crafts acylation between **4.10** and glutaric anhydride gave carboxylic acid **4.16** in good yield, and CDI coupling with *N*-methoxy-*N*-methylamine hydrochloride or esterification provided **4.8** and **4.9** respectively (Scheme 4.3). Additionally, the previously described microwave Stille conditions gave **4.17** and **4.18** in 65% and 69% yield, respectively. The relative reactivity of the Weinreb amide and the conjugated ketone of **4.8** were investigated by adding two equivalents of the lithium anion of **4.15** at -78 ^{o}C and allowing the reaction to warm to room temperature. Interestingly, only

starting keto-Weinreb amide **4.8** and alcohol **4.19** were recovered from the reaction mixture.

Clearly, the Weinreb amide functionality shows somewhat limited reactivity. Colby and co-workers showed that the complex formed when DIBALH and *N*-methoxy-*N*-methylamine hydrochloride are reacted will form a stable (yet hydrolysable) intermediate with a more reactive carbonyl in the presence of a lesser reactive carbonyl.[35] The extent of their study did not include the Weinreb amide functionality, but appeared to be a viable option to enable the desired reactivity of **4.8** and **4.18** through intermediate **4.20**. An initial trial using methyllithium as nucleophile under Colby's conditions at -78 ^{o}C provided dicarbonyl **4.21**. However, when intermediate **4.20** was treated with either the lithium anion of **4.6** or **4.14**, the desired compounds **4.22** or **4.23** were not seen by NMR or mass spectrometry in the complex mixture of products. Although unconfirmed as the culprit in our case, one of the downfalls of the *N*-methoxy-*N*-methylamide functionality is the alternative reaction by some strong bases to provide a de-*N*-methoxylated product.[36]

4.6 Potential Alternative Acylating Methods

Reaching the McMurry dicarbonyl precursor **4.5** in as few steps as possible and without generating complex mixtures is the ideal scenario. As revealed in the previous section, the second acylation step is limited by the reactivity of the Weinreb amide electrophile in the presence of a conjugated carbonyl.

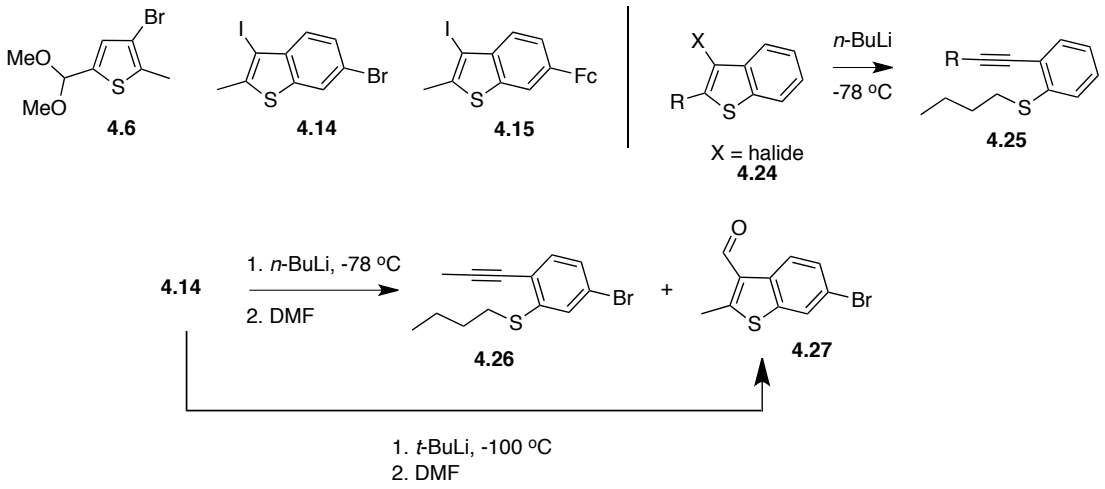

Figure 4.5 Nucleophile Precursors (top left), known side reaction involved during 3-lithiation of 3-halogenated benzo[*b*]thiophenes with *n*-BuLi (top right), and treatment of dihalide **4.14** with *n*-BuLi and the product distribution.

However, the nucleophiles involved are not innocent. The lithium anions of **4.6**, **4.14**, and **4.15** are preferred due to their ease of preparation and their generally higher reactivity. Each anion requires temperatures below 0 ^{o}C for stability issues, and if one equivalent is needed relative to its reacting partner, this necessitates a good electrophile. Dihalogen **4.14** requires temperatures at or below -78 ^{o}C to prevent "halogen dance" following selective lithium-iodo exchange. To further complicate generation of the desired lithium anion, a known reaction[37] with benzo[*b*]thiophene compounds similar to **4.24** and *n*-BuLi is the attack of base on the sulfur atom leading to ring-opening/elimination and creation of an alkynyl side product, **4.25**.

To circumvent the side-product generation, *t*-BuLi was used instead of *n*-BuLi to selectively dehalogenate **4.14**. Two separate reactions were run using *t*-BuLi: 1) quench with DMF and isolate product and 2) quench with water and analyze the crude reaction by ^{1}H-NMR. The aldehyde product was

recovered in 66% yield. Running the reaction with the same conditions and quenching with water verified selective lithiation at the 3-position by the presence of **4.10** in the proton NMR. Also, this appeared to be the exclusive product with no alkyne side-products. The selective lithium-halogen exchange of **4.14** with *n*-BuLi was also tried, and generation of **4.26** was seen by ^{1}H-NMR in significant amounts along with the desired aldehyde, **4.27** (2:1 aldehyde:alkyne by crude NMR).

4.6.1 Nucleophilic Addition to Activated Esters

With the limitations of the nucleophile understood regarding thiophene and benzo[*b*]thiophene anions, the electrophile has to be evaluated based on the results of section **4.5**: 1) the α,β-unsaturated ketone of **4.18** is more reactive than the Weinreb amide and 2) the amide is not reactive toward the desired nucleophile with *in-situ* protection of the more reactive carbonyl. This implies reversing the reactivity of the two carbonyls by generating a more electrophilic acid derivative than a Weinreb amide. The simplest carbonyl activation would be the generation of an acid chloride, but this is not a good option for reasons that will be discussed in section **4.6.2** regarding the Friedel-Crafts reaction. The carbonyl of methyl ester **4.17** is more reactive than the Weinreb amide, but this derivative would not necessarily be more activated than the unsaturated ketone, leading to undesired **4.28** and a potentially complex mixture of products.

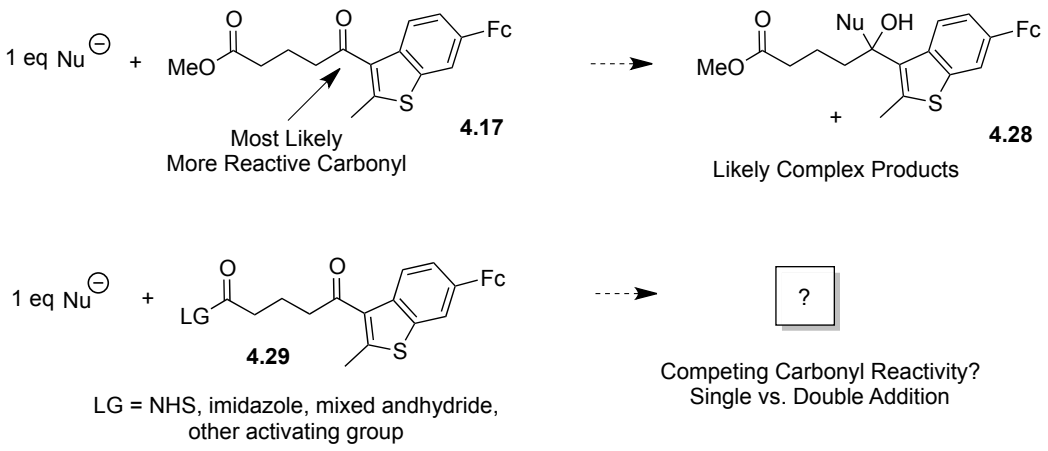

Figure 4.6 Reactivity of activated carboxylic acid derivatives to nucleophiles.

The necessity to generate peptide bonds has lead to a plethora of activating groups for the carboxylic acid. Some of the simpler derivatives include the NHS ester, carbonyl imidazole, and the mixed anhydride. The addition of lithium anions to these activated systems is not common in the literature except for simple sp^3 anions[38] and ylides.[39] Examples of sp^2 and sp lithium anion additions are very low yielding.[40,41] Regardless of whether the nucleophilic addition is regiospecific to the acid derivative of **4.29** over the conjugated ketone (even if protected), double addition is still likely, defeating the goal of avoiding mixtures.

4.6.2 Friedel-Crafts Acylation

Friedel-Crafts acylation was also considered for inclusion of the second aryl group to **4.16** (Figure 4.7). Neither the vinyl group nor the ferrocene are compatible with the Friedel-Crafts reaction and must be therefore included following the second acylation. This caveat would require differentiation of both aryl subunits to selectively introduce the vinyl and

ferrocene moieties. Additionally, the precedence for low yields of acid chloride formation with δ-benzoyl butyric acids (**4.30**) was cause for concern.[42] Shashidhar et al. investigated the mixture of pseudo acid chlorides (**4.31**) and normal acid chlorides (**4.32**) upon reaction of δ-benzoyl butyric acids with oxalyl chloride. They revealed a dependence on the electron donating/withdrawing substituents on the benzene ring, whereby the pseudo acid chloride is produced in high amounts with electron withdrawing groups. This would limit the effective addition of the second aryl group under Friedel-Crafts conditions as the pseudo acid chloride undergoes elimination to give enol lactone side products (**4.33**).

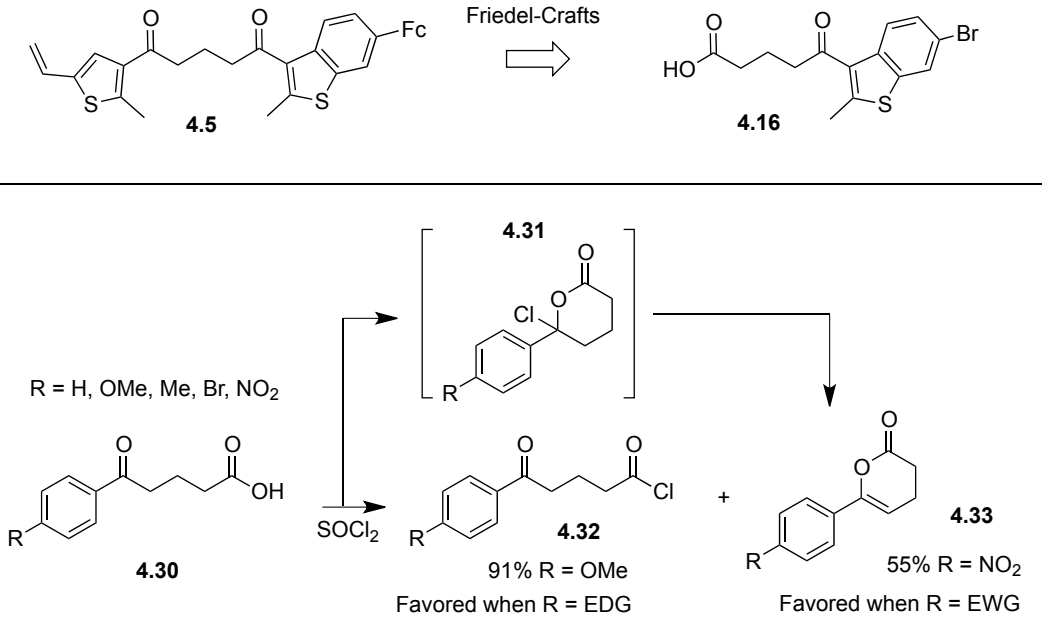

Figure 4.7 Friedel-Crafts reaction and the 1,5-keto acid system.

In the process of our research, Migulin et al.[43] published a procedure for synthesizing a mixed thiophene/benzo[*b*]thiophene photoswitch (follow up to

the previously mentioned Russian patent) functionalized differentially with chloride and bromide handles. Access to diketone **4.34** utilized a double Friedel-Crafts procedure, but acylation of **4.35** or **4.36** resulted in poor yields of 31 and 14% respectively (Figure 4.8, top). They recognized the findings of Shashidhar et al. as a possible culprit toward their low yields.

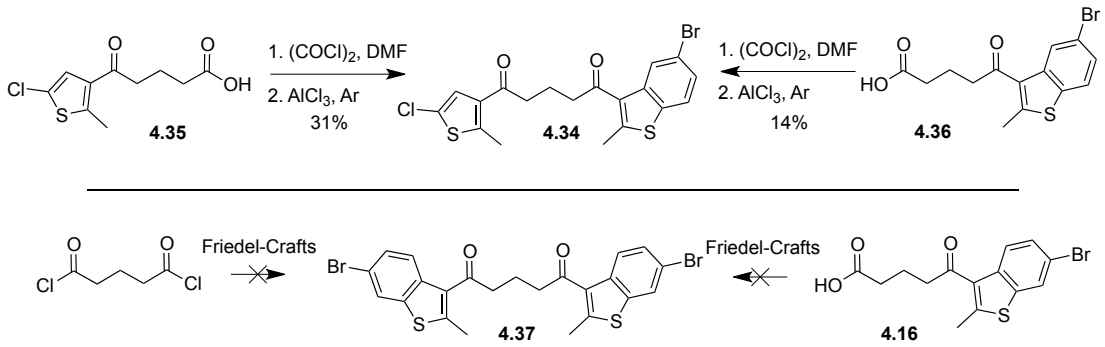

Figure 4.8 Attempts at Friedel-Crafts for second acylation .

Prior to the publication by Migulin et al., attempts at synthesizing symmetric diketone **4.37** via Friedel-Crafts (Figure 4.8, bottom) using the procedure of Krayushkin et al.[44] were unsuccessful (glutaryl dichloride route). Treatment of acid **4.16** was also unsuccessful in yielding **4.37**.

4.6.3 Pd-Catalyzed Cross-Coupling of *in-situ* Activated Carboxylic Acids

Another attractive route considered for the second acylation was the Pd cross-coupling of an *in-situ* activated carboxylic acid **4.38** with a thiophene boronic acid. This method would potentially provide **4.22**, a compound only two steps away from the desired photoswitch (Figure 4.9). Cross-coupling of carboxylic acids and boronic acids have been primarily researched by the

Lukas Gooßen[45] and Akio Yamamoto[46] groups. The Gooßen group has optimized the conditions for many applications in a series of publications.[47,48,49]

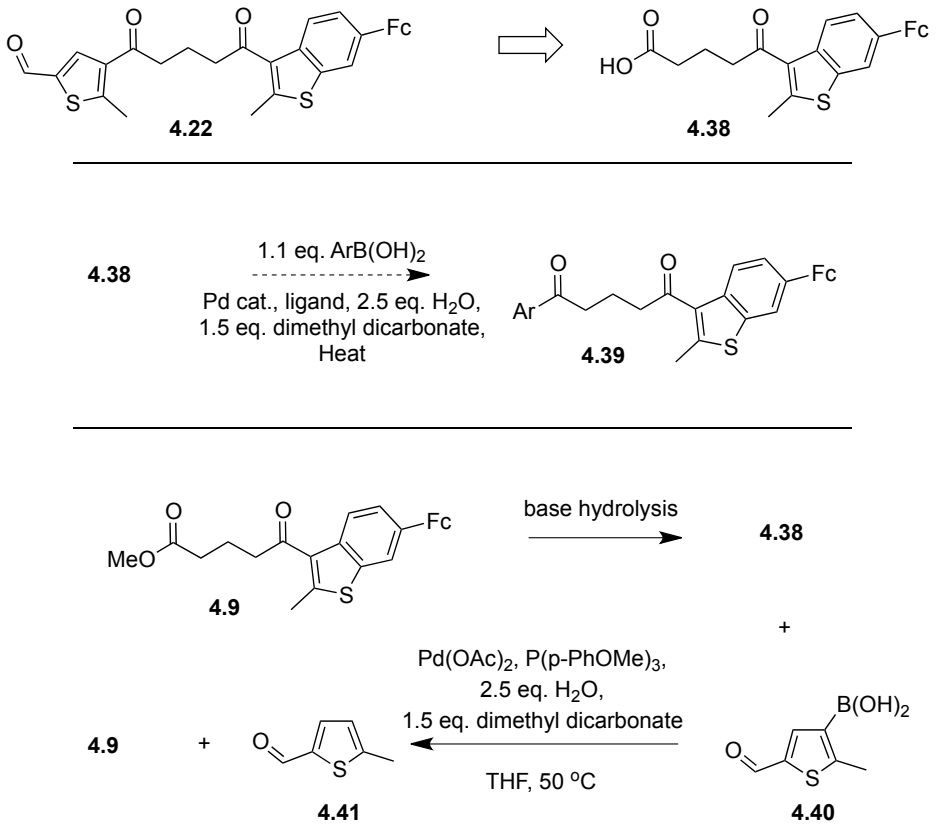

Figure 4.9 Cross Coupling Proposed acylation method utilizing Pd-catalyzed cross-coupling of in-situ generated mixed anhydride and thiophene-boronic acid.

Essentially, the carboxylic acid is activated to Pd insertion following *in-situ* reaction with dimethyl dicarbonate to generate a mixed anhydride (Figure 4.9). Pivalic anhydride, Boc-anhydride, and acetic anhydride also work as activators, but they do not work nearly as well. Gooßen and Yamamoto propose a mechanism similar to the Suzuki-Miyaura reaction (without the need for base) leading to acyl compounds similar to **4.39**. Another attractive

aspect of this reaction is that it uses one of the cheaper and more stable Pd (II) catalysts, $Pd(OAc)_2$.

Access to the ferrocenylated carboxylic acid **4.38** must pass through methyl ester **4.9** due to the inability of the carboxylic acid to undergo the Stille reaction. After base hydrolysis of the ferrocenylated methyl ester, Gooßen's conditions were attempted to couple the known boronic acid **4.40**. Interestingly, crude NMR showed no remaining starting material. However, the acid was converted to methyl ester **4.9** and the thiophene was deborylated to give **4.41**. Both of these products were also confirmed by mass spectrometry. Further optimization of this reaction was not pursued.

4.7 Lactol 4.7 Generation and Utility

One of the main purposes of our alternative synthesis of an unsymmetrical photoswitch was to avoid the possibility of mixtures of compounds leading to a decreased potential yield of desired product. Methyl ester **4.17** or Weinreb amide **4.18** would still allow us to pursue this goal without the need to directly protect the ketone portion of the molecule. Reduction of both carbonyl functionalities of **4.17** or **4.18** with DIBALH provides lactol **4.7**, which bears the desired functionality in the form of a masked aldehyde that is revealed in the presence of at least two equivalents of the lithium anion of **4.6** (Scheme 4.4). Precedence for this type of reaction with complex anions is seen in the work towards the total synthesis of (+)-macbecin I by Martin and co-workers.[50] Multiple equivalents of nucleophile

were necessary to give a good yield of diol **4.42** as a noticeable color change from red to brown above -40 ^{o}C signified possible anion decomposition. It should be noted that the dimethyl acetal was readily hydrolyzed during acidic workup to give diol **4.42**. The utility of this particular nucleophilic addition should be highly advantageous for the creation of a variety of mixed photoswitches.

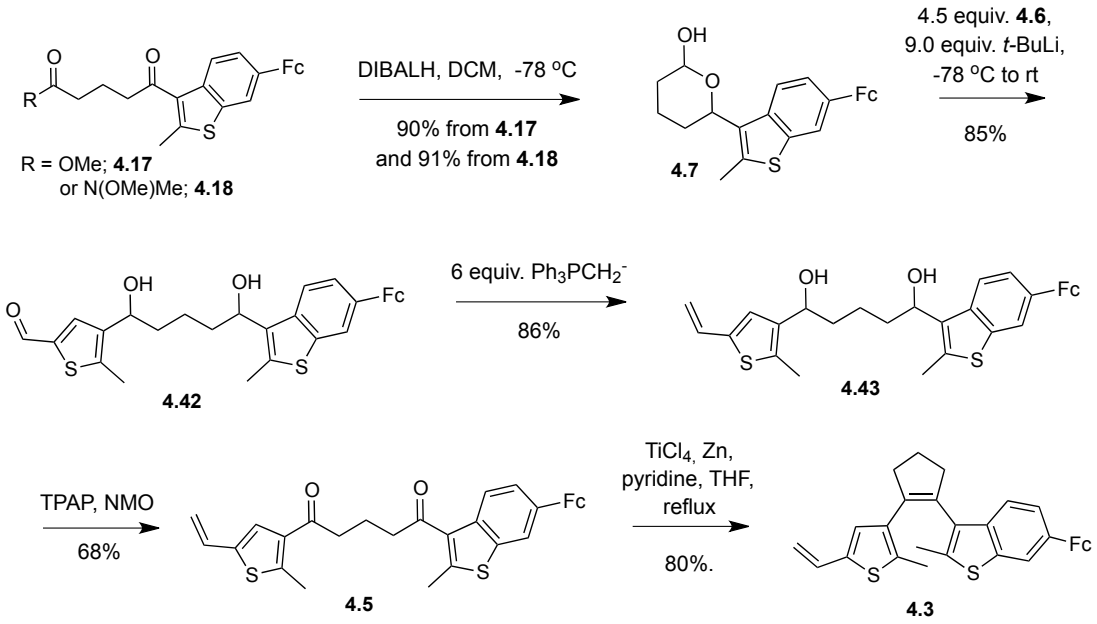

Scheme 4.4 Synthesis of 4.3 via lactol **4.7**.

Aldehyde **4.42** was treated with excess methylenetriphenylphosphorane to give alkene **4.43** in 85% yield. Oxidation of diol **4.43** did not proceed well under PCC, Swern, or Dess-Martin conditions providing mostly decomposed product. However, Ley conditions provided a 68% yield of diketone **4.5**. The McMurry reaction proceeded smoothly to furnish **4.3** in 80% yield as orange crystals.[11,43]

4.8 Photochromic Properties of 4.3 in Solution and the Solid State

Unlike the majority of molecular photoswitch compounds that are colorless in the open form, crystals of compound **4.3** appear orange due to the presence of the ferrocene moiety (Figure 4.10b). Compounds containing ferrocene range in color from pale yellow to dark red depending on the degree of conjugation.

4.8.1 Photocyclization of 4.3

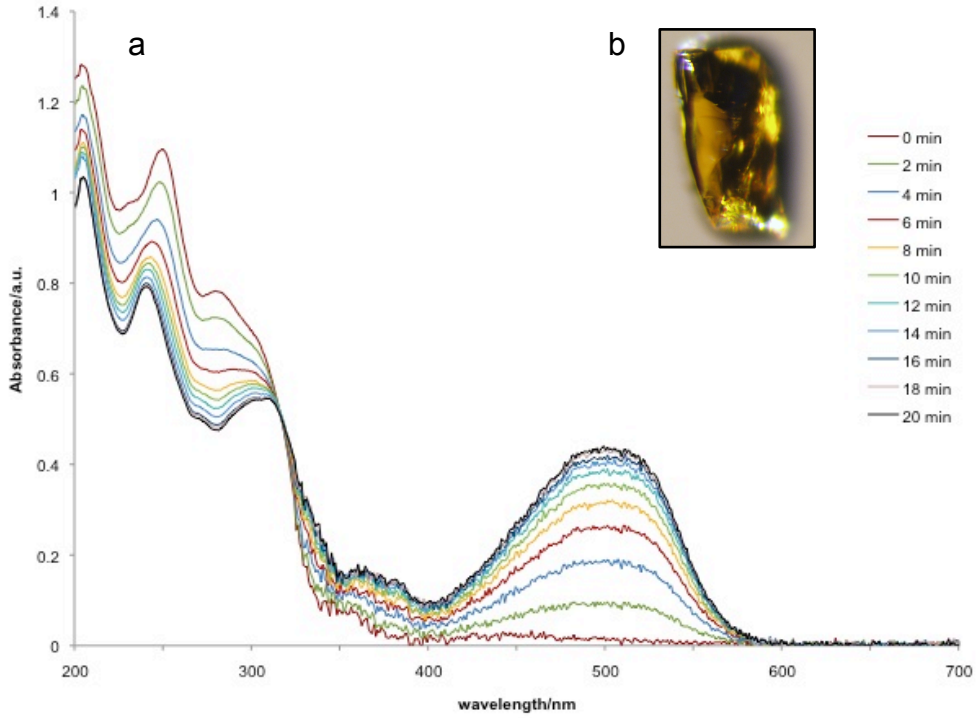

Figure 4.10 Open to Closed a) UV-Vis spectra of interval irradiation of **4.3** in heptane (4.5 x 10^{-5} M) with 306 nm light. b) Mechanically chopped (razorblade) single crystal of **4.3**.

To investigate the degree of photocyclization, solutions of **4.3** were irradiated with either monochromatic light via a xenon light source (306 nm), or a handheld UV lamp commonly used for TLC (254 or 365 nm). The UV/Vis

spectrum of **4.3** in heptanes displays distinct maxima typical to dithienylethene compounds in the UV at 206 and 252 nm, as well as shoulders at 284 and 360 nm (Figure 4.10a). There is also a weaker intensity peak that extends from the UV into the visible region (maximum 450 nm), which can be attributed to ferrocene. Irradiation of a dilute solution of **4.3** with UV light turns the solution from colorless to red and gives rise to a new peak at 505 nm (Figure 4.10a). Over time, as the sample is irradiated with monochromatic light, the intensity of the peaks below 350 nm decrease and there is a noticeable hypsochromic shift from 252 to 242 nm. Also, the shoulder at 284 nm is replaced with a more defined peak at 310 nm.

4.8.2 Attempts at Cycloreversion of 4.4

Photoisomerization of compound **4.4** to **4.3** was conducted in toluene, but cyclization of **4.3** was first carried out using a high pressure Hg vapor lamp. After 60 minutes of irradiation the photostationary state was reached, as judged by UV/Vis (Figure 4.11). Cycloreversion of the same sample using a white LED visibly bleached the red solution, but after 90 minutes of irradiation the solution still had a tinge of yellow color. Monitoring the sample by UV/Vis showed no change in the sample at 90 minutes, but the profile did not directly overlay with the spectrum of the open form at zero minutes of irradiation. It would appear from this result that complete cycloreversion did not occur.

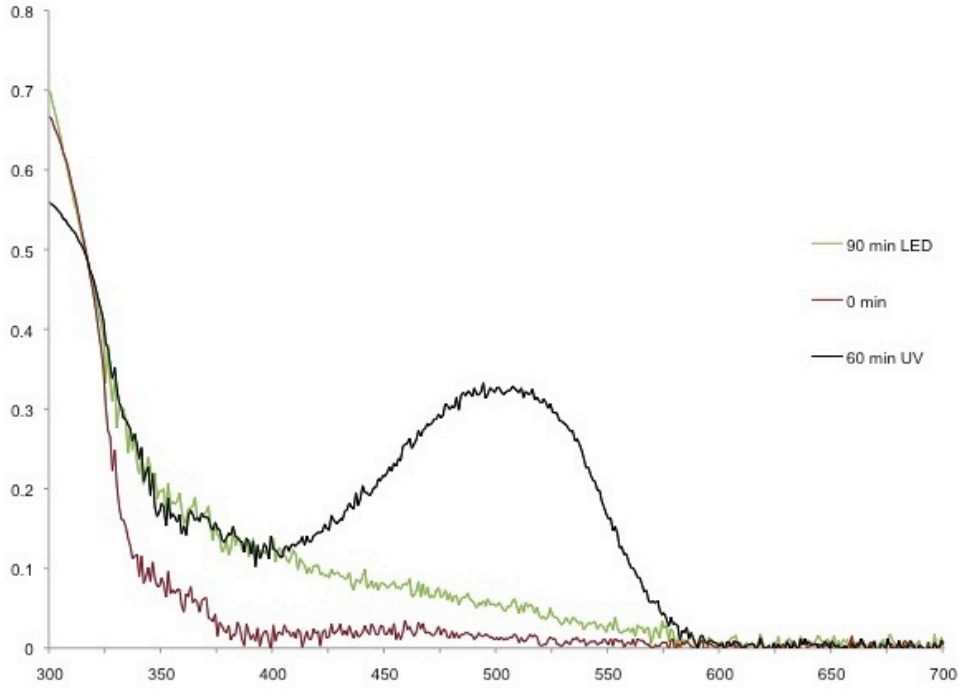

Figure 4.11 Photocyclization and Cycloreversion of **4.3** in toluene (7.6 x 10^{-5} M). Cyclization was conducted with a 250 W high pressure Hg vapor lamp. Cycloreversion of the sample was conducted with a white LED (I = 12.6 mW/cm^2). The spectra were normalized to the isosbestic point at 317 nm.

4.8.3 Characterization of Photoisomerization and Isolation of 4.4

In order to determine the degree of conversion and to eventually isolate **4.4** in the pure form, a solution of **4.3** in an NMR tube (6.9 x 10^{-3} M deuterobenzene) was irradiated with the handheld UV lamp. After 35 minutes of irradiation with 365 nm light, ^{1}H-NMR did not show the appearance of any new peaks despite a clear color change from yellow to red (Figure 4.12 inset). An additional irradiation with 254 nm light for 20 min did not change the color of the solution by eye, but did begin to show the appearance of two new peaks assigned to the methyl protons in the ^{1}H-NMR spectrum. However, any further irradiation did not increase the percent conversion. The same sample

was then evaporated and redissolved in heptanes (1.0×10^{-3} M), chosen for its lower UV-cutoff, and was irradiated with the monochromatic light source for a period of 5 h. The percent conversion of this sample was determined by ^{1}H-NMR in deuterobenzene by comparing the integration of the new methyl proton peaks to that of **4.3**, and it was found that 43% conversion was attained (Figure 4.12c). Lastly, the effect of concentration on photoconversion efficiency of **4.3** was evaluated with the monochromatic light source. At a 0.03 M concentration, cyclohexane had to be substituted for heptanes due to low solubility. After 5 hours of irradiation, the sample was red in color, but by ^{1}H-NMR showed no detectable formation of **4.4**.

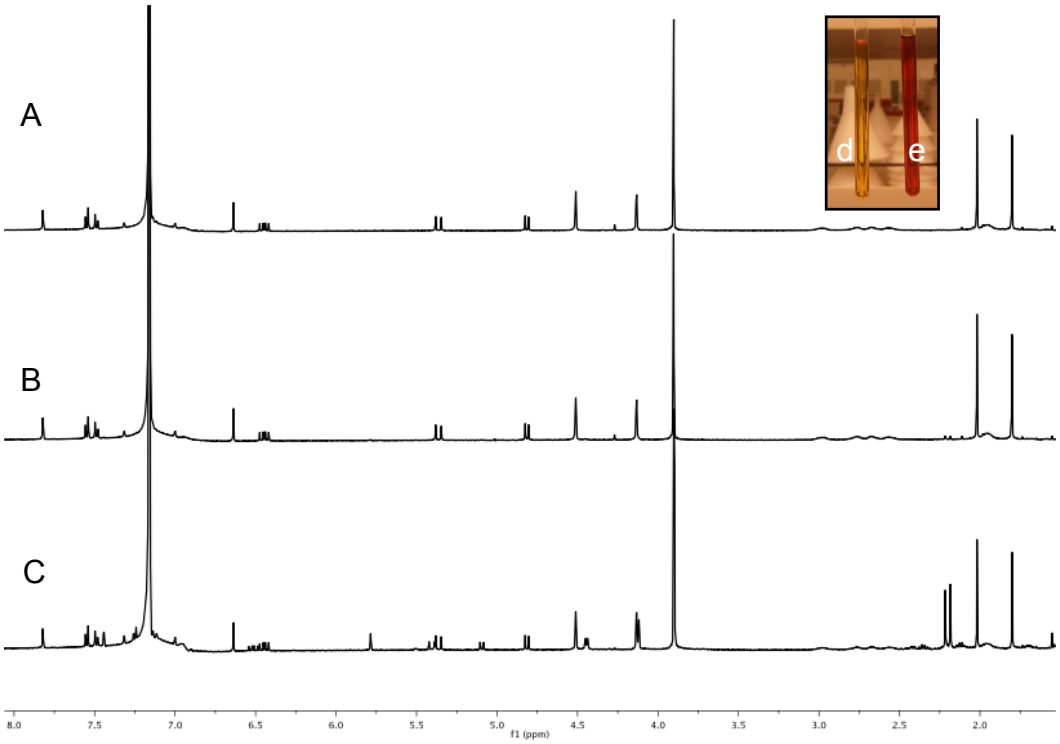

Figure 4.12 Stacked ^{1}H-NMR (500 MHz, benzene-D_6) spectra of the same sample of **4.3**: A) with no UV; 6.9 x 10^{-3} M B) with 365 nm (35 min) and 254 nm (20 min) irradiation; 6.9 x 10^{-3} M in deuterobenzene, and C) 306 nm monochromatic light; 1.0 x 10^{-3} M in heptanes (5 h).*Inset:* d) **4.3** with no UV irradiation; 6.9 x 10^{-3} M, e) with 365 nm (35 min) and 254 nm (20 min) irradiation; 6.9 x 10^{-3} M in deuterobenzene.

The importance of solvent, light source, and a dilute concentration of **4.3** for a semi-efficient photocyclization to **4.4** were determined from the prior experiments. Thus, conversion of **4.3** (52 mg scale) was set forth to prepare analytically pure **4.4**. After evaporation of the solvent, a clean portion of **4.4** was successfully separated via flash column chromatography, despite the similar polarities of **4.3** and **4.4**. However, only 7 mg of **4.4** was recovered along with 12.5 mg of a mixture of **4.3** and **4.4**. The overall mass recovery of 38% indicates decomposition during the photocyclization as well as the presence of black baseline material on the column. Additionally, when purified

4.4 was left in a foil-coated vial for weeks, the residue darkened from its original deep red color. After passing **4.4** through a short plug of silica, there was again an appearance of black baseline material in addition to the red fraction. Analysis of the red fraction by ^{1}H-NMR revealed a mixture of compounds. The cause of degradation is unknown and occurred before a ^{13}C-NMR could be acquired.

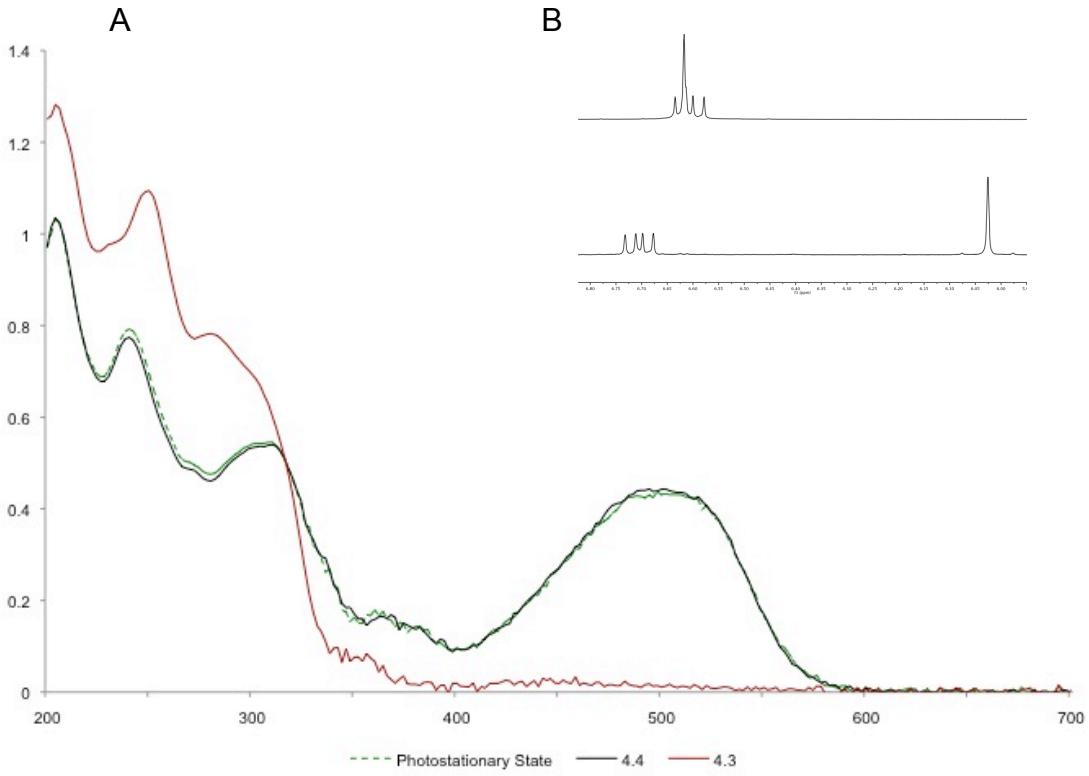

Figure 4.13 Photocyclization Conversion A) UV-Vis spectra of pure **4.4** isolated by flash chromatography vs 0 min (**4.3**) and 20 min 306 nm (photostationary state)**.** (4.5 x 10^{-5} M heptane). B) Stacked ^{1}H-NMR (500 MHz, $CDCl_3$) spectra showing thiophene and vinyl protons of **4.3** (top of inset) vs. pure **4.4** (bottom of inset). The spectra were normalized to the isosbestic point at 317 nm.

Prior to degradation, **4.4** was characterized by ^{1}H-NMR. The drastic shielding of the thiophene proton from **4.3** to **4.4** is shown in Figure 4.12b and

is typical to molecular switches in the literature.[16] The UV/Vis profile (Figure 4.13a) of purified **4.4** matched that of the 20 min spectrum seen in Figure 4.11a (overlayed in Figure 4.13a). This reinforces the seeming concentration dependence on the degree of photocyclization as a dilute sample (10^{-5} mM) can be converted nearly in quantitative yield to the closed isomer **4.4**.

4.9 X-ray of 4.3

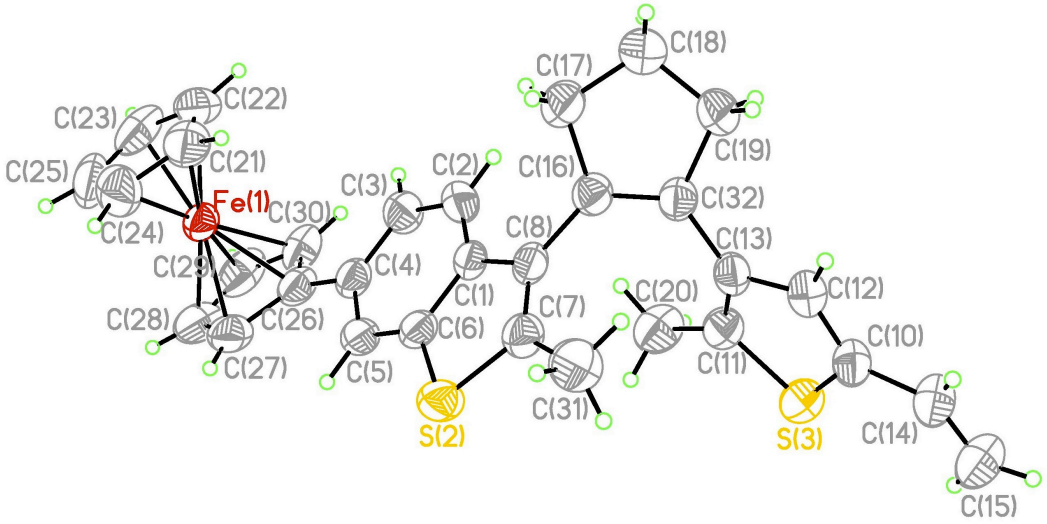

Figure 4.14 ORTEP of the ferrocenylated photoswitch, **4.3**.

Compound **4.3** was highly crystalline and formed yellow, x-ray quality single crystals upon slow evaporation from a mixture of hexanes and dichloromethane (Figure 4.14). The distance between the reactive carbon atoms, 3.67 Å, is well below the determined necessary distance for solid-state cyclization (~4.2 Å).[51] Interestingly, crystals of **4.3** do not appear to undergo photocyclization upon UV irradiation (306 nm Xe lamp or 254 nm handheld UV), unlike similar compounds recently reported.[43] However, this finding does

seem to corroborate the fact that concentrated solutions of **4.3** do not undergo complete cyclization.

4.10 CONCLUSION

A new synthetic route towards unsymmetrical benzo[*b*]thienyl-thienylethene photoswitches, which allows the potential for an extensive variation of subunits, was described. Each aryl subunit was functionalized prior to the McMurry cyclization, which reduced the handling of the photoactive compound. Attachment of the ferrocene moiety directly to the benzo[*b*]thiophene subunit appears to affect the photocyclization event adversely (solid and concentrated solution), as other ferrocene containing photoswitches are reported to cyclize in the crystalline form. Complete cyclization is apparent at low concentrations, while low photoconversion occurs at higher concentrations. Cycloreversion does not appear to go to completion. The stability of the closed form is in question due to reduced mass recovery during photocyclization and unknown degradation processes of the purified closed isomer in the dark. Investigation of the photoswitch on Ru nanoparticles is ongoing in the Chen lab.

Experimentals

Photoisomerization. Ring closing experiments used irradiation from a handheld UV lamp (254 or 365 nm) or a 250W Xe lamp with a monochromator (306 nm, 12 nm slit, I = 13.5 mW/cm^2). Ring opening was conducted by irradiation with an LED lamp (I = 12.6 mW/cm^2). UV/Vis

spectroscopic studies were performed with an ATI Unicam UV4 spectrometer using a 1 cm quartz cuvette with a resolution of 2 nm.

0.1 mmol Scale Photocyclization: Compound **4.3** (52.0 mg, 0.1 mmole) was dissolved in cyclohexane (20 mL) and split evenly amongst eight scintillation vials. Each aliquot was diluted to a final volume of 20 mL with heptane (6.3 x 10^{-4} M) and irradiated for 1 h through the top of the open vial with the Xe lamp (306 nm). All of the vials were combined and evaporated to give a dark red residue, which was pre-loaded onto silica gel and purified via flash column chromatography (2% DCM in hexanes) yielding 7.2 mg of **4.4** and 12.5 mg of **4.3/4.4** as a mixture.

General Procedure A: Microwave Stille Reaction to provide 4.13, 4.17 and 4.18. To a microwave reaction vessel with a stirbar was added halide (**4.10**, **4.9**, or **4.8**; 1.0 equiv), CuO powder (1.0 equiv), and $PdCl_2$(dppf) (10 mol%). DMF (4 mL/mmol halide) was added to the sealed reaction vessel and was evacuated and purged with dry N_2 (repeat 5x). Tributylstannylferrocene[33] (1.5 equiv) was added to the reaction mixture prior to microwave heating (200W, 140 ^{o}C, 25 min). The black mixture was diluted with EtOAc and vacuum filtered through a pad of celite and silica gel. After rinsing with additional EtOAc, the orange solution was washed with water (5x) and brine prior to drying ($MgSO_4$) and filtration. The resulting ferrocenylated compounds were purified by flash column chromatography (silica) or recrystallized. In the

case of chromatography, the non-polar tin byproducts were removed by mixing the semi-pure product with 10% KF/silica and DCM. This slurry was filtered and rinsed with DCM, EtOAc, and THF until the silica was no longer orange in color.

General Procedure B: Iodination to provide 4.14 and 4.15. The appropriate benzothiophene (**4.10** or **4.13**; 1.0 equiv) was suspended in glacial acetic acid (5 mL/0.44 mmol benzothiophene), and to this mixture was added 20% H_2SO_4 (0.43 mL/0.44 mmol benzothiophene), $NaIO_4$ (0.25 equiv), and I_2 (0.5 equiv). The light purple mixture was heated at 70-80 ^oC for 3 h, after which time the deep purple solution was cooled to room temperature and diluted with water. The reaction mixture was extracted with DCM (3x), and the combined organic layers were washed with water (2x), sat. sodium bicarbonate (2x), brine, and 10% $Na_2S_2O_3$ solution. The organic layer was dried ($MgSO_4$), filtered, and evaporated to give the crude iodide, which was purified via flash column chromatography.

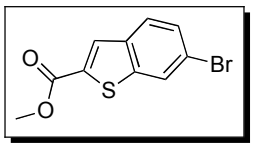

6-Bromobenzo[*b*]thiophene-2-carboxylic acid methyl ester (4.11). The literature procedure of Fedi et al.[52] was followed for the synthesis of **4.11**. To a two-neck round bottom flask fitted with a condenser was added 4-bromo-2-fluorobenzaldehyde (14.8 g, 72.9 mmol) and DMSO (100 mL, anhydrous). Methyl thioglycolate (8 mL, 89.5 mmol) and triethylamine (30 mL, 215.2

mmol) were added and the reaction heated to 80-90 ^{o}C over 2 h. The reaction was allowed to cool before being poured into vigorously stirring ice-water (3500 mL). After 1 h of stirring, the solid was filtered and dried before recrystallization from ethanol (250 mL) to give pale yellow crystals (16.1 g, 81% yield), mp 113-115 ^{o}C. IR (thin-film, cm^{-1}) 3012, 2952, 2913, 2849, 1717, 1510, 1434, 1384, 1307, 1259, 1168, 1090, 1060, 858, 803, 752, 713; ^{1}H NMR ($CDCl_3$) δ 8.013 (d, *J* = 1.5 Hz, 1H), 7.73 (d, *J* = 9.0 Hz, 1H), 7.51 (dd, *J* = 1.5, 9.0 Hz, 1H), 3.95 (s, 3H); ^{13}C NMR ($CDCl_3$) δ 163.0, 143.6, 137.5, 134.1, 130.3, 128.8, 126.7, 125.5, 121.4, 52.8.

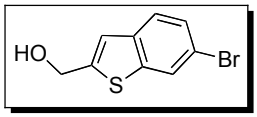

(6-Bromobenzo[*b*]thiophen-2-yl)methanol (4.12a). Ester **4.11** (6.8 g, 25.0 mmol) was dissolved in THF (anhydrous, 50 mL) and cooled to 0 ^{o}C. Lithium dimethylammonium borohydride[53] (50 mL, 50.0 mmol, 1.0 *M* THF/hexane) was added drop-wise. After 5 min of stirring, the reaction was complete as judged by TLC and was quenched with HCl (3.0 *M*) under vigorous stirring until the evolution of gas ceased. The organic layer was separated, and the aqueous layer extracted with EtOAc (3x). The combined organic layers were washed with water and brine followed by drying (Na_2SO_4). Evaporation of solvent gave a yellow solid, which was recrystallized from isopropanol/water to give **4.12a** as white crystals. (5.7 g, 94% yield), mp 111-113 ^{o}C. IR (thin film, cm^{-1}) 3203, 3071, 2901, 2853, 1577, 1523, 1444, 849, 841; ^{1}H NMR ($CDCl_3$) δ 7.95 (d, *J* = 1.5

Hz, 1H), 7.57 (d, *J* = 8.5 Hz, 1H), 7.44 (dd, *J* = 1.5, 8.5 Hz, 1H), 7.17 (d, *J* = 1.0 Hz, 1H), 4.91 (s, 2H), 1.97 (br s, 1H); ^{13}C NMR ($CDCl_3$) δ 145.8, 141.6, 138.5, 128.0, 125.1, 124.8, 121.1, 118.3, 60.9; HRMS (EI) for C_9H_7BrOS $[M]^+$ calcd, 241.9401, found, 241.9404 (error = 1.2 ppm).

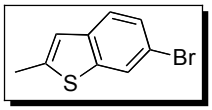

6-Bromo-2-methylbenzo[*b*]thiophene (4.10). The preparation of the mesylate was adapted from a previously published procedure by Hay et al.[54] Primary alcohol **4.12a** (5.3 g, 22 mmol) was dissolved in DCM (anhydrous, 100 mL) and stirred under dry nitrogen. Triethylamine (8.0 mL, 57 mmol) and methanesulfonyl chloride (4.3 mL, 55 mmol) were then added and the resulting mixture was allowed to stir at room temperature for 16 h. The reaction was then diluted with DCM and washed with water and brine. The combined organic layer was dried with $MgSO_4$, filtered and evaporated to give the mesylate, which was taken on without purification. The crude mesylate was dissolved in THF (anhydrous, 100 mL) and cooled to 0 ^oC followed by the drop-wise addition of lithium triethylborohydride (44 mL, 44 mmol, 1.0 *M* in hexanes). The solution was allowed to warm to room temperature and stirring was continued for 5 h. After the reaction was deemed to be complete by TLC, the reaction mixture was cooled to 0 ^oC and carefully quenched with HCl (1.0 *M*, 100 mL). The mixture was extracted with EtOAc (3x), dried (Na_2SO_4) and evaporated to give the crude benzothiophene **4.10**. After dry loading onto silica, **4.10** was passed

through a plug of silica using hexanes as eluent to give 4.5 g (91% yield) of the desired product, mp 66-67 ^{o}C. IR (thin-film, cm^{-1}) 3054, 2932, 1522, 1438, 1386, 1197, 1120, 866, 841, 794; ^{1}H NMR ($CDCl_3$) δ 7.87 (d, *J* = 1.5 Hz, H), 7.49 (d, *J* = 8.5 Hz, 1H), 7.40 (dd, *J* = 1.5, 8.5 Hz, 1H), 6.93 (t, *J* = 1.0 Hz, 1H), 2.57 (d, *J* = 1.0 Hz, 1H); ^{13}C NMR ($CDCl_3$) δ 141.8, 141.3, 139.3, 127.6, 124.6, 123.8, 121.4, 117.2, 16.3; HRMS (EI) for $C_9H_7BrS[M]^+$ calcd, 225.9452, found, 225.9449 (error = -1.3 ppm).

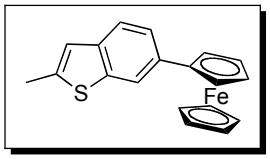

6-Ferrocenyl-2-methylbenzo[*b*]thiophene (4.13). Compound **4.10** (227.1 mg, 1.0 mmol) was subjected to General Procedure A and **4.13** (red-orange crystals) was purified via flash column chromatography (hexanes) to give 251 mg (76% yield) of the desired product, mp 85-88 ^{o}C. IR (thin-film, cm^{-1}) 3293, 3090, 2929, 2865, 1730, 1703, 1641, 1599, 1554, 1437, 1120, 1105, 818; ^{1}H NMR ($CDCl_3$) δ 7.86 (d, *J* = 1 Hz, 1H), 7.59 (d, *J* = 8.0 Hz, 1H), 7.48 (dd, *J* = 1.0 , 8.0 Hz, 1H), 6.96 (t, *J* = 1.0 Hz, 1H), 4.71 (t, *J* = 2.0 Hz, 2H), 4.35 (t, *J* = 2.0 Hz, 2H), 4.07 (s, 5H), 2.60 (d, *J* = 1.0 Hz, 3H); ^{13}C NMR ($CDCl_3$) δ 140.32, 140.27, 138.8, 134.8, 123.3, 122.4, 121.7, 119.0, 85.9, 69.7, 69.0, 66.6, 16.4; HRMS (ESI) for $C_{19}H_{16}NaSFe$ $[M + H]^+$ calcd, 333.03949, found, 333.03939 (error = -0.2948 ppm).

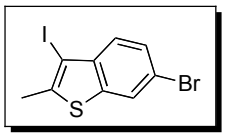

6-Bromo-3-iodo-2-methylbenzo[*b*]thiophene (4.14). Iodination of **4.10** (250 mg, 1.1 mmol) was conducted according to General Procedure B to give **4.14** (252 mg, 65% yield) as white crystals, mp 67-69 ^{o}C. IR (thin-film, cm^{-1}) 3067, 2911, 2847, 1882, 1712, 1619, 1580, 1545, 1445, 1435, 1386, 1284, 1236, 1155, 902, 858, 802; ^{1}H NMR ($CDCl_3$) δ 7.82 (t, *J* = 1.0 Hz, 1H), 7.47 (d, *J* = 1.0 Hz, 2H), 2.56 (s, 3H); ^{13}C NMR ($CDCl_3$) δ 140.4, 140.0, 139.6, 128.6, 126.1, 124.6, 118.8, 80.7, 18.9; HRMS (ESI) for C_9H_6BrIS $[M]^+$ calcd, 351.8418, found, 351.8425 (error = 2.0 ppm).

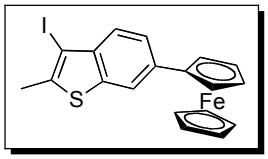

6-Ferrocenyl-3-iodo-2-methylbenzo[*b*]thiophene (4.15). Iodination of **4.13** (32 mg, 0.10 mmol) was conducted according to General Procedure B to give **4.15** (40 mg, 90% yield) as red crystals, mp 196-198 ^{o}C turned black between 160-170 ^{o}C. IR (thin-film, cm^{-1}) 3293, 3089, 2927, 2867, 1703, 1642, 1598, 1553, 1435, 1105, 817; ^{1}H NMR ($CDCl_3$) δ 7.79 (dd, *J* = 0.5, 1.5 Hz, 1H), 7.56 (m, 2H), 4.71 (t, *J* = 2.0 Hz, 2H), 4.36 (t, *J* = 2.0 Hz, 2H), 4.05 (s, 5H), 2.59 (s, 3H); ^{13}C NMR ($CDCl_3$) δ 139.8, 138.8, 138.5, 136.7, 124.8, 124.2, 118.9, 81.0, 69.8, 69.3, 66.8, 18.9; HRMS (ESI) for $C_{19}H_{15}FeIS$ $[M]^+$ calcd, 457.9289, found, 457.9293 (error = 0.9 ppm).

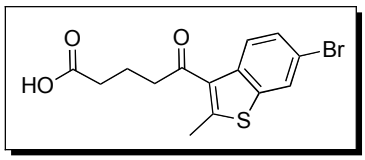

5-(6-Bromo-2-methylbenzo[*b*]thiophen-3-yl)-5-oxopentanoic acid (4.16). Glutaric anhydride (2.24 g, 19.3 mmol; 98%) was dissolved in DCM (anhydrous, 20 mL) and added drop-wise to $AlCl_3$ (g, 67.4 mmol) in DCM (100 mL) cooled to 0 ^{o}C. The reaction mixture was allowed to warm to room temperature and stirred for 30 min. A solution of **4.10** (3.97 g, 17.5 mmol) in DCM (100 mL) was added drop-wise to the solution of $AlCl_3$ and went from yellow to dark green in color. The reaction was stirred at room temperature for 2 h and was poured onto cracked ice upon completion. Concentrated HCl was added drop-wise until the disappearance of the white precipitate (became homogeneous white solution) followed by extraction with DCM (4x). The combined DCM layers were washed with water and extracted with minimal amounts of NaOH (2.0 *M*, 5x). The first few NaOH extractions created an insoluble precipitate (sodium salt of **4.16**) and was filtered away and put aside. The NaOH extractions were combined with the precipitate in an Erlenmeyer flask. The flask was cooled to 0 ^{o}C and with vigorous stirring, HCl (3.0 *M*) was added drop-wise until pH 1 and a white precipitate persisted. Acid **4.16** (4.58 g, 77% yield) was filtered and dried under vacuum, mp 136-138 ^{o}C. IR (thin-film, cm^{-1}) 3034, 2909, 2750, 2573, 1696, 1649, 1578, 1501, 1445, 1406, 1378, 1243, 1170, 931, 819, 768; ^{1}H NMR (CD_3OD) δ 8.04 (d, *J* = 8.5 Hz, 1H), 7.96 (d, *J* = 2.0 Hz, 1H), 7.49 (dd, *J* = 2.0, 8.5 Hz, 1H), 3.02 (t, *J* = 7.0 Hz, 2H), 2.74 (s, 3H), 2.41 (t, *J* = 7.0 Hz, 2H), 2.01 (p, *J* = 7.0 Hz, 2H);

^{13}C NMR (CD_3OD) δ 199.9, 177.2, 150.4, 140.4, 138.9, 138.8, 129.7, 126.4, 125.4, 119.3, 43.9, 34.2, 20.8, 17.0; HRMS (ESI) for $C_{14}H_{13}O_3NaSBr$ [M + Na]$^+$ calcd, 362.96610, found, 362.96606 (error = -0.1059ppm).

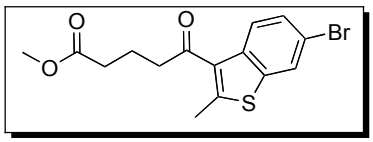

5-(6-Bromo-2-methylbenzo[*b*]thiophen-3-yl)-5-oxopentanoic acid methyl ester (4.9). Acid **4.16** (1.00 g, 2.93 mmol) was dissolved in methanol (anhydrous, 50 mL) along with 3 drops of sulfuric acid. The solution was refluxed for 3 h and cooled to room temperature prior to evaporation of the solvent. The residue was taken up in EtOAc, washed with sat. aq. sodium bicarbonate solution, water and brine. The organic layer was dried with Na_2SO_4, filtered and evaporated to yield methyl ester **4.9** as a white solid (1.02 g, 98% yield), mp 69-71 ^{o}C. IR (thin-film, cm^{-1}) 3337, 3067, 2950, 1734, 1664, 1581, 1447, 1174, 818; ^{1}H NMR ($CDCl_3$) δ 8.01 (d, *J* = 9.0 Hz, 1H), 7.86 (d, *J* = 2.0 Hz, 1H), 7.48 (dd, *J* = 2.0, 9.0 Hz, 1H), 3.67 (s, 3H), 2.98 (t, *J* = 7.0 Hz, 2H), 2.74 (s, 3H), 2.45 (t, *J* = 7.0 Hz, 2H), 2.10 (p, *J* = 7.0 Hz, 2H); ^{13}C NMR ($CDCl_3$) δ 197.8, 173.8, 148.6, 138.9, 137.4, 132.7, 128.8, 125.2, 124.3, 118.5, 51.8, 42.8, 33.2, 19.6, 17.2; HRMS (ESI) for [M + Na]$^+$ calcd, 376.98175, found, 376.98448 (error = 7.2455 ppm).

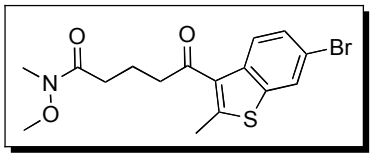

5-(6-Bromo-2-methylbenzo[b]thiophen-3-yl)-N-methoxy-N-methyl-5-oxopentanamide (4.8). Acid **4.16** (1.27 g, 3.73 mmol) was dissolved in DCM (anhydrous, 35 mL) and cooled to 0 ^{o}C. CDI (726 mg, 4.48 mmol) was added gradually and the reaction was allowed to warm to room temperature over 45 min. *N*-methoxy-*N*-methylamine hydrochloride (437 mg, 4.48 mmol) was added in one portion to the activated acid and stirring was continued for 16 h. The reaction mixture was quenched with HCl (1.0 *M*, 9.0 mL), diluted with water, and extracted with EtOAc (3x). The combined organic layers were washed with brine, dried (Na_2SO_4), filtered, and evaporated to yield **4.8** as a white solid (1.43 g, quantitative yield), mp 95-96 ^{o}C. IR (thin-film, cm^{-1}) 3321, 3066, 2962, 2936, 2819, 1662, 1581, 1505, 1447, 1414, 1383, 1341, 1175, 995, 864, 818, 765, 733; ^{1}H NMR ($CDCl_3$) δ 8.03 (d, *J* = 9.0 Hz, 1H), 7.85 (d, *J* = 2.0 Hz, 1H), 7.48 (dd, *J* = 2.0, 9.0 Hz, 1H), 3.66 (s, 3H), 3.17 (s, 3H), 3.01, (t, *J* = 7.0 Hz, 2H), 2.75 (s, 3H), 2.56 (t, *J* = 7.0 Hz, 2H), 2.10 (p, *J* = 7.0 Hz, 2H); ^{13}C NMR ($CDCl_3$) δ 198.4, 148.5, 138.9, 137.5, 132.8, 128.7, 125.2, 124.3, 118.4, 61.4, 43.0, 32.3, 31.0, 19.3, 17.2; HRMS (ESI) for $C_{16}H_{18}NO_3NaSBr$ $[M + Na]^+$ calcd, 406.0083, found, 406.01014 (error = 4.5377 ppm).

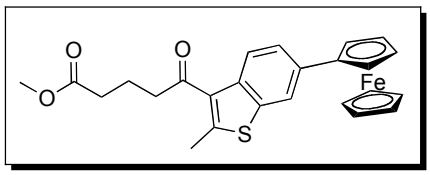

5-(6-Ferrocenyl-2-methylbenzo[b]thiophen-3-yl)- 5-oxopentanoic acid methyl ester (4.17). Compound **4.9** (50 mg, 0.14 mmol) was subjected to General Procedure A and **4.17** (42 mg, 65 % yield) was purified via recrystallization (isopropanol), mp 116-118 ^{o}C. IR (thin-film, cm^{-1}) 3152, 3088, 2929, 1737, 1654, 1600, 1438, 1171, 812; ^{1}H NMR ($CDCl_3$) δ 8.02 (d, *J* = 8.5 Hz, 1H), 7.79 (d, *J* = 1.5 Hz, 1H), 7.54 (dd, *J* = 1.5, 8.5 Hz, 1H), 4.69 (t, *J* = 2.0 Hz, 2H), 4.34 (t, *J* = 2.0 Hz, 2H), 4.04 (s, 5H), 3.69 (s, 3H), 3.02 (t, *J* = 7.0 Hz, 2H), 2.75 (s, 3H), 2.48 (t, *J* = 7.0 Hz, 2H), 2.13 (p, *J* = 7.0 Hz, 2H); ^{13}C NMR ($CDCl_3$) δ 198.2, 173.8, 147.5, 138.0, 136.6, 136.2, 133.0, 124,2, 123.5, 118.4, 85.0, 69.8, 69.3, 66.7, 51.8, 42.8, 33.3, 19.7, 17.2; HRMS (ESI) for $C_{25}H_{24}O_3NaSFe$ $[M + Na]^+$ calcd, 483.06878, found, 483.06821 (error = -1.1739 ppm).

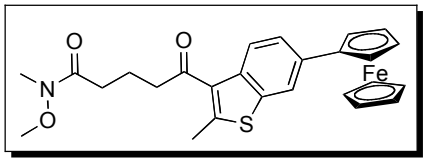

5-(6-Ferrocenyl-2-methylbenzo[b]thiophen-3-yl)-*N*-methoxy-*N*-methyl-5-oxopentanamide (4.18). Compound **4.8** (250 mg, 0.65 mmol) was subjected to General Procedure A and **4.18** (220 mg, 69% yield) was purified via recrystallization (methanol/ethanol), mp 174-176 ^{o}C. IR (thin-film, cm^{-1}); ^{1}H NMR ($CDCl_3$) δ 8.05 (d, *J* = 8.5 Hz, 1H), 7.81 (d, *J* = 1.5 Hz, 1H), 7.55 (dd, *J* = 1.5, 7.0 Hz, 1H), 4.71 (t, *J* = 1.5 Hz, 2H), 4.36 (t, *J* = 1.5 Hz, 2H), 4.06 (s, 5H), 3.69 (s,

3H), 3.20 (s, 3H), 3.07 (t, *J* = 7.0 Hz, 2H), 2.77 (s, 3H), 2.60 (t, *J* = 7.0 Hz, 2H), 2.16 (p, *J* = 7.0 Hz, 2H); ^{13}C NMR ($CDCl_3$) δ 198.7, 147.3, 138.0, 136.7, 136.1, 133.1, 124.2, 123.5, 118.4, 85.0, 69.8, 69.2, 66.6, 61.4, 43.0, 32.3, 31.1, 19.4, 17.1; HRMS (ESI) for $C_{26}H_{27}NO_3NaSFe$ $[M + Na]^+$ calcd, 512.09533, found, 512.09264 (error = -5.2456 ppm).

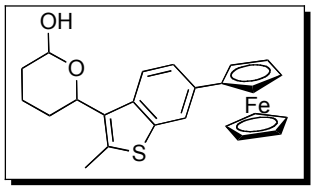

6-(6-Ferrocenyl-2-methylbenzo[*b*]thiophen-3-yl)tetrahydro-2H-pyran-2-ol (4.7). Weinreb amide **4.18** (500 mg, 1.02 mmol) was dissolved in DCM (anhydrous, 20 mL) and DIBALH (4.0 mL, 4.0 mmol, 1.0 *M* in hexanes) was added drop-wise at -78 ^{o}C. Stirring was continued at this temperature for 2 h followed by quenching with a 10% aq. sol. of Rochelle's salt. The mixture was allowed to warm to room temperature and stirring was continued for 30 minutes. The biphasic solution was vacuum filtered through celite (large surface area) and the gel-cake rinsed with EtOAc. The DCM layer was separated in a separatory funnel, while the aqueous layer was extracted with DCM (3x). The combined organic layers were washed with brine, dried (Na_2SO_4), filtered and evaporated to give a red solid. The crude solid was purified by flash column chromatography (3:1 hexanes/EtOAc) and the red band was collected (mixture of diastereomers, 402 mg, 91% yield), mp ^{o}C. IR (thin-film, cm^{-1}); ^{1}H NMR ($CDCl_3$) see spectra; ^{13}C NMR ($CDCl_3$) see spectra;

HRMS (ESI) for $C_{24}H_{24}O_2NaSFe$ $[M + Na]^+$ calcd, 455.07386, found, 455.07540 (error = 3.3787 ppm).

Reduction of ester **4.17** (0.10 g, 0.22 mmol) using only 2 equivalents of DIBALH (0.44 mL, 0.44 mmol, 1.0 *M* in hexanes) and otherwise following the same procedure as for the reduction of **4.18**, gave 0.85 g (90% yield) of lactol **4.7**. The spectral data for **4.7** was equivalent regardless of starting substrate.

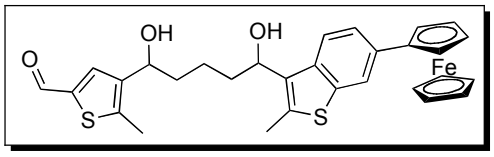

4-(5-(6-Ferrocenyl-2-methylbenzo[*b*]thiophen-3-yl)-1,5-dihydroxypentyl)-5-methylthiophene-2-carbaldehyde (4.42). Halide **4.6** (525 mg, 2.09 mmol) was dissolved in THF (anhydrous, 6 mL) and cooled to -78 ^oC. *t*-BuLi (1.6 *M* in pentane, 2.6 mL, 4.2 mmol) was added drop-wise to the halide and was stirred for 20 min. Lactol **4.7** (199 mg, 0.46 mmol) was added drop-wise to the red lithium anion and stirred for 15 min before removal from the dry ice bath. As the reaction warmed above -40 ^oC the solution turned from red to brown and began to darken as the solution warmed to room temperature. After 30 min at room temperature, the black mixture was quenched with sat. aq. NH_4Cl and extracted with EtOAc (3x). The combined organic layers were washed with water (1x), HCl (1.0 *M*, 2x) and brine prior to drying (Na_2SO_4). After filtration and evaporation of solvent, the crude diol/aldehyde **4.42** was purified by flash column chromatography (3:1 hexanes/EtOAc, then 1:1 hexanes/EtOAc) and

the red band was collected (mixture of diastereomers, 219 mg, 85% yield). IR (thin-film, cm^{-1}) 3400, 3082, 2924, 1656, 1440, 819; ^{1}H NMR ($CDCl_3$) see spectra; ^{13}C NMR ($CDCl_3$) see spectra; HRMS (ESI) for $C_{30}H_{30}O_3NaS_2Fe$ [M + Na]$^{+}$ calcd, 581.08780, found, 581.08986 (error = 3.5465 ppm).

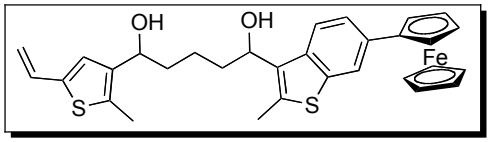

1-(6-Ferrocenyl-2-methylbenzo[*b*]thiophen-3-yl)-5-(2-methyl-5-vinylthiophen-3-yl)pentane-1,5-diol (4.43). Methyltriphenylphosphonium bromide (837 mg, 2.34 mmol) was dissolved in THF (anhydrous, 10 mL) and cooled to 0 ^{o}C. *n*-BuLi (2.5 *M* in hexanes, 0.94 mL, 2.34 mmol) was added drop-wise and the solution became yellow in color. After complete addition of base, the reaction was stirred for 1 h and diol **4.42** (219 mg, 0.39 mmol) was added in THF (5 mL). The reaction mixture was stirred at room temperature for 1 h and became orange in color. When judged to be complete by TLC, the reaction was quenched with sat. aq. NH_4Cl sol. and extracted with EtOAc (3x). The combined organic layers were washed with brine, dried (Na_2SO_4), filtered, and evaporated to give the crude alkene, which was purified by flash column chromatography (1:1 hexanes/EtOAc; the red band was collected) to give 187 mg (86% yield) of the desired material as a mixture of diastereomers. IR (thin-film, cm^{-1}) 3368, 3087, 2939, 2857, 1619, 1599, 1440, 819; ^{1}H NMR ($CDCl_3$) see spectra; ^{13}C

NMR ($CDCl_3$) see spectra; HRMS (ESI) for $C_{31}H_{32}O_2NaS_2Fe$ $[M + Na]^+$ calcd, 579.10853, found, 581.10630 (error = -3.8587 ppm).

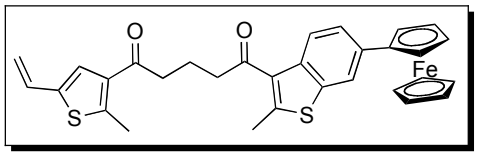

1-(6-Ferrocenyl-2-methylbenzo[*b*]thiophen-3-yl)-5-(2-methyl-5-vinylthiophen-3-yl)pentane-1,5-dione (4.5). Oxidation of diol **4.43** was conducted under Ley conditions. Oven-dried molecular sieves were flame activated and cooled under dry N_2 in a two-necked round bottom flask. The diol (264 mg, 0.474 mmol) was added to the round bottom along with NMO (167 mg, 1.42 mmol) and DCM (anhydrous, 10 mL) with stirring. After cooling the orange solution to 0 ^oC, TPAP (16.7 mg, 0.047 mmol) in DCM was added slowly, followed by warming to room temperature and continued stirring for 2 h. The reaction was vacuum filtered through a pad of silica gel and rinsed with DCM. Purification of the diketone was conducted by flash column chromatography (1:1, DCM/hexanes) to yield **4.5** as a bright orange solid (179 mg, 68% yield), mp 151-152 ^oC. IR (thin-film, cm^{-1}) 3082, 2928, 2857, 1662 (br), 817; ^1H NMR ($CDCl_3$) δ 8.03 (d, *J* = 8.0 Hz, 1H), 7.78 (d, *J* = 1.5 Hz, 1H), 7.53 (dd, *J* = 1.5, 8.0 Hz, 1H), 7.21 (s, 1H), 6.68 (dd, *J* = 10.5, 17.5 Hz, 1H), 5.47 (d, *J* = 17.5 Hz, 1H), 5.15 (d, *J* = 10.5 Hz, 1H), 4.70 (t, *J* = 2.0 Hz, 2H), 4.35 (t, *J* = 2.0 Hz, 2H), 4.05 (s, 5H), 3.06 (t, *J* = 7.0 Hz, 2H), 2.95 (t, *J* = 7.0 Hz, 2H), 2.75 (s, 3H), 2.70 (s, 3H), 2.19 (p, *J* = 7.0 Hz, 2H); ^{13}C NMR ($CDCl_3$) δ 198.7, 195.9,

148.7, 147.5, 138.6, 138.0, 136.7, 136.2, 135.9, 133.1, 129.4, 126.8, 124.3, 123.5, 118.5, 114.0, 85.1, 69.9, 69.3, 66.7, 42.9, 40.8, 19.0, 17.2, 16.6; HRMS (ESI) for $C_{31}H_{28}O_2NaS_2Fe$ $[M + Na]^+$ calcd, 575.07723, found, 575.07620 (error = -1.7987 ppm).

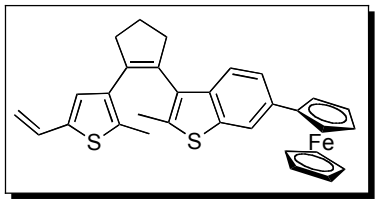

6-Ferrocenyl-2-methyl-3-(2-(2-methyl-5-vinylthiophen-3-yl)cyclopent-1-enyl)benzo[*b*]thiophene (4.3). Photoswitch **4.3** was synthesized similarly to the procedures of Huang et al. and Migulin et al.[9,43] To a cooled (-10 ^oC) slurry of Zn powder (177 mg, 2.7 mmol) in THF (anhydrous, 5 mL) with vigorous stirring was added $TiCl_4$ (77 mL, 0.7 mmol) drop-wise. The slurry was stirred in the dark and refluxed for 1 h. The solution became blue in color and was cooled to room temperature. Pyridine (57 mL, 0.7 mmol) was added to the blue solution prior to addition of diketone **4.5** (100 mg, 0.18 mmol) in a minimal amount of THF, and the reaction was refluxed for 4 h. After cooling to room temperature, the reaction was quenched with water, filtered, and rinsed with THF. Pure compound was obtained after passing through a plug of silica (hexanes). X-ray quality single crystals were obtained from slow evaporation of a hexanes/DCM mixture (75 mg, 80% yield), mp 168-170 ^oC. IR (thin-film, cm^{-1}) 3087, 2945, 2846, 2241, 1619, 1599, 1438, 1407, 818, 732; ^1H NMR ($CDCl_3$) δ 7.76 (s, 1H), 7.43-7.39 (m, 2H), 6.61-6.56 (dd, *J* = 17.0, 10.5 Hz, 1H), 6.60 (s, 1H), 5.31 (d, *J* = 17.0,

10.5 Hz,1H), 4.66 (t, *J* = 2.0 Hz, 2H), 4.31 (t, *J* = 2.0 Hz, 2H), 4.03 (s, 5H), 3.08-2.90 (br m, 2H), 2.84-2.62 (br m, 2H), 2.14 (p, *J* = 7.5 Hz, 2H), 2.10 (s, 3H), 1.84 (s, 3H); ^{13}C NMR ($CDCl_3$) δ 138.9, 138.7, 138.0, 137.5, 135.6, 135.2, 134.8, 134.4, 133.9, 130.9, 130.2, 127.2, 123.1, 122.2, 119.0, 112.0, 86.0, 69.8, 69.0, 66.6, 38.2, 38.1, 23.8, 14.93, 14.87; HRMS (ESI) for $C_{31}H_{28}S_2KFe$ $[M + K]^+$ calcd, 559.06134, found, 569.06317 (error = 3.2674 ppm).

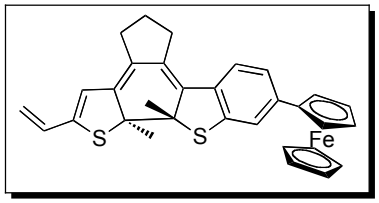

Closed form of 4.3 (4.4). The closed isomer was isolated according to the description above for the photocyclization of 0.1 mmole of **4.3**. IR (thin-film, cm^{-1}) 3071, 2917, 2846, 1736, 1651, 1459, 1067; ^{1}H NMR ($CDCl_3$) δ 7.31 (d, *J* = 1.5 Hz, 1H), 7.26 (d, *J* = 8.0 Hz, 1H), 7.16 (dd, *J* = 1.5, 8.0 Hz, 1H), 6.70 (dd, *J* = 10.5, 17.0 Hz, 1H), 6.02 (s, 1H), 5.30 (d, *J* = 17.0 Hz, 1H), 5.31 (d, *J* = 10.5 Hz, 1H), 4.61 (t, *J* = 2.0 Hz, 2H), 4.32 (t, *J* = 2.0 Hz, 2H), 4.07 (s, 5H), 2.74-2.63 (m, 2H), 2.54-2.49 (m, 1H), 2.44-2.37 (m, 1H), 1.92-1.83 (m, 2H), 1.91 (s, 3H), 1.89 (s, 3H); HRMS (ESI) for $C_{31}H_{28}S_2NaFe$ $[M + Na]^+$ calcd, 543.08740, found, 543.08500 (error = -4.4287 ppm).

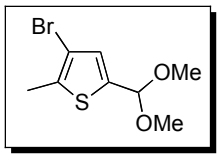

3-Bromo-5-(dimethoxymethyl)-2-methylthiophene (4.6). 2-Methylthiophene (10.5 mL, 122 mmol) was dissolved in glacial acetic acid (50 mL) and cooled to 0 ^{o}C. Bromine

(14.5 mL, 282 mmol) in acetic acid (20 mL) was added drop-wise and the reaction was stirred for 16 h in the dark. The reaction was poured onto water and slowly quenched with sat. $NaHCO_3$ solution. The mixture was then extracted with ether (5x), the organic layers combined, and washed with water. The organic layer was washed further with sat. $NaHCO_3$ solution (2x), water, 10% aq. $Na_2S_2O_3$ and then dried with Na_2SO_4. 3,5-dibromo-2-methylthiophene was distilled under vacuum to yield a pale yellow liquid. (22.5 g, 72% yield).[55] ^1H NMR ($CDCl_3$) δ 6.84 (s, 1H), 2.32 (s, 3H); ^{13}C NMR ($CDCl_3$) δ 136.2, 132.1, 108.9, 108.7, 15.0;

3,5-Dibromo-2-methylthiophene (4.94 g, 19.3 mmol) was dissolved in THF (anhydrous, 50 mL) and cooled to -78 ^oC. *n*-BuLi (2.5 *M* in hexanes, 7.72 mL, 19.3 mmol) was added drop-wise and the reaction stirred for 20 min. DMF (2.24 mL, 28.95 mmol) was added and the reaction mixture stirred for an additional 20 min prior to warming to room temperature (stir 1 h). The reaction was cooled to 0 ^oC and quenched with sat. aq. NH_4Cl, extracted with ether (3x). The combined organic layers were washed with brine, dried (Na_2SO_4), filtered, and evaporated. The resulting solid was dissolved in hot hexanes and decanted from a brown precipitate. The supernatant was evaporated and the solid redissolved in hot hexanes. If any brown precipitate remained, the process was repeated until the entire solid was soluble in hot hexanes, which was again evaporated. Recrystallization from heptanes gave 5-methyl-2-thiophenebenzaldehyde as yellow to clear/colorless crystals. (2.76 g, 70%

yield), mp 57-58 °C (lit. 58 °C)[26] IR (thin-film, cm^{-1}); ^1H NMR ($CDCl_3$) δ 9.78 (s, 1H), 7.59 (s, 1H), 2.49 (s, 3H); ^{13}C NMR ($CDCl_3$) δ 181.7, 146.0, 140.3, 138.9, 111.4, 16.1.

The dimethylacetal of 5-methyl-2-thiophenebenzaldehyde was synthesized according to the procedure of Lehn and co-workers.[26] 5-Methyl-2-thiophenebenzaldehyde (4.0 g, 19.5 mmol) was dissolved in MeOH (anhydrous, 25 mL) and trimethyl orthoformate (3 mL, 27.4 mmol). PTSA monohydrate (30 mg) was added and the reaction mixture refluxed for 4 h. The reaction was cooled to room temperature and the solvent removed under reduced pressure. The resulting oil was taken up in ether and washed with sat. aq. $NaHCO_3$ solution (2x), dried (Na_2SO_4), and evaporated. Bulb-to-bulb distillation yielded the fragrant dimethyl acetal **4.6** as a clear colorless liquid and was stored in a desiccator to avoid hydrolysis. (4.8 g, 97% yield). IR (thin-film, cm^{-1}) 3080, 2993, 2831, 1546, 1346, 1187, 1092, 996; ^1H NMR ($CDCl_3$) δ 6.88 (s, H), 5.51 (s, 1H), 3.34 (s, 6H), 2.37 (s, 3H); ^{13}C NMR ($CDCl_3$) δ 138.5, 134.9, 130.0, 128.2, 108.6, 99.6, 52.7, 14.9.

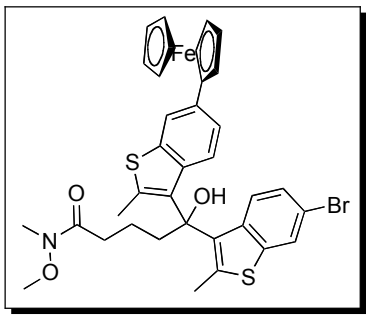

5-(6-Bromo-2-methylbenzo[*b*]thiophen-3-yl)-5-(6-ferrocenyl-2-methylbenzo[*b*]thiophen-3-yl)-5-hydroxy-*N*-methoxy-*N*-methylpentanamide (4.19). Halide **4.15** (38 mg, 0.084 mmol) was dissolved in THF (anhydrous, 1.5 mL) and cooled

to -78 °C. *n*-BuLi (2.5 *M* in hexanes, 67 mL, 0.168 mmol) was added drop-wise and the red-orange solution was allowed to stir for 30 min. Weinreb amide **4.8** (15 mg, 0.042 mmol) was added drop-wise in THF (0.5 mL) and the solution was stirred for an additional 30 min at -78 °C before warming to room temperature (1 h). The reaction was quenched at 0 °C with aq. sat. NH_4Cl and extracted with EtOAc (3x). Evaporation of solvent and purification by flash column chromatography (1:1 hexanes/EtOAc) gave **4.19** as a red-orange residue (9.1 mg, 15% yield). Compound **4.19** was recrystallized from methanol to give orange crystals, mp = 194-195 °C, IR (thin-film, cm^{-1}) 3391, 3092, 2965, 1640, 1445, 817, 735; ^1H NMR ($CDCl_3$) δ 7.81 (d, *J* = 9.0 Hz, 1H), 7.78 (d, *J* = 2.0 Hz, 1H), 7.70 (d, *J* = 2.0 Hz, 1H), 7.63 (d, *J* = 9.0 Hz, 1H), 7.255 (under solvent peak, 1H), 7.24 (t, *J* = 1.5 Hz, 1H), 4.59 (dd, *J* = 1.5, 3.5 Hz, 2H), 4.28 (t, *J* = 2.0 Hz, 2H), 3.61 (s, 3H), 3.15 (s, 3H), 2.87 (s, 1H), 2.65-2.62 (m, 2H), 2.61 (s, 3H), 2.56 (s, 3H), 2.46 (t, *J* = 7.0 Hz, 2H), 1.91-1.82 (m, 1H), 1.78-1.69 (m, 1H); MS (ESI) for $C_{35}H_{34}BrFeNO_3S_2$ $[M]^+$ calcd, 715.0507, found, 715.0518 (error = 1.48 ppm).

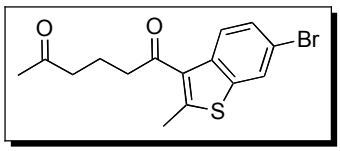

1-(6-Bromo-2-methylbenzo[*b*]thiophen-3-yl)hexane-1,5-dione (4.21). The general procedure of Colby and co-workers for in-situ masking was followed.[35] *N*-methoxy-*N*-methylamine hydrochloride (12.7 mg, 0.13 mmol) was dissolved in THF (anhydrous, 4 mL) and DIBALH (1.0 *M* in

hexanes, 130 mL, 0.13 mmol) was added drop-wise at 0 ^{o}C. The complex was formed over 1 h at room temperature and was added to a solution of **4.8** (50 mg, 0.13 mmol) in THF (10 mL) at 0 ^{o}C. The solution was stirred for 2 h at room temperature, followed by cooling to 0 ^{o}C and addition of *i*PrMgCl (1.73 *M* in THF, 75 mL, 0.13 mmol). After stirring for 1 h at 0 ^{o}C the reaction was cooled to -78 ^{o}C and methyllithium (1.6 *M* in ether, 41 mL, 0.65 mmol) was added. TLC showed no starting material after 30 min of stirring and the reaction was quenched with aq. sat. NH_4Cl and warmed to room temperature. The solvent was evaporated and the residue purified by flash column chromatography (1:1 hexanes/EtOAc) to give **4.21** (22.7 mg, 50% yield), mp 110-111 ^{o}C. IR (thin-film, cm^{-1}) 3100, 3049, 2938, 1713, 1658, 1439, 1376, 899, 831; ^{1}H NMR ($CDCl_3$) δ 8.01 (d, *J* = 9.0 Hz, 1H), 7.86 (d, *J* = 1.5 Hz, 1H), 7.48 (dd, *J* = 1.5, 9.0 Hz, 1H), 2.94 (t, *J* = 7.0 Hz, 2H), 2.74 (s, 3H), 2.58 (t, *J* = 7.0 Hz, 2H), 2.15 (s, 3H), 2.03 (p, *J* = 7.0 Hz, 2H); ^{13}C NMR ($CDCl_3$) δ 208.5, 198.1, 148.6, 138.9, 137.4, 132.7, 128.8, 125.2, 124.3, 118.5, 42.8, 42.7, 30.1, 18.4, 17.2; HRMS (ESI) for $C_{15}H_{15}O_2NaSBr$ $[M + Na]^+$ calcd, 360.98683, found, 360.98810 (error = 3.5073 ppm).

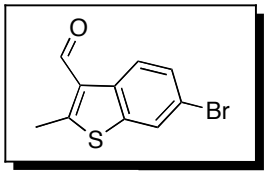

(4.27). Dihalide **4.14** (62.9 mg, 0.18 mmol) was dissolved in THF (anhydrous, 1 mL) and cooled to -100 ^{o}C in a dry ice/liquid N_2 bath. *t*-BuLi in hexanes (1.6 M, 223 μL, 0.36 mmol) was added drop wise and stirred for 5 min prior to the

addition of DMF (anhydrous, 25 μL, 0.30 mmol). The reaction was stirred for an additional 10 minutes before warming to 0 ^{o}C and quenching with water. Dilute mixture with water and extract with EtOAc (3x). The organic layers were combined and washed with water/brine before drying with $MgSO_4$. Filtration, evaporation and purification of the residue by flash column chromatography (3:1 hexanes/EtOAc; collect the fraction that stained with 2,4-DNPH by TLC) gave **4.27** (30.4 mg, 66% yield). Running the same experiment and quenching with water confirmed the addition of the aldehyde to the 3-position. Analysis of the product by NMR showed compound **4.10**, which is consistent with selective lithiation at the 3-position, mp 97-99^{o}C. IR (thin-film, cm^{-1}) 3100, 2922, 2845, 2751, 1671, 1581, 1521, 1551, 1174, 858, 819, 775; ^{1}H NMR ($CDCl_3$) δ 10.30 (s, 1H), 8.44 (d, *J* = 8.5 Hz, 1H), 7.86 (d, *J* = 2.0 Hz, 1H), 7.52 (dd, *J* = 2.0, 8.5 Hz, 1H), 2.89 (s, 3H); ^{13}C NMR ($CDCl_3$) δ 184.24, 158.17, 138.23, 136.03, 129.81, 129.4, 125.2, 124.2, 119.2, 14.3; HRMS (ESI) did not ionize with Mariner HRMS, positive mode.

4.12 Crystal Structure Data

Acknowledgement

The single crystal X-ray diffraction data in this work were recorded on an instrument supported by the National Science Foundation, Major Research Instrumentation (MRI) Program under Grant No. CHE-0521569.

Table 4.1 Crystal data and structure refinement for 4.3.

Identification code	**4.3**	
Empirical formula	C31 H28 Fe S2	
Formula weight	520.50	
Temperature	298(2) K	
Wavelength	0.71073 Å	
Crystal system	Triclinic	
Space group	P-1	
Unit cell dimensions	a = 10.350(4) Å	α = 74.781(4)°
	b = 11.367(4) Å	β = 79.632(4)°
	c = 11.575(4) Å	γ = 78.724(4)°
Volume	1276.7(8) $Å^3$	
Z	2	
Density (calculated)	1.354 $g.cm^{-3}$	
Absorption coefficient (μ)	0.772 mm^{-1}	
F(000)	544	
Crystal size	0.195 × 0.170 × 0.085 mm^3	
ω range for data collection	1.88 to 26.73°	
Index ranges	$-13 \leq h \leq 13$, $-14 \leq k \leq 14$, $-14 \leq l \leq 14$	
Reflections collected	13050	
Independent reflections	5362 [R_{int} = 0.0293]	
Completeness to θ = 26.73°	98.9 %	
Absorption correction	Empirical	
Max. and min. transmission	0.7455 and 0.6965	
Refinement method	Full-matrix least-squares on F^2	
Data / restraints / parameters	5362 / 0 / 319	
Goodness-of-fit on F^2	1.017	
Final R indices [I>2σ(I)]	R_1 = 0.0401, wR_2 = 0.0901	
R indices (all data)	R_1 = 0.0681, wR_2 = 0.1053	
Largest diff. peak and hole	0.280 and -0.221 $e^-.Å^{-3}$	

Table 4.2 Atomic coordinates and equivalent isotropic displacement parameters ($Å^2$) for **4.3**. U(eq) is defined as one third of the trace of the orthogonalized U_{ij} tensor.

	x	y	z	U(eq)
Fe(1)	0.34630(4)	0.69660(3)	0.09847(3)	0.047(1)
S(2)	0.24206(7)	1.21632(7)	0.31586(7)	0.056(1)
S(3)	-0.17402(8)	1.63219(7)	0.15284(7)	0.061(1)
C(1)	0.0560(2)	1.1134(2)	0.2790(2)	0.041(1)
C(8)	-0.0076(2)	1.1976(2)	0.3541(2)	0.043(1)
C(5)	0.2737(3)	1.0392(2)	0.1790(2)	0.047(1)
C(26)	0.3010(3)	0.8846(2)	0.0562(2)	0.052(1)
C(6)	0.1938(2)	1.1136(2)	0.2508(2)	0.044(1)
C(2)	0.0010(3)	1.0362(2)	0.2319(2)	0.051(1)
C(13)	-0.2252(2)	1.4398(2)	0.3150(2)	0.044(1)
C(16)	-0.1519(3)	1.2108(2)	0.3969(2)	0.046(1)
C(4)	0.2181(3)	0.9631(2)	0.1341(2)	0.046(1)
C(7)	0.0788(3)	1.2588(2)	0.3803(2)	0.049(1)
C(11)	-0.1634(3)	1.4743(2)	0.1998(2)	0.049(1)
C(3)	0.0807(3)	0.9632(2)	0.1619(3)	0.055(1)
C(12)	-0.2808(3)	1.5445(2)	0.3647(3)	0.051(1)
C(30)	0.2545(3)	0.8335(2)	-0.0254(2)	0.060(1)
C(10)	-0.2606(3)	1.6543(3)	0.2892(3)	0.055(1)
C(27)	0.4408(3)	0.8465(3)	0.0490(3)	0.063(1)
C(19)	-0.3782(3)	1.2862(3)	0.4451(3)	0.058(1)
C(21)	0.2650(3)	0.6371(3)	0.2718(3)	0.067(1)
C(14)	-0.3059(3)	1.7769(3)	0.3127(4)	0.070(1)
C(17)	-0.2133(3)	1.1018(3)	0.4749(3)	0.067(1)
C(22)	0.2121(3)	0.5872(3)	0.1942(3)	0.072(1)
C(29)	0.3656(4)	0.7663(3)	-0.0839(3)	0.072(1)
C(28)	0.4789(4)	0.7734(3)	-0.0383(3)	0.075(1)
C(24)	0.4333(4)	0.5247(3)	0.1756(4)	0.082(1)
C(23)	0.3172(4)	0.5186(3)	0.1353(3)	0.081(1)

C(15)	-0.2969(4)	1.8824(4)	0.2360(5)	0.090(1)
C(18)	-0.3582(3)	1.1483(3)	0.4933(4)	0.098(1)
C(25)	0.4017(3)	0.5972(3)	0.2593(3)	0.075(1)
C(32)	-0.2432(2)	1.3135(2)	0.3815(2)	0.044(1)
C(20)	-0.0925(3)	1.3936(3)	0.1167(2)	0.064(1)
C(31)	0.0531(3)	1.3513(3)	0.4561(3)	0.066(1)
H(5A)	0.3647	1.0410	0.1614	0.057
H(2A)	-0.0900	1.0345	0.2481	0.061
H(3A)	0.0424	0.9119	0.1318	0.066
H(12A)	-0.3268	1.5376	0.4424	0.061
H(30A)	0.1619	0.8433	-0.0391	0.072
H(27A)	0.5003	0.8669	0.0953	0.076
H(19A)	-0.4076	1.3281	0.5104	0.070
H(19B)	-0.4435	1.3118	0.3893	0.070
H(21A)	0.2146	0.6890	0.3255	0.080
H(17A)	-0.1955	1.0343	0.4347	0.081
H(17B)	-0.1785	1.0733	0.5515	0.081
H(22A)	0.1181	0.5987	0.1839	0.086
H(29A)	0.3628	0.7212	-0.1446	0.086
H(28A)	0.5695	0.7342	-0.0620	0.090
H(24A)	0.5226	0.4848	0.1493	0.099
H(23A)	0.3102	0.4735	0.0757	0.097
H(18A)	-0.3926	1.1278	0.5786	0.117
H(18B)	-0.4052	1.1105	0.4508	0.117
H(25A)	0.4649	0.6171	0.3023	0.090
H(20A)	-0.0959	1.3087	0.1569	0.096
H(20B)	-0.0014	1.4064	0.0951	0.096
H(20C)	-0.1347	1.4142	0.0451	0.096
H(31A)	-0.0401	1.3653	0.4856	0.099
H(31B)	0.0800	1.4275	0.4081	0.099
H(31C)	0.1029	1.3206	0.5232	0.099
H(15A)	-0.331(4)	1.952(4)	0.265(3)	0.101(13)
H(14)	-0.339(3)	1.775(3)	0.389(3)	0.081(12)
H(15B)	-0.251(4)	1.881(4)	0.148(4)	0.113(15)

Table 4.3 Anisotropic displacement parameters $(Å)^2$ for **4.3**. The anisotropic displacement factor exponent takes the form:
$-2\pi^2[h^2 a^{*2} U_{11} + ... + 2 h k a^* b^* U_{12}]$

	U_{11}	U_{22}	U_{33}	U_{23}	U_{13}	U_{12}
Fe(1)	0.0479(2)	0.0358(2)	0.0525(2)	-0.0106(2)	0.0007(2)	-0.0026(2)
S(2)	0.0501(4)	0.0494(4)	0.0736(5)	-0.0256(4)	0.0030(4)	-0.0133(3)
S(3)	0.0594(5)	0.0469(4)	0.0679(5)	-0.0002(4)	-0.0062(4)	-0.0090(3)
C(1)	0.0405(14)	0.0306(13)	0.0466(14)	-0.0077(11)	-0.0032(11)	0.0002(10)
C(8)	0.0459(15)	0.0324(13)	0.0452(14)	-0.0051(11)	-0.0040(11)	0.0005(11)
C(5)	0.0438(15)	0.0386(14)	0.0547(16)	-0.0117(12)	0.0076(12)	-0.0068(11)
C(26)	0.0604(18)	0.0343(14)	0.0543(16)	-0.0100(12)	0.0059(13)	-0.0059(12)
C(6)	0.0479(15)	0.0324(13)	0.0494(15)	-0.0094(11)	-0.0012(12)	-0.0072(11)
C(2)	0.0406(15)	0.0472(16)	0.0646(18)	-0.0169(14)	-0.0047(13)	-0.0021(12)
C(13)	0.0385(14)	0.0419(15)	0.0487(15)	-0.0086(12)	-0.0081(11)	0.0013(11)
C(16)	0.0476(15)	0.0420(15)	0.0440(14)	-0.0103(12)	-0.0004(11)	-0.0043(12)
C(4)	0.0505(16)	0.0322(13)	0.0524(15)	-0.0111(12)	-0.0010(12)	-0.0020(11)
C(7)	0.0504(16)	0.0421(15)	0.0526(16)	-0.0155(12)	-0.0005(12)	-0.0039(12)
C(11)	0.0496(16)	0.0450(16)	0.0494(15)	-0.0052(12)	-0.0059(12)	-0.0059(12)
C(3)	0.0515(17)	0.0458(16)	0.0709(19)	-0.0234(14)	-0.0081(14)	-0.0049(13)
C(12)	0.0441(15)	0.0459(16)	0.0592(17)	-0.0120(13)	-0.0060(13)	0.0009(12)
C(30)	0.083(2)	0.0400(16)	0.0499(16)	-0.0099(13)	-0.0052(15)	0.0017(14)
C(10)	0.0454(16)	0.0437(16)	0.074(2)	-0.0142(14)	-0.0140(14)	0.0023(12)
C(27)	0.0578(18)	0.0465(17)	0.082(2)	-0.0248(16)	0.0181(16)	-0.0143(14)
C(19)	0.0473(16)	0.0555(18)	0.0636(18)	-0.0127(14)	0.0063(13)	-0.0012(13)
C(21)	0.068(2)	0.067(2)	0.0512(17)	-0.0038(15)	0.0087(15)	-0.0067(16)
C(14)	0.059(2)	0.047(2)	0.103(3)	-0.021(2)	-0.014(2)	0.0032(15)
C(17)	0.063(2)	0.0468(17)	0.074(2)	0.0003(15)	0.0099(16)	-0.0018(14)
C(22)	0.061(2)	0.068(2)	0.080(2)	0.0089(18)	-0.0122(17)	-0.0267(17)
C(29)	0.109(3)	0.0460(18)	0.0511(18)	-0.0151(14)	0.0119(18)	-0.0074(18)
C(28)	0.079(2)	0.0466(18)	0.085(2)	-0.0206(17)	0.037(2)	-0.0133(16)
C(24)	0.076(2)	0.056(2)	0.088(3)	0.0042(19)	-0.004(2)	0.0191(18)
C(23)	0.118(3)	0.0363(17)	0.079(2)	-0.0037(16)	-0.008(2)	-0.0107(19)

C(15)	0.086(3)	0.046(2)	0.137(4)	-0.018(3)	-0.023(3)	-0.0065(19)
C(18)	0.060(2)	0.062(2)	0.139(4)	0.010(2)	0.018(2)	-0.0060(17)
C(25)	0.068(2)	0.084(3)	0.066(2)	-0.0015(19)	-0.0215(17)	-0.0067(18)
C(32)	0.0452(14)	0.0404(14)	0.0421(14)	-0.0085(11)	-0.0031(11)	-0.0016(11)
C(20)	0.084(2)	0.0596(19)	0.0436(16)	-0.0103(14)	0.0047(15)	-0.0134(16)
C(31)	0.066(2)	0.068(2)	0.074(2)	-0.0362(17)	-0.0019(16)	-0.0115(16)

Table 4.4 Bond lengths [Å] for **4.3.**

atom-atom	distance	atom-atom	distance
Fe(1)-C(21)	2.024(3)	Fe(1)-C(25)	2.024(3)
Fe(1)-C(22)	2.026(3)	Fe(1)-C(23)	2.026(3)
Fe(1)-C(28)	2.028(3)	Fe(1)-C(24)	2.028(3)
Fe(1)-C(30)	2.029(3)	Fe(1)-C(27)	2.031(3)
Fe(1)-C(29)	2.039(3)	Fe(1)-C(26)	2.042(3)
S(2)-C(6)	1.733(3)	S(2)-C(7)	1.749(3)
S(3)-C(11)	1.721(3)	S(3)-C(10)	1.723(3)
C(1)-C(2)	1.396(3)	C(1)-C(6)	1.405(3)
C(1)-C(8)	1.446(3)	C(8)-C(7)	1.351(4)
C(8)-C(16)	1.478(3)	C(5)-C(4)	1.374(4)
C(5)-C(6)	1.392(3)	C(26)-C(27)	1.421(4)
C(26)-C(30)	1.422(4)	C(26)-C(4)	1.480(3)
C(2)-C(3)	1.368(3)	C(13)-C(11)	1.363(3)
C(13)-C(12)	1.433(3)	C(13)-C(32)	1.470(3)
C(16)-C(32)	1.344(3)	C(16)-C(17)	1.506(4)
C(4)-C(3)	1.400(4)	C(7)-C(31)	1.496(4)
C(11)-C(20)	1.500(4)	C(12)-C(10)	1.352(4)
C(30)-C(29)	1.418(4)	C(10)-C(14)	1.461(4)
C(27)-C(28)	1.428(4)	C(19)-C(18)	1.505(4)
C(19)-C(32)	1.507(4)	C(21)-C(25)	1.392(4)
C(21)-C(22)	1.412(4)	C(14)-C(15)	1.299(5)
C(17)-C(18)	1.486(4)	C(22)-C(23)	1.393(5)

C(29)-C(28)	1.393(5)	C(24)-C(23)	1.385(5)
C(24)-C(25)	1.387(5)		

Table 4.5 Bond angles [°] for **4.3**.

atom-atom-atom	angle	atom-atom-atom	angle
C(21)-Fe(1)-C(25)	40.24(12)	C(21)-Fe(1)-C(22)	40.83(13)
C(25)-Fe(1)-C(22)	67.75(14)	C(21)-Fe(1)-C(23)	68.03(14)
C(25)-Fe(1)-C(23)	67.43(15)	C(22)-Fe(1)-C(23)	40.20(14)
C(21)-Fe(1)-C(28)	156.80(16)	C(25)-Fe(1)-C(28)	121.76(16)
C(22)-Fe(1)-C(28)	160.70(15)	C(23)-Fe(1)-C(28)	124.33(14)
C(21)-Fe(1)-C(24)	67.65(14)	C(25)-Fe(1)-C(24)	40.04(14)
C(22)-Fe(1)-C(24)	67.41(15)	C(23)-Fe(1)-C(24)	39.94(15)
C(28)-Fe(1)-C(24)	108.05(15)	C(21)-Fe(1)-C(30)	124.24(13)
C(25)-Fe(1)-C(30)	160.28(13)	C(22)-Fe(1)-C(30)	108.52(14)
C(23)-Fe(1)-C(30)	123.14(15)	C(28)-Fe(1)-C(30)	68.31(14)
C(24)-Fe(1)-C(30)	158.30(15)	C(21)-Fe(1)-C(27)	120.65(13)
C(25)-Fe(1)-C(27)	106.76(15)	C(22)-Fe(1)-C(27)	157.18(13)
C(23)-Fe(1)-C(27)	160.21(15)	C(28)-Fe(1)-C(27)	41.18(12)
C(24)-Fe(1)-C(27)	123.57(16)	C(30)-Fe(1)-C(27)	68.74(13)
C(21)-Fe(1)-C(29)	161.52(15)	C(25)-Fe(1)-C(29)	157.19(15)
C(22)-Fe(1)-C(29)	125.17(15)	C(23)-Fe(1)-C(29)	109.05(14)
C(28)-Fe(1)-C(29)	40.07(14)	C(24)-Fe(1)-C(29)	122.69(14)
C(30)-Fe(1)-C(29)	40.80(12)	C(27)-Fe(1)-C(29)	68.51(14)
C(21)-Fe(1)-C(26)	106.94(12)	C(25)-Fe(1)-C(26)	123.30(14)
C(22)-Fe(1)-C(26)	122.21(13)	C(23)-Fe(1)-C(26)	158.25(15)
C(28)-Fe(1)-C(26)	68.74(11)	C(24)-Fe(1)-C(26)	159.69(16)
C(30)-Fe(1)-C(26)	40.88(11)	C(27)-Fe(1)-C(26)	40.83(11)
C(29)-Fe(1)-C(26)	68.62(11)	C(6)-S(2)-C(7)	91.98(12)
C(11)-S(3)-C(10)	92.63(13)	C(2)-C(1)-C(6)	117.7(2)
C(2)-C(1)-C(8)	129.9(2)	C(6)-C(1)-C(8)	112.4(2)
C(7)-C(8)-C(1)	112.8(2)	C(7)-C(8)-C(16)	125.4(2)
C(1)-C(8)-C(16)	121.7(2)	C(4)-C(5)-C(6)	120.0(2)

C(27)-C(26)-C(30)	107.5(2)	C(27)-C(26)-C(4)	126.6(3)
C(30)-C(26)-C(4)	125.9(3)	C(27)-C(26)-Fe(1)	69.17(15)
C(30)-C(26)-Fe(1)	69.09(15)	C(4)-C(26)-Fe(1)	127.01(19)
C(5)-C(6)-C(1)	121.5(2)	C(5)-C(6)-S(2)	127.8(2)
C(1)-C(6)-S(2)	110.66(18)	C(3)-C(2)-C(1)	120.2(2)
C(11)-C(13)-C(12)	111.5(2)	C(11)-C(13)-C(32)	126.3(2)
C(12)-C(13)-C(32)	122.0(2)	C(32)-C(16)-C(8)	128.5(2)
C(32)-C(16)-C(17)	110.9(2)	C(8)-C(16)-C(17)	120.5(2)
C(5)-C(4)-C(3)	118.5(2)	C(5)-C(4)-C(26)	120.8(2)
C(3)-C(4)-C(26)	120.7(2)	C(8)-C(7)-C(31)	129.2(2)
C(8)-C(7)-S(2)	112.18(19)	C(31)-C(7)-S(2)	118.6(2)
C(13)-C(11)-C(20)	128.4(2)	C(13)-C(11)-S(3)	111.4(2)
C(20)-C(11)-S(3)	120.3(2)	C(2)-C(3)-C(4)	122.1(3)
C(10)-C(12)-C(13)	114.4(3)	C(29)-C(30)-C(26)	108.2(3)
C(29)-C(30)-Fe(1)	69.95(18)	C(26)-C(30)-Fe(1)	70.03(17)
C(12)-C(10)-C(14)	127.4(3)	C(12)-C(10)-S(3)	110.1(2)
C(14)-C(10)-S(3)	122.5(3)	C(26)-C(27)-C(28)	107.5(3)
C(26)-C(27)-Fe(1)	69.99(15)	C(28)-C(27)-Fe(1)	69.29(17)
C(18)-C(19)-C(32)	104.4(2)	C(25)-C(21)-C(22)	107.2(3)
C(25)-C(21)-Fe(1)	69.91(18)	C(22)-C(21)-Fe(1)	69.66(17)
C(15)-C(14)-C(10)	127.0(4)	C(18)-C(17)-C(16)	104.9(2)
C(23)-C(22)-C(21)	107.7(3)	C(23)-C(22)-Fe(1)	69.93(19)
C(21)-C(22)-Fe(1)	69.51(17)	C(28)-C(29)-C(30)	108.2(3)
C(28)-C(29)-Fe(1)	69.55(19)	C(30)-C(29)-Fe(1)	69.25(17)
C(29)-C(28)-C(27)	108.6(3)	C(29)-C(28)-Fe(1)	70.38(18)
C(27)-C(28)-Fe(1)	69.53(16)	C(23)-C(24)-C(25)	108.4(3)
C(23)-C(24)-Fe(1)	69.96(19)	C(25)-C(24)-Fe(1)	69.84(19)
C(24)-C(23)-C(22)	108.2(3)	C(24)-C(23)-Fe(1)	70.1(2)
C(22)-C(23)-Fe(1)	69.87(18)	C(17)-C(18)-C(19)	108.0(3)
C(24)-C(25)-C(21)	108.5(3)	C(24)-C(25)-Fe(1)	70.13(19)
C(21)-C(25)-Fe(1)	69.85(18)	C(16)-C(32)-C(13)	128.7(2)
C(16)-C(32)-C(19)	111.0(2)	C(13)-C(32)-C(19)	120.3(2)

Table 4.6 Torsion angles [°] for **4.3**.

atom-atom-atom-atom	angle	atom-atom-atom-atom	angle
C(2)-C(1)-C(8)-C(7)	-178.9(3)	C(6)-C(1)-C(8)-C(7)	0.3(3)
C(2)-C(1)-C(8)-C(16)	2.0(4)	C(6)-C(1)-C(8)-C(16)	-178.8(2)
C(21)-Fe(1)-C(26)-C(27)	117.56(19)	C(25)-Fe(1)-C(26)-C(27)	76.6(2)
C(22)-Fe(1)-C(26)-C(27)	159.57(19)	C(23)-Fe(1)-C(26)-C(27)	-169.4(3)
C(28)-Fe(1)-C(26)-C(27)	-38.3(2)	C(24)-Fe(1)-C(26)-C(27)	46.4(4)
C(30)-Fe(1)-C(26)-C(27)	-119.3(2)	C(29)-Fe(1)-C(26)-C(27)	-81.5(2)
C(21)-Fe(1)-C(26)-C(30)	-123.15(19)	C(25)-Fe(1)-C(26)-C(30)	-164.16(18)
C(22)-Fe(1)-C(26)-C(30)	-81.1(2)	C(23)-Fe(1)-C(26)-C(30)	-50.1(4)
C(28)-Fe(1)-C(26)-C(30)	81.0(2)	C(24)-Fe(1)-C(26)-C(30)	165.6(3)
C(27)-Fe(1)-C(26)-C(30)	119.3(2)	C(29)-Fe(1)-C(26)-C(30)	37.84(19)
C(21)-Fe(1)-C(26)-C(4)	-3.3(3)	C(25)-Fe(1)-C(26)-C(4)	-44.3(3)
C(22)-Fe(1)-C(26)-C(4)	38.8(3)	C(23)-Fe(1)-C(26)-C(4)	69.8(5)
C(28)-Fe(1)-C(26)-C(4)	-159.1(3)	C(24)-Fe(1)-C(26)-C(4)	-74.5(4)
C(30)-Fe(1)-C(26)-C(4)	119.9(3)	C(27)-Fe(1)-C(26)-C(4)	-120.8(3)
C(29)-Fe(1)-C(26)-C(4)	157.7(3)	C(4)-C(5)-C(6)-C(1)	-0.1(4)
C(4)-C(5)-C(6)-S(2)	-179.6(2)	C(2)-C(1)-C(6)-C(5)	-0.4(4)
C(8)-C(1)-C(6)-C(5)	-179.7(2)	C(2)-C(1)-C(6)-S(2)	179.2(2)
C(8)-C(1)-C(6)-S(2)	-0.2(3)	C(7)-S(2)-C(6)-C(5)	179.5(3)
C(7)-S(2)-C(6)-C(1)	0.0(2)	C(6)-C(1)-C(2)-C(3)	0.7(4)
C(8)-C(1)-C(2)-C(3)	179.9(3)	C(7)-C(8)-C(16)-C(32)	57.3(4)
C(1)-C(8)-C(16)-C(32)	-123.7(3)	C(7)-C(8)-C(16)-C(17)	-118.6(3)
C(1)-C(8)-C(16)-C(17)	60.4(4)	C(6)-C(5)-C(4)-C(3)	0.3(4)
C(6)-C(5)-C(4)-C(26)	179.2(2)	C(27)-C(26)-C(4)-C(5)	21.3(4)
C(30)-C(26)-C(4)-C(5)	-158.8(3)	Fe(1)-C(26)-C(4)-C(5)	111.6(3)
C(27)-C(26)-C(4)-C(3)	-159.9(3)	C(30)-C(26)-C(4)-C(3)	20.0(4)
Fe(1)-C(26)-C(4)-C(3)	-69.6(4)	C(1)-C(8)-C(7)-C(31)	-178.9(3)
C(16)-C(8)-C(7)-C(31)	0.2(5)	C(1)-C(8)-C(7)-S(2)	-0.4(3)
C(16)-C(8)-C(7)-S(2)	178.7(2)	C(6)-S(2)-C(7)-C(8)	0.2(2)
C(6)-S(2)-C(7)-C(31)	179.0(2)	C(12)-C(13)-C(11)-C(20)	179.6(3)
C(32)-C(13)-C(11)-C(20)	-4.2(5)	C(12)-C(13)-C(11)-S(3)	-0.4(3)

C(32)-C(13)-C(11)-S(3)	175.9(2)	C(10)-S(3)-C(11)-C(13)	0.7(2)
C(10)-S(3)-C(11)-C(20)	-179.2(2)	C(1)-C(2)-C(3)-C(4)	-0.5(4)
C(5)-C(4)-C(3)-C(2)	0.0(4)	C(26)-C(4)-C(3)-C(2)	-178.9(3)
C(11)-C(13)-C(12)-C(10)	-0.3(3)	C(32)-C(13)-C(12)-C(10)	-176.8(2)
C(27)-C(26)-C(30)-C(29)	-1.1(3)	C(4)-C(26)-C(30)-C(29)	178.9(2)
Fe(1)-C(26)-C(30)-C(29)	-59.8(2)	C(27)-C(26)-C(30)-Fe(1)	58.71(19)
C(4)-C(26)-C(30)-Fe(1)	-121.3(3)	C(21)-Fe(1)-C(30)-C(29)	-165.3(2)
C(25)-Fe(1)-C(30)-C(29)	161.6(4)	C(22)-Fe(1)-C(30)-C(29)	-122.8(2)
C(23)-Fe(1)-C(30)-C(29)	-80.8(2)	C(28)-Fe(1)-C(30)-C(29)	36.92(19)
C(24)-Fe(1)-C(30)-C(29)	-47.5(4)	C(27)-Fe(1)-C(30)-C(29)	81.3(2)
C(26)-Fe(1)-C(30)-C(29)	119.1(3)	C(21)-Fe(1)-C(30)-C(26)	75.7(2)
C(25)-Fe(1)-C(30)-C(26)	42.6(5)	C(22)-Fe(1)-C(30)-C(26)	118.15(19)
C(23)-Fe(1)-C(30)-C(26)	160.15(18)	C(28)-Fe(1)-C(30)-C(26)	-82.14(19)
C(24)-Fe(1)-C(30)-C(26)	-166.5(3)	C(27)-Fe(1)-C(30)-C(26)	-37.73(16)
C(29)-Fe(1)-C(30)-C(26)	-119.1(3)	C(13)-C(12)-C(10)-C(14)	179.2(3)
C(13)-C(12)-C(10)-S(3)	0.8(3)	C(11)-S(3)-C(10)-C(12)	-0.9(2)
C(11)-S(3)-C(10)-C(14)	-179.4(3)	C(30)-C(26)-C(27)-C(28)	0.7(3)
C(4)-C(26)-C(27)-C(28)	-179.3(3)	Fe(1)-C(26)-C(27)-C(28)	59.4(2)
C(30)-C(26)-C(27)-Fe(1)	-58.66(19)	C(4)-C(26)-C(27)-Fe(1)	121.3(3)
C(21)-Fe(1)-C(27)-C(26)	-80.3(2)	C(25)-Fe(1)-C(27)-C(26)	-121.90(19)
C(22)-Fe(1)-C(27)-C(26)	-49.6(4)	C(23)-Fe(1)-C(27)-C(26)	168.4(4)
C(28)-Fe(1)-C(27)-C(26)	118.7(3)	C(24)-Fe(1)-C(27)-C(26)	-162.45(19)
C(30)-Fe(1)-C(27)-C(26)	37.77(17)	C(29)-Fe(1)-C(27)-C(26)	81.7(2)
C(21)-Fe(1)-C(27)-C(28)	160.9(2)	C(25)-Fe(1)-C(27)-C(28)	119.4(2)
C(22)-Fe(1)-C(27)-C(28)	-168.3(3)	C(23)-Fe(1)-C(27)-C(28)	49.7(5)
C(24)-Fe(1)-C(27)-C(28)	78.8(3)	C(30)-Fe(1)-C(27)-C(28)	-80.9(2)
C(29)-Fe(1)-C(27)-C(28)	-37.0(2)	C(26)-Fe(1)-C(27)-C(28)	-118.7(3)
C(22)-Fe(1)-C(21)-C(25)	118.1(3)	C(23)-Fe(1)-C(21)-C(25)	80.6(2)
C(28)-Fe(1)-C(21)-C(25)	-46.5(4)	C(24)-Fe(1)-C(21)-C(25)	37.3(2)
C(30)-Fe(1)-C(21)-C(25)	-163.4(2)	C(27)-Fe(1)-C(21)-C(25)	-79.5(2)
C(29)-Fe(1)-C(21)-C(25)	165.0(4)	C(26)-Fe(1)-C(21)-C(25)	-121.9(2)
C(25)-Fe(1)-C(21)-C(22)	-118.1(3)	C(23)-Fe(1)-C(21)-C(22)	-37.6(2)
C(28)-Fe(1)-C(21)-C(22)	-164.6(3)	C(24)-Fe(1)-C(21)-C(22)	-80.8(2)
C(30)-Fe(1)-C(21)-C(22)	78.5(2)	C(27)-Fe(1)-C(21)-C(22)	162.3(2)

C(29)-Fe(1)-C(21)-C(22)	46.9(5)	C(26)-Fe(1)-C(21)-C(22)	120.0(2)
C(12)-C(10)-C(14)-C(15)	-173.1(4)	S(3)-C(10)-C(14)-C(15)	5.1(5)
C(32)-C(16)-C(17)-C(18)	6.6(4)	C(8)-C(16)-C(17)-C(18)	-176.8(3)
C(25)-C(21)-C(22)-C(23)	-0.4(4)	Fe(1)-C(21)-C(22)-C(23)	59.7(2)
C(25)-C(21)-C(22)-Fe(1)	-60.1(2)	C(21)-Fe(1)-C(22)-C(23)	-118.9(3)
C(25)-Fe(1)-C(22)-C(23)	-80.9(2)	C(28)-Fe(1)-C(22)-C(23)	42.7(5)
C(24)-Fe(1)-C(22)-C(23)	-37.4(2)	C(30)-Fe(1)-C(22)-C(23)	119.8(2)
C(27)-Fe(1)-C(22)-C(23)	-161.2(3)	C(29)-Fe(1)-C(22)-C(23)	77.6(3)
C(26)-Fe(1)-C(22)-C(23)	162.8(2)	C(25)-Fe(1)-C(22)-C(21)	38.0(2)
C(23)-Fe(1)-C(22)-C(21)	118.9(3)	C(28)-Fe(1)-C(22)-C(21)	161.5(4)
C(24)-Fe(1)-C(22)-C(21)	81.5(2)	C(30)-Fe(1)-C(22)-C(21)	-121.33(19)
C(27)-Fe(1)-C(22)-C(21)	-42.3(4)	C(29)-Fe(1)-C(22)-C(21)	-163.55(18)
C(26)-Fe(1)-C(22)-C(21)	-78.3(2)	C(26)-C(30)-C(29)-C(28)	1.1(3)
Fe(1)-C(30)-C(29)-C(28)	-58.8(2)	C(26)-C(30)-C(29)-Fe(1)	59.84(19)
C(21)-Fe(1)-C(29)-C(28)	161.4(4)	C(25)-Fe(1)-C(29)-C(28)	-44.2(4)
C(22)-Fe(1)-C(29)-C(28)	-162.91(19)	C(23)-Fe(1)-C(29)-C(28)	-121.1(2)
C(24)-Fe(1)-C(29)-C(28)	-79.0(2)	C(30)-Fe(1)-C(29)-C(28)	119.9(3)
C(27)-Fe(1)-C(29)-C(28)	37.96(17)	C(26)-Fe(1)-C(29)-C(28)	81.98(19)
C(21)-Fe(1)-C(29)-C(30)	41.5(5)	C(25)-Fe(1)-C(29)-C(30)	-164.1(3)
C(22)-Fe(1)-C(29)-C(30)	77.2(2)	C(23)-Fe(1)-C(29)-C(30)	119.0(2)
C(28)-Fe(1)-C(29)-C(30)	-119.9(3)	C(24)-Fe(1)-C(29)-C(30)	161.1(2)
C(27)-Fe(1)-C(29)-C(30)	-81.9(2)	C(26)-Fe(1)-C(29)-C(30)	-37.91(18)
C(30)-C(29)-C(28)-C(27)	-0.6(4)	Fe(1)-C(29)-C(28)-C(27)	-59.2(2)
C(30)-C(29)-C(28)-Fe(1)	58.6(2)	C(26)-C(27)-C(28)-C(29)	0.0(3)
Fe(1)-C(27)-C(28)-C(29)	59.8(2)	C(26)-C(27)-C(28)-Fe(1)	-59.8(2)
C(21)-Fe(1)-C(28)-C(29)	-165.1(3)	C(25)-Fe(1)-C(28)-C(29)	161.48(19)
C(22)-Fe(1)-C(28)-C(29)	46.6(5)	C(23)-Fe(1)-C(28)-C(29)	78.6(2)
C(24)-Fe(1)-C(28)-C(29)	119.7(2)	C(30)-Fe(1)-C(28)-C(29)	-37.57(17)
C(27)-Fe(1)-C(28)-C(29)	-119.6(3)	C(26)-Fe(1)-C(28)-C(29)	-81.65(19)
C(21)-Fe(1)-C(28)-C(27)	-45.5(4)	C(25)-Fe(1)-C(28)-C(27)	-78.9(2)
C(22)-Fe(1)-C(28)-C(27)	166.2(4)	C(23)-Fe(1)-C(28)-C(27)	-161.8(2)
C(24)-Fe(1)-C(28)-C(27)	-120.7(2)	C(30)-Fe(1)-C(28)-C(27)	82.1(2)
C(29)-Fe(1)-C(28)-C(27)	119.6(3)	C(26)-Fe(1)-C(28)-C(27)	37.98(19)
C(21)-Fe(1)-C(24)-C(23)	82.0(2)	C(25)-Fe(1)-C(24)-C(23)	119.5(3)

C(22)-Fe(1)-C(24)-C(23)	37.7(2)	C(28)-Fe(1)-C(24)-C(23)	-122.3(2)
C(30)-Fe(1)-C(24)-C(23)	-45.7(5)	C(27)-Fe(1)-C(24)-C(23)	-165.1(2)
C(29)-Fe(1)-C(24)-C(23)	-80.7(3)	C(26)-Fe(1)-C(24)-C(23)	160.3(3)
C(21)-Fe(1)-C(24)-C(25)	-37.5(2)	C(22)-Fe(1)-C(24)-C(25)	-81.8(2)
C(23)-Fe(1)-C(24)-C(25)	-119.5(3)	C(28)-Fe(1)-C(24)-C(25)	118.2(2)
C(30)-Fe(1)-C(24)-C(25)	-165.2(3)	C(27)-Fe(1)-C(24)-C(25)	75.4(2)
C(29)-Fe(1)-C(24)-C(25)	159.9(2)	C(26)-Fe(1)-C(24)-C(25)	40.8(5)
C(25)-C(24)-C(23)-C(22)	-0.3(4)	Fe(1)-C(24)-C(23)-C(22)	-59.7(2)
C(25)-C(24)-C(23)-Fe(1)	59.5(2)	C(21)-C(22)-C(23)-C(24)	0.4(4)
Fe(1)-C(22)-C(23)-C(24)	59.9(2)	C(21)-C(22)-C(23)-Fe(1)	-59.5(2)
C(21)-Fe(1)-C(23)-C(24)	-81.0(2)	C(25)-Fe(1)-C(23)-C(24)	-37.3(2)
C(22)-Fe(1)-C(23)-C(24)	-119.1(3)	C(28)-Fe(1)-C(23)-C(24)	76.6(3)
C(30)-Fe(1)-C(23)-C(24)	161.6(2)	C(27)-Fe(1)-C(23)-C(24)	39.2(5)
C(29)-Fe(1)-C(23)-C(24)	118.5(2)	C(26)-Fe(1)-C(23)-C(24)	-161.6(3)
C(21)-Fe(1)-C(23)-C(22)	38.1(2)	C(25)-Fe(1)-C(23)-C(22)	81.8(2)
C(28)-Fe(1)-C(23)-C(22)	-164.3(2)	C(24)-Fe(1)-C(23)-C(22)	119.1(3)
C(30)-Fe(1)-C(23)-C(22)	-79.3(2)	C(27)-Fe(1)-C(23)-C(22)	158.3(4)
C(29)-Fe(1)-C(23)-C(22)	-122.4(2)	C(26)-Fe(1)-C(23)-C(22)	-42.5(4)
C(16)-C(17)-C(18)-C(19)	-9.3(4)	C(32)-C(19)-C(18)-C(17)	8.7(4)
C(23)-C(24)-C(25)-C(21)	0.0(4)	Fe(1)-C(24)-C(25)-C(21)	59.5(2)
C(23)-C(24)-C(25)-Fe(1)	-59.5(2)	C(22)-C(21)-C(25)-C(24)	0.2(4)
Fe(1)-C(21)-C(25)-C(24)	-59.7(2)	C(22)-C(21)-C(25)-Fe(1)	60.0(2)
C(21)-Fe(1)-C(25)-C(24)	119.4(3)	C(22)-Fe(1)-C(25)-C(24)	80.9(2)
C(23)-Fe(1)-C(25)-C(24)	37.2(2)	C(28)-Fe(1)-C(25)-C(24)	-80.2(3)
C(30)-Fe(1)-C(25)-C(24)	163.8(4)	C(27)-Fe(1)-C(25)-C(24)	-122.6(2)
C(29)-Fe(1)-C(25)-C(24)	-48.4(5)	C(26)-Fe(1)-C(25)-C(24)	-164.3(2)
C(22)-Fe(1)-C(25)-C(21)	-38.5(2)	C(23)-Fe(1)-C(25)-C(21)	-82.2(2)
C(28)-Fe(1)-C(25)-C(21)	160.4(2)	C(24)-Fe(1)-C(25)-C(21)	-119.4(3)
C(30)-Fe(1)-C(25)-C(21)	44.3(5)	C(27)-Fe(1)-C(25)-C(21)	117.9(2)
C(29)-Fe(1)-C(25)-C(21)	-167.8(3)	C(26)-Fe(1)-C(25)-C(21)	76.3(2)
C(8)-C(16)-C(32)-C(13)	2.1(5)	C(17)-C(16)-C(32)-C(13)	178.3(3)
C(8)-C(16)-C(32)-C(19)	-177.4(3)	C(17)-C(16)-C(32)-C(19)	-1.2(3)
C(11)-C(13)-C(32)-C(16)	50.2(4)	C(12)-C(13)-C(32)-C(16)	-133.9(3)
C(11)-C(13)-C(32)-C(19)	-130.3(3)	C(12)-C(13)-C(32)-C(19)	45.6(4)

C(18)-C(19)-C(32)-C(16)	-4.7(4)	C(18)-C(19)-C(32)-C(13)	175.8(3)

References

[1] Irie, M. *Chem. Rev.* **2000**, *100*, 1685-1716.

[2] Jakobsson, F. L. E.; Marsal, P.; Braun, S.; Fahlman, M.; Berggren, M.; Cornil, J.; Crispin, X. *J. Phys. Chem. C* **2009**, *113*, 18396-18405.

[3] Tsujioka, T.; Onishi, I.; Natsume, D. *Appl. Opt.* **2010**, *49*, 3894-3899.

[4] Sevez, G.; Gan, J.; Delbaere, S.; Versmeerch, G.; Sanguinet, L.; Levillain, E.; Pozzo, J.-L. *Photochem. Photobiol. Sci.* **2010**, *9*, 131-135.

[5] Peters, A.; Branda, N. R. *J. Am. Chem. Soc.* **2003**, *125*, 3404-3405.

[6] Irie, M. *Photochem. Photobiol. Sci.* **2010**, *9*, 1535-1542.

[7] Hiroto, S.; Suzuki, K.; Kamiya, H.; Shinokubo, H. *Chem. Commun.* **2011**, *47*, 7149-7151.

[8] Singer, M.; Jäschke, A. *J. Am. Chem. Soc.* **2010**, *132*, 8372-8377.

[9] Huang, Z.-N.; Xu, B.-A.; Jin, S.; Fan, M.-G. *Synthesis*, **1998**, *8*, 1092-1094.

[10] Lucas, L. N.; van Esch, J. H.; Kellogg, R. M.; Feringa, B. L. *Chem. Commun.* **1998**, 2313.

[11] Xu, B. A.; Huang, Z. N.; Jin, S.; Ming, Y. F.; Fan, M. G.; Yao, S. D. *J. Photochem. Photobiol. A: Chem.* 1997, *110,* 35-40.

[12] Lucas, L. N.; de Jong, J. J. D.; van Esch, J. H.; Kellog, R. M.; Feringa, B. L. *Eur. J. Org. Chem.* **2003**, 155-166.

[13] Krayushkin, M. M.; Migulin, V. A.; Yarovenko, V. N.; Barachevskii, V. A.; Vorontsova, L. G.; Starikova, Z. A.; Zavarzin, I. V.; Bulgakova, V. N. *Mendeleev Commun.* **2007**, *17*, 125-127.

[14] Sun, L.; Tian, H. *Tetrahedron Lett.* **2006**, *47*, 9227-9231.

[15] Guerchais, V.; Ordronneau, L.; Le Bozec, H. *Coord. Chem. Rev.* **2010**, *254*, 2533-2545.

[16] Fernàndez-Acebes, A.; Lehn, J.-M. *Chem. Eur. J.* **1999**, *5*, 3285-3292.

[17] Yin, J.; Yu, G.-A.; Tu, H.; Liu, S. H. *Appl. Organometal. Chem.* **2006**, *20*, 869-873.

[18] Sun, L.; Tian, H. *Tetrahedron Lett.* **2006**, *47*, 9227-9231.

[19] Sun, L.; Wang, S.; Tian, H. *Chem. Lett.* **2007**, *36*, 250-251.

[20] Guirado, G.; Coudret, C.; Launay, J.-P. *J. Phys. Chem. C* **2007**, *111*, 2770-2776.

[21] Zhong, Y.-W.; Vila, N.; Henderson, J. C.; Flores-Torres, S.; Abruña, H. D. *Inorg. Chem.* **2007**, *46*, 10470-10472.

[22] Sénéchal-David, K.; Zaman, N.; Walko, M.; Halza, E.; Rivière, E.; Guillot, R.; Feringa, B. L.; Boillot, M.-L. *Dalton Trans.* **2008**, 1932-1936.

[23] Chen, W.; Chen, S. W.; Ding, F.; Wang, H.; Brown, L. E.; Konopelski, J. P. *J. Am. Chem. Soc.* **2008,** *130,* 12156-12162.

[24] Kang, X.; Zuckerman, N. B.; Konopelski, J. P.; Chen, S. W. *J. Am. Chem. Soc.* **2012,** *134,* 1412-1415.

[25] Krayushkin, M. M.; Migulin, V. A. Russian Patent No. RU 2421453 C1, **2011**.

[26] Gilat, S. L.; Kawai, S. H.; Lehn, J.-M. *Chem. Eur. J.* **1995**, *1*, 275-284.

[27] Plaumann, D. E.; Fitzsimmons, B. J.; Ritchie, B. M.; Fraser-Reid, B. *J. Org. Chem.* **1982**, *47*, 941.

[28] Gronowitz, S.; Björk, P.; Malm, J.; Hörnfeldt, A.-B. *J. Organomet. Chem.* **1993**, *460*, 127-129.

[29] Krayushkin, M. M.; Lichitsky, B. V.; Kozhinov, D. V.; Ivanov, S. N.; Dudinov, A. A. *ARKIVOC* **2003**, *13*, 147-156.

[30] Mamane, V. *Mini Rev. Org. Chem.* **2008**, *5*, 303-312.

[31] Liu, C.-M.; Luo, S.-J.; Liang, Y.-M.; Ma, Y.-X. *Synth. Commun.* **2000**, *30*, 2281-2285.

[32] Liu, C.-M.; Chen, B.-H.; Liu, W.-Y.; Wu, X.-L.; Ma, Y.-X. *J. Organomet. Chem.* **2000**, *598*, 348-352.

[33] Guillaneux, D.; Kagan, H. B. *J. Org. Chem.* **1995**, *60*, 2502-2505.

[34] Impagnatiello, N.; Heynderickx, A.; Moustrou, C.; Samat, A. *Mol. Cryst. Liq. Cryst.* **2005**, *430*, 243-248.

[35] Barrios, F. J.; Zhang, X.; Colby, D. A. *Org. Lett.* **2010**, *12*, 5588-5591.

[36] Graham, S. L.; Scholz, T. H. *Tetrahedron Lett.* **1990,** *31,* 6269

[37] Belley, M.; Douida, Z.; Mancuso, J.; De Vleeschauwer, M. *Synlett*, **2005**, *2*, 247-250.

[38] Villuendas, I.; Parilla, A.; Guerrero, A. *Tetrahedron*, **1994**, *50*, 12673-12684.

[39] Alvarez Ibarra, C.; Cuervo Rodriguez, R.; Fernandez Monreal, M. C.; Garcia Navarro, F. J.; Martin Tesorero, J. *J. Org. Chem.* **1989**, *54*, 5620-5623.

[40] Heckert, S. J.; Heathcock, C. H. *J. Org. Chem.* **1985**, *50*, 5159-5166.

[41] Chiu, C. C.; Frank, J. *J. Org. Chem.* **1994**, *59*, 5763-5766.

[42] Shashidhar, M. S.; Bhatt, M. V. *J. Chem. Soc. Perkin Trans. II*, **1986**, 355-358.

[43] Migulin, V. A.; Krayushkin, M. M.; Barachevsky, V. A.; Kobelva, O. I.; Valova, T. M.; Lyssenko, K. A. *J. Org. Chem.* **2012**, *77*, 332-340.

[44] Krayushkin, M. M.; Migulin, V. A.; Yarovenko, V. N.; Barachevskii, V. A.; Vorontsova, L. G.; Starikova, Z. A.; Zavarzin, I. V.; Bulgakova, V. N. *Mendeleev Commun.* **2007**, *17*, 125-127.

[45] Gooßen, L. J.; Ghosh, K. *Angew. Chem. Int. Ed.* **2001,** *40,* 3458-3460.

[46] Kakino, R.; Yasumi, S.; Shimizu, I.; Yamamoto, A. *Bull. Chem. Soc. Jpn.* **2002,** *75,* 137-148.

[47] Gooßen, L. J.; Ghosh, K. *Eur. J. Org. Chem* **2002**, 3254-3267.

[48] Gooßen, L. J.; Winkel, L.; Döhring, A.; Ghosh, K.; Paetzold, J. *Synlett*, **2002**, *8*, 1237-1240.

[49] Gooßen, L. J.; Koley, D.; Hermann, H. L.; Thiel, W. *J. Am. Chem. Soc.* **2005**, *127*, 11102-11114.

[50] Martin, S. F.; Dodge, J. A.; Burgess, L. E.; Hartmann, M. *J. Org. Chem.* **1992**, *57*, 1070-1072.

[51] Kobatake, S.; Uchida, K.; Tsuchida, E.; Irie, M. *Chemm. Commun.* **2002**, 2804-2805.

[52] Fedi, V.; Altamura, M.; Catalioto, R.-M.; Giannotti, D.; Giolitti, A.; Giuliani, S.; Guidi, A.; Harmat, N. J. S.; Lecci, A.; Meini, S.; Nannicini, R.; Pasqui, F.; Tramontana, M.; Triolo, A.; Maggi, C. A. *J. Med. Chem.* **2007**, *50*, 4793-4807.

[53] Collins, C. J.; Fisher, G. B.; Reem, A.; Goralski, C. T.; Singaram, B. *Tetrahedron Lett.* **1997**, *38*, 529-532.

[54] Hay, M. P.; Pchalek, K.; Prujin, F. B.; Hicks, K. O.; Slim, B. G.; Anderson, R. F.; Shinde, S. S.; Phillips, V.; Denny, W. A.; Wilson, W. R. *J. Med. Chem.* **2007**, *50*, 6654-6664.

[55] Yang, T.; Pu, S.; Chen, B.; Xu, J. *Can. J. Chem.* **2007**, *85*, 12-20.

APPENDIX: Selected ^{1}H and ^{13}C-NMR Spectra

^{1}H and ^{13}C NMR

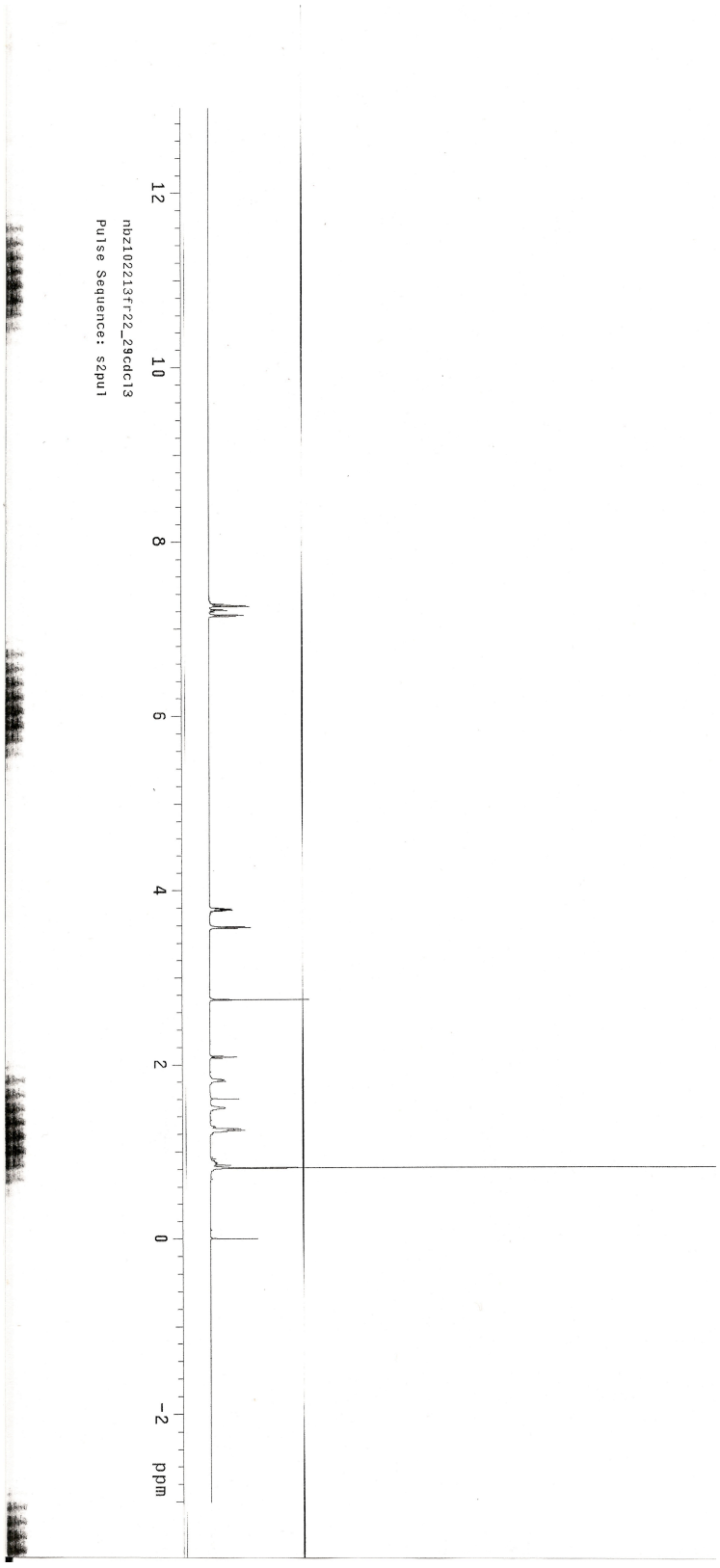

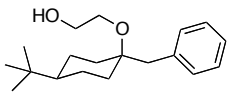

***cis*-1.11**
500 MHz, $CDCl_3$

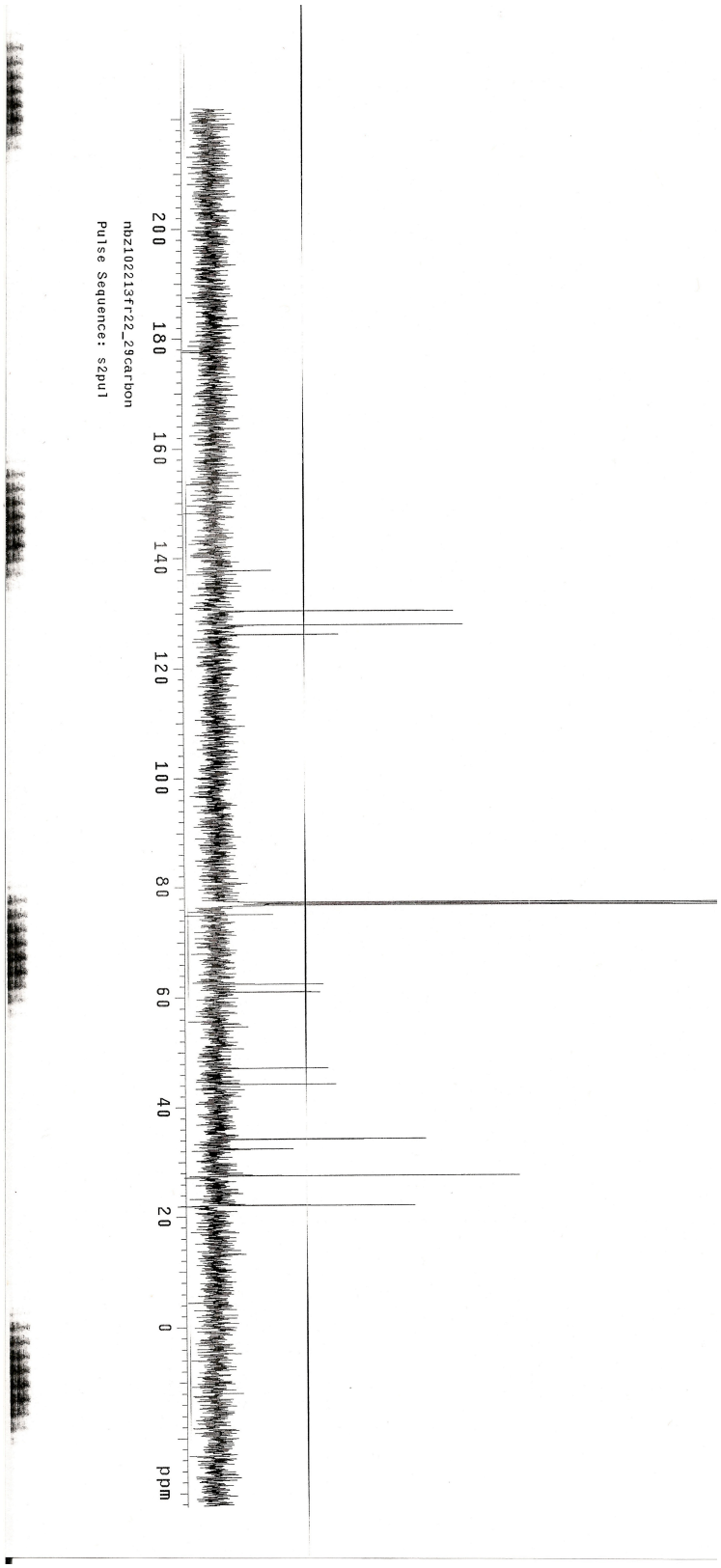

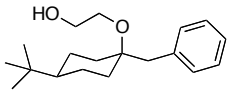

***cis*-1.11**
125 MHz, $CDCl_3$

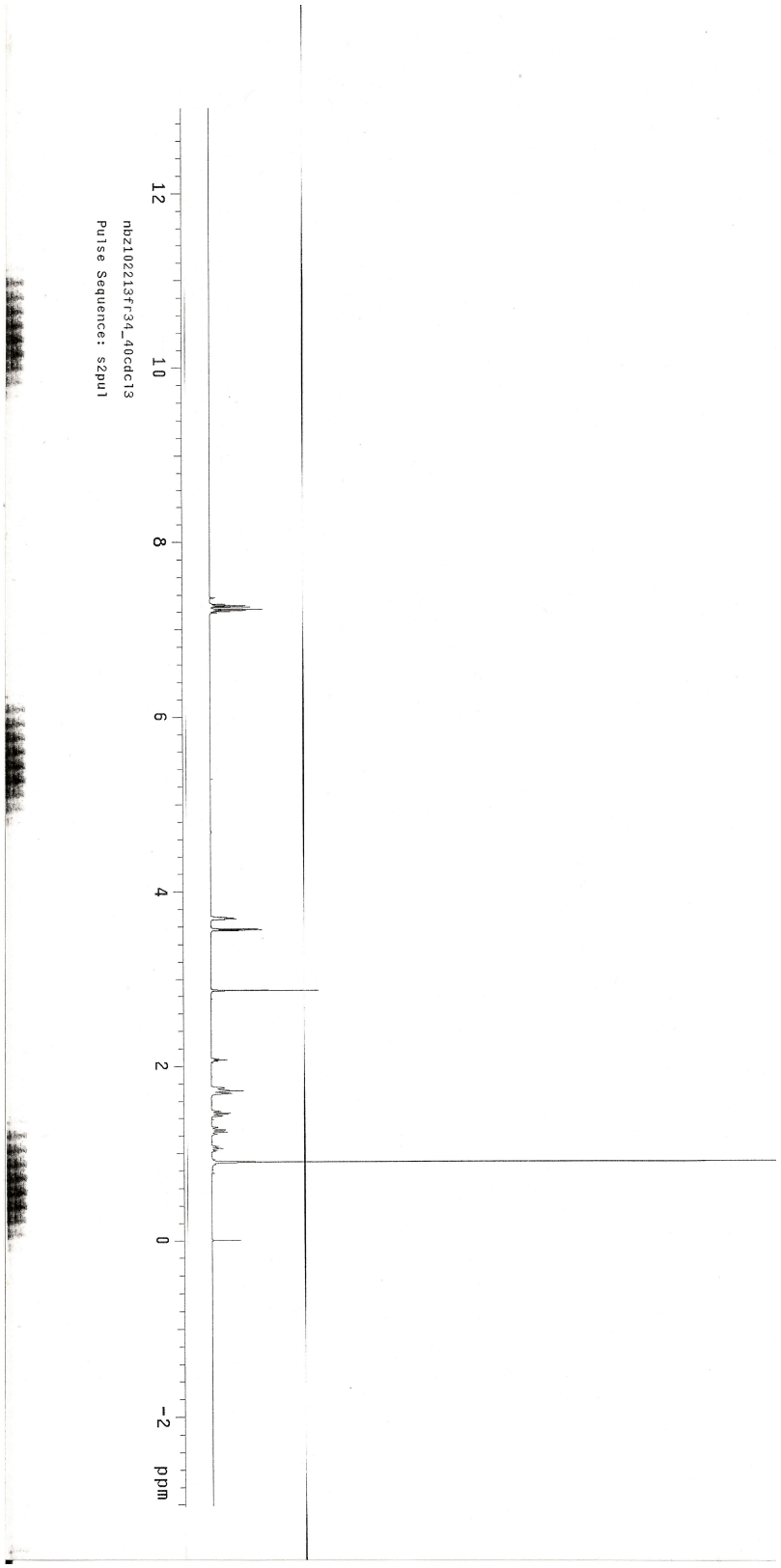

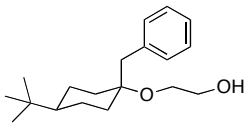

trans-**1.11**
500 MHz, $CDCl_3$

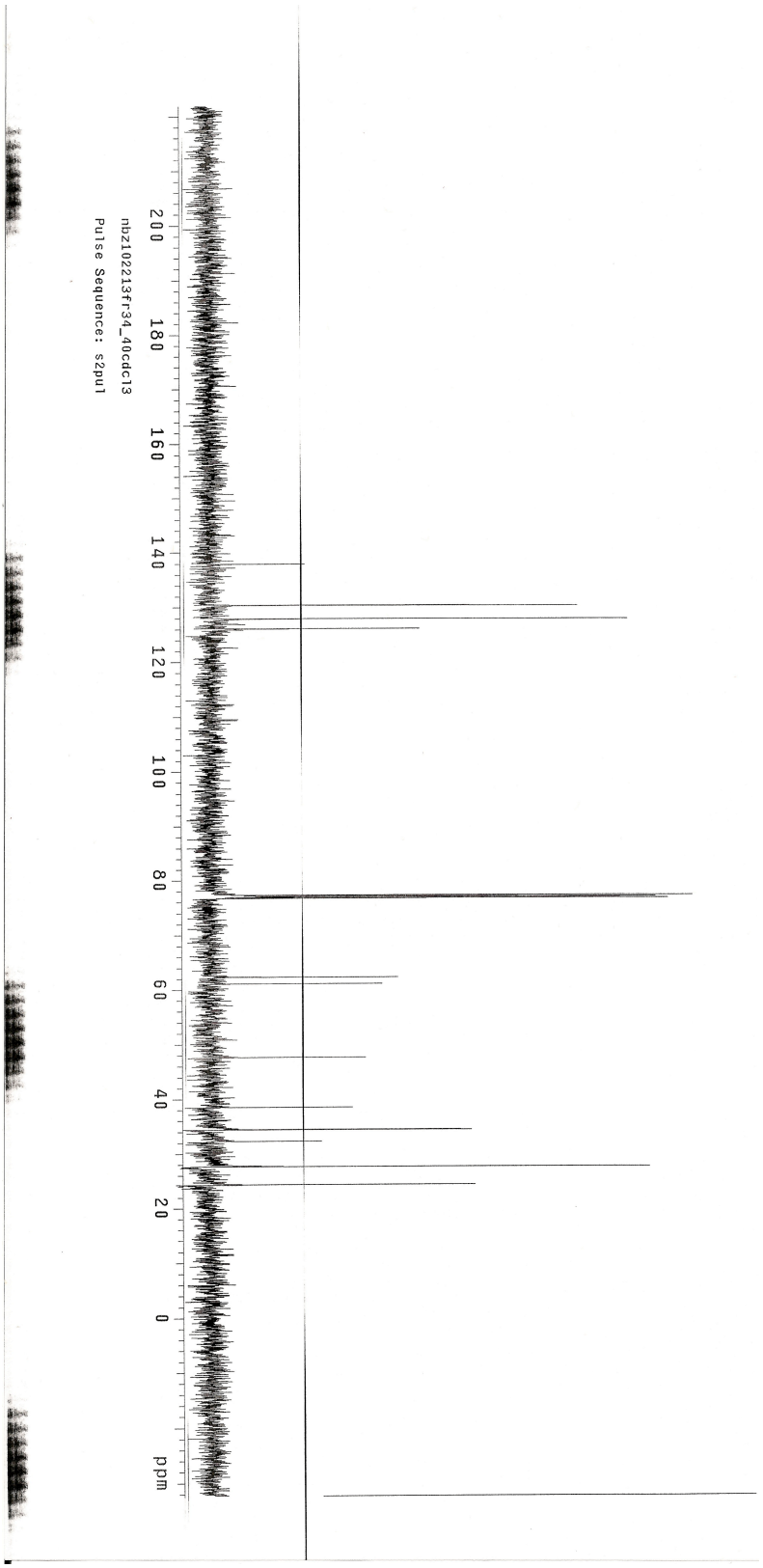

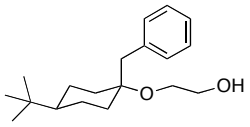

trans-**1.11**
125 MHz, $CDCl_3$

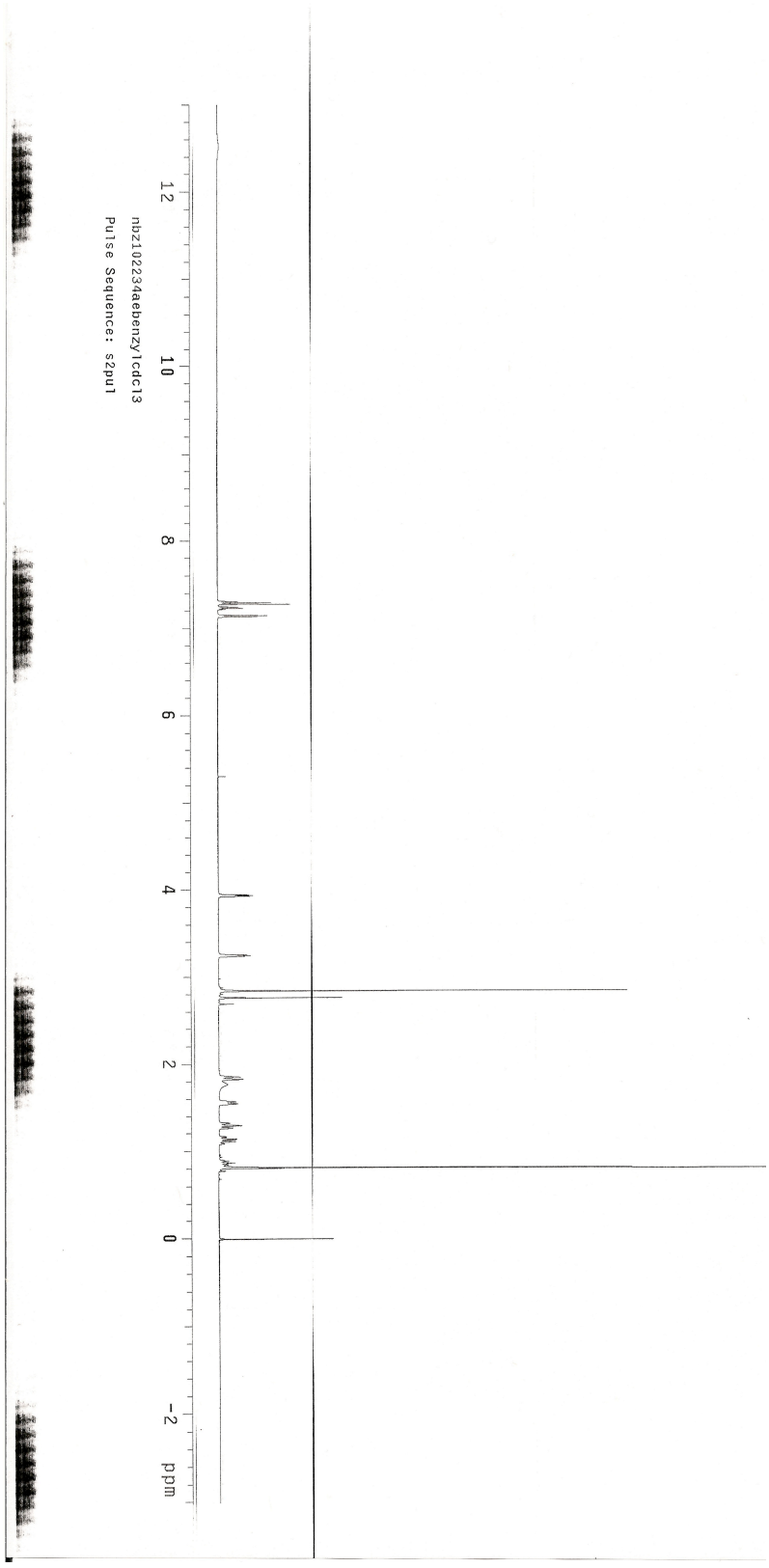

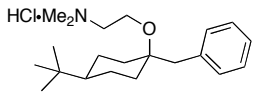

***cis*-1.12**
500 MHz, $CDCl_3$

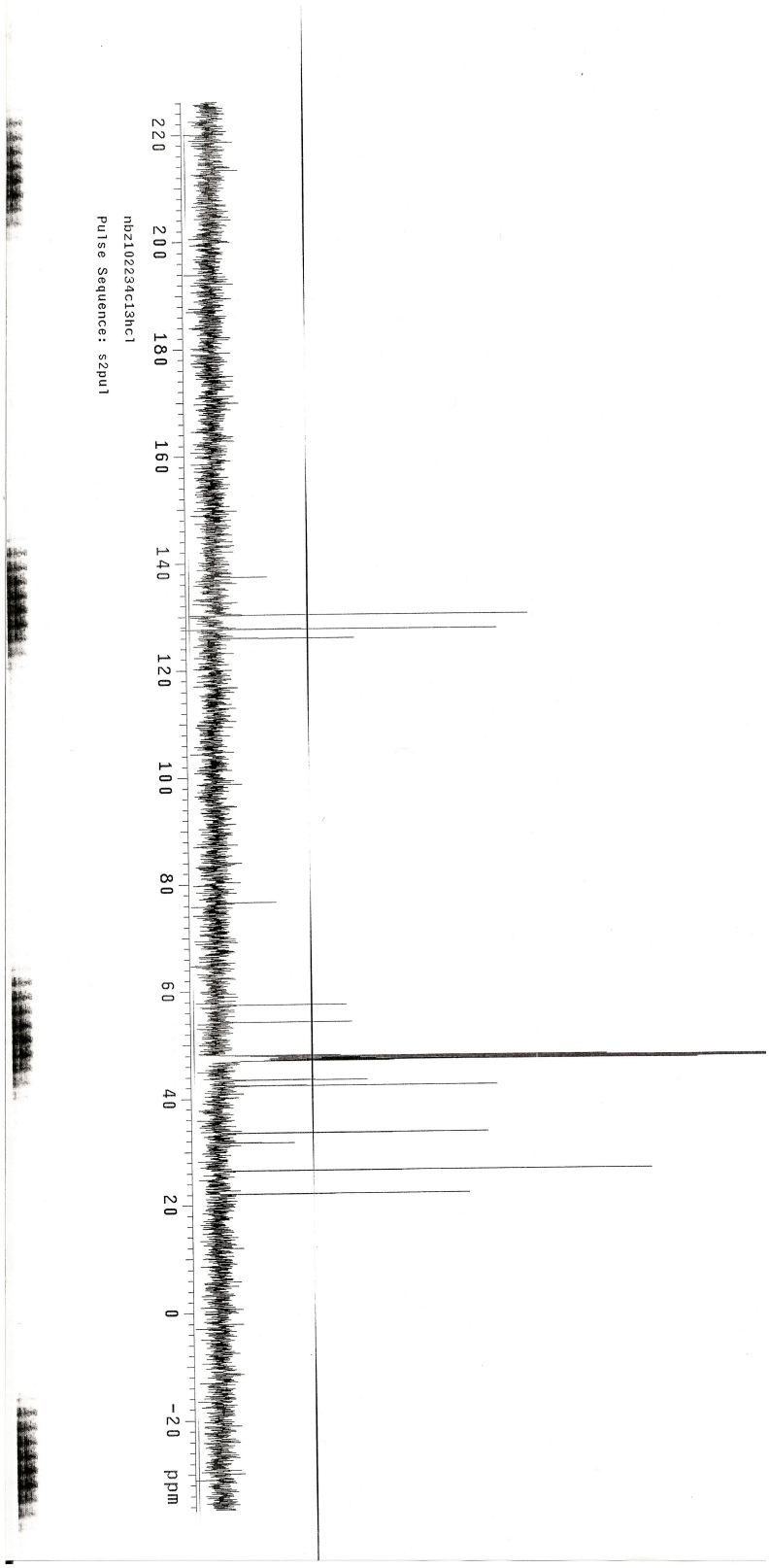

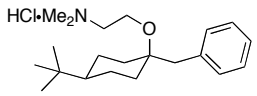

***cis*-1.12**
125 MHz, CD_3OD

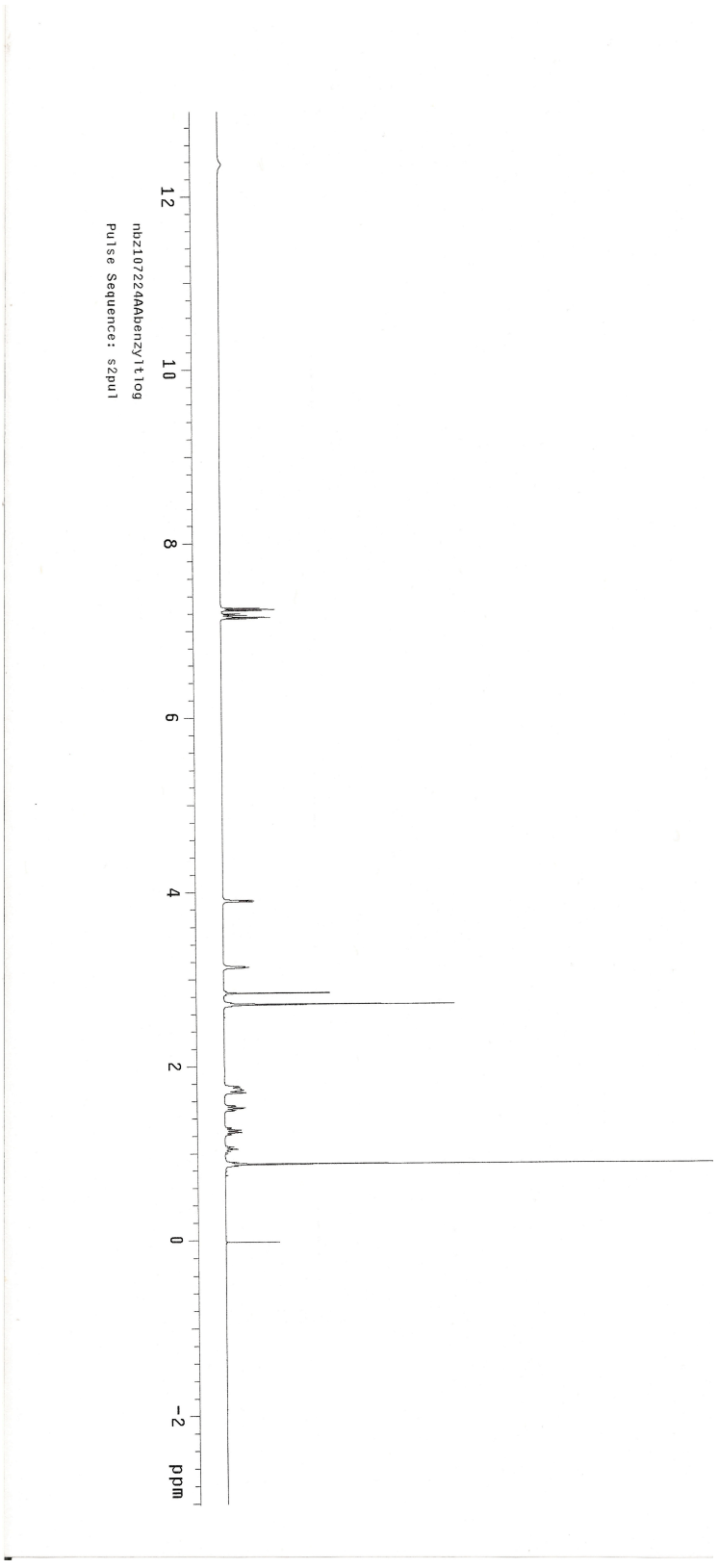

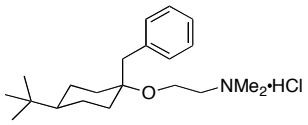

trans-**1.12**
500 MHz, $CDCl_3$

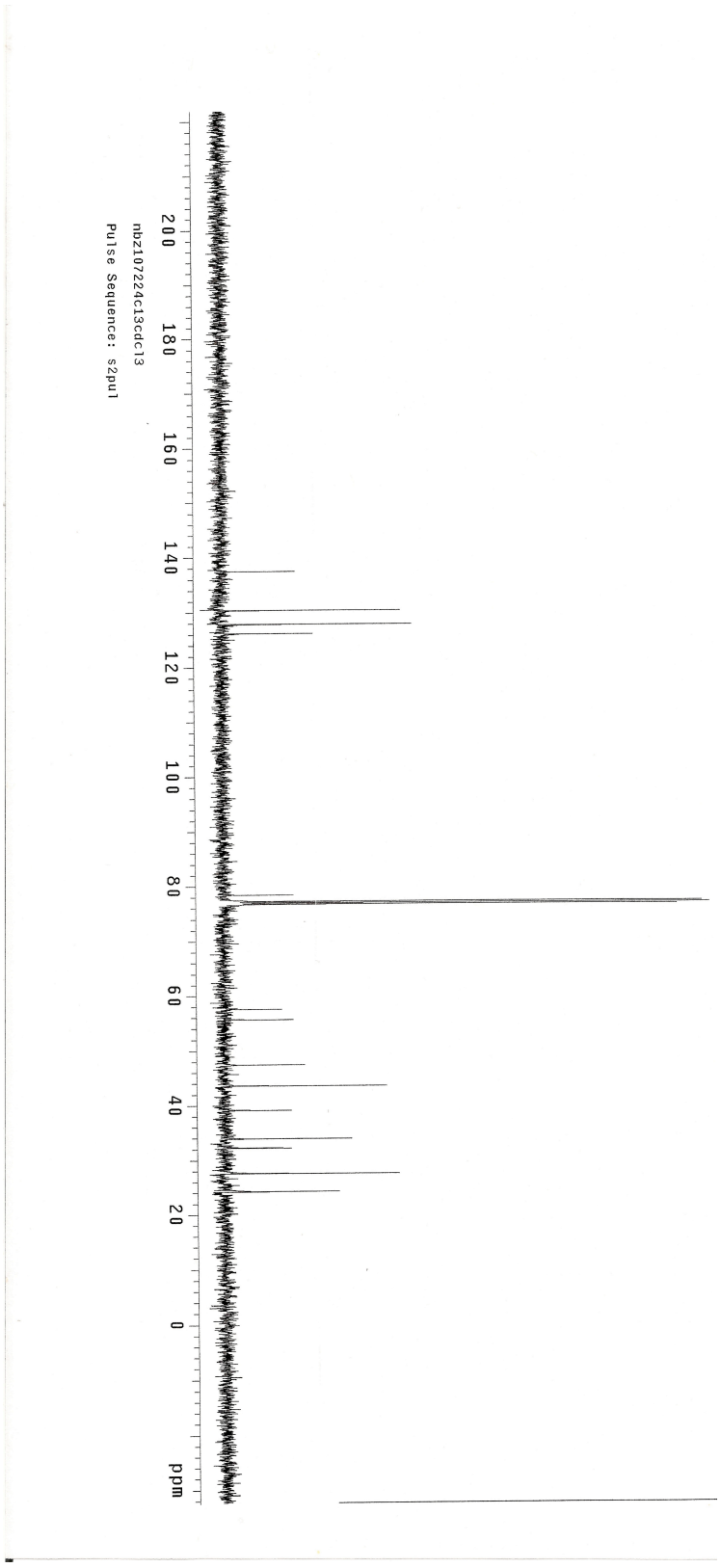

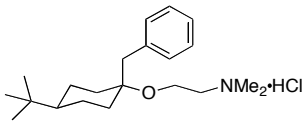

trans-**1.12**
125 MHz, $CDCl_3$

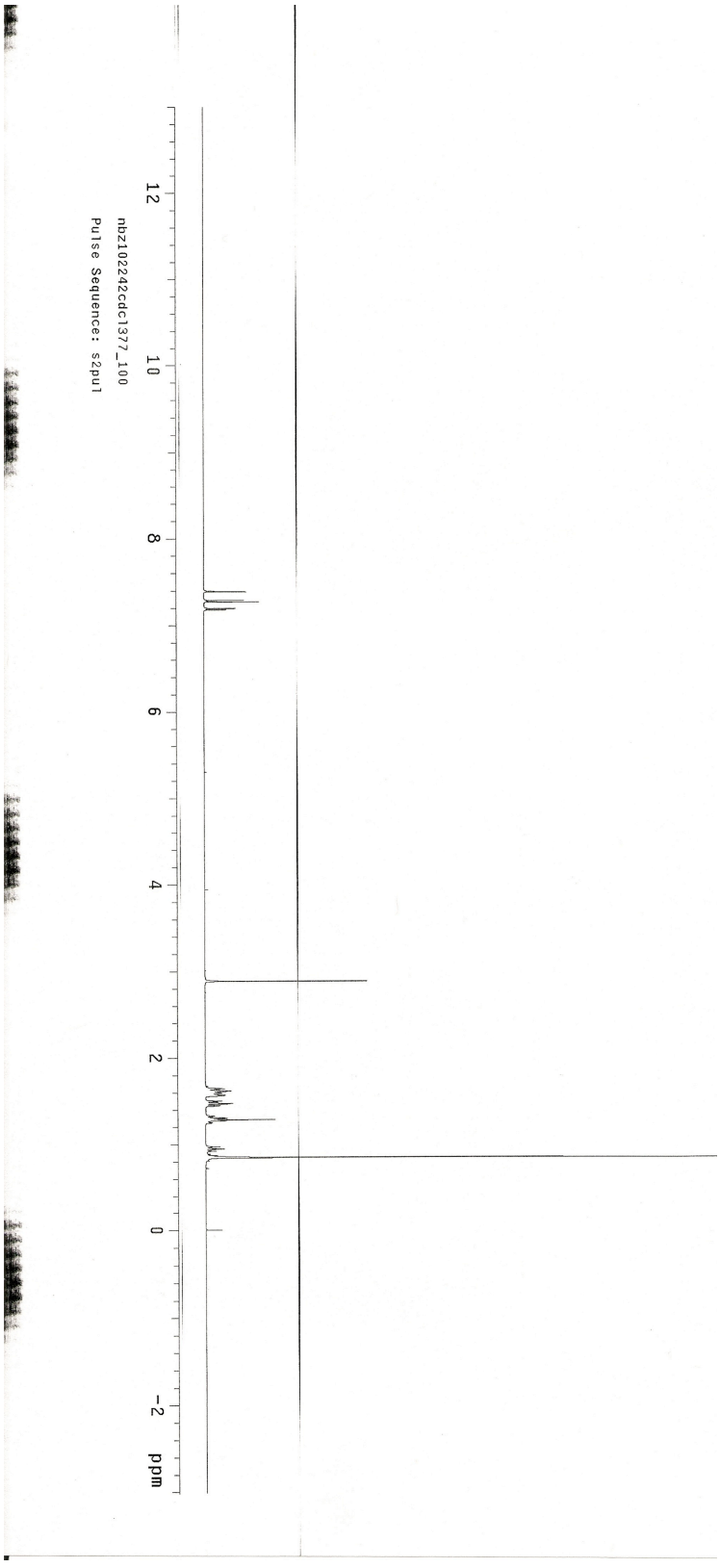

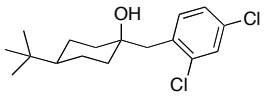

***cis*-1.9**
500 MHz, $CDCl_3$

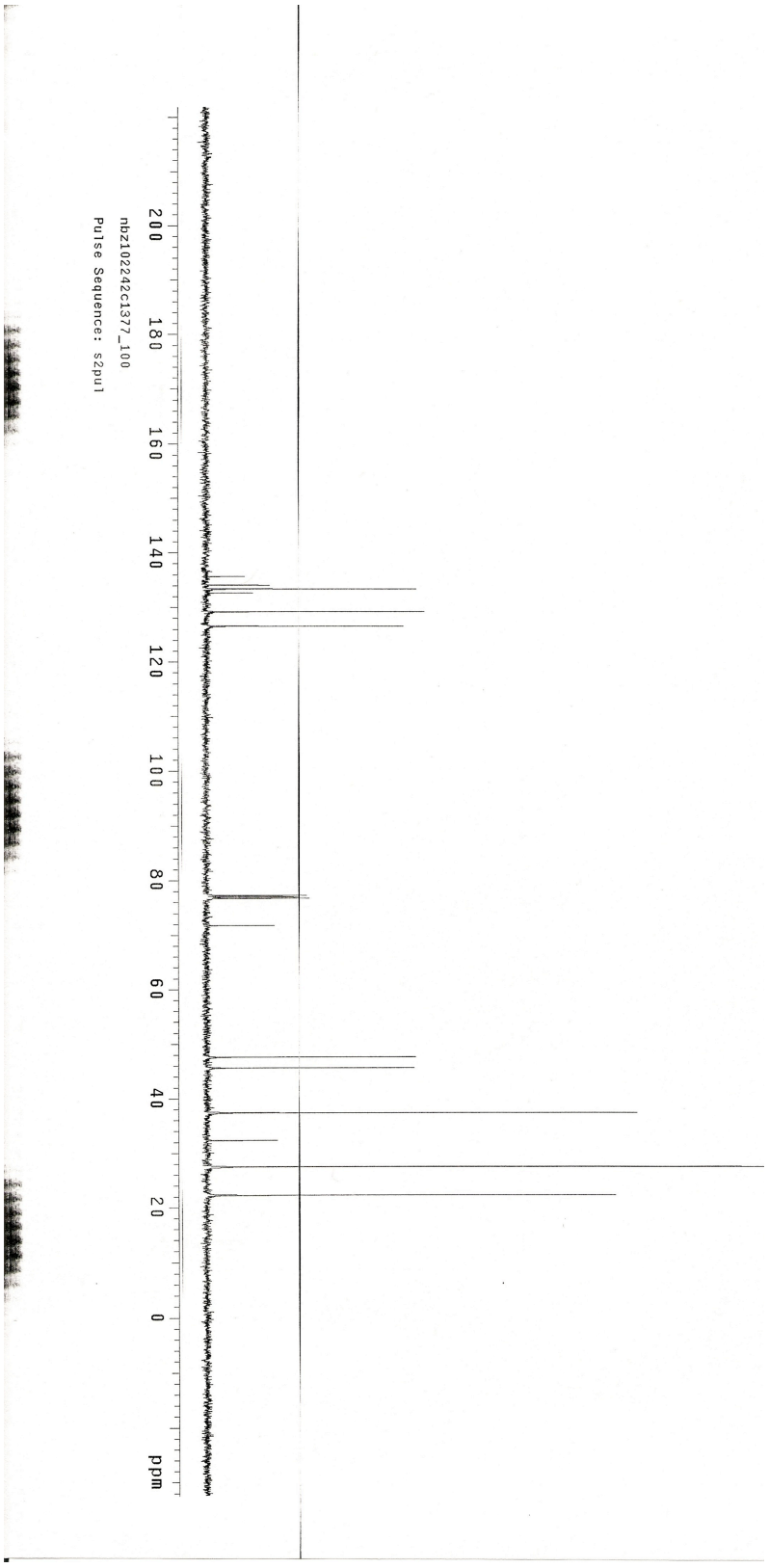

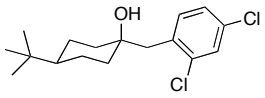

***cis*-1.9**
125 MHz, $CDCl_3$

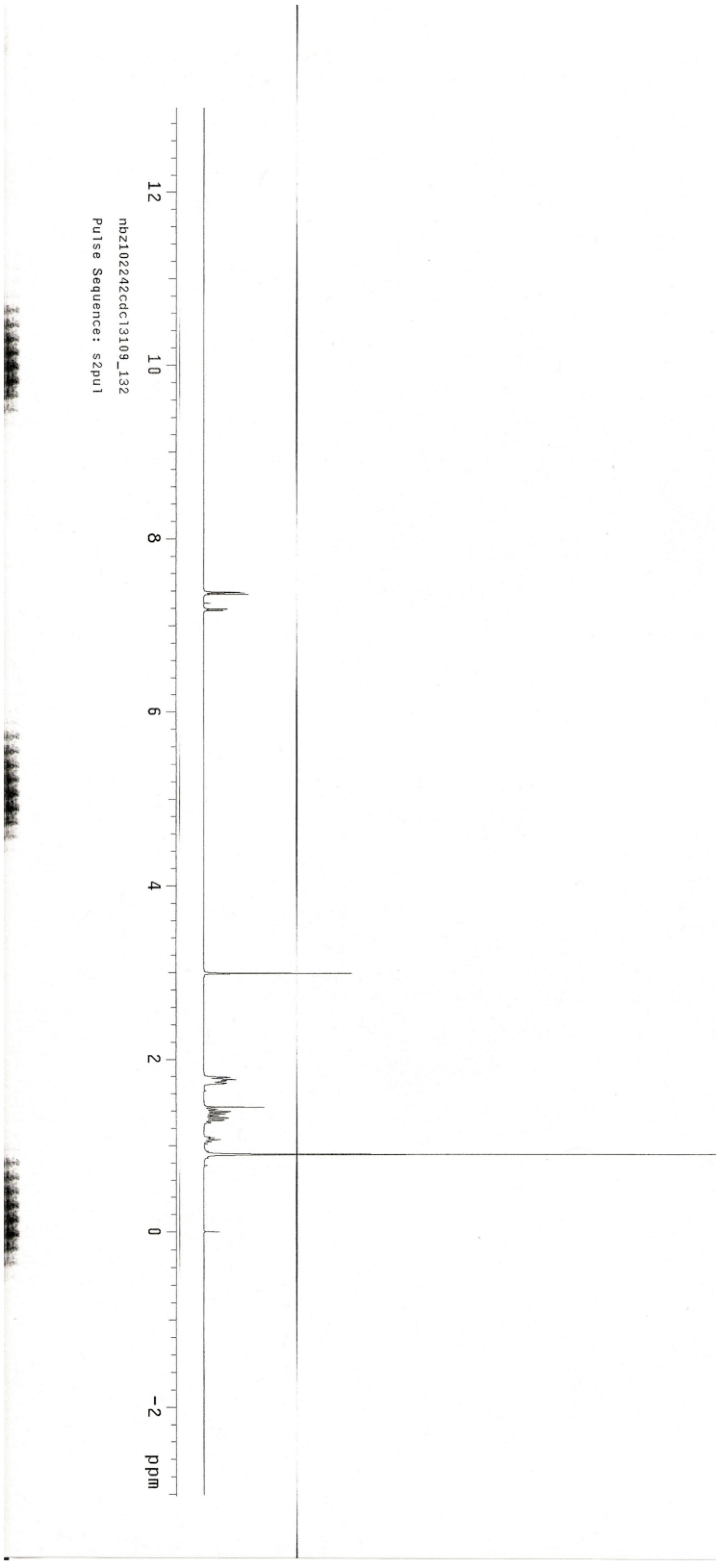

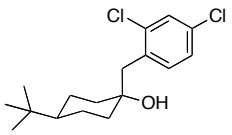

trans-**1.9**
500 MHz, $CDCl_3$

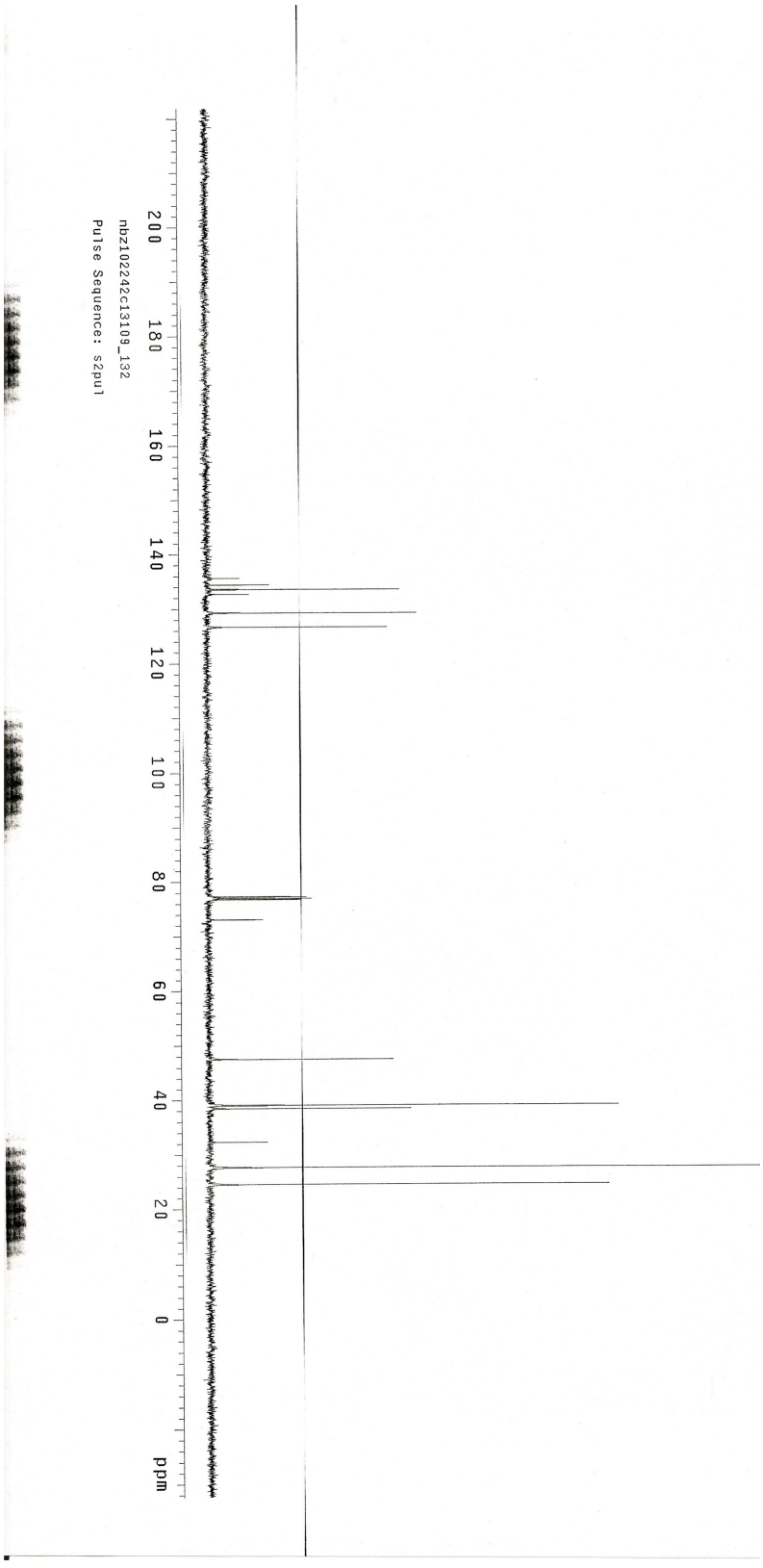

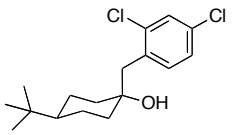

trans-**1.9**
125 MHz, $CDCl_3$

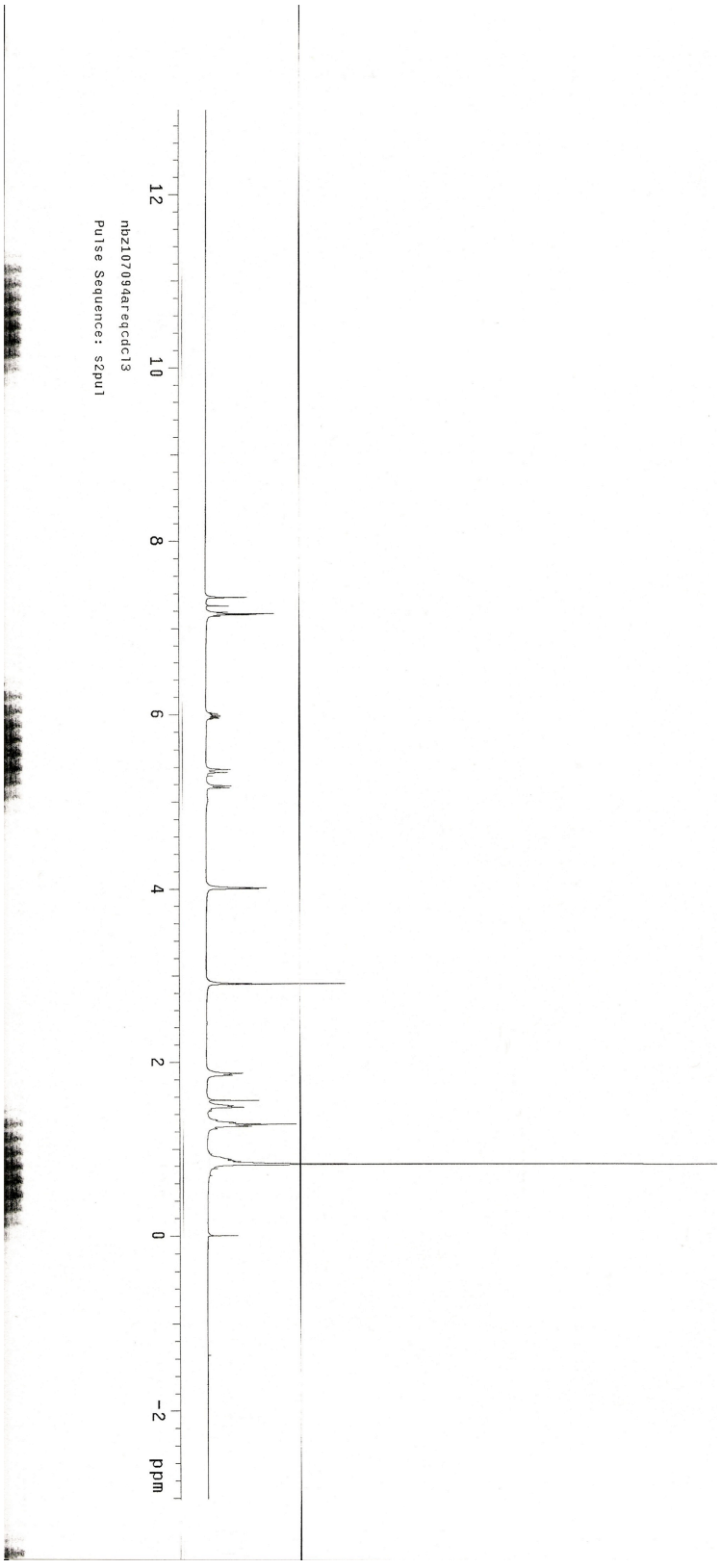

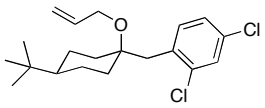

***cis*-1.18**
500 MHz, $CDCl_3$

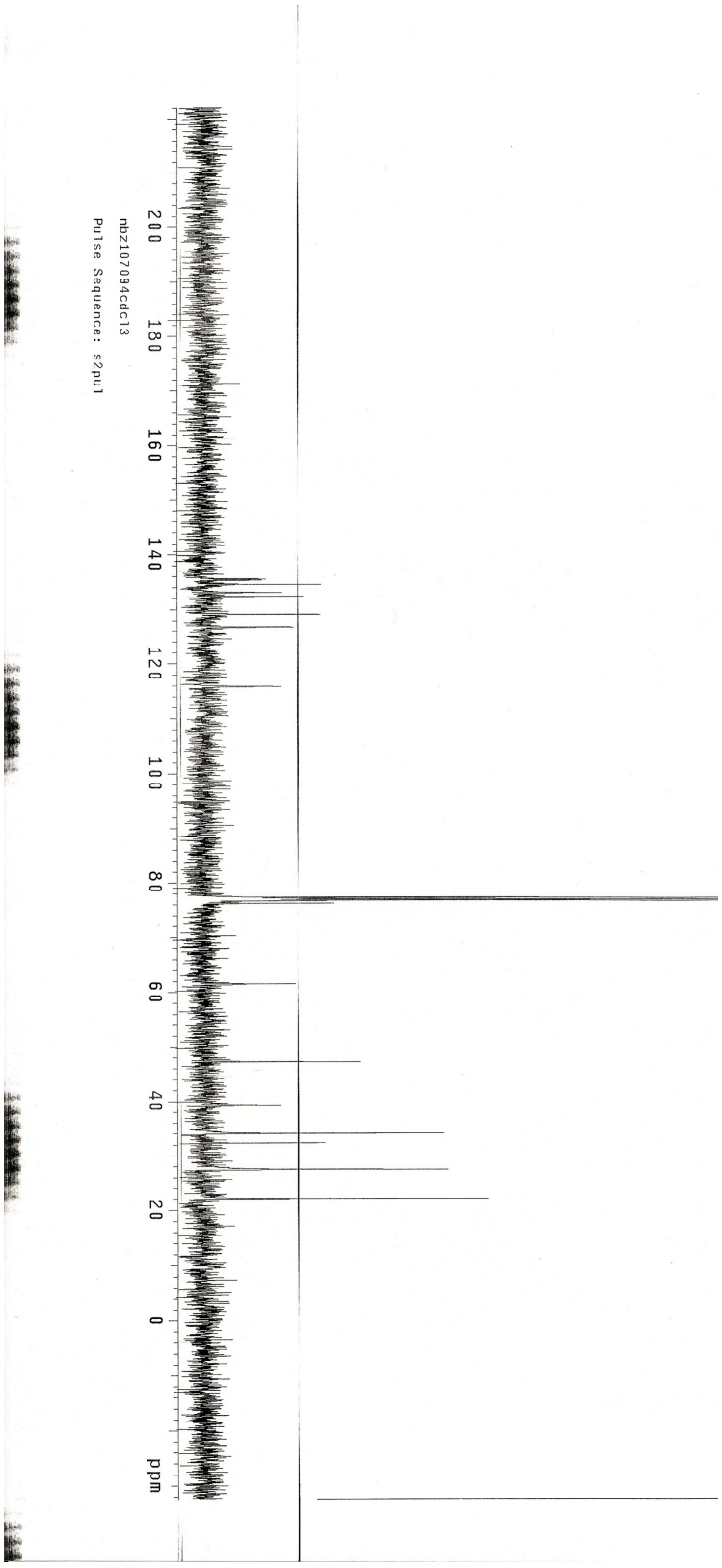

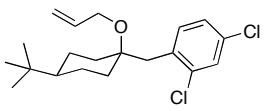

***cis*-1.18**
125 MHz, $CDCl_3$

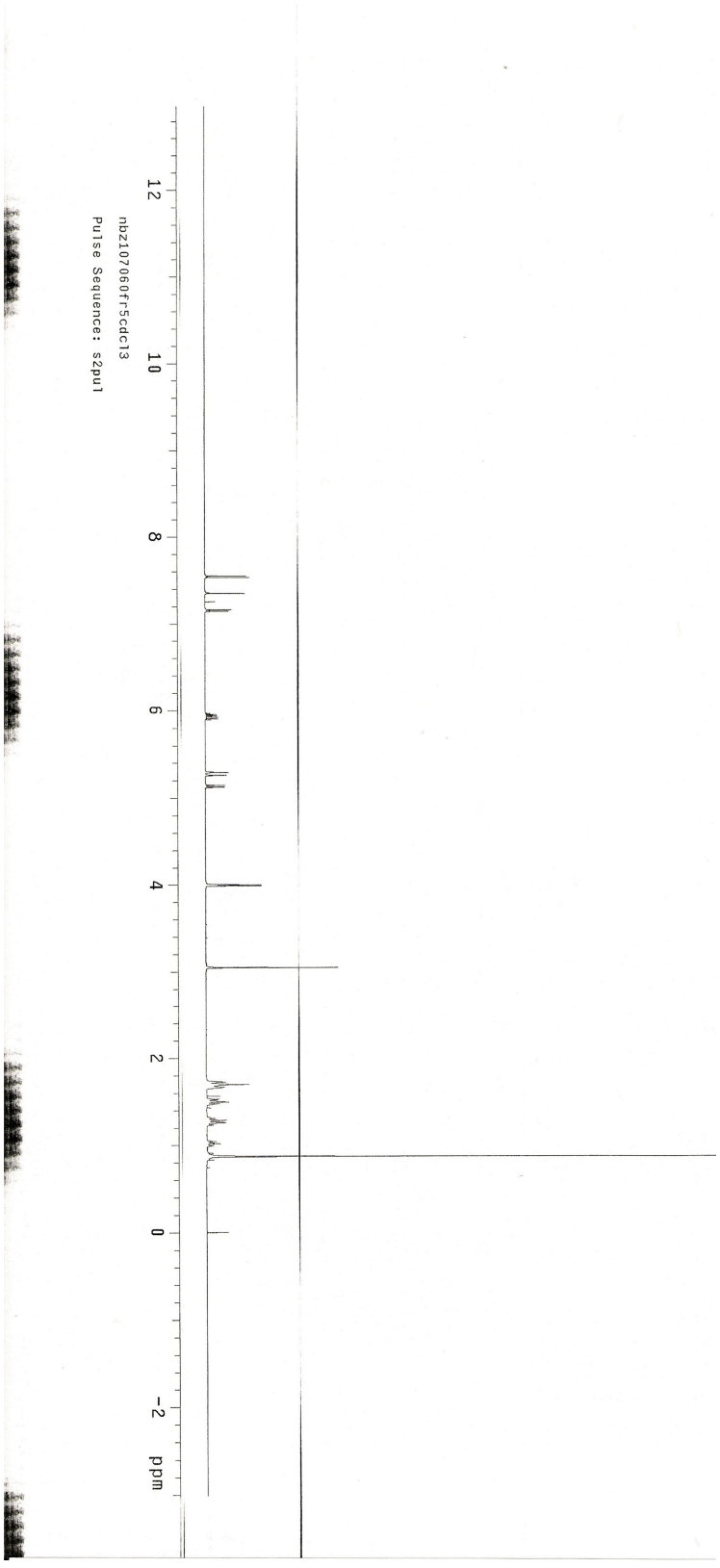

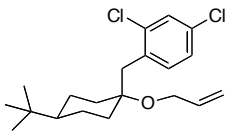

trans-**1.18**
500 MHz, $CDCl_3$

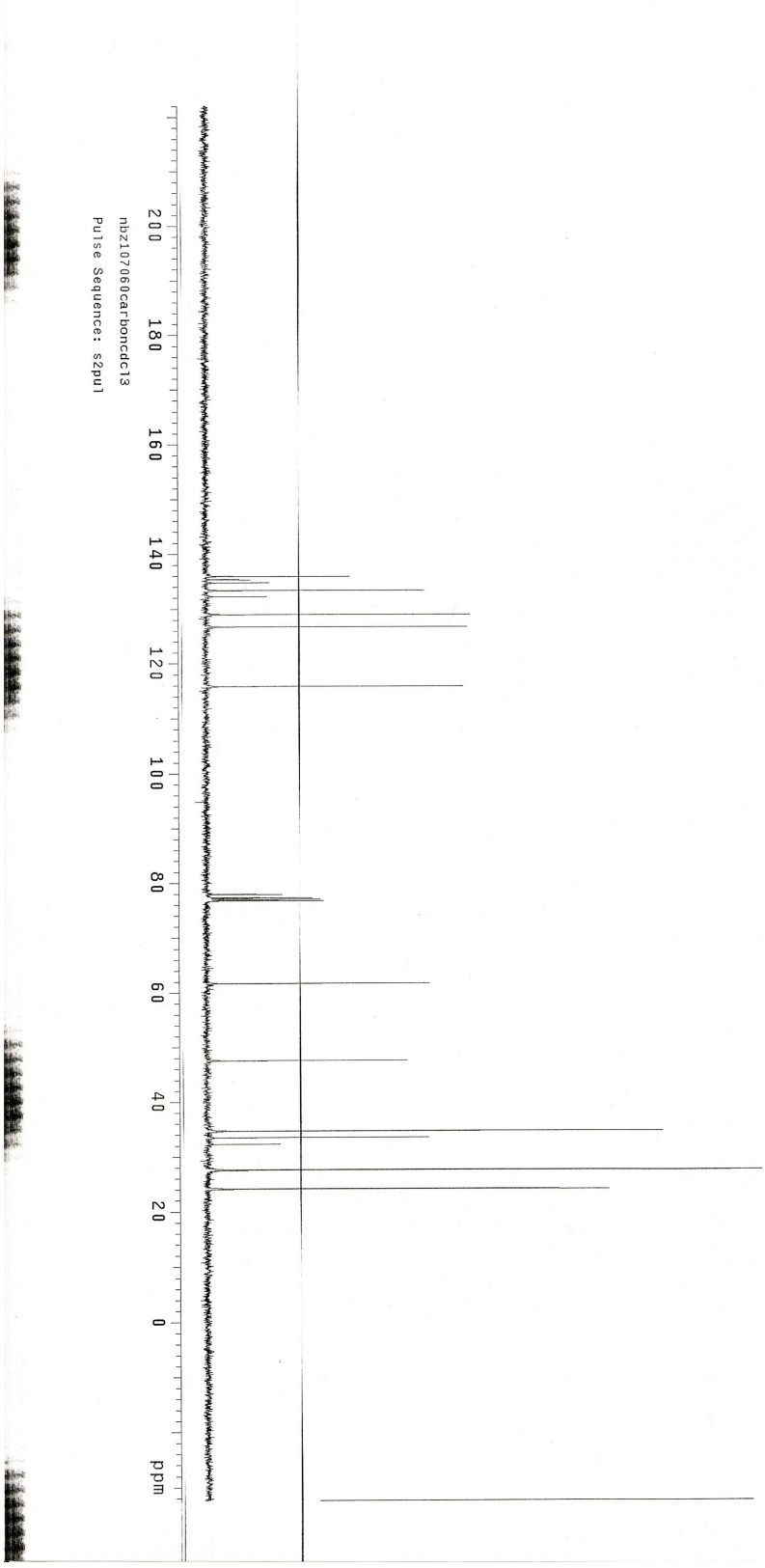

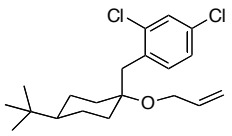

trans-**1.18**
125 MHz, $CDCl_3$

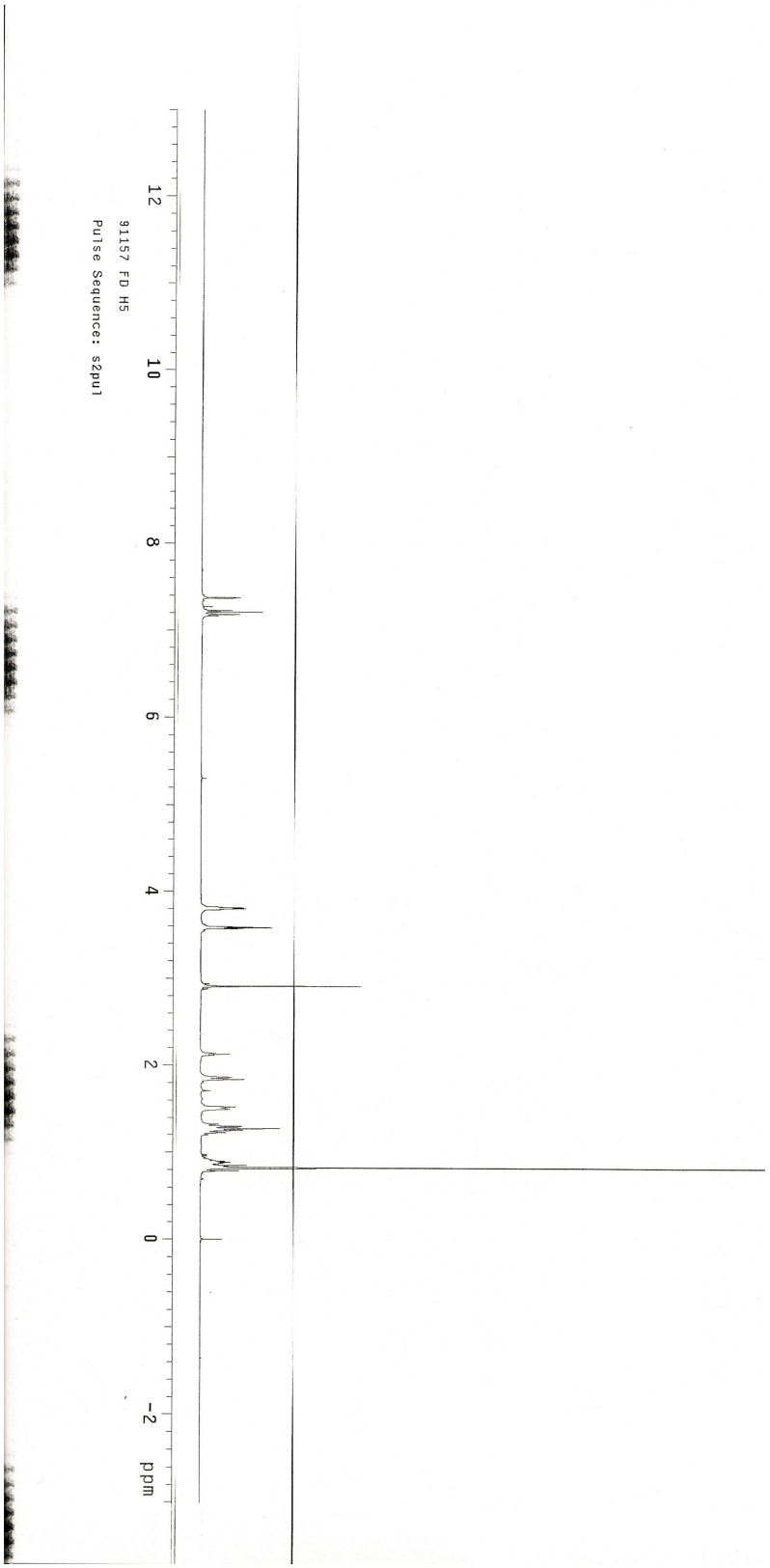

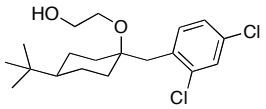

***cis*-1.6**
500 MHz, $CDCl_3$

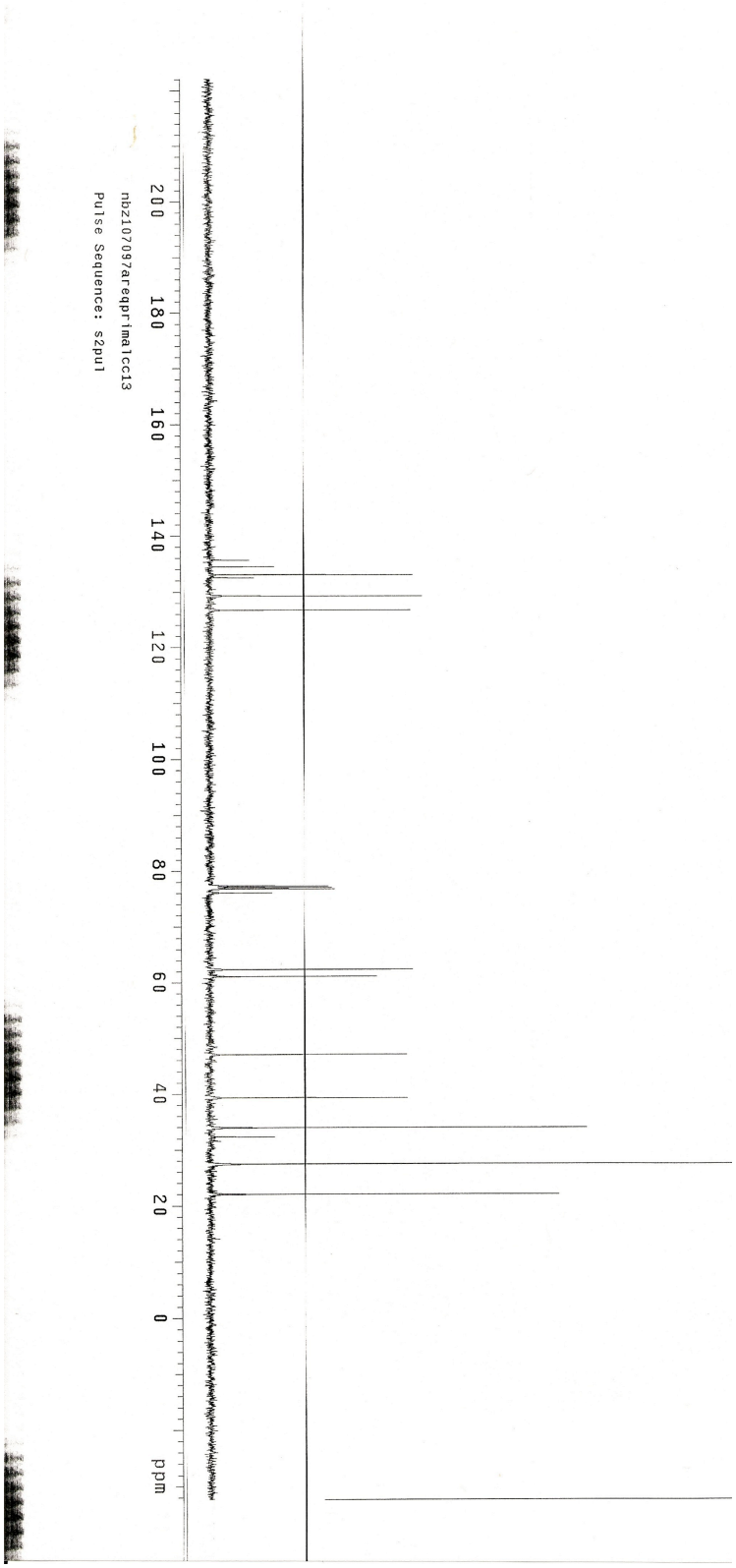

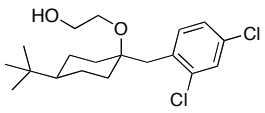

***cis*-1.6**
125 MHz, $CDCl_3$

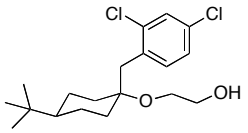

trans-**1.6**
500 MHz, $CDCl_3$

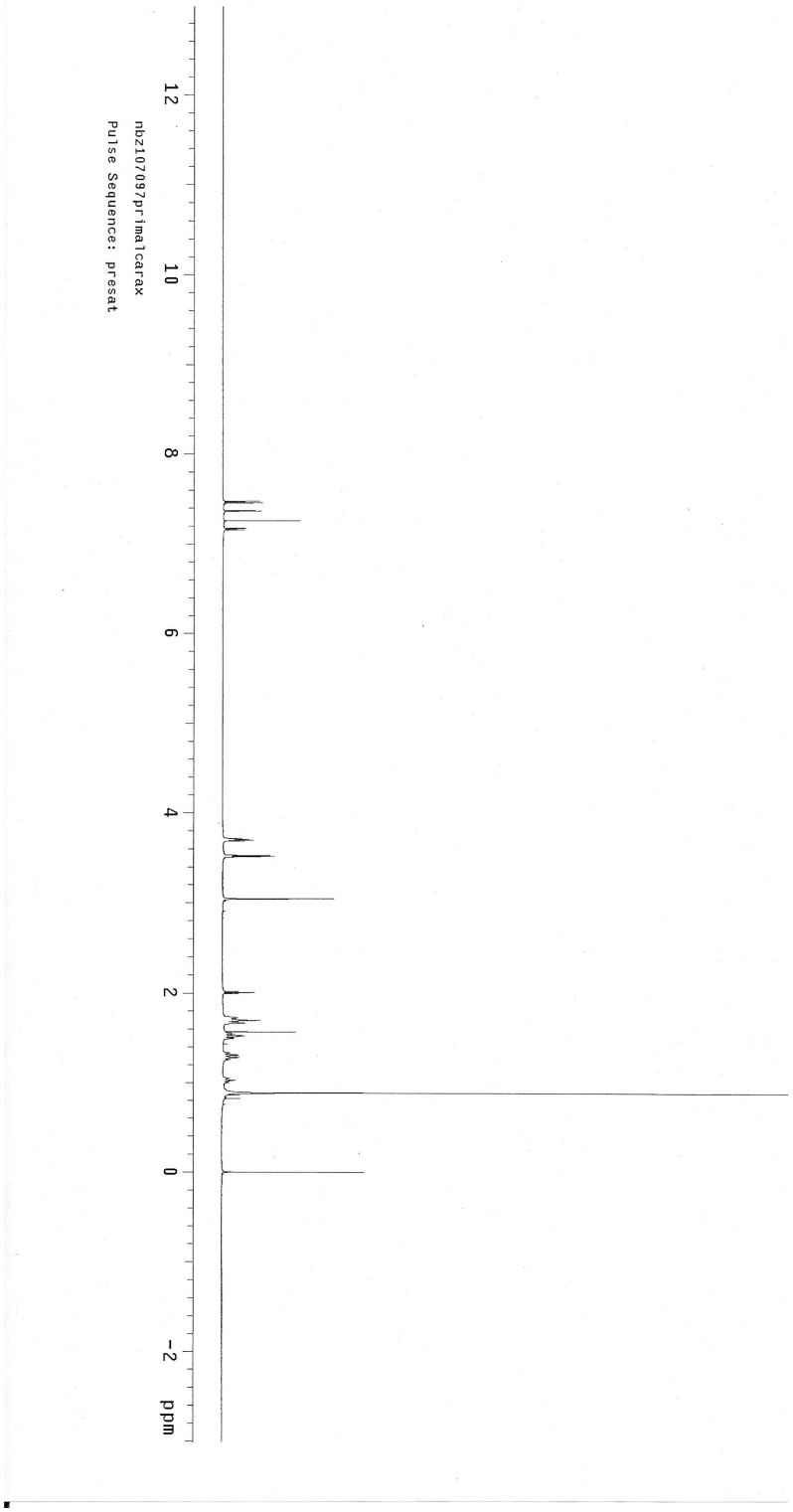

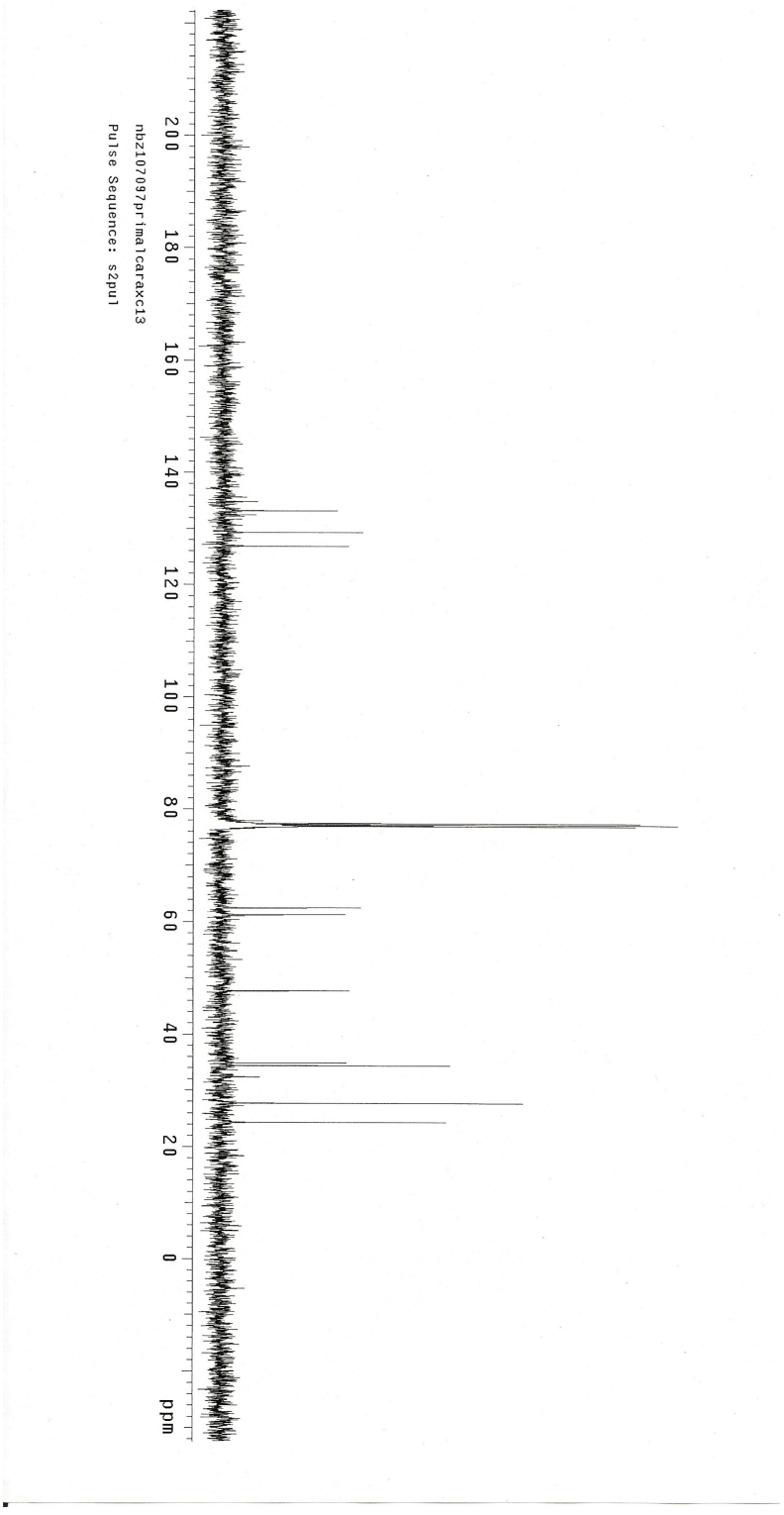

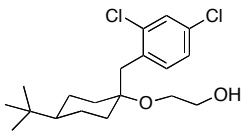

trans-**1.6**
125 MHz, $CDCl_3$

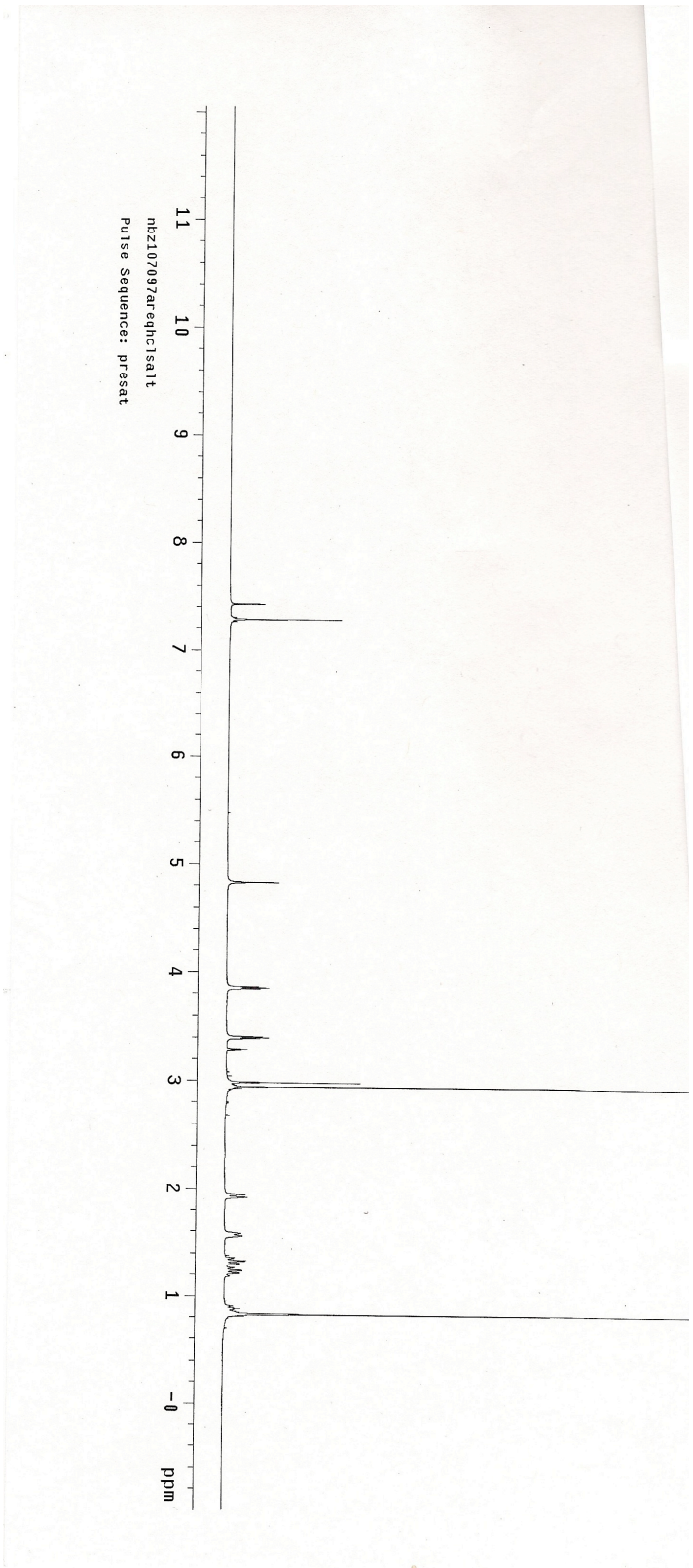

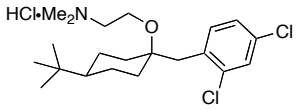

***cis*-1.13**
500 MHz, CD_3OD

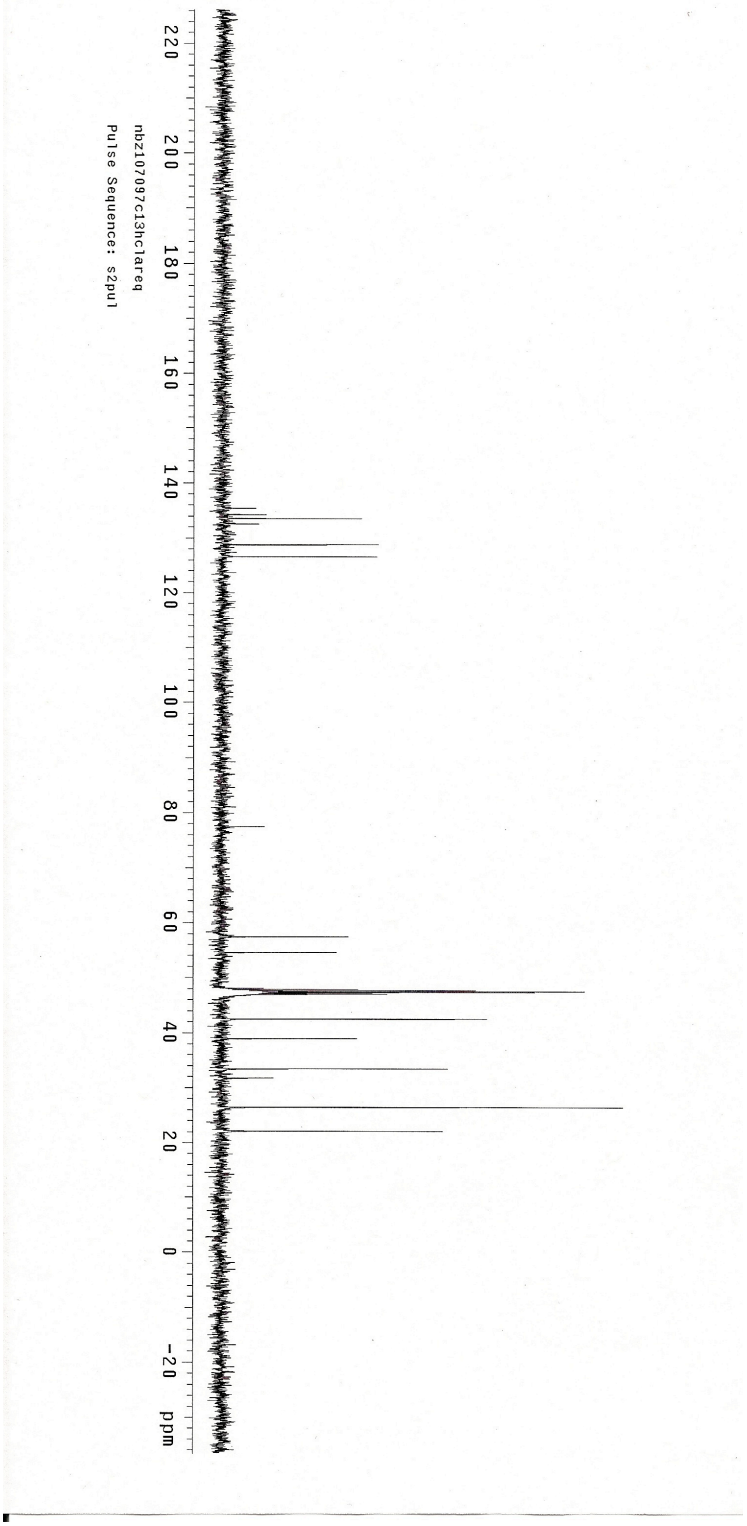

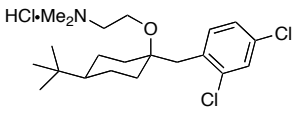

***cis*-1.13**
125 MHz, CD_3OD

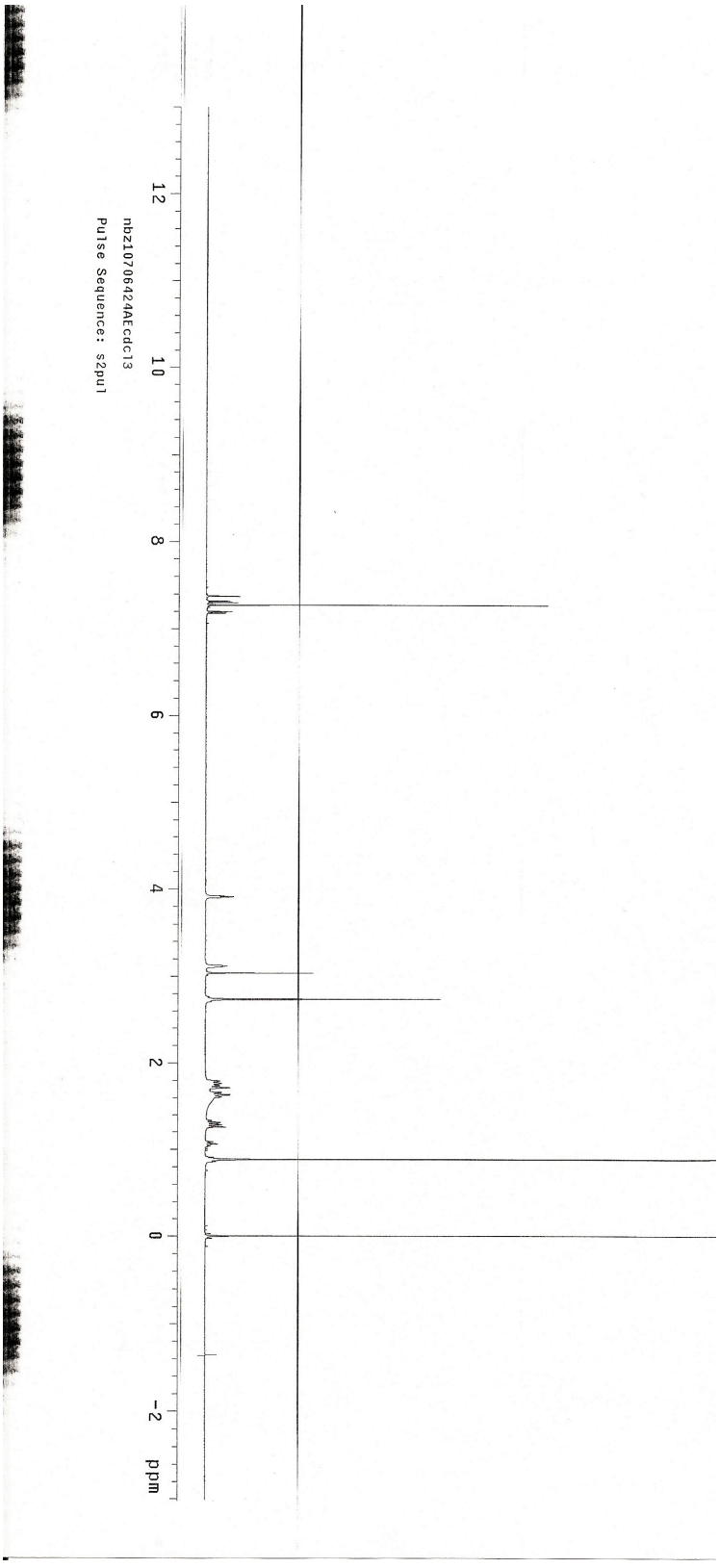

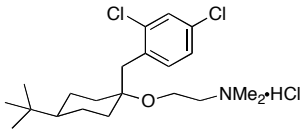

trans-**1.13**
500 MHz, $CDCl_3$

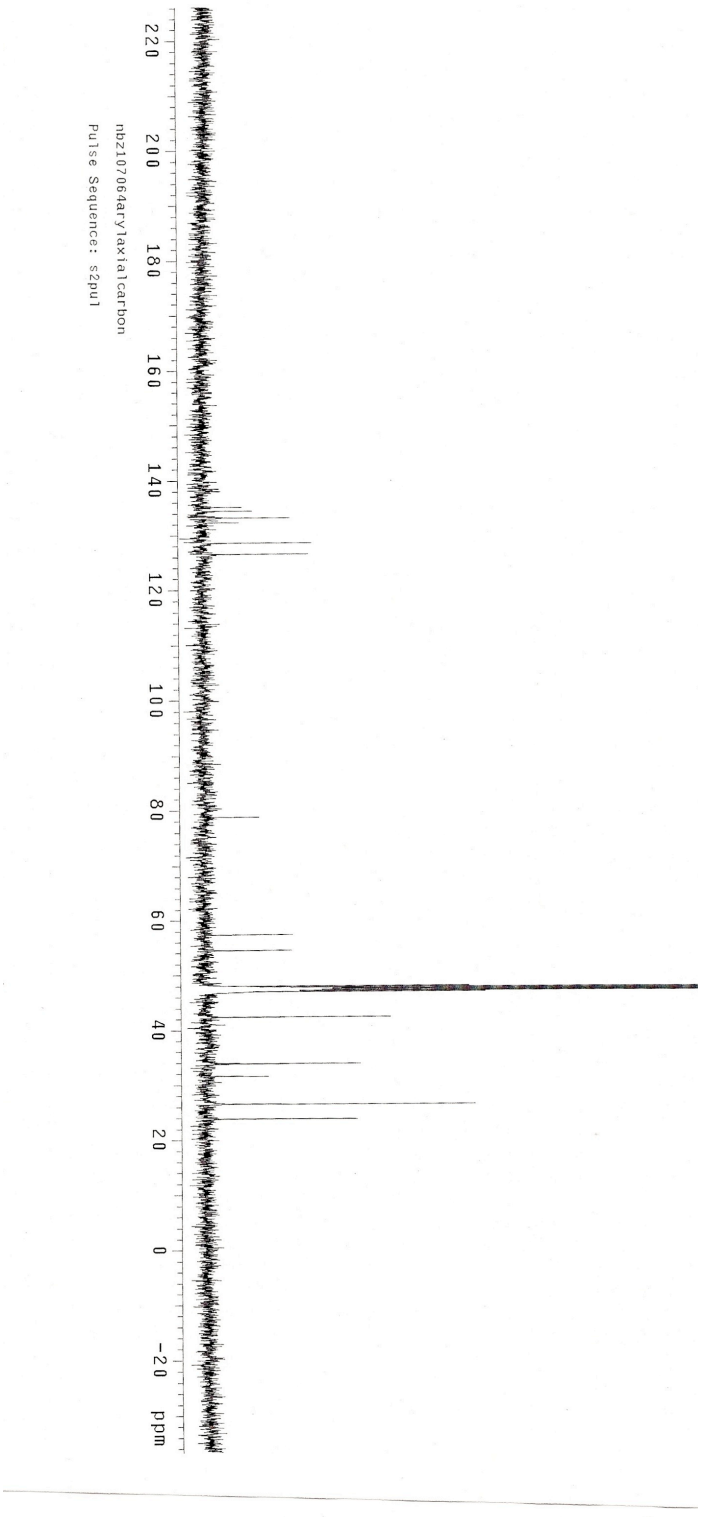

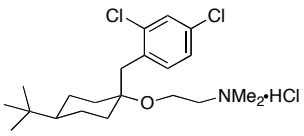

trans-**1.13**
125 MHz, CD_3OD

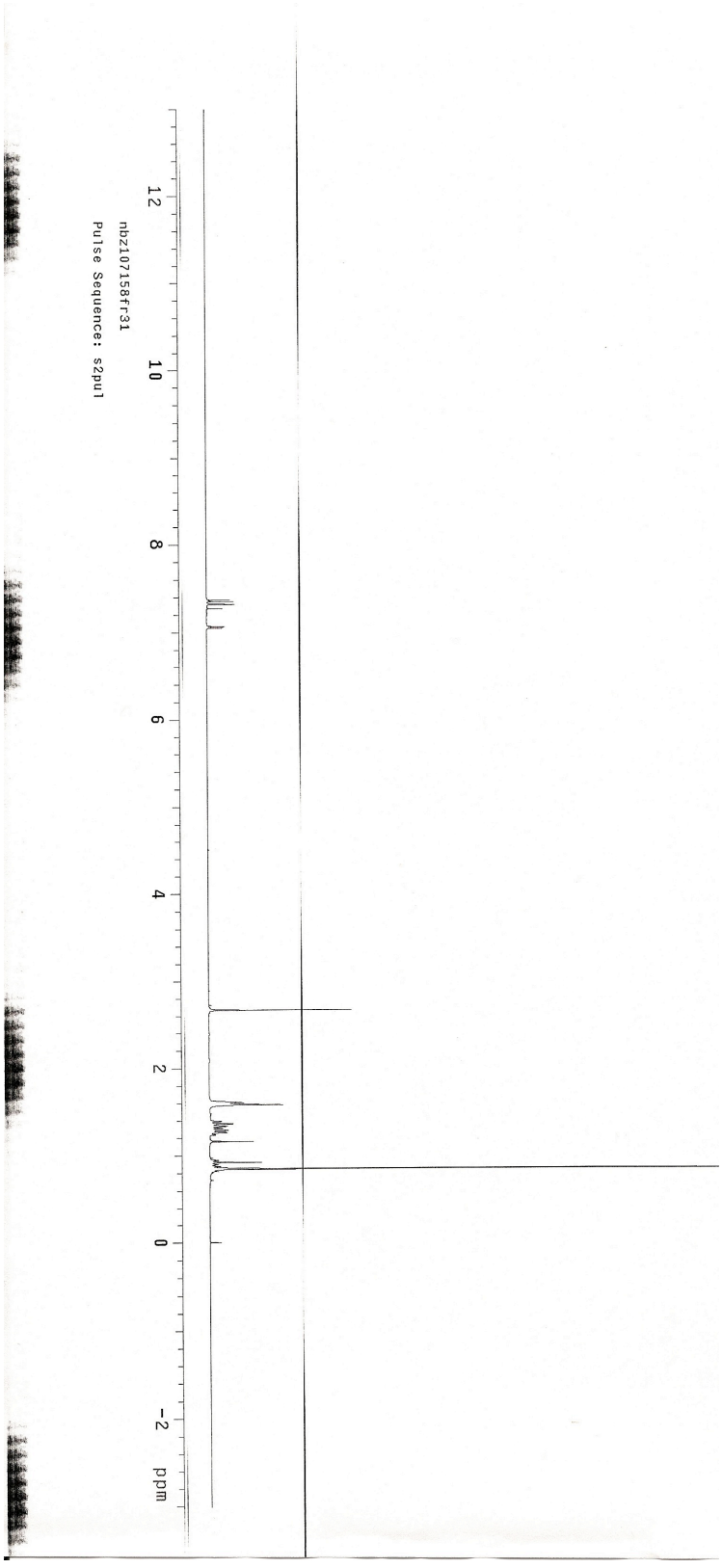

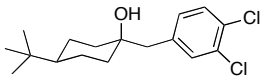

***cis*-1.20**
500 MHz, $CDCl_3$

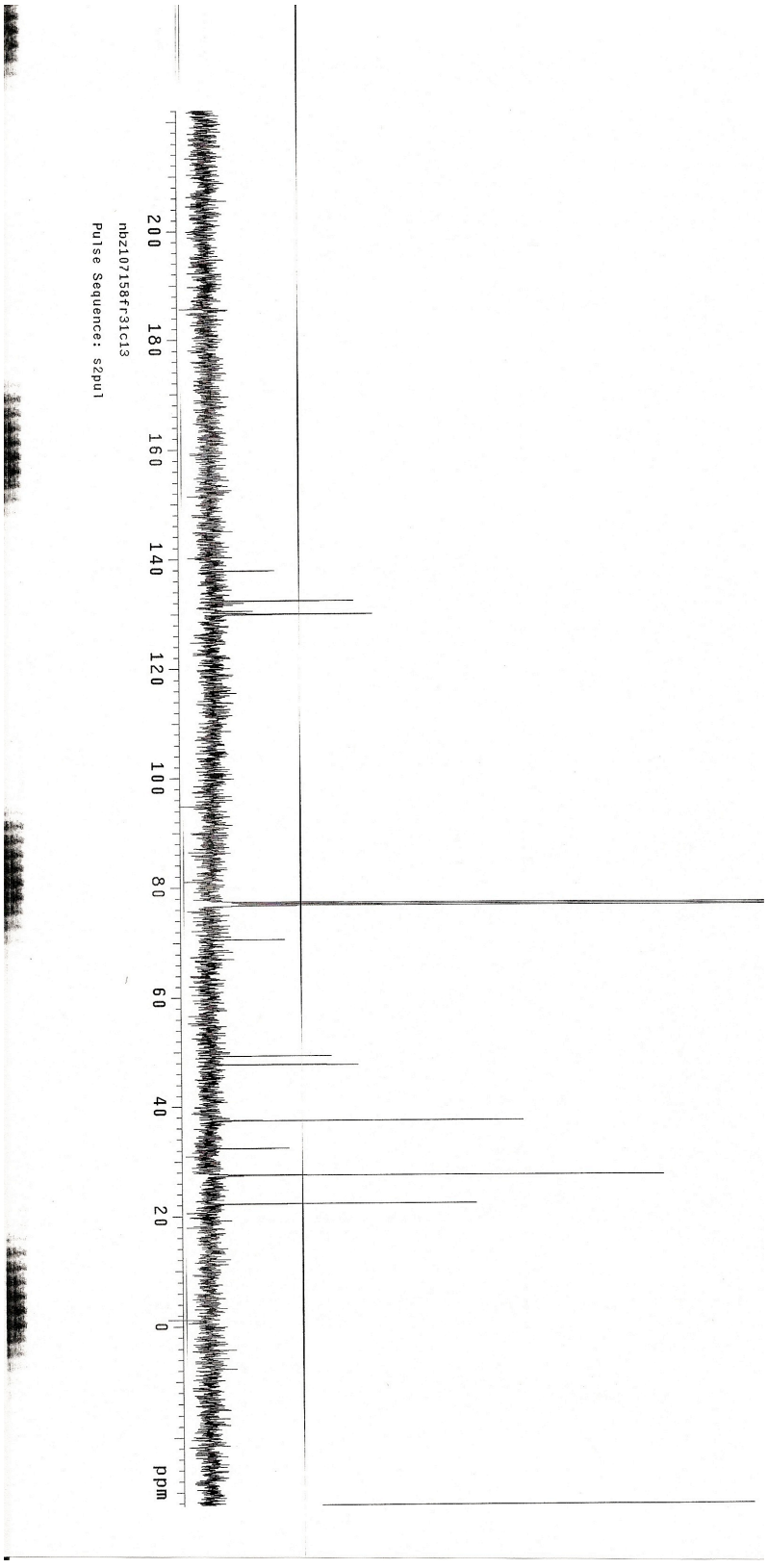

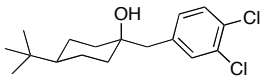

cis-**1.20**
125 MHz, $CDCl_3$

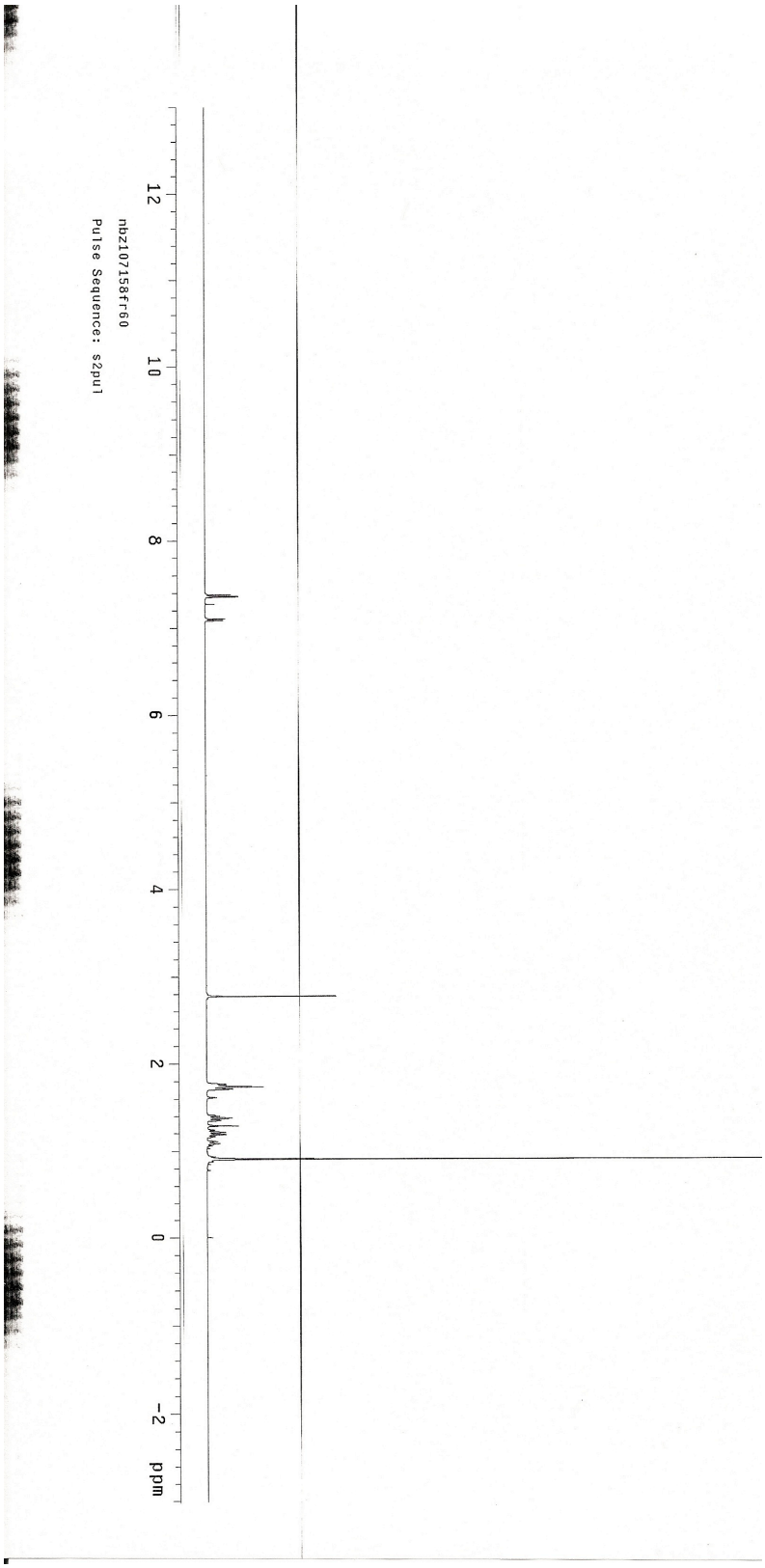

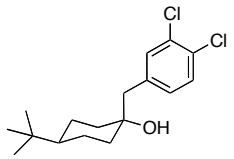

trans-**1.20**
500 MHz, $CDCl_3$

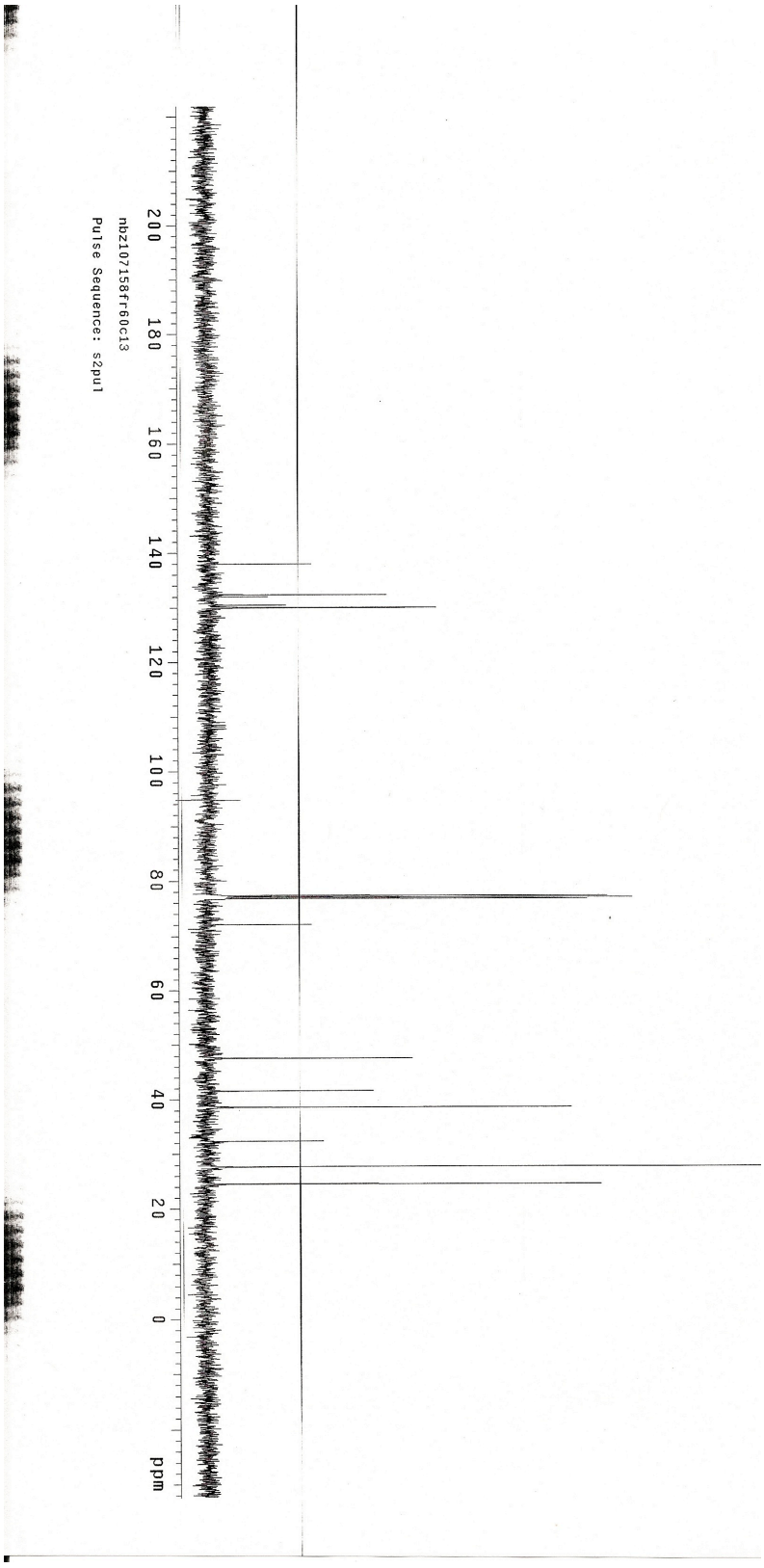

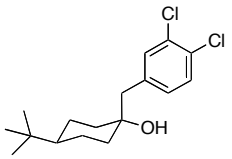

trans-**1.20**
125 MHz, $CDCl_3$

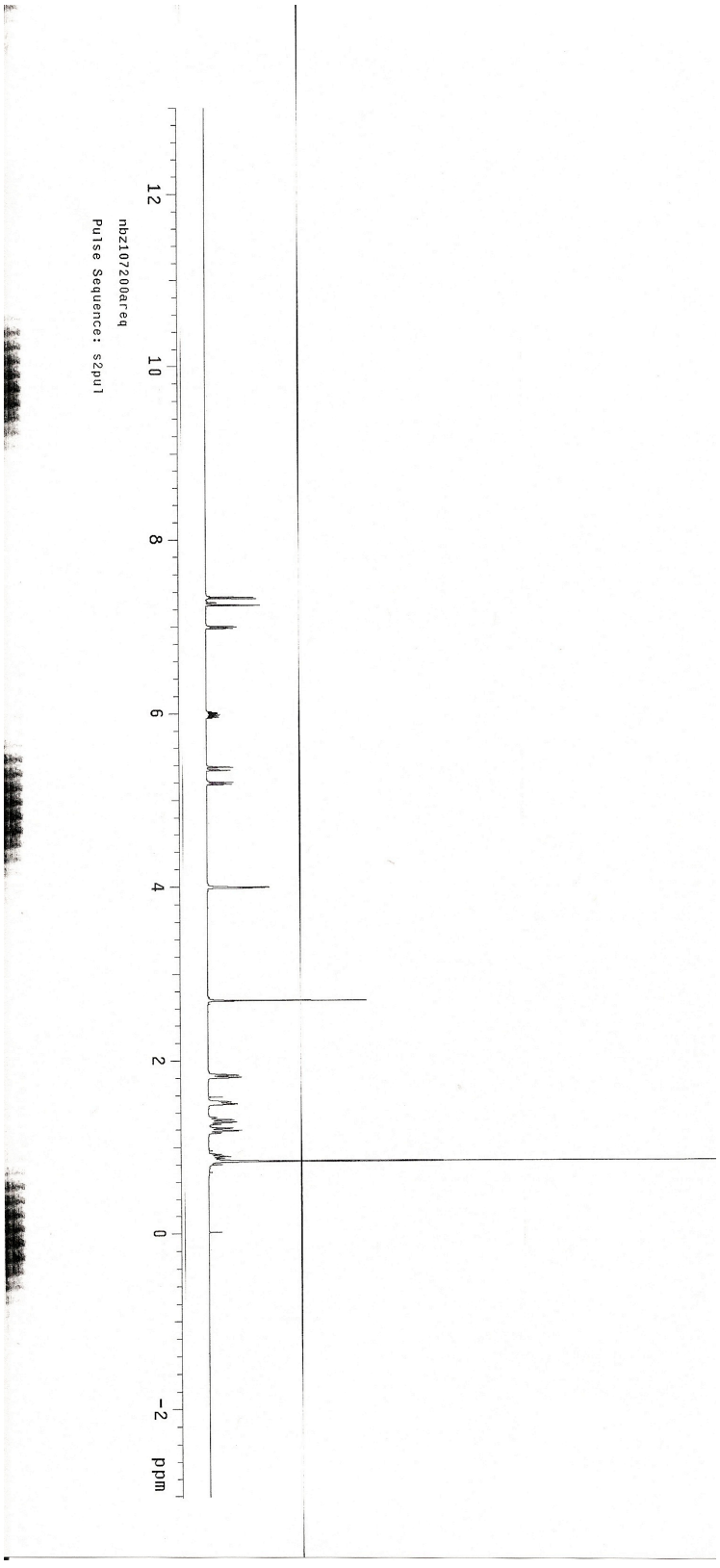

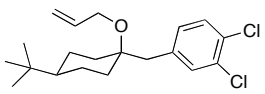

***cis*-1.21**
500 MHz, $CDCl_3$

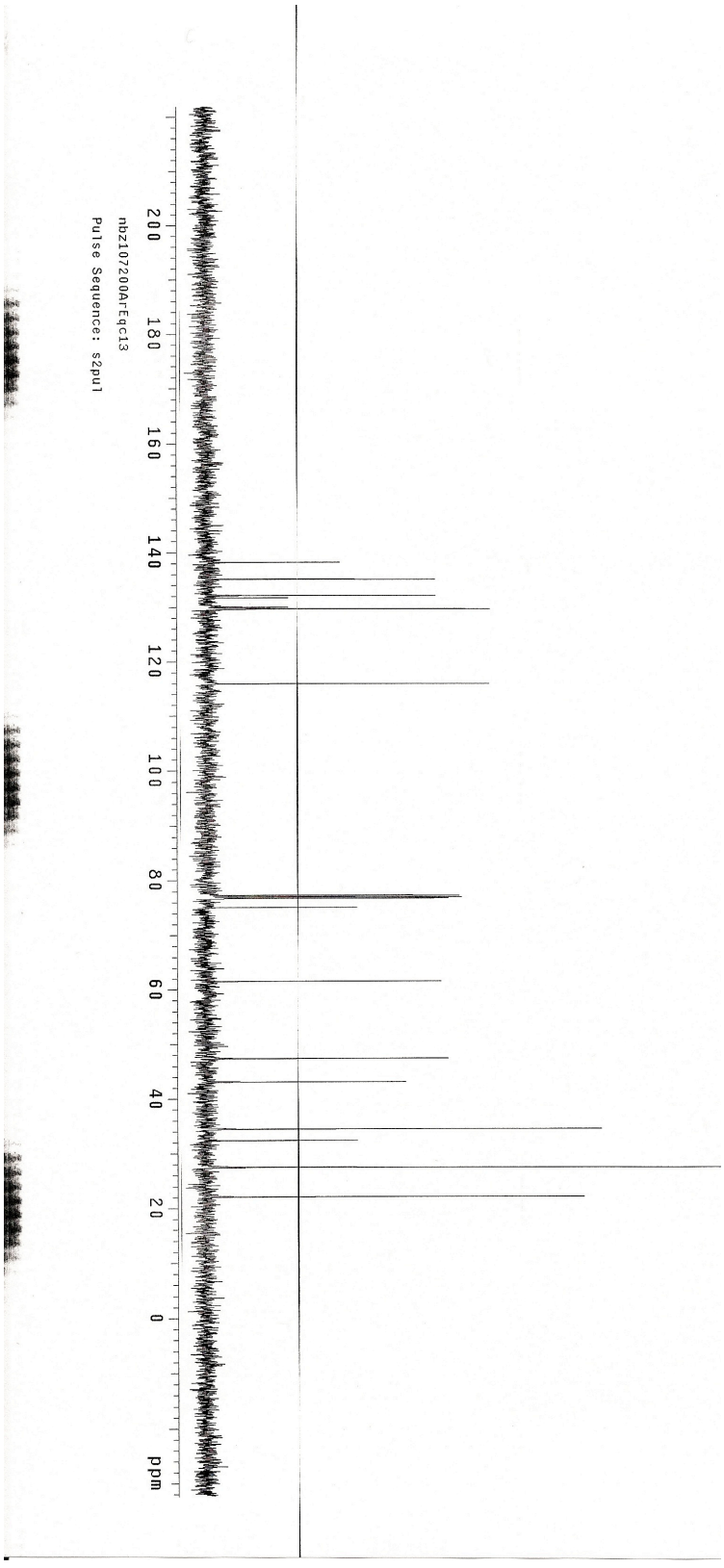

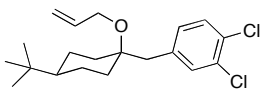

cis-**1.21**
125 MHz, $CDCl_3$

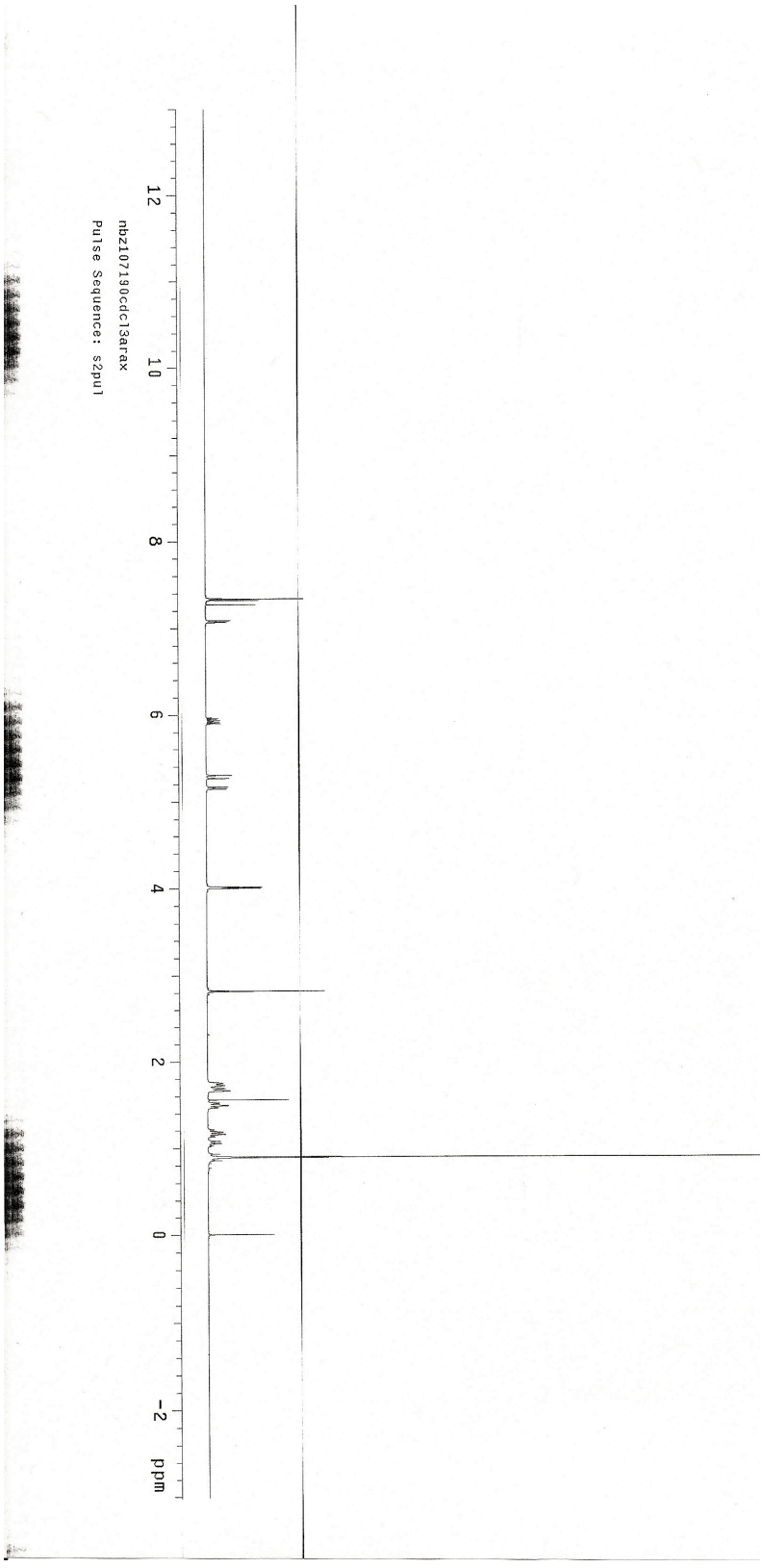

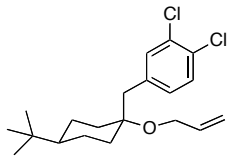

trans-**1.21**
500 MHz, $CDCl_3$

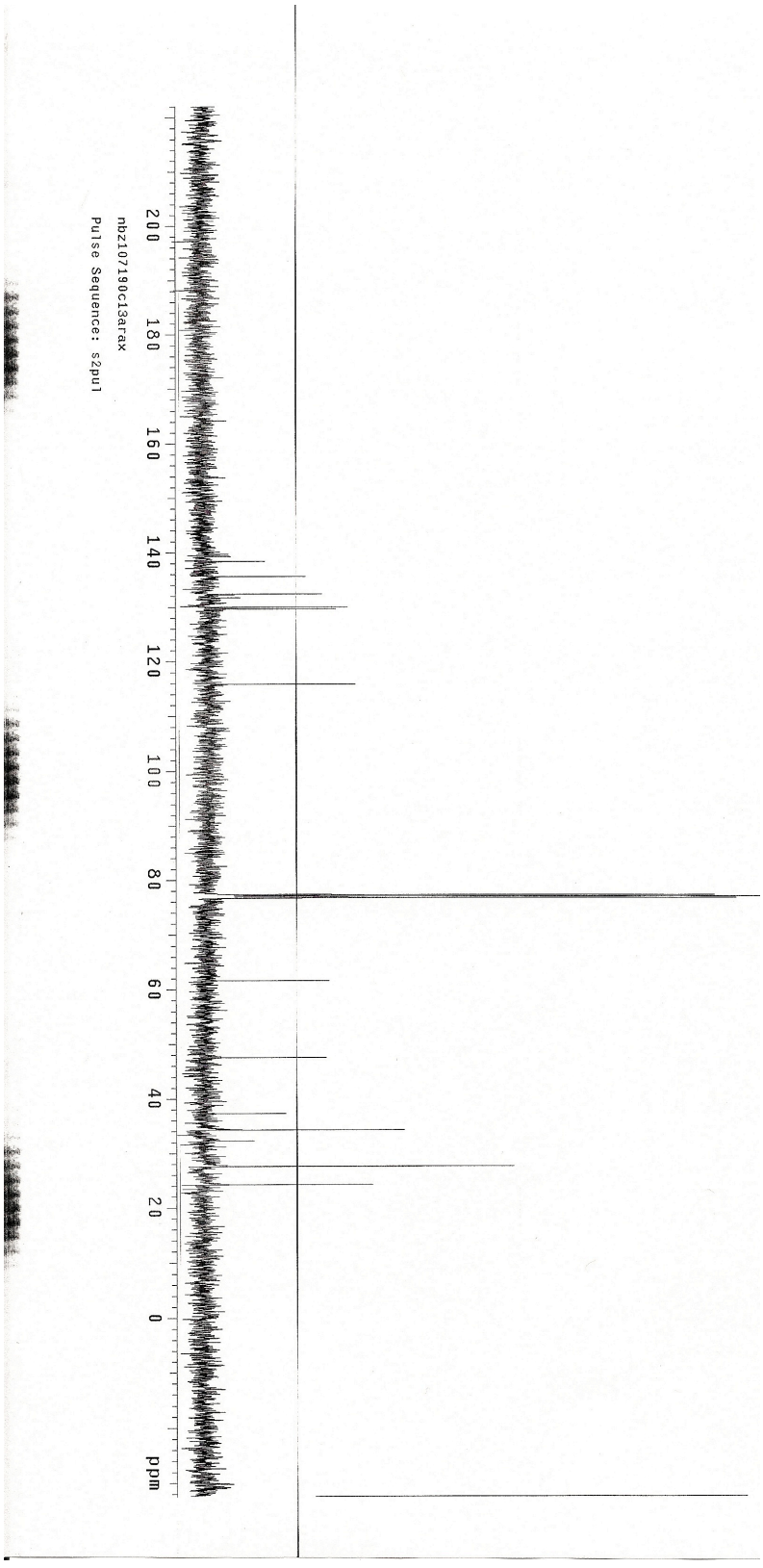

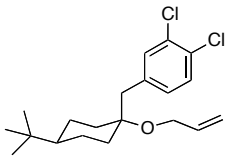

trans-**1.21**
125 MHz, $CDCl_3$

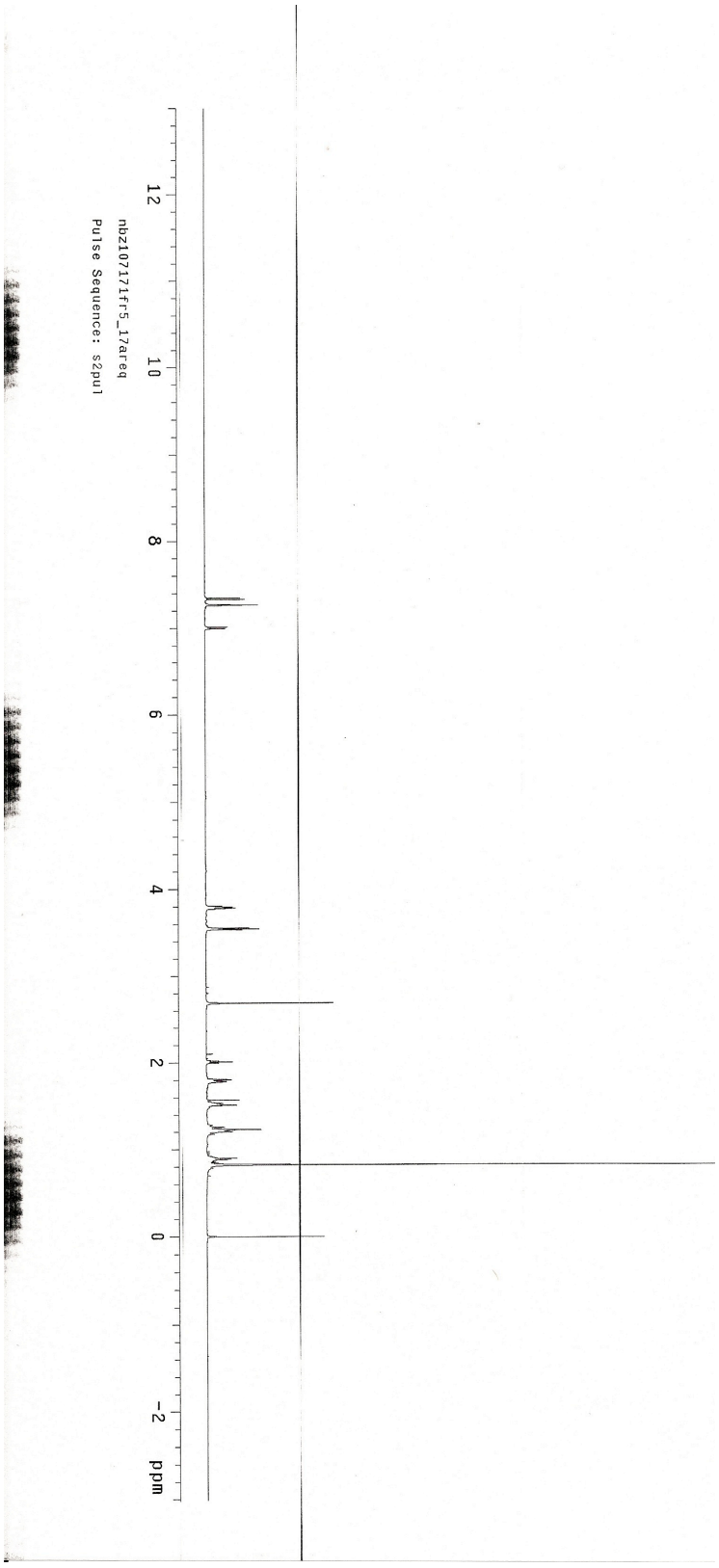

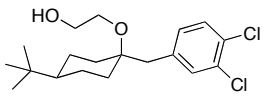

cis-**1.22**
500 MHz, $CDCl_3$

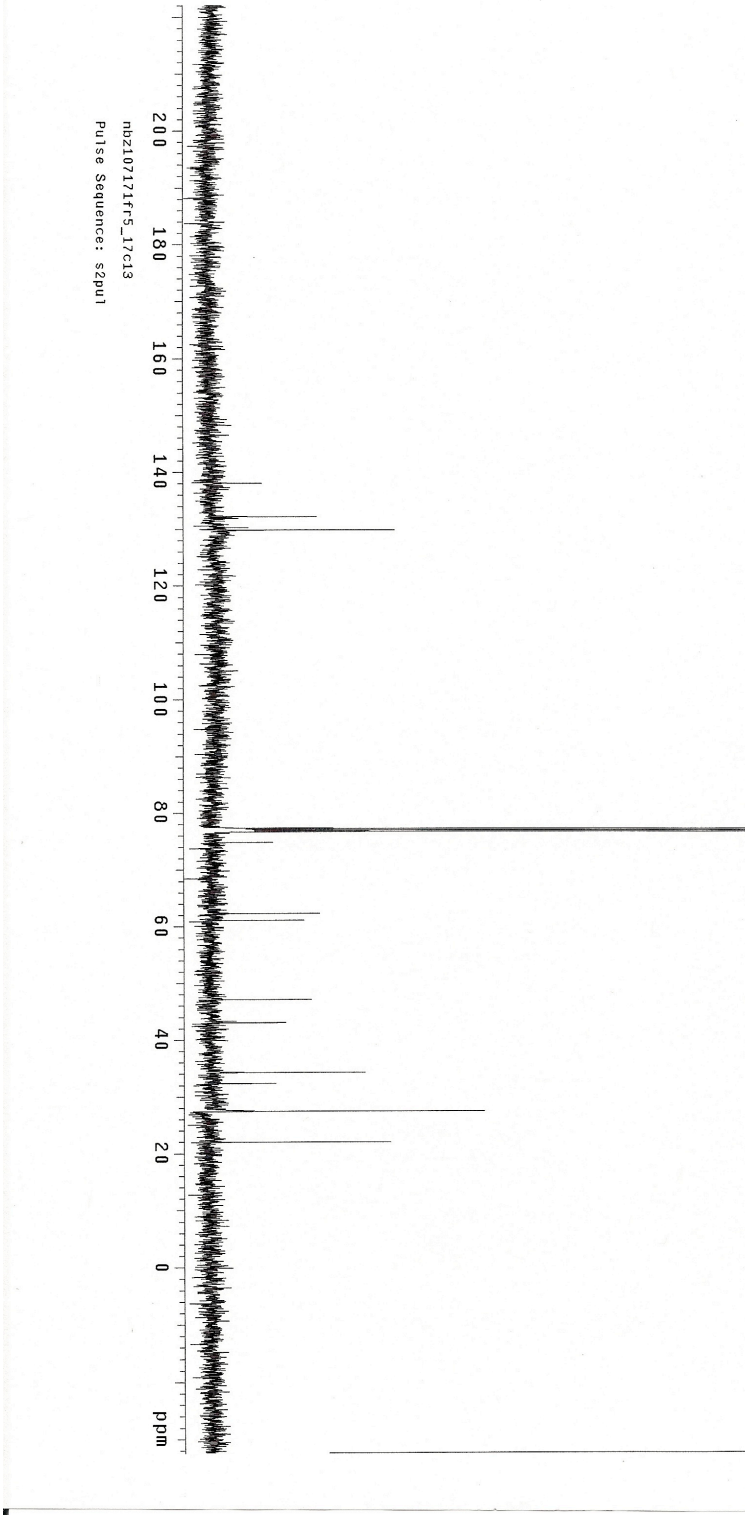

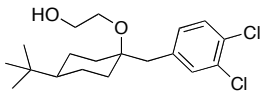

***cis*-1.22**
125 MHz, $CDCl_3$

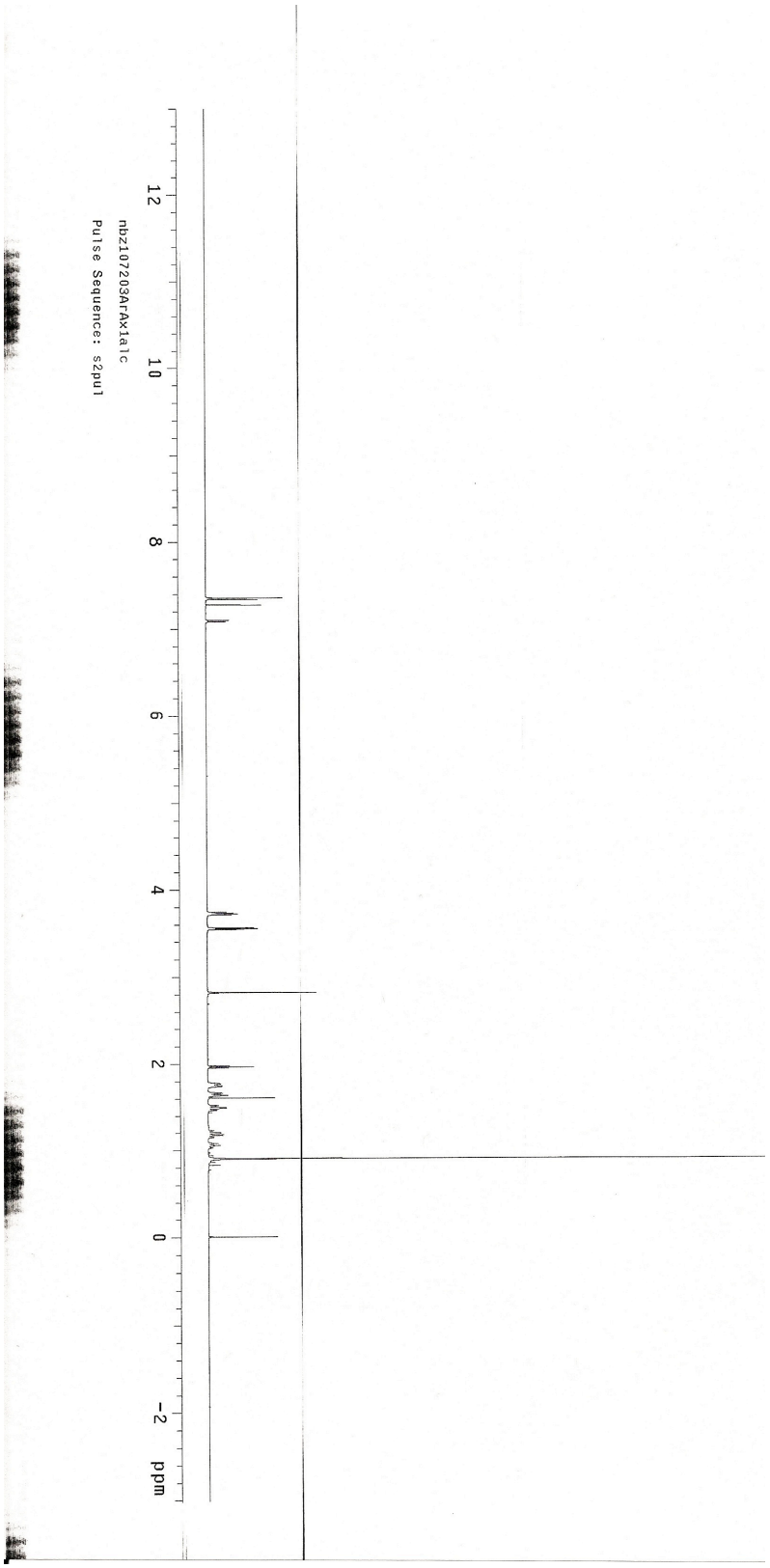

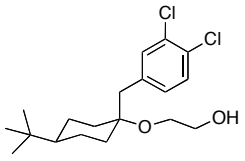

trans-**1.22**
500 MHz, $CDCl_3$

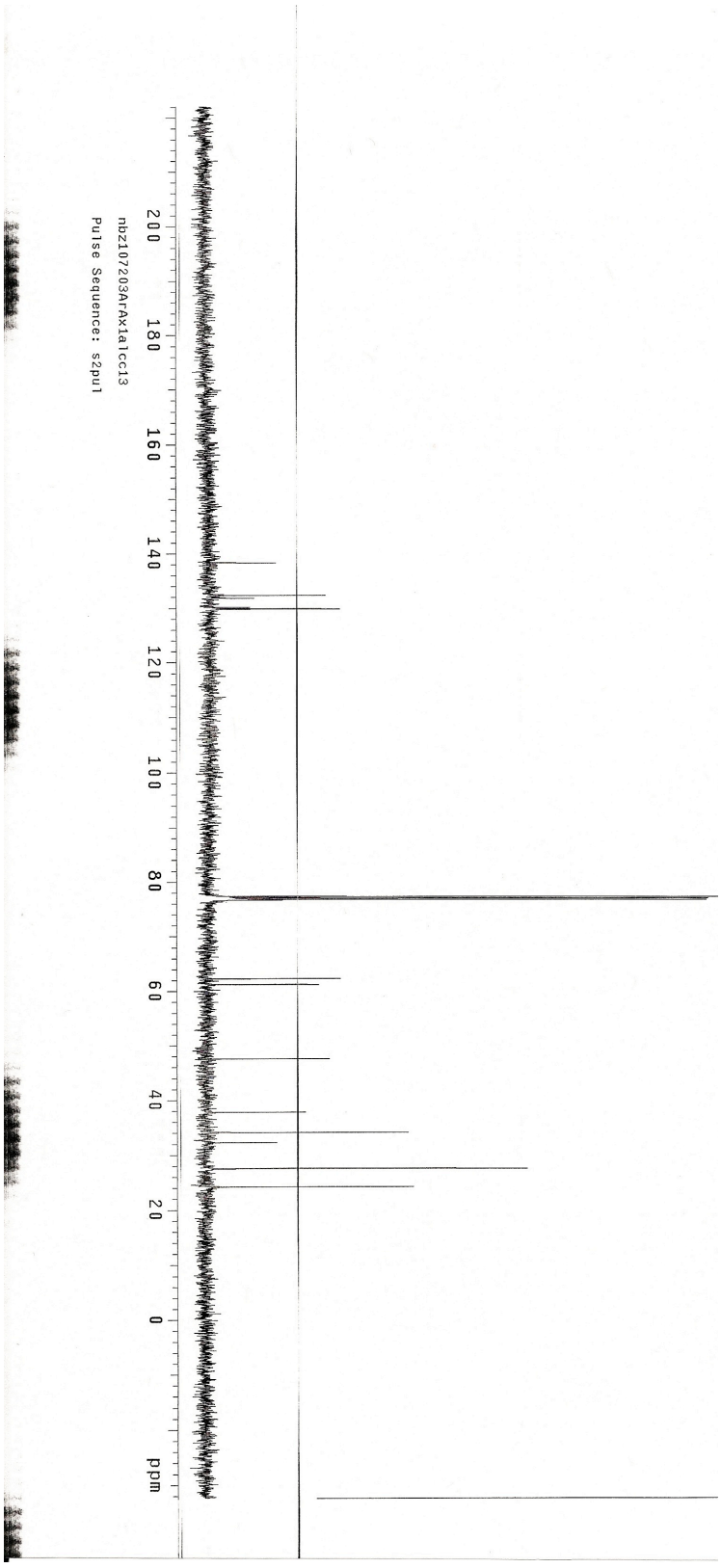

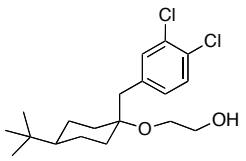

trans-**1.22**
125 MHz, $CDCl_3$

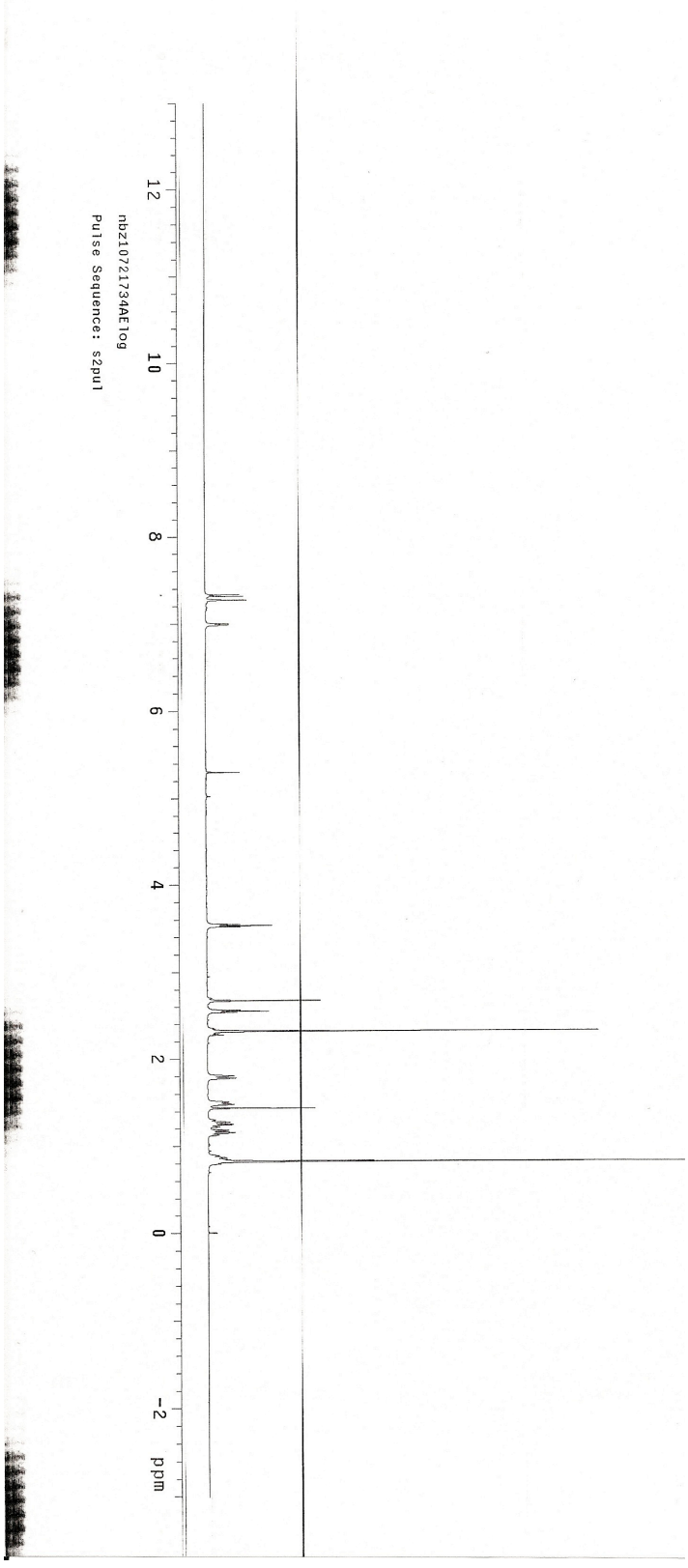

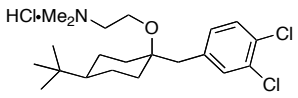

***cis*-1.23**
500 MHz, $CDCl_3$

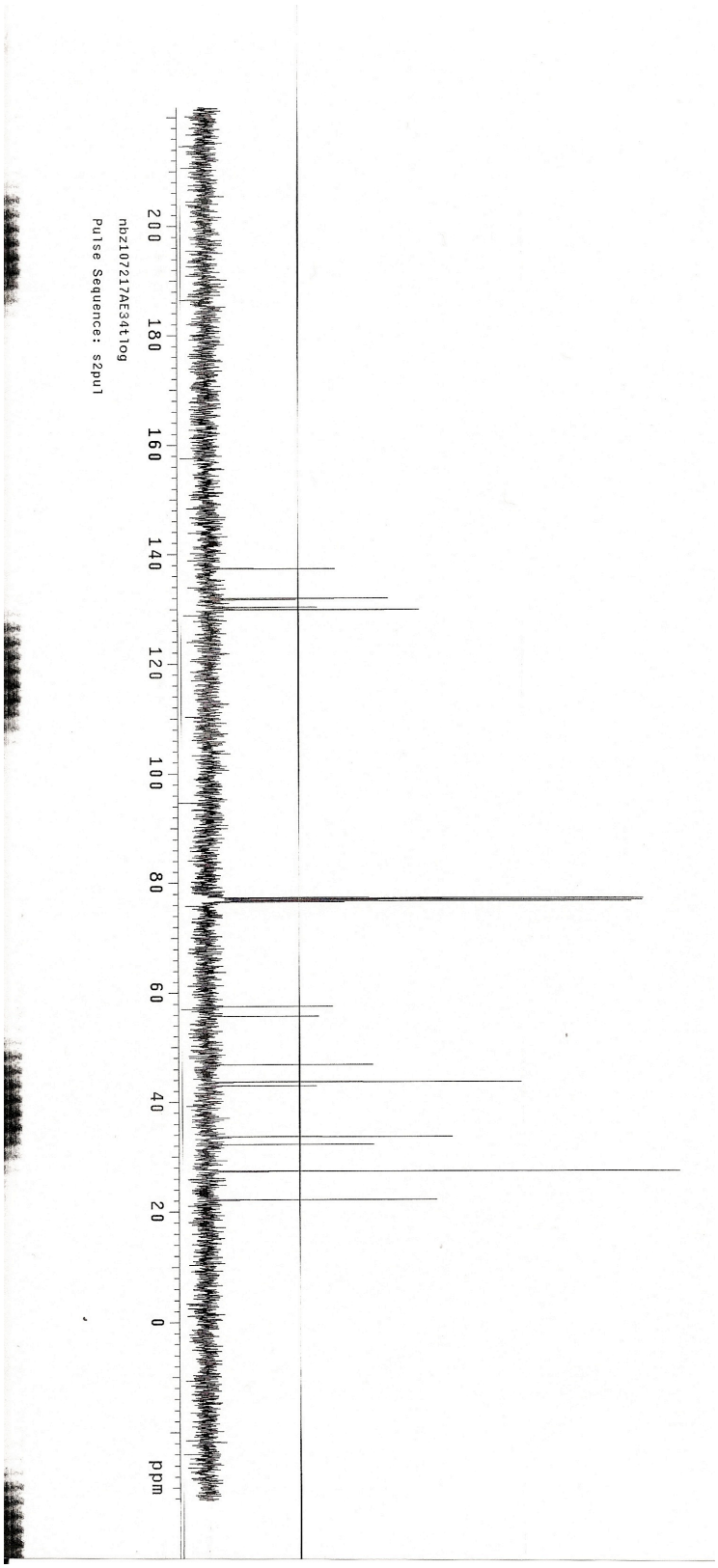

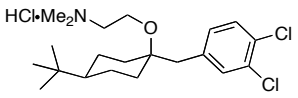

***cis*-1.23**
125 MHz, $CDCl_3$

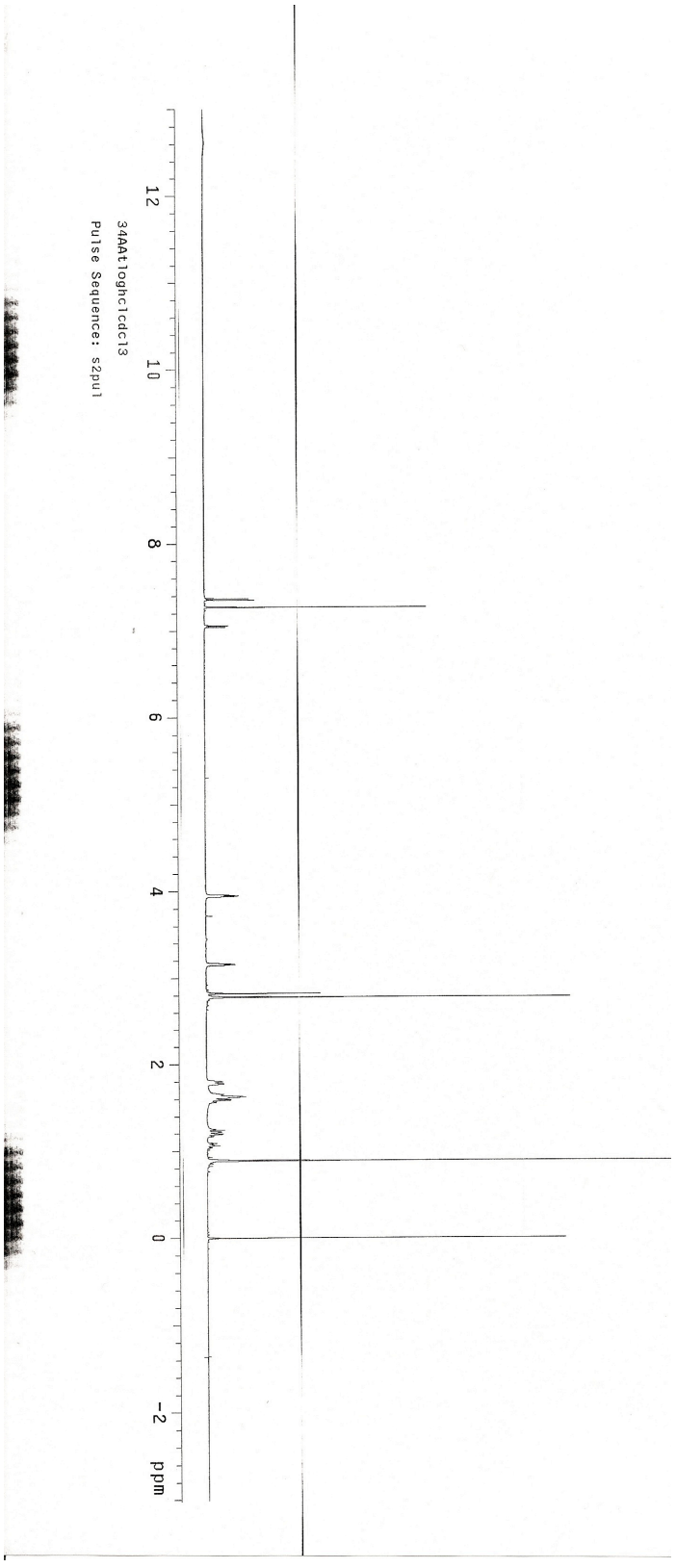

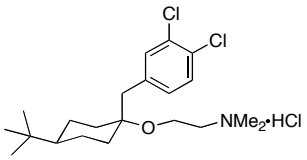

trans-**1.23**
500 MHz, $CDCl_3$

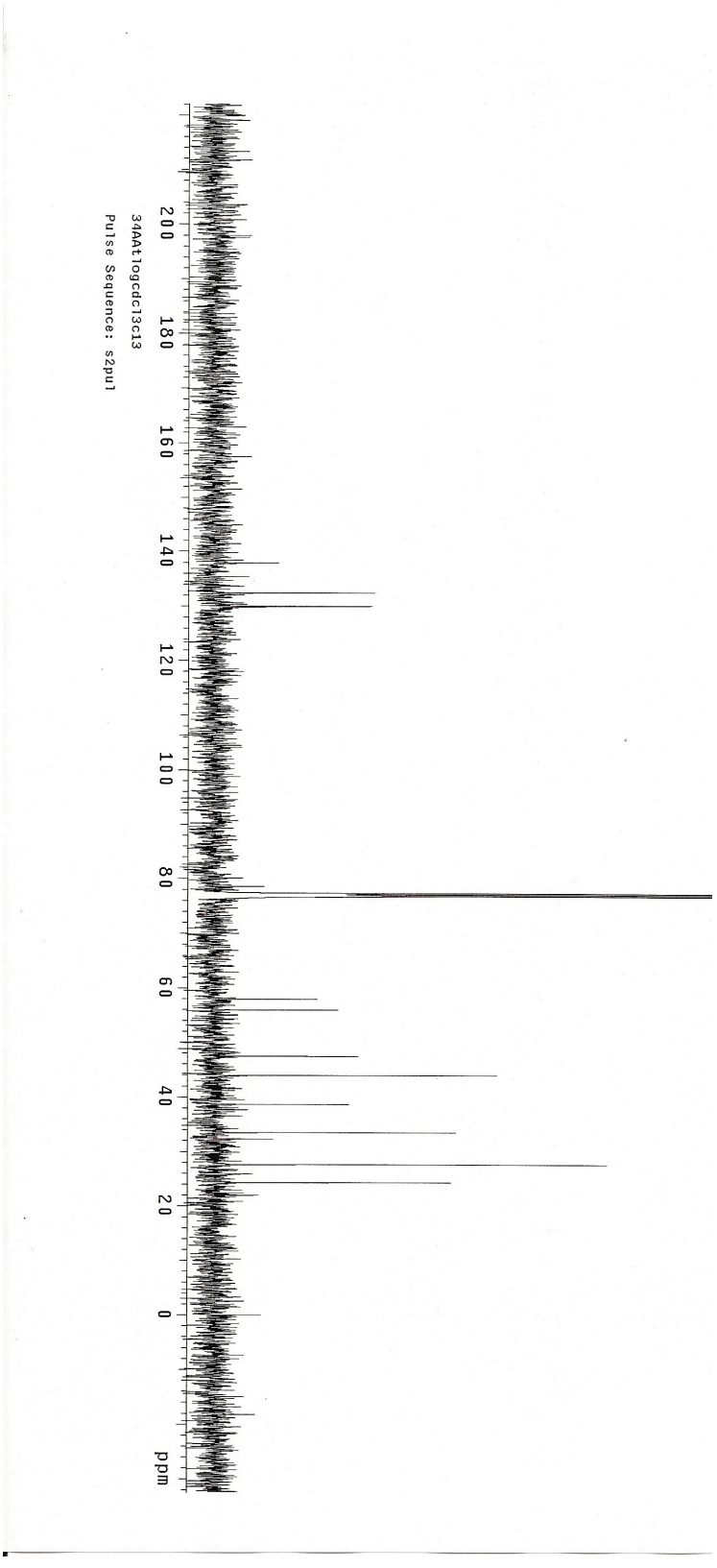

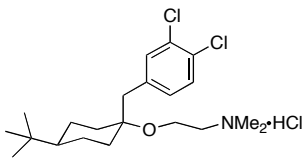

trans-**1.23**
125 MHz, $CDCl_3$

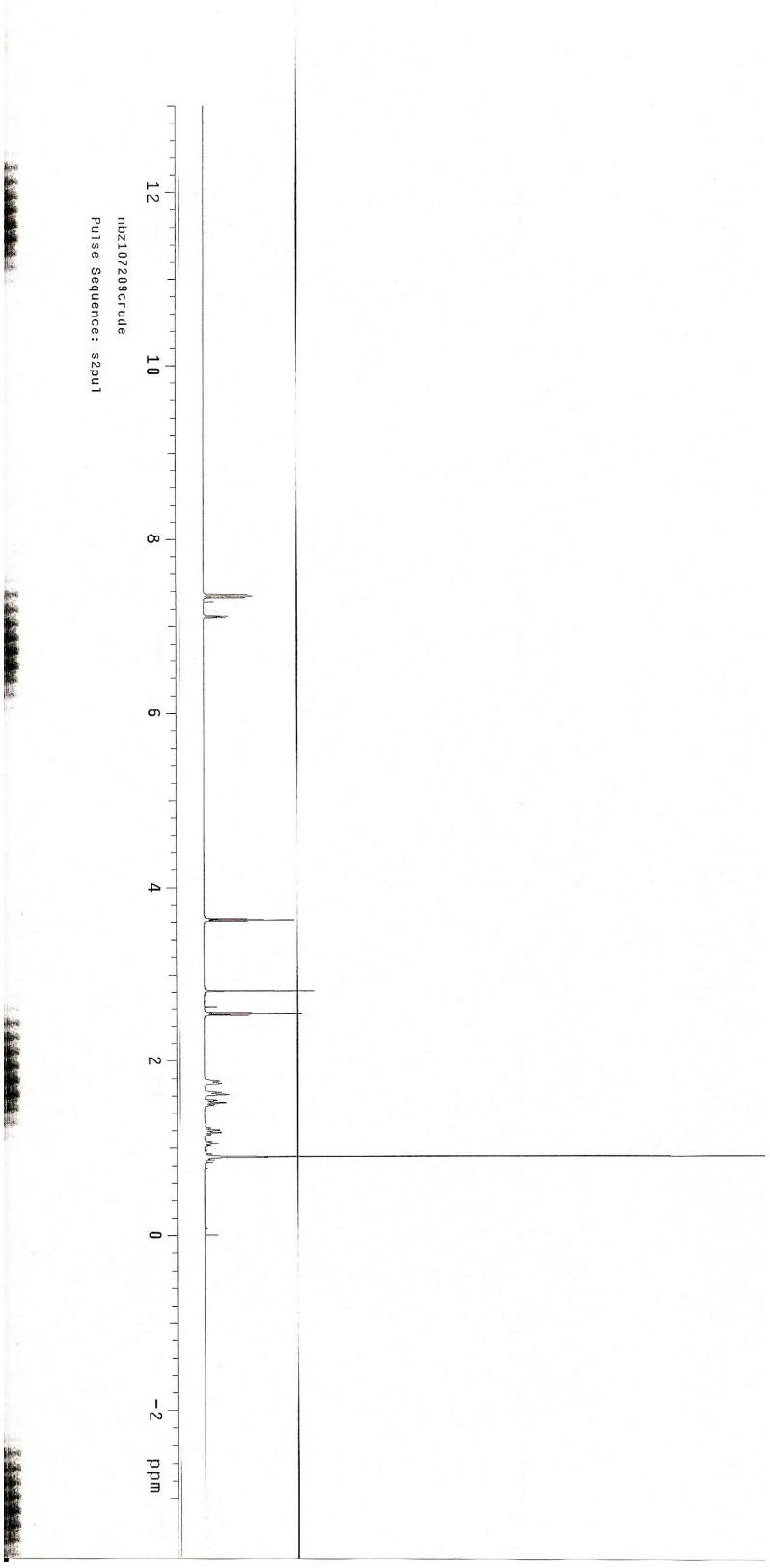

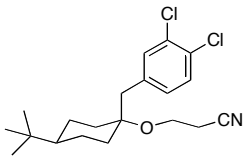

1.24
500 MHz, $CDCl_3$

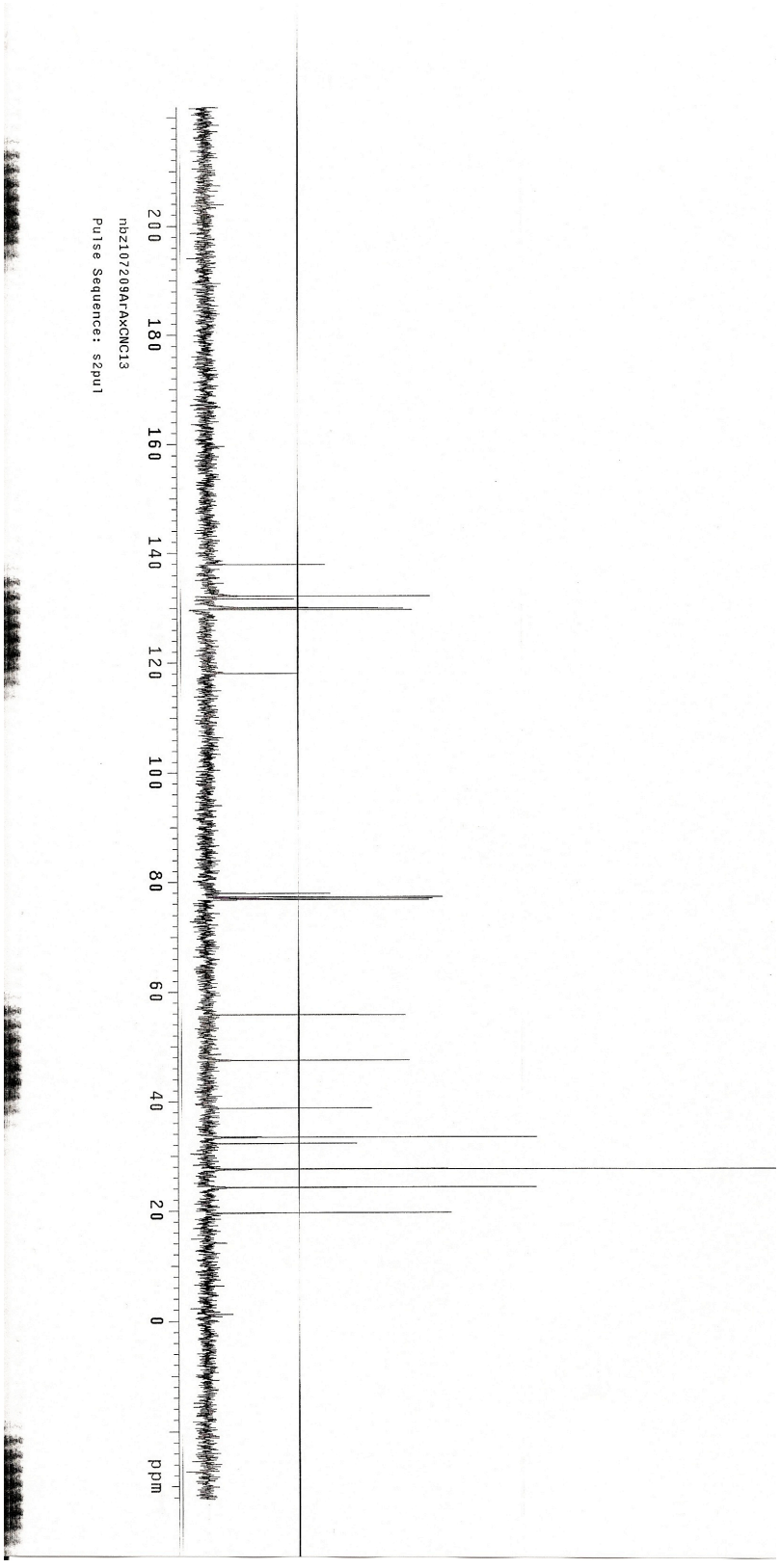

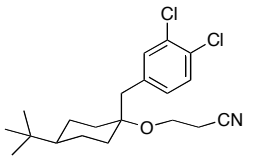

1.24
125 MHz, $CDCl_3$

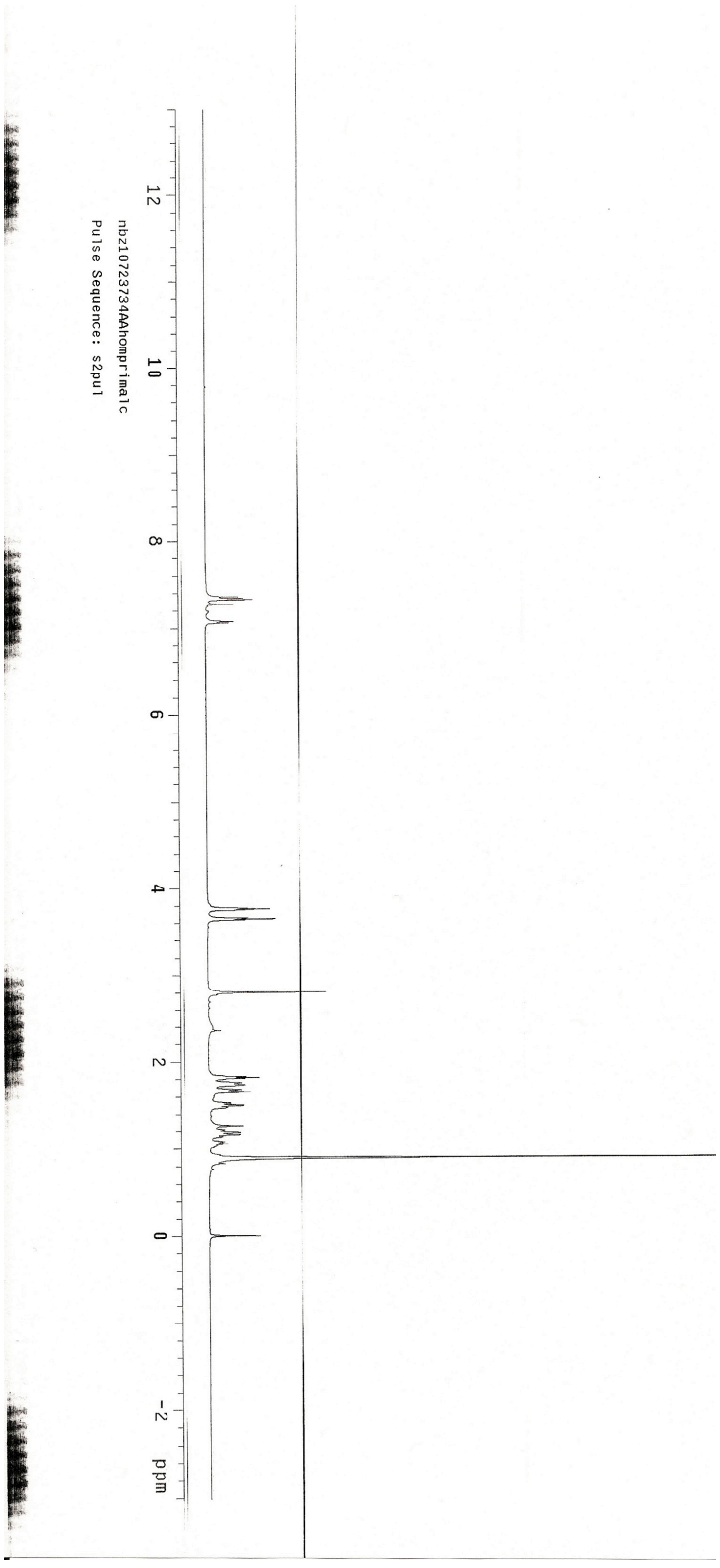

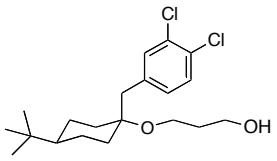

1.25
500 MHz, $CDCl_3$

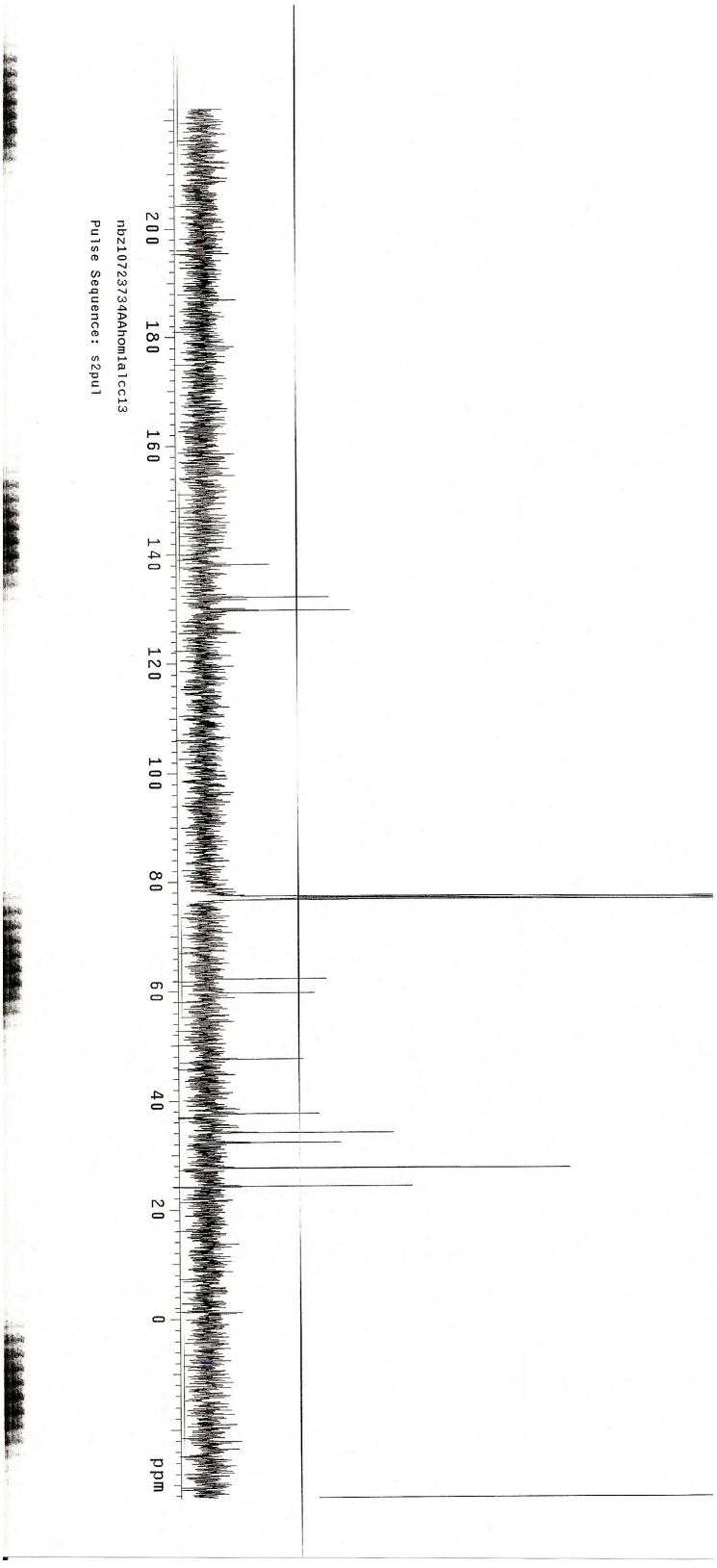

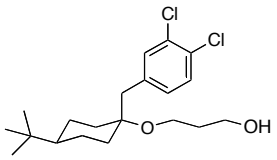

1.25
125 MHz, $CDCl_3$

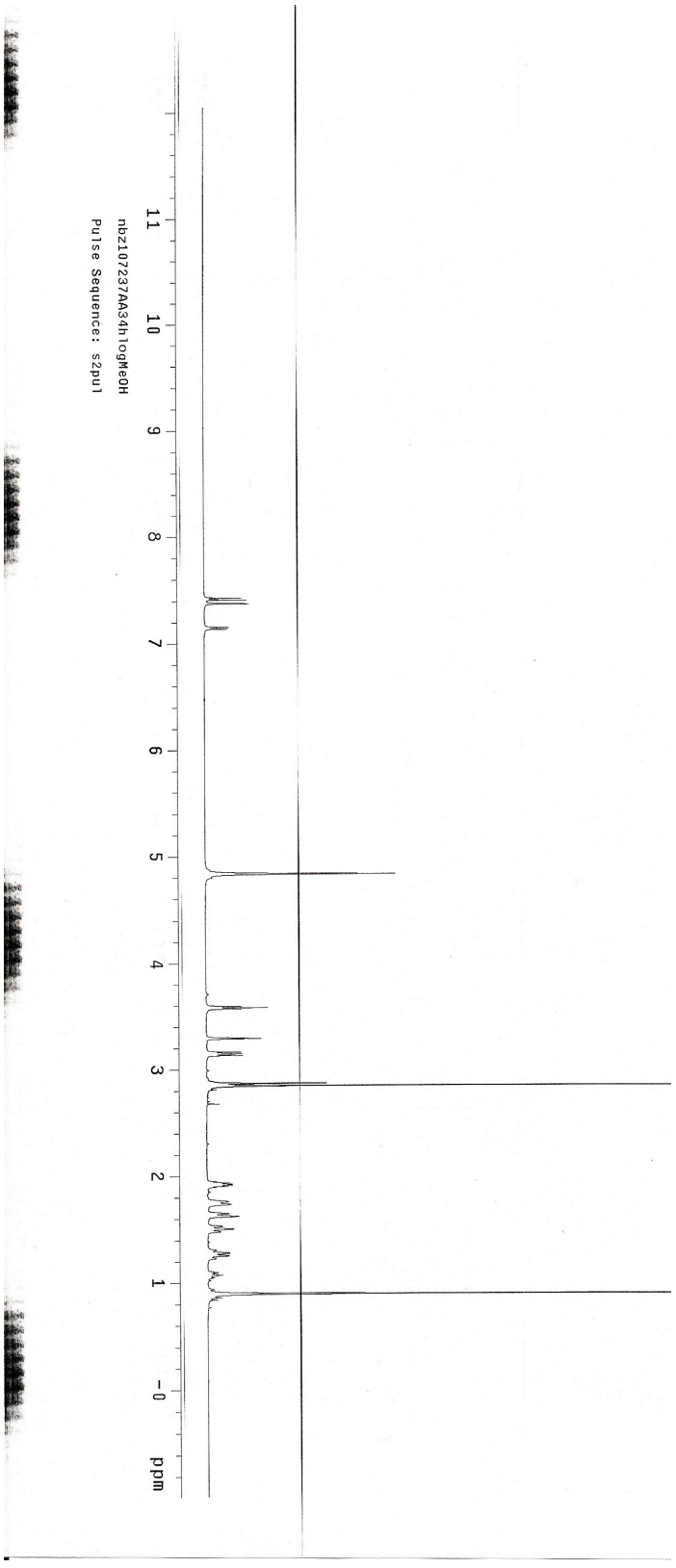

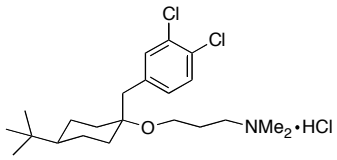

1.26
500 MHz, CD_3OD

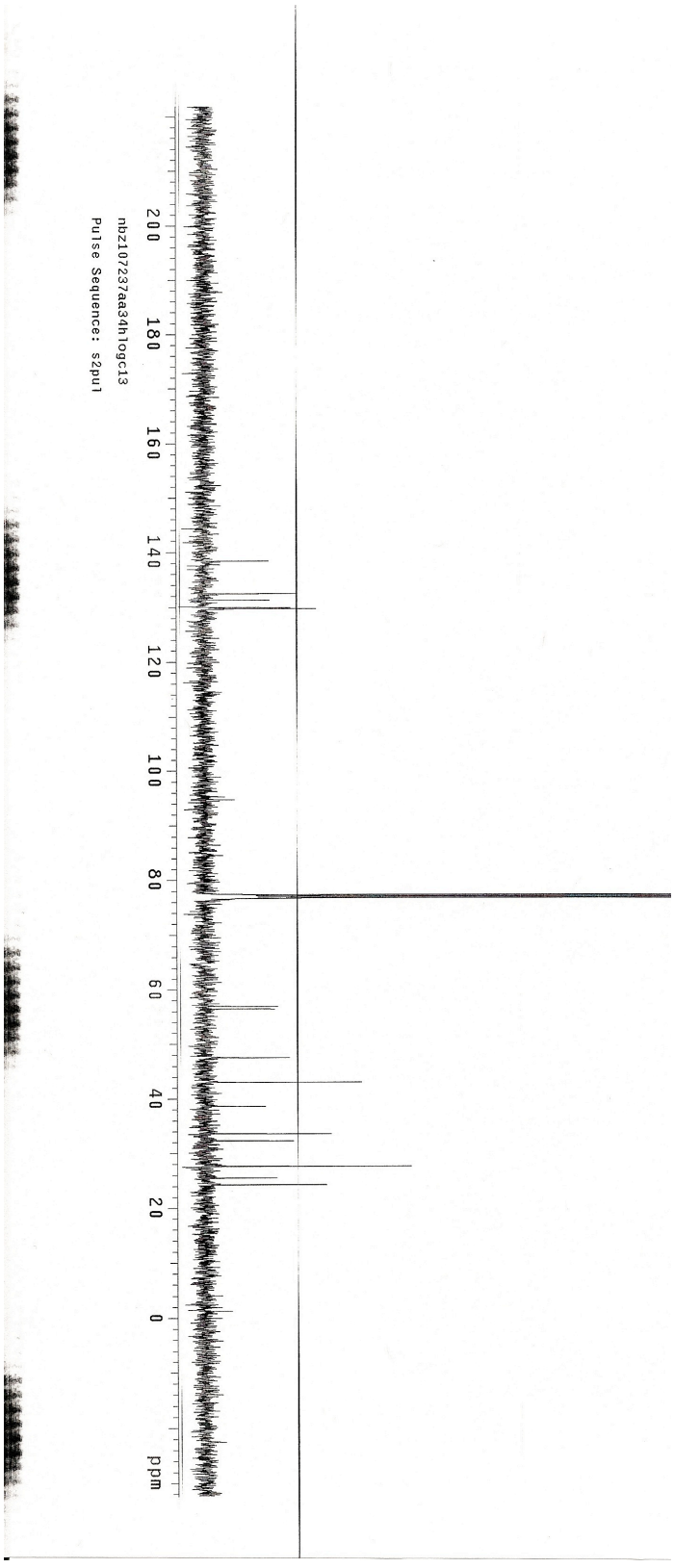

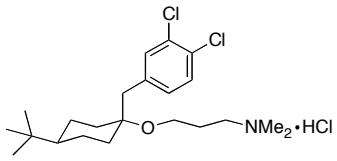

1.26
125 MHz, $CDCl_3$

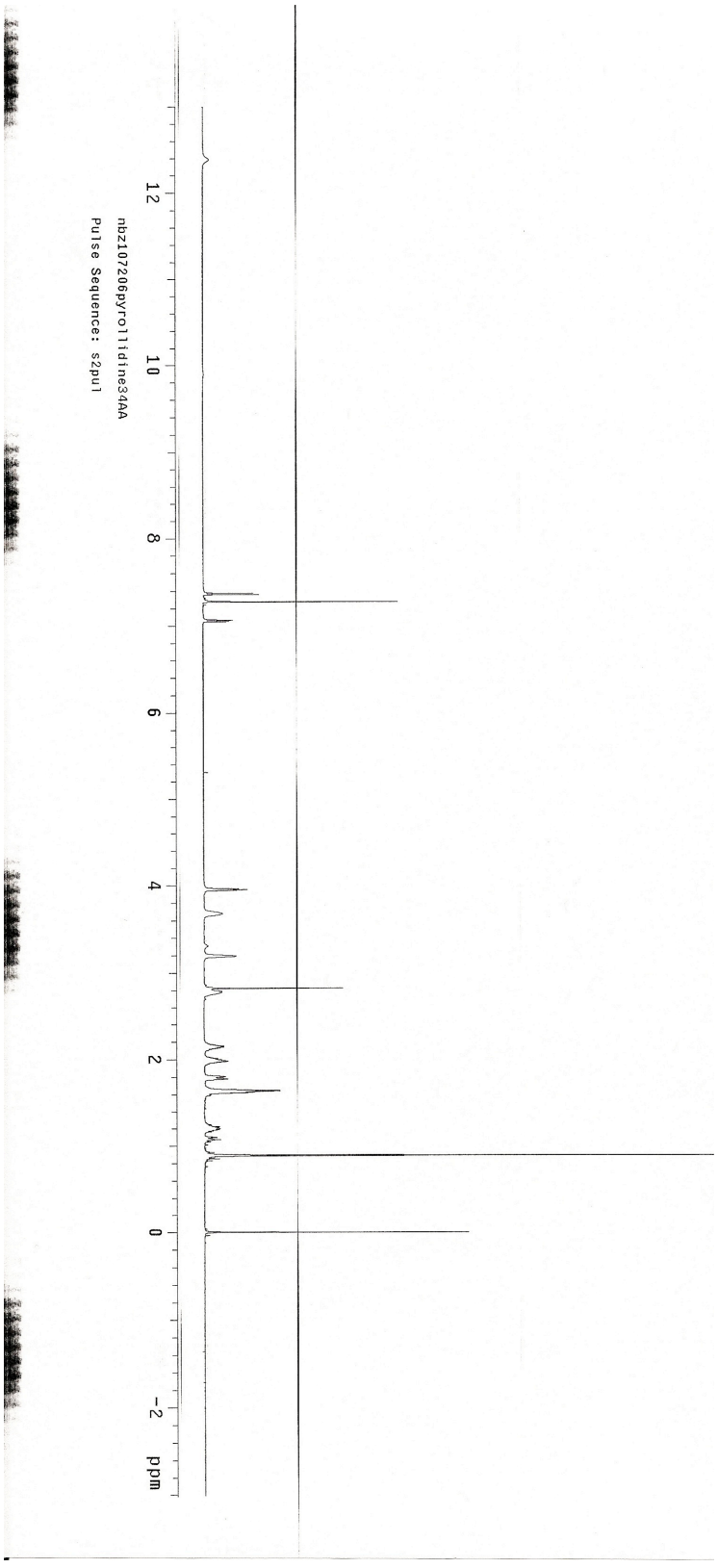

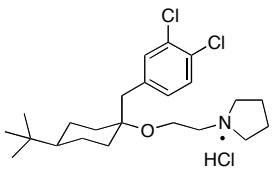

1.27
500 MHz, $CDCl_3$

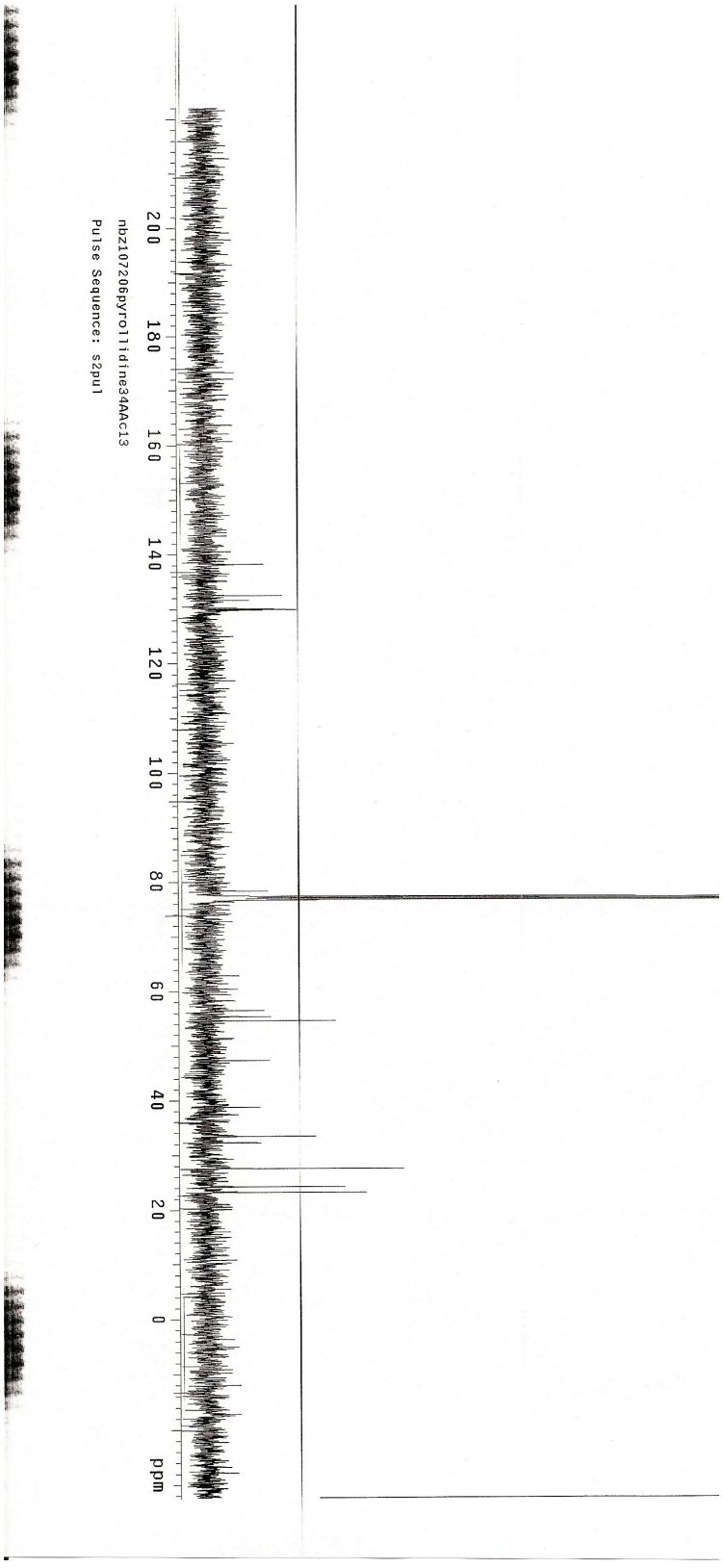

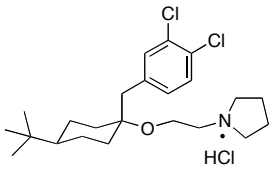

1.27
125 MHz, $CDCl_3$

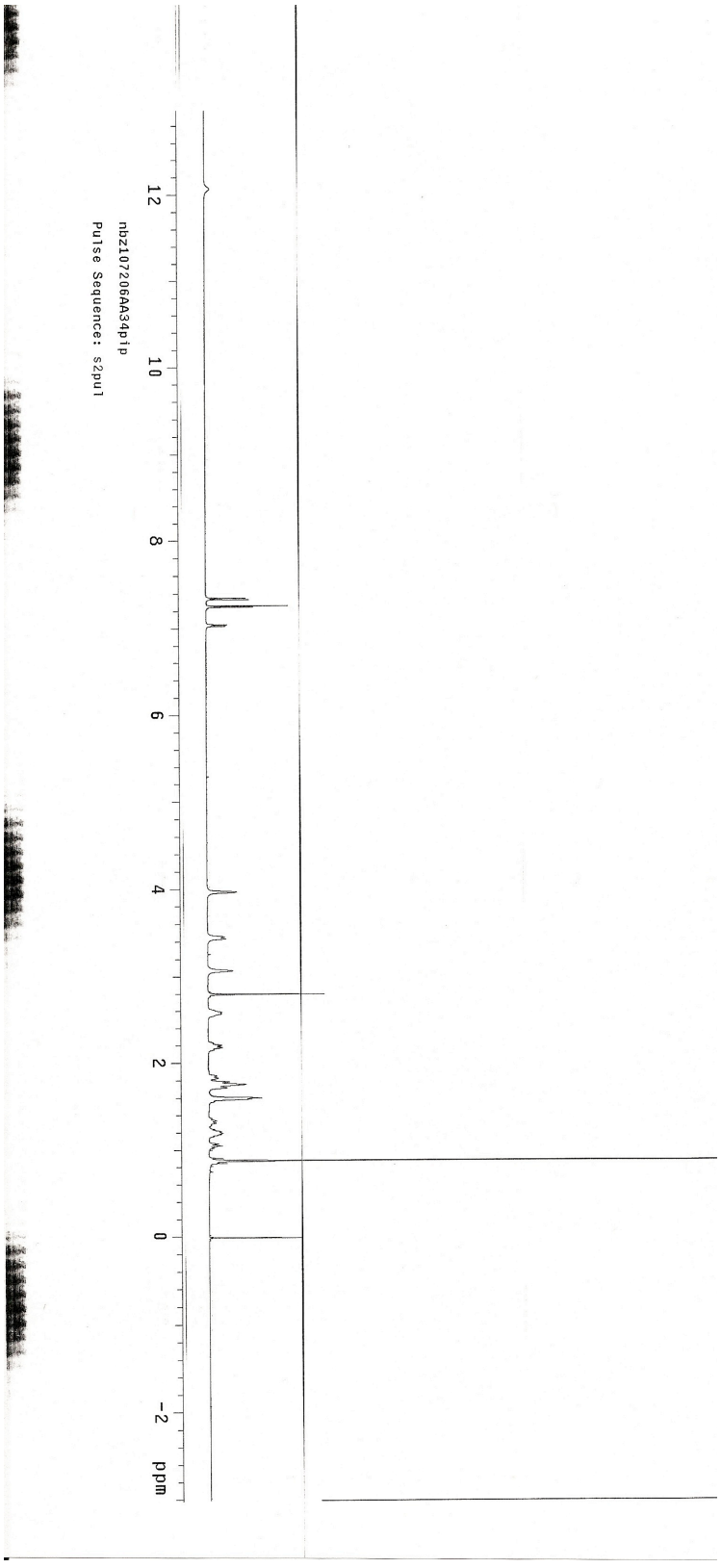

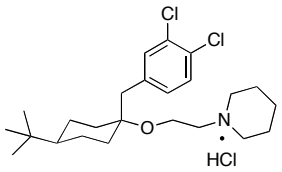

1.28
500 MHz, $CDCl_3$

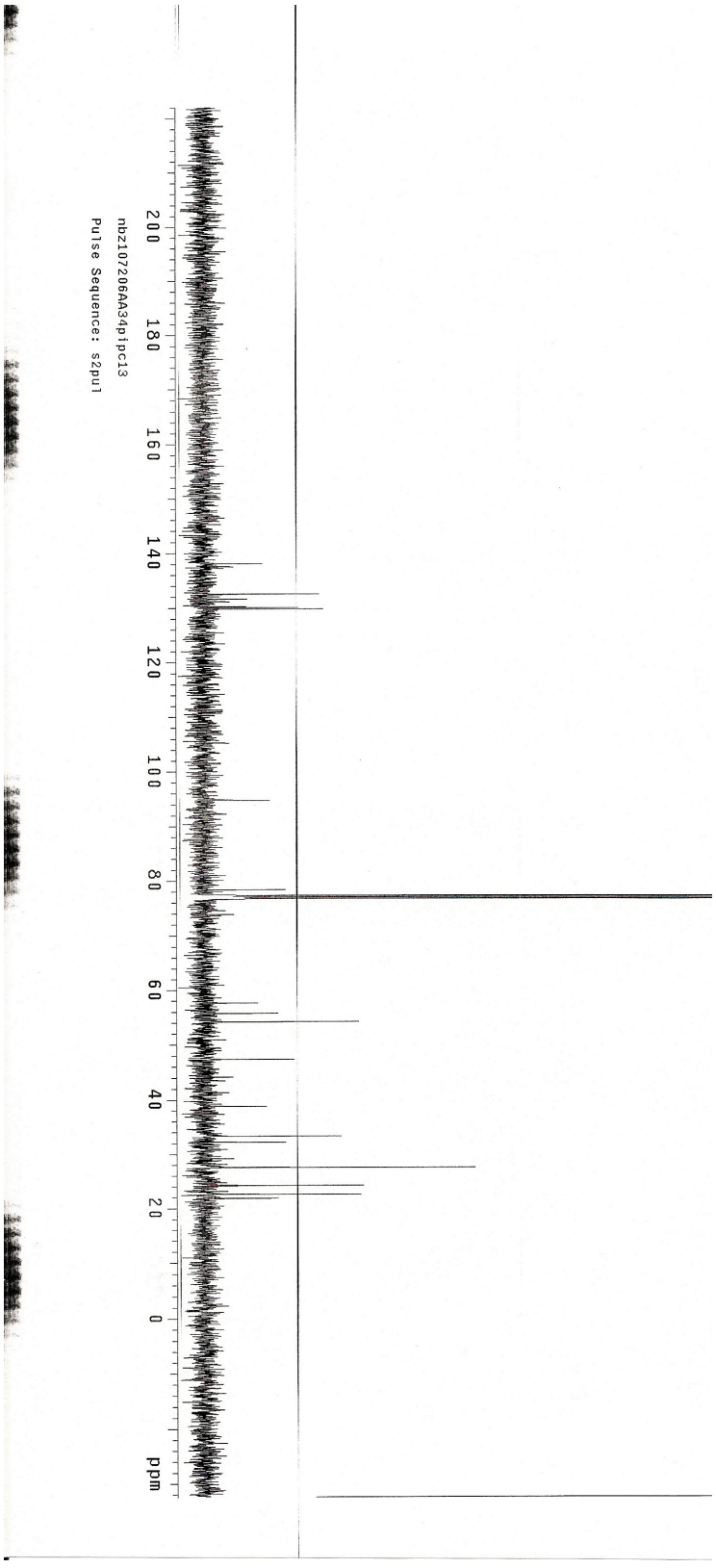

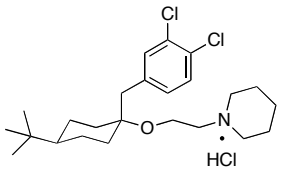

1.28
125 MHz, $CDCl_3$

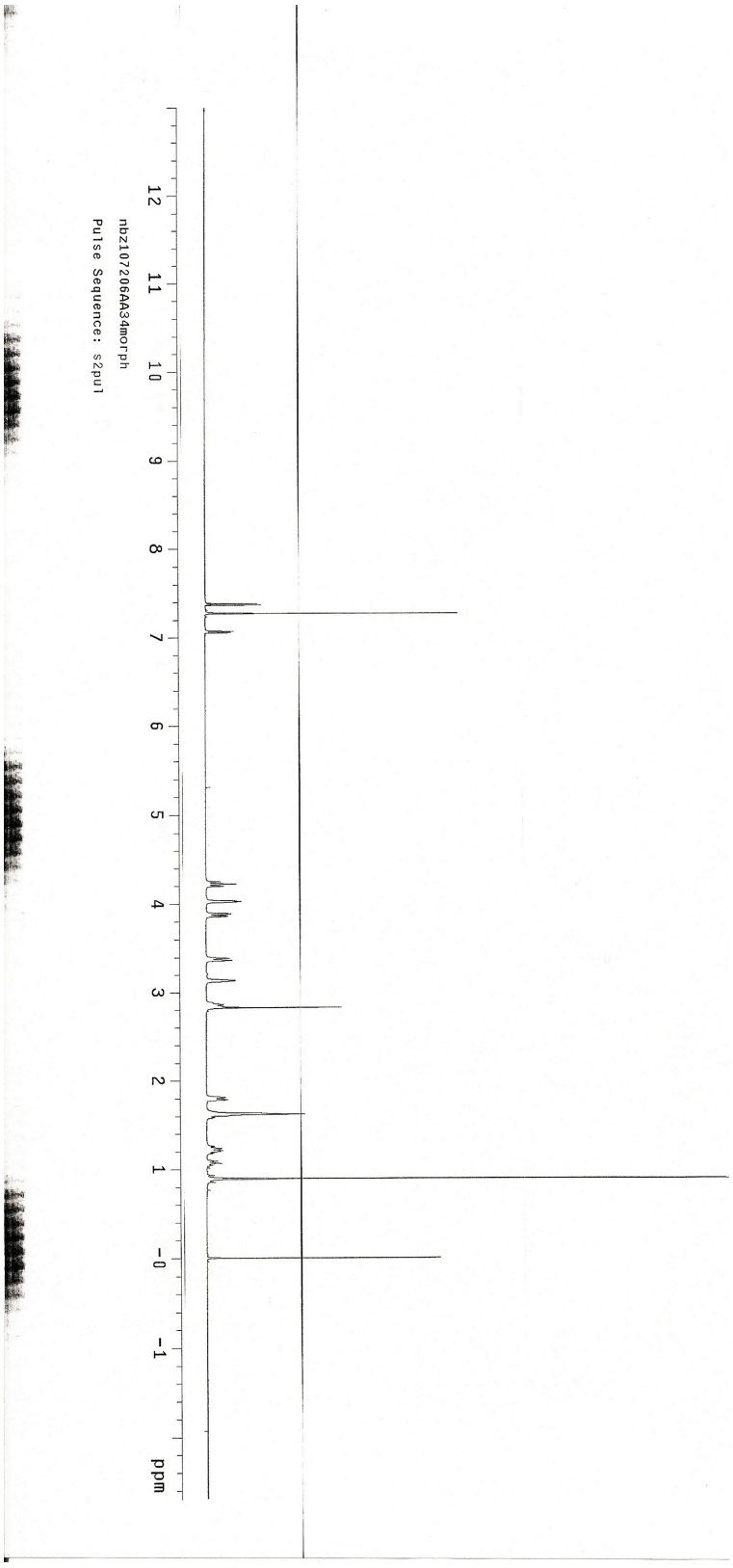

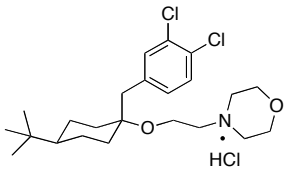

1.29
500 MHz, $CDCl_3$

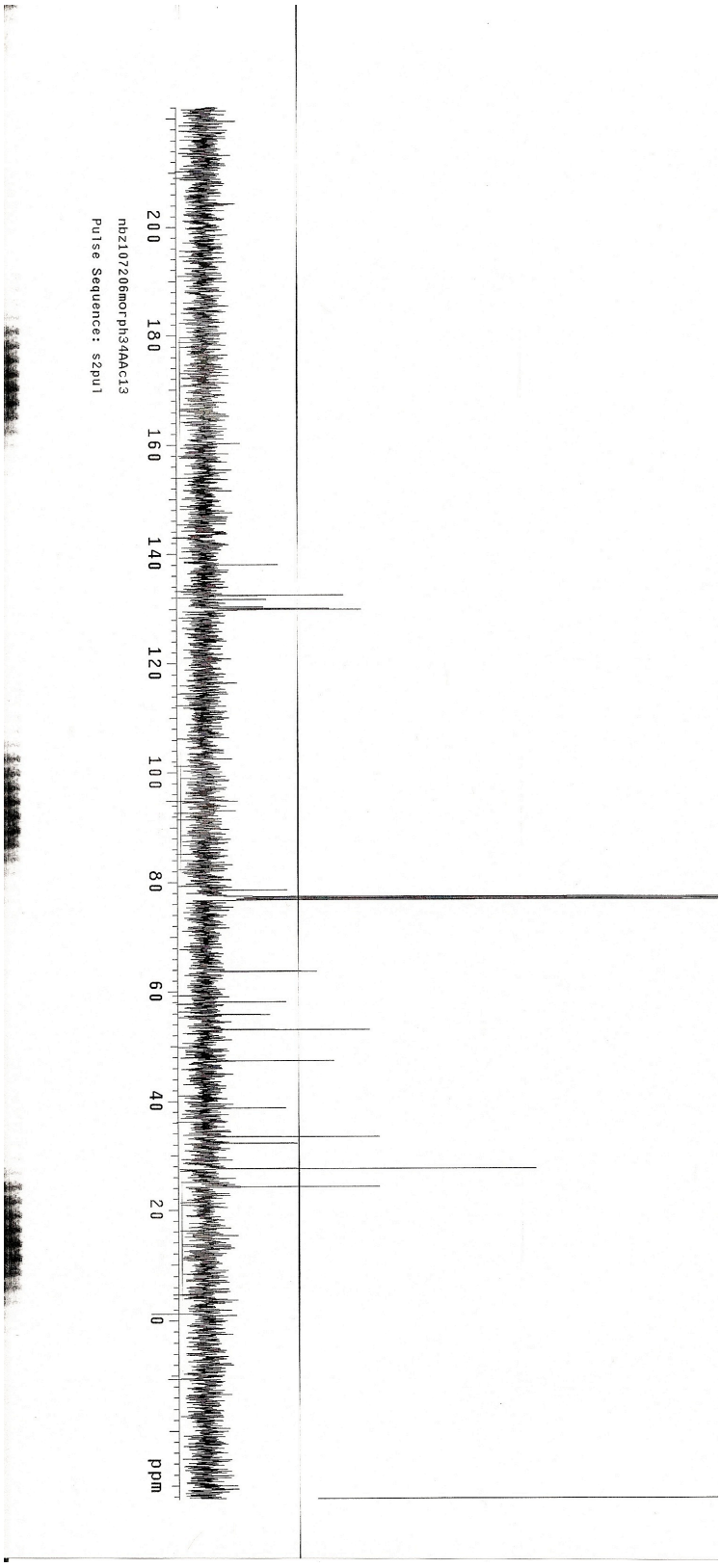

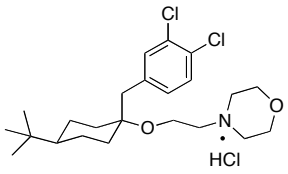

1.29
500 MHz, $CDCl_3$

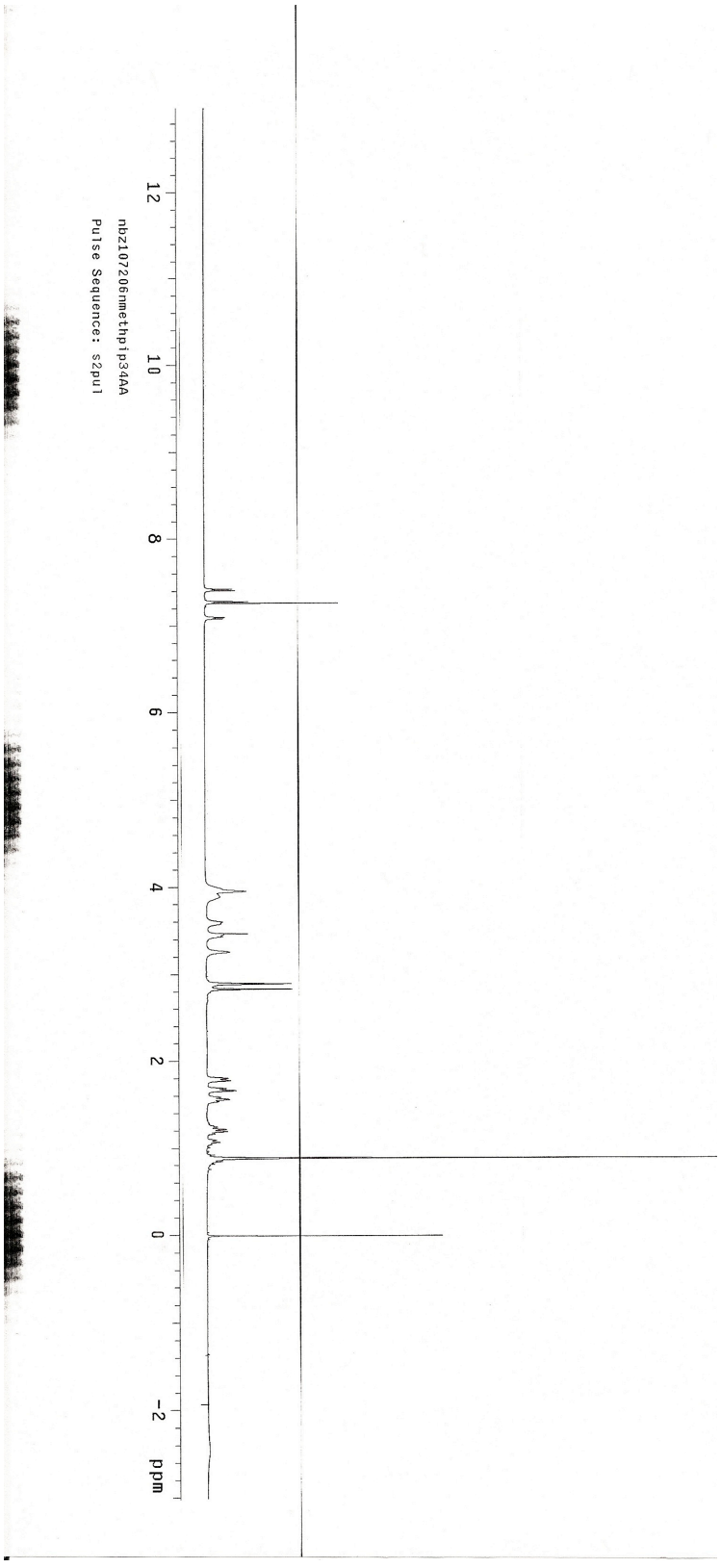

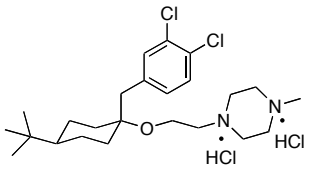

1.30
500 MHz, $CDCl_3$

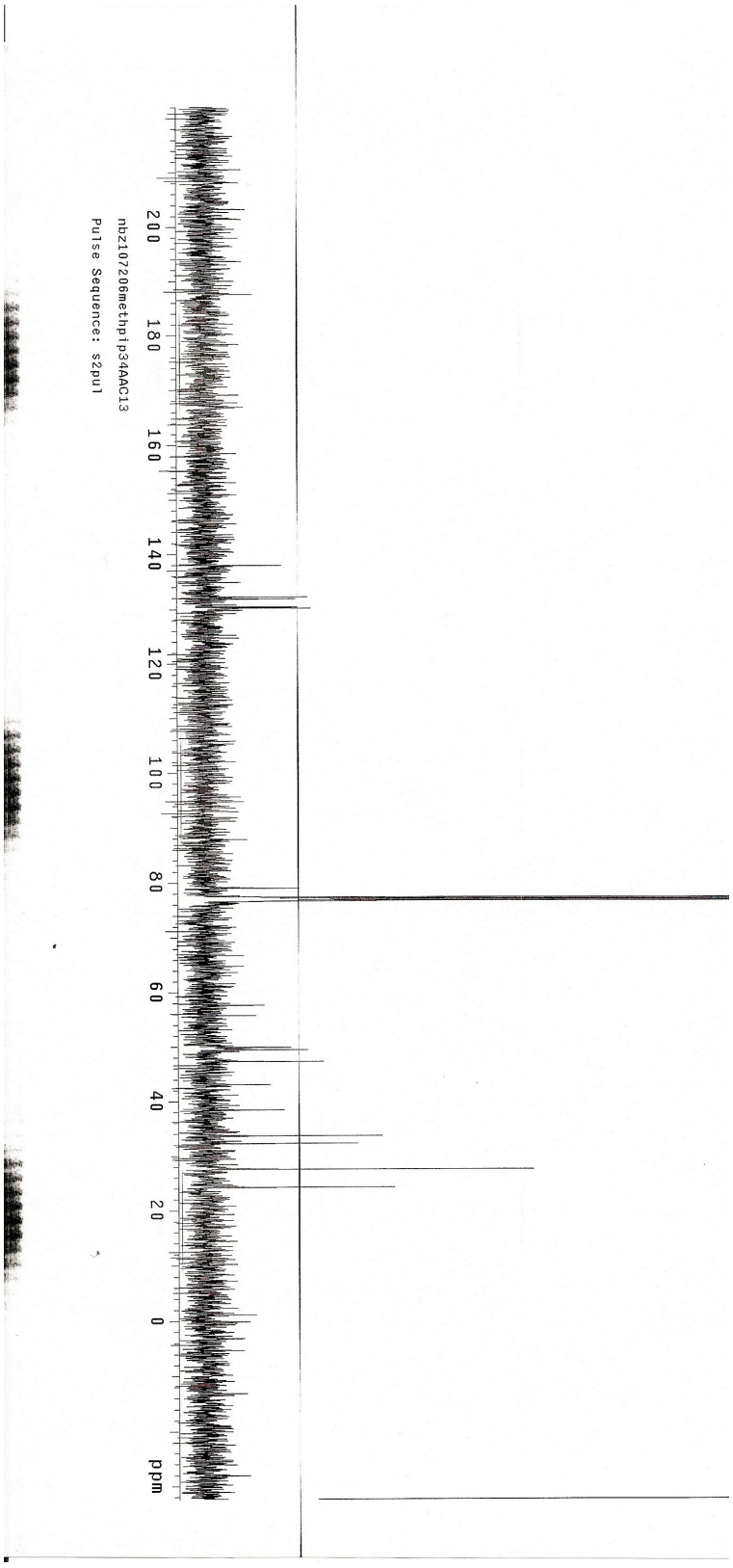

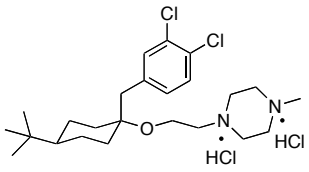

1.30
125 MHz, $CDCl_3$

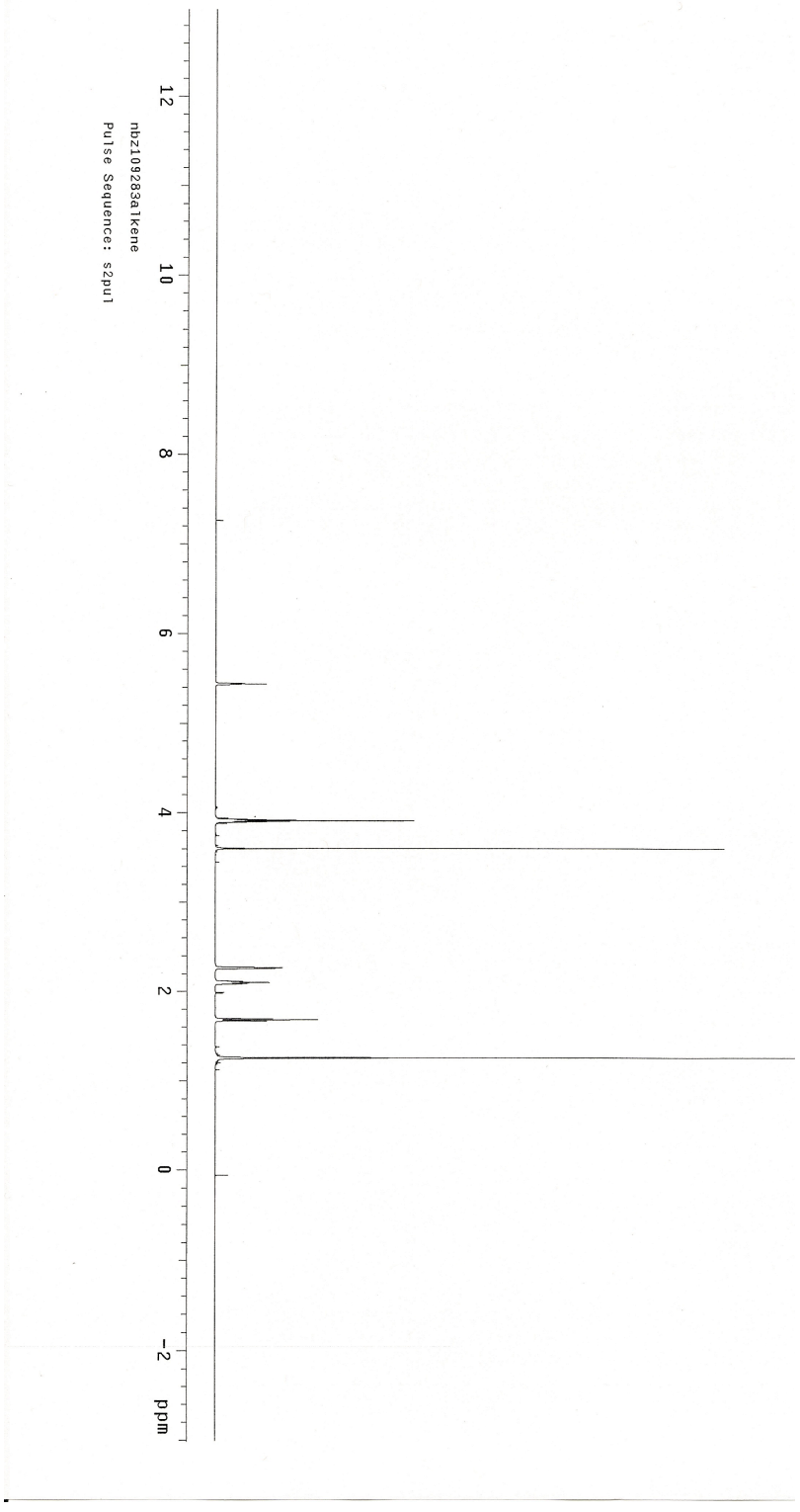

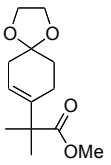

1.31
500 MHz, $CDCl_3$

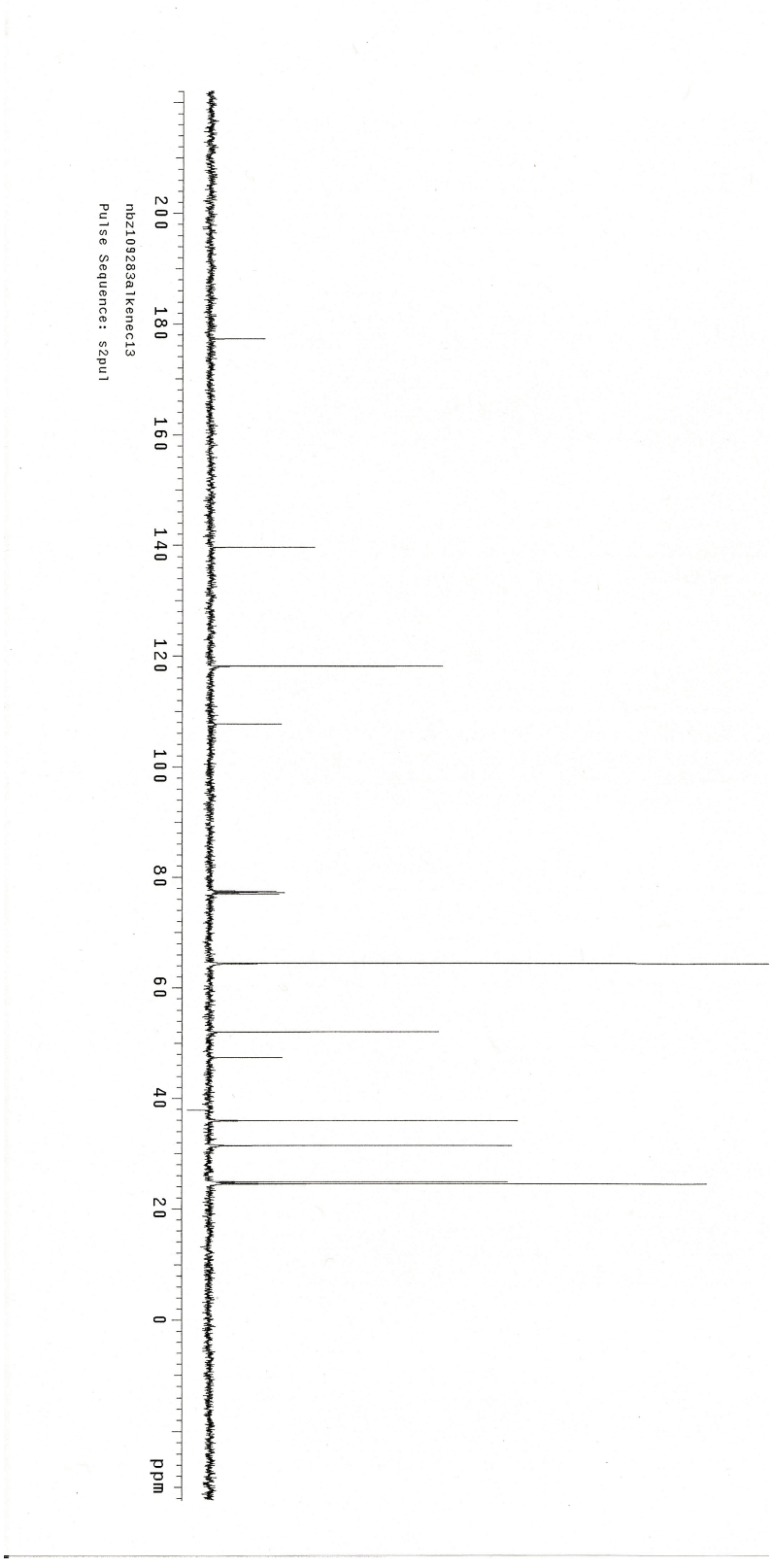

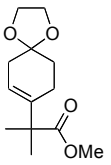

1.31
125 MHz, $CDCl_3$

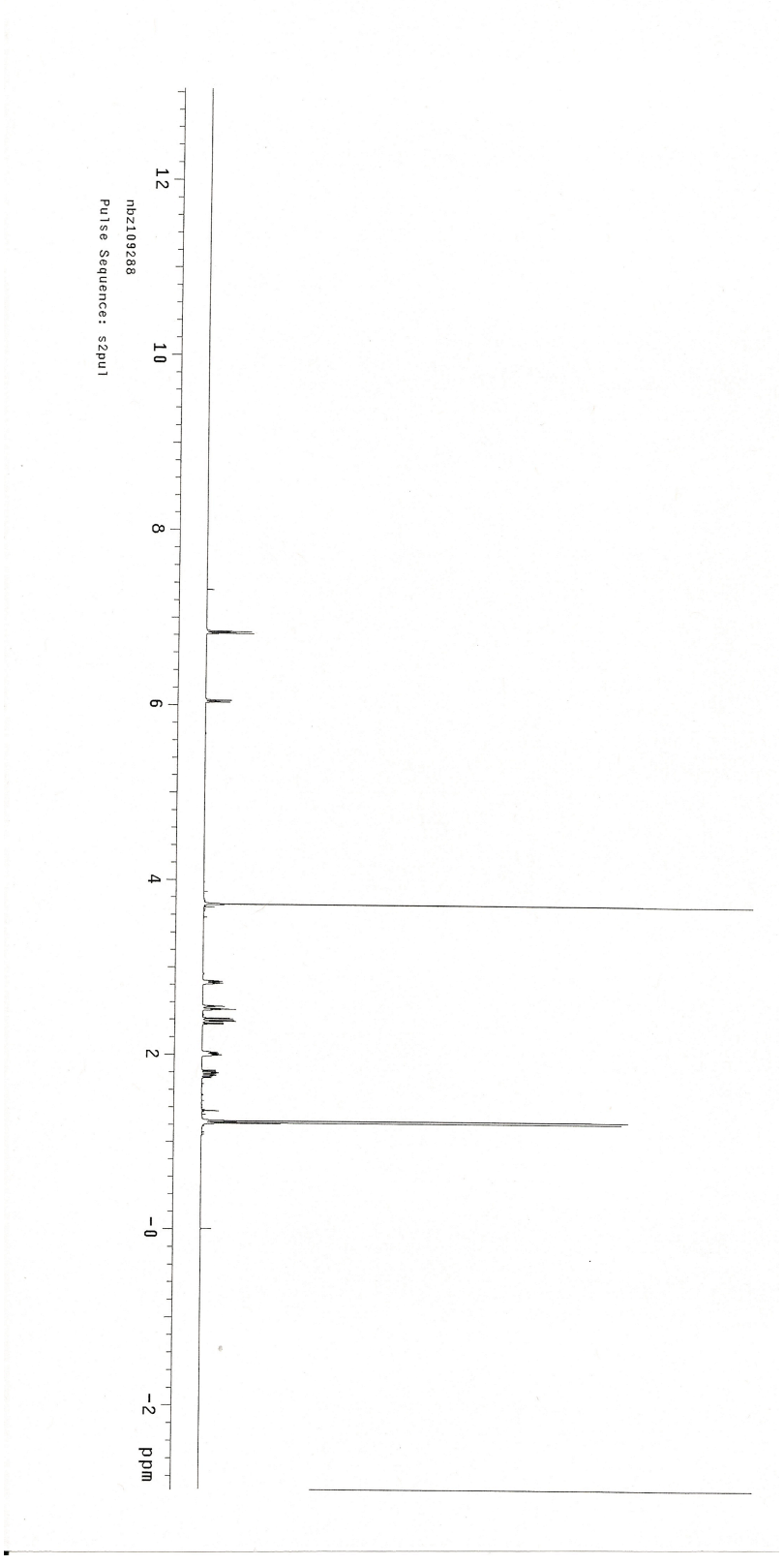

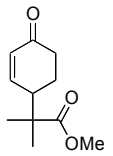

1.32
500 MHz, $CDCl_3$

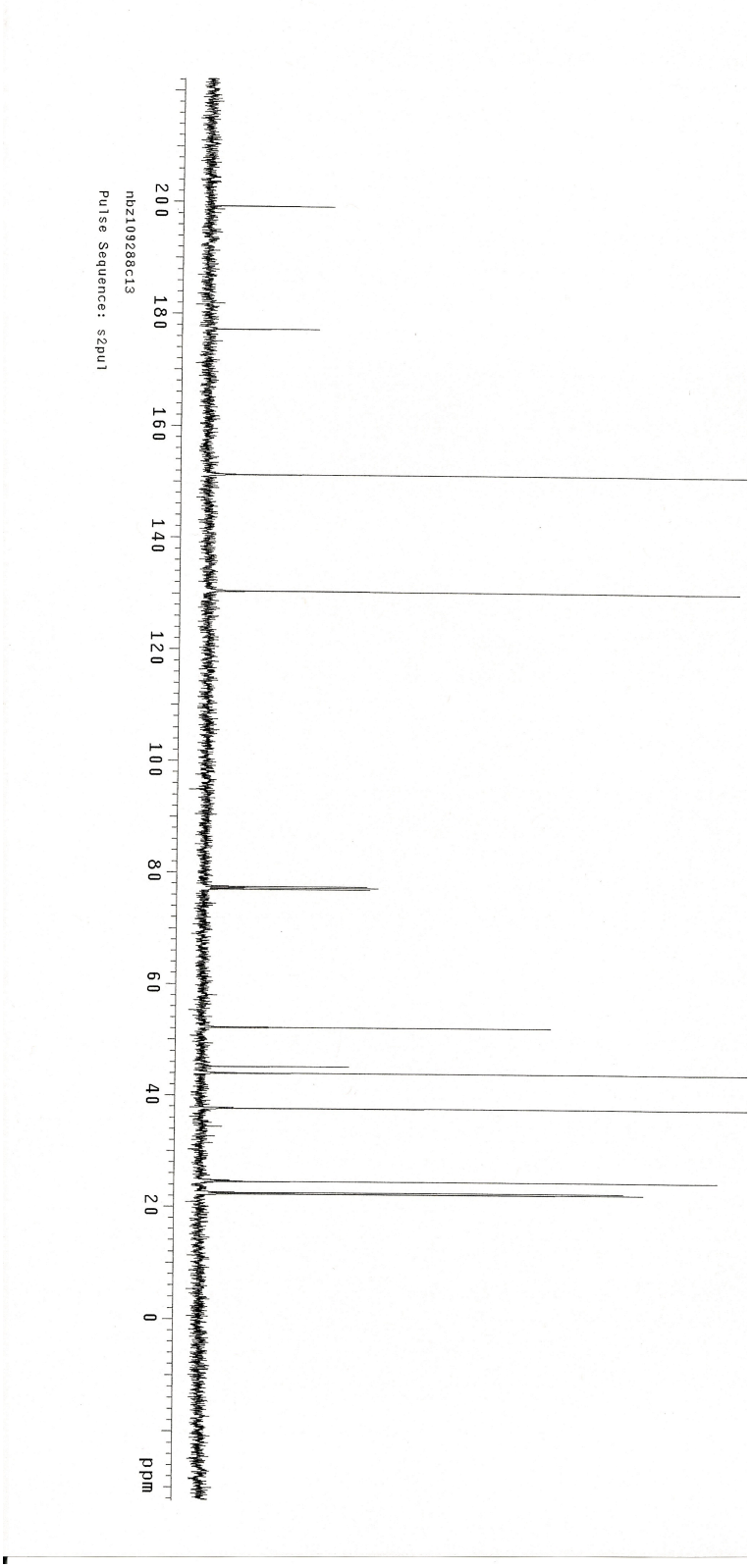

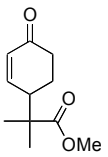

1.32
125 MHz, $CDCl_3$

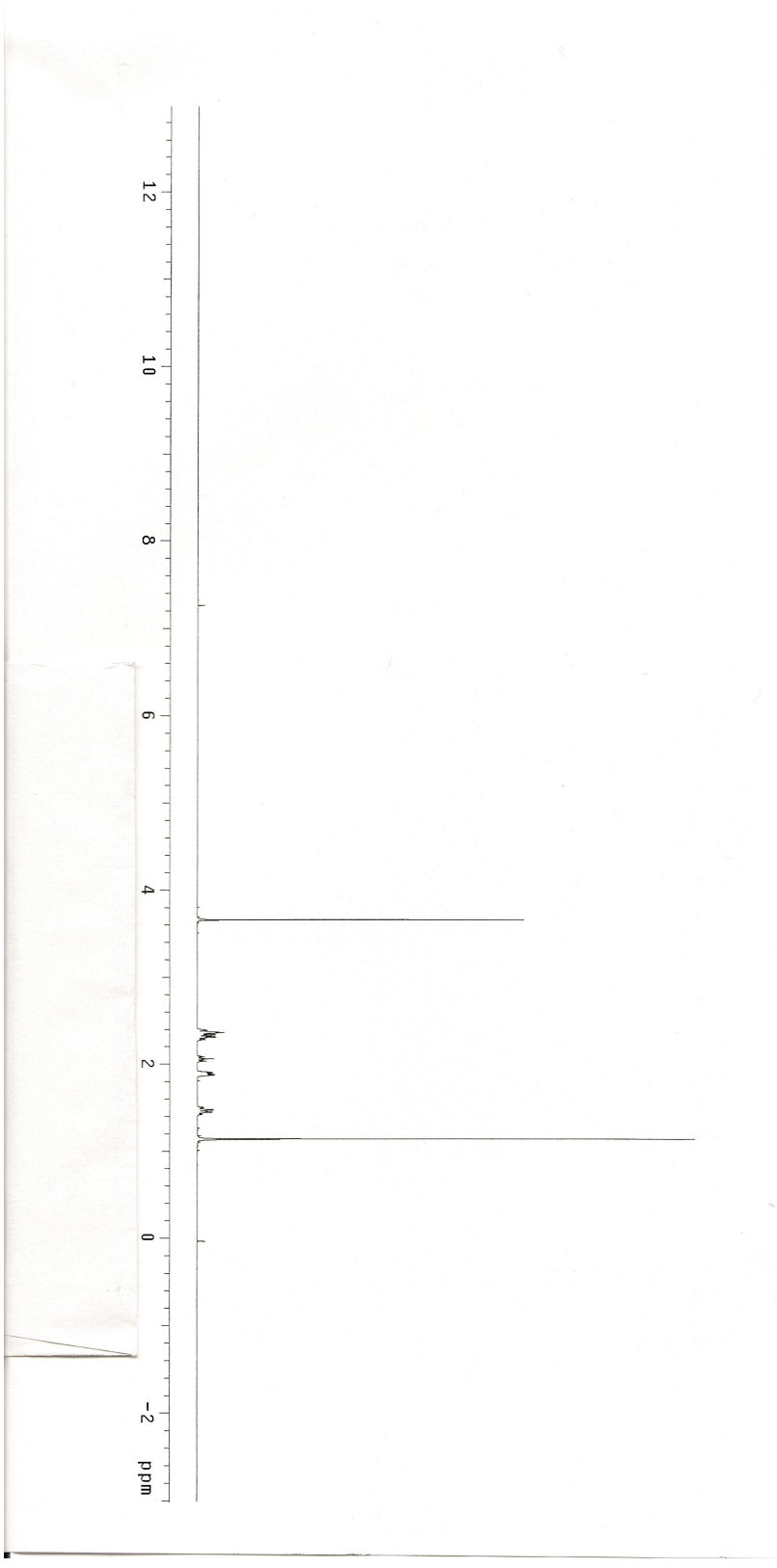

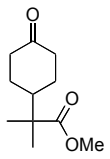

1.33
500 MHz, $CDCl_3$

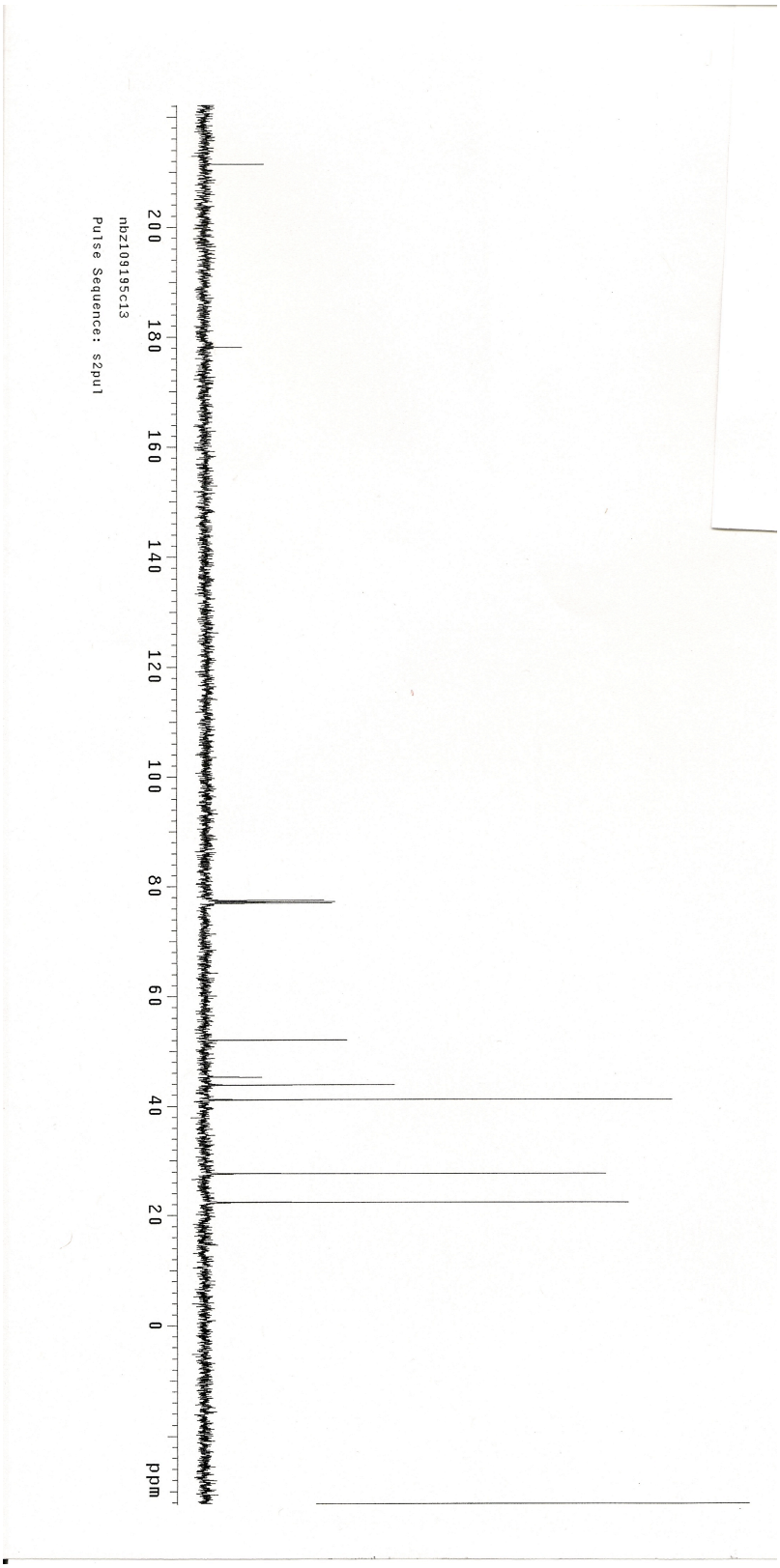

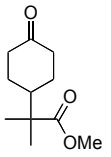

1.33
125 MHz, $CDCl_3$

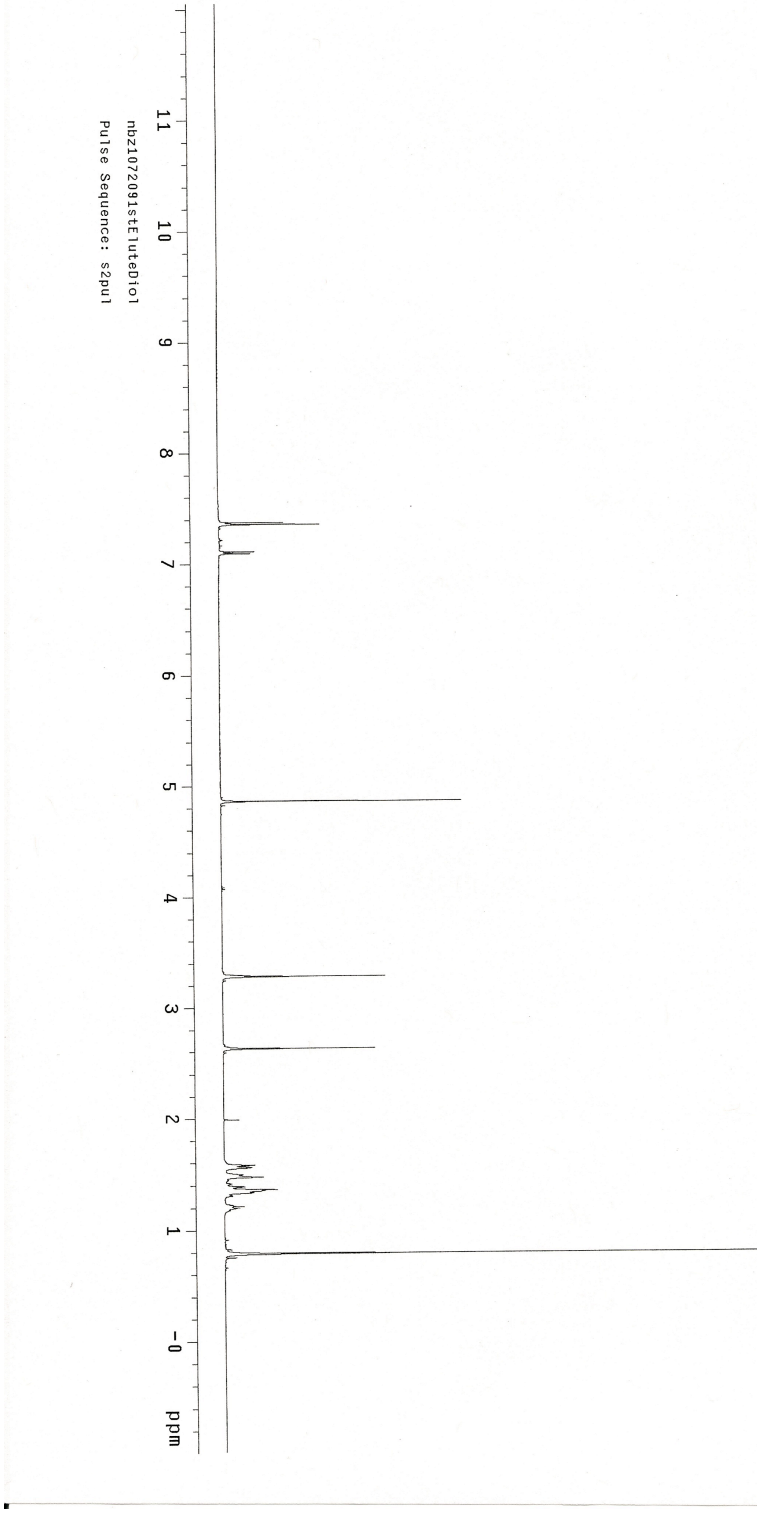

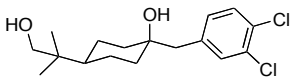

***cis*-1.34**
500 MHz, CD_3OD

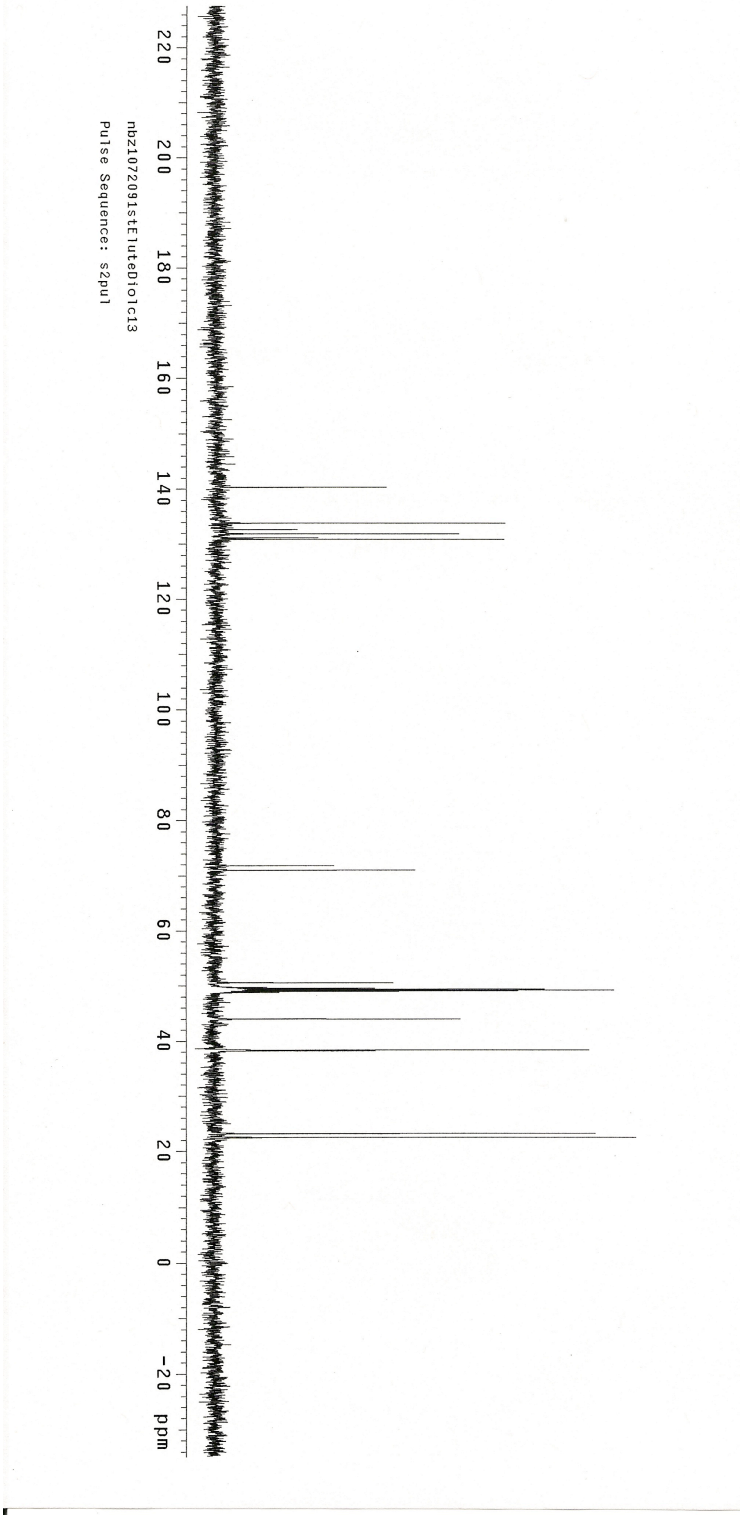

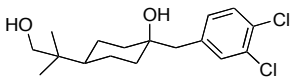

***cis*-1.34**
125 MHz, CD_3OD

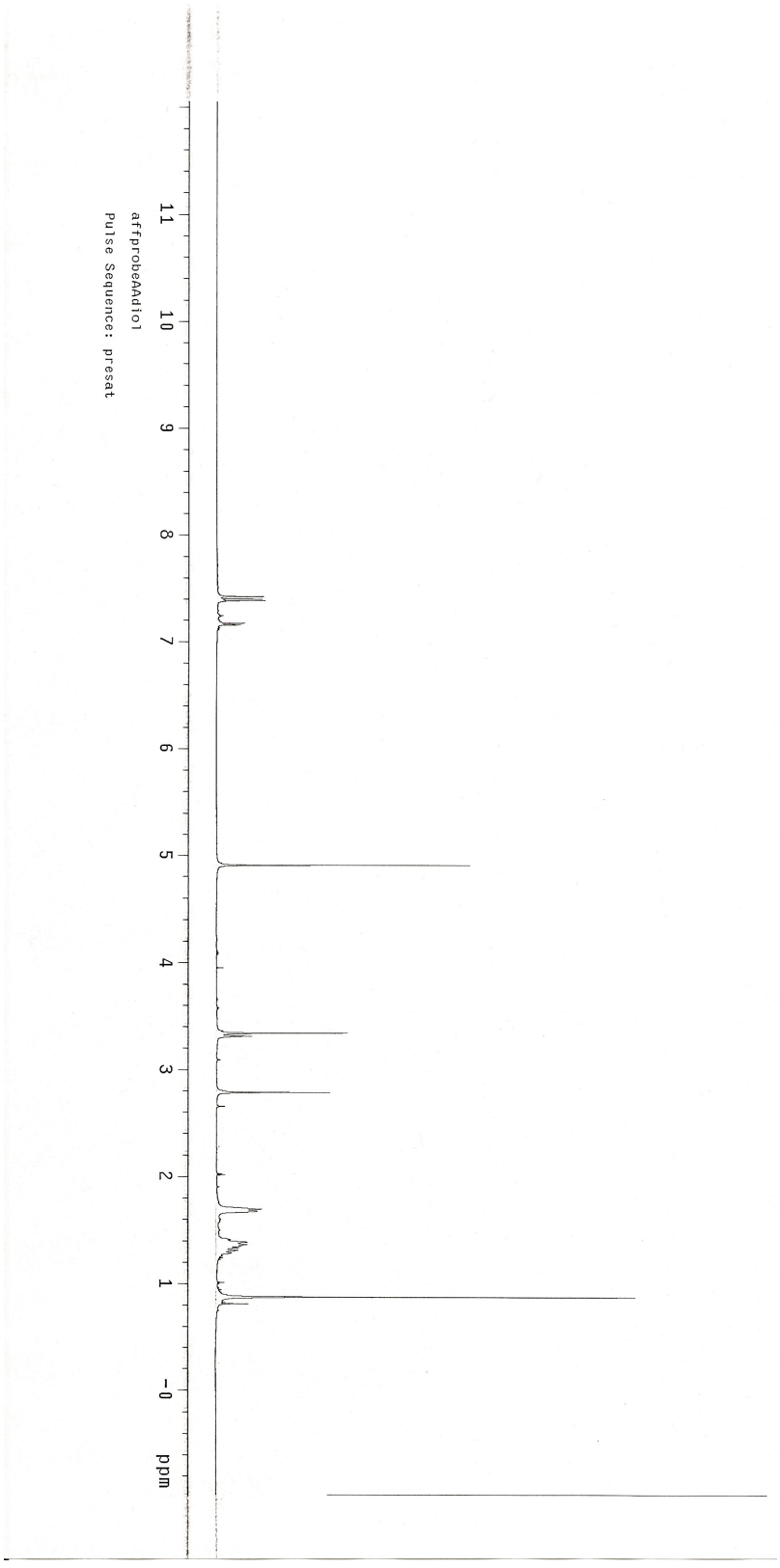

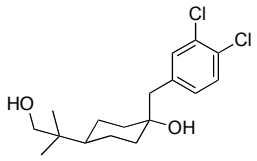

trans-**1.34**
500 MHz, CD_3OD

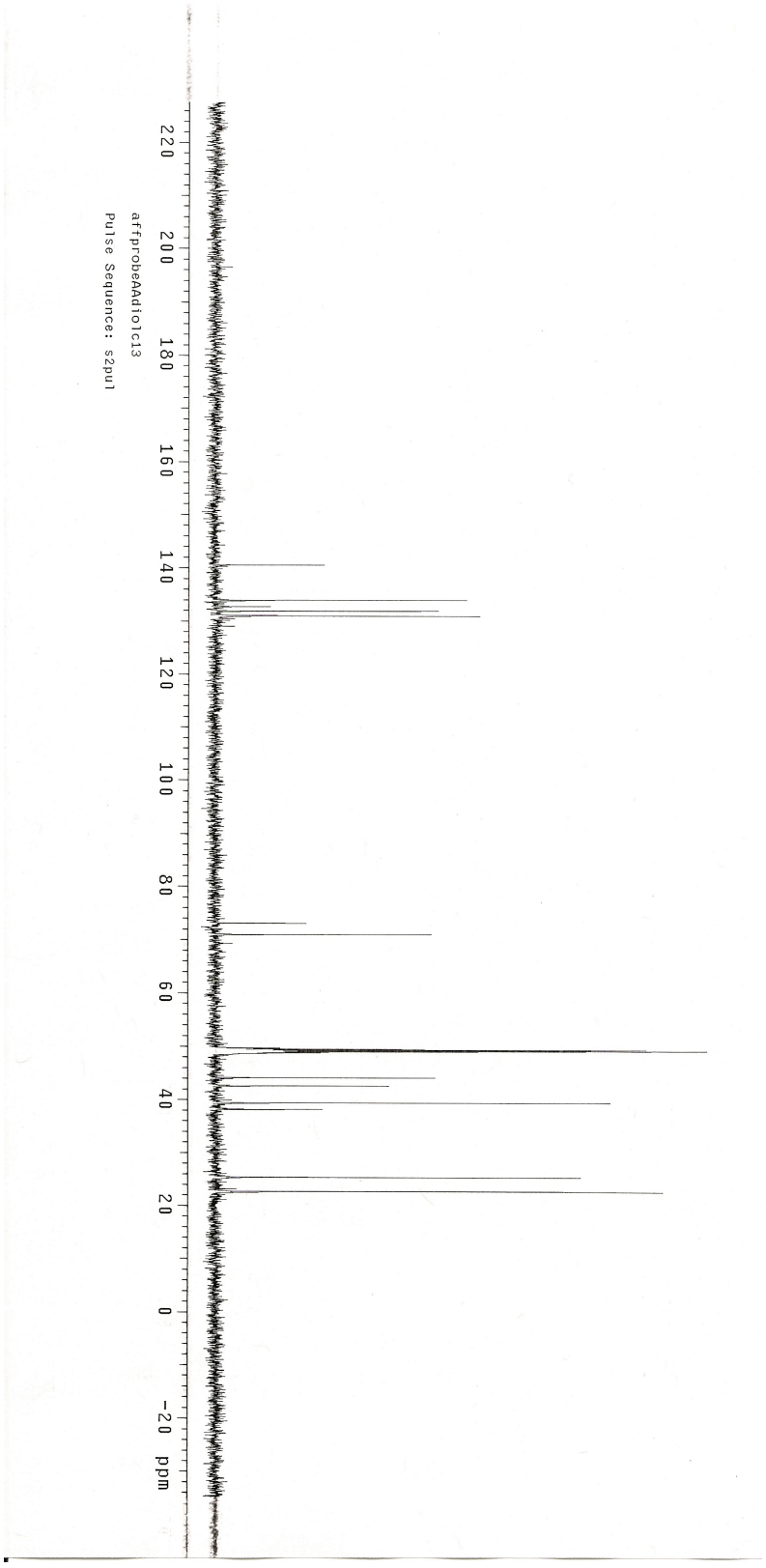

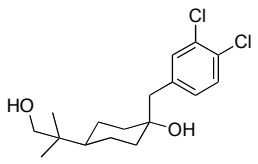

trans-**1.34**
125 MHz, CD_3OD

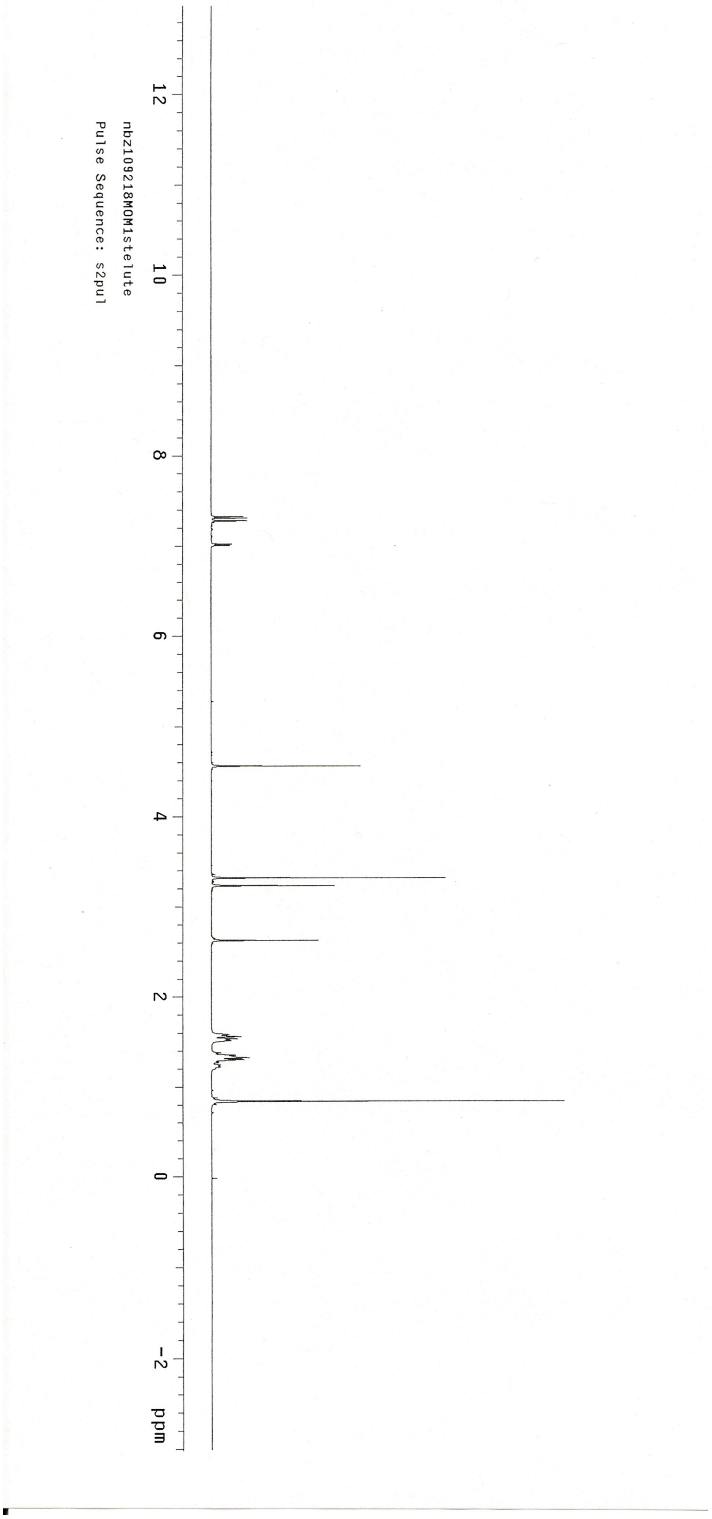

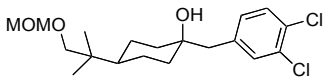

***cis*-1.35**
500 MHz, $CDCl_3$

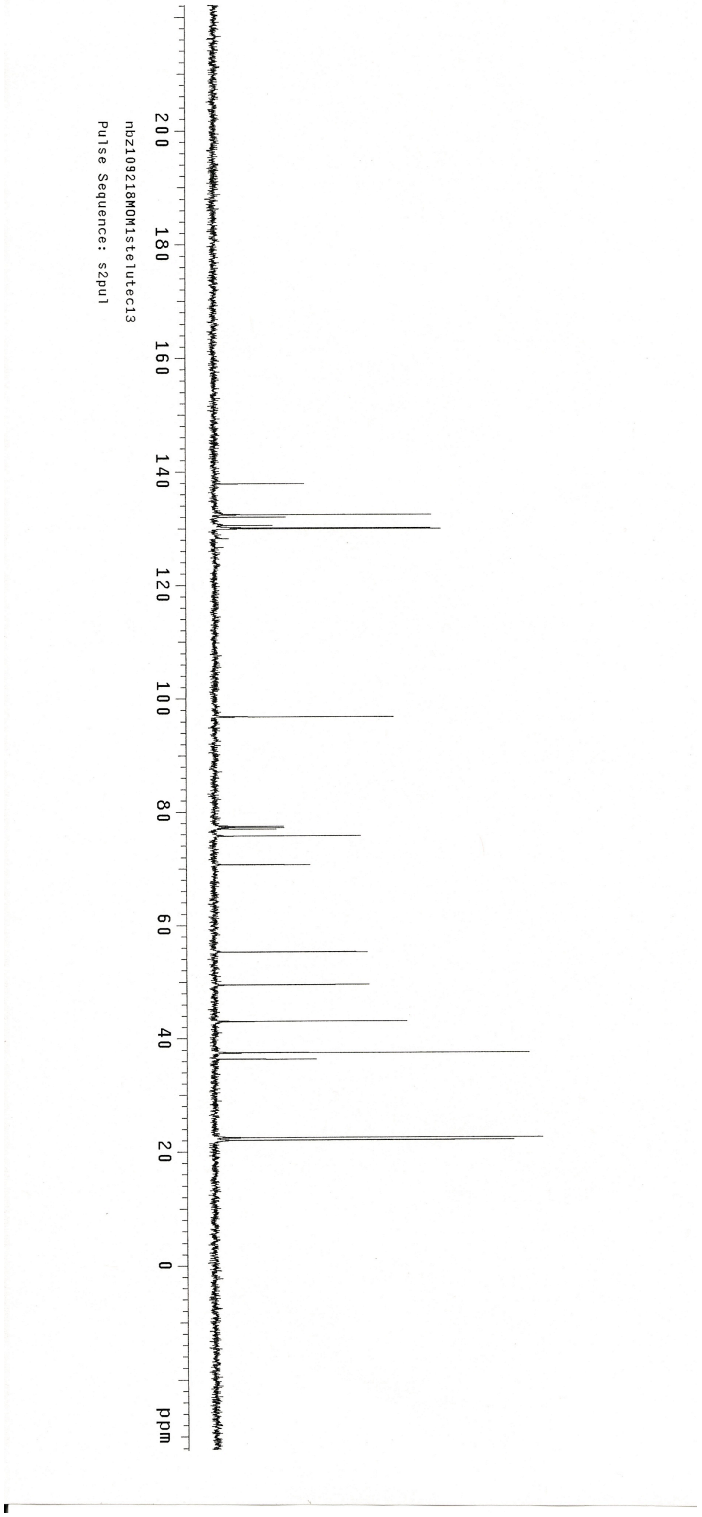

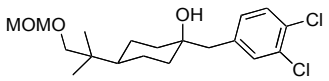

***cis*-1.35**
125 MHz, $CDCl_3$

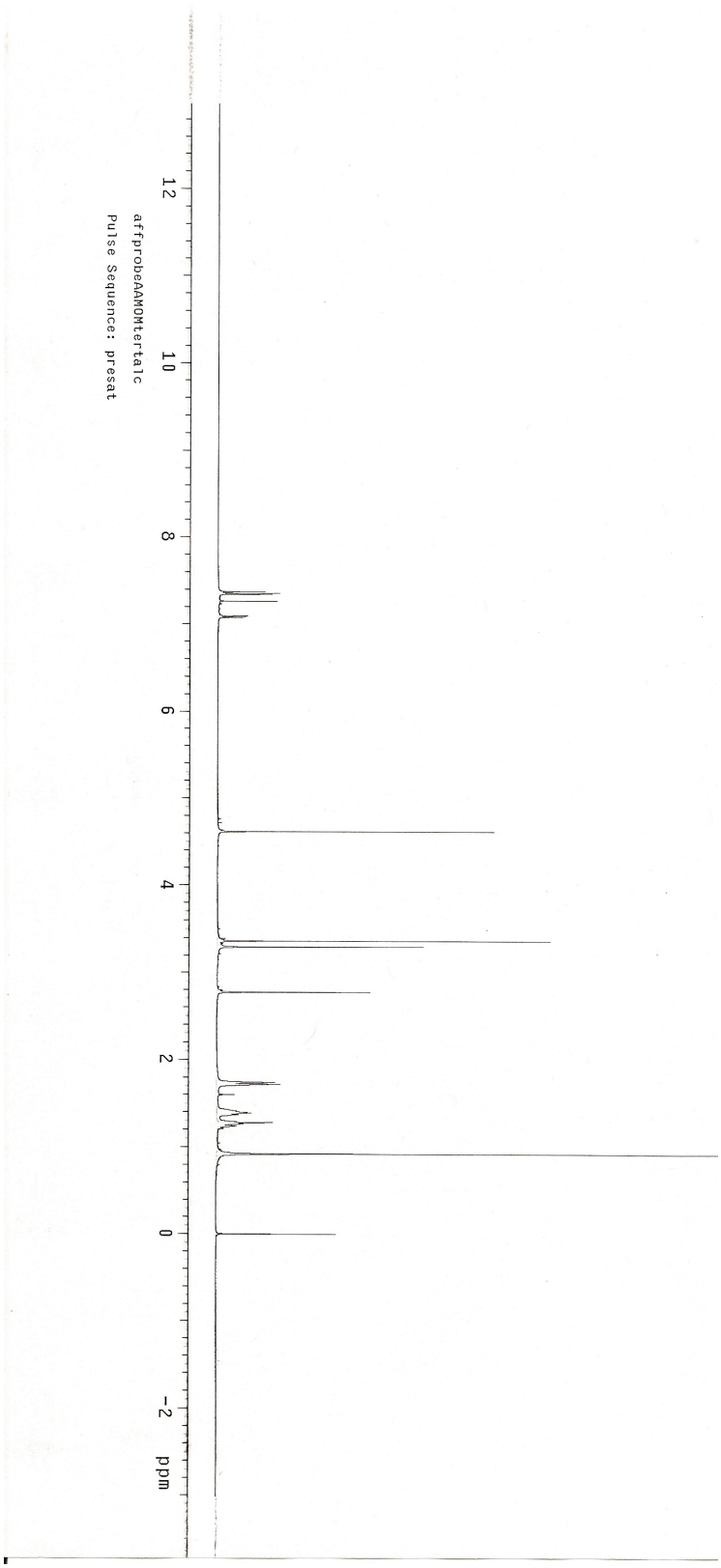

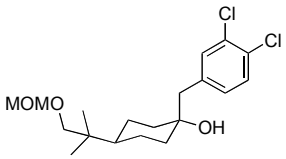

trans-**1.35**
500 MHz, $CDCl_3$

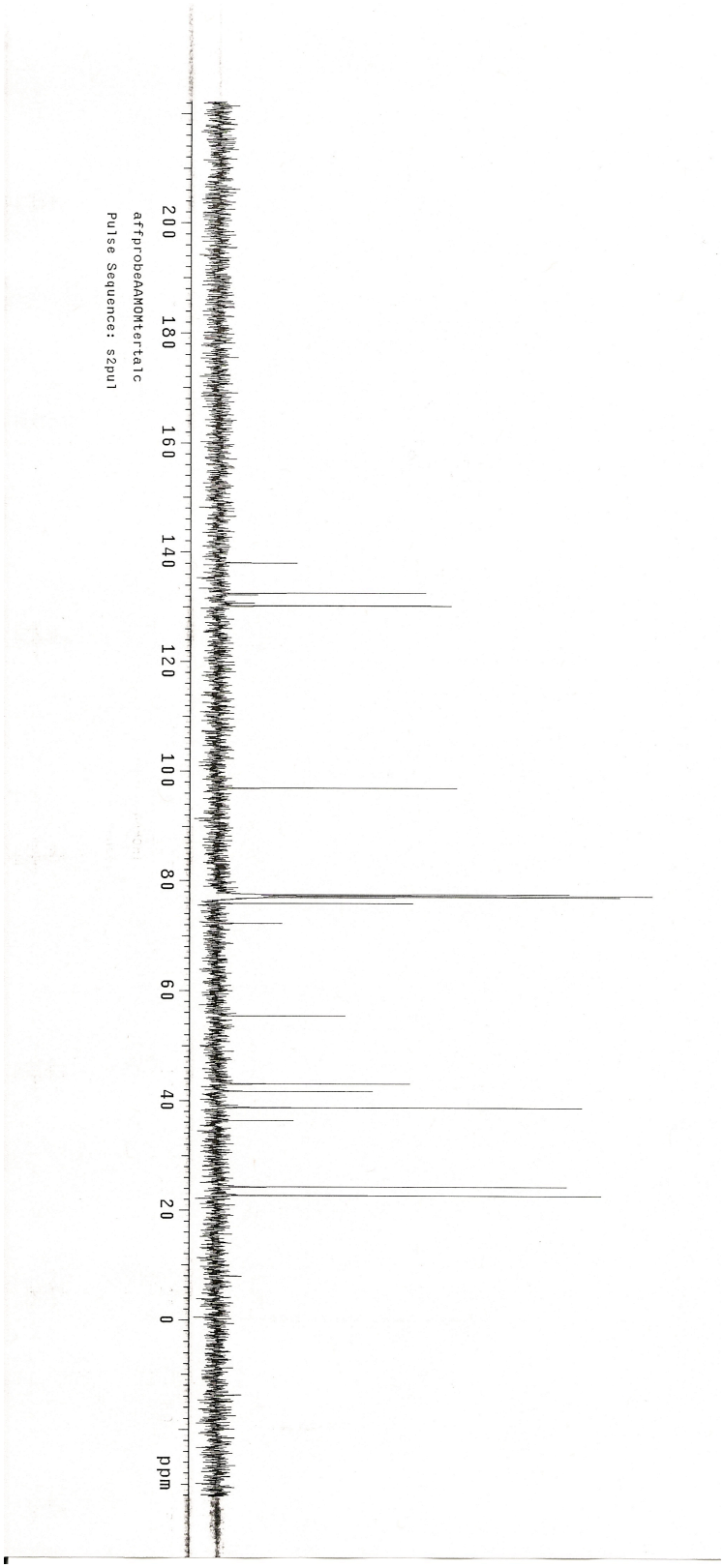

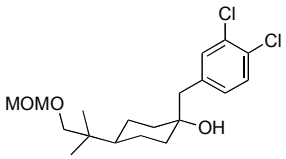

trans-**1.35**
125 MHz, $CDCl_3$

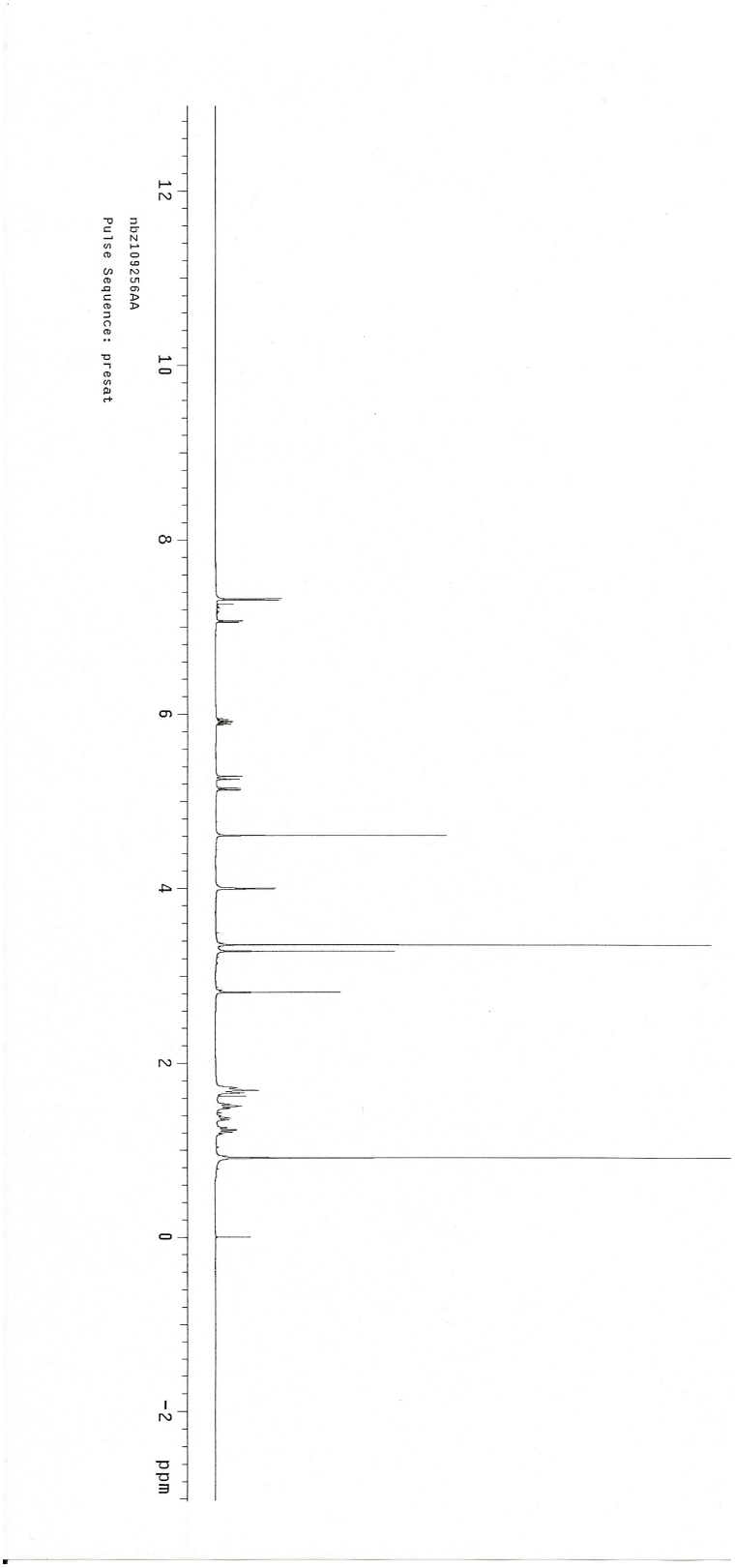

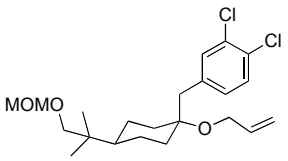

1.36
500 MHz, $CDCl_3$

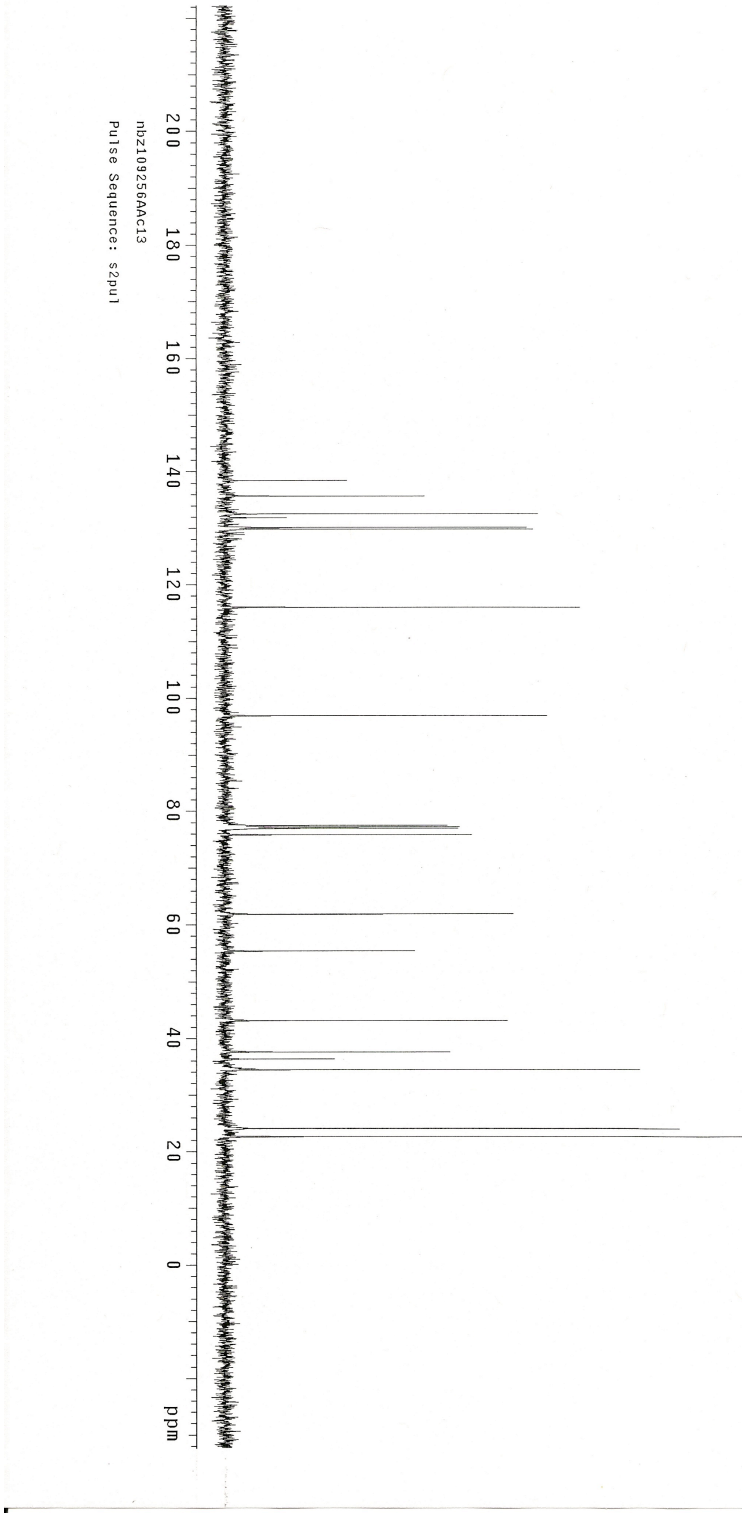

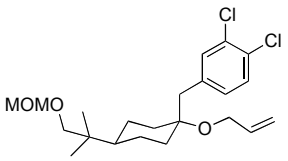

1.36
125 MHz, $CDCl_3$

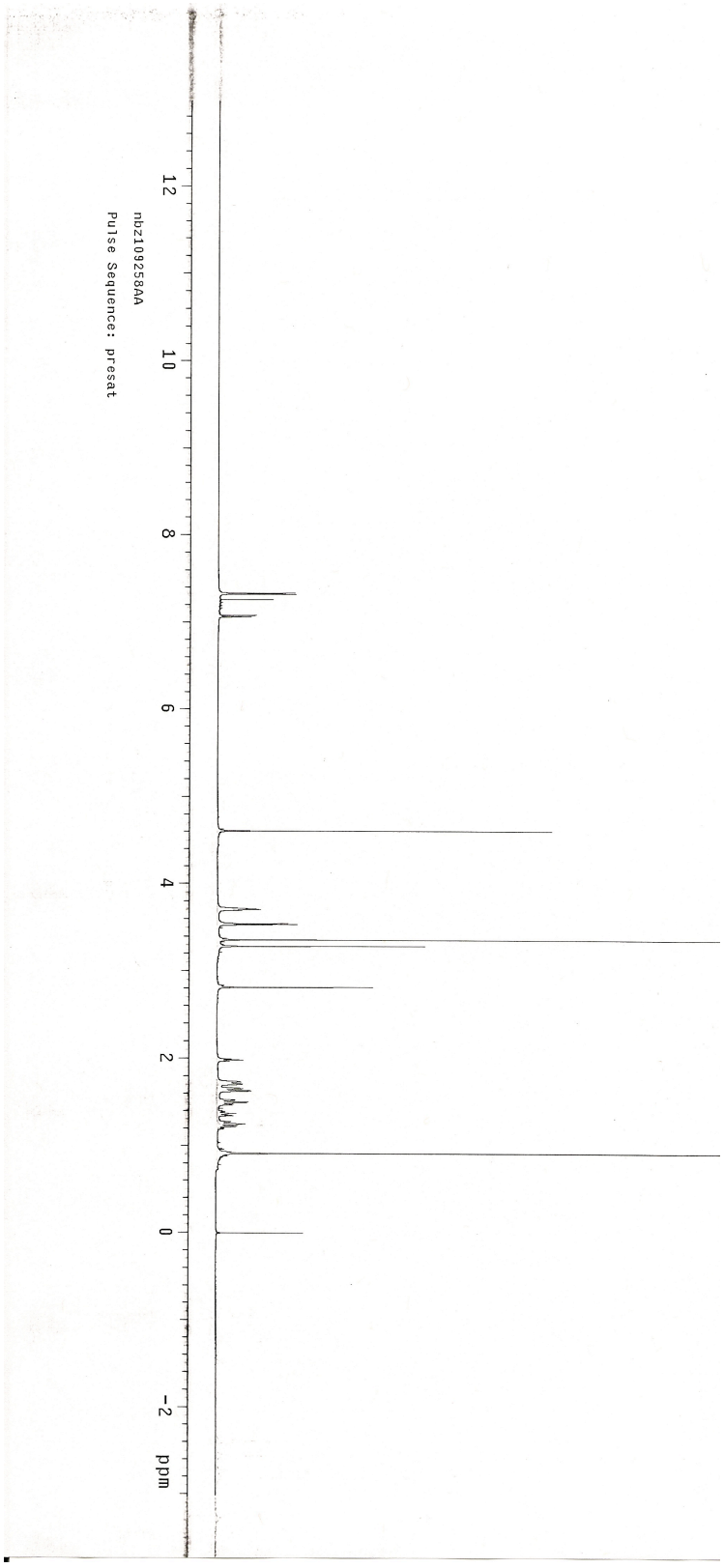

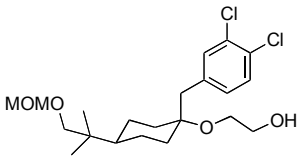

1.37
500 MHz, $CDCl_3$

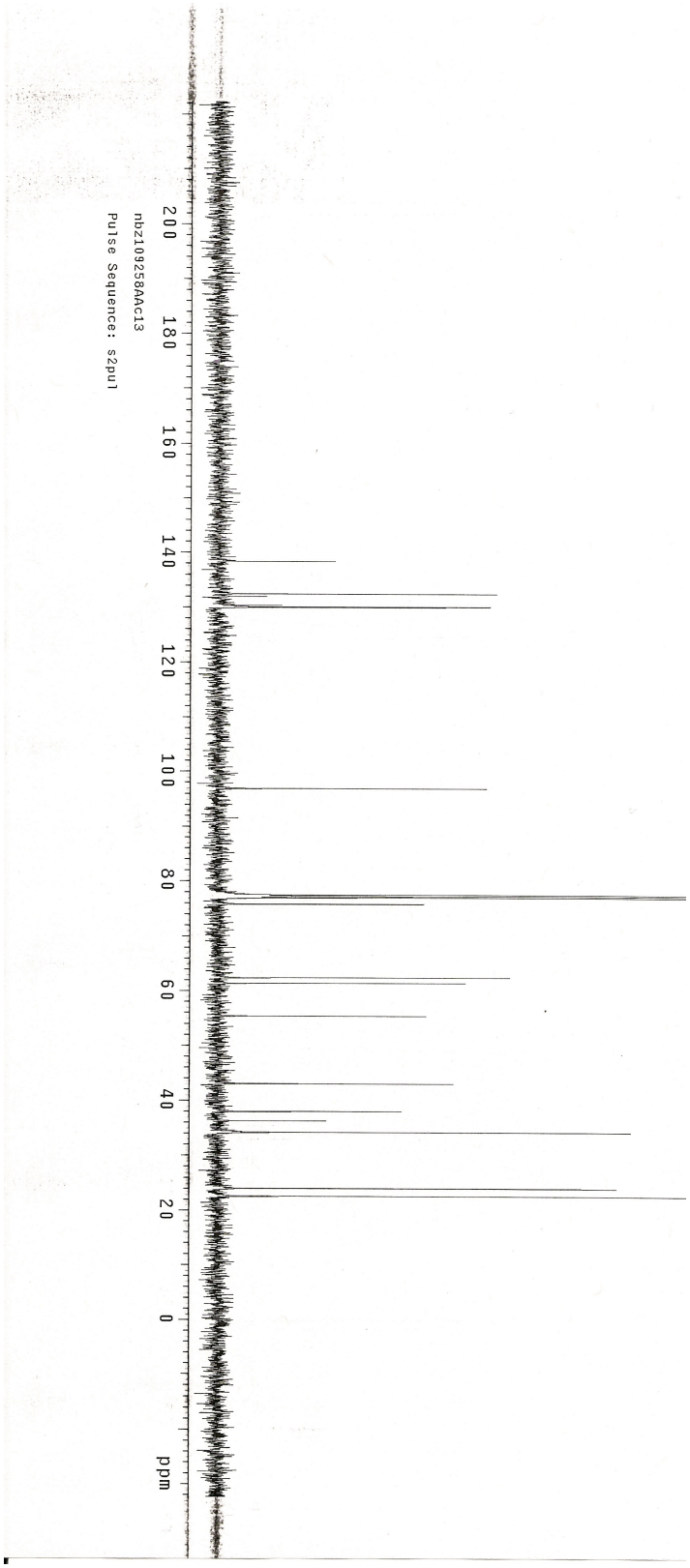

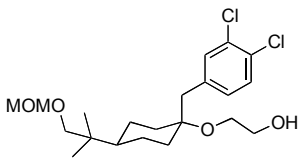

1.37
125 MHz, $CDCl_3$

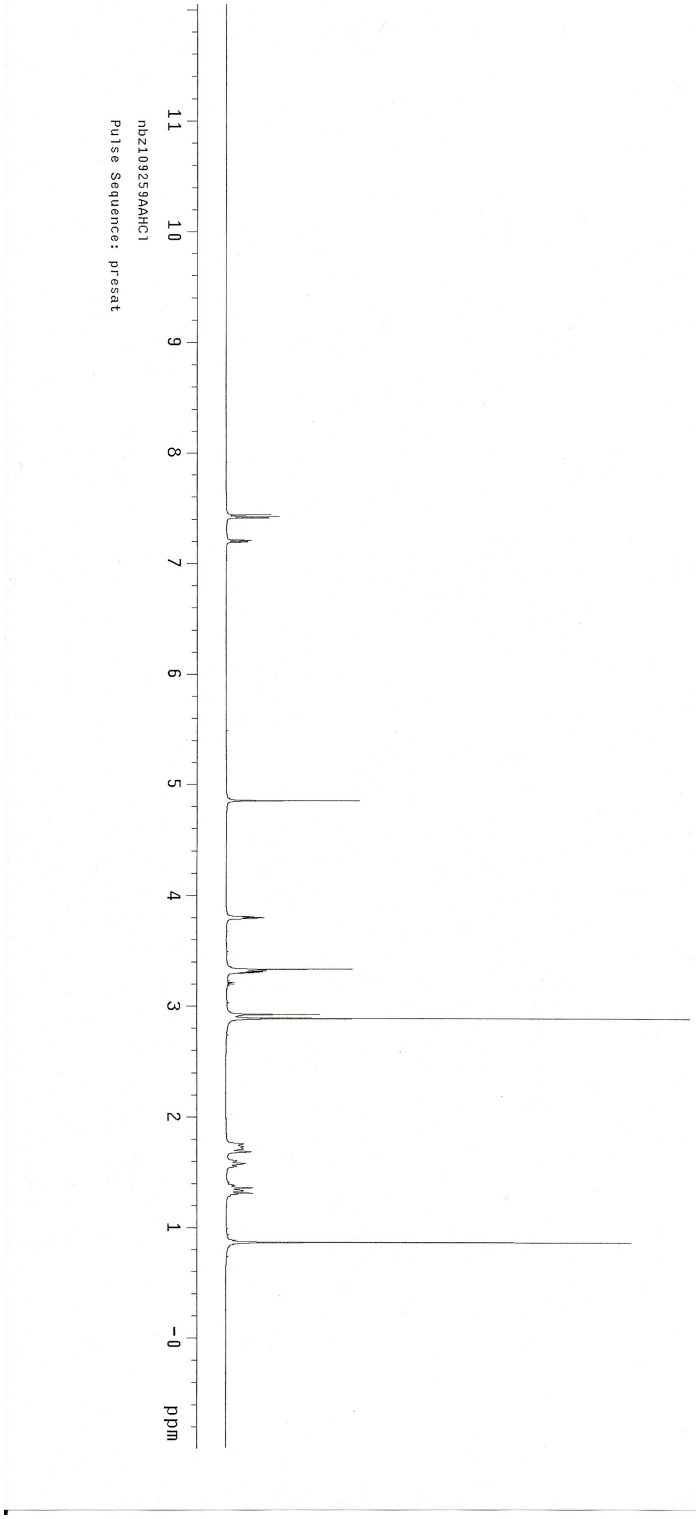

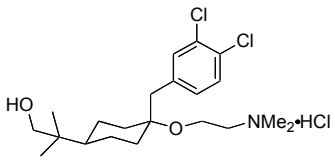

1.38
500 MHz, CD_3OD

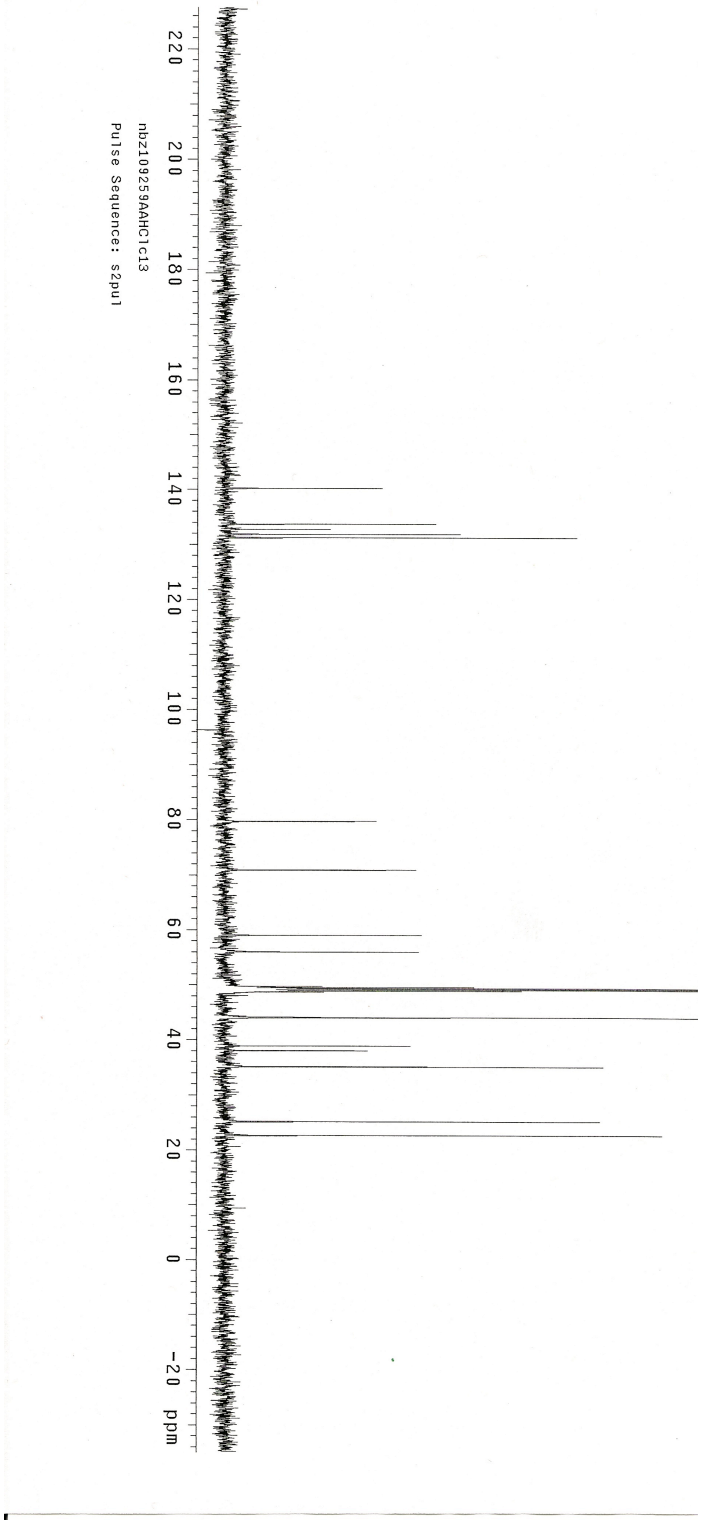

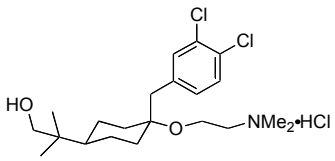

1.38
125 MHz, CD_3OD

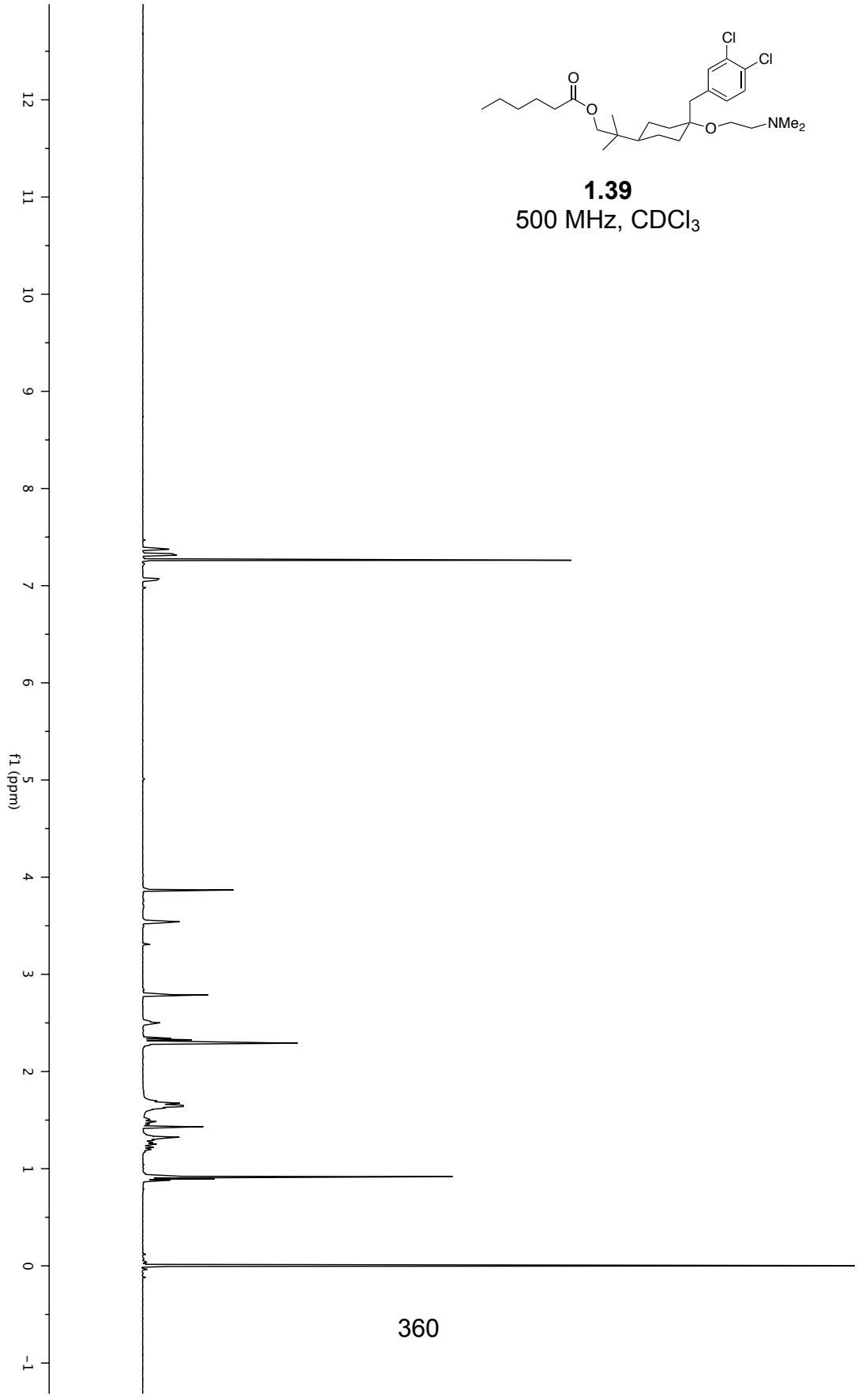

1.39
500 MHz, $CDCl_3$

1.39
125 MHz, $CDCl_3$

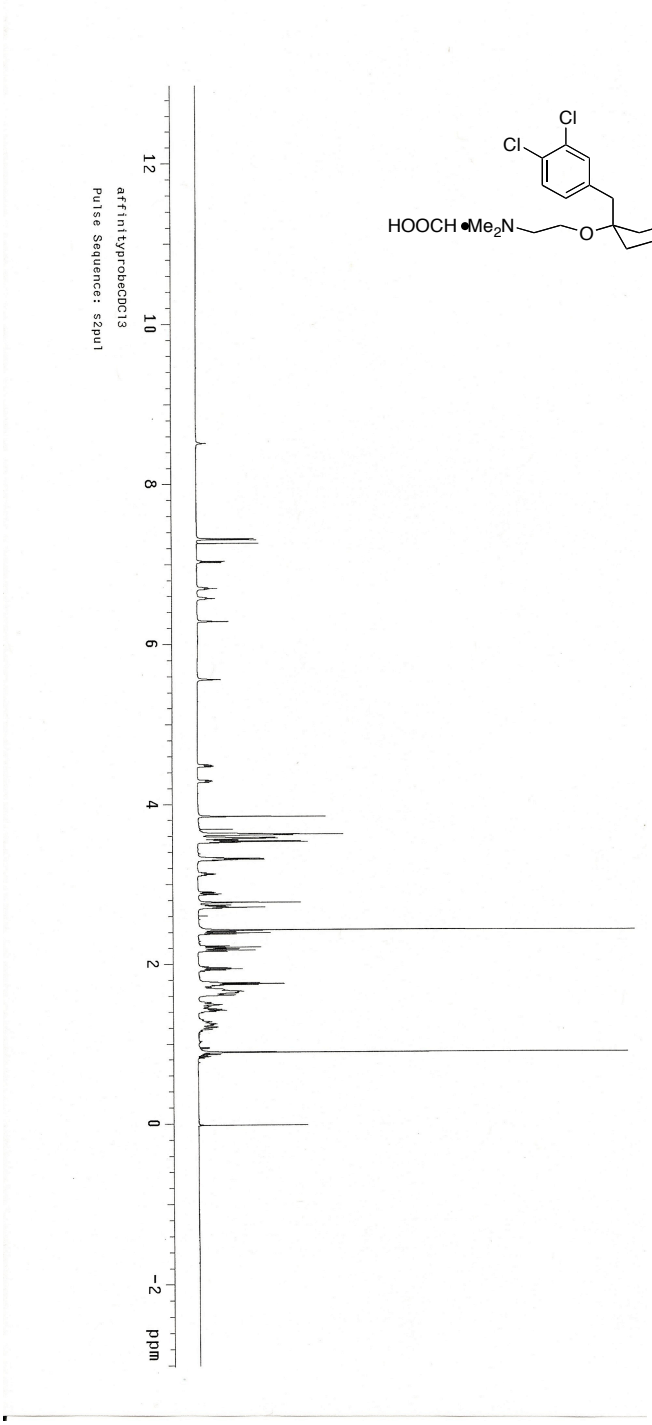

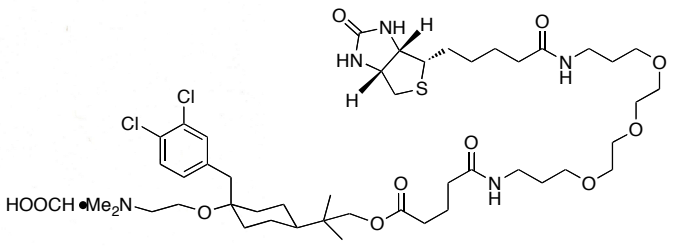

1.41
500 MHz, $CDCl_3$

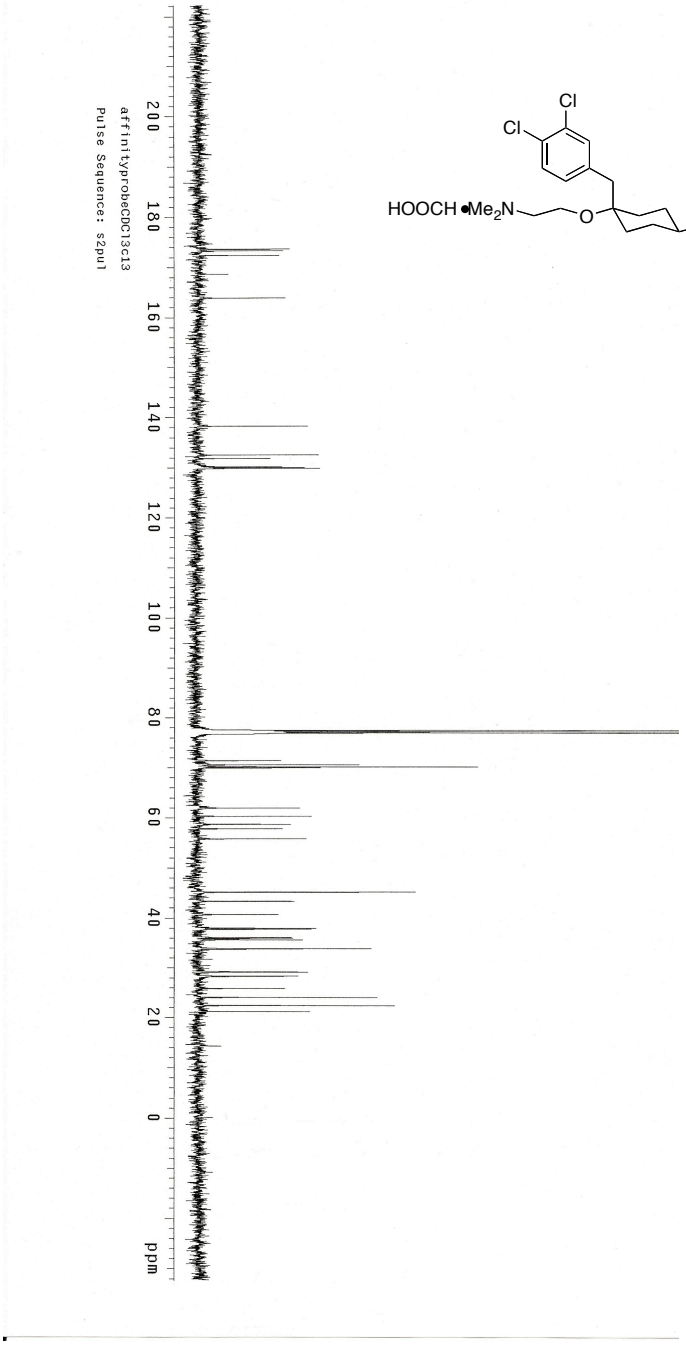

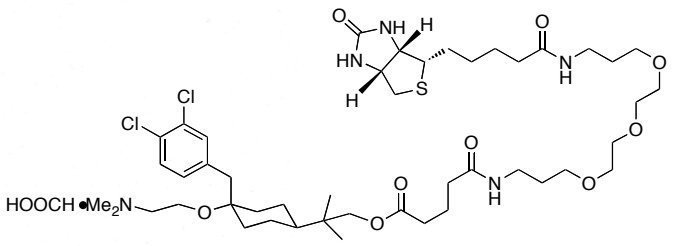

1.41
125 MHz, $CDCl_3$

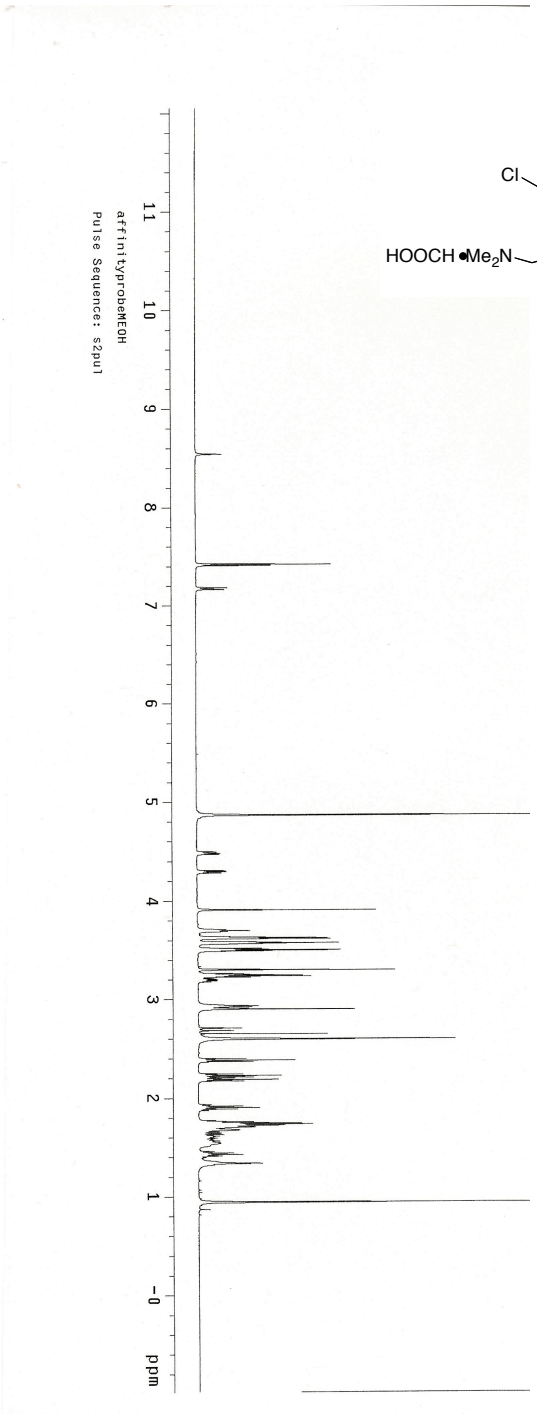

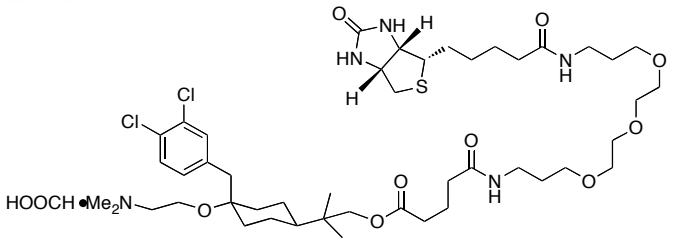

1.41
500 MHz, CD_3OD

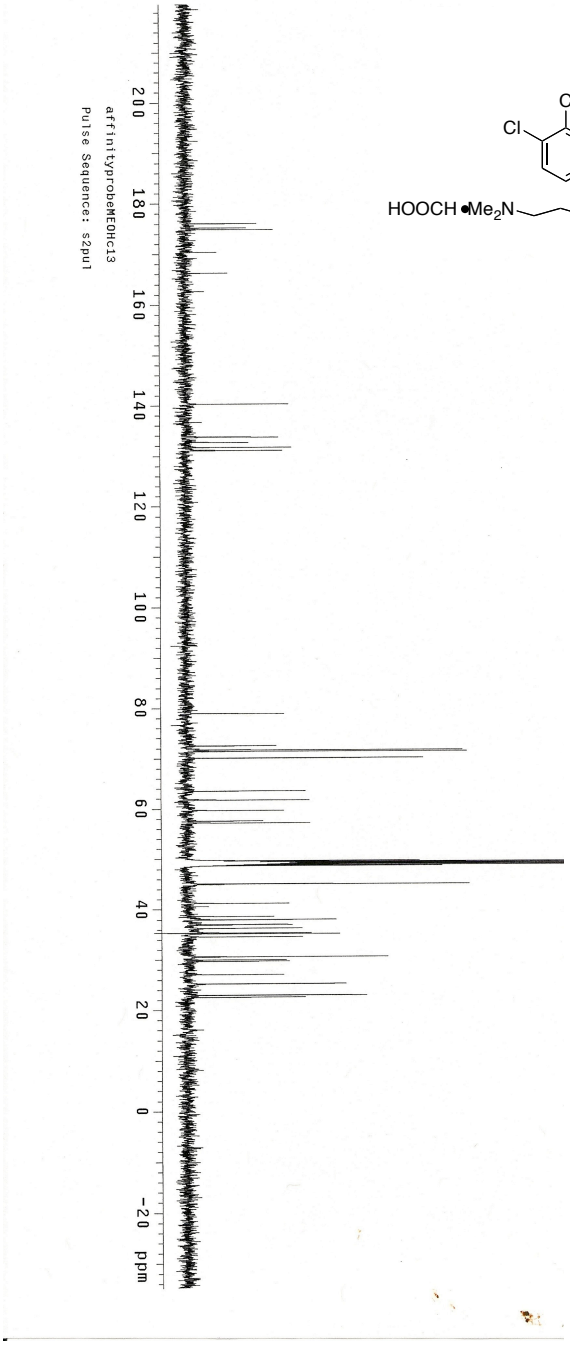

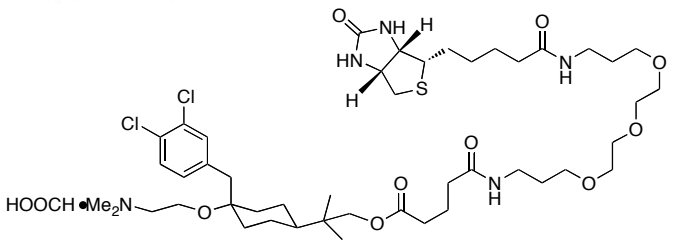

1.41
125 MHz, CD_3OD

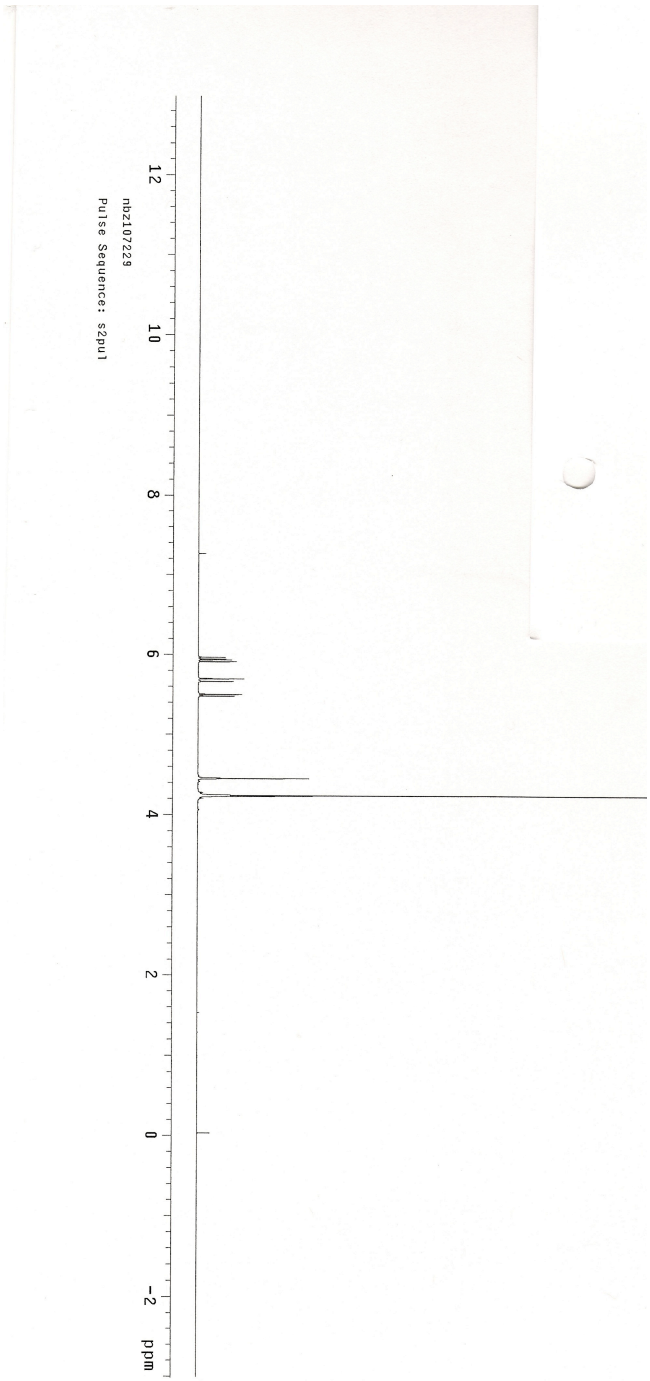

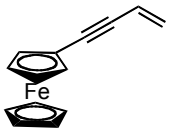

2.16
500 MHz, $CDCl_3$

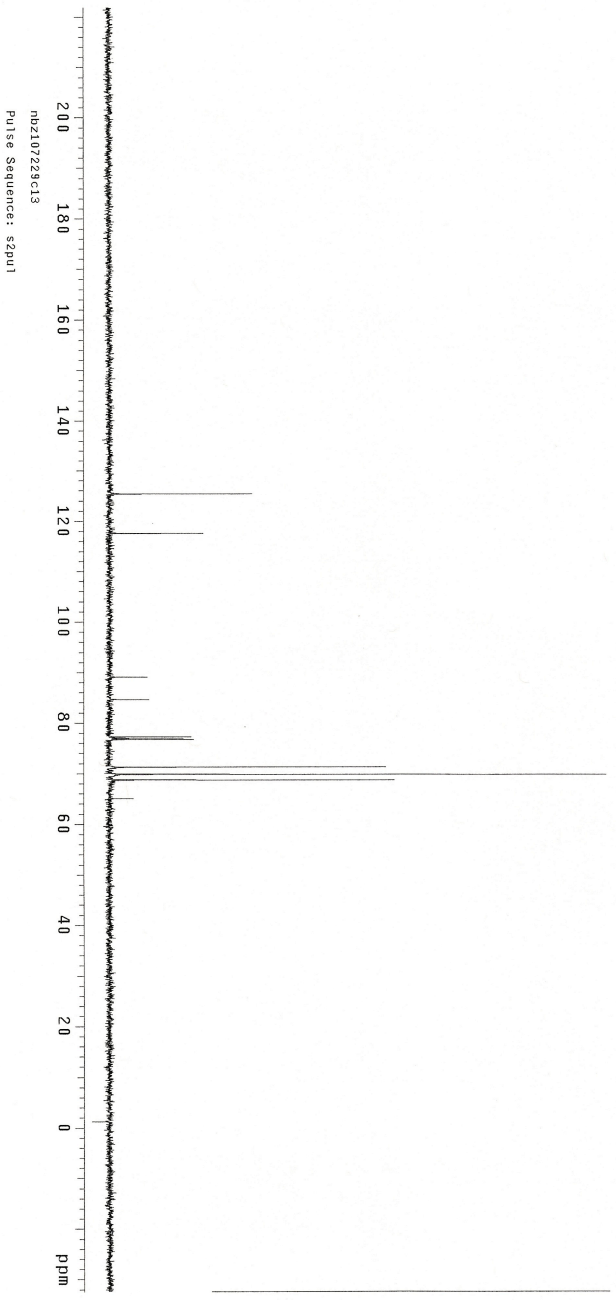

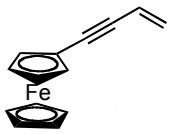

2.16
125 MHz, $CDCl_3$

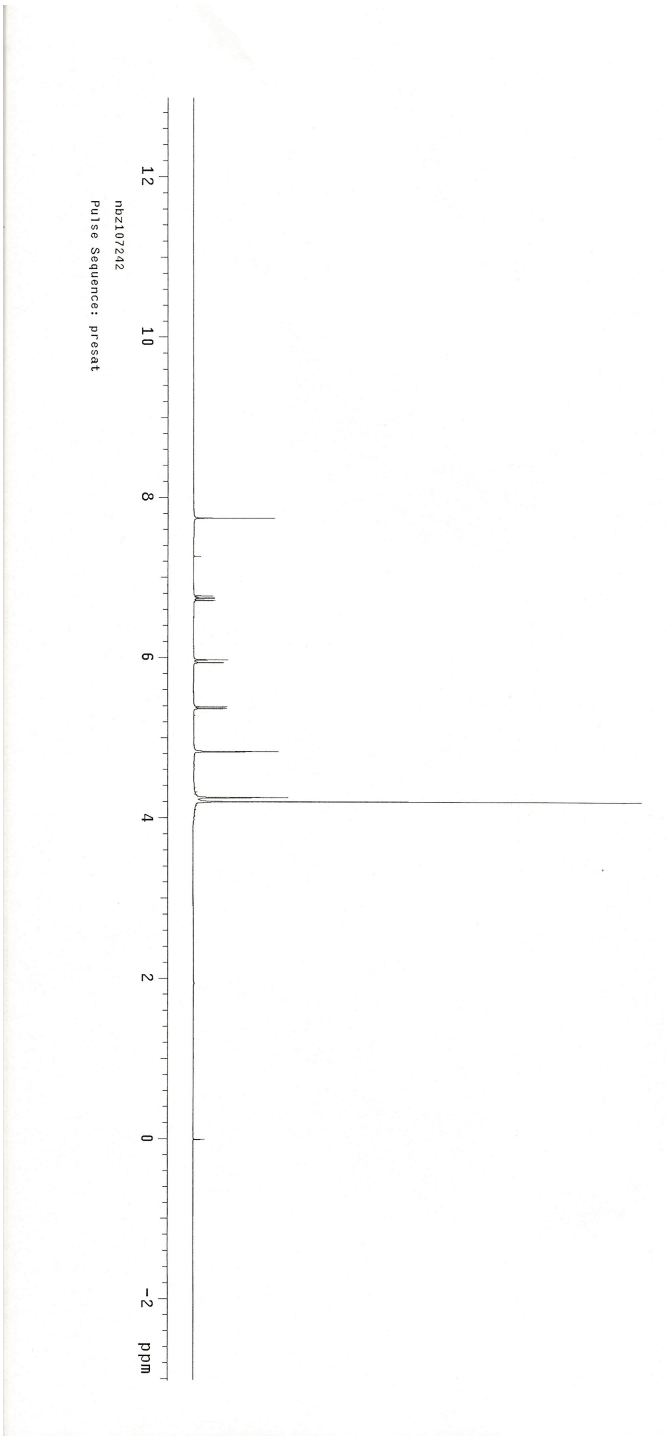

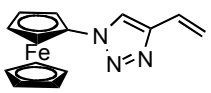

2.18
500 MHz, $CDCl_3$

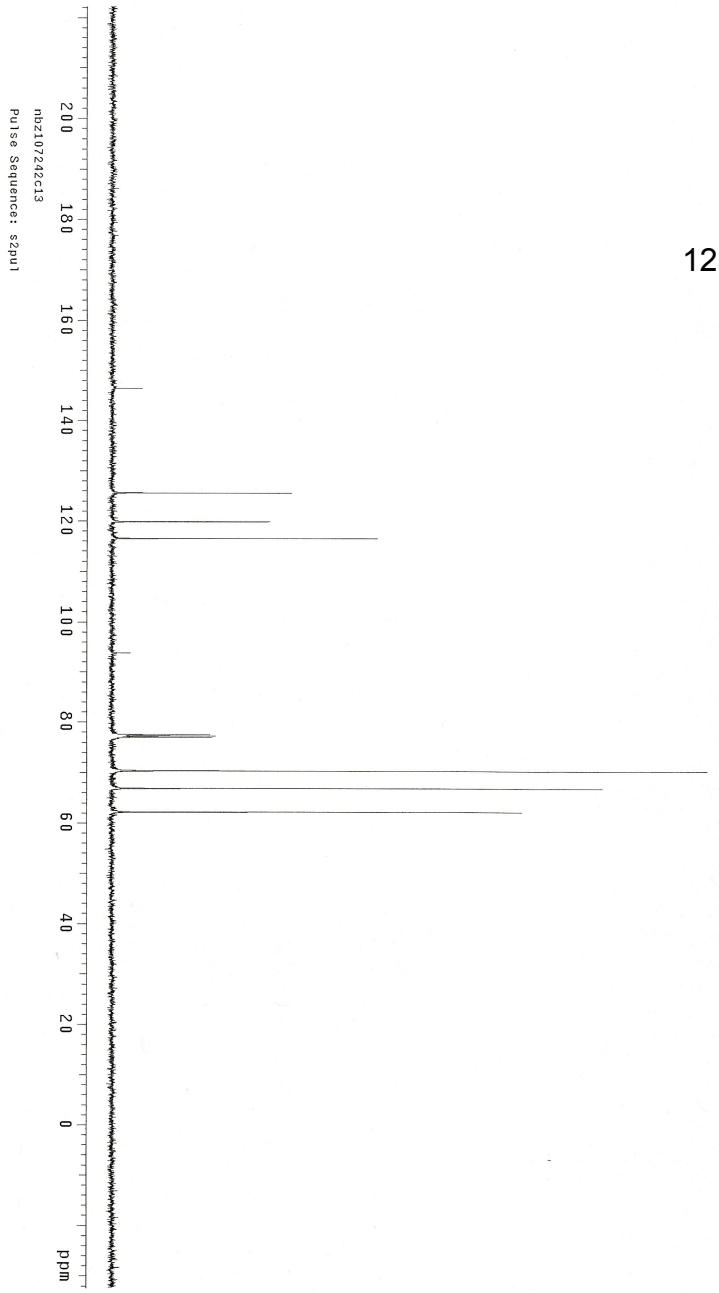

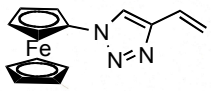

2.18
125 MHz, $CDCl_3$

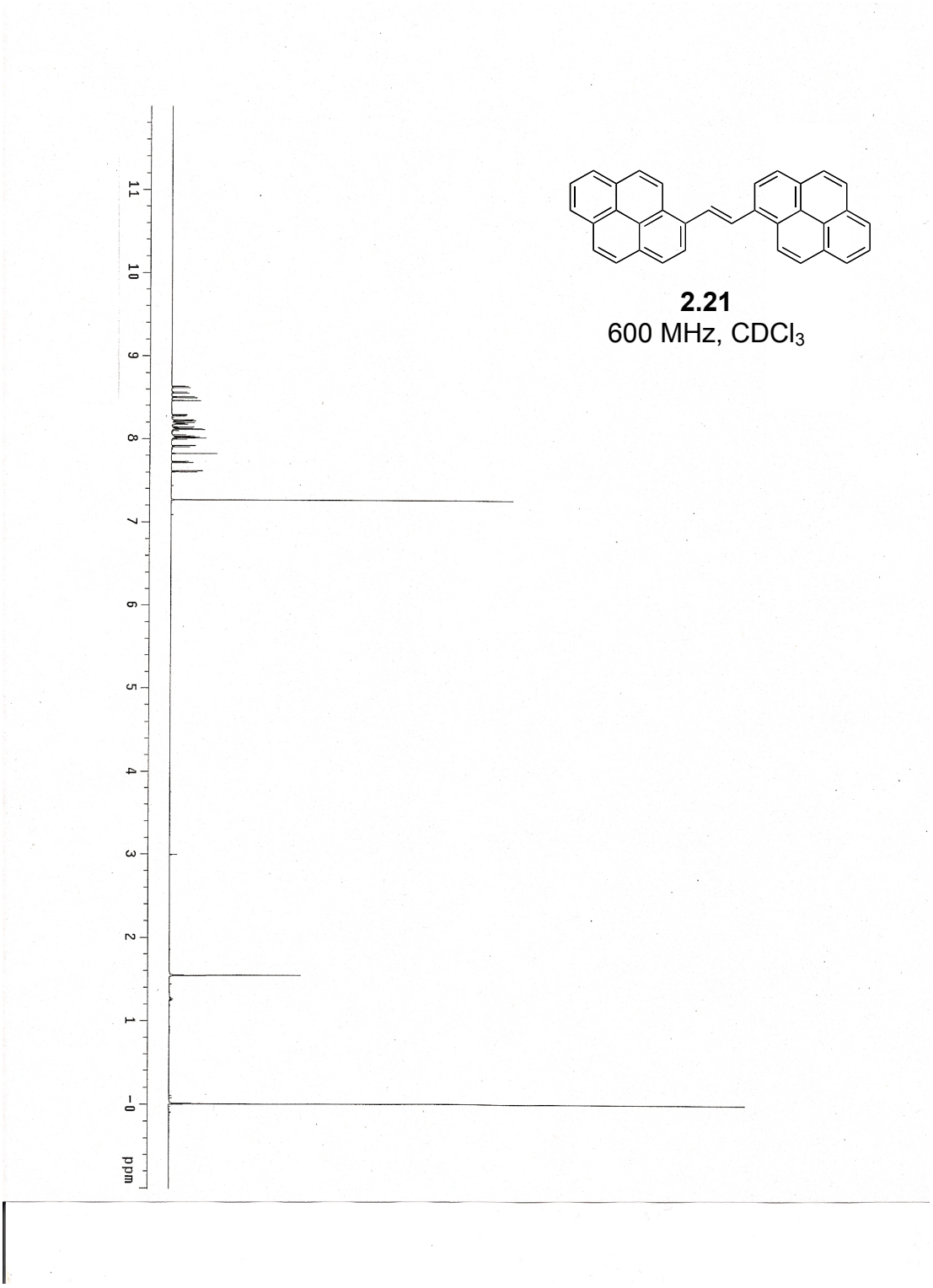

2.21
600 MHz, $CDCl_3$

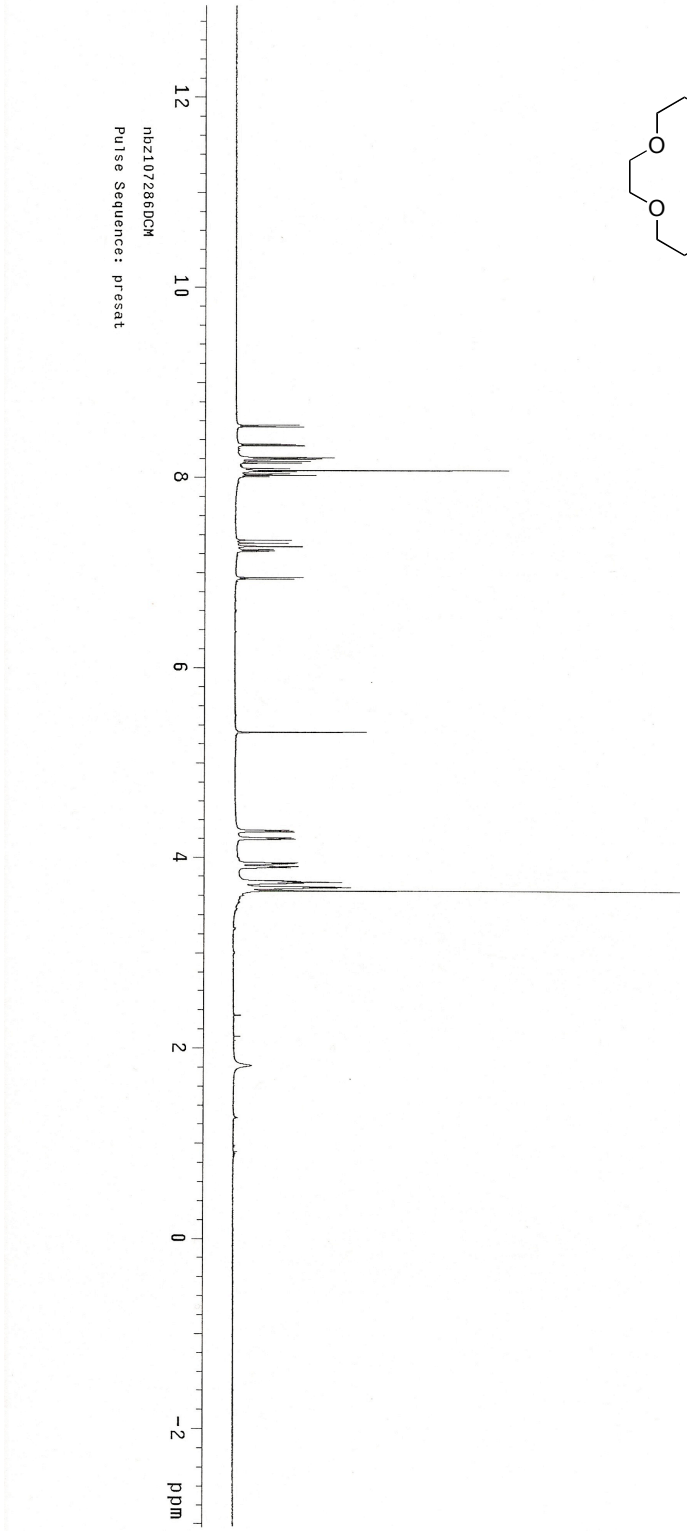

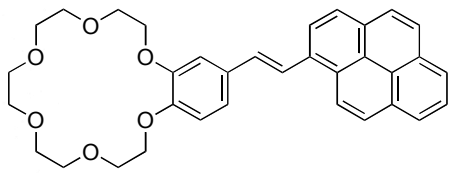

2.26
500 MHz, $CDCl_3$

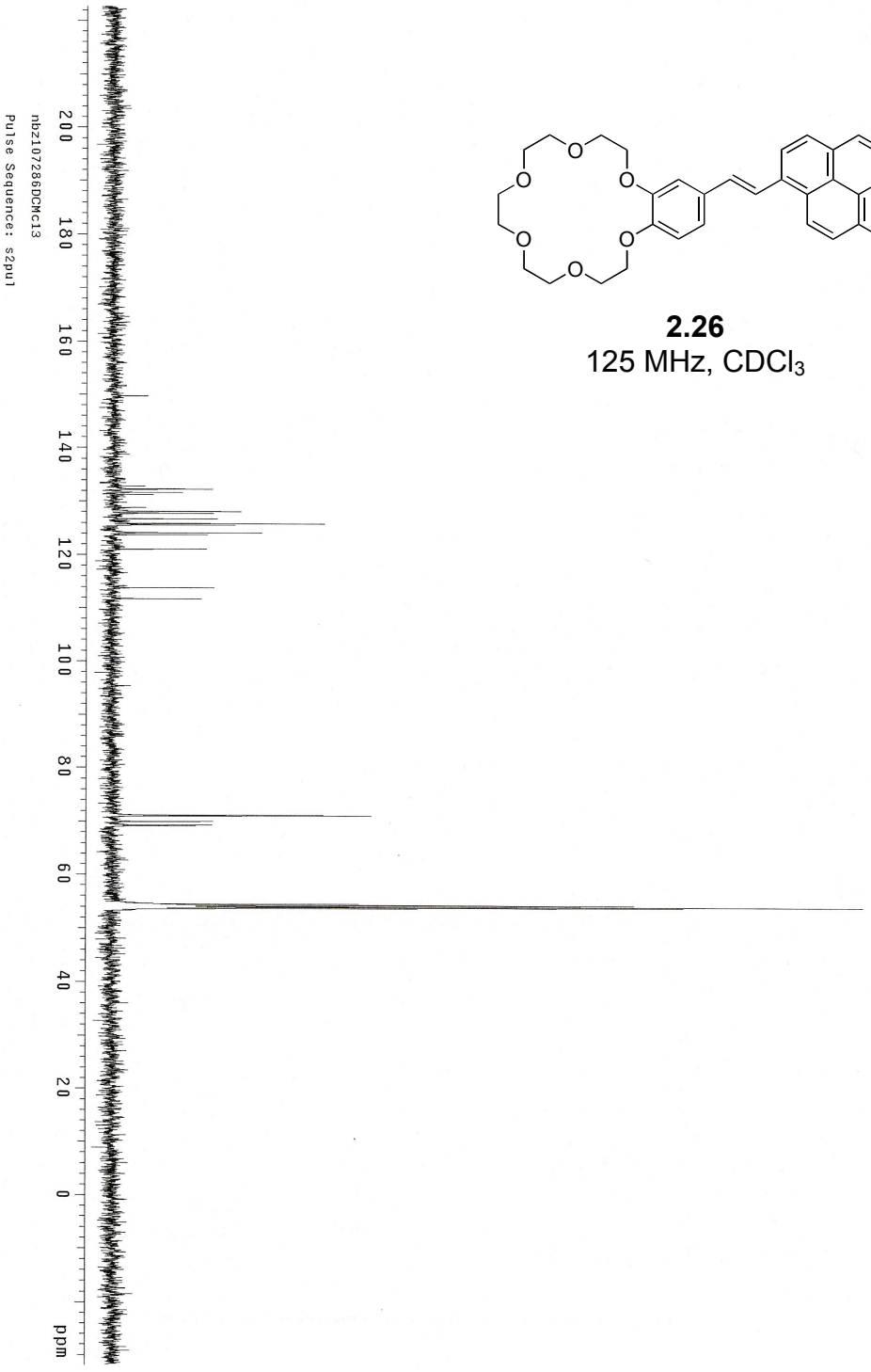

2.26
125 MHz, $CDCl_3$

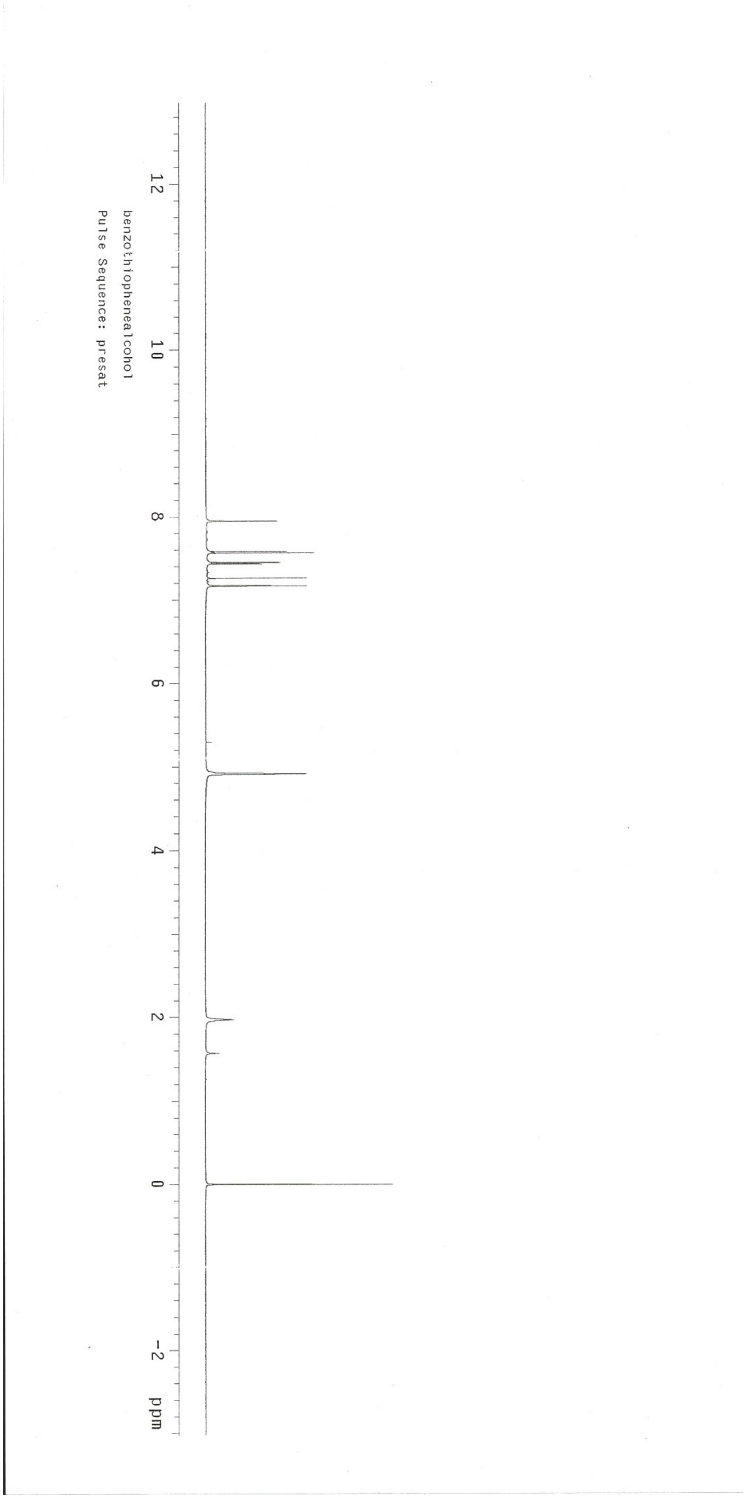

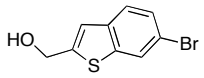

4.12a
500 MHz, CD_3OD

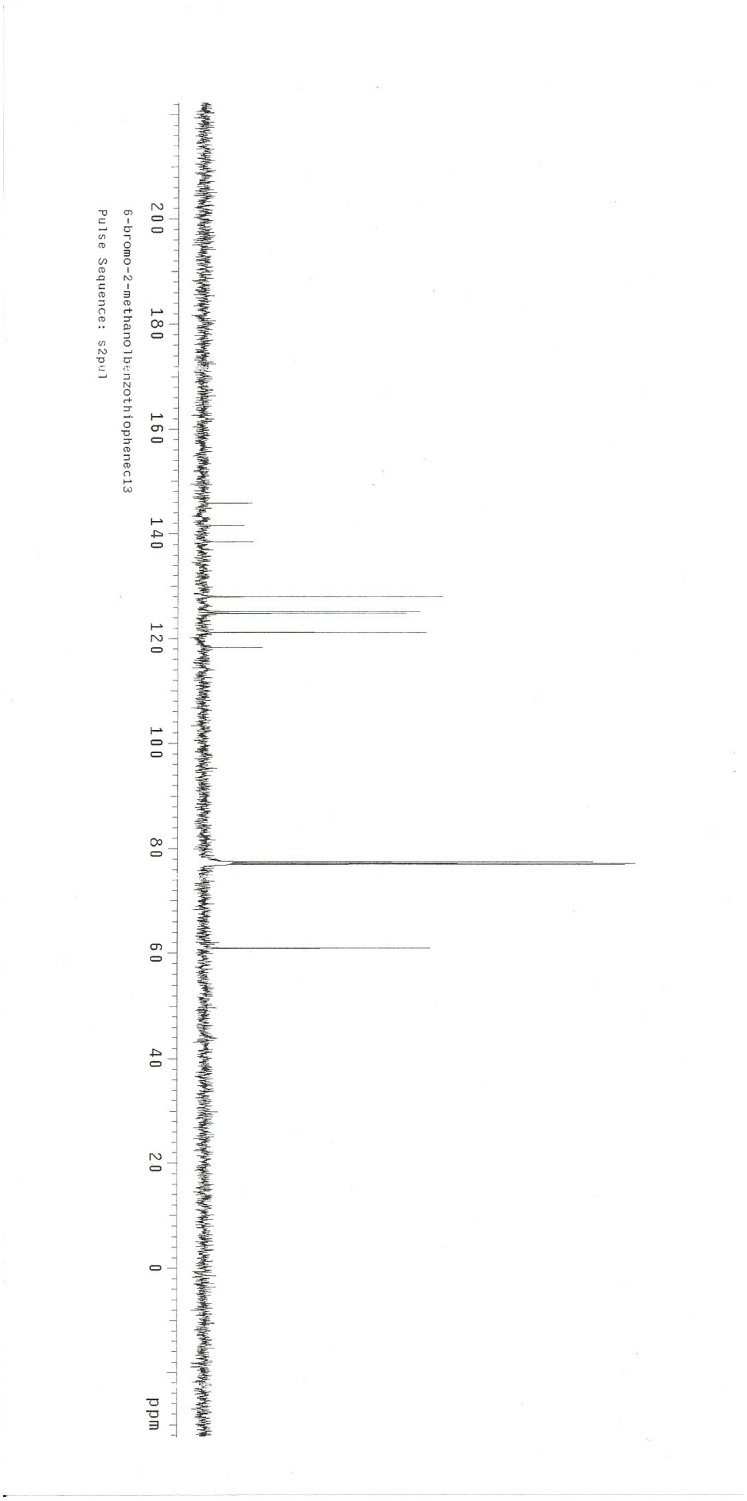

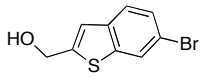

4.12a
125 MHz, CD_3OD

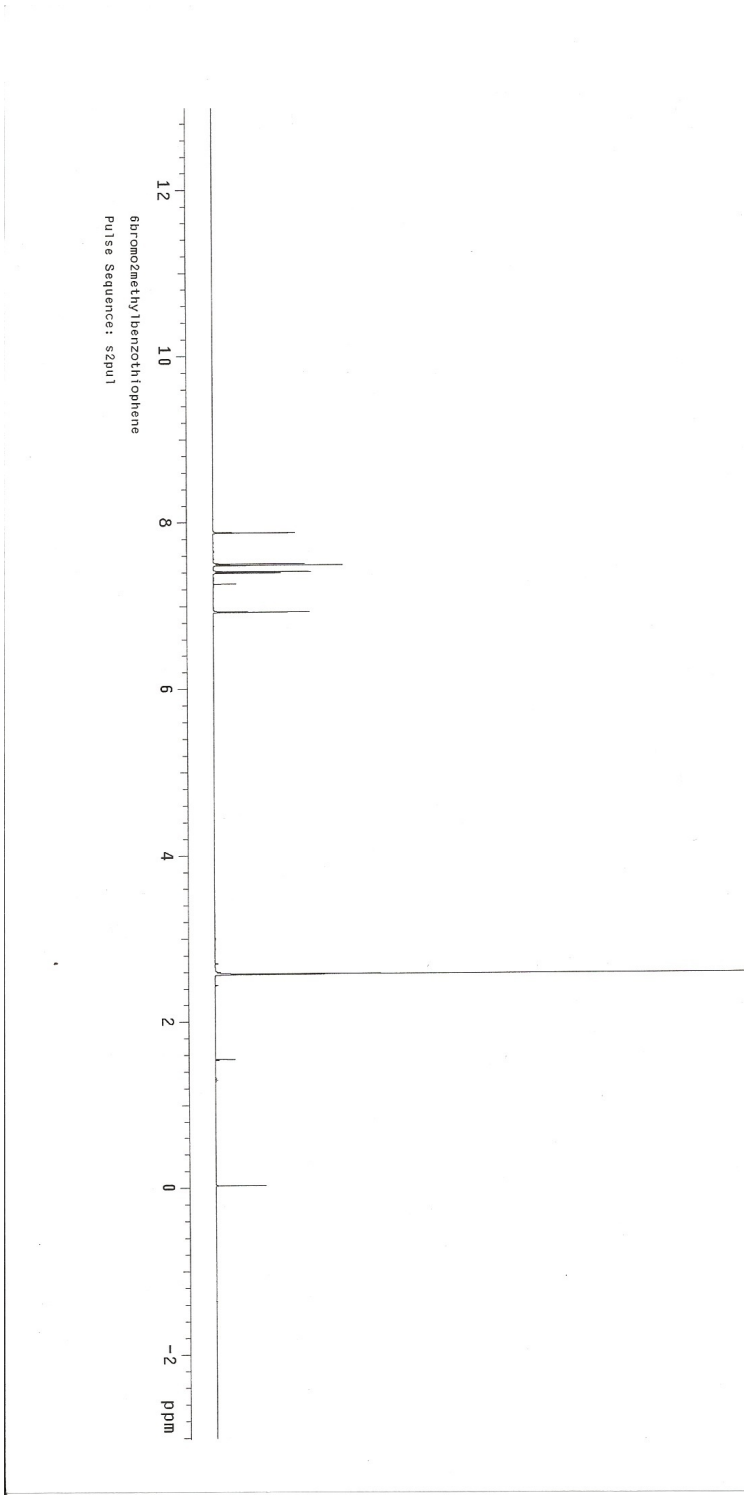

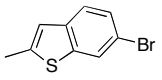

4.10
500 MHz, $CDCl_3$

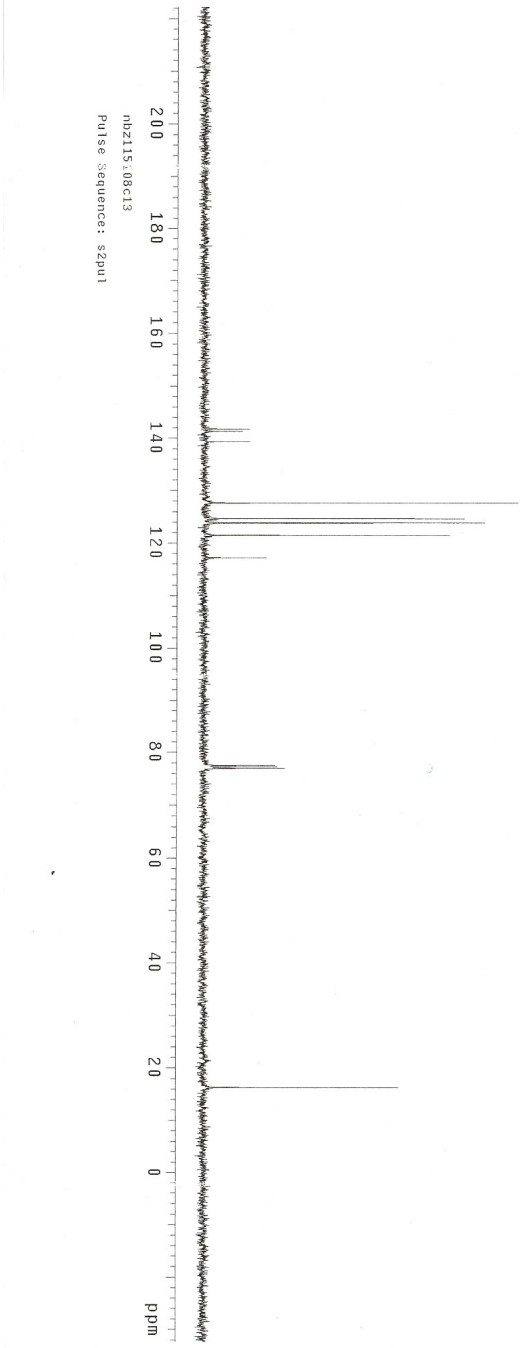

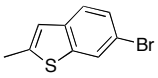

4.10
125 MHz, $CDCl_3$

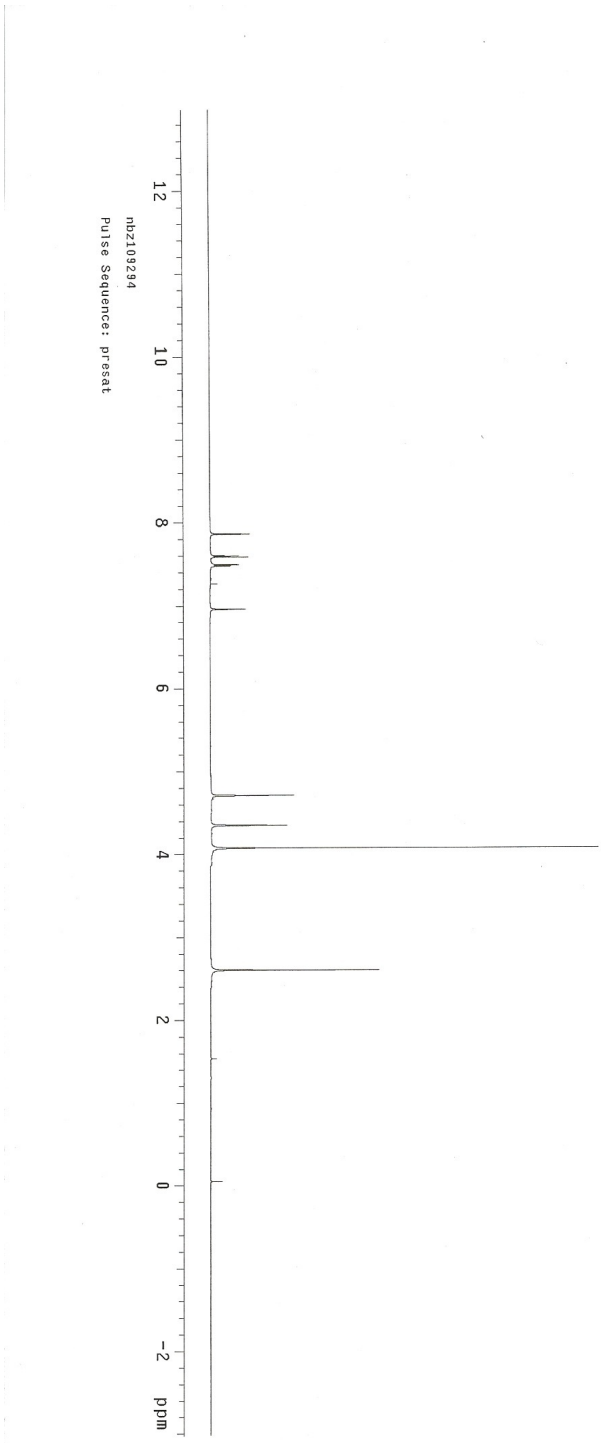

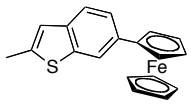

4.13
500 MHz, $CDCl_3$

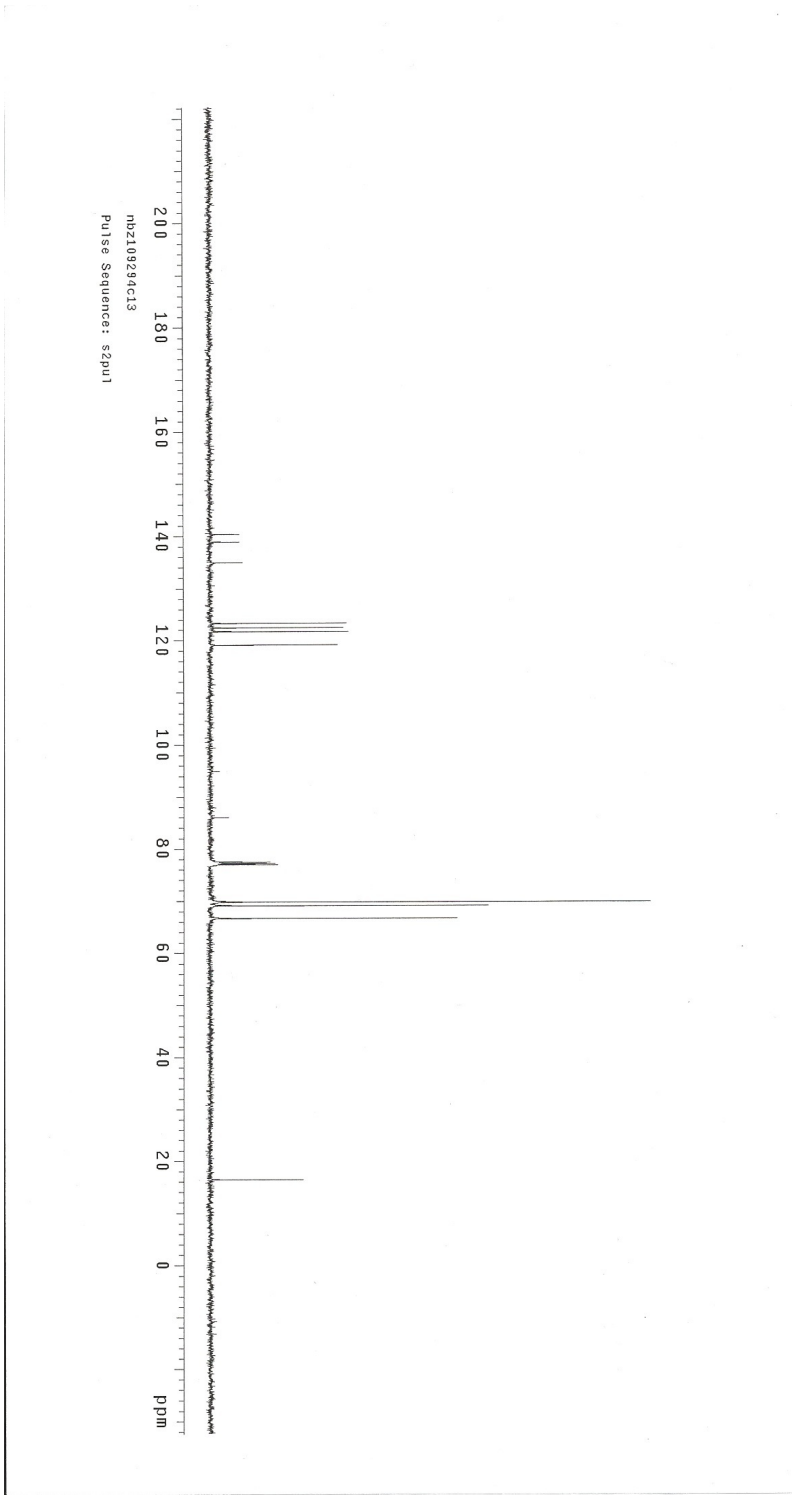

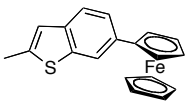

4.13
125 MHz, $CDCl_3$

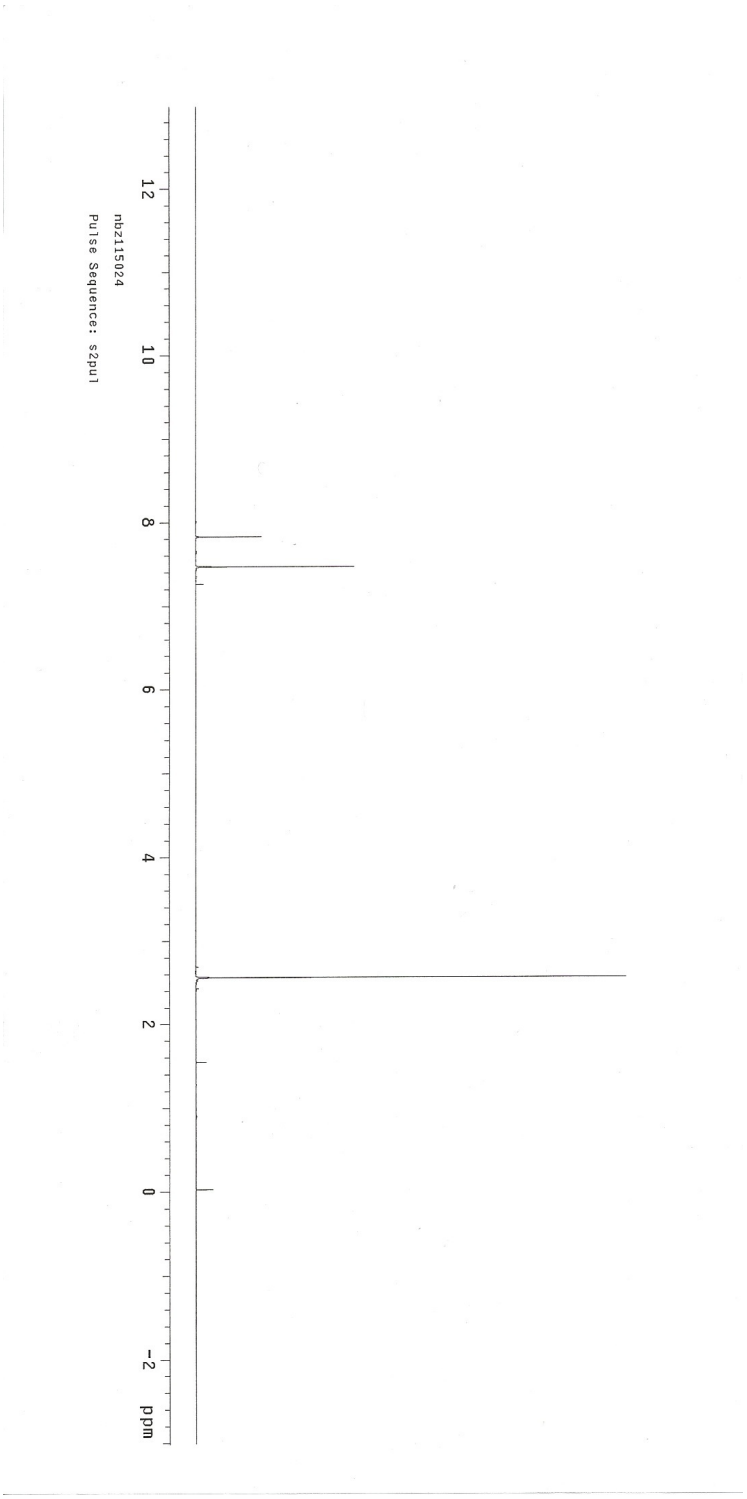

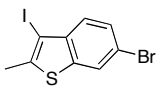

4.14
500 MHz, $CDCl_3$

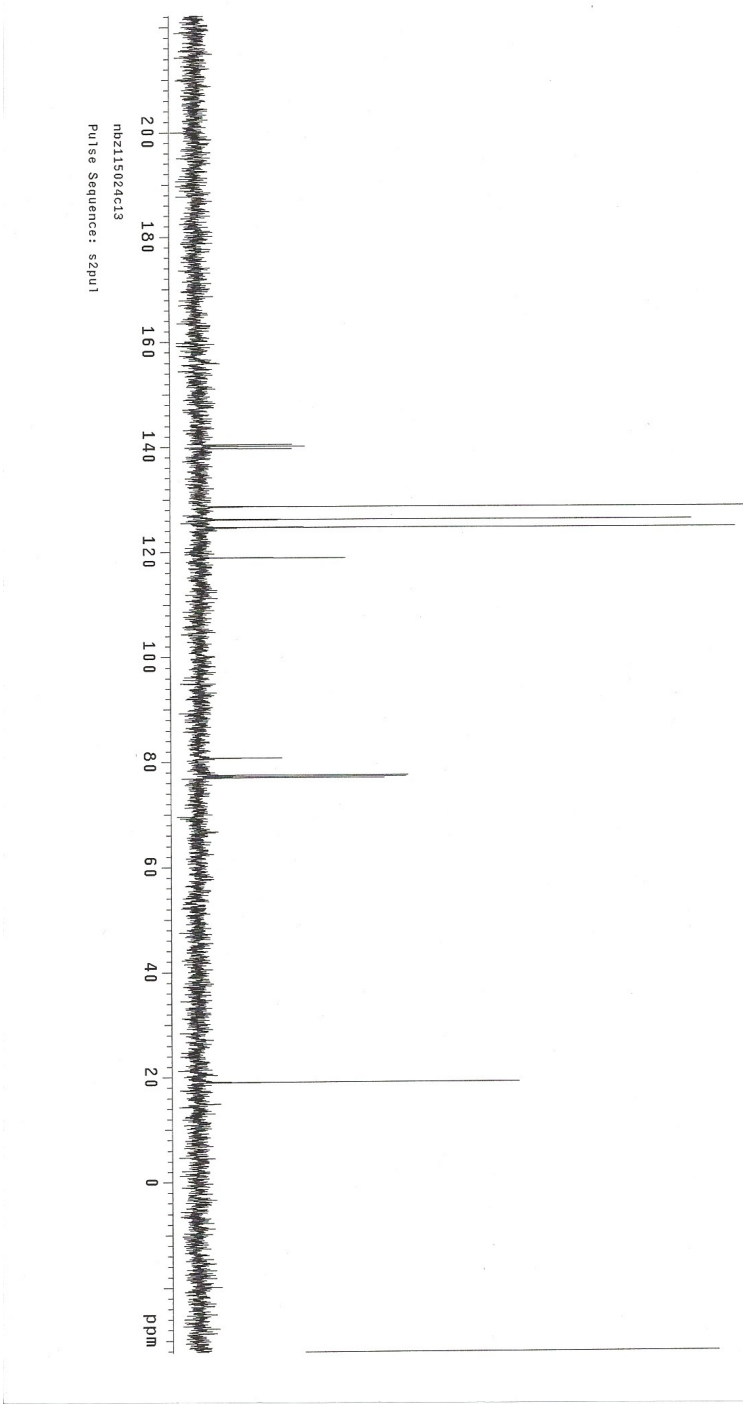

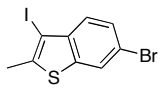

4.14
125 MHz, $CDCl_3$

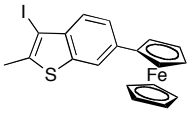

4.15
500 MHz, $CDCl_3$

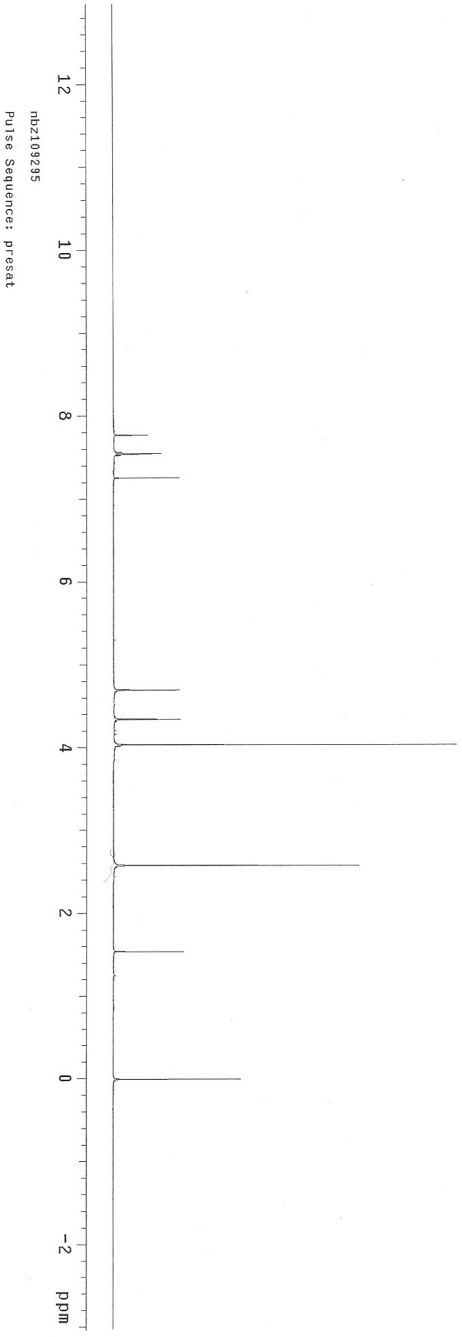

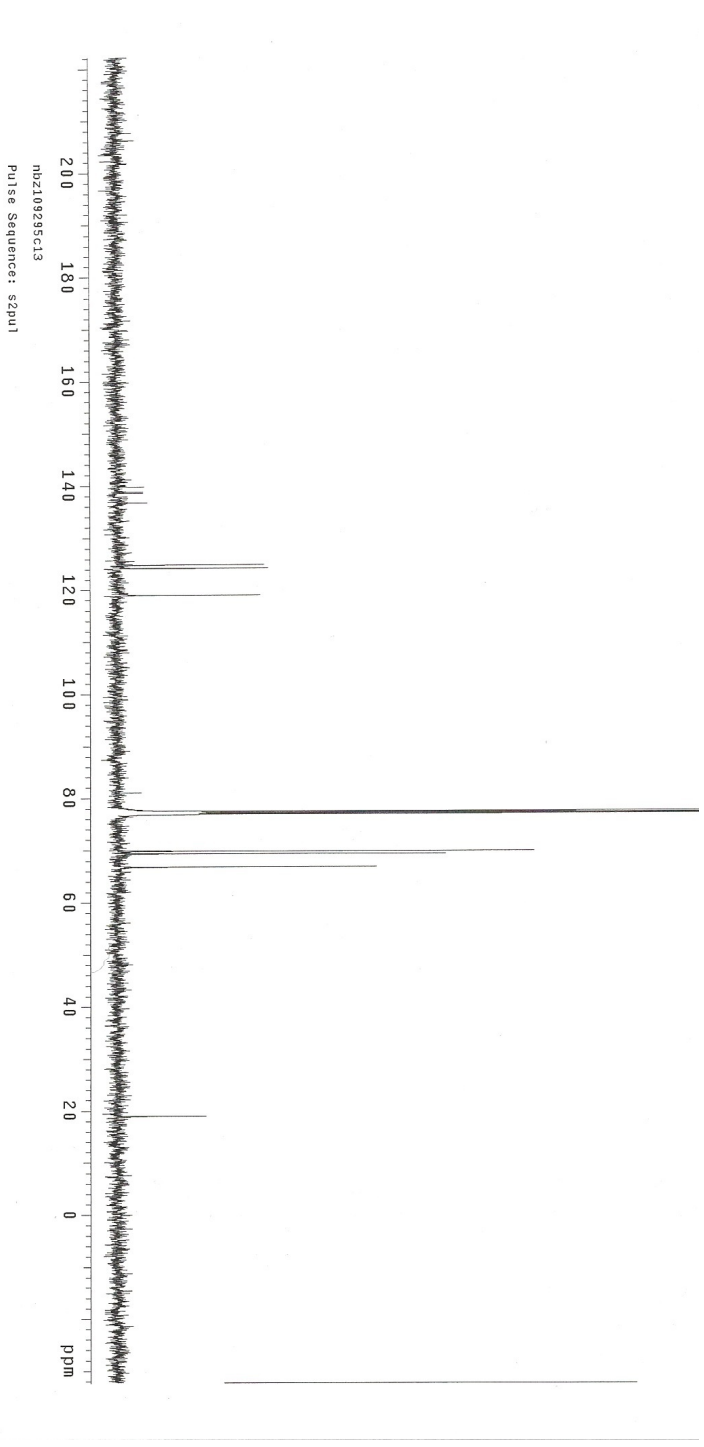

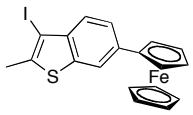

4.15
125 MHz, $CDCl_3$

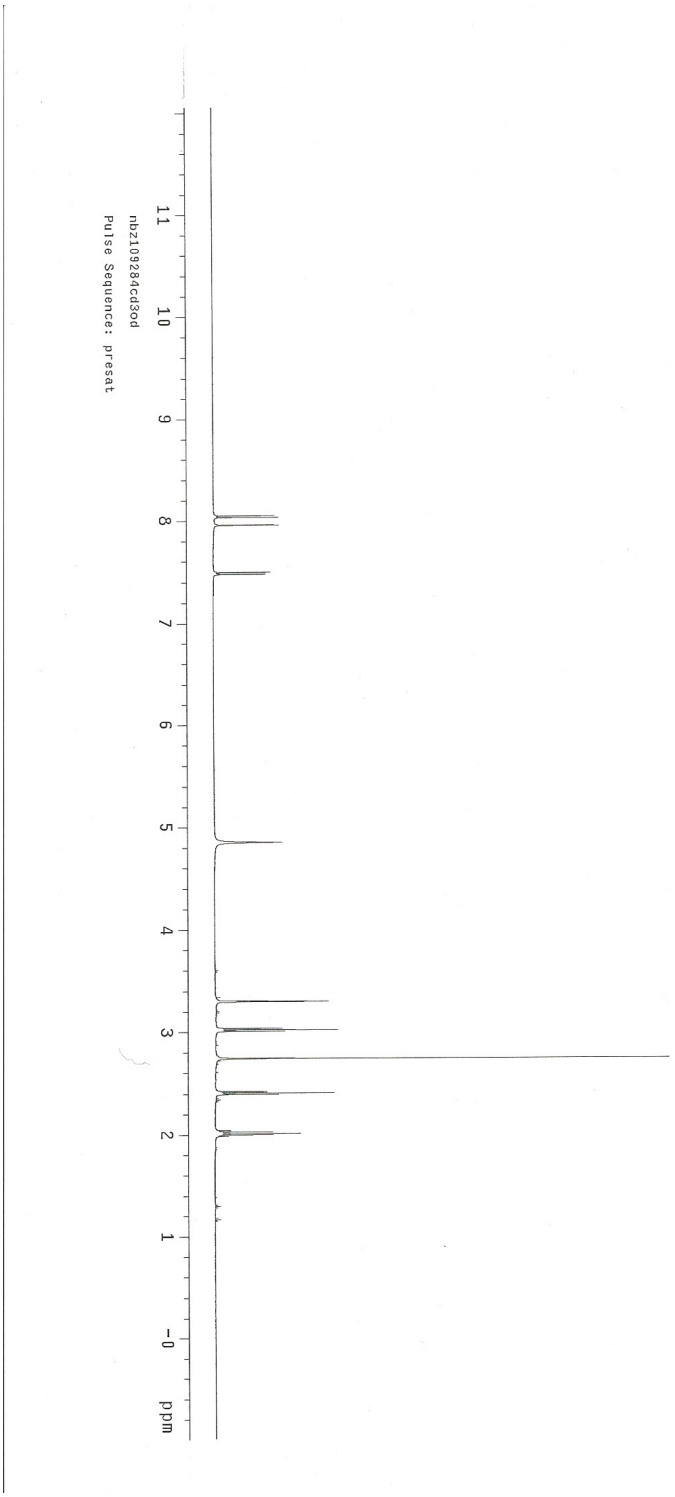

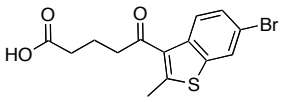

4.16
500 MHz, CD_3OD

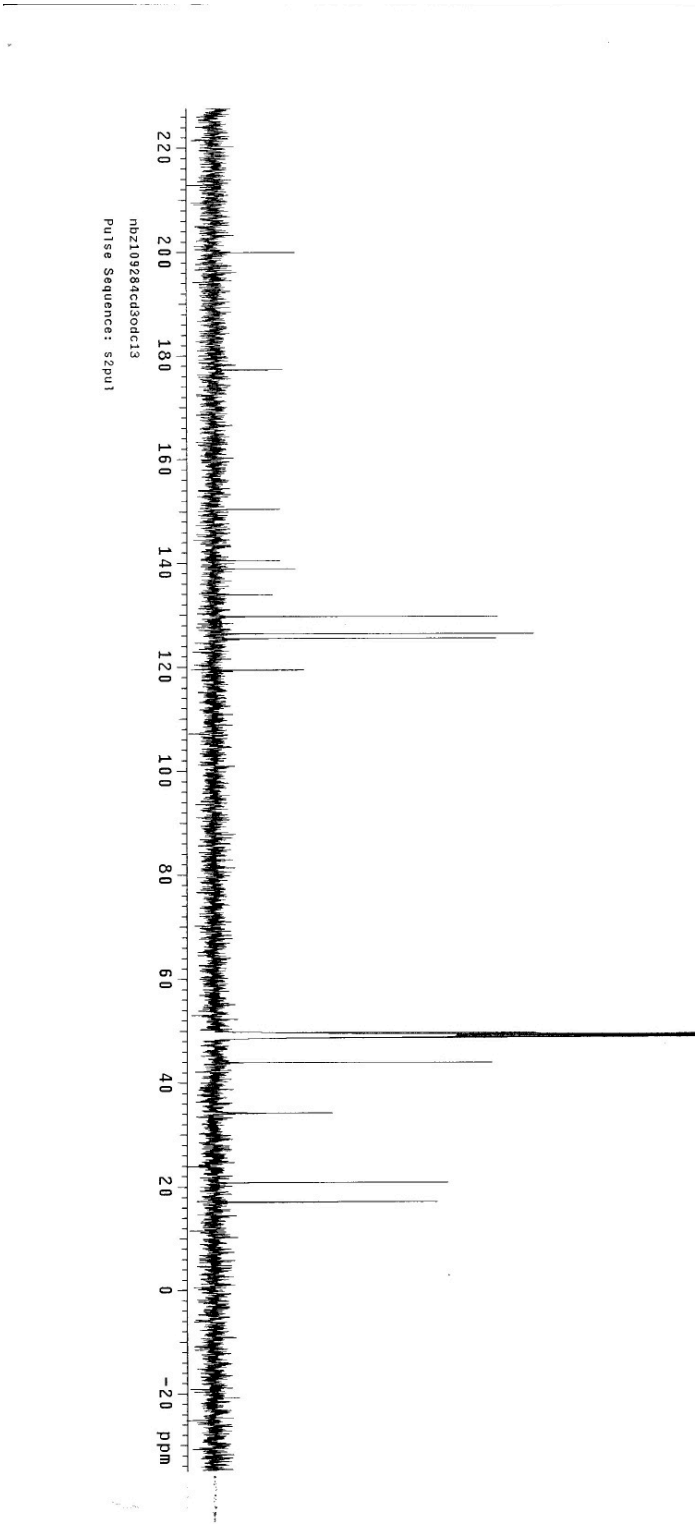

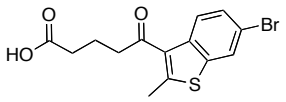

4.16
125 MHz, CD_3OD

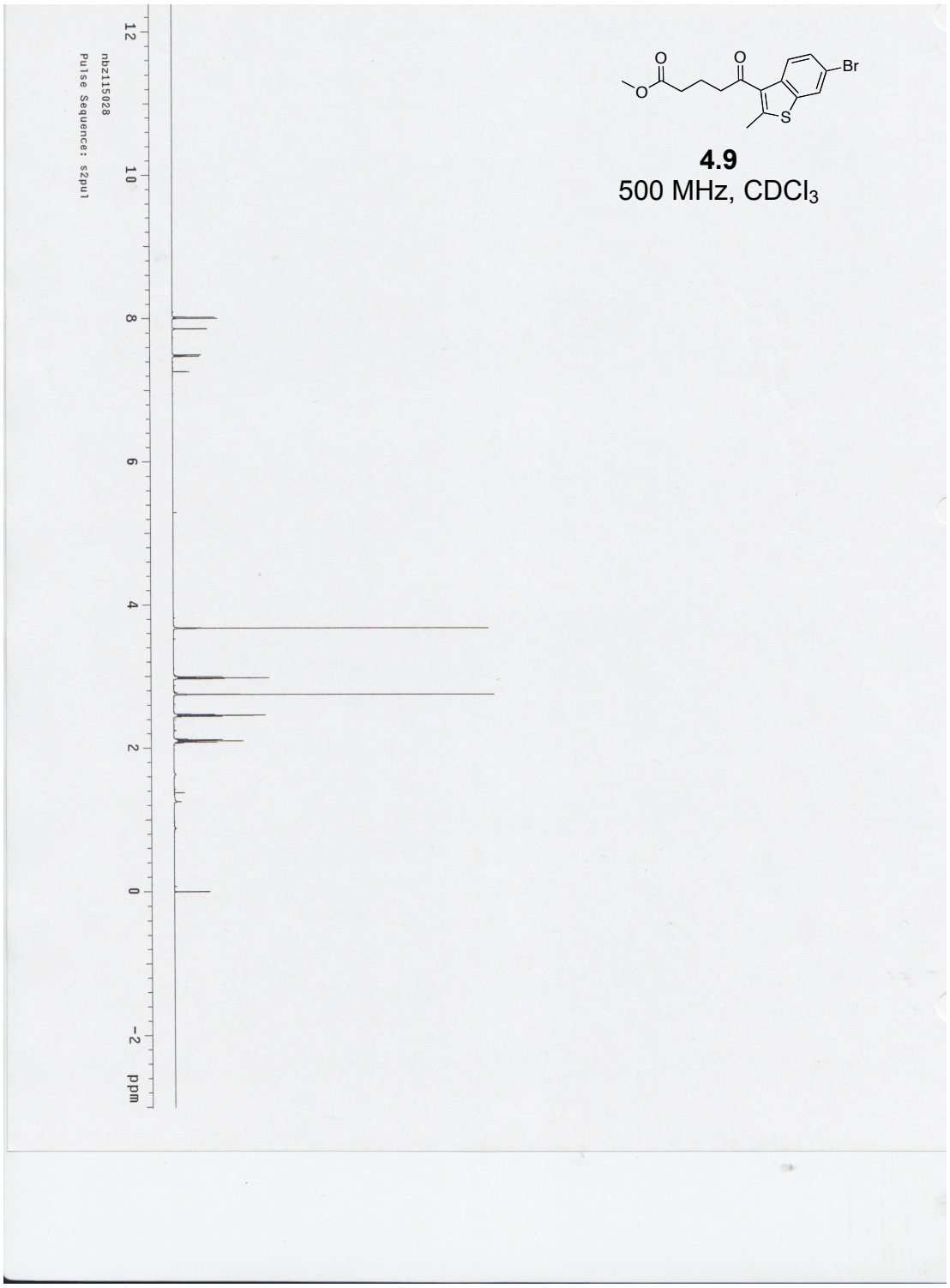

4.9
500 MHz, $CDCl_3$

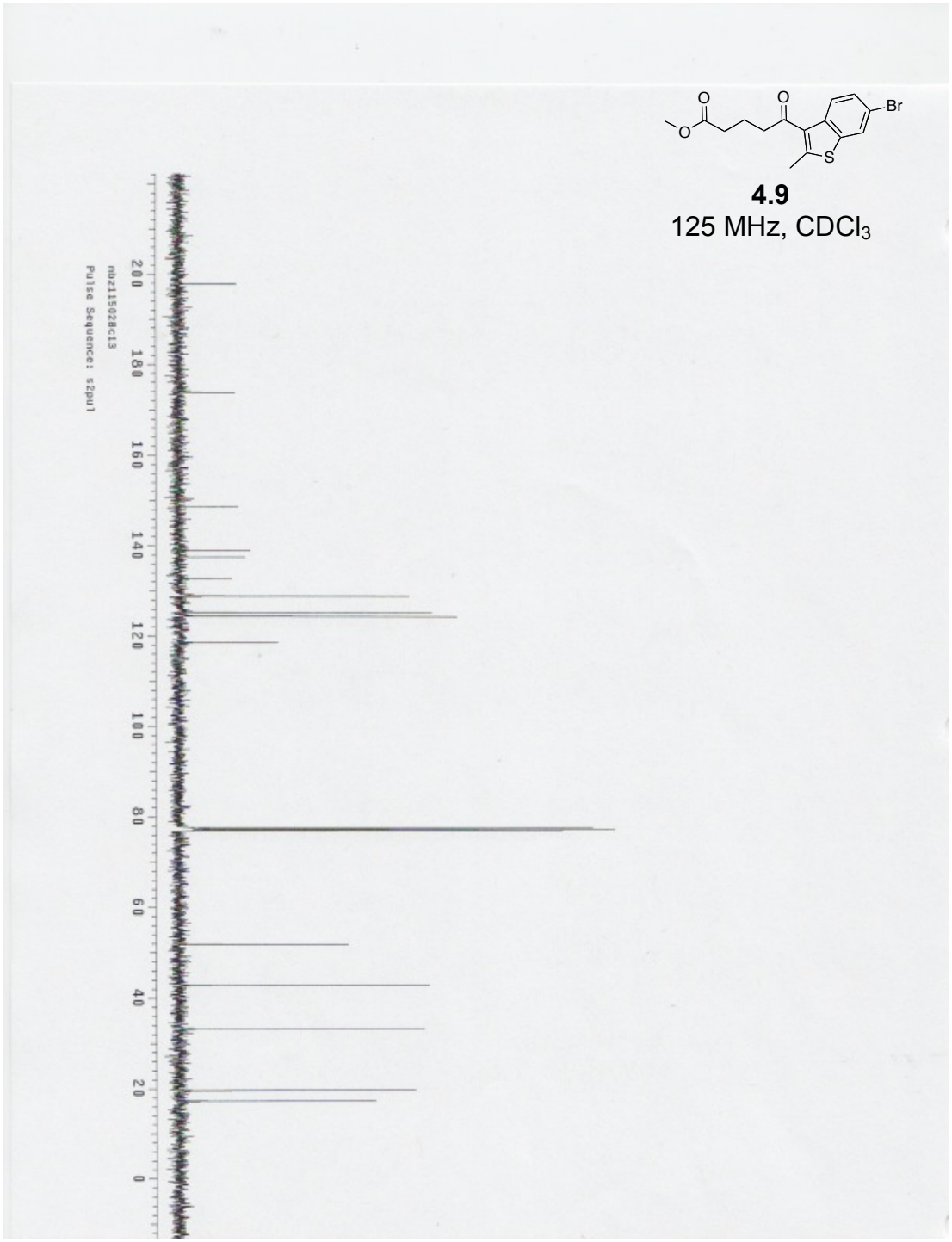
O
O
Br
O
S
4.9
125 MHz, CDCl3
nbz115028c13
Pulse Sequence: s2pul
200
180
160
140
120
100
80
60
40
20
0

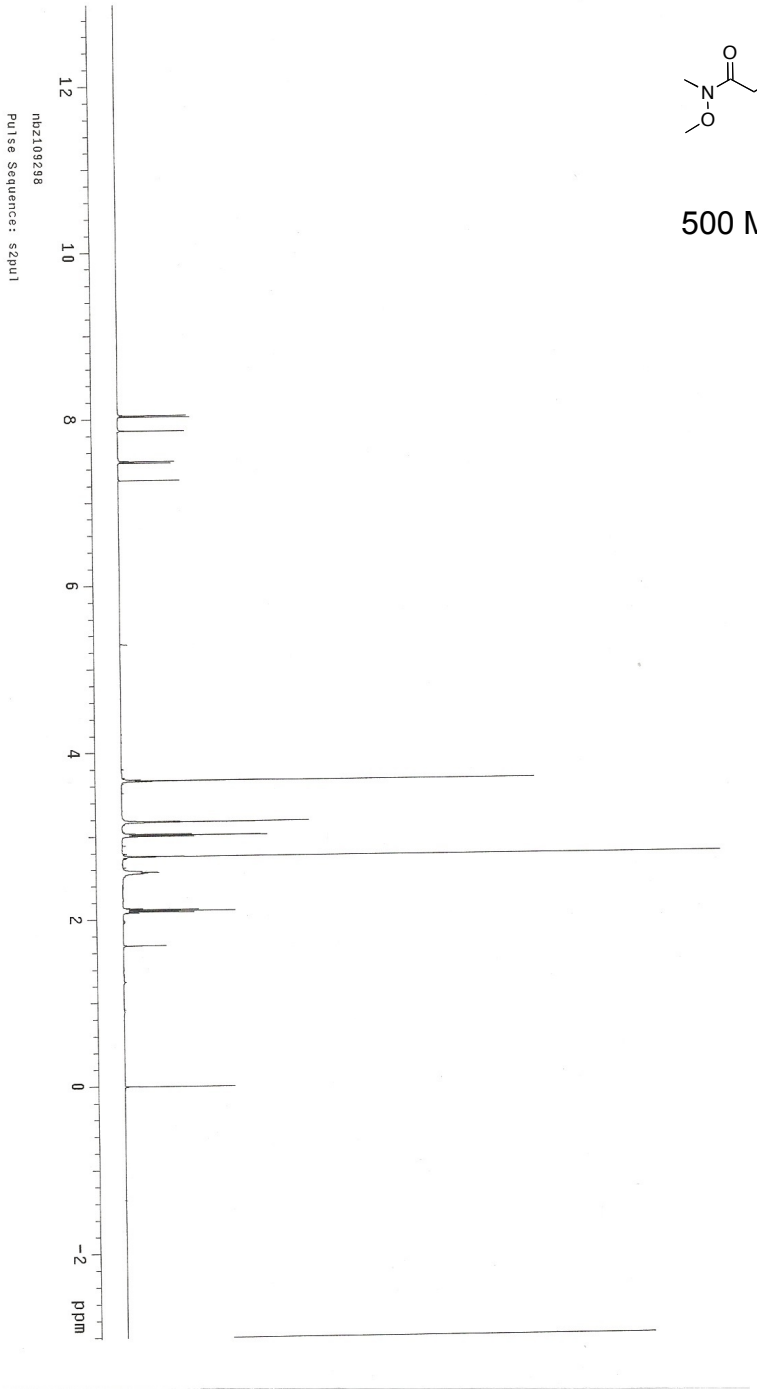

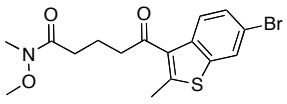

4.8
500 MHz, $CDCl_3$

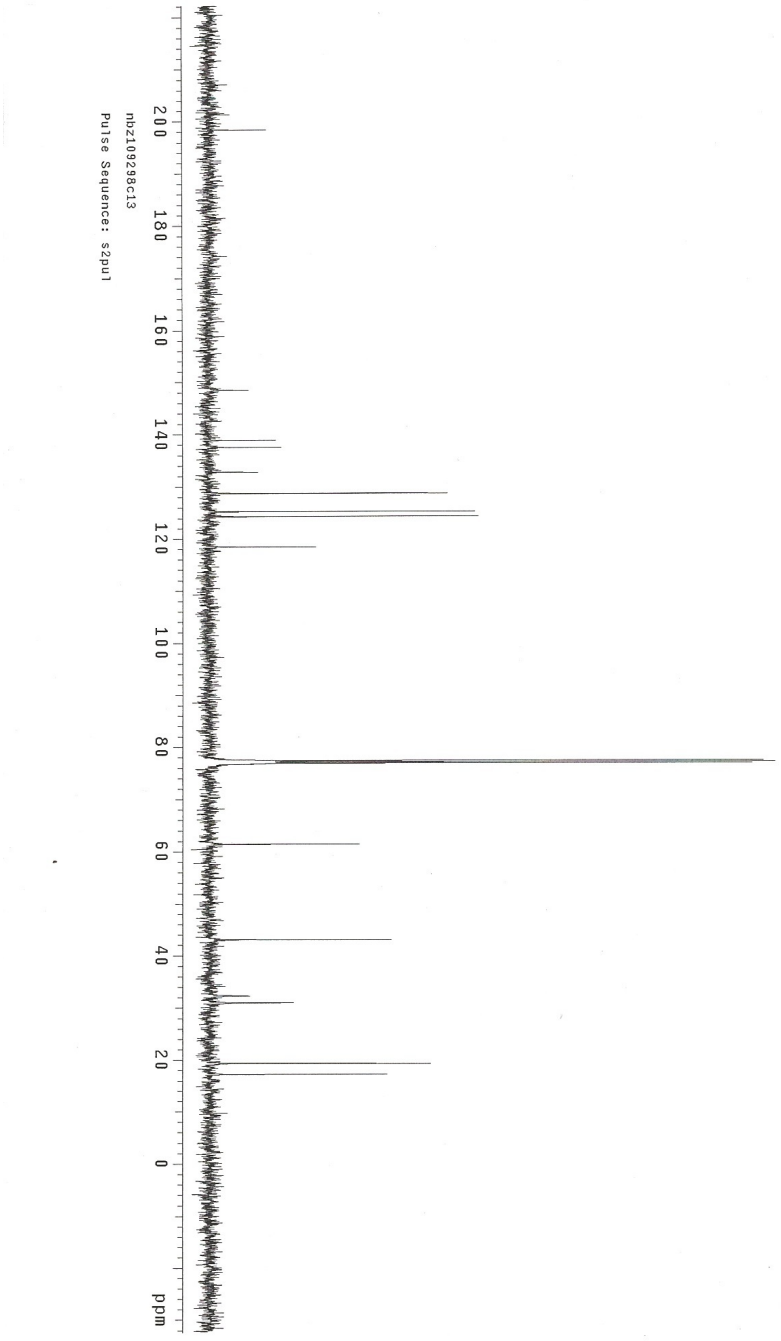

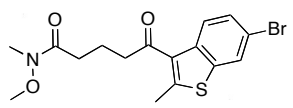

4.8
125 MHz, $CDCl_3$

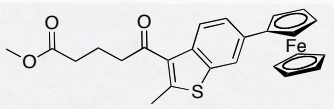

4.17
500 MHz, $CDCl_3$

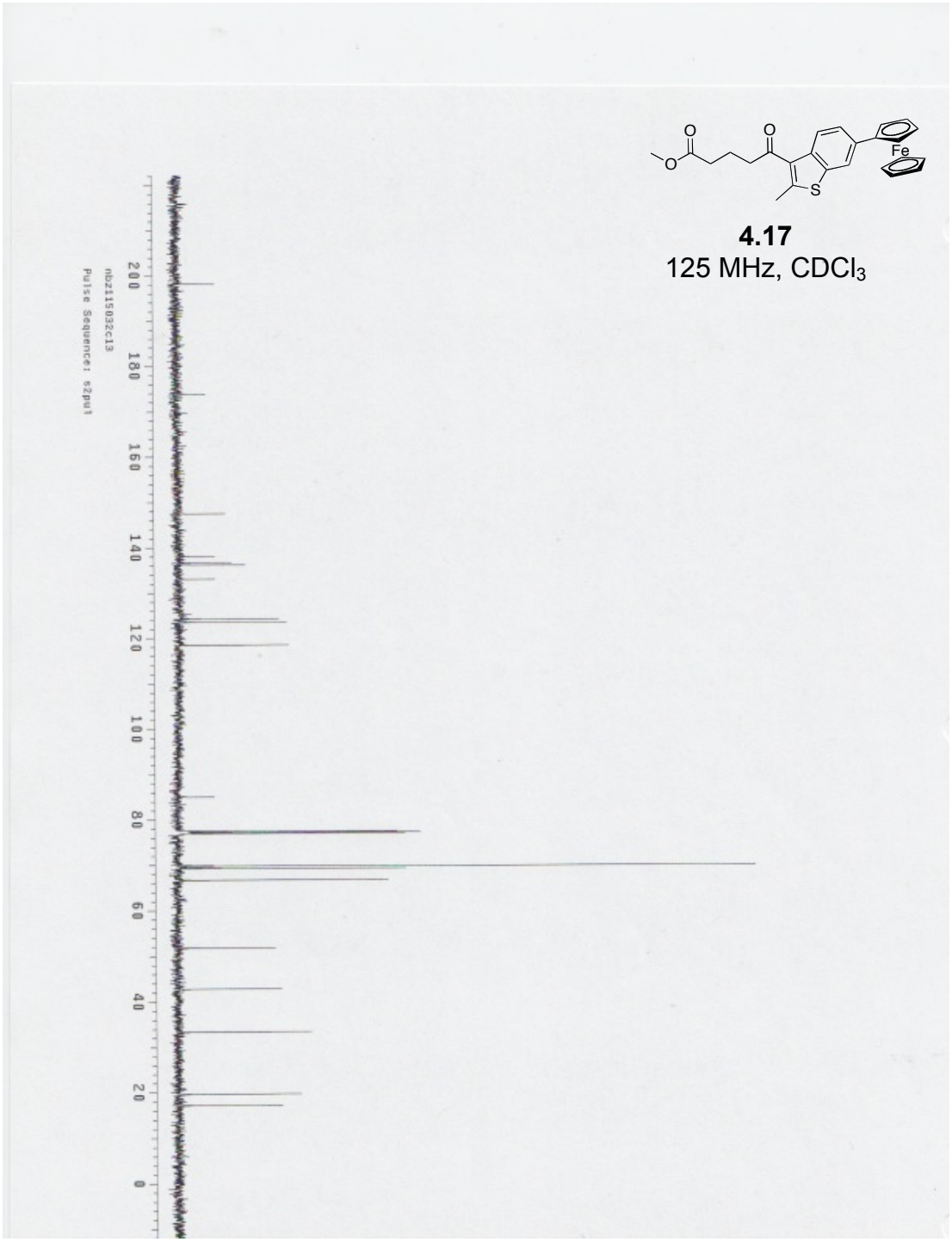

4.17
125 MHz, $CDCl_3$

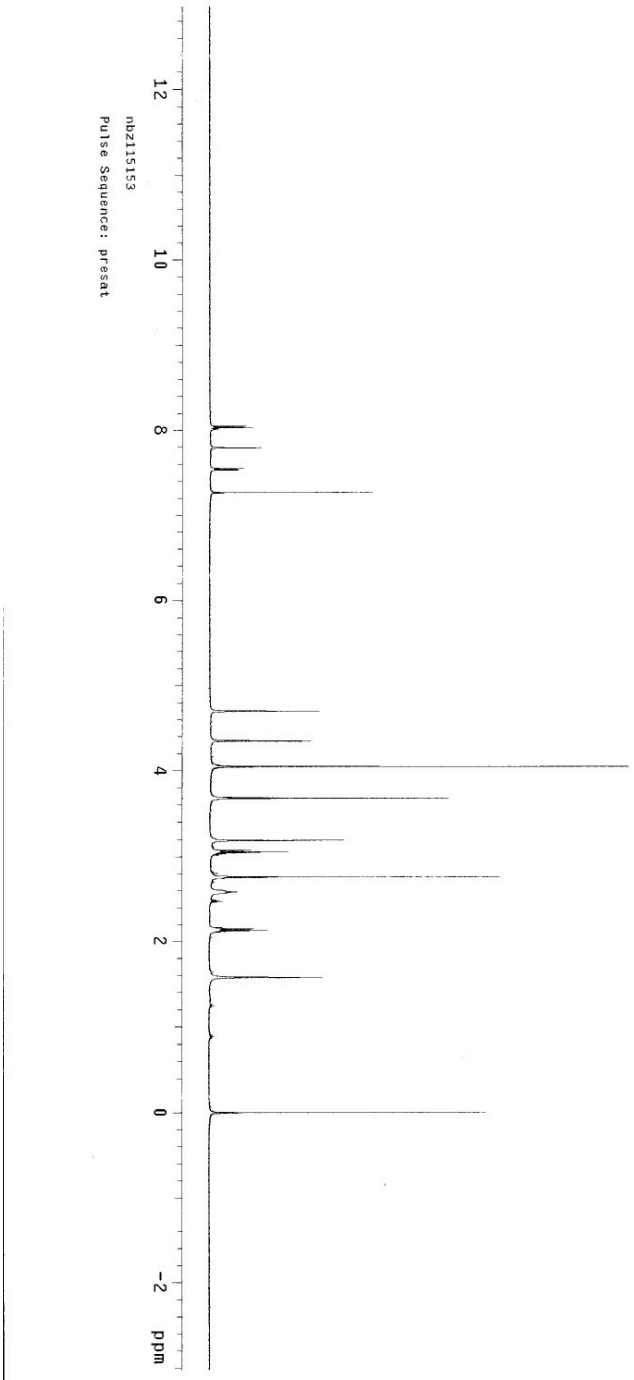

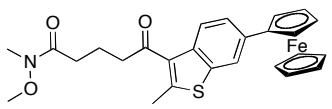

4.18
500 MHz, $CDCl_3$

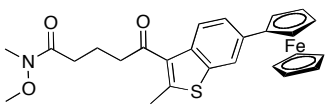

4.18
125 MHz, $CDCl_3$

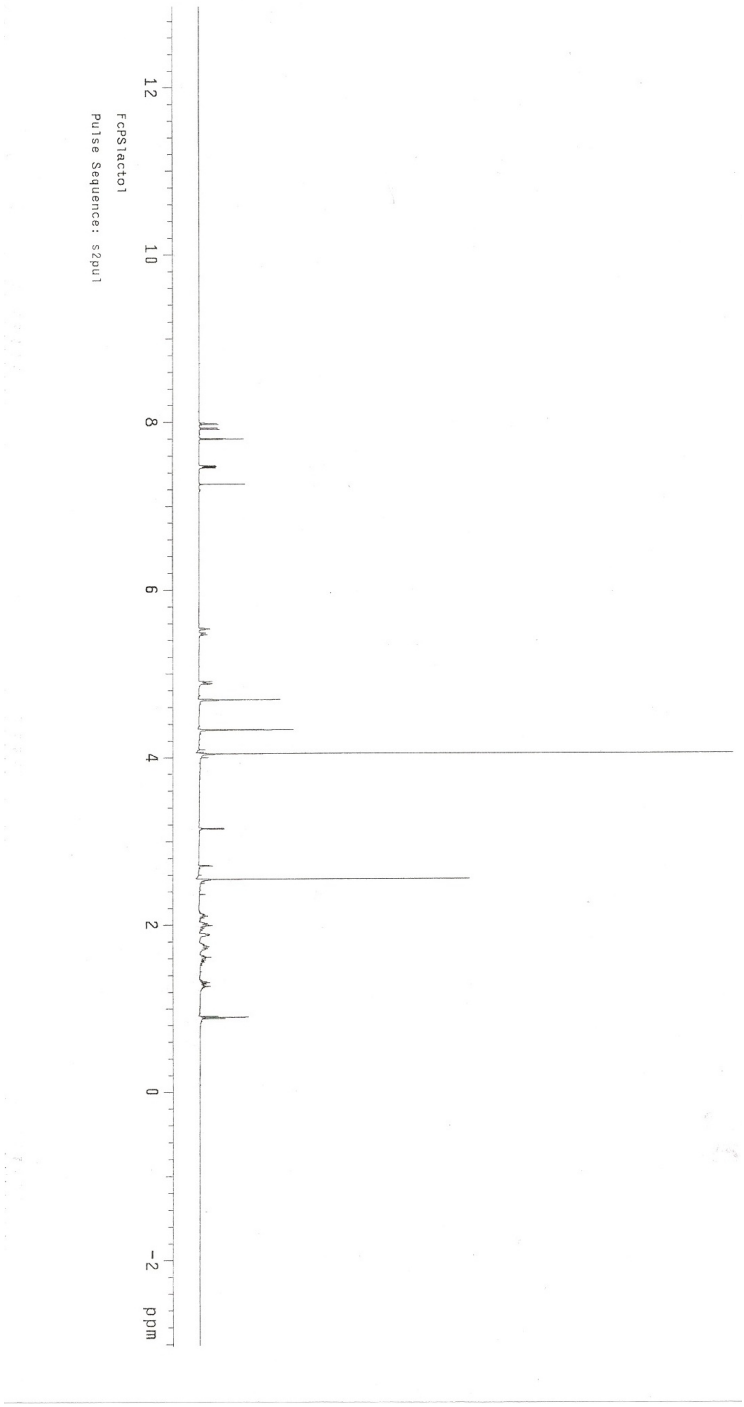

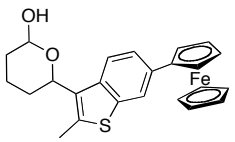

4.7
500 MHz, $CDCl_3$

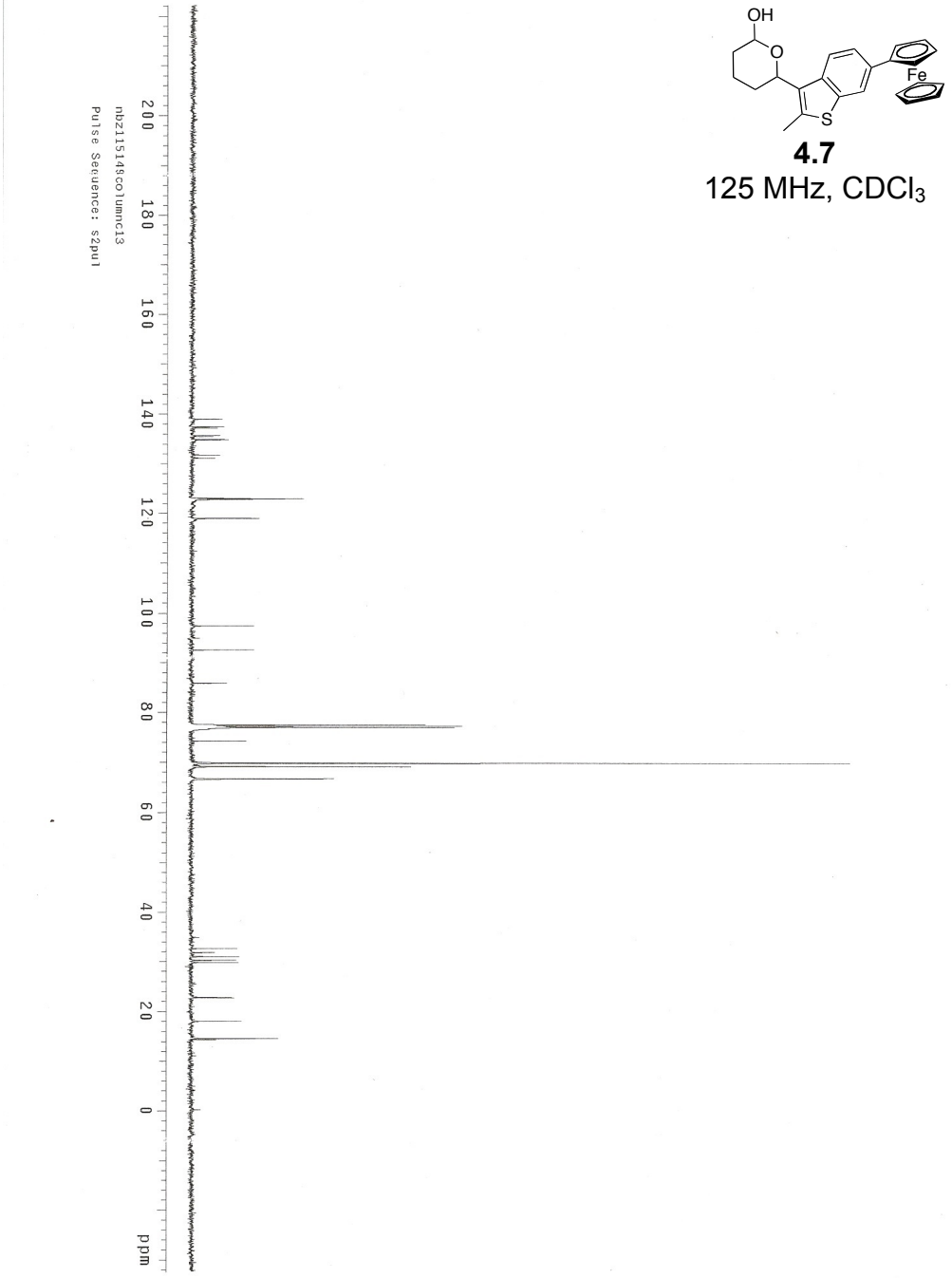

4.7

125 MHz, $CDCl_3$

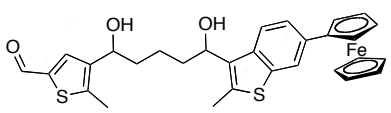

4.42

500 MHz, $CDCl_3$

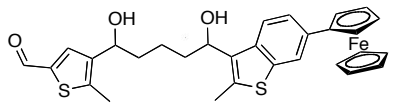

4.42

125 MHz, $CDCl_3$

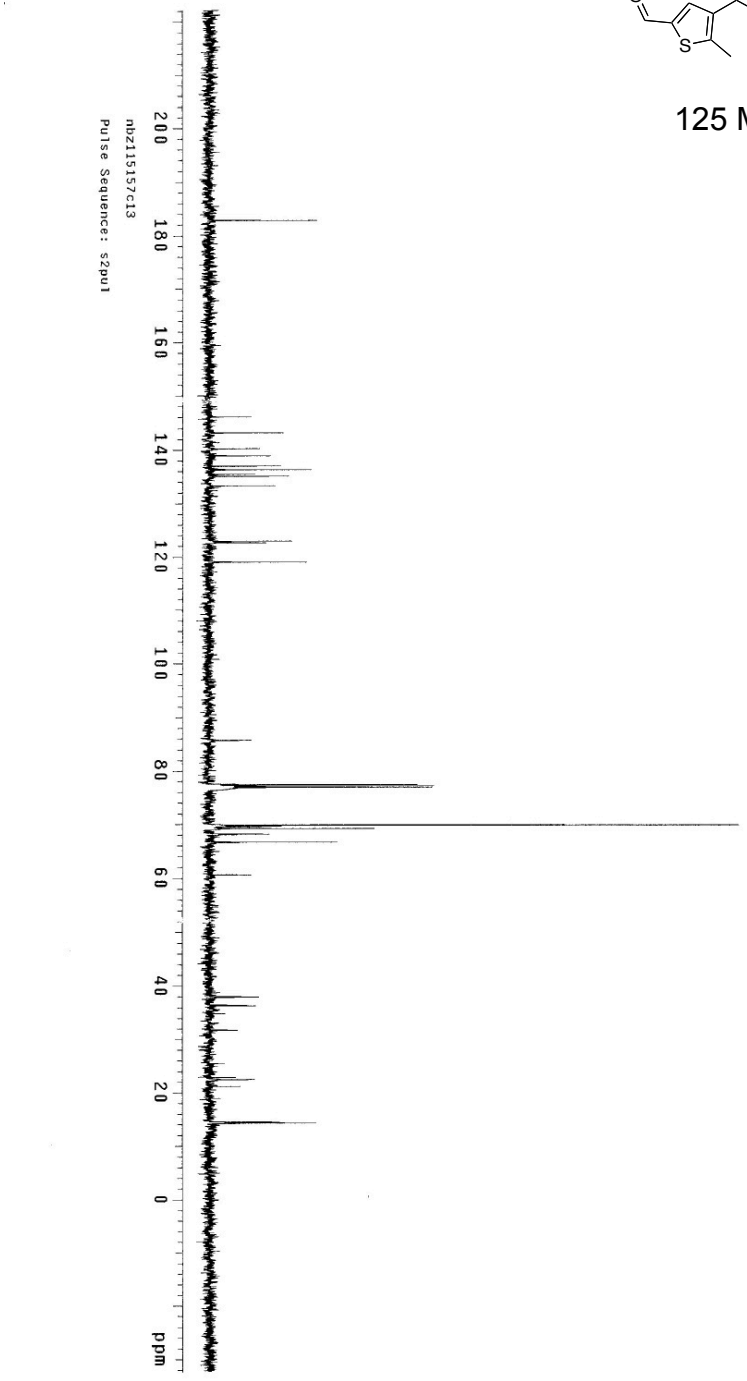

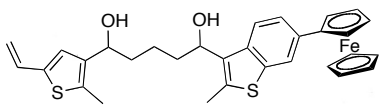

4.43
500 MHz, $CDCl_3$

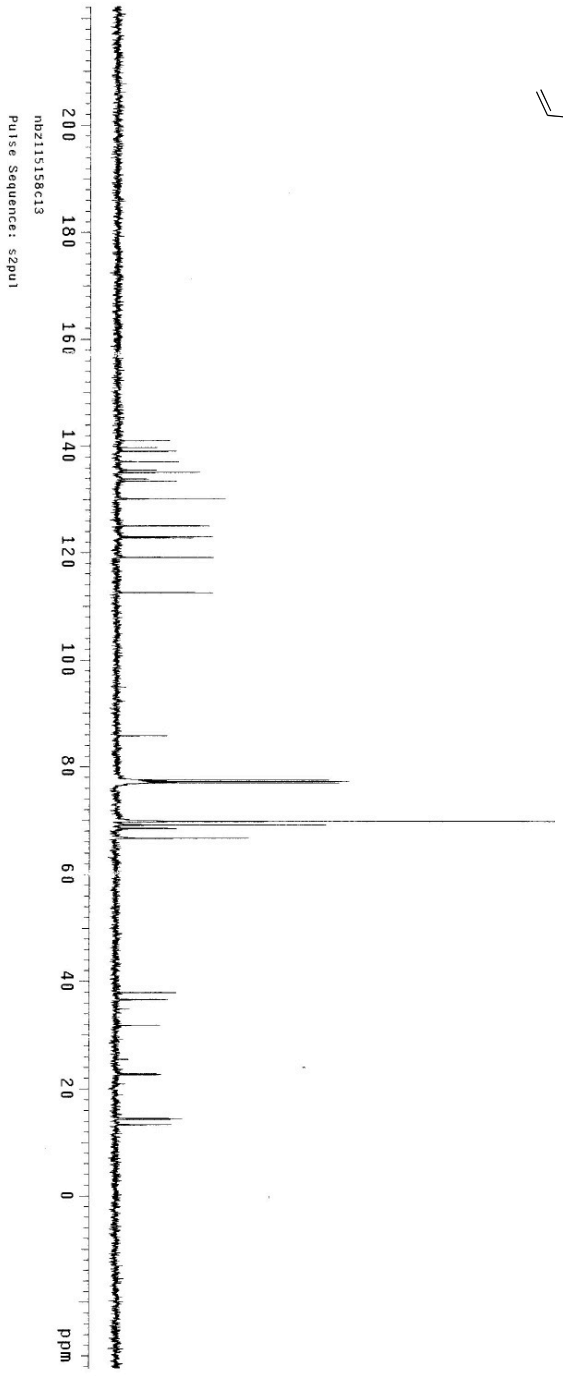

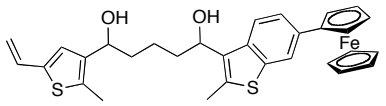

4.43
125 MHz, $CDCl_3$

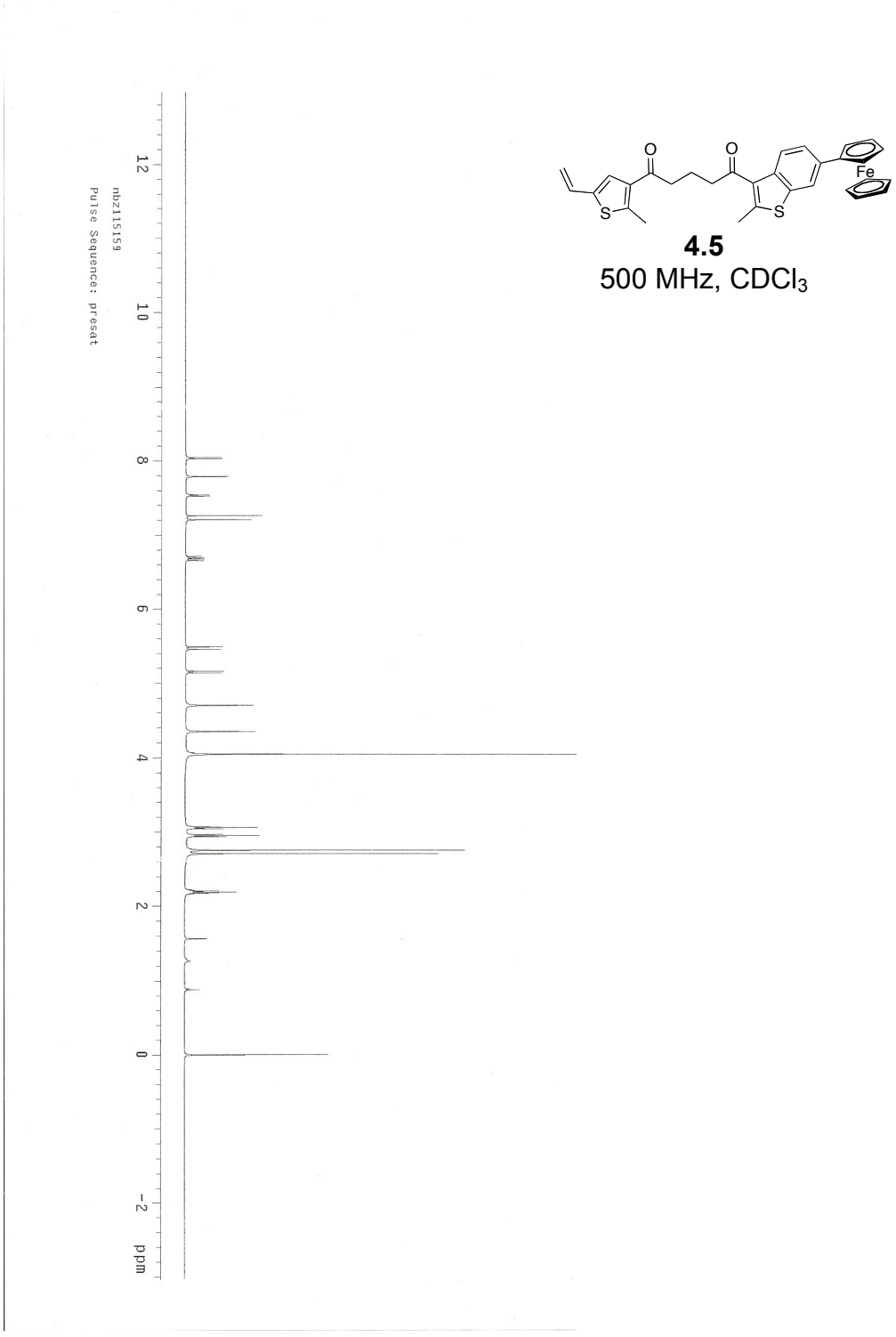

4.5
500 MHz, $CDCl_3$

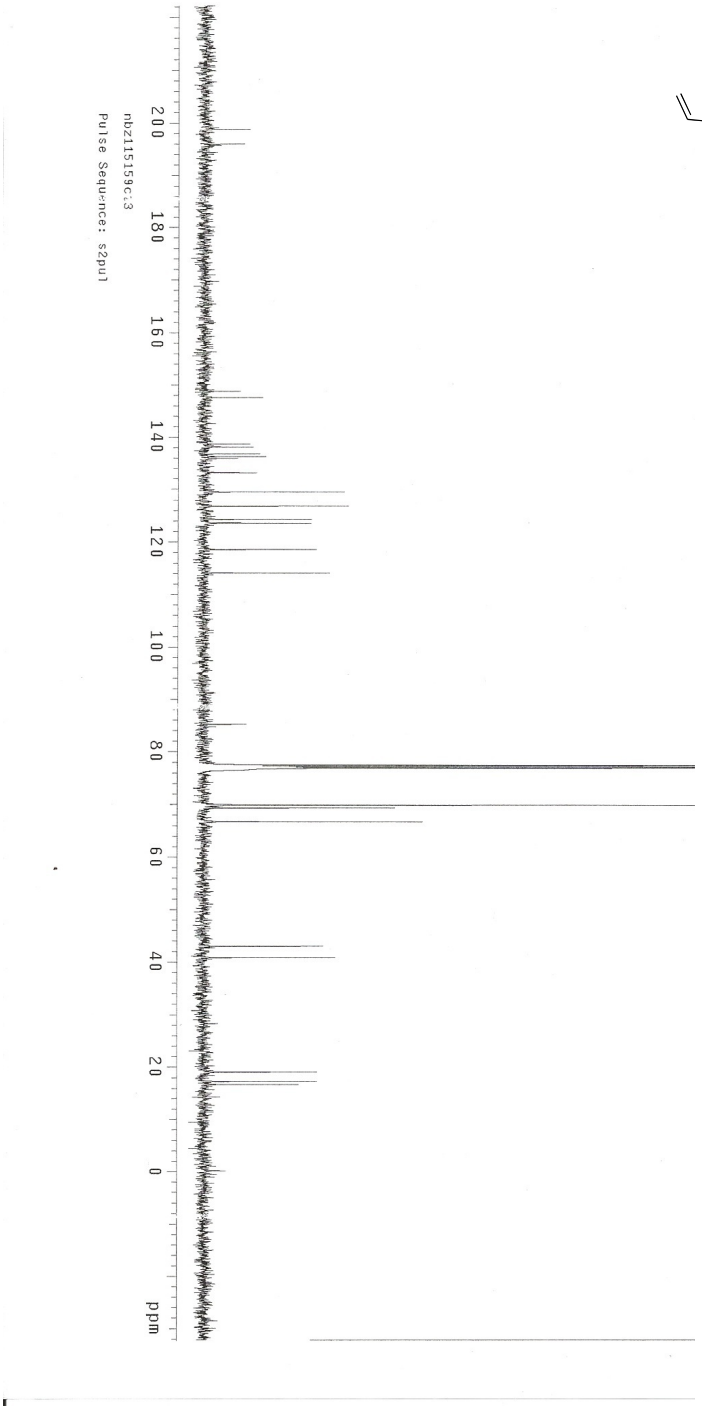

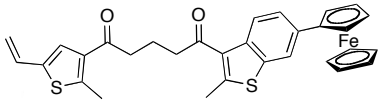

4.5
125 MHz, $CDCl_3$

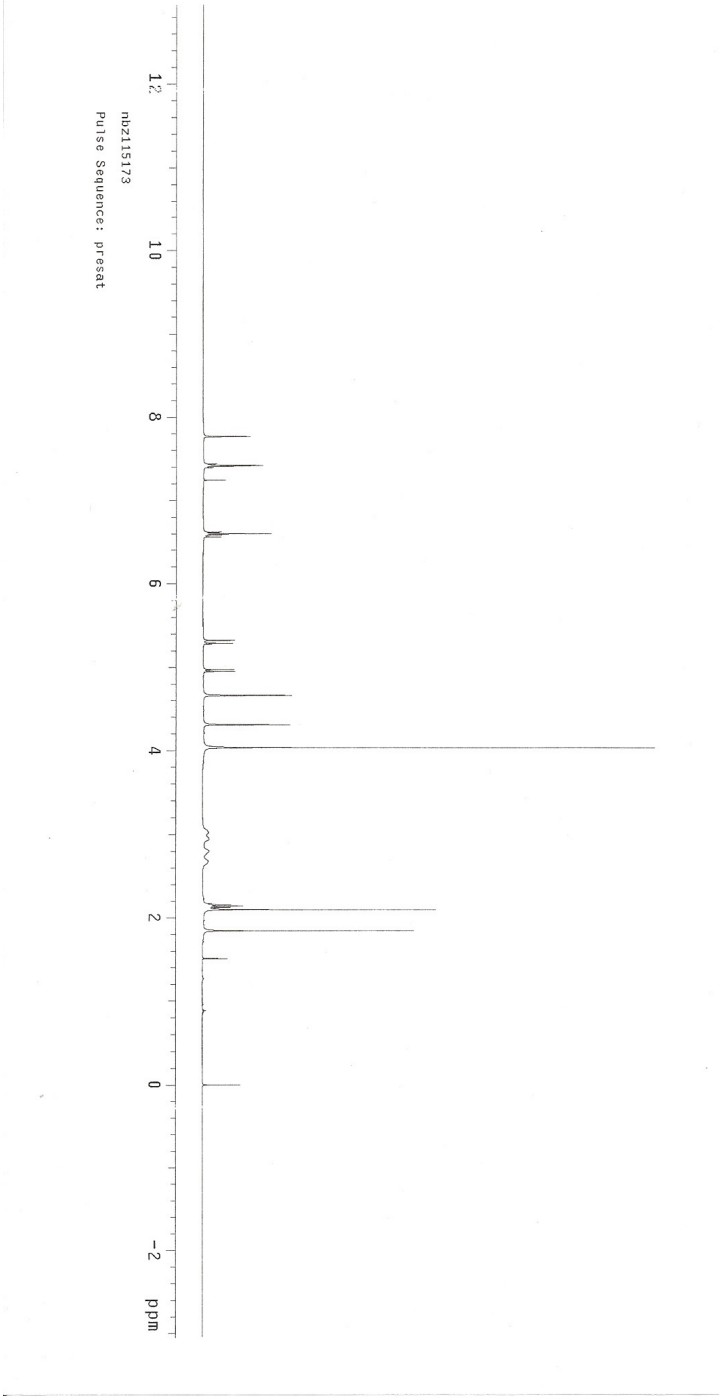

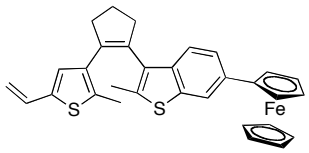

4.3
500 MHz, $CDCl_3$

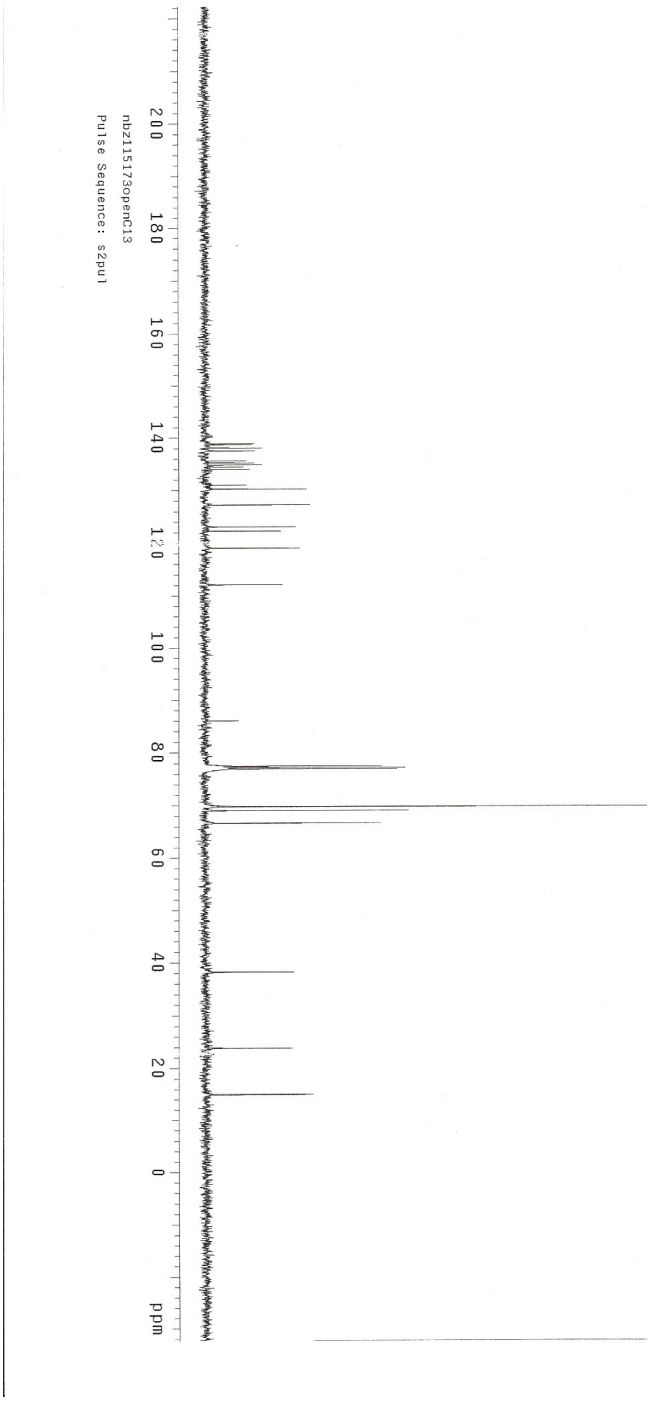

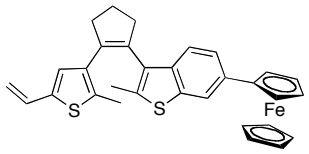

4.3
125 MHz, $CDCl_3$

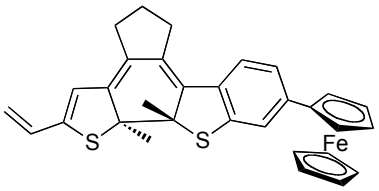

4.4
500 MHz, $CDCl_3$

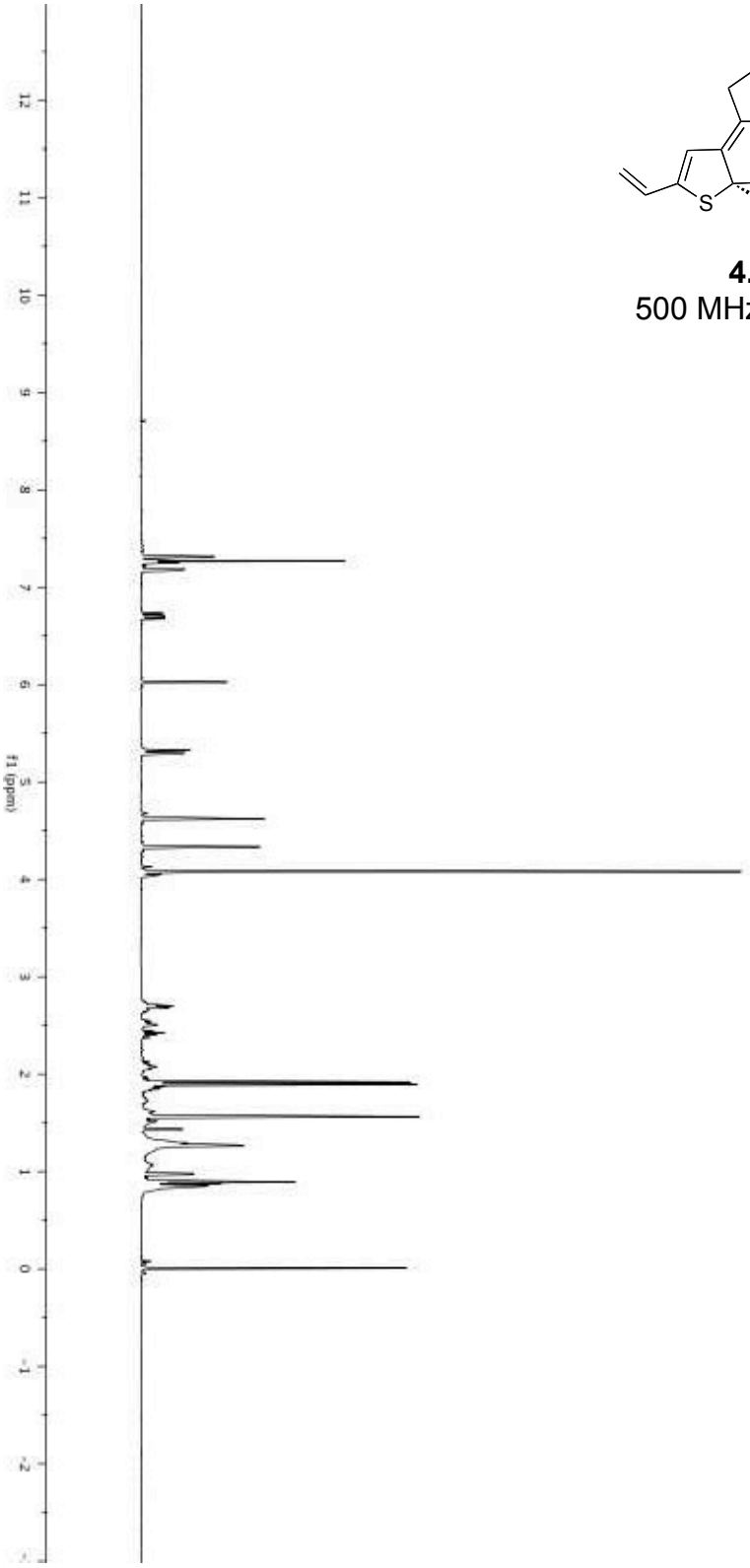

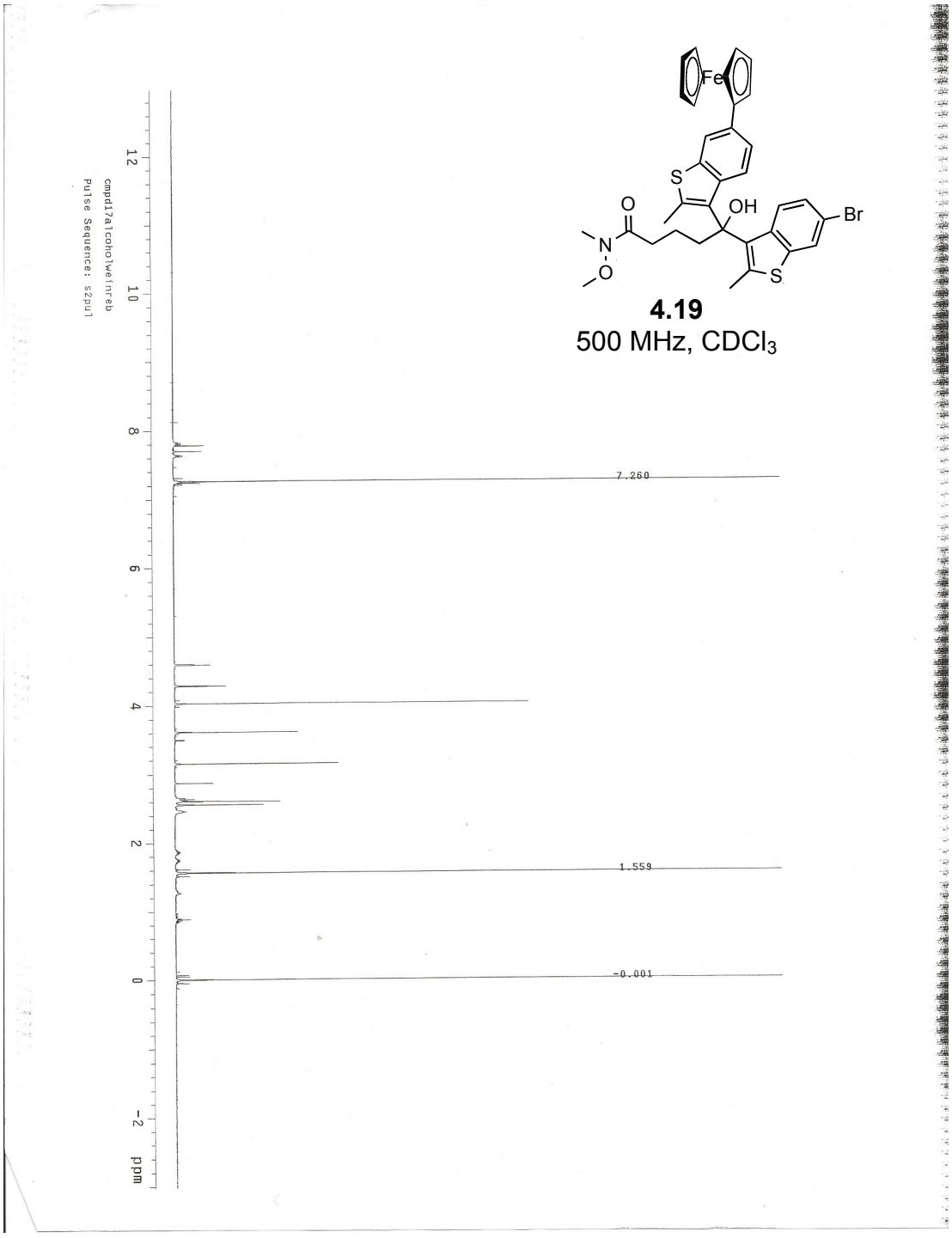
Fe
S
O
OH
Br
N
O
S
4.19
500 MHz, CDCl3
cmpd17alcoholweinreb
Pulse Sequence: s2pul
12
10
8
6
4
2
0
-2
ppm
7.260
1.559
-0.001

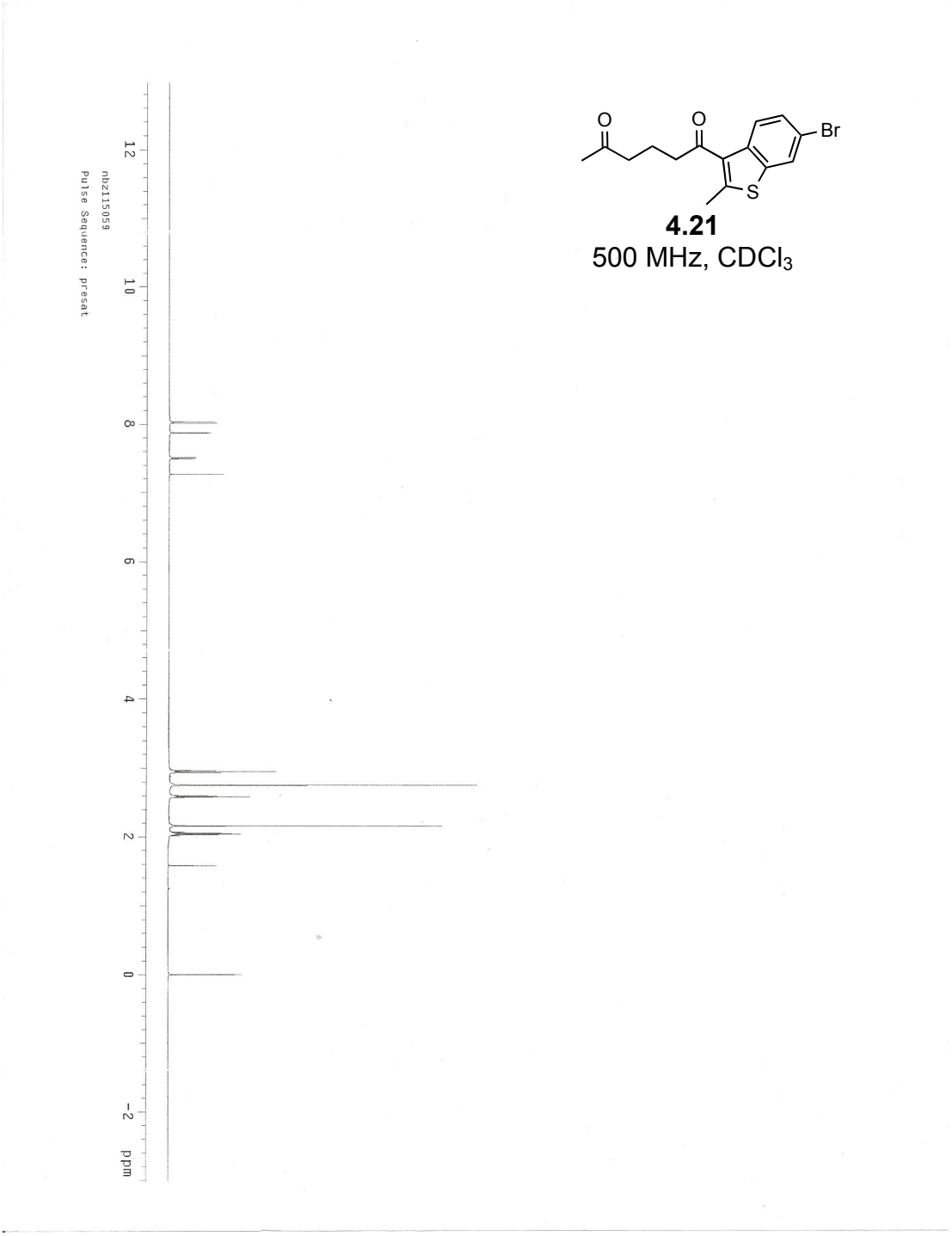

4.21
500 MHz, $CDCl_3$

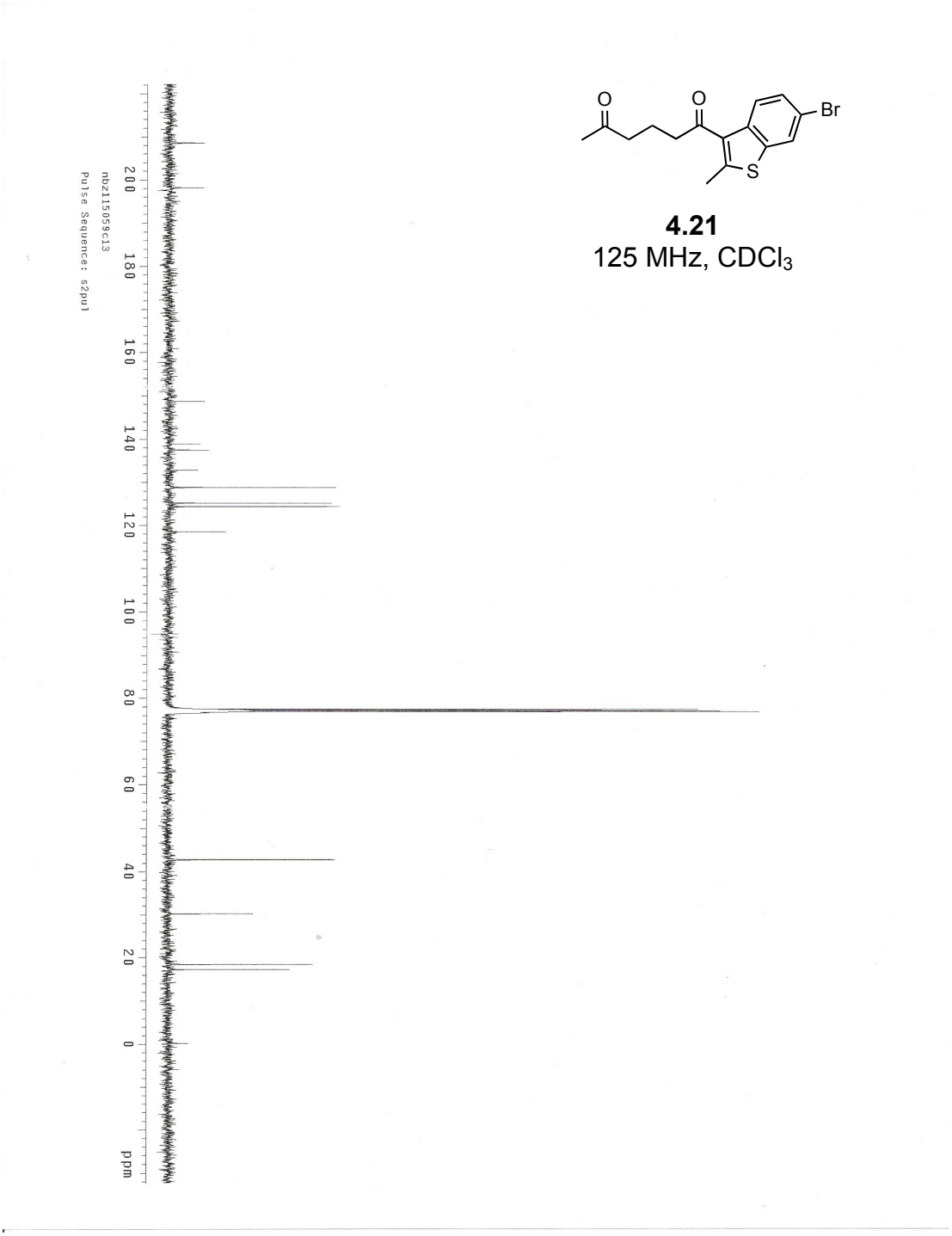

4.21
125 MHz, $CDCl_3$

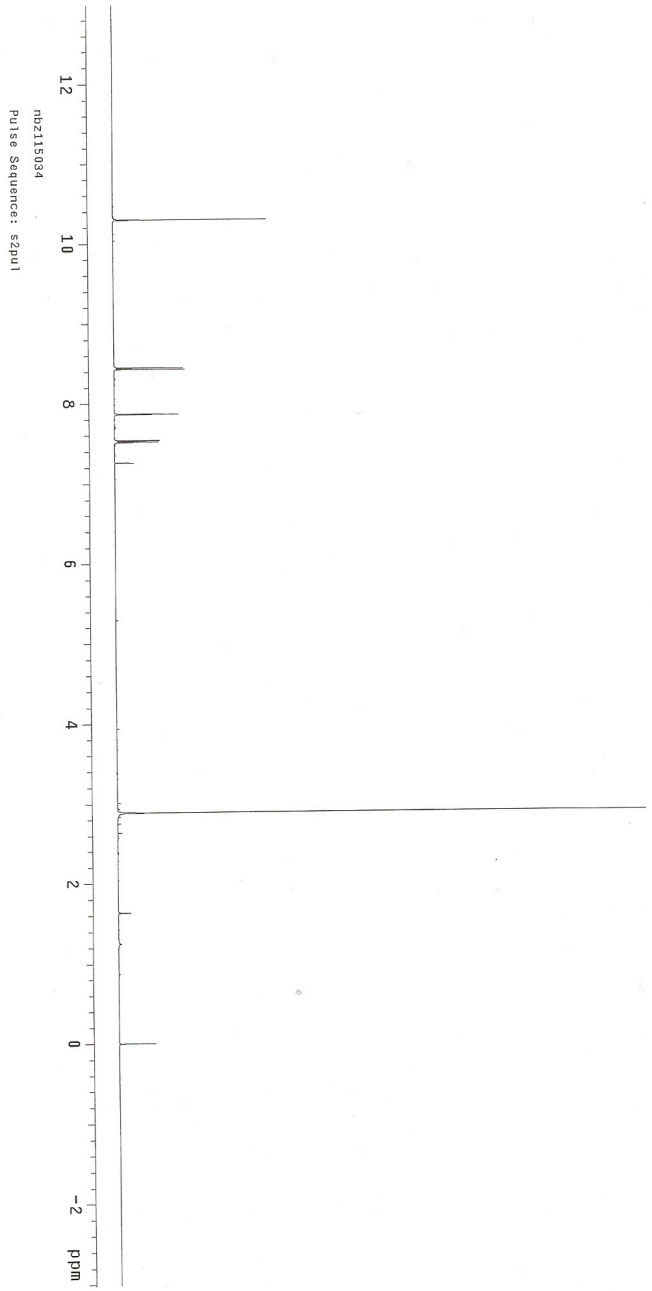

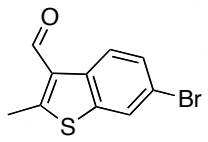

4.27

500 MHz, $CDCl_3$

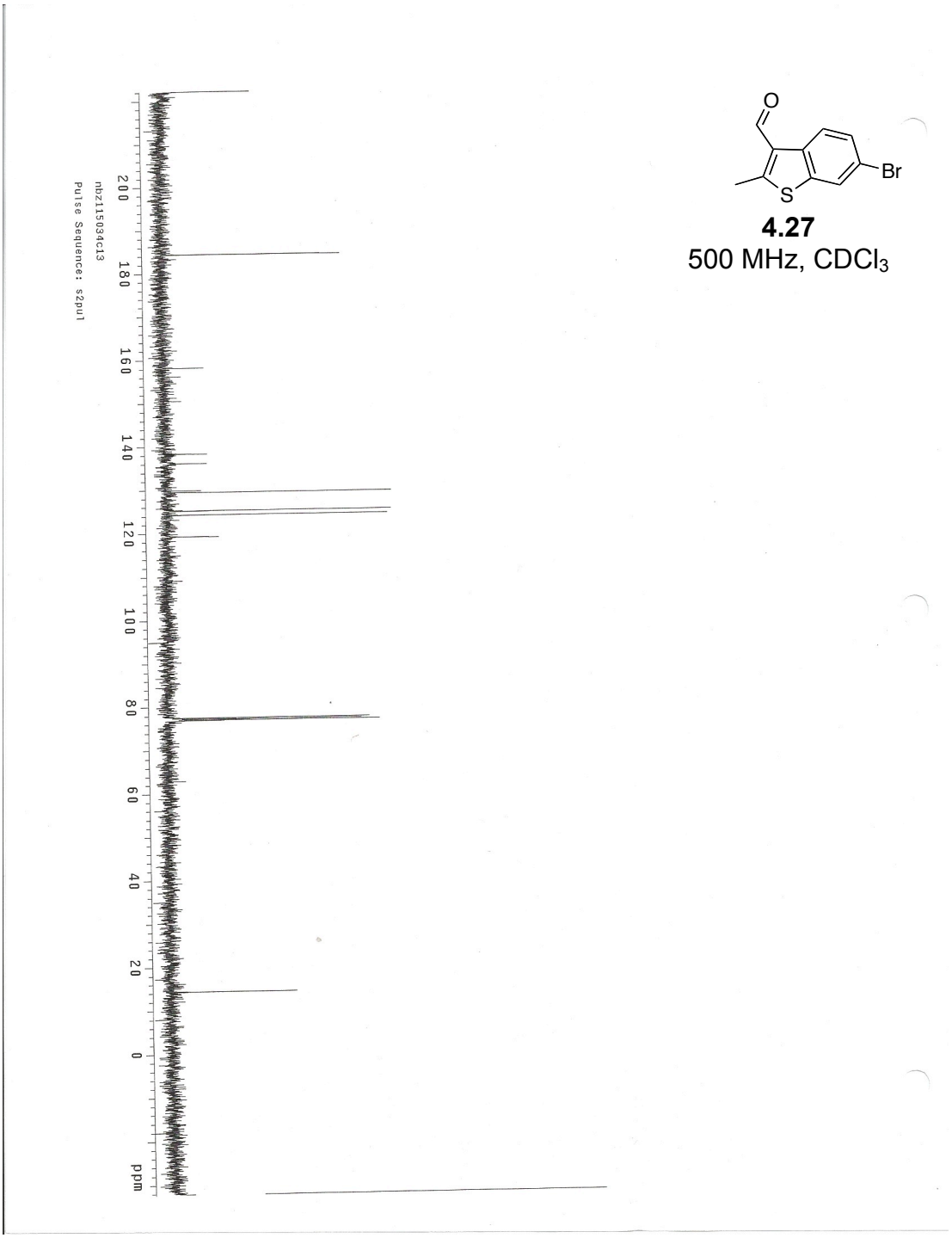

4.27
500 MHz, $CDCl_3$

BIBLIOGRAPHY

Alvarez Ibarra, C.; Cuervo Rodriguez, R.; Fernandez Monreal, M. C.; Garcia Navarro, F. J.; Martin Tesorero, J. *J. Org. Chem.* **1989**, *54*, 5620-5623.

Ast, S.; Müller, H.; Flehr, R.; Klamroth, T.; Walz, B.; Holdt, H.-J. *Chem. Commun.* **2011**, *47*, 4685-4687.

Bachmann, W. E.; Carmack, M. *J. Am. Chem. Soc.* **1941**, *63*, 2494-499.

Balogh, J.; Kegl, T.; Parkanyi, L.; Kollar, L.; Ungvary, F.; Skoda-Foldes, R. *J. Organomet. Chem*. **2011**, *696*, 1394-1403.

Barrios, F. J.; Zhang, X.; Colby, D. A. *Org. Lett.* **2010**, *12*, 5588-5591.

Belley, M.; Douida, Z.; Mancuso, J.; De Vleeschauwer, M. *Synlett*, **2005**, *2*, 247-250.

Bianchini, C.; Masi, D.; Romerosa, A.; Zanobini, F.; Peruzzini, M. *Organometallics* **1999**, *18*, 2376-2386.

Bok, P. R.; Sambanis, A. British Patent 1 549 122, **1979**.

Brachmann, C. B.; Davies, A.; Cost, G. J.; Caputo, E.; Li, J.; Hieter, P.; Boeke, J. D. *Yeast* **1998**, *14*, 115-132.

Brust, M.; Fink, J.; Bethell, D.; Schiffrin, D. J.; Kiely, C. *J. Chem. Soc., Chem. Commun.* **1995,** 1655-1656.

Brust, M.; Walker, M.; Bethell, D.; Schiffrin, D. J.; Whyman, R. *J. Chem. Soc. Chem. Commun.* **1994**, 801-802.

Burshell, A.; Stathis, P. A.; Do, Y.; Miller, S. C.; Feldman, D. *J. Biol. Chem.* **1984**, *259*, 3450-3456.

Bustelo, E.; de los Ríos, I.; Tenorio, M. J.; Puerta, M. C.; Valerga, P. *Monatsh. Chem.* **2000**, *131*, 1311-1320.

Cardenas, M. E.; Cruz, M. C.; Del Poeta, M.; Chung, N.; Perfect, J. R.; Heitman, J. *Clin. Microbiol. Rev.* **1999**, *12*, 583-611.

Carson, C. A.; Kerr, M. A. *Org. Lett.* **2009**, *11*, 777–779.

Caruso, F.; Gittins, D. I. *J. Phys. Chem. B*, **2001**, *105*, 6846-6852.

Chen, S. W.; Konopelski, J. P.; Wang, H. “CRC: Nanoparticle-Mediated Electronic Communication,” **2008**, NSF CHE-0832065.

Chen, S. W.; Sommers, J. M. *J. Phys. Chem. B* **2001**, *105*, 8816-8820.

Chen, W.; Chen, S. W.; Ding, F.; Wang, H.; Brown, L. E.; Konopelski, J. P. *J. Am. Chem. Soc.* **2008,** *130,* 12156-12162.

Chen, W.; Chen, S. W.; Ding, F.; Wang, H.; Brown, L. E.; Konopelski, J.P. *J. Am. Chem. Soc.* **2008**, *130*, 12156-12162.

Chen, W.; Davies, J. R.; Ghosh, D.; Tong, M. C.; Konopelski, J. P.; Chen, S. *Chem. Mater.* **2006**, *18*, 5253-5259.

Chen, W.; Zuckerman, N. B.; Kang, X.; Ghosh, D.; Konopelski, J. P.; Chen, S. W. *J. Phys. Chem. C* **2010**, *114*, 18146-18152.

Chen, W.; Zuckerman, N. B.; Konopelski, J. P.; Chen, S. W. *Anal. Chem.* **2010**, *82*, 461-465.

Chen, W.; Zuckerman, N. B.; Lewis, J. W.; Konopelski, J. P.; Chen, S. W. *J. Phys. Chem. C*, **2009**, *113*, 16988-16995.

Chidsey, C. E. D.; Bertozzi, C. R.; Putvinkski, T. M.; Mujsce, A. M. *J. Am. Chem. Soc.* **1990**, *112*, 4301-4306.

Chiu, C. C.; Frank, J. *J. Org. Chem.* **1994**, *59*, 5763-5766.

Collins, C. J.; Fisher, G. B.; Reem, A.; Goralski, C. T.; Singaram, B. *Tetrahedron Lett.* **1997**, *38*, 529-532.

Couldwell, W. T.; Hinton, D. R.; He, S.; Chen, T. C.; Sebat, I.; Weiss, M. H.; Law, R. E. *FEBS Lett.* **1994**, *345, 43-46.*

Cowan, D. O.; LeVanda, C.; Park, J.; Kaufman, F. *Acc. Chem. Res.* **1973**, *6*, 1-7.

Creighton, J. A.; Eadon, D. G. *J. Chem. Soc. Faraday Trans.* **1991**, *87*, 3881-3891.

Cumming, W. J.; Gaudiana, R. A.; Ingwall, R. T.; Kolb, E. S.; Mehta, P. G.; Minns, R. A. Polaroid Corporation, Cambridge Mass. U. S. Patent 5,414,069; **1995**.

D'Souza, F.; Chitta, R.; Gadde, S.; Zandler, M. E.; McCarty, A. L.; Sandanayaka, A. S. D.; Araki, Y.; Ito, O. *Chem. Eur. J.* **2005**, *11*, 4416-4428.

de los Ríos, I.; Tenorio, M. J.; Puerta, M. C.; Valerga, P. *J. Am. Chem. Soc.* **1997**, *119*, 6529-6538.

Diamandis, E. P.; Christopoulos, T. K. *Clin. Chem.* **1991**, *37*, 625-636.

Ding, F.; Wang, H.; Wu, Q.; Van Voorhis, T.; Chen, S. W.; Konopelski, J. P. *J. Phys. Chem. A* **2010**, *114*, 6039-6046.

Egger, H.; Schloegel, K. *Monatsh. Chem.* **1964**, *6*, 1750-1758.

Engel, P. S.; Schexnayder, M. A. *J. Am. Chem. Soc.* **1975**, *97*, 145–153.

Faulkner, C. W.; Ingham, S. L.; Khan, M. S.; Lewis, J.; Long, N. J.; Raithby, P. R. *J. Organomet. Chem.* **1994**, *482*, 139-145.

Fedi, V.; Altamura, M.; Catalioto, R.-M.; Giannotti, D.; Giolitti, A.; Giuliani, S.; Guidi, A.; Harmat, N. J. S.; Lecci, A.; Meini, S.; Nannicini, R.; Pasqui, F.; Tramontana, M.; Triolo, A.; Maggi, C. A. *J. Med. Chem.* **2007**, *50*, 4793-4807.

Fernàndez-Acebes, A.; Lehn, J.-M. *Chem. Eur. J.* **1999**, *5*, 3285-3292.

Ferrié, L.; Boulard, L.; Pradaux, F.; Bouzbouz, S.; Reymond, S.; Capdevielle, P.; Cossy, J. *J. Org. Chem.* **2008**, *73*, 1864–1880.

Fischer, H.; Zayed, M. A. *J. Therm. Anal. Calorim.* **2000**, *61*, 897-908.

Fisher, B.; Constantino, J. P.; Wickerham, D. L.; Redmond, C.; Kovanah, M.; Cronin, W. M.; Vogel, V.; Robidoux, A.; Dimitrov, N.; Atkins, J.; Daly, M.; Wiend, S.; T.-C., E.; Ford, L.; Wolmark, N. *J. Natl. Cancer Inst* **1998**, *90*, 1371-1388.

Flowers, R. G.; Nichols, F. S. *J. Am. Chem. Soc.* **1949**, *71*, 3104.

Focsanneanu, K.-S.; Scaiano, J. C. *Photochem. Photobiol. Sci*, **2005**, *4*, 817-821.

Ford, M. J.; Hoft, R. C.; McDonagh, A. *J. Phys. Chem. B* **2005**, *109*, 20387-20392.

Fulton, J. R.; Aggarwal, V. K.; de Vicente, J. *Eur. J. Org. Chem.* **2005**, 1479-1492.

Fuwa, H.; Ishigai, K.; Goto, T.; Suzuki, A.; Sasaki, M. *J. Org. Chem.* **2009**, *74*, 4024-4040.

Gassner, N. C.;Tamble, C. M.; Bock, J. E.; Cotton, N.; White, K. N.; Tenney, K.; St. Onge, R. P.; Proctor, M. J.; Giaever, G.; Davis, R. W.; Crews, P.; Holman, T. R.; Lokey, R. S. *J. Nat. Prod.* **2007,** *70,* 383-390.

Geerts, J. P.; Martin, R H. *Bull. Soc. Chim. Belg.* **1960**, *69*, 563-569.

Giaever, G.; Chu, A. M.; Ni, L.; Connelly, C.; Riles, R.; Véronneau, S.; Dow, S.; Lucau-Danila, A.; Anderson, K.; André, B.; Arkin, A. P.; Astromoff, A.; El Bakkoury, M.; Bangham, R.; Benito, R.; Brachat, S.; Campanaro, S.; Curtiss, M.; Davis, K.; Deutschbauer, A.; Entian, K.-D.; Flaherty, P.; Foury, F.; Garfinkel, D. J.; Gerstein, M.; Gotte, D.; Güldener, U.; Hegemann, J. H.; Hempel, S.; Herman, Z.; Jaramillo, D. F.; Kelly, D. E.; Kelly, S. L.; Kötter, P.; LaBonte, D.; Lamb, D. C.; Lan, N.; Liang, H.; Liao, H.; Liu, L.; Luo, C.; Lussier, M.; Mao, R.; Menard, P.; Ooi, S. L.; Revuelta, J. L.; Roberts, C. J.; Rose, M.; Ross-Macdonald, P.; Scherens, B.; Schimmack, G.; Shafer, B.; Shoemaker, D. D.; Sookhai-Mahadeo, S.; Storms, R. K.; Strathern, J. N.; Valle, G.; Voet, M.; Volckaert, G.; Wang, C.-Y.; Ward, T. R.; Wilhelmy, J.; Winzeler, E. A.; Yang, Y.; Yen, G.; Youngman, E.; Yu, K.; Bussey, H.; Boeke, J. D.; Snyder, M.;Philippsen, P.; Davis, R. W.; Johnston, M. *Nature*, **2002**, *418*, 387-391.

Gilat, S. L.; Kawai, S. H.; Lehn, J.-M. *Chem. Eur. J.* **1995**, *1*, 275-284.

Glendening, E. D.; Feller, D.; Thompson, M. A. *J. Am. Chem. Soc.* **1994**, *116*, 10657-10669.

Gooßen, L. J.; Ghosh, K. *Angew. Chem. Int. Ed.* **2001,** *40,* 3458-3460.

Gooßen, L. J.; Ghosh, K. *Eur. J. Org. Chem* **2002**, 3254-3267.

Gooßen, L. J.; Koley, D.; Hermann, H. L.; Thiel, W. *J. Am. Chem. Soc.* **2005**, *127*, 11102-11114.

Gooßen, L. J.; Winkel, L.; Döhring, A.; Ghosh, K.; Paetzold, J. *Synlett*, **2002**, *8*, 1237-1240.

Gottardis, M. M.; Robinson, S. P.; Satyaswaroop, P. G.; Jordan, V. C. *Cancer Res.* **1988**, *48*, 812-815.

Graham, S. L.; Scholz, T. H. *Tetrahedron Lett.* **1990,** *31,* 6269

Gromov, A.; Enev, V.; Mulzer, J. *Org. Lett.* **2009**, *11*, 2884–2886.

Gronowitz, S.; Björk, P.; Malm, J.; Hörnfeldt, A.-B. *J. Organomet. Chem.* **1993**, *460*, 127-129.

Guerchais, V.; Ordronneau, L.; Le Bozec, H. *Coord. Chem. Rev.* **2010**, *254*, 2533-2545.

Guillaneux, D.; Kagan, H. B. *J. Org. Chem.* **1995**, *60*, 2502-2505.

Guirado, G.; Coudret, C.; Launay, J.-P. *J. Phys. Chem. C* **2007**, *111*, 2770-2776.

Hall, L. A. R.; Stephens, V. C.; Burckhalter, J. H. *Org. Syn.* **1951**, *31*.

Haobin Wang group website: www.chemistry.nmsu.edu/hwang_new.html

Hariharan, M.; Karunakaran, S. C.; Ramaiah, D. *Org. Lett.* **2007**, *9*, 417-420.

Harvey, S.; Junk, P. C.; Raston, C. L.; Salem, G. *J. Org. Chem.* **1988**, *53*, 3134-3140.

Hashmi, A. S. K.; Hutchings, G. J. *Angew. Chem. Int. Ed.* **2006**, *45*, 7896-7936.

Hauser, C. R.; Pruett, R. L.; Mashburn, T. A. *J. Org. Chem.* **1961**, *26*, 1800-1801.

Hay, M. P.; Pchalek, K.; Prujin, F. B.; Hicks, K. O.; Slim, B. G.; Anderson, R. F.; Shinde, S. S.; Phillips, V.; Denny, W. A.; Wilson, W. R. *J. Med. Chem.* **2007**, *50*, 6654-6664.

Hay, M. P.; Pchalek, K.; Prujin, F. B.; Hicks, K. O.; Slim, B. G.; Anderson, R. F.; Shinde, S. S.; Phillips, V.; Denny, W. A.; Wilson, W. R. *J. Med. Chem.* **2007**, *50*, 6654-6664.

Heckert, S. J.; Heathcock, C. H. *J. Org. Chem.* **1985**, *50*, 5159-5166.

Hiramatsu, H.; Osterloh, F. E. *Chem. Mater.* **2004**, *16*, 2509-2511.

Hiroto, S.; Suzuki, K.; Kamiya, H.; Shinokubo, H. *Chem. Commun.* **2011**, *47*, 7149-7151.

Hu, P.; Zhao, K. Q.; and Xu, H. B. *Molecules* **2001**, *6*, M249.

Hu, P.; Zhao, K. Q.; and Xu, H. B. *Molecules* **2001**, *6*, M250.

Huang, Z.-N.; Xu, B.-A.; Jin, S.; Fan, M.-G. *Synthesis*, **1998**, *8*, 1092-1094.

Hughes, T. R. *Funct. Integr. Genomics* **2002**, *2*, 199-211.

Impagnatiello, N.; Heynderickx, A.; Moustrou, C.; Samat, A. *Mol. Cryst. Liq. Cryst.* **2005**, *430*, 243-248.

Ipaktschi, J.; Hosseinzadeh, R.; Sclaf, P.; Dreiseidler, E. *Helv. Chim. Acta* **1998**, *81*, 1821-1834.

Irie, M. *Chem. Rev.* **2000**, *100*, 1685-1716.

Irie, M. *Photochem. Photobiol. Sci.* **2010**, *9*, 1535-1542.

Itami, K.; Kamei, T.; Yoshida, J. *J. Am. Chem. Soc.* **2003**, *125*, 14670-14671.

Jakobsson, F. L. E.; Marsal, P.; Braun, S.; Fahlman, M.; Berggren, M.; Cornil, J.; Crispin, X. *J. Phys. Chem. C* **2009**, *113*, 18396-18405.

Jordan, V. C. *Breast Cancer Res. Treat.* **1988**, *11*, 197-209.

Jordan, V. C.; Jaspan, T. *J. Endocrinol.* **1976**, *68*, 453-460.

Jordan, V. C.; Morrow, M. *Endocr. Rev.* **1999**, *20*, 253-278.

Kaim, W.; Klein, A.; Glöckle, M. *Acc. Chem. Res.* **2000**, *33*, 755-763.

Kakino, R.; Yasumi, S.; Shimizu, I.; Yamamoto, A. *Bull. Chem. Soc. Jpn.* **2002,** *75,* 137-148.

Kang, X.; Chen, W.; Zuckerman, N. B.; Konopelski, J. P.; Chen, S. W. *Langmuir* **2011**, *27,* 12636-12641.

Kang, X.; Li, X.; Hewitt, W. M.; Zuckerman, N. B.; Konopelski, J. P.; Chen, S. W. *Anal. Chem*. **2012**, *84*, 2025-2030.

Kang, X.; Zuckerman, N. B.; Konopelski, J. P. Chen, S. W. *Angew. Chemie Int. Ed.* **2010**, *49*, 9496-9499.

Kang, X.; Zuckerman, N. B.; Konopelski, J. P.; Chen, S. W. *J. Am. Chem. Soc.* **2012,** *134,* 1412-1415.

Kang, X.; Zuckerman, N. B.; Konopelski, J. P.; Chen, S. W. *J. Am. Chem. Soc.* **2012**, *134*, 1412-1415.

Kim, H. N.; Ren, W. X.; Kim, J. S.; Yoon, J. *Chem. Soc. Rev.* **2012**, *41*, 3210-3244.

Kim, S.-H.; Rieke, R. D. *J. Org. Chem.* **2000**, *65*, 2322-2330.

Kobatake, S.; Uchida, K.; Tsuchida, E.; Irie, M. *Chemm. Commun.* **2002**, 2804-2805.

Kolb, H. C.; Sharpless, K. B. *Drug Discovery Today*, **2003**, *8*, 1128-1137.

Krayushkin, M. M.; Lichitsky, B. V.; Kozhinov, D. V.; Ivanov, S. N.; Dudinov, A. A. *ARKIVOC* **2003**, *13*, 147-156.

Krayushkin, M. M.; Migulin, V. A. Russian Patent No. RU 2421453 C1, **2011**.

Krayushkin, M. M.; Migulin, V. A.; Yarovenko, V. N.; Barachevskii, V. A.; Vorontsova, L. G.; Starikova, Z. A.; Zavarzin, I. V.; Bulgakova, V. N. *Mendeleev Commun.* **2007**, *17*, 125-127.

Krayushkin, M. M.; Migulin, V. A.; Yarovenko, V. N.; Barachevskii, V. A.; Vorontsova, L. G.; Starikova, Z. A.; Zavarzin, I. V.; Bulgakova, V. N. *Mendeleev Commun.* **2007**, *17*, 125-127.

Lai, L-L.; Ho, C-H.; Lin, Y-J.; Wang, E.; Liu, Y-H.; Wang, Y.; Lin, Y-C.; Cheng, K-L. *Helv. Chim. Acta.* **2002**, *85*, 108-114.

Landaverry, Y. R. Ph.D. Dissertation, University of California, Santa Cruz, **2007**.

Lara, P.; Rivada-Wheelaghan, O.; Conejero, S.; Poteau, R.; Philippot, K.; Chaudret, B. *Angew. Chem. Int. Ed.* **2011**, *50* , 12080-12084.

Lerner, L. J.; Holthaus, J. F.; Thompson, C. R.; *Endocrinology* **1958**, *63*, 295-318.

Liu, C.-M.; Chen, B.-H.; Liu, W.-Y.; Wu, X.-L.; Ma, Y.-X. *J. Organomet. Chem.* **2000**, *598*, 348-352.

Liu, C.-M.; Luo, S.-J.; Liang, Y.-M.; Ma, Y.-X. *Synth. Commun.* **2000**, *30*, 2281-2285.

Lucas, L. N.; de Jong, J. J. D.; van Esch, J. H.; Kellog, R. M.; Feringa, B. L. *Eur. J. Org. Chem.* **2003**, 155-166.

Lucas, L. N.; van Esch, J. H.; Kellogg, R. M.; Feringa, B. L. *Chem. Commun.* **1998**, 2313.

Lum, P. K.; Armour, C. D.; Stepaniante, S. B.; Cavet, G.; Wolf, M. K.; Butler, J. S.; Hinshaw, J. S.; Garnier, P.; Prestwich, G. D.; Leonardson, A.; Garrett-Engele, P.; Rush, C. M.; Bard, M.; Schimmack, G.; Phillips, J. W.; Roberts, C. J.; Shoemaker, D. D. *Cell*, **2004**, 121-137.

Luo, S-J.; Liu, Y-H.; Liu, C-M.; Liang, Y-M; Ma, Y-X. *Synth. Commun.* **2000**, *30*, 1569-1572.

Luo, S.-J.; Liu, Y.-H.; Liu, C.-M.;Liang, Y.-M.; Ma, Y.-X. *Synth. Commun.* **2000**, *30*, 1569-1572.

Lynam, J. M. *Chem. Eur. J.* **2010**, *16*, 8238-8247.

Madani, N. D.; Malloy, P. J.; Rodriguez-Pombo, P.; Krishnan, A. V.; Feldman, D. *Microbiology* **1994**, *91*, 922-926.

Maity, P.; Tsunoyama, H.; Yamauchi, M.; Xie, S.; Tsukuda, T. *J. Am. Chem. Soc.* **2011**, *133*, 20123-20125.

Malashikhin, S.; Finney, N. S. *J. Am. Chem. Soc.* **2008**, *130*, 12846-12847.

Mamane, V. *Mini Rev. Org. Chem.* **2008**, *5*, 303-312.

Marshall, J. A.; Andersen, N. H.; Schlicher, J. W. *J. Org. Chem.* **1970**, *35*, 858-861.

Martin, S. F.; Dodge, J. A.; Burgess, L. E.; Hartmann, M. *J. Org. Chem.* **1992**, *57*, 1070-1072.

McDonagh, A. M.; Deeble, G. J.; Hurst, S.; Cifuentes, M. P.; Humphrey, M. G. *J. Chem. Ed.* **2001**, *78*, 232-234.

McDonald, C. C.; Alexander, F. E.; Whyte, B. W.; Forest, A. P. Steward, H. J.; *Br. Med. J.***1995***, 311*, 977-980.

Mendes-Pereira, A. M.; Sims, D.; Dexter, T.; Fenwick, K.; Assiotis, I.; Kozarewa, I.; Mitsopoulos, C.; Hakas, J.; Zvelebil, M.; Lord, C. J.; Ashworth, A. *Proc. Natl. Acad. Sci. USA* **2011**, *Early Edition*.

Metzger, A.; Piller, F. M.; Knochel, P. *Chem. Commun.* **2008**, 5824-5826.

Migulin, V. A.; Krayushkin, M. M.; Barachevsky, V. A.; Kobelva, O. I.; Valova, T. M.; Lyssenko, K. A. *J. Org. Chem.* **2012**, *77*, 332-340.

Miller, G. *Science* **2010**, *329*, 502-504.

Mirkhalaf, F.; Paprotny, J.; Schiffrin, D. J. *J. Am. Chem. Soc.* **2006,** *128,* 7400–7401.

Moore, L. L.; Fulton, A. M.; Harrison, M. L.; Geahlen, R. L. *J. Proteome Res.* **2004**, *3*, 1184-1190.

Nesmeyanov, A. N.; Drozd, V. N.; Sazonova, V. A. *Dokl. Akad. Nauk SSSR*, **1963**, *150,* 321-324.

Norris, J. R.; Ribbons, D. W., Eds.; Yeast Gene Analysis, Volume 36, Methods in Microbiology; Academic Press: London, **2007**.

Osborne, C. K.; Coronado, E.; Allred, D. C.; Wiebe, V.; DeGregorio, M. *J. Natl. Cancer Inst.* **1991**, *83*, 1477-1482.

Pandey, R. J.; Wakharkar, R. D.; Kumar, P. *Synth. Commun.* **2005**, *35*, 2795-2800.

Parsons, A. B.; Lopez, A.; Givoni, I. E.; Williams, D. E.; Gray, C. A.; Porter, J.; Chua, G.; Sopko, R.; Brost, R. L.; Ho, C.-H.; Wang, J.; Ketela, T.; Brenner, C.; Brill, J. A.; Fernandez, G. E.; Lorenz, T. C.; Payne, G. S.; Ishihara, S.; Ohya, Y.; Andrews, B.; Hughes, T. R.; Frey, B. J.; Graham, T. R.; Andersen, R. J.; Boone, C. *Cell* **2006**, *126*, 611-625.

Patterson, J.; Furr, M. B. B.; Wakeling, A.; Battersby, L. *Breast Cancer Res. Treat.* **1982**, *2*, 363-374.

Perrier, T.; Saulnier, P.; Benoît, J.-P. *Chem. Eur. J.* **2010**, *16*, 11516-11529.

Peters, A.; Branda, N. R. *J. Am. Chem. Soc.* **2003**, *125*, 3404-3405.

Petros, R. A.; DeSimone, J. M. *Nat. Rev. Drug Discovery*, **2010**, *9*, 615-627.

Piller, F. M.; Metzger, A.; Schade, M. A.; Haag, B. A.; Gavryushin, A.; Knochel, P. *Eur. J. Org. Chem.* **2009**, *15*, 7192-7202.

Plaumann, D. E.; Fitzsimmons, B. J.; Ritchie, B. M.; Fraser-Reid, B. *J. Org. Chem.* **1982**, *47*, 941.

Powers, M. J.; Meyer, T. J. *J. Am. Chem. Soc.* **1978**, *100*, 4393-4398.

Professor Grant A. Hartzog website: mcd.ucsc.edu/faculty/hartzog.html

Professor Joshua M. Stuart website: http://sysbio.soe.ucsc.edu/

Professor Ronald W. Davis website: http://genomics.Stanford.edu/

Pruchnik, F. P. Organometallic Chemistry of the Transition Elements; Plenum Press: New York, 1990.

Quan,T. K.; Zuckerman, N. B.; Bray, W. M.; Weber, R. J.; Roguev, A.; Krogan, N.J.; Li, R.; Stuart, J. M.; Konopelski, J. P.; Hartzog, G. A.; Lokey, R. S. *Manuscript in Progress* **2011**.

Robertson, D. W.; Katzenellenbogen, J. A. *J. Org. Chem.* **1982**, *47*, 2387-2393.

Robertson, D. W.; Katzenellenbogen, J. A.; Long, D. J.; Rorke, E. A.; Katzenellenbogen, B. S. *J. Steroid Biochem.* **1982**, *16*, 1-13.

Sato, S.; Murata, A.; Shirakawa, T.; Uesugi, M. *Chem. Biol.* **2010**, *17*, 616-623.

Sauer, E. L. O.; Hooper, J.; Woo, T.; Barriault, L. *J. Am. Chem. Soc.* **2007**, *129*, 2112-2119.

Schenone, S.; Bruno, O.; Ranise, A.; Bondavalli, F.; Cenicola, M. L.; Losasso, C.; Carnevale, M.; Ottavo, R.; D'Antonio, M. *Farmaco* **1990**, *12*, 1309-1325.

Sénéchal-David, K.; Zaman, N.; Walko, M.; Halza, E.; Rivière, E.; Guillot, R.; Feringa, B. L.; Boillot, M.-L. *Dalton Trans.* **2008**, 1932-1936.

Sevez, G.; Gan, J.; Delbaere, S.; Versmeerch, G.; Sanguinet, L.; Levillain, E.; Pozzo, J.-L. *Photochem. Photobiol. Sci.* **2010**, *9*, 131-135.

Shaowei Chen group website: www.chem.ucsc.edu/~schen/

Sharpless, K. B.; Amberg, W.; Bennani, Y. L. Crispino, G. A.; Hartung, J.; Jeong, K.-Y.; Kwong, H.-L.; Morikawa, K.; Wang, S.-M.; Xu, D.; Zhang, X.-L. *J. Org. Chem.* **1992**, *57*, 2768-2771

Shashidhar, M. S.; Bhatt, M. V. *J. Chem. Soc. Perkin Trans. II*, **1986**, 355-358.

Shin, E. J. *Chem. Lett.* **2002**, 686-687.

Siemeling, U.; Rother, D. *J. Organomet. Chem.* **2009**, *694*, 1055-1058.

Simonian, A. L.; Good, T. A.; Wang, S.-S.; Wild, J. R. *Analytica Chimica Acta*, **2005**, *534*, 69-77.

Singer, M.; Jäschke, A. *J. Am. Chem. Soc.* **2010**, *132*, 8372-8377.

Smid, J. *Org. Prep. Proceed. Intl.* **1976**, *8*, 193-196.

Song, Y.; Kang, X.; Zuckerman, N. B.; Phebus, B. D.; Konopelski, J. P.; Chen, S. W. *Nanoscale* **2011**, *3*, 1984-1989.

Song, Z.; Chrisope, D. R.; Beak, P. *J. Org. Chem.* **1987**, *52*, 3940-3941.

Sun, L.; Tian, H. *Tetrahedron Lett.* **2006**, *47*, 9227-9231.

Sun, L.; Tian, H. *Tetrahedron Lett.* **2006**, *47*, 9227-9231.

Sun, L.; Wang, S.; Tian, H. *Chem. Lett.* **2007**, *36*, 250-251.

Takuwa, A.; Kanaue, T.; Yamashita, K.; Nishigaichi, Y. *J. Chem. Soc., Perkin Trans. 1*, **1998**, 1309-1314.

Tall, A. R.; Yvan-Charvet, L.; Wang, N. *Arterioscler. Thromb. Vasc. Biol.* **2007**, *27*, 257-260.

Tamble, C. M.; St. Onge, R. P.; Giaever, G.; Nislow, C.; Williams, A. G.; Stuart, J. M.; Lokey, R. S. *Mol. Biosyst.* **2011**, *7*, 2019-2030.

Thomas, K. G.; Zajicek, J.; Kamat, P. V. *Langmuir*, **2002**, *18*, 3722-3727.

Todo, H.; Terao, J.; Watanabe, H.; Kuniyasu, H.; Kambe, N. *Chem. Commun.* **2008**, 1332-1334.

Tong, A. H.; Lesage, G.; Bader, G. D.; Ding, H.; Xu, H.; Xin, X.; Young, J.; Berriz, G. F.; Brost, R. L.; Chang, M.; Chen, Y.; Cheng, X.; Chua, G.; Friesen, H.; Goldberg, D. S.; Haynes, J.; Humphries, C.; He, G.; Hussein, S.; Ke, L.; Krogan, N.; Li, Z.; Levinson, J. N.; Lu, H.; Ménard, P.; Munyana, C.; Parsons, A. B.; Ryan, O.; Tonikian, R.; Roberts, T.; Sdicu, A.-M.; Shapiro, J.; Sheikh, B.; Suter, B.; Wong, S. L.; Zhang, L. V.; Zhu, H.; Burd, C. G.; Munro, S.; Sander, C.; Rine, J.; Greenblatt, J.; Peter, M.; Bretscher, R.; Bell, G.; Roth, F. P.; Brown, G. W.; Andrews, B.; Bussey, H.; Boone, C. *Science* **2004**, *303*, 808-813.

Torok, D. S.; Figueroa, J. J.; Scott, W. J. *J. Org. Chem.* **1993**, *58*, 7274-7276.

Traylor, T. G.; Ware, J. C. *J. Am. Chem. Soc.* **1967**, *89*, 2304-2316.

Tsujioka, T.; Onishi, I.; Natsume, D. *Appl. Opt.* **2010**, *49*, 3894-3899.

Tsutsui, M.; Courtney, A. *Adv. Organomet. Chem.* **1977**, *16*, 241–282.

Tulevski, G. S.; Myers, M. B.; Hybertsen, M. S.; Steigerwald, M. L.; Nuckolls, C. *Science*, **2005**, *309*, 591-594.

Varma, S.; Sabo, D.; Rempe, S. B. *J. Mol. Biol.* **2008**, *376*, 13-22.

Viau, G.; Brayner, R.; Poul, L.; Chakroune, N.; Lacaze, E.; Fievet-Vincent, F.; Fievet, F. *Chem. Mater.* **2003**, *15*, 486-494.

Vignolle, J.; Tilley, T. D. *Chem. Commun.* **2009**, 7230-7232.

Villuendas, I.; Parilla, A.; Guerrero, A. *Tetrahedron*, **1994**, *50*, 12673-12684.

Ward, H. W. C. *Br. Med. J.* **1973**, *1*, 13-14.

Warta, R.; Sixl, H. *J. Chem. Phys.* **1988**, *88*, 95-99.

Winzeler, E. A.; Shoemaker, D. D.; Astromoff, A.; Liang, H.; Anderson, K.; André, B.; Bangham, R.; Benito, R.; Boeke, J. D.; Bussey, H.; Chu, A. M.; Connelly, C.; Davis, K.; Dietrich, F.; Dow, S. W.; El Bakkoury, M.; Foury, F.; Friend, S. H.; Gentalen, E.; Giaever, G.; Hegemann, J. H.; Jones, T.; Laub, M.; Liao, H.; Liebundguth, N.; Lockhart, D. J.; Lucau-Danila, A.; Lussier, M.; M'Rabet, N.; Menard, P.; Mittmann, M.; Pai, C.; Rebischung, C.; Revuelta, J. L.; Riles, L.; Roberts, C. J.; Ross-MacDonald, P.; Scherens, B.; Snyder, M.; Sookhai-Mahadeo, S.; Storms, R. K.; Véronneau, S.; Voet, M.; Volckaert, G.; Ward, T. R.; Wysocki, R.; Yen, G. S.; Yu, K.; Zimmermann, K.; Philippsen, P.; Johnston, M.; Davis, R. W. *Science*, **1999**, *285*, 901-906.

Xu, B. A.; Huang, Z. N.; Jin, S.; Ming, Y. F.; Fan, M. G.; Yao, S. D. *J. Photochem. Photobiol. A: Chem.* 1997, *110,* 35-40.

Xu, G. L.; Crutchley, R. J.; DeRosa, M. C.; Pan, Q. J.; Zhang, H. X.; Wang, X. P.; Ren, T. *J. Am. Chem. Soc.* **2005**, *127*, 13354-13363.

Yang, J.; Lee, J. Y.; Too, H.-P. *Analytica Chimica Acta* **2006**, *571*, 206-210.

Yang, T.; Pu, S.; Chen, B.; Xu, J. *Can. J. Chem.* **2007**, *85*, 12-20.

Yang, Y. F.; Zhou, Y. H.; Cha, C. S. *Electrochim. Acta* **1995**, *40*, 2579- 2586.

Yee, C. K.; Jordan, R.; Ulman, A.; White, H.; King, A.; Rafailovich, M.; Sokolov, J. *Langmuir* **1999,** *15,* 3486-3491.

Yee, C.; Scotti, M.; Ulman, A.; White, H.; Rafailovich, M.; Sokolov, S. *Langmuir*, **1999**, *15*, 4314-4316.

Yin, J.; Yu, G.-A.; Tu, H.; Liu, S. H. *Appl. Organometal. Chem.* **2006**, *20*, 869-873.

Zhai, J.; Zhai, Y.; Dong, S. *Colloids Surf. A*, **2009**, *335*, 207-210.

Zhang, S.; Chandra, K. L.; Gorman, C. B. *J. Am. Chem. Soc.* **2007**, *129*, 4876-4877.

Zhang, S.; Chandra, K. L.; Gorman, C. B. *J. Am. Chem. Soc.* **2007**, *129*, 4876-4877.

Zhang, Y.-L.; Shing, T. K. M. *J. Org. Chem.* **1997**, *62*, 2622-2624.

Zhong, Y.-W.; Vila, N.; Henderson, J. C.; Flores-Torres, S.; Abruña, H. D. *Inorg. Chem.* **2007**, *46*, 10470-10472.

Zuckerman, N. B.; Myers, A. S.; Quan, T. K.; Bray, W. M.; Lokey, R. S.; Hartzog, G. M.; Konopelski, J. P. *ChemMedChem*, **2012**, accepted.